THE ASTROPHYSICAL JOURNAL

An International Review of Spectroscopy and Astronomical Physics

FOUNDED IN 1895 BY GEORGE E. HALE AND JAMES E. KEELER

EDITORS

OTTO STRUVE
Managing Editor

S. CHANDRASEKHAR
Associate Managing Editor

Yerkes Observatory of the University of Chicago

PAUL W. MERRILL
Mount Wilson Observatory of the
Carnegie Institution of Washington

HARLOW SHAPLEY
Harvard College Observatory
Cambridge, Massachusetts

N. U. MAYALL
Lick Observatory
University of California

With the Collaboration of the American Astronomical Society

COLLABORATING EDITORS

CECILIA H. PAYNE-GAPOSCHKIN, *Harvard College Observatory;* H. N. RUSSELL, *Princeton University;* R. H. BAKER, *University of Illinois;* C. S. BEALS, *Dominion Astrophysical Observatory, Victoria;* LUIS E. ERRO, *Astrophysical Observatory, Tonanzintla;* O. C. WILSON, *Mount Wilson Observatory;* LYMAN SPITZER, JR., *Yale University;* A. N. VYSSOTSKY, *Leander McCormick Observatory;* ALBERT E. WHITFORD, *Washburn Observatory*

VOLUME 105

JANUARY–MAY 1947

THE UNIVERSITY OF CHICAGO PRESS
CHICAGO, ILLINOIS

CAMBRIDGE UNIVERSITY PRESS, LONDON

PUBLISHED JANUARY, MARCH, MAY, 1947

COMPOSED AND PRINTED BY THE UNIVERSITY OF CHICAGO PRESS
CHICAGO, ILLINOIS, U.S.A.

Astron. Obs
Wahr.

CONTENTS

NUMBER 1

CHROMOSPHERIC SPECTRUM FROM TEN ECLIPSE EXPEDITIONS. S. A. Mitchell 1

AN INTERPRETATION OF THE HEIGHTS OF LINES IN THE SOLAR CHROMOSPHERE. Rupert WILDT 36

A SEARCH FOR FAINT BLUE STARS. M. L. Humason and F. Zwicky 85

THE RELATIVE INTENSITIES OF THE CORONAL AND OTHER FORBIDDEN LINES. I. S. Bowen and P. Swings 92

RADIAL VELOCITIES AND SPECTRAL TYPES OF 181 DWARF STARS. Alfred H. Joy . . . 96

ZEEMAN EFFECT IN STELLAR SPECTRA. H. W. Babcock 105

THE SPECTRUM OF Z ANDROMEDAE IN AUGUST, 1946. Paul W. Merrill 120

EXTENDED SUM RULES FOR TRANSITION ARRAYS. Donald H. Menzel 126

THE ELECTRON VELOCITY DISTRIBUTION IN GASEOUS NEBULAE AND STELLAR ENVELOPES. David Bohm and Lawrence H. Aller 131

ON THE RADIATIVE EQUILIBRIUM OF A STELLAR ATMOSPHERE. XIII. S. Chandrasekhar . 151

ON THE RADIATIVE EQUILIBRIUM OF A STELLAR ATMOSPHERE. XIV. S. Chandrasekhar . 164

SPECTRAL TYPES OF STARS IN THE GLOBULAR CLUSTERS MESSIER 3 AND MESSIER 13. Daniel M. Popper 204

INFRARED SPECTRA OF EARLY-TYPE STARS. W. A. Hiltner 212

NOTES

BARNARD'S PHOTOGRAPHS OF MARS. Gerard P. Kuiper and Mary R. Calvert . . . 215

REVIEWS 216

ERRATUM 216

NUMBER 2

A PHOTOELECTRIC STUDY OF THE ECLIPSING VARIABLE, TX URSAE MAJORIS. C. M. Huffer and Olin J. Eggen 217

SPECTROSCOPIC OBSERVATIONS OF RIGEL WITH HIGH DISPERSION. Roscoe F. Sanford . . 222

THE SPECTROSCOPIC ORBIT OF σ PISCIUM. Emilia Pisani Belserene 229

INTERPRETATION OF RADIO RADIATION FROM THE MILKY WAY. Charles Hard Townes . 235

THE PHYSICS OF COSMIC GRAINS. Felix Cernuschi 241

SMALL DARK NEBULAE. Bart J. Bok and Edith F. Reilly 255

THE ECLIPSING SYSTEM UX MONOCEROTIS. Sergei Gaposchkin 258

LUMINOSITY FUNCTIONS OF THE BRIGHTER STARS. John W. Abrams 268

A STUDY OF THE SPECTRUM VARIABLES OF TYPE A. Armin J. Deutsch 283

STELLAR MODELS WITH CONVECTION AND WITH DISCONTINUITY OF THE MEAN MOLECULAR WEIGHT. P. Ledoux 305

STELLAR MODELS WITH ISOTHERMAL CORES AND POINT-SOURCE ENVELOPES. Marjorie Hall Harrison 322

ON THE BROADENING OF NEUTRAL HELIUM LINES IN STELLAR SPECTRA. Margaret K. Krogdahl 327

NOTES

AW PEGASI. Lois T. Slocum 350

ERRATUM 352

NUMBER 3

FINE STRUCTURE OF THE INFRARED ATMOSPHERIC OXYGEN BANDS. L. Herzberg and G. Herzberg 353

ATOMIC LINES IN THE SPECTRUM OF R ANDROMEDAE. Paul W. Merrill 360

RELATIVE *gf*-VALUES FOR LINES OF *V* I. Robert B. King 376

THE SPACE MOTIONS OF THE R STARS. Noah W. McLeod 390

ON THE ORIGIN OF THE HEAVY ELEMENTS. G. B. van Albada 393

ATMOSPHERIC TEMPERATURES FROM INFRARED EMISSION SPECTRA OF THE MOON AND EARTH. I. THE OZONE LAYER. Arthur Adel 406

A SLOW CORPUSCULAR RADIATION FROM THE SUN. K. O. Kiepenheuer 408

ON THE RADIATIVE EQUILIBRIUM OF A STELLAR ATMOSPHERE. XV. S. Chandrasekhar . 424

ON THE RADIATIVE EQUILIBRIUM OF A STELLAR ATMOSPHERE. XVI. S. Chandrasekhar and FRANCES H. BREEN 435

ON THE RADIATIVE EQUILIBRIUM OF A STELLAR ATMOSPHERE. XVII. S. Chandrasekhar . 441

ON THE RADIATIVE EQUILIBRIUM OF A STELLAR ATMOSPHERE. XVIII. S. Chandrasekhar and Frances H. Breen 461

ZODIACAL LIGHT IN THE SOLAR CORONA. H. C. van de Hulst 471

RADIAL VELOCITIES AND ABSOLUTE MAGNITUDES OF Be STARS. Burke Smith 489

THE M-TYPE SUPERGIANT MEMBERS OF THE DOUBLE CLUSTER IN PERSEUS. W. P. Bidelman 492

NOTES

A NEW SPECTROSCOPIC TRIPLE STAR, HD 157978–9. Dean B. McLaughlin . . . 497

THE ECLIPSING SYSTEM RY PERSEI. Frank Bradshaw Wood 498

NOTE ON THE ECLIPSING SYSTEM OF RX GEMINORUM. Sergei Gaposchkin 499

THE TRUMPLER STARS. O. Struve 499

CHANGES IN THE INFRARED SPECTRUM OF VV CEPHEI. P. C. Keenan and J. A. Hynek 500

RECENT CHANGES IN THE SPECTRUM OF β MONOCEROTIS A. Arne Slettebak . . . 502

THE SPECTRAL TYPE AND LUMINOSITY OF β CANIS MAJORIS. Anne B. Underhill . . 502

THE PERIOD OF THE SPECTRUM VARIABLE 56 ARIETIS. Armin J. Deutsch 503

REVIEWS 505

INDEX 507

THE ASTROPHYSICAL JOURNAL

AN INTERNATIONAL REVIEW OF SPECTROSCOPY AND ASTRONOMICAL PHYSICS

VOLUME 105 JANUARY 1947 NUMBER 1

CHROMOSPHERIC SPECTRUM FROM TEN ECLIPSE EXPEDITIONS

S. A. MITCHELL
Leander McCormick Observatory
Received July 23, 1946

ABSTRACT

The heights in kilometers and the intensities are given for 3500 lines. For 5000 A to the red side of 3066 A the photographs of the flash spectrum have a uniform dispersion of 10.8 A/mm and for an additional 800 A the dispersion is 80 A/mm. The spectra includes 35 lines of the Balmer series of hydrogen and from *H* 11 to *H* 40 of the Paschen series.

Since the date of the earlier publication by the author, successful photographs have been obtained at the eclipses of 1930 and 1937, both expeditions being in the Pacific Ocean. The heights and intensities from the earlier eclipses were re-estimated, and an attempt was made to secure uniformity in the observed material.

Throughout my life as an eclipse observer I have experienced rare good luck. In one hundred thousand miles of travel by land and sea, I have had an accumulated duration of totality of less than one-half hour, or 26 minutes, for securing the observations. From my ten eclipses I have secured measurable spectra at five different eclipses—in 1901, 1905, 1925, 1930, and 1937—while, in addition, in 1918 a few of the stronger lines were photographed through clouds.

Three times heretofore I have published wave lengths and associated data from my photographs of the flash spectrum. In each case the original was published in the *Astrophysical Journal*, the most recent discussion being in 1930, in Volume **71**, and in *Publications of the Leander McCormick Observatory*, Volume **5**, Part II. The spectra taken in 1905 and 1925 were included together with a region of 250 A of short wave lengths photographed at the 1926 eclipse by Davidson and Stratton. A total of 3250 lines was tabulated between 3066 A and 7065 A.

Since the date of the preparation of the material for publication, I have been on three additional expeditions, on two of which I obtained successful spectra.

For the 1930 eclipse on Niuafoou, or Tin-Can Island, in the South Pacific, the plane mirrors for the coelostats used were aluminized for the first time; with two concave gratings of dispersion 10.8 A/mm, the region from the extreme ultraviolet to 7800 A in the infrared was covered. There was a considerable overlap from 4650 A to 6800 A between the spectra taken by the two gratings. In 1937, on Canton Island, again in the South Pacific Ocean, instead of the concave grating always kindly loaned by Professor F. A. Saunders and used in eclipses from 1905 to 1930 inclusive, I had a grating of similar dispersion, 10.8 A/mm, loaned by Mount Wilson Observatory. The grating was aluminized,

and all coelostat mirrors were likewise coated with aluminum. Through the kindness of H. D. Curtis, I had the use of the concave-grating spectrograph constructed by him for the 1925 eclipse. The spectra for the extreme infrared gave a dispersion of about 80 A/mm. Curtis had been invited and had accepted the invitation to be a member of the 1937 expedition, but an unfortunate illness prevented his participation.

All spectra in the present discussion were photographed on fixed plates, or rather, on heavy celluloid films. The exposures for first and second flash at each eclipse were timed through observations with a direct-vision spectrograph, consisting of old-fashioned binoculars with a replica grating over the lens to be used for the right eye and dark glass over the lens for the left eye. At each eclipse since 1905 the celluloid films have been coated specially at the Research Laboratories of Eastman Kodak Company, through the sympathetic co-operation of Dr. C. E. K. Mees.

THE CHROMOSPHERIC SPECTRA

Included in the present compilation are photographs of four eclipses—1905, 1925, 1930, and 1937. There is a total of 3500 lines. For 5000 A to the long-wave-length side of 3066 A, the dispersion is 10.8 A/mm, and for the balance of 800 A the spectra are at the smaller dispersion of 80 A/mm. The two later eclipses of 1930 and 1937 added very materially to the results of the two earlier eclipses already published. With grating and coelostat mirror both aluminized, the spectra in 1937 were in greater strength in the extreme ultraviolet than previously, with the result that heights in the chromosphere in kilometers are given for most of the spectrum lines of shortest wave lengths. The spectra of 1930 and 1937 were specially valuable in the region of wave lengths greater than 5000 A. The 1937 spectra extend to *H* 11 of the Paschen series of hydrogen; and this series, up to and including *H* 40, was photographed for the first time at an eclipse. Also in this long-wave-length region are the strong Ca^+ triplet, lines of *He* and *O* and of a few metals, and the coronium line at 7892 A.

For much of the region included in the tabular material, the spectra from the four eclipses were available for intercomparison, together with the considerable overlap from 4650 A to 6800 A from the 1930 eclipse. It goes without saying that both the heights in the chromosphere and the intensities depend greatly on the sensitivity of the emulsion at different wave lengths. It also goes without saying that vast improvements have been made in photographic emulsions in the quarter-century since the Spanish eclipse of 1905. Hence, with the additional material available, it became desirable to re-estimate both the intensities and the heights of the two earlier eclipses of 1905 and 1925 and then to try to put the results of the four eclipses on as uniform a system as possible. The technique for estimating intensities was simple enough and followed the practice of A. S. King through his long years of work at Mount Wilson. The spectra to be compared, on celluloid films $1\frac{1}{4}$ inches in width, were placed parallel to each other, film side down, on a frame of glass illuminated from beneath. With the dispersion of 10.8 A/mm, it was a simple matter to clamp to the eclipse film a transparent millimeter scale, in order to keep track of the wave lengths. After completing estimates on a few hundred angstroms, the millimeter scale could be gradually shifted.

As all chromospheric spectra were normal in scale, I had the use of two photographic prints on exactly the same scale for wave lengths; the upper print of the two being the Rowland Atlas of the Fraunhofer spectrum reduced sixfold, and immediately below a fivefold enlargement of the flash spectrum. A reproduction appears in *Ap. J.*, **71**, 48 1930. One could see at a glance, therefore, the striking differences in intensities between the Fraunhofer and the chromospheric spectra. In adopting a scale of intensities for the chromosphere, it seemed the wisest plan to follow as closely as possible the Rowland scale, which has become the standard for solar work. At certain sections of wave lengths, where strong ionized lines became bunched, it was a difficult task to keep to the scale thus established.

The eye and the memory of the observer had to be gradually trained. As a matter of fact, the estimates of differences of intensities of spectral lines resemble the technique of estimating the differences of stellar magnitudes, either visually directly at the telescope or in the office on a photographic plate. The present writer has had experience spread over many years in making thousands and thousands of estimates in deriving the magnitudes of all comparison stars for all the regions adopted by the American Association of Variable Star Observers. As stars approximate points of light and have no peculiarities except that of color, it is a much simpler undertaking to estimate differences of stellar magnitudes than to estimate intensities of spectral lines. With slitless spectra, especially for the stronger chromospheric lines, it is necessary to combine both the blackness and the width in order to furnish the integrated intensity. After long-continued training and experience that started with the spectra of the 1901 eclipse and after consulting many observers, particularly those of Mount Wilson, it is the considered opinion of the present writer that estimates by a trained observer have as high, or even a higher, accuracy than measures by microphotometer of any kind.

To secure the tabular material has been a long-drawn-out task, spread throughout a great number of years. To keep the scales of heights and intensities on as uniform a scale as possible, one might go back and forth to the regions of wave lengths done yesterday, last week, or six months previously. For obvious reasons, the work proceeded from shorter to longer wave lengths.

Both the intensities and the heights in the chromosphere depend on a large number of different factors. For the first flash at the beginning of totality, the chromospheric arcs of lowest levels above the photosphere are covered up by the advancing moon within a small fraction of a second of time. Hence the timing of the exposure is of the very greatest importance. With slitless spectra the character of the seeing is almost equally important. The low-level lines are always superposed on a strong continuous background, and hence, under poorer conditions of seeing, the spectrum line becomes broader and weaker compared with the continuous background and practically disappears. Needless to say, perfect focus is required to obtain the best results. Then, in addition, the mountains on the projected moon are very bothersome, as also are prominences, Baily's beads, "hot spots," or affected areas of the sun.

When two things are compared, such, for instance, as chronometers on ship board, and differences are noted, it is difficult to decide which chronometer is the faulty performer. When scientists compare physical data and differences are noted, it is always so easy to blame the other fellow. With spectra from four different eclipses to compare, differences between eclipses were continually observed, and notes were made on the observing sheets. The problem then arose to know what was best to do with these notes. For the reasons given in the preceding paragraph, differences between one chromospheric spectrum and another were to be expected. The tabular material herewith presented represents what might be called a "weighted average" of the four eclipses.

Chiefly on account of the fine qualities of the seeing and of fortunate timing of the exposures, I regard the 1905 flash spectrum as my best. It reaches lower levels in the photosphere than any of the others. Almost equally good, however, are the 1930 and the 1937 spectra. These two later spectra extended the region of investigation at the ultraviolet end, but most particularly at the red end, up to 8863 A.

Attention should be called to the fact that the heights in kilometers in the present publication at wave lengths greater than 5000 A are usually greater than those appearing in the previous publication of 1930. The reason is obvious, namely, the greater sensitivity of the photographic emulsion in the later years.

DIFFERENCES NOTED AT DIFFERENT ECLIPSES

Attention might be called also to some of the differences between the various eclipses. It must be confessed that it was a continual surprise, while the detailed comparisons of

the spectra at the four eclipses were being made, that there were comparatively so few differences in heights and intensities between the different spectra. However, there were certain differences noted, and some of the more pronounced ones are given here. Perhaps the greatest difference of all was in the *CN* band at 3883 A, the 1905 eclipse showing the banded spectrum in greater strength than in 1930. As the year 1905 was near sun-spot maximum, one is tempted to conclude that the increased solar activity caused greater relative strength to the low-lying *CN* bands. A simpler explanation seems to be the fortunate timing of the exposure in 1905.

The relative intensities of *He* and He^+ at different elevations above the photosphere have been noted by other observers, particularly by Menzel. The He^+ line at 4686 A has an intensity 2 close to the photosphere, but a greater intensity of 8 at 1000 km and higher. The three eclipses of 1905, 1930, and 1937 tell the same story. The neutral *He* line at 4713 A has an intensity of 15 at lower heights and 25 at greater heights. The note regarding *He* 5016 states: "Weak at low heights in both years 1905 and 1930, most intense at 'hot spot' in 1930 with intensity 20 at 1000 kms." The *He* line at 4388 A had an intensity 2 at 500 km, but at 1500 km the intensity was 10 for the three eclipses of 1905, 1930, and 1937. Interesting differences of intensities were noted between the *He* line at 3819.6 and the *Fe* line 3820.4.

Differences in intensities at different eclipses were observed for the stronger lines of certain metallic spectra. For instance, all lines of the strong multiplet, No. 3, of Mn^+ (given in the accompanying tabulation) had greater intensities and extended to greater heights in 1930 as compared with 1905.

Wave Length	1905	1930	Wave Length	1905	1930
3441.98	20	25	3488.68	12	18
3460.31	18	25	3495.83	6	12
3474.04	15	25	3496.81	4	5
3474.12			3497.54	5	8
3482.90	15	20			

On the average, the stronger lines of Fe^+ and Ni^+ are more intense and extend to greater heights in 1930 than in 1905 and 1925. Many intercomparisons were made between the heavier lines of Fe^+ and Ti^+ and Cr^+. As a general rule, the Fe^+ lines do not extend as high as do the Cr^+ and Ti^+ lines of the same intensity, while the Cr^+ lines are more intense at greater heights than are Ti^+ lines of the same average intensities. The strong La^+ line at 3988.5 had an intensity of 10 in 1905 and the smaller intensity 5 in 1925, 1930, and 1937. It was interesting to note the relative increase in intensities at a "hot spot," for instance, the Sc^+ line at 5657.87A and other lines in the same multiplet and for many lines of Fe^+ in the strong multiplet, No. 74, where the strongest line is at 6456.38 A. Similar effects are found in the strong Si^+ lines at 6347A and 6371 A. It seems unnecessary to record here further differences of the many noted in the intercomparisons of the spectra of the four eclipses. As already stated, most of these differences can be explained by differences in the qualities of seeing and exposure times and by factors noted in the article, "The Relative Distribution and Abundance of the Elements in the Lower Chromosphere," by S. A. Mitchell and Emma T. R. Williams (*Ap. J.*, **77**, 1, 1933).

In preparing the present material for publication, the author would again like to express his high appreciation for the rare good luck that has stayed with him throughout the many years of his observations of total eclipses. In the pioneer days of four decades ago, relatively little was known (compared with present-day information) regarding the laboratory spectra of the elements. Lockyer had already pointed out the greater strength of the enhanced lines in the chromosphere, as compared with the Fraunhofer

spectrum; but what were the enhanced lines other than that, for some reason then unknown, they had a greater intensity in the spark than in the arc spectrum? For interpreting the flash spectrum, there was then nothing to do but to draw one's own conclusions by slowly and painfully going to the published literature, by tabulating the results, and then deciding from the estimated intensities, frequently on different scales, just which lines were enhanced and which were not. With this condition as a background, it is little wonder that the author should regard himself as most fortunate in the recent appearance of *A Multiplet Table of Astrophysical Interest* by Charlotte E. Moore (Princeton Observatory, 1945). It was a great joy to have a publication from the highest authority in order to decide on the element both in photosphere and in chromosphere corresponding to a particular wave length.

The chromospheric spectrum is a reversal of that of the photosphere, but with striking differences in intensities. In forming the Fraunhofer line, the radiation from the photosphere passes *radially* through the relatively cooler gases of the chromosphere, while for the flash spectrum the radiation takes place in a direction *tangential* to the photosphere. As the intensity of radiation, both in absorption and in emission spectra, depends on the total number of atoms encountered, it is of the highest importance to be able to evaluate the relative numbers of atoms involved. For deriving this information the heights in kilometers that atoms extend above the photosphere become of major interest. Hence it seems indisputable that the greatest contribution to be made by spectroscopic observations at a total eclipse to our knowledge of conditions in the sun is information regarding the heights that the atoms of the elements extend in kilometers above the photosphere. The heights given in Table 1 cannot record the maximum heights attained by the atoms involved but, rather, the heights where the atoms may be detected, depending on the threshold value of the photographic emulsion. In other words, the number of atoms involved in the tip of a chromospheric arc of *Fe* extending to 400 km is exactly the same number of atoms as are involved in the tip of the 3933 A line of Ca^+ extending to 14,000 km.

In attempting to interpret the differences between flash and Fraunhofer spectra, it was early recognized—and that long before there was any knowledge of multiplet structure—that the strongest lines of any element, like neutral *Fe*, extended to the greatest heights above the photosphere. The greater the heights, the greater became the relative differences in the numbers of atoms involved in the radial and the tangential paths. The Saha theory of ionization explained in quite simple fashion the difficulties that had been so perplexing in the earlier interpretations of eclipse spectra. Hence for a neutral element like *Fe* the spectral lines of greatest strength are those that extended to the greatest heights above the photosphere. The strongest lines of *Fe* are those that involve the greatest number of atoms, and these are the resonance lines and those of low excitation potentials. Similarly, the greatly increased strengths of the enhanced lines in the chromospheric spectrum have the simple explanation of the great heights above the photosphere reached by the ionized atoms. Hence the strongest lines of a neutral element have increased strengths over their intensities in the Fraunhofer spectrum, and they therefore behave almost like enhanced lines.

In making the final draft for Table 1 the writer was again under deep obligation to Charlotte Moore Sitterly in the use of her own revision of the *Revised Rowland*. This revision was particularly helpful in giving the latest reliable information regarding identification of elements, but specially for the intensities given in Rowland. As is well known, these revisions of hers were from spectra taken at the Mount Wilson Observatory. At the greatest wave lengths there are many remarkable alterations in the intensities published in the *Revised Rowland*.

The first column of Table 1 is the wave length measured from eclipse spectra and on the system of the *Revised Rowland*. In giving the "Element" it seemed the wisest plan to confine attention, corresponding to any one wave length, to no more than two elements.

With the help of the *Rowland Atlas* printed on the same scale as the enlarged flash spectrum, with the Allegheny *Map of the Solar Spectrum* for the greater wave lengths, with the *Revised Rowland*, and any other published material, but especially with the *Multiplet Table of Astrophysical Interest*, the author gives what he considers the element, or elements, chiefly responsible for the spectral line of each wave length. The element of greatest importance *in the interpretation of the chromospheric spectrum* is given first.

In the third and fourth columns, the intensities from Rowland and from the flash spectrum are given, the former called "Sun." For blended lines, the superior figure to the right of the solar intensity gives the number of lines in Rowland blended together. The fifth column gives the heights in kilometers of the vapors of the chromosphere. The excitation potentials recorded are those corresponding to the high atomic level (and taken from the *Multiplet Table*) for the first of the two elements, if two elements are given. When blanks are found in the column of excitation potentials, it is an indication that the line in question is still unclassified. This is true for thirty lines of neutral *Fe*, for a few lines of other elements, and for the carbon molecules *CN*, *CH*, and C_2. The low value of the excitation potential belonging to a line of any praticular wave length may usually be found by referring to the earlier publication on the spectrum of the chromosphere in *Ap. J.*, Volume **71**, or to the *Revised Rowland*.

The diminished intensity in the flash spectrum of the last line in the tabular material at 8862.9 A is the result of the diminished sensitivity of the emulsion.

TABLE 1

Chromosphere	Element	Sun	Flash	Height in Km	High E.P.	Chromosphere	Element	Sun	Flash	Height in Km	High E.P.
3066.32....	Ti^+	3^2	3	1000	4.02	3187.71....	He-V^+	2	10	1500	23.61
3072.16....	Ti^+	3	3	1000	4.05	3188.45....	V^+-Fe	6	3	800	4.96
3072.97....	Ti^+	6	5	1000	4.02	3190.82....	Ti^+-V^+	7^3	12	1200	4.95
3075.24....	Ti^+	3	5	1000	4.02	3191.91....	Zr^+-Ti	2^2	2	800	4.66
3078.64....	Ti^+	8	8	1500	4.04	3192.88....	Fe^+-Fe	3^2	7	1000	5.53
3088.02....	Ti^+	7	12	2000	4.05	3193.79....	Fe^+	1	7	1000	5.58
3092.88....	V^+-Al	8^4	2	.....	4.38	3195.71....	V^+-Ti^+	3^2	2	.....	3.97
3102.24....	V^+	3	3	1000	4.34	3196.04....	Fe^+	3	7	1000	5.52
3106.23....	Ti^+	3	2	1000	5.21	3197.01....	Cr^+-Fe	6^3	8	1000	6.39
3110.71....	Ti^+-V^+	5	4	1000	5.19	3197.51....	Ti^+-Fe	1	2	.....	3.89
3117.75....	Ti^+-Ti	5^3	1	.....	5.18	3200.23....	V^+-Fe	9^3	3	800	3.99
3118.41....	V^+	3	2	.....	4.29	3202.50....	Ti^+-Fe	2	10	1000	4.93
3118.62....	Cr^+	2	12	1500	6.37	3203.32....	V^+-Ti^+	3^2	4	800	3.96
3119.74....	Ti^+	1	2	.....	5.19	3206.01....	Ti^+	1	2	800	4.93
3120.36....	Cr^+	3	10	1500	6.38	3208.47....	Cr^+-V^+	3^3	2d	600	6.38
3121.02....	V^+-Cr^+	4	1	.....	4.34	3209.17....	Cr^+	1	7	1000	6.38
3125.00....	Cr^+-	4	15	1500	6.39	3210.49....	Fe^+	2	8	1000	5.56
3125.34....	V^+	5	1	.....	4.27	3211.98....	Fe	4^3	2	600	6.23
3126.20....	V^+-Zr^+	6^2	2	1000	4.31	3213.27....	Fe^+-Ti^+	4^2	12	1200	5.53
3128.68....	Cr^+	2	6	1500	6.37	3214.12....	Zr^+-Fe	7^4	3	800	3.93
3129.12....	Zr^+	0	1	.....	4.47	3214.78....	Ti^+-V^+	3	6	1000	3.89
3129.74....	Zr^+	0	2	.....	3.98	3215.34....	Ca-V	3^2	1	600	5.72
3130.40....	V^+-Be^+	4^2	3	1000	4.29	3215.89....	Fe-	3^2	1	600	6.30
3130.76....	Ti^+-Ti	3	4	1000	3.95	3216.70....	V^+	1	4	800	3.97
3131.13....	Be^+	1	1	.....	3.94	3217.10....	Ti^+-V^+	3^2	10	1500	3.86
3132.05....	Cr^+	4	20	1500	6.41	3217.40....	Cr^+-Fe	2	8	1000	6.37
3133.38....	V^+-Zr^+	3^2	2	.....	4.27	3218.25....	Ti^+	2	5	1000	5.40
3134.17....	Ni-Fe	8	0	.....	4.15	3219.77....	Fe-Cr	5^2	2	600	6.25
3135.01....	V^+	2	1	.....	6.45	3222.00....	Fe	4^2	1	600	6.30
3135.42....	Fe^+-Fe	2^2	1	.....	7.81	3222.89....	Ti^+	4	10	1500	3.84
3136.67....	Cr^+-Co	3	6	1000	6.38	3223.51....	Ti	0	1	600	5.84
3138.66....	Zr^+	1	2	.....	4.03	3224.26....	Ti^+	2	5	1000	5.40
3143.75....	Ti^+	4	3	1000	3.95	3225.77....	Fe	3	2	600	6.21
3147.22....	Cr^+	3	5	1000	6.39	3226.79....	Ti^+-Fe	3^2	3	1000	3.85
3148.04....	Ti^+	2	6	1000	3.92	3227.74....	Fe^+-Fe	4^2	12	1200	5.49
3149.96....	Cr^+-Fe^+	4^3	2	800	8.04	3228.59....	Ti^+	2	7	1000	4.90
3152.24....	Ti^+	5	3	800	4.04	3229.23....	Ti^+-Fe	5^2	9	1500	3.82
3154.19....	Ti^+-Fe^+	3	6	1000	4.02	3229.43....	Ti^+	2	5	1000	4.95
3155.63....	Ti^+	3	2	800	4.05	3231.32....	Ti^+	2	4	1000	3.95
3157.51....	Ti^+-	2^2	1	.....	3.92	3231.80....	Zr^+-V^+	2^2	2	600	3.86
3158.89....	Ca^+	2	7	1000	7.02	3232.29....	Ti^+	2	6	1000	4.93
3161.19....	Ti^+	3	7	1000	4.02	3232.82....	Fe^+-Ni	3^2	2	600	7.95
3161.80....	Ti^+	3	8	1000	4.02	3234.49....	Ti^+	10	30	2000	3.86
3162.56....	Ti^+	4	10	1000	4.04	3236.15....	Ti^+	1	4	1000	4.89
3163.11....	Fe^+	2^2	2	.....	5.57	3236.59....	Ti^+	7	25	2000	3.84
3165.98....	Zr^+-Fe^+	2	2	.....	4.06	3237.90....	V^+-Fe^+	2	3	1000	5.84
3166.40....	Zr^+-Fe	3^3	2	.....	4.70	3239.03....	Ti^+	6	20	2000	3.82
3167.84....	Fe^+-Fe	5^2	4	800	7.69	3239.69....	Ti^+	2	8	1000	4.89
3168.49....	Ti^+	4	12	1200	4.05	3241.12....	Zr^+	1	2	800	3.85
3170.31....	Fe^+	2	3	800	5.58	3242.00....	Ti^+	7	25	2000	3.81
3177.56....	Fe^+	2	2	600	7.77	3243.06....	Ni	6	2	600	3.83
3179.33....	Ca^+	5	8	1000	7.02	3243.74....	Fe^+-Mn	2	3	1000	7.94
3180.24....	Fe	3	2	.....	6.32	3245.10....	La^+	— 1	2	600	3.98
3180.67....	Cr^+-Cr	4^2	10	1000	6.41	3246.05....	Fe	7^2	2	600	3.91
3181.30....	Ca^+-Cr^+	4^2	4	1000	7.02	3247.22....	Fe^+-Fe	4^2	3	800	7.94
3183.11....	Fe^+	2	5	1000	5.57	3247.56....	Cu	10	3	800	3.80
3184.08....	Ti^+-V	3^2	2	.....	3.89	3248.64....	Ti^+	1	6	1500	5.04
3185.26....	Fe^+	2	4	1000	5.59	3249.40....	Ti^+	2	2	600	4.87
3186.01....	Ce^+	1^2	1	.....	4.59	3251.21....	Fe	3	2	600	5.98
3186.72....	Fe^+	3	7	1000	5.56	3251.96....	Ti^+-V^+	7^2	10	1500	3.81
3187.37....	Fe^+	1	2	.....	8.00	3252.94....	Ti^+-Mn	9^2	12	1500	3.82

TABLE 1—*Continued*

Chromosphere	Element	Sun	Flash	Height in Km	High E.P.	Chromosphere	Element	Sun	Flash	Height in Km	High E.P.
3254.24....	Ti^{+}-Fe	11^{3}	10	1200	3.84	3312.21....	Co-Fe	3	1	500	5.67
3254.72....	V^{+}-V	5	4	800	5.81	3312.75....	Fe^{+}-Ti	2	4	800	4.80
3255.88....	Fe^{+}	6	12	1200	4.77	3313.97....	Fe^{+}	1	7	1000	4.82
3256.46....	Zr^{+}-Fe	1	2	800	4.50	3314.54....	Ti-Mn	5^{2}	2	500	4.77
3256.89....	Fe	4^{2}	1	600	.....	3315.32....	Ti^{+}	3	7	1000	4.94
3257.41....	Fe-	10^{3}	2	600	4.77	3315.68....	Ni	7	2	500	3.83
3257.91....	V^{+}	0	2	600	6.27	3317.30....	Fe-Mn	4^{3}	2d	500	5.99
3258.34	Mn	3	1	600	5.96	3318.03....	Ti^{+}	6	8	1000	3.84
3258.73....	Fe^{+}	3	3	1000	7.66	3319.09....	Fe-Ti^{+}	6^{3}	2	500	6.70
3259.06....	Fe^{+}	3	3	1000	7.67	3320.29....	Ni	7	2	500	3.88
3260.25....	Ti^{+}-Mn	5	2	800	4.94	3321.71....	Ti^{+}	4	12	1200	4.94
3261.57....	Ti^{+}	7^{2}	12	1500	5.01	3322.29....	Ni	3	2	500	4.14
3262.37....	Fe	3	2	500	.....	3322.91....	Ti^{+}	8^{2}	22	1500	3.86
3263.58....	Ti^{+}-Fe	8^{2}	3d	1000	4.94	3323.75....	Fe	3	2	500	6.53
3264.76....	Fe^{+}-Zr^{+}	11^{4}	4	1000	4.82	3324.06....	Cr^{+}	4	4	1000	8.47
3265.06....	Fe	2	3	500	5.95	3324.54....	Fe	4^{2}	3	500	6.11
3265.64....	Fe-La^{+}	6^{2}	2	600	3.87	3325.50....	Fe	3	2	500	6.15
3266.95....	Fe^{+}	1	1	600	7.53	3326.75....	Ti^{+}	5	9	1000	3.82
3267.71....	V^{+}	6	7	1200	4.84	3327.87....	V^{+}	2	3	1000	4.12
3270.15....	Cr^{+}-Co	1	3	800	6.23	3328.40....	Cr^{+}	2	3	1000	6.12
3271.11....	V^{+}-Zr^{+}	11^{2}	10	1200	4.86	3328.88....	Fe	3	2	500	6.96
3271.62....	Ti^{+}-Fe	6	5	1200	5.01	3329.42....	Ti^{+}-Co	8^{2}	20	1500	3.84
3272.17....	Ti^{+}-Zr^{+}	7^{2}	6	1200	4.99	3329.99....	Mg	5^{2}	4	1000	6.40
3273.03....	Zr^{+}	2	4	800	5.93	3331.73....	Fe	4^{2}	3	500	6.13
3274.00....	Cu	10	3	800	3.77	3332.08....	Ti^{+}	3	15	1200	4.94
3275.29....	Ti^{+}	3	3	800	4.84	3334.17....	Zr^{+}-Co	6^{3}	3d	600	4.70
3276.12....	V^{+}	5	10	1200	4.89	3334.62....	Zr^{+}	0	2	600	4.26
3276.82....	Ti^{+}	5^{2}	4	800	4.84	3335.18....	Ti^{+}	6^{2}	20	1500	3.82
3277.36....	Fe^{+}	7	20	1200	4.75	3336.30....	Cr^{+}-Fe	4^{2}	8	1000	6.11
3278.26....	Ti^{+}	5	6	1000	4.99	3336.66....	Mg	8	5	800	6.40
3278.90....	Ti^{+}	4	8	1000	4.84	3336.90....	Ti^{+}-Ni	2^{3}	2	600	4.87
3279.31....	Zr^{+}	2	4	800	3.86	3337.38....	La^{+}-Co	2^{2}	3	600	4.10
3279.93....	Ti^{+}-V^{+}	3^{2}	3	800	4.87	3337.87....	Ti^{+}	3^{2}	4	800	4.93
3281.32....	Fe^{+}	5	15	1200	4.80	3339.16....	Fe-Ni	3^{2}	2	500	6.14
3282.33....	Ti^{+}	5	8	1000	4.98	3339.79....	Cr^{+}	3	15	1200	6.12
3282.86....	Zr^{+}-Ni	6^{3}	2	800	5.58	3340.33....	Ti^{+}	5^{2}	20	1500	3.81
3284.70....	Zr^{+}	1	4	600	3.76	3341.88....	Ti^{+}-Fe	8^{2}	35	2000	4.26
3285.41....	Fe^{+}	2	6	1000	4.83	3342.27....	Fe	6^{2}	2	500	5.96
3286.78....	Fe	7	2	600	5.92	3342.61....	Cr^{+}	3	10	1000	6.14
3287.65....	Ti^{+}	5	12	1000	5.64	3343.74....	Ti^{+}	4	10	1000	3.84
3288.18....	Ti^{+}	3	2	600	3.89	3344.50....	La^{+}-Ca	2	3	600	3.92
3288.60....	Ti^{+}-Zr^{+}	6^{4}	4	800	4.98	3344.82....	Zr^{+}	0	3	600	4.70
3289.34....	V^{+}-Fe^{+}	7^{2}	4	600	4.84	3344.99....	Zn-Ti	4^{2}	1	400	7.75
3290.83....	Fe	6^{2}	1	500	5.96	3346.73....	Ti^{+}	5^{2}	10	1000	3.82
3292.05....	Fe-Cr^{+}	8^{3}	3	600	6.99	3347.89....	Cr^{+}-Fe	6^{2}	8d	1000	6.11
3295.49....	Cr^{+}	2	3	800	7.90	3349.00....	Ti^{+}-Cr	9^{3}	30	1500	3.81
3295.83....	Fe^{+}	6	15	1200	4.82	3349.41....	Ti^{+}	9^{2}	40	2500	3.73
3298.73....	V^{+}-Co	5^{2}	2	600	4.86	3350.46....	Ti^{+}-Ni^{+}	3^{2}	3	600	4.84
3299.41....	Ti	2	1	500	4.64	3351.60....	Fe-Ti	3^{2}	2	500	5.87
3302.14....	Ti^{+}	4	2	600	3.89	3352.11....	Ti^{+}	2	4	800	4.90
3302.81....	Fe^{+}-Na	8^{2}	15	1200	4.77	3353.11....	Cr^{+}-Fe	4^{3}	3	500	6.10
3303.51....	Fe^{+}-Fe	5^{2}	10	800	4.83	3353.74....	Sc^{+}	4	12	1000	3.99
3305.14....	Zr^{+}-Fe	2	2	500	3.77	3354.35....	Zr^{+}-Co	3	4	500	4.43
3306.04....	Fe-	8^{3}	2	500	5.92	3354.66....	Ti	3	3	400	3.70
3306.31....	Zr^{+}-Fe	6^{2}	4	600	3.77	3355.22....	Fe	4	2	400	6.97
3307.08....	Cr^{+}-La^{+}	4^{3}	4	600	7.88	3356.11....	Zr^{+}	1	4	600	3.77
3307.74....	Ti^{+}-Cr	4	2	500	3.85	3357.37....	Zr^{+}-Cr^{+}	3^{2}	4	600	3.68
3308.80....	Ti^{+}-Mn	7^{2}	7	1000	3.86	3358.50....	Cr^{+}	4	15	1200	6.12
3309.54....	Ti-Ti^{+}	2	1	400	4.78	3359.72....	Sc^{+}	2	3	800	3.68
3310.55....	Fe-Cr^{+}	6^{3}	1	400	6.97	3360.05....	Zr^{+}-	3^{2}	2	500	5.15
3311.87....	Cr^{+}-Mn	2	3	600	7.86	3360.35....	Cr^{+}	2	12	1000	6.76

TABLE 1—*Continued*

Chromo-sphere	Element	Sun	Flash	Height in Km	High E.P.	Chromo-sphere	Element	Sun	Flash	Height in Km	High E.P.
3361.24....	Ti^{+}-Sc^{+}	5^{2}	30	2500	3.70	3412.46....	*Co*	9^{2}	2	400	3.62
3361.98....	Sc^{+}-*Ca*	3^{2}	6d	600	3.67	3413.14....	*Fe*	5	3	500	5.80
3362.69....	Ti^{+}-Zr^{+}	1	2	500	4.89	3413.51....	*Ni*-	4^{2}	2	400	3.78
3363.75....	Cr^{+}-*Ni*	3^{3}	3	800	6.09	3413.99...	*Ni*	4	3	400	3.72
3364.62....	*Ni*	3	1	500	7.03	3414.78....	*Ni*	15	8	1000	3.64
3365.77....	*Ni*	6	2	500	4.09	3415.54....	*Fe*	3	3	600	5.83
3366.21....	Ti^{+}-*Ni*	6	6	1000	4.89	3416.03....	Fe^{+}	3	4	800	5.88
3366.82....	*Fe*-*Ni*	6^{2}	3	500	5.85	3416.99....	Ti^{+}	1	3	800	4.84
3368.07....	Cr^{+}	5	20	1500	6.14	3417.84....	*Fe*	4^{2}	2	400	5.82
3368.92....	Sc^{+}	3	8	800	3.67	3418.48....	*Fe*	5	2	600	5.82
3369.22....	Ti^{+}	1	3	800	4.89	3419.70....	*Fe*	2	1	400	6.44
3369.63....	*Ni*	6	3	500	3.66	3421.25....	Cr^{+}	4	25	1500	6.02
3370.82....	*Fe*	4	2	400	6.34	3422.71....	Cr^{+}-*Fe*	7^{2}	25	1500	6.05
3371.76....	*Ni*-*Ti*	7^{2}	2d	400	3.82	3423.71....	*Ni*	7	4	500	3.82
3372.21....	Ti^{+}-Sc^{+}	3^{2}	6	800	4.26	3424.27....	*Fe*	4	2	500	5.77
3372.84....	Ti^{+}	10^{2}	40	2500	3.67	3425.00....	*Fe*	4	2	500	6.64
3374.32....	Ti^{+}-*Ni*	6^{2}	6	1000	4.89	3425.56....	Fe^{+}	2	3	500	5.27
3374.64....	Zr^{+}-*Ni*	3^{2}	4	600	4.65	3426.32....	*Fe*	6^{2}	4	600	4.59
3376.40....	La^{+}-*Ni*	4^{2}	2	400	3.98	3426.70....	*Fe*	5^{2}	2	600	5.79
3377.56....	*Ti*	6^{2}	2	400	3.67	3427.12....	*Fe*	6^{3}	4	600	5.77
3378.34....	Cr^{+}-Zr^{+}	2	7	1000	6.74	3428.18....	*Fe*	4	2	500	5.79
3379.35....	Cr^{+}-Sc^{+}	2	4	800	6.74	3428.46....	*Ni*	2^{2}	1	400	7.28
3379.87....	Cr^{+}-Ti^{+}	4^{2}	7	1000	6.74	3430.57....	Zr^{+}	1	5	1000	4.06
3380.25....	Ti^{+}-*Fe*	9^{3}	15	1500	3.70	3431.59....	*Co*	4	3	500	3.70
3380.70....	La^{+}-*Sr*	12^{3}	4	600	3.97	3432.43....	Zr^{+}	— 1	2	500	4.52
3382.40....	*Fe*-*Ti*	4^{3}	3	600	5.82	3433.34....	Cr^{+}	3	22	1500	6.02
3382.72....	Cr^{+}	4	15	1500	6.09	3434.09....	*Fe*-*Cr*	2	1	400	6.34
3383.84....	Ti^{+}-*Fe*	9^{3}	40	2500	3.65	3435.49....	*Ni*	1	1	400	5.26
3385.08....	*Co*-	5^{3}	3	500	4.16	3436.00....	Fe^{+}-*Cr*	4^{4}	2d	400	7.54
3385.95....	*Ti*	3	2	500	3.69	3437.19....	*Ni*-*Fe*	8^{3}	3d	500	3.59
3387.40....	*Fe*	2	1	400	6.39	3438.22....	Zr^{+}	2	8	1000	3.68
3387.88....	Ti^{+}-Zr^{+}	5	20	1500	3.67	3438.97....	Mn^{+}-*Fe*	4^{2}	6	1000	4.76
3388.80....	Ti^{+}	2	4	600	4.87	3440.62....	*Fe*	20	15	1500	3.59
3389.75....	*Fe*	2	2	400	5.85	3441.01....	*Fe*	15	12	1500	3.64
3391.05....	*Ni*-*Cr*	6^{2}	2	400	3.64	3441.97....	Mn^{+}	6	25	1500	5.35
3391.42....	Cr^{+}	2	5	800	6.05	3443.22....	Ti^{+}-*Fe*	3^{3}	3	800	5.62
3391.96....	Zr^{+}	2	6	800	3.80	3443.87....	*Fe*	8	8	1000	3.67
3392.60....	*Fe*-*Ti*	3^{2}	3	500	5.80	3444.30....	Ti^{+}	4	15	1500	3.73
3392.98....	*Ni*	3	3	800	3.66	3445.09....	*Fe*	5	3	500	5.07
3393.14....	Cr^{+}-Zr^{+}	2^{2}	8	1000	6.73	3445.58....	*Cr*	2	2	400	6.11
3393.80....	Cr^{+}	2	6	800	6.73	3446.27....	*Ni*	15	8	800	3.69
3394.30....	Cr^{+}	2	4	800	6.74	3447.30....	*Fe*	4	3	600	5.77
3394.56....	Ti^{+}-*Fe*	6^{2}	20	1500	3.65	3448.87....	V^{+}-*Fe*	1^{2}	3	600	3.99
3395.37....	*Co*-Fe^{+}	5^{2}	2	400	4.51	3449.21....	*Co*	5	3	400	4.16
3396.37....	Zr^{+}-*Fe*	1^{2}	3	800	4.59	3449.48....	*Co*	6	3	400	4.01
3397.00....	*Fe*	3	2	400	4.59	3450.31....	*Fe*	5	2	500	5.79
3399.30....	Zr^{+}-*Fe*	5^{2}	5	800	3.95	3451.90....	*Fe*	3	2	400	5.79
3401.51....	*Fe*	3	2	400	4.54	3452.47....	Ti^{+}	1	6	800	5.61
3402.27....	*Fe*	3	2	400	6.85	3452.89....	*Ni*	6	5	800	3.68
3402.43....	Ti^{+}-Cr^{+}	3	10	1200	4.84	3453.32....	*Cr*	0	1	400	6.11
3403.35	Cr^{+}-*Ni*	6^{3}	18	1500	6.05	3453.56	*Co*	5	3	400	4.00
3404.35....	*Fe*	5^{2}	3	500	5.81	3454.19....	Ni^{+}	1	3	600	6.51
3404.80....	Zr^{+}-*Fe*	2^{2}	4	800	3.98	3455.30....	*Co*-	5	2	400	3.80
3406.44....	*Fe*	3	2	400	6.88	3456.44....	Ti^{+}	3	12	1000	5.62
3406.78....	*Fe*	5	3	500	5.84	3457.64....	Zr^{+}	0	2	400	4.13
3407.21....	Ti^{+}-Ni^{+}	4^{2}	8	1000	3.67	3458.40....	*Ni*-*Fe*	11^{2}	10d	1000	3.78
3407.52....	*Fe*	7^{2}	3	500	5.79	3459.43....	*Fe*	2	1	400	6.25
3408.81....	Cr^{+}	3	25	1500	6.09	3459.92....	Mn^{+}-*Fe*	6^{3}	6	800	4.74
3409.79....	Ti^{+}	2	6	800	3.65	3460.32....	Mn^{+}	4	25	1500	5.37
3410.22....	Zr^{+}-*Fe*	3^{2}	4	800	4.03	3461.46....	Ti^{+}	5	15	1500	3.70
3411.33....	*Fe*	3	2	400	6.33	3461.68....	*Ni*	8	6	800	3.59

TABLE 1—*Continued*

Chromo-sphere	Element	Sun	Flash	Height in Km	High E.P.	Chromo-sphere	Element	Sun	Flash	Height in Km	High E.P.
3462.79....	*Co*	6	3	400	4.19	3511.86 ...	*Cr*$^+$	2	4	600	5.99
3463.18....	*Zr*$^+$-*Fe*	2^2	4d	600	5.04	3512.63....	*Co*	6	3	400	4.09
3464.12....	*Sr*$^+$-*Fe*	4^3	4d	800	6.59	3513.52....	*Co*	5	2	400	3.61
3465.79....	*Ti*$^+$-*Co*	12^4	12d	1000	5.61	3513.85....	*Fe*	7	4	600	4.37
3466.67....	*Fe*	6^3	2	400	4.42	3514.03....	*Ni*$^+$-*Ni*	7^2	9	800	6.36
3467.61....	*Ni-Cr*	5^2	3	400	3.72	3515.01....	*Ni*	12	10	800	3.62
3468.78....	*Fe*$^+$-*Fe*	4^3	5	800	7.69	3516.22....	*Ni*	2	1	400	7.03
3469.49....	*Ni*	3	2	400	3.83	3516.55....	*Fe*	4^2	2	400	6.36
3469.84....	*Fe*	2	2	400	6.15	3517.33....	*V*$^+$	3	9	1000	4.63
3471.36....	*Fe-Co*	6^2	4d	600	5.82	3518.32....	*Co*	5	3	500	4.55
3472.60....	*Ni-*	7^2	6	800	3.66	3518.81....	*Fe*	6^2	3	600	5.70
3473.61....	*Fe-Cr*	3^3	2	400	4.54	3519.74....	*Ni*	7	5	600	3.78
3474.11....	*Mn*$^+$	4^2	25	1500	5.35	3520.23....	*Ti*$^+$	2	12	1000	5.54
3475.15....	*Cr*$^+$	2	6	1000	5.97	3520.88....	*Zr*$^+$	2	2	400	4.06
3475.44....	*Fe*	10	10	1000	3.64	3521.32....	*Fe*	8	6	600	4.42
3476.68....	*Fe*	8	7	800	3.67	3521.57....	*Co*	7^2	3	400	3.93
3476.99....	*Ti*$^+$	3	8	1000	3.70	3521.77....	*Fe-V*$^+$	2	1	400	5.72
3477.17....	*Ti*$^+$	5	15	1500	3.67	3522.90....	*Fe*	2	2	400	6.37
3478.60....	*Fe*$^+$-*Zr*$^+$	3^5	3d	500	5.88	3523.47....	*Co-Ni*	4	3	400	4.13
3479.40....	*Zr*$^+$	2	6	800	4.26	3524.12....	*Fe*	6^2	3	400	5.77
3480.39....	*Zr*$^+$-*Ti*	3^3	2	600	4.47	3524.50....	*Ni*	20	15	1000	3.53
3480.90....	*Ti*$^+$	2	3	600	4.62	3524.78....	*V*$^+$-	1	2	400	4.59
3481.20....	*Zr*$^+$	2	8	800	4.34	3525.77....	*Zr*$^+$-*Co*	6^2	6	800	3.86
3482.95....	*Mn*$^+$	5	20	1500	5.37	3526.31....	*Fe*	9^4	4d	800	5.77
3483.65....	*Ni-Co*	9^3	4	500	3.82	3526.75....	*Co-Fe*	10^2	4	600	3.50
3484.16....	*Cr*$^+$	4	3	500	5.99	3527.79....	*Fe*	5	3	500	6.34
3484.96....	*Fe-Ni*	4^3	2	400	5.96	3529.02....	*Co-Ni*	4^2	3	500	3.67
3485.37....	*Fe-Co*	6	3	500	5.73	3529.71....	*Co-Fe*	9^3	4d	600	4.01
3485.94....	*V*$^+$-*Ni*	5	3	500	4.63	3530.72....	*V*$^+$	3	10	1000	4.56
3488.09....	*Fe*$^+$-*Ni*	3^2	6	800	5.23	3531.63....	*Mn-Fe*	6^3	6	600	5.77
3488.68....	*Mn*$^+$	4	18	1200	5.38	3532.00....	*Mn*	7^2	6	600	5.77
3489.42....	*Co*	5	2	400	4.46	3532.50....	*Fe*	4	2	400	.....
3489.76....	*Ti*$^+$	2	8	1000	3.67	3533.21....	*Fe-Co*	17^3	4	600	6.36
3490.60....	*Fe*	10	10	800	3.59	3533.89....	*Ti*$^+$	1	5	800	5.54
3491.03....	*Ti*$^+$	5	15	1200	3.65	3534.91....	*Fe-*	3	2	400	5.97
3492.93....	*Ni*	10	8	1000	3.64	3535.41....	*Ti*$^+$	4	25	1200	5.54
3493.14....	*V*$^+$	0	4	800	4.60	3535.69....	*Sc*$^+$	3	4	800	3.80
3493.46....	*Fe*$^+$-*Ti*	3^2	2	600	7.66	3536.56 ...	*Fe*	7	4	500	6.35
3494.18....	*Fe*	2	2	500	5.95	3537.80....	*Fe*	9^3	3	400	6.31
3494.64....	*Fe*$^+$-*Cr*$^+$	3^2	8	800	5.80	3538.26....	*V*$^+$-*Fe*	2^2	3	400	4.61
3495.34....	*Cr*$^+$-*Fe*	5^2	3	600	5.97	3540.08....	*Fe*	5	2	400	6.34
3495.68....	*Mn*$^+$-*Co*	7^3	12	1200	5.38	3540.75....	*Fe*	5^2	3	600	4.40
3496.18....	*Zr*$^+$-*V*$^+$	3^2	15	1200	3.57	3541.08....	*Fe*	7	6	600	6.32
3497.00....	*Mn*$^+$-*Fe*	9^4	5	800	5.35	3542.16....	*Fe*	9^2	6d	600	6.34
3497.57....	*Mn*$^+$	3	8	1000	5.37	3543.36....	*Co-Fe*	4^2	3d	400	5.36
3497.87....	*Fe*	8	8	800	3.64	3544.63....	*Fe*	3	2	400	6.08
3499.12....	*Ti-Er*$^+$	0	3	500	4.59	3545.23....	*V*$^+$	4	10	1000	4.57
3500.43....	*Ti*$^+$-*Fe*	5^2	6d	800	3.65	3545.69....	*Fe*	8^2	4	400	6.32
3500.89....	*Ni*	6	2	500	3.69	3547.25....	*Fe*	6^2	2d	400	6.28
3501.72....	*Co*$^+$	1^2	2	500	5.72	3547.98....	*Mn-Ni*	13^3	6d	500	5.77
3502.26....	*Co*	6^2	3	500	3.95	3549.05....	*Y*$^+$	2	8	1000	3.61
3502.65....	*Ni-Co*	4^2	3	600	3.52	3550.59....	*Co*	4	3	400	3.65
3504.44....	*V*$^+$	2	3	800	4.61	3551.41....	*Ni-Fe*	5^2	2	400	3.64
3504.88....	*Ti*$^+$-*Fe*	5^2	20	1500	5.40	3551.92....	*Zr*$^+$	1	7	800	3.57
3505.63....	*Zr*$^+$	2^2	4	600	3.68	3552.92....	*Fe-Co*	7^3	2	500	6.34
3506.43....	*Co-Fe*	9^3	3d	600	4.03	3553.63....	*Fe-Ni*	8^2	3	500	7.03
3507.57....	*Ni-Fe*	4^2	3	400	3.68	3554.12....	*Fe*	5	4	600	4.43
3508.40....	*Fe-Fe*$^+$	6^3	3	600	6.50	3554.92....	*Fe*	9	6	600	6.29
3509.86....	*Co-Ti*$^+$	4	2	400	4.10	3556.71....	*V*$^+$-*Zr*$^+$	11^4	15d	1200	4.59
3510.33....	*Ni-Zr*$^+$	10^2	6	800	3.73	3558.52....	*Sc*$^+$-*Fe*	8	12	1000	3.48
3510.87....	*Ti*$^+$	5	20	1500	5.40	3559.10....	*Fe-CN*	1	1	400	.....

TABLE 1—*Continued*

Chromosphere	Element	Sun	Flash	Height in Km	High E.P.	Chromosphere	Element	Sun	Flash	Height in Km	High E.P.
3559.50....	*Fe*	3	2	400	6.53	3602.50....	*Fe*	7^2	4	500	6.28
3560.67....	*Fe-V*$^+$	3^2	2	500	6.70	3603.17....	*Fe*	5	4	500	6.11
3560.91....	*Co*	4	3	500	4.09	3603.84....	*Cr*$^+$*-Fe*	7^3	12	1000	6.12
3561.72....	*Ti*$^+$*-Ni*	5^3	5d	800	4.04	3604.38....	*Fe-Ti*	3^2	2	400	6.29
3564.15....	*Fe-Co*	4	3	600	5.06	3605.33....	*Cr-Co*	16^3	12d	1000	3.42
3564.49....	*Fe*	5^2	3	400	5.90	3606.69....	*Fe*	6	6	600	6.10
3565.37....	*Fe-Ti*$^+$	15^2	15	1200	4.42	3607.46....	*Mn-Zr*$^+$	3^2	2	500	5.55
3565.94....	*Ti*$^+$	1	3	600	4.62	3608.17....	*Fe*	4	3	500	6.26
3566.15....	*V*$^+$*-Cr*	2	3	600	4.53	3608.86....	*Fe*	20	18	1500	4.43
3566.43....	*Ni*	10	10	600	3.88	3609.36....	*Ni*	5	3	400	3.53
3567.00....	*Fe-*	3^2	3	500	6.32	3609.53....	*Cr*	2	2	400	5.95
3567.73....	*Sc*$^+$	6^2	12	1000	3.46	3610.18....	*Fe-Ti*	7^2	5	600	6.21
3568.59....	*Fe-Co*	6^2	3d	500	6.32	3610.63....	*Ni-Fe*	8^2	3	600	3.53
3569.55....	*Co-Mn*	11^3	4d	600	4.38	3611.06....	*V*$^+$	2	10	1000	3.55
3570.14....	*Fe-Mn*	24^2	18	1200	4.37	3611.81....	*Zr*$^+$*-Co*	2^2	3	400	5.15
3571.96	*Ni-Fe*	11^2	5	500	3.62	3612.72....	*Ni*	6	2	400	3.69
3572.52....	*Sc*$^+$*-Zr*$^+$	10^2	20	1200	3.48	3613.09....	*Zr*$^+$*-Fe*	6^3	8	800	3.45
3573.39	*Ti*$^+$*-Fe*	12^5	7d	800	4.02	3613.82....	*Sc*$^+$	7^2	30	1500	3.44
3573.97						3614.75....	*Zr*$^+$	2	8	800	3.77
3574.43....	*V*$^+$*-Cr*	1	1	400	5.81	3615.71....	*Cr-Fe*	3	2	400	3.41
3575.00....	*Co-Fe*	8^2	3	500	4.03	3616.20....	*Fe-*	3^2	2	400	5.83
3575.35....	*Co-Fe*	4^2	2	500	3.55	3616.57....	*Fe*	4	3	400	.....
3576.00....	*Fe*	4	3	500	6.31	3617.34....	*Cr*$^+$*-Fe*	5^2	2	500	8.32
3576.38....	*Sc*$^+$	7^2	20	1200	3.46	3617.82....	*Fe*	6	3	400	6.42
3576.89....	*Zr*$^+$	1	6	800	3.86	3618.77....	*Fe*	20	20	1500	4.40
3577.83....	*Mn*	5	3	500	5.55	3619.42....	*Ni*	8	12	800	3.83
3578.25....	*Fe-Zr*$^+$	5^2	5	400	6.32	3619.76....	*Fe*	2	1	400	5.80
3578.73....	*Cr*	10	12	1200	3.45	3620.23....	*Fe*	2	1	400	6.25
3579.83....	*Fe*	2	2	500	6.67	3620.46....	*V*$^+$*-Fe*	3	2	400	6.52
3580.96....	*Sc*$^+$	5	10	1000	3.45	3621.14....	*V*$^+$*-Fe*	5^2	3	800	5.77
3581.22....	*Fe*	30	25	1500	4.30	3621.49....	*Fe*	6	6	800	6.12
3581.76....	*Fe-*	5^3	2	400	6.13	3621.99....	*Fe*	6	4	800	6.15
3582.20....	*Fe-*	7^2	3	400	6.67	3623.30....	*Fe*	7^2	5d	800	5.30
3582.60....	*Fe*	5^2	2	400	6.31	3623.89....	*Fe-Mn*	5^2	2	600	6.26
3583.87....	*CN*-*	3	3d	600	.....	3624.39....	*Ni-Ca*	10^3	5d	600	3.40
3584.62....	*V*$^+$*-Fe*	8^2	8	800	3.55	3624.84....	*Ti*$^+$	5	18	1200	4.62
3584.95....	*Fe*	6	4	600	6.43	3626.86....	*Fe*	4^2	2d	400	6.96
3585.30....	*Fe-Co*	12^2	10	1200	4.40	3627.85....	*Co*	4	2	400	3.91
3585.63....	*Fe-Cr*$^+$-†	8^2	12	1200	4.35	3628.71....	*V*$^+$	2	7	1000	3.53
3586.53....	*Mn*	4	3	500	5.57	3630.01....	*Zr*$^+$	1	4	800	3.76
3586.85....	*Fe-*	11^2	5	800	4.43	3630.73....	*Sc*$^+$*-Ca*	7^2	30	1500	3.41
3587.20....	*Ti*$^+$*-Co*	9^2	12	800	4.05	3631.48....	*Fe*	15	20	1500	4.35
3587.59....	*Fe*	8^2	3	400	5.85	3632.01....	*Fe-Co*	5^2	2	400	6.46
3587.98....	*Zr*$^+$*-Ni*	6	5	600	3.76	3632.60....	*Fe-Cr*	4^2	2	400	6.33
3588.62....	*Fe*	7^2	2	400	6.26	3632.96....	*Fe-*	6^2	2	400	5.87
3589.13....	*Fe*	8^3	5	600	4.29	3633.13....	*V*$^+$	2	10	1000	3.40
3589.72....	*V*$^+$*-Sc*$^+$	10^2	12	800	4.50	3633.85....	*Fe*	5^2	2	400	6.37
3590.48....	*Sc*$^+$-‡	4^2	12	800	3.46	3634.25....	*He-Fe*	6^2	4d	1200	24.27
3591.43....	*Fe*	4^2	5	600	6.28	3634.71....	*Co-Fe*	4	2	400	6.26
3592.00....	*V*$^+$	2	12	800	4.53	3635.34....	*Ti-Fe*	6^2	4d	500	3.39
3592.67....	*Fe*	3	4	400	6.66	3636.18....	*Fe*	5^2	4	500	5.58
3593.41....	*V*$^+$*-Cr*	12^2	15	1000	4.56	3636.56....	*Zr*$^+$*-Cr*	3^2	3	500	3.86
3594.78....	*Fe-Co*	9^2	5d	500	6.27	3636.81....	*Fe-Co*	6^3	3	500	5.97
3595.20....	*Fe-Mn*	3^2	2	400	6.30	3637.84....	*Fe*	4	3	500	6.32
3596.03....	*Ti*$^+$	4	15	1200	4.04	3638.31....	*Fe*	3	3	400	6.14
3597.03....	*Fe-*	5	3	400	6.68	3639.43....	*Co*	4^3	2	400	5.34
3597.71....	*Ni*	8	6	600	3.64	3639.80....	*Cr*	2	2	400	5.92
3599.00....	*Fe*	6^3	4d	600	6.30	3640.41....	*Fe-Cr*	6	4	600	6.11
3599.58....	*Fe*	3	3	600	6.99	3641.35....	*Ti*$^+$	4	25	1500	4.62
3600.77....	*V*$^+$	3	18	1200	3.61	3641.81....	*Cr-Co*	2^2	2	500	5.92
3601.89....	*V*$^+$	1	12	1000	3.53	3642.74....	*Sc*$^+$*-Ti*	12^3	25	1500	3.39

* Third head of fourth *CN* band. † Second head of fourth *CN* band. ‡ First head of fourth *CN* band.

TABLE 1—*Continued*

Chromo-sphere	Element	Sun	Flash	Height in Km	High E.P.	Chromo-sphere	Element	Sun	Flash	Height in Km	High E.P.
3643.75....	*Fe-*	9^3	3	500	6.31	3685.25....	Ti^+	10	90	6000	3.92
3644.41....	*Ca*	5	3	500	5.28	3686.10....	*Fe-V*	9^2	4	600	6.28
3644.83....	*Ca-Fe*	9^3	4	500	5.28	3686.83....	*H* 19	.....	35	3000	13.50
3645.34....	Sc^+-	6^2	12	1200	3.41	3687.62....	*Fe*	10^2	8	600	4.20
3646.17....	*Ti-Gd*$^+$	1	3	400	3.38	3688.48....	*Ni-Fe*	7^2	3	500	3.62
3647.41....	*Fe*	4	3	400	4.93	3689.50....	*Fe-*	9^2	4	500	6.18
3647.81....	*Fe*	12	18	1500	4.29	3689.90....	*Ti-Fe*	3^2	3	400	3.39
3649.35....	*Fe-Co*	7^2	4	600	3.38	3690.70....	*Co-Fe*	4	3	400	5.38
3649.56....	*Fe*	5	3	600	6.06	3691.62....	*H* 18	.....	40	3500	13.50
3650.19....	*Fe*	9^2	4	600	5.80	3692.24....	*V*	1	1	400	3.62
3651.08....	*Fe-*	6	4	400	6.22	3692.67....	*Fe-Er*$^+$	2	4	800	.....
3651.47....	*Fe*	7	4	500	6.13	3693.02....	*Fe*	3	2	400	6.35
3651.77....	Sc^+	4	15	1200	3.39	3693.48....	*Co*	1	3	400	5.37
3652.55....	*Co*	3	2	400	3.55	3694.13....	*Fe-Ni*	10^4	10	800	6.37
3653.48....	*Ti*	5	2	400	3.43	3695.00....	*Fe*	5	5	600	5.92
3653.93....	*Fe-Cr*	6^3	3	400	5.80	3695.67....	*Fe-V*	4^3	3	600	5.89
3654.66....	*Ti-Fe*	3^2	2	400	3.38	3696.34....	Ti^+-	1^2	4	600	4.90
3655.64....	*Fe*	6^2	3	500	6.20	3697.21....	*H* 17	.....	40	4000	13.49
3656.19....	*Cr-Fe*	5^2	3	500	5.91	3698.14....	Zr^+-*Ti*	2	8	800	4.34
3656.66....	*H* 37	.....	2	600	13.53	3698.60....	*Fe*	4	3	400	6.34
3657.26....	*H* 36	.....	4	800	13.53	3699.16....	*Fe*	3	3	400	6.34
3658.05....	*H* 35	.....	3	800	13.53	3700.39....	V^+	1	4	600	5.84
	Ti	1			3.39	3701.09....	*Fe*	8	5	600	6.32
3658.66....	*H* 34	.....	2	800	13.53	3702.27....	*Fe-Co*	12^4	6d	600	4.93
3659.42....	*H* 33	.....	3	1000	13.53	3703.89....	*H* 16	.....	45	4500	13.49
3659.70....	Ti^+-*Fe*	10^2	12d	1000	4.95	3704.97....	*He*	.....	5	1200	24.21
3660.33....	*H* 32	.....	4	800	13.53	3705.57....	*Fe*	9	12	1200	3.38
	Fe	2			6.22	3706.11....	Ca^+-Ti^+	9^2	25	1200	6.44
3661.28....	*H* 31	.....	6	1000	13.53	3707.08....	*Fe*	5	4	600	6.31
3662.23....	Ti^+	5	18	1500	4.93	3707.48....	*Ti-Co*	4^2	2	400	5.34
	H 30	.....			13.52	3707.94....	*Fe*	10^2	8	800	3.42
3662.90....	*Cr-Fe*	4	3	500	5.90	3708.69....	*Co-Fe*	2^2	3	400	5.36
3663.42....	*Fe*	9^3	10	1200	5.92	3709.32....	*Fe*	8	10	800	4.24
	H 29	.....			13.52	3709.90....	*Ti*	0	2	400	4.37
3664.66....	Y^+	2	15	1500	3.55	3710.34....	V^+	3	20	1200	3.51
	H 28	.....			13.52	3712.06....	*H* 15	.....	50	5000	13.48
3666.09....	*H* 27	.....	12	1500	13.52	3712.89....	Cr^+-*Mn*	5^2	15	800	6.02
3666.74....	Sc^+-*Fe*	4^2	3	500	3.39	3713.51....	La^+	− 2	2	400	3.50
3667.26....	*Fe*	4	3	400	6.56	3714.85....	Zr^+	0	2	500	3.85
3667.74....	*H* 26	.....	15	1800	13.52	3715.17....	Cr^+	2	7	800	6.41
3668.53....	Zr^+-Y^+	0^2	4	600	3.77	3715.43....	V^+	4	10	800	4.89
3669.46....	*H* 25	.....	22	1800	13.52	3716.40....	*Fe*	7	6	500	6.25
3670.08....	*Fe-Co*	5^2	2	400	6.20	3717.40....	*Ti*	2	2	400	3.32
3670.46....	*Ni*	5	5	500	3.53	3718.40....	*Fe*	4	3	600	6.07
3671.33....	Zr^+	0	20	2000	4.07	3719.94....	*Fe*	40	35	2000	3.32
	H 24	.....			13.52	3721.64....	Ti^+	4	6	2000	3.89
3671.68....	*Ti*	3	2	400	3.41	3722.00....	*H* 14	.....	60	5500	13.47
3673.08....	*Fe*	3	3	400	.....	3722.55....	*Fe-Ni*	9^2	12	1200	3.40
3673.82....	*H* 23	.....	22	2000	13.51	3723.55....	Ti^+	1	4	600	4.87
3674.74....	Zr^+-*Fe*	3^2	8	800	3.68	3724.06....	Ti^+	1	6	600	4.89
3675.34....	Sc^+-*Ca*	1	3	400	3.67	3724.40....	*Fe*	6	6	600	5.58
3676.34....	*Fe-Cr*	6	25	2500	5.91	3725.00....	*Ti-Ni*	2^2	2	400	4.37
	H 22	.....			13.51	3725.50....	*Fe*	3	2	400	6.35
3677.37....	*Fe*	7^2	4	500	5.62	3726.98....	*Fe*	7^2	4	600	6.34
3677.79....	Cr^+-*Fe*	13^4	20	1200	6.05	3727.39....	V^+-Cr^+	3^3	8	800	4.99
3679.34....	*H* 21	.....	30	2500	13.51	3727.68....	*Fe-Zr*$^+$	5^2	10	800	4.26
3679.96....	*Fe*	9	10	1000	3.35	3728.38....	V^+-Ce^+	5^2	3	400	5.81
3680.97....	*Fe-*	10^3	4d	600	6.55	3729.86....	*Ti*	3	3	400	3.31
3682.21....	*Fe*	7^2	4	500	6.34	3730.39....	*Co-Fe*	5^2	5	500	5.18
3682.82....	*H* 20	.....	30	2500	13.51	3731.20....	Zr^+-*Fe*	7^3	5	500	5.04
3684.12....	*Fe*	7	4	500	6.07	3731.98....	*Cr-Mn*	3^2	2	400	3.31

TABLE 1—*Continued*

Chromo-sphere	Element	Sun	Flash	Height in Km	High E.P.	Chromo-sphere	Element	Sun	Flash	Height in Km	High E.P.
3732.40....	*Fe-Co*	6	4	500	5.49	3779.59....	*Fe-Fe*$^+$	3^2	2	450	5.48
3732.76....	*V*$^+$	2	4	600	4.86	3780.48....	*Zr-CN*	1^2	2	450	3.26
3733.33....	*Fe*	7	8	1000	3.42	3780.95....	*Fe-*	6^2	2	450	5.45
3734.45....	*H* 13	.....	70	6000	13.46	3781.66....	*Ce*$^+$*-CN*	1^2	2	450	3.79
3734.91....	*Fe*	40	20	2000	4.16	3782.26....	*V*$^+$*-CN*	0^2	2	450	6.87
3735.46....	*Fe-Nd*$^+$	5^2	5	600	6.23	3783.47....	*Ni-Fe*$^+$	8^2	10	750	3.69
3737.00....	*Ca*$^+$*-Ni*	8^2	50	2000	6.44	3784.15....	*CN*	2^4	2	500	.....
	Fe	30			3.35	3785.36....	*CN*	2^3	2	500	.....
3738.29....	*Fe-Cr*$^+$	6^2	5	600	6.55	3785.58....	*CN*	1^2	2	500	.....
3739.15....	*Ni-Fe*	5^2	4	800	3.47	3785.90....	*Fe-*	5^3	4	600	5.68
3739.75....	*Fe-Ni*	6	6d	800	6.33	3786.17....	*Fe-Ti*	4	4	600	6.08
3741.06....	*Ti*	4	4	500	3.32	3786.68....	*Fe*	5	4	600	4.27
3741.64....	*Ti*$^+$	4	30	2000	4.87	3787.11....	*Fe-CN*	1	2	450	6.88
3742.70....	*Fe-Cr*	6^3	4	600	6.22	3787.94....	*Fe*	9	8	800	4.26
3743.49....	*Fe-Cr*	12^5	12d	1000	4.28	3788.66....	*Y*$^+$	2	15	1000	3.36
3744.11....	*Fe*	4	4	400	6.32	3789.56....	*Fe-*	4^2	2	450	5.85
3745.78....	*Fe*	14^2	30d	2000	3.38	3790.09....	*Fe*	5	6	800	4.24
3746.53....	*Fe*	3^2	3	400	5.48	3790.42....	*V-Cr*	4^3	2	400	4.63
3747.60....	*Y*$^+$	1	6	600	3.40	3790.78....	*La*$^+$*-Fe*	3^2	4	800	3.38
3748.25....	*Ti*$^+$	1	20	1500	4.88	3791.36....	*Cr*	1	1	400	6.25
	Fe	10			3.40	3792.22....	*Fe-Cr*	4^2	4	600	5.97
3749.50....	*Fe*	20	18	1500	4.20	3792.78....	*Fe-CN*	4^2	3	600	5.47
3750.25....	*H* 12	.....	75	6000	13.45	3793.35....	*Cr-Fe*	2^2	2	400	6.25
3751.65....	*Zr*$^+$	1	3	500	4.26	3793.60....	*Ni-Fe*	6^2	3	400	3.53
3752.21....	*Fe*	4^2	3	500	6.31	3794.31....	*Fe-CN*	4	3	400	5.70
3752.86....	*Ti*	4	4	400	3.34	3794.76....	*La*$^+$	1	6	800	3.50
3753.55....	*Fe-Ti*	6	5	400	5.45	3795.01....	*Fe*	8	8	800	4.24
3754.51....	*Fe-Cr*$^+$	4^2	4	400	6.27	3796.25....	*Zr*$^+$*-CN*	1^3	3d	500	4.26
3755.41....	*Co*	1	2	400	5.36	3798.02....	*H* 10	.....	100	6000	13.40
3756.04....	*Fe*	3	3	400	5.45	3799.52....	*Fe*	7	8	800	4.20
3757.16....	*Fe-Cr*	7^3	4	400	6.84	3800.06....	*CN*	2^4	3	400	.....
3757.66....	*Ti*$^+$*-Cr*	4	15	1200	4.84	3801.37....	*Ce*$^+$*-CN*	2^3	2	400	4.14
3758.25....	*Fe*	15	15	1200	4.24	3801.74....	*Fe*	5^2	6	600	6.07
3759.33....	*Ti*$^+$	12	65	6000	3.89	3802.28....	*Fe*	2	2	400	6.53
3760.07....	*Fe-V*$^+$	6^2	5	600	5.68	3802.71....	*CN*	1^2	3	400	.....
3760.54....	*Fe*	4	4	400	5.49	3803.00....	*Ce*$^+$*-CN*	1^2	4	400	3.60
3761.33....	*Ti*$^+$	7	75	6000	3.85	3803.42....	*V-CN*	0	3	400	3.53
3761.88....	*Ti*$^+$	3			5.86	3804.00....	*Fe*	3	2	400	6.56
3762.35....	*Fe-CN*	5^4	4	400	6.63	3804.65....	*Cr-V*	4^3	4	400	6.24
3763.80....	*Fe*	10	15d	1200	4.26	3805.32....	*Fe*	6	4	600	6.53
3764.12....	*Fe*$^+$*-Ce*$^+$	1	4	500	5.85	3806.15....	*Fe-CN*	3^2	2	400	6.64
3764.54....	*Zr-CN*	1^5	3	400	3.28	3806.75....	*Fe-Mn*	8	3	400	6.50
3765.49....	*Fe*	6	10	800	6.50	3807.31....	*Fe-Ni*	12^2	8d	800	5.45
3766.68....	*Zr*$^+$*-Fe*	4^2	5	600	3.68	3808.09....	*Cr-Fe*	4^4	3	500	6.24
3767.15....	*Fe*	8	12	1200	4.28	3808.85....	*Fe-CN*	4^2	6d	600	5.79
3768.21....	*Cr-CN*	6^3	6d	600	5.81	3809.51....	*Mn-V*	4	3	400	5.37
3769.46....	*Ni*$^+$	3	8	600	6.36	3810.84....	*Fe-CN*	4^2	5	500	6.53
3770.72....	*H* 11	.....	80	6000	13.43	3811.40....	*Ti-Ni*	2^2	2	400	5.10
3771.66....	*Ti*	2	2	400	3.32	3812.00....	*Fe-CN*	3^3	3	400	4.19
3772.57....	*Ni-*	3^2	4	400	3.48	3813.10....	*Fe*	7^2	10	1000	5.81
3773.76....	*Fe-CN*	4^5	4d	500	6.30	3813.49....	*Ti*$^+$*-Fe*	4^2	8	1000	3.84
3774.38....	*Y*$^+$	3	20	1000	3.40	3814.53....	*Ti*$^+$*-Fe*	7^2	12	1000	3.81
3774.85....	*Fe*	4	3	400	5.48	3815.38....	*V*$^+$*-Cr*	2^2	2	400	6.12
3775.54....	*Ni*	7	7	800	3.69	3815.82....	*Fe*	15	20	1500	4.71
3776.02....	*Ti*$^+$	2	7	800	4.84	3816.33....	*Fe-Co*	3	2	400	5.42
3776.48....	*V*$^+$*-Fe*	4^2	4	600	3.40	3817.65....	*Zr*$^+$*-Fe*	3	4	600	3.76
3777.42....	*Fe*	3	3	500	5.82	3818.31....	*Y*$^+$*-V*	2^2	4	600	3.36
3777.98....	*Ni-CN*	3^3	3	500	3.29	3819.15....	*CN*	3^3	3d	700	.....
3778.30....	*V*$^+$*-Fe*	3	4	500	4.94	3819.63....	*He*	.....	15	4000	24.11
3778.70....	*Fe-CN*	6^3	3	500	5.45	3820.43....	*Fe*	25	25	1600	4.09
3779.39....	*Fe*	4	4	500	5.81	3821.16....	*Fe*	4	3	500	6.48

TABLE 1—*Continued*

Chromosphere	Element	Sun	Flash	Height in Km	High E.P.	Chromosphere	Element	Sun	Flash	Height in Km	High E.P.
3821.79	*Fe-CN*	5^2	4d	600	5.83	3864.36	*Fe-CN*	4^2	4	600	5.77
3822.81	*V-CN*	1	3	500	3.51	3864.87	*V*	3	4	600	3.21
3823.56	*Mn-Cr*	4	3	500	5.36	3865.12	*CN*	3	4	600	.....
3823.99	*Mn-Fe*	2^2	3d	500	5.38	3865.51	*Fe-Cr*$^+$	7	8	1000	4.20
3824.46	*Fe*	6	20	1500	3.23	3866.00	*CN*	3	3	600	.....
3825.32	*CN*	1^2	3	600	.....	3866.79	*CN*	2	3	600	.....
3825.86	*Fe*	20	20	1500	4.14	3867.20	*Fe*	3	3	800	6.20
3826.60	*CN-Fe*	4^3	4d	400	5.67	3867.62	*He-V*	1	3	800	24.07
3827.31	*Zr*$^+$*-CN*	2^2	3	600	.....	3867.94	*Fe-CN*	2	4	800	5.77
3827.79	*Fe*	8	15	1200	4.77	3868.38	*CN-Ti*	1	3	600	5.16
3829.35	*Mg*	10	40	5000	5.92	3868.75	*CN*	1	3	600	.....
3830.68	*Fe-CN*	5^4	6	600	5.82	3869.13	*CN*	1	3	600	.....
3831.06	*Cr-V*$^+$	3d	6	600	4.22	3869.51	*Fe-CN*	3	4	600	5.91
3832.34	*Mg*	15	50	5000	5.92	3869.89	*CN*	1	3	600	.....
3832.89	*Ni*	3	3	800	3.38	3871.09	*CN*	3^4	6	800	.....
3833.32	*Fe*	4	4	800	5.77	3871.37	*CN*¶	2d	6	800	.....
3833.74	*CN*	1^3	2	500	.....	3871.80	*Fe-La*$^+$	3^2	3	600	6.12
3834.26	*Fe-Mn*	14^2	15	1200	4.17	3872.20	*CN*	3^3	3	600	.....
3835.54	*H* 9	.....	120	7000	13.37	3872.55	*Fe*	6	7	1000	4.17
3836.08	*Ti*$^+$	2	4	700	3.82	3872.73	*V-CN*	1	2	600	4.26
3836.42	*Fe-CN*	5^3	5	800	6.50	3873.05	*Co-Fe*	6^3	4	600	3.62
3836.77	*Zr*$^+$	1	3	800	3.77	3873.90	*Co-Fe*	8^2	6	600	3.70
3838.30	*Mg*	25	60	6000	5.92	3874.75	*CN*	3^2	3	500	.....
3839.65	*Fe-Mn*	4^2	3	600	7.16	3875.19	*Ti-V*	4^2	4	500	3.18
3840.44	*Fe-CN*	8	12	1200	4.20	3875.78	*CN*	2	2	500	.....
3840.74	*V-La*$^+$	1	2	600	3.25	3876.05	*Fe*	5	6	700	4.19
3841.07	*Fe-Mn*	10	12	1200	4.81	3876.35	*CN*	2^3	3	600	.....
3841.88	*Co-CN*	6^4	5	600	4.13	3876.92	*CN-Co*	8^2	4	600	3.61
3843.13	*Zr*$^+$*-Fe*	10^4	10d	800	3.57	3878.01	*Fe-CN*	8	8	1500	4.14
3844.00	*Mn-CN*	2	2	500	5.39	3878.65	*Fe-V*$^+$	11^3	25	1500	3.27
3844.29	*CN-V*	4^2	3	500	3.21	3879.59	*CN*	4^4	3	600	.....
3845.14	*Fe-CN*	5^3	3	600	5.62	3880.19	*CN*	3^5	3	600	.....
3845.44	*Co-CN*	8	6	600	4.13	3880.68	*CN*	1	4	600	.....
3846.26	*Fe-Ti*	5^3	2	500	6.86	3881.25	*CN*	5^5	5	600	.....
3846.79	*Fe-CN*	8^4	8	700	6.45	3881.91	*CN-Co*	2	4	600	3.76
3847.92	*CN*	3^3	2	600	.....	3882.25	*CN*	2	6	600	.....
3848.30	*Fe-Ti*	2	4	600	5.80	3882.50	*CN*	3^3	10	800	.....
3848.93	*La*$^+$*-Cr-*	4^2	5	700	3.21	3883.29	*CN-Cr***	3^2	10	800	4.16
3849.45	*Cr*	2^2	3	500	4.18	3884.32	*Fe-*	3^2	4	500	5.86
3849.93	*Fe*	10	10	1000	4.21	3885.32	*Fe-Cr*	8^3	4d	500	5.59
3850.82	*Fe*	4	7	700	4.19	3886.32	*Fe-La*$^+$	15	25	1500	3.23
3851.22	*CN*	2	3	600	.....	3887.02	*Fe*	7	6	800	4.09
3851.60	*CN*	1^3	3d	600	.....	3889.20	*H*ζ	.....	140	8000	13.33
3852.50	*Fe-CN*	7^3	4d	600	5.37	3890.41	*Fe*	2	2	400	6.40
3853.39	*Fe-CN*	3^2	3d	600	6.14	3890.85	*Fe*	3	4	500	5.89
3854.01	*CN*	1^2	3	600	.....	3891.41	*Zr-Nd*$^+$	2^3	5	600	3.32
3854.45	*CN-Fe*	4^2	6	800	6.40	3891.93	*Ba*$^+$*-Fe*	5^2	5d	600	5.67
3854.81	*CN*§	1	4	600	.....	3893.02	*V-Fe*	4^3	2	500	3.21
3855.58	*Cr-Fe*	5^2	4	600	5.90	3893.38	*Fe*	4	4	500	6.11
3856.26	*Fe-Si*$^+$	9^2	25	1500	3.25	3894.12	*Co-Cr*	8^2	7	800	4.21
3856.84	*CN*	3^2	2d	600	.....	3895.06	*Co-Ti*	8^3	5	600	3.80
3857.70	*Cr-CN*	6	4	600	5.90	3895.68	*Fe*	7	20	1500	3.28
3858.36	*Ni*	7	6	800	3.62	3896.20	*V*$^+$*-V*	1^2	6	800	4.56
3858.72	*CN*	2	4	500	.....	3896.70	*Fe-Ce*$^+$	2^3	2	500	6.81
3859.87	*Fe*	20	40	2500	3.20	3897.75	*Fe-Cr*	6^4	5	700	5.85
3860.60	*CN*	3	3	600	.....	3898.05	*Fe*	5	6	800	4.17
3861.23	*Co-Fe*	7^2	5	600	4.24	3898.40	*Ti-Co*	3^2	3	500	3.17
3861.73	*CN*‖	7^5	5	600	.....	3899.09	*V*$^+$*-Fe*	5^2	5	800	4.96
3862.49	*Si*$^+$*-CN*	3^2	6	300	10.02	3899.70	*Fe*	8	18	1500	3.25
3863.42	*Nd*$^+$*-CN*	3	5	600	3.19	3900.54	*Ti*$^+$	5	35	2000	4.29

§ Fourth head of third *CN* band.
‖ Third head of third *CN* band.
¶ Second head of third *CN* band.
** First head of third *CN* band.

TABLE 1—*Continued*

Chromosphere	Element	Sun	Flash	Height in Km	High E.P.	Chromosphere	Element	Sun	Flash	Height in Km	High E.P.
3901.72....	*Nd*$^+$-	5^2	5d	500	.....	3945.97....	*Cr*	2^3	1	400	6.13
3902.39....	*V*-	6^3	3	500	3.23	3946.90....	*Fe-Co*	4^2	3	500	6.32
3902.97....	*Fe-Cr*	10	8	1000	4.71	3947.66....	*Fe-Ti*	7^3	6	600	5.95
3903.19....	*V*$^+$-*Cr*	3^2	6	1000	4.63	3948.13....	*Fe*	5	3	600	6.35
3903.82....	*Fe*-	7^2	4	600	6.14	3948.67....	*Ti-Fe*	8^2	4	600	3.13
3904.77....	*Ti*	3	4	500	4.06	3949.07....	*La*$^+$-*Ca*	1	8	800	3.53
3905.53....	*Si*	12	12	1000	5.06	3949.96....	*Fe*	5	5	600	5.29
3905.92....	*Nd*$^+$-	4^2	3	500	.....	3950.33....	*Y*$^+$	2	10	1000	3.23
3906.48....	*Fe*	10	12	1000	3.27	3951.20....	*Fe-Nd*$^+$	5	3	700	6.38
3906.72....	*Fe-V*	3	6	600	6.45	3951.97....	*V*$^+$	2	6	600	4.59
3906.99....	*Eu*$^+$	2^2	3	600	3.36	3952.66....	*Fe*	7^2	4	600	5.80
3907.45....	*Sc-Fe*	3	3	600	3.16	3953.03....	*Fe-Co*	10^4	4	600	6.13
3907.91....	*Fe*	4	5	600	5.90	3954.53....	*Fe*-	3^2	1	400	6.37
3908.77....	*Cr*	4	3	500	4.16	3955.37....	*Fe*-	5	2	400	6.39
3909.65....	*Fe*-	4	3	500	6.43	3956.39....	*Ti-Fe*	8^2	5	600	3.14
3909.90....	*Fe-Co*	8^2	5	600	5.99	3956.72....	*Fe*	6	8	600	5.80
3910.68....	*Fe-V*	6^2	3	500	5.90	3957.05....	*Ca-Fe*	7	8	750	5.00
3911.15....	*Ti-Nd*$^+$	0	2	500	5.19	3958.23....	*Zr*$^+$-*Ti*	5	15	1000	3.64
3911.84....	*Sc*	2	2	500	3.18	3959.48....	*Gd*$^+$-	0^2	1d	400	3.84
3912.18....	*Ni-Cr*	4^2	4	500	6.93	3960.33....	*Fe*	4	3	400	6.74
3913.55....	*Ti*$^+$-*Fe*	9^2	40	2500	4.26	3961.51....	*Al*	20	35	2000	3.13
3914.45....	*V*$^+$-*Fe*$^+$	8^5	10d	800	4.94	3962.98....	*Fe-Ti*	6^2	6	800	6.38
3915.33....	*Fe-Co*	2^2	3	500	5.43	3964.39....	*Fe-Ti*	5^2	4	600	5.95
3915.72....	*Cr*-	6^2	8	800	6.15	3964.72....	*He*	.....	8	1200	23.64
3915.96....	*Zr*$^+$-*La*$^+$	2^2	6	800	3.68	3966.58....	*Fe-Zr*	6^3	4	500	5.86
3916.34....	*V*$^+$-*Cr*	5^2	3	600	4.57	3968.70....	*Ca*$^+$	700	180	14000	3.11
3916.74....	*Fe*	5	3	600	6.37	3970.25....	*H*ϵ	5	120	8000	13.26
3917.24	*Fe*	5	4	700	4.14	3971.33....	*Fe*	5	4	400	5.79
3918.34....	*Fe*	8^2	7	800	5.62	3971.89....	*Eu*$^+$-*Fe*	1^2	3	600	3.31
3918.66	*Fe*	5	4	600	6.15	3972.27....	*Ni*-	4^3	2	400	3.53
3919.12....	*Fe-Cr*	6^2	3	600	6.13	3973.60....	*V*$^+$-*Ca*	6^3	6	800	4.53
3920.25....	*Fe*	10	20	1500	3.27	3974.56....	*Co-Fe*	13^4	6d	600	3.62
3921.11....	*Cr*	3	4	600	4.13	3975.21....	*Fe*-	3^2	2	400	5.56
3921.59....	*La*$^+$-*Ce*$^+$	9^3	4	600	3.38	3976.73....	*Fe-Cr*	8^3	5d	500	6.50
3922.46	*Zr*$^+$-*V*	3^3	2	500	5.63	3977.77....	*Fe*	6	6	700	5.29
3922.92....	*Fe*	12d	20	1500	3.20	3978.40....	*Fe*	3^2	3	500	5.92
3924.09....	*Mn-Ni*	2^2	2	400	.....	3978.70....	*Co-Ce*$^+$	3	4	500	3.61
3924.53	*Ti*	4	3	400	3.17	3979.49....	*Co-Fe*	7^2	5d	600	3.20
3925.20....	*V-Fe*	4	3	500	3.31	3980.97....	*Fe-Cr*	5^4	4d	500	5.51
3925.61....	*Fe*	5	4	500	5.96	3981.81....	*Ti*$^+$-*Fe*	6^2	10	800	3.67
3925.98....	*Fe*	7^2	4	600	5.99	3982.55....	*V*$^+$-*Ti*	5^2	12	1000	3.23
3926.86....	*V*$^+$-*Cr*	2^3	3d	600	4.61	3983.17....	*Cr-Ce*$^+$	5^3	2	500	6.53
3927.96....	*Fe*	10^2	20	1500	3.25	3983.90....	*Fe-Cr*	7^2	6	600	5.81
3929.16....	*Fe-La*$^+$	4^2	4	500	5.85	3984.30....	*Cr-Mn*	4^2	3	600	5.63
3929.86....	*Ti*	2	2	500	3.14	3984.64....	*Ce*$^+$	2	2	600	4.05
3930.26....	*Fe*	8	20	1500	3.23	3985.36....	*Fe*-	4^2	3	400	6.38
3931.15....	*V-Fe*	2^2	2	400	3.21	3986.18....	*Fe*	3	4	500	6.33
3933.90....	*Ca*$^+$	1000	200	14000	3.14	3986.73....	*Mg*	6	6	600	7.42
3935.90....	*Fe-Co*	4^2	3	500	5.96	3987.15....	*Mn-Co*	5^3	4	500	6.22
3937.36....	*Fe*	3	3	500	5.82	3987.56....	*Mn-Ti*$^+$	3^2	3	500	6.22
3938.35....	*Mg-Fe*$^+$	6^2	10	1000	7.46	3988.47....	*La*$^+$	0	8	600	3.50
3939.43....	*Sc*$^+$-*Fe*$^+$	2^4	3	600	3.45	3989.09....	*Sc*$^+$-	5^2	2	500	3.41
3940.17....	*Fe-Ce*$^+$	3^2	2	500	6.53	3989.77....	*Ti-Fe*	7^2	6	600	3.11
3940.87....	*Fe-Co*	5	4	700	4.09	3990.00....	*Cr-Nd*$^+$	2^2	4	600	6.97
3941.30....	*Fe*	3	2	500	6.38	3990.35....	*Fe-V*	3^3	2	600	6.13
3941.89....	*Co-Ce*$^+$	6^4	3	600	3.56	3991.16....	*Zr*$^+$-*Cr*	3	10	800	3.85
3942.43....	*Fe*	5^2	4d	600	5.96	3991.65....	*Co-Cr*	3^3	4	500	3.67
3943.24....	*Fe*-	7^3	5	600	5.32	3992.29....	*Fe-Ce*$^+$	3^2	3	400	6.38
3944.03....	*Al*	15	25	2000	3.13	3992.86....	*Cr-V*	2	2	400	5.79
3944.71....	*Fe-Dy*$^+$	3^2	4	600	5.96	3993.13....	*Fe*	2	1	400	.....
3945.19....	*Fe-Fe*$^+$	6^2	8	800	5.87	3993.80....	*Cr-Ce*$^+$	2^3	2	400	5.79

TABLE 1—*Continued*

Chromo-sphere	Element	Sun	Flash	Height in Km	High E.P.	Chromo-sphere	Element	Sun	Flash	Height in Km	High E.P.
3994.15....	*Fe*	4	4	400	6.12	4031.92....	*Fe-Mn*	4^2	3	600	6.32
3994.68....	*Co-Nd*$^+$	4^2	4	500	3.72	4032.61....	*Fe*	6^2	5	700	4.54
3995.31....	*Co*	5	6	600	4.01	4033.07....	*Mn*	7	20	1500	3.06
3995.76....	*La*$^+$	1	8	800	3.26	4033.68....	*Mn*	2	3	500	.....
3996.57....	*Sc-*	1^3	2	400	3.09	4034.47....	*Mn*	6	18	1200	3.06
3996.96....	*V*$^+$*-Fe*	3^2	5	600	5.46	4035.57....	*V*$^+$	2	5	800	4.84
3997.41....	*Fe-*	6^2	6	600	5.80	4035.78....	*Mn*	4	7	800	5.19
3997.97....	*Co-Fe*	8^2	6	600	4.13	4036.82....	*V*$^+$	1	2	400	4.53
3998.74....	*Zr*$^+$*-Ti*	5^2	10	800	3.64	4037.08....	.....	2	1	400	.....
3999.21....	*Ce*$^+$*-Cr*$^+$	1^2	10	800	3.38	4037.65....	*Fe*	1	2	400	5.33
4000.38....	*Fe*	4^2	6d	600	6.06	4038.56....	*Fe-V*$^+$	4^4	2	400	6.34
4001.15....	*V*$^+$*-*	3	3	500	6.83	4040.02....	*Fe-V*	4^3	2	400	5.77
4001.65....	*Fe*	3	4	500	5.25	4040.62....	*Fe*	3	2	500	6.34
4002.34....	*Ti-Fe*$^+$	3^4	2	400	5.19	4040.82....	*Ce*$^+$*-Nd*$^+$	1	12	800	3.50
4002.91....	*V*$^+$	2	4	500	4.50	4041.38....	*Mn-Fe*	9^3	8d	800	5.16
4003.81....	*Ti-Fe*	3	4	500	5.21	4042.62....	*Ce*$^+$	0	4	700	3.55
4004.95....	*Fe-*	3^3	4	600	6.09	4042.87....	*La*$^+$*-Sm*$^+$	1	8	700	3.98
4005.28....	*Fe*	7	10	1000	4.63	4043.98....	*Fe-*	5^2	4	600	5.77
4005.74....	*V*$^+$	3	7	1000	4.89	4044.64....	*Fe*	3	3	500	5.87
4006.29....	*Fe*	2	3	600	6.33	4045.37....	*Co*	5	3	500	4.10
4006.73....	*Fe*	5^2	5	600	5.95	4045.84....	*Fe*	30	40	2000	4.53
4007.34....	*Fe*	3	4	600	5.83	4047.34....	*Fe*	2	2	400	5.32
4008.00....	*Ti-V*$^+$	1^3	1	400	5.19	4047.89....	*V*$^+$*-Sc*	2^3	3d	600	3.23
4008.84....	*Ti-Fe*	5^2	7	600	3.10	4048.65....	*Zr*$^+$	1	4	800	3.85
4009.34....	*He*	.....	2	1000	24.21	4048.80....	*Mn-Cr*	5	10	600	5.20
4009.73....	*Fe-Ti*	5^2	5	800	5.29	4049.46....	*Fe-Gd*$^+$	4^3	3d	500	5.62
4010.44....	*Fe-*	4^2	1	400	5.67	4050.32....	*Zr*$^+$	0	4	500	3.76
4011.19....	*Fe*	7^3	4d	500	5.62	4050.91....	*V*$^+$*-Fe*	3^3	2	400	4.84
4011.96....	*Fe-Nd*$^+$	4^3	3	500	5.52	4052.10....	*Fe-Cr*$^+$	5^2	3	500	6.43
4012.41....	*Ti*$^+$*-Ce*$^+$	4	25	1500	3.65	4052.48....	*Fe-Mn*	7^3	3	500	6.31
4013.62....	*Ti-Fe*	3	3	600	5.20	4053.32....	*Cr*$^+$	3^2	4	600	6.14
4013.86....	*Fe*	5	4	600	6.08	4053.84....	*Ti*$^+$	2	8	1000	4.93
4014.53....	*Sc*$^+$*-Fe*	5	10	800	3.39	4054.83....	*Fe*	5^2	5	500	6.26
4014.94....	*Ce*$^+$	0	2	500	3.60	4055.08....	*Ti-Fe*	3	3	500	4.09
4015.55....	*Ni-Ti*	4^3	4	500	7.09	4055.60....	*Mn*	6	5	500	5.18
4016.46....	*Fe*	2	2	400	6.43	4056.16....	*Ti*$^+$*-Cr*	1^2	3	500	3.65
4017.19....	*Fe*	7^2	6	500	6.11	4056.55....	*Fe-Sr*$^+$	1^2	2	400	5.90
4017.60....	*Ti-Ni*	4^3	3	500	5.15	4057.20....	*Fe-Co*	7^3	5	400	5.79
4018.28....	*Mn-Fe*	10^3	7	500	5.18	4057.49....	*Mg*	7	5	800	7.37
4019.04....	*Ni-Ce*$^+$	1	3	500	5.00	4058.18....	*Co-Fe*	4	3	400	3.55
4019.32....	*Co*	0	1	400	3.65	4058.93....	*Fe-Mn*	6^2	6d	600	5.45
4020.08....	*Fe-*	4^3	3	400	6.32	4059.43....	*Mn-*	2^3	1	400	6.10
4020.44....	*Sc-Fe*	2^2	4	500	3.07	4059.74....	*Fe*	2	2	400	6.57
4020.88....	*Co*	3	3	500	3.50	4060.32....	*Ti*	1	1	400	4.09
4021.50....	*Fe-Nd*$^+$	3^3	4	600	5.48	4061.06....	*Nd*$^+$*-*	3	8	800	3.51
4021.91....	*Fe*	5	6	700	5.82	4061.90....	*Mn-*	4^2	2	400	6.10
4023.42....	*V*$^+$	3	6	800	4.86	4062.50....	*Fe*	5	6	600	5.87
4023.66....	*Sc*	2	6	800	3.09	4063.26....	*Fe*	4	3	600	6.24
4024.06....	*Zr-Fe*	3^2	2	500	3.75	4063.62....	*Fe*	20	25	1800	4.59
4024.61....	*Fe-Ti*	7^2	8	800	6.29	4064.30....	*Ti*$^+$*-Fe*	5^4	3	500	5.62
4025.14....	*Ti*$^+$	3	10	800	3.67	4065.15....	*Ti-V*$^+$	2	1	400	4.08
4026.28....	*He*	.....	35	6000	23.94	4065.45....	*Fe*	3	3	500	6.29
4026.52....	*Ti-Mn*	3^2	3	500	5.17	4066.50....	*Co-Fe*	4^2	3	500	3.95
4027.26....	*Zr-V*$^+$	1^2	2	400	3.68	4067.07....	*Fe*	8^2	8	700	5.85
4027.95....	.....	0	2	600	.....	4067.43....	*La*$^+$	− 2	1	500	3.21
4028.36....	*Ti*$^+$	4	15	1000	4.95	4068.00....	*Fe*	6	4	500	6.23
4029.60....	*Zr*$^+$*-Fe*	5	6	600	3.77	4068.63....	*Co-Ce*$^+$	1^2	3	450	4.98
4030.48....	*Fe-Ti*	5	5	600	6.26	4069.20....	*Ti-Nd*$^+$	3^2	4	450	5.78
4030.79....	*Mn*	9	25	1500	3.06	4070.30....	*Mn*	3	3	400	5.21
4031.26....	*Fe-Ce*$^+$	2^2	4	500	6.27	4070.90....	*Fe-Cr*$^+$	5^2	4	400	6.26
4031.69....	*La*$^+$	2	8	600	3.38	4071.75...	*Fe*	15	25	1500	4.63

TABLE 1—*Continued*

Chromosphere	Element	Sun	Flash	Height in Km	High E.P.	Chromosphere	Element	Sun	Flash	Height in Km	High E.P.
4072.36....	*Fe-*	3^3	2	400	6.28	4114.58....	*Fe*	6^2	4	500	5.82
4073.35....	Ce^+	1^2	3	500	3.03	4115.20....	*V*	3	4	600	3.28
4073.75....	*Fe*	4	5	500	6.28	4115.99....	*Ni*	3	2	400	7.13
4074.79....	*Fe*	5^2	5	500	6.06	4116.63....	*V-*	3^3	3	500	3.27
4075.18....	Nd^+-	3^3	2d	500	3.09	4117.87....	*Fe-*	2	2	400	6.40
4076.07....	*Cr-*Fe^+	4^2	4	500	5.72	4118.15....	Ce^+	0	3	500	3.21
4076.66....	*Fe*	8^3	5	500	6.22	4118.70....	*Fe-Co*	11^3	12	800	6.25
4077.35....	La^+-*Y*	1	3	800	3.26	4119.38....	*Fe*	1	1	400	.....
4077.83....	Sr^+	8	80	6000	3.03	4119.78....	Ce^+-*Fe*	2^3	3	400	3.60
4078.47 ...	*Fe-Ti*	7^2	5	500	5.62	4120.30....	*Fe*	4	3	400	5.97
4079.16....	*Mn-Fe*	5^2	4	500	5.16	4120.78....	*He*	.....	4	2500	23.87
4079.45....	*Mn*	3	4	500	5.20	4121.31....	*Co*	6	5	600	3.91
4079.88....	*Fe*	3	3	500	5.87	4121.87....	*Fe-Cr*	4^2	3d	600	5.81
4080.30....	*Fe*	3	4	500	6.29	4122.60....	Fe^+-*Fe*	4^2	6d	600	5.57
4081.22....	*Zr-*Ce^+	2^2	4	500	3.75	4123.30....	La^+	1	7	800	3.31
4082.23....	*Fe*	3^2	2	400	6.26	4123.47....	*V*	2^2	2	500	3.26
4082.44....	*Sc-Ti*	3	2	400	3.04	4123.78....	*Fe*	4	4	800	5.59
4083.00....	*Mn*	4	4	500	5.19	4124.81....	V^+-Fe^+	1^2	5d	800	3.40
4083.58....	*Mn-Fe*	6^2	6	500	5.18	4125.78....	*Fe*	7^3	4	500	5.82
4083.82....	*Fe-V*	3	2	400	6.42	4126.20....	*Fe*	4	3	400	6.31
4084.50....	*Fe*	5	4	400	6.22	4126.51....	*Cr*	2	2	400	5.52
4085.02....	*Fe*	4	3	400	5.85	4127.71....	*Fe*	8^2	8	800	5.84
4085.30....	*Fe-*Ce^+	5^2	4	500	6.25	4128.10....	*V-*Mn^+	6	6	800	3.26
4086.30....	*Co-*Cr^+	4^2	3	400	4.89	4128.76....	Fe^+	2	2	500	5.56
4086.66....	La^+	1	10	800	3.02	4129.26....	*Cr-Fe*	5^2	2	500	5.89
4087.08....	*Fe*	3	3	500	6.34	4129.73....	Eu^+	1	10	800	2.99
4087.28....	Fe^+	− 1	3	500	5.59	4130.68....	Ba^+	2	4	500	5.20
4088.57....	*Fe*	3	3	400	6.64	4131.31....	*Cr*	0	2	400	6.82
4089.23....	*Fe*	3	3	400	5.95	4131.91....	*V-Fe*	2	2	500	3.27
4090.55....	Zr^+-*V*	2^2	3	600	3.77	4132.13....	*Fe*	10	12	900	4.59
4090.97....	*Fe-*Ce^+	3	4	600	6.37	4132.91....	*Fe*	4	4	500	5.82
4091.54....	*Fe*	3	3	500	5.84	4133.78....	*Fe-*Ce^+	5^2	4d	500	6.22
4092.39....	*Fe-Co*	6^3	7	500	3.93	4134.36....	*Fe-V*	6^2	6	500	2.99
4092.62....	*V-Ca*	3	2	500	3.30	4134.69....	*Fe*	5	6	500	5.80
4094.36....	Gd^+-	2	1	400	3.53	4135.41....	Nd^+-	1^2	3	500	.....
4094.90....	*Ca*	4	3	400	5.53	4135.84....	*Zr-*	1^2	2	400	3.61
4095.37....	*V-Fe*	2^3	2	400	4.07	4136.54....	*Fe*	3	3	500	6.34
4096.02....	*Fe*	5^2	5	500	5.59	4137.06....	*Fe*	4	5	500	6.38
4097.06....	*Fe*	2	4	400	6.28	4137.64....	Ce^+	1	5	500	3.02
4098.18....	*Fe-Cr*	5	5	600	6.24	4138.06....	*Fe-*	1^2	1d	400	5.80
4098.56....	*Ca-*Cr^+	6^2	5	600	5.53	4139.89....	*Fe*	4	3	400	3.97
4098.83....	Gd^+	− 2	1	400	3.83	4140.36....	*Fe*	3	1	400	6.36
4099.83....	*V*	2	4	500	3.28	4141.66....	La^+	0	1	400	3.38
4101.85....	*Hδ*	40	140	8000	13.16	4141.88....	*Fe*	3	2	400	5.98
4102.95....	*Si*	5	4	500	4.91	4142.41....	*Cr-Ti*	8^4	2	400	6.09
4103.50....	*Fe-*Dy^+	1^2	2	400	6.24	4143.11....	*Ti-*	1^3	2	400	5.27
4104.12....	*Fe-*	5	5	600	6.26	4143.90....	*He*	.....	4	2000	24.11
4105.06....	*V-Fe*	3^2	6d	600	3.27		*Fe*	15	10		4.53
4106.24....	*Fe*	2	3	500	5.58	4144.48....	Ce^+	0	1	450	2.98
4106.44....	*Fe*	2	3	500	6.39	4144.98....	Ce^+	0	2	450	3.20
4107.49....	*Fe*	5	6	600	5.82	4145.22....	*Fe*	1	1	400	5.66
4108.54....	*Ca*	2	2	400	5.70	4146.08....	*Fe*	3	4	400	5.95
4109.21....	*Fe-*Nd^+	4^2	5	600	6.28	4146.46....	*Cr-*	3^4	3	400	5.93
4109.73....	*V-Fe*	5^2	6	600	3.26	4147.40....	*Fe-Mn*	3^2	3	400	6.29
4110.49....	*Co*	4	4	500	4.05	4147.69....	*Fe*	4	3	400	4.45
4111.42....	*Cr*	1	2	500	5.89	4148.83....	*V*	0	1	400	3.24
4111.82....	*V*	4	5	500	3.30	4149.24....	Zr^+	2	15d	900	3.77
4112.30....	*Fe*	2	2	400	6.38		*Fe*	4			6.29
4112.74....	*Ti*	1	1	400	3.05	4149.88....	*Fe-*Ce^+	3^2	3	600	3.03
4113.09....	*Fe-Mn*	4^2	3	400	7.16	4150.25....	*Fe*	3	2	400	6.39
4113.85....	Nd^+-*Mn*	−1	4d	500	3.18	4150.53....	*Ti-Co*	2^2	2	400	5.26

TABLE 1—*Continued*

Chromosphere	Element	Sun	Flash	Height in Km	High E.P.	Chromosphere	Element	Sun	Flash	Height in Km	High E.P.
4151.03	Zr^+-Ti	1	4	600	3.77	4189.52	Fe-CN	2^2	2	400	6.62
4151.91	La^+-Ce^+	2^2	4	500	3.21	4190.06	Cr-	1^2	1	400	5.80
4152.18	Fe-	4^2	4	500	3.93	4191.48	Fe	9^2	10d	1200	5.40
5152.53	CN††	1^3	2	400	.....	4192.54	Fe-CN	3^3	1	400	.....
4153.36	Fe	1	1	400	.....	4192.95	Ce^+-CN	0^2	2	400	3.68
4153.94	Fe-Cr	7^3	3d	500	6.35	4193.42	CN	1^3	2	400	.....
4154.51	Fe	4	4	500	5.79	4194.44	Fe-CN	1^4	1	400	5.66
4154.85	Fe	4	4	500	6.32	4194.96	Cr-CN	2^2	3d	500	6.78
4156.15	Zr^+-Nd^+	5^4	12	500	3.68	4195.50	Fe-Ni	8^3	4d	500	6.26
4156.85	Fe	4	5	500	5.79	4196.59	La^+-Fe	2	8	600	3.26
4157.85	Fe	5	5	400	6.37	4197.11	CN¶¶	2	4	500	.....
4158.05	CN‡‡	− 1	2	400	.....	4198.14	Fe-	3^2	1	500	.....
4158.85	Fe	4	3	400	6.38	4198.28	Fe	8^2	9	1000	5.33
4159.25	.....	4	2	400	.....	4198.69	Fe-V	3	2	600	6.34
4160.42	Fe	3^2	1d	400	5.90	4199.09	Fe	5	10	1200	5.97
4161.08	Zr^+-Fe	4^2	6	900	3.68	4199.94	Fe-	3^2	2d	600	3.03
4161.50	Ti^+-Fe	4	6	900	4.05	4200.53	Ni-CN	2^2	3	600	6.23
4161.80	Sr^+	1	2	800	5.89	4200.85	Fe-Ti	4^2	3	600	6.32
4162.64	CN-	2^2	2d	600	.....	4201.65	Fe-Ni	1	1	400	6.50
4163.66	Ti^+-Cr	4	15	1000	5.54	4202.11	Fe	8	12	1200	4.42
4164.30	V^+-CN	2^4	3d	500	4.99	4202.43	V^+-CN	1^2	2	400	4.63
4165.33	Fe-CN	4^2	3	500	.....	4203.00	Ce^+-Fe	4^3	5	600	3.49
4165.58	Ce^+	1	3	500	3.39	4203.59	Cr-Fe	2	2	400	5.47
4166.01	Ba^+	0	2	500	5.67	4203.98	Fe	7^2	5	800	5.77
4166.85	CN	0	2	500	.....	4204.68	Y^+-CH	3^2	6	800	2.94
4167.24	Mg	8	6	800	7.29	4205.06	V^+-Eu^+	2^2	6	800	4.96
4167.66	Y-CN§§	2^2	4	600	3.03	4205.54	Fe-Fe^+	2	3	500	6.34
4167.94	Fe	4^2	4	500	6.25	4206.69	Fe-	4^2	4d	600	2.99
4168.76	Fe-Fe^+	4^2	2	400	6.31	4207.08	Fe	3	3	500	5.75
4169.05	He	.....	1	1000	24.09	4207.44	Cr^+-CN	1	1	400	6.74
4169.37	Ti-Sm^+	0^2	2	400	4.84	4208.59	Fe	3	2	600	6.31
4169.81	Fe	2	2	400	6.34	4208.95	Zr^+	1	7	1000	3.64
4170.87	Fe	4	3	500	5.96	4209.71	V-Cr	3^4	2	500	3.23
4171.10	Ti-	4	3	500	5.10	4210.37	Fe-	7^2	6d	800	5.40
4171.95	Ti^+	2	18	1200	5.54	4211.00	CH	3	2d	500	.....
4172.16	Fe	2	2	500	6.20	4211.89	Zr^+	2	6	800	3.45
4172.68	Fe-Cr^+	6^2	3d	600	3.91	4212.73	CN	4^2	2	500	.....
4173.48	Fe^+-Ti^+	8^3	20	1200	5.53	4213.65	Fe-CH	3	5d	600	5.76
4173.95	Fe-Ti^+	4^2	2d	500	3.94	4215.70	Sr^+-CN	5	60	6000	2.93
4174.89	Fe-Cr	5^2	4	600	3.87	4216.16	Fe-				
4175.64	Fe	5	6	500	5.79		CN***	4^2	4	800	2.93
4176.58	Fe	4	3	400	6.31	4217.15	Gd^+-CH	2^2	4	600	3.59
4177.34	Ti-Nd^+	0	1	500	4.83	4217.54	Fe-La^+	5	5	600	6.34
4177.54	V^+-Fe	6^2	25	1200	3.36	4218.36	.....	1	1	400	.....
4178.87	Fe^+	3	20	1200	5.52	4218.68	CH	3	2	400	.....
4179.42	Cr^+-V	3	8	600	6.76	4219.40	Fe	7^2	6	600	5.90
4180.36	Fe-CN	1	2	400	5.67	4220.32	Fe	3	4	500	5.98
4180.82	CN|||	2	4	500	.....	4220.62	Sm^+	− 1	3	500	3.11
4181.81	Fe-	8^3	8d	800	5.77	4221.16	.....	0	1d	400	.....
4182.36	Fe	3	3	600	5.96	4222.22	Fe	5	6	800	5.36
4182.74	Fe	2	1	400	6.35	4222.70	Ce^+-Cr	1^2	4	800	3.04
4183.38	V^+-Zr	3^2	3d	400	4.99	4223.18	Pr^+-	2^2	2	500	2.98
4184.19	Ti^+-Gd^+	6^2	6d	600	4.02	4223.49	CH-	2^2	1	400	.....
4184.89	Fe-Cr	4	5	600	5.77	4224.19	Fe	4	3	500	6.28
4186.56	Ce^+	2	3	600	3.33	4224.65	Fe-CH	5^2	3	500	6.34
4187.08	Fe	6	9	1200	5.39	4225.30	Fe-V^+	4^3	6	600	6.32
4187.77	Fe	10^4	9	1200	5.36	4226.74	Ca	20	40	4000	2.92
4188.73	Ti	4	2	400	5.18	4227.50	Fe	4	4	600	6.24
4189.08	CN	2^2	2	400	.....	4227.72	Ca^+-Zr	1^2	3	400	3.14

†† Sixth head of second *CN* band.
‡‡ Fifth head of second *CN* band.
§§ Fourth head of second *CN* band.
||| Third head of second *CN* band.
¶¶ Second head of second *CN* band.
*** First head of second *CN* band.

TABLE 1—*Continued*

Chromosphere	Element	Sun	Flash	Height in Km	High E.P.	Chromosphere	Element	Sun	Flash	Height in Km	High E.P.
4228.68....	*Fe*	1	1	350	6.27	4268.67....	*Fe-V*	3^2	4d	500	6.18
4229.71....	*Fe-CH*	6^3	5d	500	4.40	4269.52....	La^+	0	1	400	4.67
4231.03....	*Ni-CH*	4	3	400	6.44	4269.70....	*CH-*	2	2	400	.....
4231.70....	Zr^+-*Fe*	2^2	2	400	4.66	4270.19....	*Ti*-Ce^+	1	1	400	5.20
4232.60....	*Fe*-Nd^+	3^2	2	400	2.99	4271.16....	*Fe*	6	10	1000	5.33
4233.22....	Fe^+	4	30	2200	5.49	4271.77....	*Fe*	15	20	2000	4.37
4233.66....	*Fe*	6	3	600	5.39	4272.77....	*Cr-*	2^2	1	400	5.78
4234.19....	V^+	0	1	400	4.59	4273.36....	Fe^+-Zr^+	5^2	10	800	5.58
4235.21....	*Mn*	5^2	6	600	5.79	4273.99....	*Fe-CH*	4^3	2	400	5.95
4235.92....	*Fe*-V^+	10^3	15d	1200	5.33	4274.77....	*Cr-Ti*	9^2	30	2000	2.89
4236.95....	V^+-*CH*	3^3	2	400	4.59	4275.55....	La^+-Cr^+	1^2	5	500	3.21
4237.21....	*Fe-*	4^2	3	500	3.87	4276.64....	*Fe-Ti*	2	2	400	6.75
4237.99....	*Fe*	4	3	500	6.31	4276.99....	*V*	1	1	400	4.23
4238.39....	La^+	1	2	500	3.31	4277.46....	*Fe-Zr*$^+$	3^2	3	400	5.48
4238.86....	*Fe*	5	4	500	6.29	4278.20....	Fe^+-*Ti*	4^2	4d	500	5.77
4239.30....	*Zr-Fe*	2	1	400	3.60	4278.76....	*Ti-*	2^2	2	400	5.18
4239.88....	*Fe-Mn*	7^3	7	600	3.86	4279.65....	*CH-Fe*	4^2	4	500	6.75
4240.40....	*Fe-Ca*	3^2	1	400	6.44	4279.98....	Sc^+-*CH*	3^3	3	500	3.48
4240.68....	*Cr*	1	1	400	5.88	4280.41....	*Cr*	1	2	400	6.72
4241.10....	*Fe*-Pr^+	2	2	500	5.73	4280.72....	Sm^+-*CH*	2^4	2	500	3.37
4242.24....	Er^+	1^2	2	500	.....	4281.07....	*Mn*	2	3	500	5.79
4242.45....	Cr^+-*Fe*	4^2	6	1000	6.76	4281.94....	*CH*	2	1	400	.....
4242.75....	*Fe*	2	2	400	6.20	4282.46....	*Fe*	5	10	1000	5.05
4243.38....	*Fe-CH*	5^3	4d	500	6.53	4282.96....	*Ca*	4	8	800	4.76
4243.87....	*Fe*	2	2	400	6.77	4284.14....	Cr^+-*V*	3^2	5d	600	6.72
4244.66....	Sm^+-Ni^+	— 1	1	400	3.18	4284.81....	*Ti-Ni*	4^3	3	400	4.61
4245.28....	*Fe*	6^2	6	500	5.75	4285.43....	*Fe*-Ce^+	5^3	3	400	6.10
4246.06....	*Fe*	2	2	400	6.17	4285.98....	*Ti-Co*	3^2	3	400	3.70
4246.90....	Sc^+	5	50	5000	3.22	4286.43....	*Fe-CH*	3	2	400	5.82
4247.41....	*Fe*	4	4	500	6.26	4286.99....	La^+-*Fe*	2	2	400	4.82
4248.26....	*Fe*	2	4	500	5.96	4287.40....	*Ti*	1	1	400	3.71
4248.68....	Ce^+-*CH*	2	4	500	3.11	4287.96....	Ti^+-*Ni*	4^3	8	1200	3.95
4249.52....	*CH*	3^2	2	400	.....	4289.09....	*Ti-Fe*	3^2	2d	500	3.69
4250.16....	*Fe*	8	10	1200	5.36	4289.60....	*Ca*	4	25	2000	4.75
4250.85....	*Fe-*	9^2	12	1200	4.45		*Cr*	5			2.88
4251.69....	*Ti*-Gd^+	1^2	3	500	4.77	4290.18....	Ti^+	2	25	2000	4.04
4252.46....	Cr^+	2^3	4d	500	6.74	4290.95....	*Ti-Fe*	4^2	4	500	3.69
4252.96....	Mn^+-	3^3	1	400	8.26	4291.32....	*Ti-Fe*	5^3	3	500	3.71
4253.39....	Ce^+-Gd^+	0^2	1	400	3.36	4292.09....	*Fe-CH*	6^4	5d	500	5.04
4254.36....	*Cr*	8	35	2000	2.90	4293.03....	Zr^+-*CH*	5^2	5d	500	4.61
4255.02....	*Fe-CH*	2	2	400	5.91	4294.07....	Ti^+-*Fe*	7^2	30	2500	3.95
4255.50....	*Fe-Cr-*	3^3	3	500	5.90	4294.80....	Sc^+	2	4	500	3.48
4255.89....	Ce^+-*CH*	2	4	500	3.60	4295.09....	*CH*	4	4	500	.....
4256.44....	Sm^+	1^2	1	500	3.28	4295.91....	*Ti*-La^+	4^3	5d	500	3.68
4257.65....	*Mn*	2	2	500	5.84	4296.67....	Fe^+-Zr^+	4^3	12	1000	5.57
4258.23....	Fe^+-*Fe*	4^3	8d	800	5.59	4297.09....	*CH-Cr*	7^4	2d	400	5.57
4258.58....	*Fe-CH*	4^3	2	400	5.72	4298.10....	*Fe-CH*	4^2	4d	800	5.91
4259.07....	*Fe-V*	4^4	3d	400	5.90	4298.72....	*Ti-Ni*	4^2	2	500	3.69
4260.11....	*Fe*	5^2	3	500	5.96	4299.02....	*Ca*	3	8	800	4.75
4260.51....	*Fe*	10	20	1500	5.29	4299.27....	*Fe-Ti*	4	4	800	5.29
4261.42....	*CH*	4^2	3	600	.....	4299.60....	*Ti*	2	2	500	3.69
4261.82....	Cr^+-*CH*	4^3	5	1000	6.74	4300.05....	Ti^+	3	35	2500	4.05
4263.19....	*Ti-Cr*	2	2	400	4.77	4300.61....	*Ti-CH*	2	2	500	3.69
4263.62....	La^+	0	1	400	4.84	4301.08....	*Ti-CH*	6^2	4d	600	3.70
4264.32....	*Fe-*	4^2	3d	500	6.25	4301.60....	*CH-*	1^2	0	400	.....
4264.76....	*Fe*	2	2	400	6.84	4301.94....	Ti^+	3	12	1200	4.02
4265.21....	*Fe-Ti*	2	1	400	6.81	4302.59....	*Ca-CH*	8^3	8	1200	4.76
4265.94....	*Mn*	2	1	400	5.82	4303.20....	Fe^+	2	10	1200	5.56
4266.82....	*Fe-Cr*	4^3	2	500	5.61	4303.56....	Nd^+-	2^2	4	600	2.87
4267.40....	*CH*	2	2	500	.....	4303.95....	*CH-*	6^2	2	400	.....
4267.76....	*Fe-CH*	4^2	3	500	5.99	4304.49....	*CH-Fe*	3^2	2d	400	5.80

TABLE 1—*Continued*

Chromosphere	Element	Sun	Flash	Height in Km	High E.P.	Chromosphere	Element	Sun	Flash	Height in Km	High E.P.
4305.46....	Sr^{+}-Fe	3	4	1000	5.89	4358.74....	Y^{+}	0	10	800	2.94
4305.82....	Ti-Sc^{+}	7^{3}	6	1000	3.71	4359.65....	Zr^{+}-Cr	4^{2}	10d	800	4.06
4306.73....	CH-Ce^{+}	2	3	500	2.90	4360.37....	Ti-CH	2^{2}	1	400	5.00
4307.39....	CH	4^{2}	1	500	.....	4360.86....	Fe-Zr	1	2	400	6.46
4307.86....	Ca	3	35	2500	4.74	4361.99....	Ni^{+}-Sm^{+}	1^{2}	2	400	6.84
	Ti^{+}-Fe	6			4.02	4362.56....	.....	1	1	400	.....
4308.89....	Fe-CH	5^{3}	1	500	6.48	4363.18....	Cr-CH	1	2d	500	5.78
4309.35....	Fe-CH	3	2	500	5.80	4364.19....	Y^{+}	1	3	500	6.78
4309.62....	V^{+}-CH	1	10	800	3.04	4364.66....	Ce^{+}-La^{+}	− 1	3	500	3.32
4310.21....	CH	5^{2}	1	400	.....	4365.84....	Fe	2	1	400	5.80
4310.76....	V^{+}-Ce^{+}	3^{2}	2	400	4.80	4366.56....	CH	2^{2}	4	400	.....
4311.12....	CH	3^{2}	2	400	.....	4367.54....	Fe	5	5	800	5.80
4311.56....	CH-Ti	6^{3}	2	400	5.01	4367.73....	Ti^{+}	2	6	800	5.40
4312.12....	CH	5^{3}	2	400	.....	4367.95....	Fe-V	3^{2}	2	400	4.43
4312.82....	Ti^{+}	3	18	1500	4.04	4368.49....	Ni-Nd^{+}	1^{2}	1d	400	6.23
4314.08....	Sc^{+}	3	18	1500	3.48	4369.39....	Fe^{+}	1	5	600	5.59
4314.97....	Ti^{+}-Fe	8^{3}	18	1500	4.02	4369.72....	Fe-Ti	5^{2}	6	600	5.86
4315.96....	La^{+}-Gd^{+}	− 1	2	400	3.26	4371.01....	Zr^{+}	1	5	600	4.03
4316.75....	Ti^{+}	1	4	600	4.90	4371.28....	Cr	2	4	600	3.82
4317.20....	Zr^{+}-	1^{2}	2	500	3.57	4371.58....	.....	1^{2}	1	400	.....
4318.73 ...	Ca-Ti	4	9d	1000	4.75	4372.26....	Ti-Fe^{+}	0	1	400	5.30
4319.55....	Cr-Fe	1^{2}	1d	400	5.73	4372.80....	CH	1^{2}	1	400	.....
4320.77....	Sc^{+}-Ti^{+}	5^{2}	25	2000	3.46	4373.57....	Fe	2	1d	400	5.37
4321.60....	Ti	0	2	500	5.08	4374.49....	Sc^{+}-Fe	3	15	1500	3.44
4322.42....	La^{+}-	1^{2}	2	500	3.03	4375.00....	Y^{+}	2	20	1500	3.23
4323.20....	Sm^{+}-CH	2	4d	500	2.96	4376.00....	Fe	6	15	1200	2.82
4323.73....	CH-	4^{2}	2	400	.....	4376.81....	Fe-Cr	1	1d	400	5.82
4325.02....	Sc^{+}	4	12	1500	3.45	4377.24....	CH	2	2	400	.....
4325.79....	Fe-Ni	10^{3}	20	2000	4.45	4377.81....	Fe	1	1	400	6.08
4326.75....	Fe	2	2	400	5.79	4378.26....	CH	2	2	400	.....
4327.05....	Fe	3	4	500	6.38	4379.25....	V	4	4	600	3.12
4327.87....	Fe	2	3	500	6.14	4379.76....	Zr^{+}-Cr	0	4	500	4.34
4328.94....	Sm^{+}-Fe	1^{3}	4d	600	3.03	4380.71....	CH	2	3	400	.....
4330.09....	Ti^{+}-V	2^{2}	5	800	4.89	4381.19....	Cr-Mn	1^{2}	1d	400	5.51
4330.66....	Ti^{+}	2	8	800	4.02	4382.16....	Ce^{+}	− 1	3d	400	3.02
4331.66....	Ni	2	4	500	4.52	4382.90....	Fe-CH	3^{2}	2	400	6.37
4332.80....	V-Cr	2^{3}	4d	500	2.87	4383.54....	Fe	15	30	2000	4.29
4333.72....	La^{+}	1	10	800	3.02	4384.27....	Fe^{+}	1	1	400	5.46
4334.84....	V^{+}-La^{+}	2^{3}	2	400	4.86	4384.69....	V-Sc^{+}	4^{2}	3	500	3.10
4337.12....	Fe	5	4	600	4.40	4385.14....	Cr-La^{+}	4^{3}	4	600	3.84
4337.98....	Ti^{+}	4	20	2500	3.92	4385.34....	Fe^{+}	2	10	1200	5.58
4338.77....	Fe^{+}-Mn	1^{2}	2	400	5.22	4386.81....	Ti^{+}	1	8	800	5.40
4340.63....	$H\gamma$	20	150	8000	13.00	4387.49....	Cr-CH	2^{3}	2	400	5.79
4342.13....	Gd^{+}	0	1d	400	3.44	4387.86....	He	.....	5	2000	23.94
4343.20....	Fe-Cr	4^{2}	3	500	6.08	4388.39....	Fe	3	2	400	6.40
4343.65....	Fe	2	2	400	5.87	4389.24....	Fe	2	2	400	2.86
4344.39....	Ti^{+}-Cr	6^{2}	12d	1200	3.92	4389.95....	V	2	2	400	3.09
4346.70....	Fe-Cr	3^{2}	2	400	6.13	4390.47....	Fe-Mg^{+}	2^{2}	1	400	5.79
4347.39....	Fe-Pr^{+}	2^{2}	2	400	2.84	4390.96....	Ti^{+}-Fe	3^{2}	8	700	4.04
4347.90....	Fe-Sm^{+}	3^{2}	3	500	6.43	4391.67....	Ce^{+}-Cr	2^{2}	6	600	3.13
4348.94....	Fe	2	3	400	5.82	4393.01....	Fe	0	1	400	5.81
4349.76....	Ce^{+}	− 1	2	400	3.53	4394.01....	Ti^{+}-Ti	3^{2}	8d	800	4.02
4351.05....	Cr-Ti^{+}	4^{2}	4d	600	3.80	4395.13....	Ti^{+}-V	6^{2}	40	3000	3.89
4351.84....	Fe^{+}-Cr	10^{2}	25	2000	5.53	4395.89....	Ti^{+}	1	6	600	4.05
4352.81....	Fe-V	5^{2}	8d	600	5.05	4397.18....	Cr	− 1	1d	400	5.80
4354.18....	Ti-Cr	1^{4}	1	400	4.99	4398.00....	Y^{+}	1	6	800	2.94
4354.74....	Sc^{+}	2^{2}	5	800	3.44	4398.32....	Ti^{+}	0	6	800	4.02
4355.08....	Ca-Eu^{+}	2	1	400	5.53	4399.79....	Ti^{+}	3	15	1200	4.04
4356.00....	Ni-CH	1^{2}	2	400	6.45	4400.52....	Sc^{+}-V	4^{2}	15	1200	3.41
4356.72....	Cr-	2^{4}	1	400	5.83	4400.92....	Ni	0	1	400	6.44
4358.13....	Nd^{+}	0	3d	400	3.15	4401.35....	Fe	3^{2}	2	400	6.39

TABLE 1—*Continued*

Chromo-sphere	Element	Sun	Flash	Height in Km	High E.P.	Chromo-sphere	Element	Sun	Flash	Height in Km	High E.P.
4401.57....	*Ni*	2	3	500	5.98	4438.23....	*Fe-Ti*	2^3	2	400	6.45
4403.36....	*Zr^+-Cr*	0	4d	500	3.98	4439.84....	*Fe*	1	1	350	5.05
4404.27....	*Ti*	1	2	400	5.04	4440.37....	*Zr^+-V^+*	1^2	4	500	3.98
4404.79....	*Fe*	10	25	1800	4.35	4440.92....	*Fe-Ce^+*	2^2	1d	400	6.72
4405.76....	*Ti*	0	1	350	3.85	4441.74....	*Ti^+-V*	3	5	600	3.95
4406.11....	*V^+-V*	0	1	350	4.59	4442.33....	*Fe*	6	4	600	4.97
4406.68....	*V*	2	2	400	3.10	4443.03....	*Zr^+-Fe*	5^3	4	500	4.26
4407.67....	*Fe-Ti^+*	6^2	4d	500	4.97	4443.85....	*Ti^+*	5	35	3000	3.85
4408.18....	*V*	2	3	500	3.07	4444.60....	*Ti^+*	2	5	600	3.89
4408.46....	*Fe-V*	5^2	4	500	4.99	4445.40....	*Fe-*	1	1	350	2.86
4408.75 ...	*V-Pr^+*	− 1	1	400	3.06	4445.69....	*Co*	− 1	1	350	5.87
4409.38....	*Ti^+*	2^3	4	600	4.02	4446.28....	*Fe^+-Nd^+*	0^2	4	600	8.71
4410.13....	*Cr-*	1^3	1	400	5.80	4446.86 ...	*Fe*	2	2	400	6.45
4410.53....	*Ni*	1	2	500	6.09	4447.19....	*Fe*	2	2	400	4.96
4411.08....	*Ti^+-Cr*	1	4	600	5.88	4447.73....	*Fe*	6	5	800	4.49
4411.84....	*Ti^+-Mn*	2^2	3	600	4.02	4449.18 ...	*Ti*	2	5d	800	4.65
4412.15....	*Cr*	1^2	1	400	3.82	4449.67....	*V-Fe^+*	− 1	1	400	4.12
4413.10....	*Zr*	− 1	1	350	4.19	4450.37....	*Ti^+-Fe*	3^2	15	1800	3.85
4413.60....	*Fe^+-Cr*	2^2	2	350	5.46	4450.77....	*Ce^+*	− 1	3	400	2.98
4414.12....	*V^+*	− 1	1	350	4.34	4450.98....	*Ti*	1	1	400	4.64
4414.63....	*Zr^+*	− 1	2	400	4.03	4451.55....	*Mn-Nd^+*	3	5	600	5.65
4415.12....	*Fe*	8	12	1500	4.40	4452.01....	*V*	0	2	400	4.63
4415.53....	*Sc^+*	3	15	1500	3.39	4452.76....	*Sm^+*	− 1	2	400	3.05
4416.43....	*V*	0	1	400	3.06	4452.98....	*Mn*	1	1	400	5.70
4416.84....	*Fe^+*	2	15	1200	5.56	4453.30....	*Ti*	2	1	400	4.19
4417.22....	*Ti*	0	1	400	4.67	4453.72....	*Ti*	1	1	350	4.54
4417.71....	*Ti^+*	3	20	1500	3.95	4454.41....	*Fe*	3	3	500	5.59
4418.36....	*Ti^+*	1	4	600	4.02	4454.77....	*Ca*	5	15	1500	4.66
4418.86....	*Ce^+-Gd^+*	1^3	2	400	3.18	4455.29....	*Ti-Mn*	2	2	400	4.21
4419.97....	*V*	− 1	1	350	3.07	4455.86....	*Ca-Mn*	5^2	5	600	4.66
4420.54....	*Sc^+-Sm^+*	0^2	3d	400	3.41	4456.50....	*Fe*	1	2	400	5.80
4421.25....	*Co-Sm^+*	0^2	0	350	5.71		*Ca-Ti^+*	2	2	400	4.66
4421.61....	*V*	0	1	350	3.07	4457.04....	*Mn*	0	1	350	5.83
4421.91....	*Ti^+*	1	3	500	4.84	4457.50....	*Zr^+-Ti*	2	4	500	3.95
4422.61....	*V^+-Fe*	3	5	600	2.89		*Mn*	2	2	500	5.83
4423.21....	*Fe-Ti^+*	2^2	2	350	5.77	4458.08....	*Fe-Mn*	4^2	3	400	6.64
4423.82....	*Fe*	2	2	350	6.43	4458.60....	*Cr-Sm^+*	0	1	400	5.77
4424.35....	*Cr-Sm^+*	1^2	4	400	5.79	4459.11....	*Fe-Ni*	5^2	6d	600	4.93
4425.35....	*Ca*	4	6	800	4.66	4459.81....	*V-Cr*	1	1	400	3.05
4426.12....	*Ti-V*	0	2	400	4.66	4460.37....	*Ce^+-V*	1^3	8	800	2.77
4427.05....	*Ti*	2	2	400	4.28	4461.12....	*Zr^+-Fe*	2^2	3	500	3.77
4427.34....	*Fe*	5	15	1200	2.84	4461.60....	*Fe*	4	12	1200	2.85
4427.75....	*Ti^+-Cr*	0^3	2	400	4.02	4461.98....	*Mn-Fe*	3	2	400	5.83
4428.39....	*V-Cr*	1^2	1	400	3.05	4462.52....	*Ni*	1	2	400	6.22
4429.17....	*Ce^+-Pr^+*	− 1	3	500	3.39	4463.02....	*Nd^+-Fe*	0^2	3	500	3.32
4429.99....	*La^+-Cr*	0^2	7	800	3.02	4463.51....	*Ti-Ni*	1^2	2	400	4.64
4430.57....	*Fe*	3	4	500	5.00	4464.56....	*Ti^+-Mn*	4^2	12d	1200	3.92
4431.29....	*Sc^+-Ti*	1^3	2	400	3.39	4465.30....	*Cr*	0	1	350	5.76
4432.21....	*Ti^+-Cr*	0^2	2	400	4.02	4465.75....	*Ti*	1	1	350	4.50
4432.70....	*Fe-*	2^2	1	400	6.34	4466.59....	*Fe*	5	8	1000	5.58
4433.21....	*Fe*	3	3	400	6.42	4466.93....	*Fe*	1	1	400	6.67
4433.88....	*Ti-Fe*	2^2	3	400	4.21	4467.30....	*Sm^+*	− 1	3	400	3.42
4434.32....	*Sm^+*	− 1	1	350	3.16	4468.48....	*Ti^+*	5	40	2500	3.89
4434.98....	*Ca-Fe*	7^2	10	1200	4.66	4469.37....	*Fe*	4	6	500	6.40
4435.60....	*Ca*	4	8	1000	4.66	4469.60....	*Co-V*	1^2	1	350	5.71
4436.20....	*Mn-V*	3^2	2d	400	5.69	4470.11....	*Mn*	1	0	350	5.69
4436.93....	*Fe-Ni*	2	2	400	5.82	4470.47....	*Ni*	2	2	400	6.15
4437.70....	*He*	.....	2d	1000	23.91	4471.54....	*He*	.....	90	7500	23.63
	V	1^2			3.07	4472.88....	*Fe^+-Fe*	2^3	7d	600	5.59
						4474.05....	*V*	− 1	0	350	4.71

TABLE 1—*Continued*

Chromosphere	Element	Sun	Flash	Height in Km	High E.P.	Chromosphere	Element	Sun	Flash	Height in Km	High E.P.
4474.74....	*V*	− 1	0	350	4.64	4519.58....	*Sm*$^+$	− 1	2	400	3.27
4474.90....	*Ti*	0	1	350	4.19	4520.22....	*Fe*$^+$	3	20	1000	5.52
4476.04....	*Fe*	7^2	9	800	5.59	4521.18....	*Cr*	0	1	400	6.81
4477.26....	*Cr-V*	0^2	1d	350	5.45	4522.34....	*La*$^+$	− 1	1	400	2.73
4477.97....	*Fe*	0	0	350	4.94	4522.67....	*Fe*$^+$*-Ti*	5^2	25	1500	5.56
4478.73....	*Gd*$^+$*-Sm*$^+$	0^2	1	350	3.35	4523.07....	*Ce*$^+$*-Sm*$^+$	0	2	500	2.77
4479.56....	*Fe-Mn*	2^3	2	400	6.43	4523.89....	*Sm*$^+$	− 1	2	500	3.16
4480.08....	*Fe-*	2^2	1	350	5.79	4524.65....	*Ti*$^+$	0	2	500	3.95
4480.54....	*Ni-Ti*	0	0	350	6.64	4525.15....	*Fe-Ba*$^+$	6^2	5	600	6.31
4481.23....	*Mg*$^+$*-Ti*	2^2	6d	600	11.58	4526.10....	*La*$^+$*-Cr*	0	1	400	3.50
4482.23....	*Fe*	8^2	10	1000	2.86	4526.46....	*Cr-Fe*	4^3	3	500	5.26
4482.71....	*Ti-Fe*	1	2	400	4.21	4526.94....	*Ca*	3	3	500	5.42
4483.87....	*Ce*$^+$*-Fe*	1^3	2	400	3.14	4527.33....	*Ti-Cr*	3	4	500	3.54
4484.25....	*Fe*	4	3	600	6.34	4528.60....	*Fe*	8	8d	800	4.89
4485.66....	*Fe*	3	4	600	6.42	4529.55....	*Ti*$^+$*-Fe*	2^2	6d	800	4.29
4486.92....	*Ce*$^+$	0	5	600	3.04	4530.92....	*Cr-Co*	4^3	5	600	5.26
4488.06....	*Fe-Cr*	2^2	1	400	6.34	4531.17....	*Fe*	5	5	600	4.20
4488.36....	*Ti*$^+$	1	5	600	5.86	4531.63....	*Fe*	2	2	400	5.92
4489.02....	*Ti-Fe*	2^2	3	400	4.48	4533.17....	*Ti-Fe*	5^2	5d	600	3.57
4489.19....	*Fe*$^+$	2	10	800	5.57	4534.03....	*Ti*$^+$*-Fe*$^+$	7^2	40	2500	3.95
4489.73....	*Fe*	4	4	600	2.87	4534.73....	*Ti*	4	3	500	3.55
4490.10....	*Mn-Fe*	3	4	600	5.69	4535.58....	*Ti-Cr*	4^2	6	800	3.54
4490.67....	*Fe-Ni*	3^2	2d	400	6.67	4535.99....	*Ti*	4^2	5	800	3.54
4491.46....	*Fe*$^+$	2	12	1000	5.59	4536.55....	*Fe-Cr*	− 1	0	350	6.35
4492.50....	*Cr-Fe*	1^2	1d	350	6.11	4537.18....	*Ti*	− 1	1	350	.....
4493.51....	*Ti*$^+$*-Fe*$^+$	1	3	400	3.82	4537.83....	*Fe-Sm*$^+$	1^2	2d	400	5.97
4493.98....	*Fe-Ce*$^+$	2^2	1	400	6.71	4539.01....	*Fe-Ti*	2^5	1d	350	4.99
4494.55....	*Fe*	6	6	600	4.93	4539.80....	*Cr-Ce*$^+$	0	4	600	5.25
4495.08....	*Ti-Cr*	0^2	1	350	5.70	4540.61....	*Cr*	4^2	3d	500	5.25
4495.49....	*Zr*$^+$*-Fe*	1^2	1	350	3.95	4541.50....	*Fe*$^+$*-Cr*	3^2	7d	800	5.56
4496.16....	*Ti*	1	2	400	4.49	4542.26....	*Fe-Zr*	2^2	2	400	6.34
4496.88....	*Cr*	3	5	600	3.68	4542.71....	*Fe-Cr*	1^2	2	400	6.39
4497.00....	*Zr*$^+$	0	5	600	3.45	4543.80....	*Co*	0	1	400	5.42
4497.95....	*Ce*$^+$-	− 2	1	350	3.22	4544.03....	*Ti*$^+$	1	4	800	3.95
4498.85....	*Mn*	1	2	400	5.67	4544.68....	*Ti-Cr*	4^2	5	500	3.53
4499.15....	.....	1	1	350	.....	4545.12....	*Ti*$^+$	1	5	500	3.84
4499.47....	*Sm*$^+$	− 2	0	350	2.99	4545.96....	*Cr*	3	5	500	3.65
4500.27....	*Ti*$^+$*-Cr*	0	1	350	3.82	4547.04....	*Fe-Ni*	4^3	4d	500	4.26
4501.28....	*Ti*$^+$	5	35	2500	3.85	4547.86....	*Fe*	3	4	500	6.24
4501.82....	*Cr*	0	1	350	5.64	4548.84....	*Ti*	2	2	500	3.54
4502.29....	*Mn*	2	1	350	5.65	4549.63....	*Ti*$^+$*-Fe*$^+$	8^2	50	2500	4.29
4503.82....	*Ti-*	0^2	0	350	4.87	4550.70....	*Fe*	2	1	350	.....
4504.84....	*Fe*	1	1	350	5.99	4551.17....	*Ni*	0	1	350	6.86
4505.40....	*Ti-*	1^3	1d	350	4.83	4552.46....	*Ti-*	2	6d	600	3.54
4506.35....	*Ni*	− 1	0	350	6.27	4553.00....	*V-Zr*	− 1	0	350	5.06
4506.76....	*Ti*$^+$-	1^3	2d	350	3.86	4554.11....	*Ba*$^+$	8	50	2500	2.71
4507.30....	*Cr*$^+$	− 1	1	350	5.83	4554.95....	*Cr*$^+$	2	1d	400	6.76
4508.32....	*Fe*$^+$	4	18	1200	5.58	4555.52....	*Ti*	3	2	400	3.55
4509.30....	*Fe-V*	0	1	350	5.77	4555.89....	*Fe*$^+$	3	25	1200	5.52
4509.87....	*Fe*	1^2	1	400	.....	4557.30....	*Sc*	0	0d	350	.....
4511.10....	*Ti-Fe*	1^2	1d	400	6.66	4558.57....	*Cr*$^+$*-Fe*$^+$	3^2	18d	1800	6.76
4511.84....	*Sm*$^+$	1	3	500	2.92	4560.09....	*Fe*	2	2	400	6.29
4512.74....	*Ti*	3	3	500	3.57	4560.33....	*Ce*$^+$	0^2	3	500	3.14
4513.05....	*Ni*	0	1	400	6.42	4560.85....	*V-Ce*$^+$	0^3	1	400	4.65
4514.40....	*Fe-V*	3^3	3d	500	5.77	4561.42....	.....	1	0	350	.....
4515.32....	*Fe*$^+$	3	18	1200	5.57	4562.30....	*Ce*$^+$	0	5	600	2.71
4516.29....	*Fe*	0	2	400	6.32	4563.76....	*Ti*$^+$	4	30	2500	3.92
4517.56....	*Fe*	3	2	400	5.79	4564.62....	*V*$^+$*-Fe*	1^2	1d	350	4.96
4518.04....	*Ti*	3	3	500	3.55	4565.50....	*Cr*	3	4	600	3.68
4518.31....	*Ti*$^+$	1	5	1000	3.81	4565.72....	*Co-Fe*	2	2	400	5.71
4518.69....	*Ti-*	1^2	0	350	4.15	4566.67....	*Fe*	2^2	0	350	5.25

TABLE 1—*Continued*

Chromo-sphere	Element	Sun	Flash	Height in Km	High E.P.	Chromo-sphere	Element	Sun	Flash	Height in Km	High E.P.
4568.35....	*Ti*$^+$	0	3	400	3.92	4617.30....	*Ti*	3	3	500	4.41
4568.85....	*Fe*	2^2	2	400	5.95	4618.81....	*Cr*$^+$-*Fe*	4	6	1000	6.73
4569.39....	*Cr*	0^2	1	400	5.81	4619.30....	*Fe*	3	2	400	6.26
4569.80....	*Cr-Co*	1^2	0	400	5.81	4619.70....	*Cr-V*	2^2	1	350	5.65
4571.08....	*Mg*	5	8	800	2.70	4620.55....	*Fe*$^+$	2	8	800	5.49
4572.00....	*Ti*$^+$	6	40	2500	4.26	4621.50....	*Cr*$^+$	− 1	1	350	6.37
4574.24....	*Fe*	1	1	350	5.90	4621.91....	*Cr*	2^2	2d	400	5.20
4574.74....	*Fe-La*$^+$	2^2	3	400	4.97	4622.40....	*Cr*	1	1	400	6.21
4576.32....	*Fe*$^+$	2	10	800	5.53	4623.10....	*Ti*	2	4	500	4.40
4577.20....	*V*	0	2	400	2.70	4624.40....	*V*	− 1	0	350	3.72
4577.68....	*Sm*$^+$-*Fe*$^+$	0^2	2	400	2.94	4625.03....	*Fe*	5	4	500	5.90
4578.54....	*Ca*	3	2	400	5.21	4626.21....	*Cr*	5	6d	800	3.63
4578.80....	*V*	− 1	1	350	4.63	4626.60....	*Mn*	0	1	350	.....
4579.24....	*Fe-*	1^2	1	350	5.52	4627.44....	*V*$^+$	1^2	1d	350	6.45
4579.99....	*Cr-La*$^+$	3	5	400	3.63	4628.16....	*Ce*$^+$	1^2	5	500	2.71
4580.42....	*V-Ti*$^+$	1	3	400	2.71	4629.42....	*Fe*$^+$-*Ti*	6	30	1200	5.46
4581.42....	*Ca-Fe*	8^2	6d	600	5.21	4630.14....	*Fe*	4	2	350	4.93
4582.32....	*Gd*$^+$	1^2	1	400	3.94	4632.18....	*Cr*	0	0	350	5.76
4582.86....	*Fe*$^+$	1	5	600	5.52	4632.85....	*Fe-*	5^2	5	500	4.26
4583.40....	*Ti*$^+$	0	1	400	3.85	4633.26....	*Cr*	0	0	350	5.78
4583.86....	*Fe*$^+$	4	30	1800	5.49	4634.04....	*Cr*$^+$	2	8	1000	6.72
4584.76....	*Fe-*	3^2	2d	400	6.28	4635.35....	*Fe*$^+$	0	1	350	8.59
4585.91....	*Ca*	4	4	500	5.21	4635.83....	*Fe*	2	2	500	5.49
4586.31....	*V-Cr*	2^2	3	500	2.73	4636.31....	*Ti*$^+$	0	2	500	3.82
4587.11....	*Fe*	2	1	400	6.25	4637.14....	*Cr*	0	0	350	5.19
4588.20....	*Cr*$^+$	3	10	1200	6.74	4637.49....	*Fe*	5	4	500	5.93
4589.93....	*Ti*$^+$	3	12	1200	3.92	4638.02....	*Fe*	4	4	500	6.25
4591.22....	*V-Fe*$^+$	− 1	0	350	5.05	4639.51....	*Ti-Cr*	5^3	3d	400	4.39
4591.39....	*Cr*	2	2	500	3.65	4640.16....	*Ti-V*	2^2	2d	400	4.39
4591.96....	*Cr*$^+$-	2^2	2d	500	6.74	4641.14....	*Fe*	1^2	1d	350	5.48
4592.50....	*Ni*	2	3	500	6.22	4642.31....	*Sm*$^+$	− 1	3d	400	3.04
4592.70....	*Fe*	4	4	500	4.24	4643.41....	*Fe*	4	3	400	6.30
4593.53....	*Fe-Sm*$^+$	1	0	350	6.61	4644.19....	*Fe*$^+$-	1^3	1d	350	5.34
4593.99....	*V-Ce*$^+$	4^3	5d	500	2.75	4645.31....	*Ti-La*$^+$	1^3	1	350	4.38
4595.28....	*Fe-Sm*$^+$	2	2	400	5.97	4646.16....	*Cr*	5	10	1000	3.68
4595.87....	*Fe-Fe*$^+$	3^3	2d	400	6.27	4646.72....	*Cr-*	2^2	1	350	5.74
4596.99....	*Co-Nd*$^+$	1^2	1d	400	6.30	4647.45....	*Fe*	4	5	500	5.59
4597.75....	*Gd*$^+$-	2^2	2	400	3.28	4648.05....	*Cr*	2^2	0	350	5.19
4598.14....	*Fe*	3	2	400	5.95	4648.86....	*Ni-Cr*	5^3	5d	500	6.06
4598.75....	*Fe*	0	0d	350	6.32	4649.45....	*Cr*	0	1	350	5.19
4599.67....	*Fe-Ti*	2^2	1d	350	.....	4650.03....	*Ti*	0	1	350	4.39
4600.17....	*V*$^+$-*Cr*	1^2	2	600	4.94	4651.29....	*Cr*	4	5	800	3.63
4600.74....	*Cr*	3	5	800	3.68	4652.16....	*Cr*	5	7	800	3.65
4601.16....	*Cr-Gd*$^+$	1^2	1	400	5.79	4653.42....	*Fe-Ti*	0^2	1	400	3.64
4602.03....	*Fe*	3	3	400	4.28	4654.11....	*Ce*$^+$	0	0	350	3.17
4602.95....	*Fe*	6	5	600	4.16	4654.64....	*Fe*	9^2	7d	600	5.85
4604.53....	*Cr*	2	1	400	5.99	4655.73....	*La*$^+$-*Ni*	1^3	2d	350	4.59
4604.96....	*Ni*	3	3	500	6.15	4656.44....	*Ti*	3	2	350	2.65
4605.66....	.....	2	0	350	.....	4657.10....	*Ti*$^+$-*Fe*$^+$	3^2	6d	800	3.89
4606.29....	*Ni-Cr*	3^2	3d	500	6.26	4660.19....	.....	1^4	0d	350	.....
4607.31....	*Sr*	1	3	500	2.68	4661.97....	*Fe-*	2	1	350	5.62
4607.67....	*Fe*	4	2	500	5.93	4662.77....	*La*$^+$-*Ti*$^+$	2^3	2d	350	2.65
4609.26....	*Ti*$^+$	0	1	350	3.85	4663.35....	*Cr-Co*	2^2	3	400	5.73
4609.92....	*Cr*	0	0	350	7.11	4663.82....	*Fe*$^+$-*Cr*	2^2	3	400	5.52
4611.29....	*Fe*	5	5d	600	6.31	4664.83....	*Cr*	3	1	350	5.76
4613.24....	*Fe*	3	2	400	5.95	4666.09....	*Cr*	2^2	1d	350	5.60
4613.42....	*Cr-La*$^+$	3	6	600	3.63	4666.74....	*Fe*$^+$-*Cr*	4^4	10d	800	5.46
4613.93....	*Zr*$^+$	1	2	400	3.64	4667.61....	*Fe-Ti*	8^3	8	500	6.23
4615.57....	*Sm*$^+$	1	2d	400	2.86	4668.13....	*Fe*	6^2	4d	400	5.90
4616.09....	*Cr*	4	6	800	3.65	4669.25....	*Fe-Cr*	4^2	3	400	6.28
4616.63....	*Cr*$^+$	1	2	500	6.73	4669.58....	*Sm*$^+$-*Ce*$^+$	0^3	2	400	2.75

TABLE 1—*Continued*

Chromosphere	Element	Sun	Flash	Height in Km	High E.P.	Chromosphere	Element	Sun	Flash	Height in Km	High E.P.
4670.38....	Sc^+	2	9	800	3.99	4718.43....	*Cr*	3	3	400	5.80
4671.40....	Cr^+	1	0	350	8.28	4719.52....	Ti^+	0	2d	350	3.85
4672.34....	.....	3	1	350	.....	4721.02....	*Fe*	2	2	350	5.59
4673.15....	*Fe*	3	2	400	6.28	4722.16....	*Zn*	3	5	500	6.63
4674.13....	.....	2^2	1	350	.....	4723.30....	*Ti-*	0^2	2d	350	3.67
4674.65....	*Fe-*Sm^+	0	2	400	4.19	4724.36....	*Cr-*La^+	0	3	400	5.69
4676.86....	Sm^+-*Ti*	− 1	1	350	2.68	4726.13....	*Fe*	0	0	350	5.60
4677.42....	*Co*	− 1	0	300	3.22	4727.44....	*Fe-Mn*	5^2	6d	600	6.28
4678.82....	*Fe*	6	3	400	6.22	4728.15....	.....	0	0	350	.....
4679.20....	*Fe*	2	1	400	5.99	4728.57....	*Fe*	4	3	400	6.25
4680.14....	*Zn*	1	3	500	6.63	4729.42....	*Fe-Cr*	2^2	1d	350	5.99
4680.72....	*Cr-*Nd^+	1^2	2	400	5.72	4730.04....	*Mg*	2	2	400	6.94
4681.46....	*Fe*	1	0	350	.....	4730.87....	*Cr-*	2^2	2	400	5.67
4681.95....	*Ti*	3	4	500	2.68	4731.48....	Fe^+	4	8	800	5.49
4682.41....	V^+-*Co*	1	3	600	3.04	4731.76....	*Ni*	1	1	350	6.42
4683.53....	*Fe*	3	2	600	5.45	4732.46....	*Ni*	1	1	350	6.70
4684.25 ...	*V*	0^2	1	350	4.53	4733.61....	*Fe*	4	4	500	4.09
4684.60....	Ce^+-*Cr*	0	1	350	3.53	4734.08....	*Fe-Sc*	1	1	350	6.88
4685.22....	*Ca-*Zr^+	3^2	2	400	5.55	4735.86....	*Fe*	3	2	350	6.66
4685.83....	He^+	.....	2N	3500	50.80	4736.79....	*Fe*	6	6	500	5.80
4686.17....	*Ni*	3	2	350	6.22	4737.33....	*Cr*	2	2	350	5.68
4687.33....	*Fe-*Sa^+	3^2	2d	350	3.59	4737.64....	*Fe-Sc*	1	1	350	5.86
4687.77....	*Zr*	0	0	300	3.36	4739.12....	*Mn*	3	3	400	5.53
4688.55....	*Zr-Ti*	1^2	1	350	2.79	4739.52....	*Zr-*Ce^+	− 1	1	350	3.25
4689.33....	*Cr*	2	2	350	5.74	4740.19....	*Ni-*La^+	− 1	4	400	6.47
4690.14....	*Fe*	4	2	350	6.30	4740.37....	*Fe-*	2^2	2	400	5.61
4690.80....	*Ti*	− 1	1	350	3.69	4741.00....	*Fe-Sc*	2^2	1	350	5.92
4691.51....	*Fe-Ti*	7^3	5d	500	5.61	4741.56....	*Fe*	3	2	350	5.42
4692.58....	La^+-	1^3	2	350	4.38	4742.75....	*Ti*	1	1	350	4.83
4693.80....	*Ti-Cr*	2^2	1	350	2.65	4743.05....	*Cr-*La^+	− 2	3	350	6.79
4694.81....	*Fe*	1	0	350	.....	4744.38....	*Fe*	3	2	350	.....
4695.27....	*Cr-*	1^2	1	350	5.60	4745.75....	*Fe*	4	4	400	6.24
4697.23....	*Cr*	2^2	2d	350	5.32	4748.18....	Sc^+	4	4	400	7.46
4698.66....	*Cr-Ti*$^+$	3^3	6d	500	5.32	4748.76....	La^+	− 2	1	350	3.52
4699.35....	.....	3	2	350	.....	4749.78....	*Fe-Co*	2^2	3d	350	7.14
4700.16....	*Fe*	4	2	350	6.30	4751.11....	*Cr-Fe*	1	1	350	6.77
4701.09....	*Fe*	1	2	350	6.30	4752.02....	*Ni-Cr*	2	1	350	6.26
4701.52....	*Ni*	1	2	350	6.70	4752.42....	*Ni*	3	3	400	6.24
4701.93....	*Fe*	0	0	350	6.04	4753.99....	*Mn*	7	6	800	4.87
4702.99....	*Mg*	10	8	800	6.95	4754.74....	*Ni-Cr*	1	1	350	6.22
4703.76....	*Ni*	3	3	400	6.27	4756.07....	*Cr*	2	2	350	5.69
4704.36....	Sm^+	1^3	1d	350	2.62	4756.49....	*Ni*	3	3	500	6.06
4704.93....	*Fe*	3	3	400	6.29	4757.55....	*Fe*	2	2	350	5.85
4705.45....	*Fe*	1	0	350	6.15	4758.11....	*Ti*	1	2	350	4.83
4706.52....	Nd^+-*V*	0	2	400	2.62	4759.32....	*Ti*	2	3	350	4.84
4707.31....	*Fe*	7^2	5d	500	5.85	4760.08....	*Fe*	− 1	1	350	5.62
4708.00....	*Cr*	2	1	350	5.78	4761.56....	*Mn*	3	4	400	5.53
4708.63....	Ti^+	2	5	600	3.85	4762.49....	*Mn-Ni*	6^2	5d	500	5.47
4708.93....	*Fe-Ti*	1	1	350	6.24	4762.86....	Ti^+	0	3	400	3.67
4709.15....	*Fe*	3	1	350	6.26	4763.98....	Ti^+-*Ni*	4	8	800	3.81
4709.71....	*Mn*	2	2	400	5.50	4764.52....	Ti^+	0	4	400	3.82
4710.24....	*Fe*	3	4	500	5.62	4765.46....	*Fe*	2	3	400	4.19
4711.50....	*Fe*	0	1	350	.....	4765.89....	*Mn*	3	3	400	5.52
4712.09....	*Fe-Ni*	0	0	350	5.62	4766.38....	*Mn*	4	4	500	5.50
4713.15....	*He*	.....	15N	5000	23.49	4768.32....	*Fe-*	5^2	4d	400	5.52
4713.99....	*Fe-*Ce^+	1^3	1	350	7.16	4769.79....	*Ti-Cr*	− 1	1	350	4.83
4714.40....	*Ni*	6	8	600	5.98	4771.13....	*Ti-Co*	− 1	1	350	3.41
4714.96....	Ce^+-Cr^+	− 2	2	400	3.20	4771.60....	*Fe-Cr*	5^2	3d	400	4.77
4715.80....	*Ni*	4	5	500	6.15	4772.79....	*Fe*	4	2	350	4.14
4716.82....	*Fe*	− 1	0	350	5.85	4773.39....	*Ni*	− 1	0	350	6.28
4717.56....	La^+-*Cr*	1^3	1d	350	4.67	4773.99....	Ce^+	− 2	0	350	3.03

TABLE 1—*Continued*

Chromosphere	Element	Sun	Flash	Height in Km	High E.P.	Chromosphere	Element	Sun	Flash	Height in Km	High E.P.
4776.11....	*Fe*	0	0	350	5.87	4843.21....	*Fe-Ni*	3	2	350	5.93
4776.40....	*V-Co*	0	3	400	4.63	4844.09....	*Fe*	1	1	350	6.08
4778.26....	*Ti*	− 1	1	350	4.81	4845.66....	*Fe*	1	0	300	5.82
4779.41....	*Fe*	1	1	350	5.98	4848.30....	*Cr*$^+$	2	7	800	6.39
4779.97....	*Ti*$^+$*-Co*	2	12	1000	4.62	4848.87....	*Fe*	1	1	300	4.81
4781.48....	*Co-*	− 2	1d	350	4.46	4849.15....	*Ti*$^+$	0	4	400	3.67
4783.47....	*Mn*	6	10	800	4.87	4851.49....	*V*	1	2	400	2.54
4783.97....	.....	0	1	350	.....	4852.59....	*Ni*	2	1	300	6.07
4786.00....	*Fe*	0	1	350	6.70	4854.82....	*Y*$^+$	1	8	600	3.53
4786.50....	*Y*$^+$*-Ni*	3	12	600	3.61	4855.37....	*Ni*	3	2	400	6.07
4786.86....	*Fe*	2	1	400	5.58	4855.70....	*Fe*	2	2	400	5.90
4787.90....	*Fe*	1	1d	350	5.56	4856.00....	*Ti*	1	0	300	4.79
4788.74....	*Fe*	3	2	350	5.80	4857.33....	*Ni*	1	2d	400	6.26
4789.31....	*Cr*	2	5	500	5.11	4859.03....	*Fe-Nd*$^+$	1[2]	1	350	6.71
4789.63....	*Fe*	3	4	500	6.11	4859.77....	*Fe*	4	4	600	5.40
4791.15....	*Fe-*	2[2]	2d	400	5.84	4861.50....	*Hβ*	30	160	9000	12.69
4792.49....	*Ti-Cr*	2	4	500	4.90	4863.65....	*Fe*	2	1	350	5.95
4792.94....	*Co*	1	3	400	5.81	4864.32....	*Cr*$^+$	1	4	500	6.38
4794.38....	*Fe*	− 1	0	300	4.99	4864.71....	*V*	0	1	300	2.55
4796.24....	*Ti-Cr*	− 1	0	300	4.90	4865.52....	*Ti*$^+$	1	2	400	3.65
4798.29....	*Fe*	1	1	350	6.74	4866.35....	*Ni*	2	2	400	6.06
4798.62....	*Ti*$^+$*-Fe*	2[2]	4d	500	3.65	4868.02....	*Co-Ti*	2[2]	3d	400	5.64
4799.46....	*Fe*	1	1	350	6.20	4870.19....	*Ti*	1	0	300	4.77
4799.80....	*Ti-V*	1	1	350	4.83	4870.80....	*Cr-Ni*	3	0	350	5.60
4800.64....	*Fe*	2	2	350	6.70	4871.36....	*Fe*	5	7	800	5.39
4801.04....	*Cr-Fe*	1	1	350	5.68	4872.17....	*Fe*	4	7	800	5.40
4802.86....	*Fe*	2	2d	350	6.20	4873.45....	*Ni*	2	2	400	6.22
4804.05....	*La*$^+$	− 2	1	350	2.80	4873.98....	*Ti*$^+$	0	5	600	5.61
4805.13....	*Ti*$^+$	3	15	1000	4.62	4875.51....	*V*	1	1	350	2.57
4807.06....	*Ni*	2	2	400	6.23	4875.93....	*Fe*	2	1	350	5.85
4807.75....	*Fe*	1	0	300	5.92	4876.41....	*Cr*$^+$	1	6	600	6.37
4808.50....	*Fe-Ti*	1[3]	1	300	5.80	4878.18....	*Fe-Ca*	7[2]	7d	600	5.40
4809.06....	*Fe-Ni*	0[2]	0	300	6.24	4881.57....	*V*	1	1	350	2.60
4810.45....	*Zn*	3	5	400	6.63	4881.75....	*Fe*	2	3	400	5.82
4811.24....	*V*$^+$*-Ti*	0[2]	0d	300	6.31	4882.18....	*Fe*	3	2	400	5.93
4812.18....	*Cr*$^+$*-Ni*	1[2]	1	300	6.41	4883.75....	*Y*$^+$	2	15	800	3.61
4813.10....	*Fe*	0	0	300	5.82	4884.66....	*Cr*$^+$	0	1	300	6.37
4813.48....	*Co-*	1	4	400	5.77	4885.07....	*Ti*	2	2	350	4.41
4814.56....	*Ni*	− 1	0	300	6.15	4885.43....	*Fe*	3	2	350	6.39
4815.74....	*Zr-Sm*$^+$	− 1[2]	2d	300	3.16	4886.37....	*Fe*	3	1	350	6.66
4817.75....	*Fe-Ni*	2	2	400	4.77	4887.11....	*Fe-Cr*	4[2]	4d	400	6.70
4820.39....	*Ti-*	1	4	400	4.06	4888.61....	*Fe*	2	1	350	6.61
4821.10....	*Ni-*	0	0	300	6.70	4889.10....	*Fe*	4[2]	4	400	4.71
4823.46....	*Mn*	5	10	1000	4.87	4890.78....	*Fe*	8	10	800	5.39
4824.09....	*Cr*$^+$*-Fe*	3	12	1000	6.41	4891.54....	*Fe*	7	12	800	5.36
4825.47....	*Nd*$^+$*-Ti*	0[3]	8	600	2.74	4892.92....	*Fe*	2	1	350	6.72
4827.50....	*V-Ti*	0[2]	1d	300	2.60	4893.85....	*Fe*$^+$*-Ce*$^+$	0[3]	2d	350	5.34
4829.00....	*Ni*	3	5	400	6.08	4894.61....	.....	− 1	0	300	.....
4829.40....	*Cr*	2	2	350	5.09	4896.50....	*Fe*	1	1	300	6.39
4831.13....	*Ni*	3	4	400	6.15	4899.89....	*Ti-La*$^+$	2	2	400	4.39
4831.70....	*V*	− 1	0	300	2.57	4900.14....	*Y*$^+$	2	20	1000	3.55
4832.40....	*V*	− 1	0	300	2.55	4901.00....	*Ni-Ti*	0	0	350	5.98
4832.76....	*Fe-Ni*	3	3	400	6.18	4902.28....	.....	0[2]	1d	350	.....
4834.56....	*Fe*	1	1	300	4.97	4903.29....	*Fe*	4	8	800	5.39
4835.84....	*Fe*	2	3	400	6.64	4904.38....	*Ni-V*	3	4	400	6.04
4836.28....	*Cr*$^+$	0	2	400	6.39	4905.15....	*Fe*	0	0	300	6.43
4838.54....	*Fe-Ni*	3[2]	3	400	5.95	4907.72....	*Fe*	2	1d	300	5.93
4839.55....	*Fe*	3	2	350	5.80	4908.02....	*Fe*	0	0	300	.....
4840.24....	*Fe-Co*	5[2]	5	400	6.69	4909.29....	*Fe*	2	1d	300	6.43
4840.83....	*Ti*	3	2	350	3.45	4910.00....	*Fe*	3	2	400	5.90
4842.83....	*Fe*	1	1	350	6.63	4910.32....	*Fe*	2	2	400	6.69

TABLE 1—*Continued*

Chromosphere	Element	Sun	Flash	Height in Km	High E.P.	Chromosphere	Element	Sun	Flash	Height in Km	High E.P.
4910.61	*Fe*	2	1	350	6.71	4978.20	*Ti*	− 1	1	300	4.44
4911.17	*Ti*$^+$	1	2	400	5.62	4978.58	*Fe*	3	3	400	6.45
4911.97	*Ni-Fe*	2[2]	1d	350	6.26	4979.62	*Fe*	− 1	0	300	6.10
4913.58	*Ti*	2	2	350	4.38	4980.17	*Ni*	4	3	400	6.07
4913.99	*Ni*	2	2	350	6.24	4981.72	*Ti*	4	4	500	3.32
4917.24	*Fe*	2	2	350	6.68	4982.51	*Fe*	4	3	500	6.56
4918.00	*Fe*	1	0	300	6.72	4983.33	*Fe*	3	3	500	6.61
4918.37	*Ni*	2	2	350	6.33	4983.97	*Fe-Ni*	5[2]	4	500	6.56
4919.02	*Fe*	6	8	800	5.36	4985.29	*Fe*	3	3	500	6.39
4919.84	*Ti*	− 1	1	300	4.66	4985.59	*Fe*	3	3	500	5.33
4920.50	*Fe*	10	12	800	5.33	4986.28	*Fe*	1	0	300	6.67
4920.92	*La*$^+$	0	3	500	2.63	4986.80	*La*$^+$	.....	1d	350	2.65
4921.80	*La*$^+$-*Ti*	1	4	500	2.75	4988.99	*Fe*	2	2	350	6.61
4922.01	*He*	.....	6	3000	23.63	4991.11	*Ti-Fe*	5[2]	6d	800	3.31
4923.09	*Fe*	0	0	300	.....	4993.47	*Fe*$^+$-	1[2]	4d	600	5.27
4923.96	*Fe*$^+$	5	35	2000	5.39	4994.08	*Fe*	3	4	600	3.38
4924.83	*Fe*	3	1	350	4.77	4996.82	*Ni*	1	1	350	6.09
4925.32	*Fe*	− 1	0	300	6.59	4997.11	*Ti*	0	1	350	2.47
4925.60	*Ni*	1	1	350	6.15	4998.22	*Ni*	1	1	350	6.06
4927.35	*Fe*	1	0	300	6.06	4999.49	*Ti-La*$^+$	3	3d	600	3.31
4927.87	*Fe*	2	2	400	.....	5000.32	*Ni*	2	2	350	6.09
4928.37	*Ti*	0	1	350	4.65	5001.04	*Ti*	0	2	350	4.46
4930.37	*Fe*	2	2	400	6.45	5001.85	*Fe*	4	3	400	6.33
4930.81	*Ni*	− 1	0	300	6.33	5002.82	*Fe*	2	1d	300	5.85
4932.02	*V*	0	1d	300	3.72	5003.72	*Ni*	0	1	350	4.14
4933.31	*Fe*	2	2	350	6.71	5004.05	*Fe*	0	1	350	6.66
4934.08	*Ba*$^+$	7	30	1800	2.50	5005.21	*Ti*$^+$	0	0	350	4.02
4935.78	*Ni*	2	2	350	6.42	5005.68	*Fe*	4	4	600	6.33
4936.25	*Cr*	1	2	350	5.60	5006.13	*Fe*	5	5	800	5.29
4937.40	*Ni*	3	2	350	6.09	5007.24	*Ti-Fe*	5[2]	4d	600	3.28
4938.12	*Fe*	2	2	350	6.43	5009.72	*Ti*	− 1	0	400	2.48
4938.84	*Fe*	4	4	600	5.36	5010.25	*Ti*$^+$	− 1	2	400	5.54
4939.24	*Fe*	2	2	400	6.70	5010.94	*Ni*	0	0	350	6.08
4939.65	*Fe*	3	4	500	3.35	5012.08	*Fe*	5[2]	5d	600	3.32
4942.49	*Cr*	2	1	350	3.43	5012.49	*Ni*	1	1	350	6.15
4945.54	*Fe-Ni*	2[2]	2d	350	6.69	5013.14	*Ti-Cr*	3[2]	2	400	4.47
4946.00	*Ni*	0	0	300	6.28	5013.67	*Ti*$^+$	0	2	400	4.04
4946.41	*Fe*	3	3	400	5.85	5014.25	*Ti-Fe*	5[2]	2	400	3.27
4950.09	*Fe*	2	2	350	5.90	5014.98	*Fe*	3	2	400	6.39
4952.34	*Ni*	1	0	350	6.08	5015.68	*He*	.....	8	3500	22.99
4952.64	*Fe*	2	1	350	6.58	5016.15	*Ti*	2	1	350	3.31
4953.20	*Ni*	2	2	350	6.22	5017.53	*Ni*	3	2	350	5.98
4954.60	*Fe*	1	1	350	.....	5018.44	*Fe*$^+$	4	40	2000	5.34
4954.86	*Cr*	2	2	350	5.60	5019.76	*Fe*	− 1	0	300	6.43
4957.30	*Fe*	5	6	800	5.33	5020.02	*Ti*	2	1	350	3.29
4957.58	*Fe*	8	12	1000	5.29	5021.67	*Fe-*	0[2]	0	300	6.66
4959.07	*Nd*$^+$	.....	3	400	2.55	5022.26	*Fe*	3	3	400	6.42
4961.91	*Fe-Sm*$^+$	0	0	300	6.11	5022.87	*Ti*	2	1	350	3.28
4962.57	*Fe*	2	1	300	6.65	5023.19	*Fe*	0	1	300	6.72
4964.88	*Cr*	1	0	300	3.42	5023.54	*Fe*	0	0	300	6.75
4965.22	*Ni*	0	1	300	6.27	5024.82	*Ti*	3	2	400	3.27
4966.15	*Fe*	4	3	400	5.80	5025.52	*Ti*	1	2	400	4.49
4967.85	*Fe*	3	3	400	6.66	5027.18	*Fe*	3	3	400	6.59
4968.62	*Fe-Ti*	2[2]	2	350	6.11	5027.76	*Fe*	1	1	300	6.65
4969.87	*Fe*	3	2	350	6.68	5028.19	*Fe*	2	2	400	6.01
4970.45	*Fe-La*$^+$	1	2	350	6.10	5029.61	*Fe*	1	1	350	5.85
4971.35	*Ni-*	1	2	350	7.00	5031.00	*Sc*$^+$	3	15	800	3.80
4973.03	*Fe-Ti*	3	4	400	6.42	5031.92	*Fe*	− 1	0	300	6.81
4975.42	*Ti-Fe*	0[2]	1d	350	4.98	5032.80	*Ni*	− 1	0	300	6.33
4976.19	*Ni*	2[2]	1	350	4.15	5033.60	C_2	− 1[2]	0	300	.....
4977.65	*Fe*	0	1	300	6.39	5033.98	C_2	− 1[2]	0	300	.....

TABLE 1—*Continued*

Chromosphere	Element	Sun	Flash	Height in Km	High E.P.	Chromosphere	Element	Sun	Flash	Height in Km	High E.P.
5035.40	*Ni*	5	3	400	6.07	5088.30	*Ni-Fe*	1^2	0	350	6.26
5035.91	*Ti-Ni*	5^2	2	400	3.90	5089.22	Fe^+	1^2	2	350	.....
5036.25	*Fe*	0	1	400	.....	5090.79	*Fe*	5	4	400	6.66
5036.49	*Ti*	2	2	400	3.89	5092.10	*Cr-C*$_2$	0^2	1	350	3.42
5036.87	Fe^+	− 1	0	300	5.27	5092.80	Nd^+	− 2	1	350	2.80
5037.75	C_2	− 1^2	0	300	.....	5093.42	Fe^+	− 2^2	1	300	9.20
5038.41	*Ti*	2	2	400	3.87	5094.40	*Ni*	0	0	300	6.24
5038.63	*Ni*	2	2	400	6.27	5095.21	C_2	0^2	2	350	.....
5039.22	*Fe-Ni*	3	1	350	5.80	5095.91	C_2	0^3	1	300	.....
5039.98	*Ti*	3	2	400	2.47	5097.01	*Fe*	3	3	400	6.69
5040.97	*Fe*	7^2	5	800	3.40	5097.50	C_2	0	1	350	.....
5041.71	*Fe-Ca*	6^2	5	800	3.93	5098.42	*Fe-*	1^2	1	350	6.33
5042.18	*Ni*	1	1	400	6.09	5098.72	*Fe*	3	2	400	4.59
5043.59	*Ti*	− 1	0	300	3.28	5099.22	*Ni-Fe*	2^2	1	400	6.06
5044.25	*Fe-Co*	3	2	400	5.29	5099.96	*Ni*	2	3	400	6.08
5045.38	*Ti-*	0^2	0d	300	3.29	5100.82	Fe^+	0^3	2	400	5.21
5047.74	*He*	.....	−1	400	23.57	5101.26	$Sc\text{-}Fe^+$	− 1^2	1	350	3.86
5048.04	*Ni*	0	0	350	6.26	5103.00	*Ni*	1	1	350	4.09
5048.47	*Fe*	3	2	400	6.39	5103.55	C_2	0^3	1	350	.....
5048.88	*Ni*	2	2	400	6.28	5104.13	*Fe*	1^2	2	350	6.58
5049.85	*Fe*	6	5	700	4.71	5105.25	C_2	1^3	1	350	.....
5051.66	*Fe*	4	6	700	3.35	5105.53	*Cu*	4	4	400	3.80
5052.91	*Ti*	0	2	400	4.61	5106.44	C_2	− 1^2	1d	350	.....
5054.70	*Fe*	1	1	300	6.07	5107.58	*Fe*	8^2	8d	800	3.40
5056.06	$Si^+\text{-}Fe$	− 1	2	400	12.47	5109.20	C_2	− 1^2	1	350	.....
5056.82	*Fe*	1	1	300	6.68	5109.70	*Fe*	2	1	400	6.70
5057.53	*Fe*	0	0	300	6.61	5110.46	*Fe*	5	12	800	2.41
5057.95	*Fe*	1	1	300	6.37	5110.74	*Cr*	0	1	350	5.11
5058.50	*Fe*	− 1	0	300	6.07	5111.33	C_2	− 1^2	1	350	.....
5060.07	*Fe*	3	2	400	2.44	5111.66	C_2	− 1^2	1	350	.....
5062.12	*Ti*	0	0	300	4.59	5112.24	Zr^+	− 2	2	350	4.07
5063.17	C_2	0^2	1	350	.....	5113.09	*Cr*	− 1	1	350	5.11
5064.57	*Ti*	4^2	4	500	2.48	5113.47	*Ti*	0	1	350	3.85
5065.00	*Fe*	4^2	4	500	6.67	5114.29	C_2	− 2	1	350	.....
5065.18	*Fe*	2	2	500	6.06	5114.55	La^+	− 2	1	350	2.65
5067.21	*Fe*	3	2	400	6.64	5115.41	*Ni*	2	2	400	6.23
5067.71	*Cr*	0	0	300	5.13	5116.17	Cr^+	− 3	1	350	6.11
5068.74	*Fe*	5	4	600	5.36	5116.68	C_2	− 1^2	1	350	.....
5070.01	C_2	0^2	2d	400	.....	5116.93	C_2	− 1	1	350	.....
5071.49	*Ti*	0	0	300	3.89	5117.97	*Mn*	− 1	1	350	5.53
5072.04	*Fe*	3	3	500	6.70	5118.17	C_2	− 2^2	1	350	.....
5072.34	Ti^+	0	2	500	5.54	5119.18	V^+	− 1	2	400	3.04
5072.64	*Fe*	2	1	350	6.64	5119.48	C_2	− 1^3	1	350	.....
5073.43	C_2	− 1	2d	350	.....	5120.43	$Ti\text{-}Fe^+$	1^3	3d	400	4.98
5074.76	*Fe*	5	3	500	6.63	5121.60	*Fe-Ni*	3^2	3	400	6.67
5075.40	$Ce^+\text{-}C_2$	− 1	2	500	2.98	5122.97	La^+	− 2	2	400	2.73
5076.24	*Fe*	3	2	400	6.71	5123.18	Y^+	0	2	600	3.40
5076.61	C_2	− 1	2	350	.....	5123.73	*Fe*	3	4	800	3.42
5079.10	*Fe*	7^2	5d	600	4.62	5125.13	*Fe-Ni*	4^2	4	400	6.61
5079.84	*Fe-Ni*	5^2	5d	600	3.42	5126.23	*Fe-Co*	2	2	400	6.65
5080.59	*Ni*	4	3	400	6.07	5126.78	C_2	− 1^2	1	350	.....
5081.09	*Ni*	3	2	400	6.26	5127.35	*Fe*	3	3	500	3.32
5081.72	*Sc-Fe*	1^3	1	300	3.87	5127.82	$Fe\text{-}Fe^+$	0^3	1	350	2.46
5082.33	*Ni*	2	1	300	6.07	5128.48	C_2	0^3	1d	350	.....
5083.37	*Fe*	4	6	600	3.38	5129.12	Ti^+	3	8	800	4.29
5084.13	*Ni*	3	3	400	6.09	5129.42	*Ni-Fe*	3^2	2	400	6.07
5084.56	*Fe-C*$_2$	− 1^2	0	300	6.11	5130.30	*Ni*	− 1	1	350	6.23
5085.54	*Sc-Ti*	1^3	1	300	3.85	5130.56	$Nd^+\text{-}C_2$	− 2	2	400	3.70
5086.26	C_2	0^2	1	300	.....	5131.49	*Fe*	2	2	400	4.62
5087.04	*Ti-Sc*	0	1	400	3.85	5131.75	*Ni*	1	2	350	6.09
5087.45	Y^+	1	8	800	3.51	5132.40	C_2	− 1^2	1	350	.....

TABLE 1—*Continued*

Chromosphere	Element	Sun	Flash	Height in Km	High E.P.	Chromosphere	Element	Sun	Flash	Height in Km	High E.P.
5132.72	Fe^+-Ti	0^2	2	350	5.20	5177.36	Fe-Cr	1^2	0	350	6.06
5133.65	Fe	4	3	400	6.56	5180.11	Fe	1	1	350	6.84
5134.47	C_2	0^3	1d	350	.....	5183.58	Mg	30	70	3500	5.09
5135.65	C_2	-1^2	0	300	.....	5184.30	Fe	2	1	350	6.65
5136.16	Fe-C_2	0^2	0	300	6.57	5185.85	Ti^+	2	7	800	4.26
5137.06	Ni	3	3	400	4.07	5187.96	Fe	1	2	350	6.50
5137.42	Fe	3	2	400	6.56	5188.69	Ti^+	2	20	1000	3.95
5137.66	C_2	-1^2	0	300	.....	5189.68	Ti	-1^2	0	300	4.61
5138.38	C_2	-1^3	0	300	.....	5191.49	Fe	4	8	800	5.40
5139.25	Fe	4	5	800	5.39	5191.93	Cr	−1	1	350	5.76
5139.43	Fe	5	6	800	5.33	5192.43	Fe	5	8	800	5.36
5139.65	Cr	−1	1	350	5.81	5192.97	Ti	2	3	350	2.40
5141.23	C_2	-1^2	0	350	.....	5194.98	Fe	4	8	500	3.93
5141.75	Fe	3	2	400	4.81	5195.48	Fe	2	2	400	6.58
5142.50	Fe	4	3	500	6.64	5196.09	Fe	1	1	300	6.61
5142.88	Fe-Ni	5^2	4	600	3.35	5196.48	Cr-Y^+	0	1	350	5.81
5144.58	Cr-C_2	0^2	0	350	5.10	5197.57	Fe^+	2	15	1000	5.59
5145.15	Fe	1	1	350	4.59	5197.94	Fe	0	0	300	6.66
5145.52	Ti	0	1	350	3.85	5198.73	Fe	3	4	400	4.59
5146.12	Fe^+-C_2	−1	1	350	5.21	5200.15	Cr	−1	0	300	5.74
5146.50	Ni	3	3	400	6.09	5200.42	Y^+	0	7	100	3.36
5147.10	C_2	−2	1	350	.....	5201.15	Ti	−2	0	300	4.46
5147.61	Ti-C_2	1^3	2	400	2.40	5202.27	Fe	6^2	6d	500	4.54
5148.13	Fe	5^2	3	400	6.64	5204.54	Cr-Fe	8^2	12d	1200	3.31
5149.13	C_2	-1^2	1	350	.....	5205.75	Y^+	0	6	600	3.40
5150.18	Fe	−1	0	350	5.97	5206.05	Cr	5	15	1200	3.31
5150.62	C_2	-1^2	1	350	.....	5208.37	Cr	5	25	1200	3.31
5150.83	Fe	4	4	500	3.38	5208.65	Fe	2	2	400	5.60
5151.88	Fe	3	3	500	3.40	5210.32	Ti	3	4d	600	3.42
5152.21	Ti	0	2	400	2.42	5211.37	Ti^+	0^2	1d	400	4.95
5153.13	Cu-C_2	2^3	3	400	6.16	5212.73	Co	−2	1d	300	5.87
5154.10	Ti^+	2	8	800	3.95	5214.12	Cr	−1	0	300	5.72
5154.40	Fe^+-C_2	-1^2	2	400	5.23	5215.19	Fe	3	3	300	5.62
5155.16	Ni	1	0	350	6.28	5216.31	Fe	3	6	800	3.97
5155.80	Ni	2	2	400	6.28	5217.40	Fe	3	2	400	5.56
5156.60	La^+-C_2	−1	1	350	2.52	5218.15	Cu-Fe	2^2	2d	400	6.17
5157.59	C_2	0^3	1	350	.....	5220.12	Ni-Pr^+	0	1d	350	6.09
5157.95	Ni	−1	1	350	5.98	5221.80	Cr	0	0	300	5.72
5158.53	C_2	-1^2	0	350	.....	5223.17	Fe	0	0	300	5.98
5159.10	Fe	2	2	400	6.66	5224.19	Ti-Cr	1^2	0	300	4.49
5159.55	C_2	-1^2	1	350	.....	5224.82	Cr-Ti	1^3	1d	350	5.80
5160.27	C_2	−1	1	350	.....	5225.47	Fe	2	2	350	2.47
5161.05	Fe^+-C_2	-1^2	1	400	5.23	5226.53	Ti^+	2	12	1000	3.92
5161.67	C_2	-1^2	1	350	.....	5227.04	Fe-Cr	9^2	12	1000	3.91
5162.31	Fe	5	3	400	6.55	5228.39	Fe	1	1	300	6.56
5162.90	C_2	-1^2	1	350	.....	5229.87	Fe	4	4	500	5.63
5163.41	C_2	-1^3	1	350	.....	5230.20	Cr-Co	−1	1	400	5.06
5164.24	C_2	-1^3	1	350	.....	5232.98	Fe	7	10	800	5.29
5164.71	C_2	-1^2	}	400	.....	5234.63	Fe^+	2	15	1000	5.57
5164.98	Fe-C_2	-1^3	6	400	6.51	5235.43	Fe-Ni	2^2	2	400	4.93
5165.18†††	C_2	-2^2	}	400	.....	5236.22	Fe	0	0	300	6.53
5166.26	Fe-Cr	3	4	600	2.39	5237.31	Cr^+	1	5	600	6.41
5167.35	Mg	15	40	2000	5.09	5238.54	Fe^+-Ti	−2	0	300	5.23
	Fe	5			3.87	5238.93	Cr	−1	0	300	5.05
5168.99	Fe^+-Fe	7^2	45	2000	5.27	5239.79	Sc^+	1	7	600	3.80
5170.70	Fe	0	1	350	.....	5242.50	Fe	2	2	400	5.97
5171.56	Fe	6	9	1000	3.86	5243.81	Fe	1	2	400	6.59
5172.65	Mg	20	60	3000	5.09	5246.72	Cr^+-Ti	-1^2	1	350	6.05
5173.73	Ti	2	3	500	2.39	5247.09	Fe	1	1	350	2.44
5175.39	Fe^+	-1^2	0	300	.....	5247.56	Cr	3	2	400	3.31
5176.57	Ni	1	1	350	6.27	5249.52	Cr^+-Nd^+	3	3d	400	6.09

††† Head of third band.

TABLE 1—*Continued*

Chromo-sphere	Element	Sun	Flash	Height in Km	High E.P.	Chromo-sphere	Element	Sun	Flash	Height in Km	High E.P.
5250.17....	*Fe*	2	1	350	2.47	5319.87....	*Nd⁺-Fe*	1^2	3d	600	2.87
5250.66....	*Fe*	3	3	400	4.54	5321.09....	*Fe*	2	1	350	6.73
5251.98....	*Ti⁺*	1	2d	350	4.93	5322.08....	*Fe*	3	2	350	4.59
5253.53....	*Fe*	2	2	350	5.62	5324.22....	*Fe*	7	8	600	5.52
5254.90....	*Fe-Fe⁺*	3	5	500	2.46	5325.59....	*Fe⁺*	2	7	600	5.52
5255.28....	*Cr-Fe*	1^2	2	350	5.80	5326.13....	*Fe*	1	0	300	5.32
5256.86....	*Fe⁺*	− 1	1	350	5.23	5326.77....	*Fe*	− 1	0	300	6.71
5257.79....	*Co-Fe*	0^2	1	350	6.30	5328.03....	*Fe*	8	12	800	3.23
5259.32....	*La⁺*	.....	2	350	2.52	5328.44....	*Fe-Cr*	10^2	10	800	3.87
5261.70....	*Ca*	3	1	400	4.86	5329.18....	*Cr*	3	2	350	5.22
5262.21....	*Ti⁺-Ca*	4^2	5	600	3.92	5329.96....	*Fe*	2	2	350	6.37
5263.39....	*Fe*	4	3	400	5.60	5330.61....	*Ce⁺*	− 2	1	350	2.71
5263.87....	*Fe*	0	2	400	5.90	5331.40....	*Co*	− 1	0	300	4.09
5264.20....	*Cr-Ca*	10^2	4	500	3.31	5332.68....	*V⁺-Co*	1	1	400	4.57
5264.77....	*Fe⁺*	1	4	500	5.56	5332.90....	*Fe*	4	6d	500	3.86
5265.70....	*Ca-Cr*	6^3	4	500	4.86	5334.22....	*Sc⁺*	− 2	1	400	3.80
5266.60....	*Fe*	6	6	500	5.33	5334.88....	*Cr⁺*	1	3	600	6.37
5268.32....	*Ni*	0	0	350	6.86	5336.77....	*Ti⁺*	4	12	1000	3.89
5268.62....	*Ti⁺*	− 1	3	350	4.93	5337.76....	*Fe⁺-Cr⁺*	1^2	4	400	5.53
5269.55....	*Fe*	8	15	1000	3.20	5339.98....	*Fe*	6	6	500	5.56
5270.32....	*Fe-Ca*	7^2	12	800	3.94	5340.46....	*Cr*	0	0	300	5.73
5272.00....	*Cr*	− 1	1	350	5.78	5341.10....	*Fe-Mn*	8^3	12d	800	3.91
5273.14....	*Fe*	4	3	400	5.62	5342.69....	*Co*	1	2	400	6.31
5273.44....	*Fe*	2	5	600	4.81	5343.46....	*Co*	3^2	3	400	6.32
5274.22....	*Ce⁺*	− 1	2	350	2.90	5345.78....	*Cr*	5	8	800	3.31
5275.01....	*Cr⁺-Fe*	0	2	350	6.39	5346.59....	*Fe⁺-Cr⁺*	0	1	350	5.52
5275.25....	*Cr-Fe*	2^2	1	350	5.22	5347.48....	*Co*	− 1	1	350	6.44
5275.99....	*Fe⁺-Cr*	6^3	20	800	5.52	5348.34....	*Cr*	4	5	500	3.31
5279.88....	*Cr⁺*	0	1	350	6.39	5349.47....	*Ca*	4	3	500	5.00
5280.33....	*Cr⁺-Fe*	1^2	2	400	6.39	5349.71....	*Fe-Sc*	1	1	350	6.67
5280.60....	*Co*	− 1	1	350	5.95	5350.17....	*Zr⁺*	1^2	3	400	4.13
5281.80....	*Fe*	5	5	400	5.36	5351.01....	*Ti*	− 1	0	300	5.07
5282.31....	*Ti*	− 1	1	350	3.38	5352.01....	*Co*	1	3	400	5.87
5283.64....	*Fe*	6	6	600	5.56	5353.43....	*Fe-Ce⁺*	4^2	8d	600	6.39
5284.12....	*Fe⁺*	2	10	800	5.21	5355.74....	*Sc*	− 1	0	300	4.25
5285.13....	*Fe*	0	0	350	6.75	5357.22....	*Sc⁺*	− 1	1	300	3.80
5288.60....	*Fe*	2	2	350	6.01	5359.21....	*Co*	− 1	0	300	6.43
5289.58....	*V⁺-*	− 1^2	0	350	3.36	5361.66....	*Fe-Nd⁺*	1	4	400	6.70
5292.50....	*Fe*	0	1	350	.....	5362.86....	*Fe⁺*	3	15	800	5.49
5293.15....	*Nd⁺*	− 1	4	400	3.15	5364.86....	*Fe*	5	5	500	6.73
5293.96....	*Fe*	0	0	350	6.46	5365.35....	*Fe*	3	4	500	5.86
5295.30....	*Fe-Sc*	0	1	350	6.73	5367.46....	*Fe*	6	6	500	6.70
5296.69....	*Cr*	3	3	400	3.31	5368.22....	*Cr⁺*	− 1^2	0d	300	6.14
5297.40....	*Cr*	2	1	400	5.22	5369.63....	*Co*	1	1	350	4.03
5298.00....	*Cr*	1	1	400	5.22	5369.98....	*Fe*	6	6	500	6.65
5298.28....	*Cr*	4	5	500	3.31	5371.51....	*Fe-*	8^2	15d	1000	3.25
5298.82....	*Fe*	0	0	300	5.96	5373.64....	*Fe-Cr*	2	2d	350	6.75
5300.82....	*Cr*	2	2	400	3.31	5377.62....	*Mn*	2	3	350	6.12
5302.05....	*La⁺*	− 2	1	400	2.73	5379.52....	*Fe*	3	2	300	5.97
5302.35....	*Fe*	5	4	400	5.60	5380.35....	.....	0	0	300	.....
5303.39....	*La⁺-V⁺*	1^2	2	350	2.65	5381.04....	*Ti⁺-La⁺*	2	8	800	3.85
5305.86....	*Cr⁺*	0	1	350	6.14	5382.20....	.....	0	0d	300	.....
5307.40....	*Fe*	3	3	500	3.93	5383.32....	*Fe*	6	6	600	6.59
5308.49....	*Cr⁺*	0	2	400	6.38	5385.57....	*Fe*	− 1	0	300	5.97
5311.79....	*Zr⁺*	− 2	1	350	4.07	5386.37....	*Fe*	1	1	350	6.43
5312.85....	*Cr*	0	0	300	5.76	5387.50....	*Fe-Cr*	0^2	0	300	6.42
5313.57....	*Cr⁺*	1	2	400	6.38	5388.36....	*Ni*	0^2	0d	300	4.22
5315.07....	*Fe*	1	1	350	6.67	5389.48....	*Fe*	3	3	400	6.69
5316.67....	*Fe⁺*	6^2	40	1200	5.46	5390.31....	*Cr-Ti*	1^3	1d	350	5.64
5318.32....	*Sc⁺-Cr⁺*	− 1	0	300	3.67	5391.42....	*Fe*	2	3	400	6.43
5318.78....	*Cr*	0	0	300	5.74	5391.65....	*Fe*	1	1	400	4.97

TABLE 1—*Continued*

Chromo-sphere	Elements	Sun	Flash	Height in Km	High E.P.	Chromo-sphere	Element	Sun	Flash	Height in Km	High E.P.
5392.10	*Ni-Sc*	0^2	0	300	6.42	5460.49	*Ti*	− 1	0	300	2.31
5393.20	*Fe*	5	5	400	5.52	5462.55	*Ni*	1	1	300	6.09
5393.42	Ce^+	− 2	2	350	2.91	5462.95	*Fe*	3	3	400	6.71
5394.67	*Mn-Fe*	2^2	3	400	2.29	5463.26	*Fe*	3	4	400	6.67
5395.18	*Fe*	0	1	300	6.71	5464.15	*Fe-Cr*	1^2	1d	350	6.38
5396.27	Ti^+	− 1	1	300	3.86	5466.41	*Fe-V*	3	3	400	6.61
5397.14	*Fe*	7	12	800	3.20	5466.97	*Fe*	1	1	300	5.82
5397.66	*Fe*	1	1	300	5.91	5468.47	Ti^+-*Ni*	0^3	1d	300	4.84
5398.27	*Fe*	3	3	400	6.71	5470.10	*Fe*	0	0	300	6.68
5399.43	*Mn*	1	2	400	6.12	5470.64	*Mn*	1^2	2	400	4.41
5400.46	*Fe*	3	5	400	6.64	5472.36	Ce^+	− 2	1	350	3.02
5401.27	*Fe*	0	0	300	6.59	5472.72	*Ti-Fe*	1	2	400	3.69
5401.99	*V-*	0^3	1d	300	4.63	5473.37	V^+	− 2	1	300	3.99
5402.76	V^+	0	2	400	4.12	5473.89	*Fe*	3	3	500	6.39
5403.88	*Fe*	2	3	500	6.34	5474.40	*Ti-*	0^2	0d	300	3.71
5404.12	*Fe*	5	6	500	6.58	5476.27	*Fe*	1	1	400	6.38
5405.39	*Fe*	1	1	300	6.65	5476.58	*Fe*	3	4	400	6.34
5405.84	*Fe*	6	12	500	3.27	5476.92	*Ni*	5	8	800	4.07
5406.80	*Fe*	1	0	300	6.64	5477.71	Fe^+-*Ti*	− 1	1	300	5.46
5407.50	Cr^+-*Mn*	1^2	3d	400	6.09	5478.42	Cr^+	− 1	2	400	6.41
5409.16	*Fe*	2	2	400	6.63		*Fe*	0	2	400	6.43
5409.81	*Cr*	5	7	800	3.31	5480.60	V^+-*Cr*	0^2	3	400	3.97
5410.89	*Fe*	4	6	400	6.73	5480.92	*Fe-Ni*	1	2	400	6.45
5411.24	*Ni*	1	2	400	6.35	5481.38	*Fe-Ti*	2^2	2	350	6.34
5412.80	*Fe*	− 1	0	300	6.70	5481.85	*Ti-Sc*	0^2	1	350	3.67
5413.69	*Mn*	− 1	0	300	6.12	5483.10	*Fe*	1	1	350	6.39
5414.04	Fe^+	0	4	400	5.49	5483.38	*Co*	1	2	350	3.95
5415.23	*Fe*	5	7	500	6.65	5483.88	*Co*	− 2	0	300	5.87
5417.05	*Fe*	0	1	300	6.67	5484.64	*Sc*	− 2	1	300	4.09
5418.80	Ti^+	1	7	800	3.85	5485.63	Nd^+	− 3	2	350	3.51
5420.30	*Mn*	1^2	2	400	4.41	5487.14	*Fe*	1	1	350	6.65
5420.94	Cr^+	− 1	1	300	6.02	5487.54	*Fe*	− 1	0	350	5.87
5421.20	.....	0	0	300	.....	5487.78	*Fe*	3	4	400	6.37
5422.02	*Fe-*	0^2	0	300	6.58	5489.75	*Fe*	0^2	0	300	6.67
5424.07	*Fe*	6	8	800	6.58	5490.11	*Ti*	0	0	300	3.70
5424.65	*Ni*	1	2	350	4.22	5490.72	Ti^+	0	3	400	3.82
5425.30	Fe^+	1	8	800	5.46	5491.90	*Fe*	− 1	0	300	6.42
5429.50	*Fe*	1	1	350	6.45	5493.51	*Fe*	1	2	350	6.33
5429.73	*Fe*	6	15	800	3.23	5494.45	*Fe*	0	0	300	6.30
5430.36	Cr^+	− 1	0	300	6.11		V^+	− 3	1	400	3.99
5431.60	Nd^+	− 2	1	300	3.39	5497.42	*Fe*	5	8	800	3.25
5432.40	*Mn-Cr*	2^2	3	400	2.29	5499.55	*Fe*	− 1	0	300	6.70
5432.90	*Fe-Fe*$^+$	2	4	400	6.70	5501.47	*Fe*	5	7	800	3.20
5433.60	.....	0^2	0	300	.....	5502.04	Cr^+	− 1	0	300	6.39
5434.54	*Fe*	5	10	800	3.28	5503.02	Cr^+	1	3	400	6.37
5435.80	Fe^+-*Ni*	1	3	350	5.49	5503.44	Fe^+	0^2	0	300	.....
5436.32	*Fe*	1	1	350	6.64	5503.98	*Ti-Ni*	1^2	1	300	4.81
5436.63	*Fe*	1	1	350	4.54	5505.84	*Mn*	1	3	350	4.41
5437.20	*Fe*	− 1	0	300	6.56	5506.81	*Fe*	5	8	800	3.23
5441.32	*Fe*	1	1	300	6.56	5508.56	Cr^+	1^2	3d	400	6.38
5444.56	*Co*	− 1	2	300	6.32	5509.96	V^+-*Ni*	2^2	7d	500	3.23
5445.03	*Fe*	4	5	400	6.63	5510.62	Cr^+	1^2	2	400	6.05
5446.86	*Fe-Ti*	8^2	12d	800	3.25	5512.27	*Fe*	1	1	350	6.59
5448.40	*Fe*	− 1	1	300	.....	5512.52	*Ti*	2	4	400	3.69
5451.07	Nd^+	− 2	1	300	.....	5513.00	*Ca*	4	3	400	5.16
5452.06	Ti^+-*Fe*	− 1	1	300	4.90	5514.29	*Ti*	2	4	400	3.66
5453.18	*Ni*	− 1	0	300	6.33	5514.57	*Ti*	2	4	400	3.67
5453.98	Ti^+-*Fe*	− 1	0	300	3.82	5516.74	*Mn*	1^2	2	350	4.41
5454.60	*Co*	− 1	0	300	6.32	5517.05	*Fe*	0	0	300	6.43
5455.59	*Fe*	6^2	12	800	3.27	5517.56	.....	− 1	0	300	.....
5457.36	*Mn*	0^3	0	300	4.42	5519.60	*Fe*	0	0d	300	.....

TABLE 1—*Continued*

Chromosphere	Element	Sun	Flash	Height in Km	High E.P.	Chromosphere	Element	Sun	Flash	Height in Km	High E.P.
5520.70	*Sc-*	0^2	0	300	4.09	5596.19	C_2	− 2	0d	300	.....
5521.18	*Fe-*	0^2	0	300	5.25	5598.43	*Ca-Fe*	6^2	8d	800	4.71
5521.64	Y^+	− 1	2	350	3.97	5599.99	*Ni*	0	0	300	6.28
5522.45	*Fe*	2	2	350	6.43	5600.24	*Fe*	0	3d	400	5.82
5525.61	*Fe*	2	3	400	6.45	5601.31	*Ca-Ce*$^+$	3	5d	500	4.72
5526.90	Sc^+	3	15	800	3.99	5602.92	*Fe-Ca*	7^2	8	800	5.62
5527.60	*V-Ti*	− 2	0	300	3.63	5603.73	C_2	− 1	1	300	.....
5528.41	*Mg*	8	9	600	6.56	5605.78	C_2	− 1	1	300	.....
5529.09	*Fe*	1^2	0d	300	5.86	5607.65	*Fe-*C_2	− 1	0	300	6.34
5530.80	*Co*	− 1	2	400	3.93	5610.14	Ce^+-C_2	− 1^2	1d	300	2.77
5532.00	*Fe*	− 1	1	400	7.12	5612.43	C_2	− 1^2	0	300	.....
5532.85	*Fe-*	2^2	2	400	5.79	5614.74	*Ni*	1	1	300	6.33
5534.86	Fe^+	2	15	800	5.46	5615.29	*Fe*	2	2	350	4.77
5535.41	*Fe-Mn*	3^2	2d	350	5.47	5615.65	*Fe*	6	12	800	5.52
5537.75	*Mn*	0^2	2d	350	4.41	5617.23	*Fe-*	1^2	0	300	5.43
5538.51	*Fe*	1	1	350	5.85	5618.66	*Fe*	1	0	300	6.39
5539.26	*Fe*	0	0	350	5.85	5619.64	*Fe*	0	0	300	6.56
5540.09	*Sr-*C_2	− 1^2	1	350	4.48	5620.53	*Fe*	0	1	300	6.33
5540.75	C_2‡‡‡	− 2	1	300	.....	5622.99	C_2	0	1	300	.....
5543.22	*Fe*	2	4	400	5.91	5624.03	*Fe*	1	1	350	6.56
5544.00	*Fe*	2	2	400	6.43	5624.55	*Fe*	4	6	600	5.60
5544.66	V^+	− 2	1	350	3.96	5625.40	*Ni-*	1^2	2d	400	6.27
5546.56	*Fe*	2	2	350	6.58	5627.61	*V*	− 1	0	300	3.27
5547.01	*Fe*	1	1	300	6.42	5627.99	C_2	− 2	0	300	.....
5549.83	*Fe*	0^2	0	300	5.90	5628.49	*Cr-Ni*	0^2	0d	300	5.60
5551.96	*Mn*	− 2	1	300	.....	5631.86	C_2	0^3	0d	300	.....
5552.24	Sc^+	− 2	0	300	3.67	5633.96	*Fe*	3	2	350	7.16
5553.61	*Fe-Ni*	2^2	2	350	6.64	5634.86	C_2	− 2^2	0	300	.....
5554.92	*Fe*	3	5	600	6.75	5635.22	C_2‖‖‖	− 2	1d	300	.....
5557.92	*Fe-*	1^2	2	350	6.67	5635.80	*Fe*	1	1	300	6.43
5558.79	*Co-V*	− 2	0d	300	5.73	5637.25	*Ni-*	2^2	2d	350	6.26
5560.17	*Fe*	2	2	350	6.64	5638.28	*Fe*	3	2	350	6.39
5561.21	.....	− 1	0	300	.....	5640.26	.....	0	0	300	.....
5562.75	*Fe*	2	3	400	6.63	5640.93	Sc^+	1	5	600	3.68
5563.59	*Fe*	3	5	400	6.39	5641.45	*Fe*	2	2	350	6.43
5565.48	*Ti*	− 1	0	300	4.44	5642.82	*Ni-Fe*	1^3	0d	300	6.33
5565.71	*Fe*	3	7	600	6.81	5644.10	*Ti*	0	4d	400	4.44
5566.11	Cr^+	0	0	300	6.11	5645.65	*Si*	1	0	300	7.09
5567.37	*Fe*	2	4	400	4.81	5646.69	*Fe*	− 1	0	300	6.43
5568.88	*Fe*	− 1	0	300	5.84	5647.23	*Co*	− 1	1	300	4.46
5569.69	*Fe*	6	8	800	5.62	5648.64	*Ti*	− 1	1	300	4.67
5572.87	*Fe-*	7^2	10	800	5.60	5649.44	*Cr*	− 1	0	300	6.01
5573.11	*Fe*	1	0	300	6.39	5649.86	*Fe-Ni*	2^2	2	400	5.80
5574.92	.....	− 2	1	300	.....	5650.65	*Fe*	1	1	300	7.25
5576.08	*Fe*	4	7	600	5.63	5651.45	*Fe*	0	1	300	6.64
5577.04	*Fe*	− 1	0d	300	7.22	5652.37	*Fe*	1	1	300	6.43
5578.69	*Ni*	1	4	500	3.88	5653.88	*Fe*	1	0	300	6.55
5582.03	*Ca*	4	3	500	4.72	5655.17	*Fe*	1	1	300	7.22
5584.42	*V-*C_2	− 2	1	350	3.27	5655.52	*Fe*	2	5	500	6.42
5584.78	*Fe-*C_2	0	2	350	5.77	5657.84	Sc^+	2	10	800	3.68
5585.60	C_2§§§	− 2	2	350	.....	5658.29	Sc^+	0	5	800	3.67
5586.83	*Fe*	7	9	800	5.56	5658.67	*Fe*	6^3	5	800	5.56
5587.59	*Fe*	0	1	300	6.33	5659.60	.....	0	0	300	.....
5587.86	*Ni*	1	5	500	4.14	5660.70	*Fe-*	1^2	1d	300	5.80
5588.74	*Ca*	6	8	800	4.72	5661.35	*Fe*	0	0	300	6.45
5589.38	*Ni*	0	1	300	6.09	5662.16	*Ti*	0	0	300	4.49
5590.10	*Ca*	3	2	400	4.72	5662.50	*Fe*	4	3	400	6.34
5590.85	*Co*	− 1^3	1	300	4.24	5662.93	V^+-*Ti*	1	7	800	4.12
5592.28	*Ni*	1	7	500	4.15	5664.02	*Ni-Cr*	1	2	300	6.70
5593.66	*Ni*	0	2d	400	6.09	5665.58	*Si*	1	1	300	7.08
5594.57	*Ca-Fe*	5^2	8	800	4.72	5666.67	*Ni*	0	1	300	6.27

‡‡‡ Third head of second band. §§§ Second head of second band. ‖‖‖ First head of second band.

TABLE 1—*Continued*

Chromosphere	Element	Sun	Flash	Height in Km	High E.P.	Chromosphere	Element	Sun	Flash	Height in Km	High E.P.
5667.20	Sc^+	0	6	600	3.67	5763.03	*Fe*	7^2	6	400	6.33
5667.49	*Fe*	2	2	300	4.77	5766.34	*Ti*	0	1	300	5.42
5669.02	Sc^+	1	6	600	3.67	5769.19	Ce^+-La^+	1^2	1d	300	2.98
5669.83	*Ni*-	1^2	1d	350	6.42	5772.18	*Si*	3	2	400	7.20
5670.78	*V*	0	0	300	3.25	5774.04	*Ti*	0	1	300	5.43
5671.89	*Sc*	0	2	350	3.62	5775.14	*Fe*	4	3	350	6.34
5675.43	*Ti*	2	3	350	4.47	5778.42	*Fe*	1	2	350	4.71
5679.04	*Fe*	3	4	350	6.81	5780.65	*Fe-Ti*	3^2	2d	350	5.36
5682.18	*Ni*	2	2	350	6.26	5782.17	*Cu*	6^2	5	400	3.77
5682.65	*Na*	5	3	350	4.27	5783.06	*Cr*	2	2	300	5.44
5684.23	Sc^+	1	5	600	5.67	5783.90	*Cr*	3	2	300	5.44
5684.49	*Si*	3	2	300	7.10	5784.67	*Fe*	1	0	300	5.52
5685.46	.....	− 1	0	300	.....	5785.11	*Cr*-Fe^+	5^2	4d	400	5.44
5686.53	*Fe*	3	4	350	6.70	5785.88	*Cr-Ti*	2^2	2	350	5.44
5688.23	*Na*	6	3	350	4.27	5787.91	*Cr*	4	3	350	5.44
5689.48	*Ti*	0	0	300	4.46	5791.02	*Cr-Fe*	7^2	5	400	5.44
5690.50	*Si*	3	1	300	7.08	5793.13	*Si*	3	2	350	7.04
5691.45	*Fe-Ni*	2	2	300	6.37	5793.93	*Fe*	2	1	300	6.33
5693.69	*Fe*	3	2	350	.....	5798.00	*Fe-Si*	7^2	4d	400	6.04
5694.89	*Ni-Cr*	3^2	4	350	6.24	5804.28	*Fe-Ti*	2^3	2d	350	5.99
5696.11	Fe^+	0	1	300	4.80	5805.27	*Ni*	4	3	350	6.28
5698.33	*Cr-Fe*	1	4	400	6.03	5806.70	*Fe*	5	3	350	6.71
5698.58	*V*	1	2	400	3.23	5809.27	*Fe*	4	3	350	5.99
5700.23	*Sc-Ni*	1^2	1	300	3.59	5811.93	*Fe*	0	1	300	6.25
5701.12	*Si*	1	1	350	7.07	5814.85	*Fe*	1	0	300	6.39
5701.50	*Fe*	4	4	500	4.71	5816.35	*Fe*	5	4	400	6.65
5702.38	*Cr*	0	1	300	5.60	5827.86	*Fe*	0	1	300	5.39
5703.57	*V*	1	2	400	3.21	5831.64	*Ni*	1	0	300	6.27
5704.74	*Fe*	0	1	300	.....	5834.04	*Fe*	0	0	300	4.71
5705.41	*Fe*	1	1	300	6.45	5838.30	*Fe*-Ce^+	1^2	1	350	6.04
5706.00	*Fe*	3	4	400	6.75	5848.16	*Fe*	3	2	350	5.36
5706.99	*Fe-V*	2^2	2d	350	5.79	5849.70	*Fe*	0	0	300	5.79
5708.10	*Fe*	1	2	400	6.58	5852.24	*Fe*	3	2	350	6.64
5708.41	*Si*	3	2	400	7.09	5853.69	Ba^+	5	15	800	2.71
5709.37	*Fe*	5	6	500	5.52	5855.07	*Fe*	1	1	350	6.70
5709.61	*Ni*	5	3	400	3.83	5856.13	*Fe*	2	2	350	6.38
5711.02	*Mg*	6	2	400	6.49	5857.51	*Ca-Ni*	11^2	10	800	5.03
5711.89	*Fe-Ni*	4	5	400	6.43	5859.54	*Fe*	5	5	500	6.64
5712.16	*Fe*	2	2	300	5.56	5861.12	*Fe*	0	0	350	6.37
5715.12	*Ni-Fe*	5	5	400	6.23	5862.42	*Fe*	6	6	600	6.63
5717.86	*Fe*	4	5	400	6.42	5864.29	*Fe*	0	1	350	6.39
5720.45	*Ti*	0	0	300	4.44	5866.46	*Ti*	3	5	400	3.17
5720.90	*Fe*	0	0	300	6.69	5867.58	*Ca*	2	1	350	5.02
5727.06	*V*	2	4	400	3.23	5873.22	*Fe*	1	1	350	6.34
5728.88	Y^+-Fe^+	− 1	0	300	3.99	5875.64	*He*	.....	100	7500	22.97
5730.90	*Fe*	0	0	300	6.35	5881.29	*Fe*	1	1	350	6.69
5731.73	*Fe*	4	3	300	6.39	5883.80	*Fe*	4	4	400	6.04
5732.33	*Fe*	0	0	300	7.12	5889.09	*Na*(D_2)	30	40	1500	2.10
5739.49	*Ti*	0	0	300	4.39	5892.86	*Ni*	4	5	400	4.07
5739.99	*Ti*	0	0	300	4.38	5895.99	*Na*(D_1)	20	35	1500	2.09
5741.82	*Fe*	2	1	300	6.39	5899.36	*Ti*	2	3	400	3.14
5747.74	.....	1	0	300	.....	5905.70	*Fe*	4	3	400	3.72
5747.92	*Fe*	2	1	300	6.73	5909.96	*Fe*	1	2	350	5.29
5748.40	*Ni*	2	2	300	3.82	5914.14	*Fe*	4	8	500	6.67
5752.00	*Fe*	4	3	350	6.67	5916.26	*Fe*	3	6	500	4.53
5753.15	*Fe*	5	5	400	6.39	5918.55	*Ti*	0	2	350	3.15
5754.64	*Ni*	5	5	400	4.07	5922.12	*Ti*	0	1	350	3.13
5756.85	*Fe*	2	1	300	.....	5927.80	*Fe*	3	1	350	6.71
5760.34	*Fe*	1	1	300	5.77	5929.68	*Fe*	2	0	350	6.61
5760.86	*Ni*	2	2	300	6.23	5930.23	*Fe*	6	7	500	6.71
5762.40	*Fe*	1	1	300	5.77	5934.70	*Fe*	5	5	400	5.99

TABLE 1—*Continued*

Chromosphere	Element	Sun	Flash	Height in Km	High E.P.	Chromosphere	Element	Sun	Flash	Height in Km	High E.P.
5937.82....	*Ti*	− 1	0	350	3.14	6122.28....	*Ca*	10	15	800	3.89
5941.75....	*Ti*	1	0	350	3.13	6125.05....	*Si*	1	1	300	7.60
5948.55....	*Si*	6	2	350	7.14	6126.28....	*Ti*	1	1	300	3.08
5949.37....	*Fe*	2	2	400	2.99	6127 92....	*Fe*	3	2	300	6.14
5952.68....	*Fe*	4	3	400	6.04	6128.99....	*Ni*	1	0	300	3.68
5953.22....	*Ti*	2	3	400	3.95	6130.15....	*Ni*	1	0	300	6.26
5956.73....	*Fe*	4	4	400	2.93	6136.78....	*Fe*	11[2]	10	800	4.45
5958.25....	*Fe*	1	0	350	3.03	6137.68....	*Fe*	7	10	800	4.59
5965.84....	*Ti*	2	4	400	3.94	6141.77....	*Ba*$^+$-*Fe*	7	40	1500	2.71
5975.31....	*Fe*	3	2	350	6.12	6142.50....	*Si*	1	2	400	7.60
5976.83....	*Fe*	4	2	350	5.99	6145.01....	*Si*	2	2	400	7.60
5978.58....	*Ti*	2	2	350	3.93	6147.78....	*Fe*$^+$-*Fe*	5[2]	6	600	5.88
5983.70....	*Fe*	5	4	400	6.59	6149.24....	*Fe*$^+$	2	6	600	5.88
5984.82....	*Fe*	6	5	400	6.77	6151.68....	*Fe*	4	2	350	4.17
5987.08....	*Fe*	5	5	400	6.84	6154.26....	*Na*	2	2	350	4.10
5991.36....	*Fe*$^+$	2	12	400	5.20	6155.22....	*Si*	5	2	350	7.60
5996.74....	*Ni*	1	1	350	6.28	6156.04....	*Ca*	− 1	0	300	4.52
5997.78....	*Fe*	3	3d	350	6.65	6157.76....	*Fe*	5	4	400	6.06
6003.05....	*Fe*	6	5	400	5.92	6159.39....	*Fe*	0	0	300	6.59
6005.54....	*Fe*	1	2	350	4.63	6160.68....	*Na*	3	1	300	4.10
6007.32....	*Ni*	1	1	350	3.72	6161.28....	*Ca*	4	2	300	4.52
6008.00....	*Fe*	4	3	400	6.69	6162.19....	*Ca*	15	25	1000	3.89
6008.58....	*Fe*	6	5	400	5.92	6163.76....	*Ca-Fe*	4[2]	3	400	4.51
6012.21....	*Ni*	1	0	350	.....	6165.30....	*Fe*	2	2	400	6.13
6013.55....	*Mn*	6	4	400	5.11	6166.44....	*Ca*	5	3	400	4.51
6016.68....	*Mn*	6	4	400	5.11	6169.02....	*Ca*	6	4	600	4.51
6020.10....	*Fe*	6[2]	6	400	6.64	6169.51....	*Ca*	7	5	600	4.51
6021.86....	*Mn*	6	5	400	5.11	6170.50....	*Fe-Ni*	4	4	600	6.77
6024.09....	*Fe*	7	6	400	6.58	6173.32....	*Fe*	5	4	400	4.21
6027.01....	*Fe*	4	4	400	6.11	6175.36....	*Ni*	3	2	400	6.07
6039.75....	*V*	0	0	350	3.10	6176.81....	*Ni*	5	3	400	6.07
6042.10....	*Fe*	3	3	400	6.75	6180.20....	*Fe*	5	2	400	4.71
6053.66....	*Ni*	0	0	350	6.26	6185.71....	*Fe*	1	0	300	.....
6056.03....	*Fe*	5	4	400	6.75	6186.70....	*Ni*	2	0	300	6.08
6062.87....	*Fe*	0	1	300	4.20	6188.04....	*Fe*	4	2	400	5.92
6065.53....	*Fe*	7	10	600	4.63	6191.13....	*Ni*	6	4	400	3.66
6076.91....	*Cr*$^+$	− 1	0	350	6.09	6191.64....	*Fe*	9	10	800	4.42
6078.47....	*Fe*	5	4	400	6.81	6194.50....	.....	0	0	350	.....
6079.05....	*Fe*	2	3	400	6.66	6195.46....	.....	0	0	350	.....
6081.44....	*V*	0	0	350	3.08	6199.14....	*V*	0	0	300	2.28
6082.75....	*Fe*	1	1	350	4.24	6200.37....	*Fe*	6	4	400	4.59
6084.12....	*Fe*$^+$	0	5	400	5.21	6204.62....	*Ni*	1	1	350	6.06
6085.23....	*Ti-Fe*	2	1	350	3.08	6213.38....	*Fe*	6	6	500	4.20
6086.29....	*Ni*	2	0	300	6.28	6215.20....	*Fe-Ti*	4	3	400	6.15
6089.60....	*Fe*	2	0	350	7.03	6216.32....	*V*	1	1	300	2.26
6090.20....	*V*	2	3	400	3.10	6219.34....	*Fe*	6	7	500	4.17
6091.18....	*Ti*	0	0	350	4.28	6220.80....	*Fe*	0	0	300	5.85
6093.70....	*Fe*	2	1	350	6.61	6224.02....	*Ni*	1	1	300	6.07
6094.41....	*Fe*	1	1	350	6.66	6226.80....	*Fe*	1	1	300	5.85
6096.65....	*Fe*	3	2	350	5.99	6229.19....	*Fe*	1	1	300	4.81
6102.15....	*Fe*	6	5	400	6.84	6230.76....	*Fe-V*	8	10	800	4.53
6102.71....	*Ca*	9	10	800	3.89	6232.70....	*Fe*	4	3	400	5.62
6103.25....	*Fe*	5[2]	3	400	6.84	6237.40....	*Si*	3	1	400	7.57
6105.14....	*Fe*	0	0	350	6.55	6238.45....	*Fe*$^+$	2	6	600	5.85
6108.15....	*Ni*	6	4	400	3.69	6239.92....	*Fe*$^+$	−1	2	400	5.85
6111.10....	*Ni*	2	1	350	6.09	6240.70....	*Fe*	3	2	300	4.19
6111.66....	*V*	0	1	350	3.06	6243.12....	*V*	1	1	300	2.28
6112.94....	.....	0	0	350	.....	6243.79....	*Si*	2	2	300	7.57
6113.33....	*Fe*$^+$	0	0	350	5.23	6244.46....	*Si-Sc*	2	1	300	7.57
6116.17....	*Ni-Fe*	4[2]	2	400	6.09	6245.64....	*Sc*$^+$	1	4	400	3.48
6119.60....	*V-Ni*	2[2]	1	350	3.08	6246.27....	*Fe*	7	6	500	5.56

TABLE 1—*Continued*

Chromosphere	Element	Sun	Flash	Height in Km	High E.P.	Chromosphere	Element	Sun	Flash	Height in Km	High E.P.
6247.56	Fe^+	2	10	800	5.85	6439.04	*Ca*	8	15	800	4.43
6252.51	*Fe*	7	8	600	4.37	6449.83	*Ca*	6	6	600	4.42
6254.28	*Fe-Si*	6[2]	7	600	4.24	6455.62	*Ca*	2	2	400	4.42
6256.43	*Fe-Ni*	6	6	600	4.42	6456.44	Fe^+	3	20	800	5.80
6258.11	*Ti*	3	2	400	3.41	6462.58	*Ca-Fe*	8[2]	12	800	4.42
6258.75	*Ti*	3	3	400	3.43	6469.26	*Fe*	2	3	400	6.72
6261.09	*Ti*	2	1	400	3.39	6471.63	*Ca*	5	3	400	4.42
6265.22	*Fe*	5	6	500	4.14	6475.58	*Fe*	2	2	400	4.45
6270.21	*Fe*	3	2	400	4.81	6481.83	*Fe*	3	3	400	4.17
6271.29	*Fe*	0	0	300	5.29	6482.76	*Ni*	1	2	400	3.83
6279.70	Sc^+	0	3	500	3.46	6491.65	Ti^+	1	6	800	3.95
6280.66	*Fe*	3	6	600	2.82	6493.74	*Ca*	6	6	800	4.41
6286.15	.....	0	0	300	.....	6494.95	*Fe*	8	10	800	4.29
6291.03	*Fe*	3	3	400	6.67	6496.40	*Fe*	2	2	400	6.67
6297.85	*Fe*	5	5	500	4.17	6496.88	Ba^+	4	30	1500	2.50
6300.23	.....	.....	1	300	.....	6499.00	*Fe*	1	1	300	2.85
6301.48	*Fe*	7	6	500	5.60	6499.68	*Ca*	4	2	300	4.41
6302.46	*Fe*	5	4	500	5.63	6501.69	*Fe*	0	0	300	.....
6311.50	*Fe*	1	1	350	4.77	6516.10	Fe^+	2	15	800	4.77
6314.73	*Ni*	4	4	400	3.88	6518.40	*Fe*	2	3	400	4.71
6315.34	*Fe*	3	3	400	6.08	6527.22	*Si*	1	0	400	7.74
6315.85	*Fe*	1	1	400	6.01	6532.89	*Ni*	0	0	300	3.82
6318.00	*Fe*	6	7	600	4.40	6546.24	*Fe-Ti*	6	4	400	4.63
6318.70	*Mg*	1	3	350	7.04	6556.09	*Ti*	1	1	400	3.34
6320.85	Sc^+	− 1	2	400	3.45	6559.59	Ti^+	0	1	400	3.92
6322.74	*Fe*	5	5	400	4.53	6569.28	*Fe*	4	3	400	6.59
6327.67	*Ni*	2	2	350	3.62	6562.80	*Hα*	40	200	12000	12.04
6330.10	*Cr*	2	0	300	2.89	6572.80	*Ce*	1	1	400	1.88
6330.85	*Fe*	2	2	350	6.66	6574.24	*Fe*	1	1	400	2.86
6335.28	*Fe*	6	7	500	4.14	6575.05	*Fe*	2	3	400	4.45
6336.90	*Fe*	7	8	500	5.62	6581.23	*Fe*	0	0	350	3.35
6338.89	*Fe*	2	2	400	6.72	6586.33	*Ni*	1	0	350	3.82
6339.12	*Ni*	2	2	400	6.08	6592.93	*Fe*	6	5	500	4.59
6344.14	*Fe*	4	3	400	4.37	6593.85	*Fe*	4	4	400	4.29
6347.05	Si^+	2	10	800	10.03	6597.58	*Fe*	2	0	350	6.65
6355.04	*Fe*	4	5	500	4.77	6598.62	*Ni*	0	0	350	6.09
6358.66	*Fe*	6	6	600	2.80	6604.58	Sc^+	1	3	400	3.22
6362.88	*Cr-Fe*	2	2	350	2.88	6609.18	*Fe*	3	2	400	4.42
6364.44	*Fe-Ni*	2[2]	2d	350	6.71	6625.05	*Fe*	1	0	350	2.87
6366.55	*Ni*	0	1	300	6.09	6627.57	*Fe*	3	0	350	6.39
6369.53	Fe^+	0	5	500	4.82	6633.79	*Fe-*	3[3]	2	400	6.40
6371.36	Si^+-*Fe*	1	7	800	10.02	6643.68	*Ni*	7	5	400	3.53
6378.26	*Ni*	7	0	350	6.07	6663.50	*Fe*	6[2]	3	400	4.27
6380.75	*Fe*	4	2	400	6.10	6678.10	*He-Fe*	8	30d	2200	22.97
6383.68	Fe^+	0	3	400	.....	6696.04	*Al*	2	2	400	4.97
6384.68	*Ni-Mn*	1	0	300	6.07	6703.60	*Fe*	3	2	300	4.59
6385.74	*Fe*	0	0	300	6.65	6705.10	*Fe*	4	3	300	6.43
6392.54	*Fe*	0	0	300	4.20	6715.40	*Fe-Cr*	2	1	350	6.43
6393.68	*Fe*	7	10	800	4.35	6717.75	*Ca*	8	3	400	4.53
6400.02	*Fe*	10[2]	12	800	5.52	6726.68	*Fe*	3	2	300	6.42
6407.28	Fe^+	0	3	500	5.80	6733.18	*Fe*	2	0	300	6.45
6408.00	*Fe*	5	6	600	5.60	6750.14	*Fe*	5	2	400	4.24
6411.72	*Fe*	7	8	600	5.56	6752.76	*Fe*	3	0	300	6.45
6414.82	*Ni-*	2[2]	2	400	6.06	6810.27	*Fe*	4	2	350	6.40
6416.98	Fe^+	1	4	600	5.80	6820.38	*Fe*	4	1	300	6.43
6419.94	*Fe*	4	3	600	6.64	6828.60	*Fe*	4	1	300	6.43
6421.45	*Fe*	7	6	600	4.19	6841.35	*Fe*	4	2	400	6.39
6430.88	*Fe*	7	8	800	4.09	6843.66	*Fe*	4	2	400	6.33
6432.63	Fe^+	1	10	800	4.80	6855.17	*Fe*	5	2	400	6.34
6433.46	*Fe*	0	0	350	6.10	6914.56	*Ni*	4	0	300	3.73
6436.45	*Fe*	0	2	400	6.09	6945.21	*Fe*	4	2	400	4.19

TABLE 1—*Continued*

Chromosphere	Element	Sun	Flash	Height in Km	High E.P.	Chromosphere	Element	Sun	Flash	Height in Km	High E.P.
6951.25....	*Fe*	6	2	350	6.31	7748.59....	*Fe-Ni*	15[2]	2	400	4.53
6978.86....	*Fe*	4	1	350	4.24	7771.95....	*O*	8	45	6000	10.69
6999.89....	*Fe*	4	1	300	5.85	7774.18....	*O*	6	30	6000	10.69
7016.07....	*Fe*	2	1	350	4.17	7775.39....	*O*	5	25	6000	10.69
7016.45....	*Fe*	4	1	350	5.90	8213.04....	*Mg*	4	2	400	7.23
7022.96....	*Fe*	4	1	350	5.93	8250.0.....	*H* 40	.....	0	500	13.53
7038.22....	*Fe*	5	1	350	5.95	8252.3.....	*H* 39	.....	0	500	13.53
7065.18....	*He*	.....	60	7500	22.62	8255.0.....	*H* 38	.....	0	500	13.53
7068.43....	*Fe*	7	2	350	5.80	8257.9.....	*H* 37	.....	1	600	13.53
7090.39....	*Fe*	7	1	350	5.95	8260.9.....	*H* 36	.....	1	600	13.53
7122.21....	*Ni*	10	2	350	5.26	8264.29....	*H* 35	.....	1	700	13.53
7130.93....	*Fe*	9	1	350	5.93	8267.95....	*H* 34	.....	1	800	13.53
7148.14....	*Ca*	12	2	300	4.42	8271.95....	*H* 33	.....	2	800	13.53
7164.43....	*Fe*	12	2	350	5.90	8276.33....	*H* 32	.....	2	900	13.53
7165.57....	*Si*	5	1	300	7.57	8381.14....	*H* 31	.....	2	1000	13.53
7187.36....	*Fe*	15	2	350	5.80	8286.43....	*H* 30	.....	2	1000	13.52
7197.02....	*Ni*	3	0	300	3.64	8292.31....	*H* 29	.....	3	1200	13.52
7202.21....	*Ca*	5	1	300	4.41	8298.84....	*H* 28	.....	4	1500	13.52
7207.40....	*Fe*	5	2	350	5.85	8306.11....	*H* 27	.....	5	1600	13.52
7281.35....	*He*	.....	5	2500	22.82	8314.27....	*H* 26	.....	6	1800	13.52
7307.96....	Fe^{+}-*Fe*	3	3	400	5.56	8323.43....	*H* 25	.....	6	2000	13.52
7310.20....	Fe^{+}	2	2	400	5.56	8327.06....	*Fe*	6	2	400	3.67
7320.69....	Fe^{+}-*Fe*	4	2	400	5.56	8333.79....	*H* 24	.....	8	1800	13.52
7326.16....	*Ca*	9	3	400	4.60	8345.55....	*H* 23	.....	10	2000	13.51
7389.39....	*Fe*	7	2	350	5.95	8346.13....	*Mg*	5	2	500	7.40
7393.61....	*Ni*	9	2	300	5.26	8359.01....	*H* 22	.....	12	2500	13.51
7400.19....	*Cr*	9	1	300	4.55	8374.49....	*H* 21	.....	15	2500	13.51
7405.80....	*Si*	9	2	350	7.26	8387.78....	*Fe*	9	2	400	3.64
7409.10....	*Si*	7	2	350	7.26	8392.41....	*H* 20	.....	18	2500	13.51
7411.16....	*Fe*	6	1	300	5.93	8413.33....	*H* 19	.....	20	3000	13.50
7415.96....	*Si*	8	2	350	7.26	8437.96....	*H* 18	.....	18	3500	13.50
7422.29....	*Ni*	6	1	300	5.28	8446.33....	*O*	.....	25	3000	10.94
7423.51....	*Si*	8	2	350	7.26	8446.76....	*O*	.....			10.94
7445.76....	*Fe*	8	2	350	5.90	8467.27....	*H* 17	.....	20	4500	13.49
7462.34....	*Cr*-Fe^{+}	10	3	400	4.55	8498.06....	Ca^{+}	.....	140	10000	3.14
7495.08....	*Fe*	9	2	300	5.85	8502.50....	*H* 16	.....	.....	.....	13.49
7511.03....	*Fe*	10	3	350	5.80	8542.14....	Ca^{+}	.....	160	12000	3.11
7555.61....	*Ni*	6	2	300	5.46	8545.39....	*H* 15	.....	.....	.....	13.48
7586.03....	*Fe*	10	2	300	5.92	8598.40....	*H* 14	.....	25	6000	13.47
7664.87....	*K*	12	2	400	1.61	8662.17....	Ca^{+}	.....	180	12000	3.14
7698.98....	*K*	10	2	400	1.61	8665.03....	*H* 13	.....	.....	.....	13.46
7711.74....	Fe^{+}	4	2	500	5.49	8736.04....	*Mg*	.....	2	500	7.33
7714.31....	*Ni*	8	1	300	3.53	8750.47....	*H* 12	.....	25	6500	13.45
7727.62....	*Ni*	8	1	300	5.26	8806.78....	*Mg*	.....	2	500	5.73
7742.62....	*Fe*	9	2	350	6.56	8862.9.....	*H* 11	.....	10	.....	13.43

AN INTERPRETATION OF THE HEIGHTS OF LINES IN THE SOLAR CHROMOSPHERE

RUPERT WILDT
Leander McCormick Observatory*
Received August 5, 1946

ABSTRACT

General theory.—The heights of different emission lines in the chromosphere, estimated from slitless flash spectrograms taken on a stationary plate, depend on the total number of emitting atoms contained in a column along the line of sight, on the threshold sensitivity of the photographic emulsion, and on the transparency of the earth's atmosphere and of the optical system. Theoretical intensities of a group of related lines originating from the same element are plotted against the estimated heights, H, and this plot is represented by a continuous function, $E(H)$. The transformation of $E(H)$ into the spatial density of the emitting atoms would be a straight problem of geometry if it were not for the interference of two physical effects introduced by the process of observation.

First, the extra-terrestrial surface brightness of the chromosphere is distorted by atmospheric scintillation, which produces a tremor disk around every surface element of the chromosophere as it appears in projection. Second, since during the photographic exposure the moon covers, or uncovers, part of the lower chromosphere, the light emitted at different levels is recorded with different exposure times; and, for lack of optical resolving-power, the chromospheric crescents portrayed on a flash spectrogram are an aggregate of superimposed images taken with varying exposure times. The correction of the observed function $E(H)$, obtained with a finite exposure time, to an infinitesimally short exposure, as it were, requires the solution of a certain integral equation, which can be effected simply by repeated differentiation. The resulting function, $f(H)$, can then be freed from the distortion by scintillation, which proves to be numerically insignificant. This procedure has been applied to the comprehensive list of heights of flash lines estimated by S. A. Mitchell.

Density gradients.—The radial decay of the density of hydrogen in the chromosphere is strictly exponential up to heights of the order of 15,000 km, numerically proportional to $\exp(-0.92 \times 10^{-8}\ \mathrm{cm}^{-1} H)$; the density gradients derived from the Balmer and the Paschen series are in good agreement. The same density gradient of hydrogen results from a comparison of the electron density at the base of the chromosphere with that at the elevation of 15,000 km, deduced by Baumbach from the absolute intensity of the continuous spectrum of the solar corona, because the free electrons are nearly all produced by the ionization of hydrogen, by far the most abundant element in the solar atmosphere.

The density laws of the metals can be represented as a sum of two or three exponentials. At heights less than 2000 km, their gradients are much steeper than that of hydrogen: but between 3000 and 6000 km they seem to approach the hydrogen gradient. The density gradients of *Fe* I and *Fe* II are compatible with the existence of ionization equilibrium with constant temperature throughout the chromosphere. Excitation temperatures for *Fe* I and *Ti* II are of the order of 3000°–4000° K and increase with increasing excitation potentials.

The density gradient of *He* I between 2000 and 6000 km is about one-quarter of that of hydrogen; the observations do not yield any confirmation of the density maximum of *He* I below the 2000 km claimed by other investigators.

Absolute densities.—On the Teller-Inglis theory, the quantum number ($n = 40$) of the last resolved member of the Paschen series implies an electron pressure of 0.11 dynes/cm^{-2} at the level $H = 500$ km. From this figure the partial pressure of hydrogen can be found if the abundance ratio, A, of hydrogen to all the electron-producing metals is known.

Relative abundances of *Na, Mg, Al, Ca, Fe, Cu,* and *Sr* in the chromosphere are derived from the estimated heights and from absolute transition probabilities; these ratios agree quite well with those found by Russell from the Fraunhofer spectrum. While the chromosphere appears to be well mixed as regards the metals, the abundance ratio, A, of hydrogen to the sum of the metals increases greatly with height. This variation of A is evaluated by a comparison of lines of *Fe* I and the Balmer series; and the extrapolated value of A at the base of the chromosphere agrees as to order of magnitude with that resulting from B. Strömgren's model of the solar photosphere. The numbers of atoms per cubic centimeter at the level $H = 500$ km are: $\log c_H = +15.63$ for neutral hydrogen, and $\log c_{Fe} = +9.53$ for neutral iron.

* Now at Yale University, Sloane Physics Laboratory and University Observatory.

The absolute densities of hydrogen and the metals thus determined lead to the conclusion that self-absorption in the tips of the chromospheric crescents is negligibly small.

Constitution of the chromosphere.—In the absence of a generally accepted theory of chromospheric support, it is of interest to point out that the chromospheric density gradient of hydrogen, which amounts to only 14 per cent of the hydrostatic gradient at the boundary temperature of the sun, corresponds to a kinetic temperature of the order of 35,000° K. This very figure also represents the line profiles, after careful correction for the instrumental pattern, of $H\beta$, $H\gamma$, and $H\delta$ as observed by Redman at the 1940 eclipse. The fact that the density gradients of the metals below 2000 km are about five times greater than that of hydrogen rules out the existence of any marked chromospheric turbulence distinguishable from thermal motions, i.e., of a kind which affects all atoms equally, irrespective of atomic weight.

Since the opacity of the solar atmosphere originates from the ionization continuum of the negative hydrogen ion, the radial distribution of continuous radiation at the extreme solar limb is determined by the density gradient of hydrogen. The predicted sharpness of the solar limb is seven times greater on the assumption of hydrostatic equilibrium at 5000° K than in the hypothetical case that the chromospheric gradient of hydrogen would continue downward unchanged for 500 km below the range covered by observations. Photometric observations of the sharpness of the solar limb, made by Lindblad at the 1945 eclipse, are in excellent agreement with the predicted hydrostatic gradient. Hence the chromosphere appears to have a rather well-defined lower boundary.

Some years ago S. A. Mitchell and E. T. R. Williams[1] discussed at length the density gradients in the solar chromosphere, which were derived from estimated "heights" of lines in the flash spectrum, and the relative abundance of elements in the chromosphere, which they deduced from the estimated total intensities of flash lines. They clearly enunciated the physical principles determining the heights attained by emission lines of the chromosphere; but, in evaluating the eclipse observations, they were handicapped by lack of many requisite spectroscopic data.

The present investigation has the advantage of being based on a revised system of estimated heights of flash lines, including the results obtained at the 1930 and 1937 eclipses. Especially valuable are the observations of the Paschen series of hydrogen, made in 1937. Moreover, a large amount of new spectroscopic data is now available, comprising the recent term analyses of numerous elements and also some theoretical and experimental values of transition probabilities. As regards the latter, there is still an unfortunate scarcity of data, and therefore no exhaustive discussion of the chromospheric heights is possible even now.

The writer is indebted to Dr. S. A. Mitchell for generously having placed at his disposal the extensive observational material assembled in the preceding paper.[2] Thanks are also due to Dr. Charlotte E. Moore, who kindly made available in draft form her Revised Multiplet Table; the definitive version of this work was invaluable, during the last stages of this investigation, for a final check on many dubious points.

I. THEORY OF THE HEIGHTS OF LINES IN THE FLASH SPECTRUM

The procedure followed by Mitchell and Williams was to plot the estimated heights of flash lines against the respective relative intensities predicted by spectroscopic theory, and then to match this graph with one of a series of similar graphs computed on different assumptions concerning the density gradients of the emitting atoms. Instead of this solution by trial and error, an explicit solution of the problem of finding the chromospheric density gradient from the observed emission gradient will be presented here. This analysis will include the discussion of the influence of two disturbing effects introduced by the process of observation: the distortion of the observed emission gradient by the atmospheric tremor disk and by the variation along the solar radius of the exposure time of the flash spectrum resulting from the moon's motion. However, for sake of clarity, a more elementary theory will be sketched first, and discussion of the scintillation and exposure-time effects will be taken up subsequently.

[1] *Ap. J.*, **77**, 1, 1933.

[2] *Ap. J.*, **105**, 1, 1947.

A. THE H_i-LOG I_i DIAGRAM

The surface brightness of the chromosphere in monochromatic light, of a certain line distinguished by the subscript i, is the energy emitted per unit time interval, into the unit solid angle, from the unit projected area:

$$I_i = \frac{A_i}{4\pi} h\nu_i n_i(x) \text{ [erg cm}^{-2} \text{ sec}^{-1} \text{ steradian}^{-1}\text{]}, \tag{1-1}$$

where A_i is the Einstein coefficient measuring the spontaneous transition probability downward from the atomic state under consideration; $h\nu_i$ is the energy of one quantum of radiation; and $n_i(x)$ is the number of atoms contained in a column of 1 cm^2 cross-section, extending along the line of sight through the chromosphere that passes above the solar limb at an elevation x. Equation (1-1) neglects the phenomena of self-absorption in the chromosphere, which will be considered later on. Quite generally, the height of a line attained on a slitless photograph of the flash spectrum, say $x = H_i$, is determined by that value of the surface brightness which corresponds to the threshold sensitivity of the photographic emulsion. Consequently, at the *tips* of the crescents of all chromospheric lines, photographed on the same plate with the same exposure time, the condition

$$I_i = \frac{A_i}{4\pi} h\nu_i n_i\,(H_i) = \text{const} \tag{1-2}$$

is satisfied, provided that the resolving-power of the optical system is such that the radial gradient of the surface brightness of the chromosphere is distinctly portrayed. If the resolving-power is insufficient, $n_i(H_i)$ in equation (1-2) has to be replaced by the integral over all the chromospheric strata contributing to the line, or

$$\int_{H_i}^{\infty} n_i\,(x)\,dx = N_i\,(H_i)\,; \tag{1-3}$$

so that the condition expressing the height attained by different flash lines now reads

$$\int_{H_i}^{\infty} I_i\,(x)\,dx = \frac{A_i}{4\pi} h\nu_i N_i\,(H_i) = \text{const}\,. \tag{1-4}$$

Equation (1-4) rather than equation (1-2) will apply to the optical systems conventionally used for photographing slitless flash spectra. It should be noted that the integration involved in equation (1-3) neglects the curvature of the solar limb; but, since the height of flash lines, with very few exceptions, is less than 1 per cent of the solar radius, no significant error can result from this simplification.

For any group of lines belonging to the same element and the same ionization stage, condition (1-4) assumes the form

$$\frac{A_i}{4\pi} h\nu_i N_{i0}\,(H_i)\,\frac{g_i'}{u_i\,(T)}\,e^{-\chi_i/kT} = \text{const} \tag{1-5}$$

if the existence of thermodynamic equilibrium be postulated; here $N_{i0}(H_i)$ is the *total* number of atoms (contained in the column specified above) in the ionization stage under consideration; g_i' is the statistical weight of the upper atomic state; $u_i(T)$ is the partition function; and χ_i is the excitation energy. Condition (1-5) can now be written as a difference equation,

$$\frac{\Delta \log\,[A_i\nu_i\,(g_i'/u_i)\,e^{-\chi_i/kT}]}{\Delta H_i} = -\frac{\Delta \log\,N_{i0}\,(H_i)}{\Delta H_i}\,, \tag{1-6}$$

which may be translated as follows: "If the logarithms of the theoretical intensities I_i of a group of related chromospheric lines of the same element—say, a multiplet or a series—are plotted against the heights H_i, the resulting graph can be read as a curve representing the radial stratification of this element, as appearing in projection on the plane perpendicular to the line of sight."

The "constant" appearing in equation (1-5) is really a function of the extinction in the terrestrial atmosphere, the transmission properties of the optical system, and the sensitivity of the photographic plate, all of which vary considerably with the wave length. Hence the theoretical intensities on the left side of equation (1-6) may require further corrections for instrumental effects in case the multiplet or series under discussion covers a wide range of wave lengths. For the numerical computation of the theoretical intensities, the equivalence of the following expressions should be remembered:

$$I_i \sim A_i \nu_i g_i' e^{-\chi_i/kT} \sim \nu_i^3 g_i f_i e^{-\chi_i/kT} \sim \nu_i^4 \left[S \frac{s}{\Sigma s} \right] e^{-\chi_i/kT}, \tag{1-7}$$

in which g_i' and g_i are the statistical weights of the upper and lower level, respectively, and f_i is the absorption oscillator strength. The product $g_i f_i$ in equation (1-7) is identical with the gf-values measured by R. B. King and A. S. King for numerous lines of *Fe* I and *Ti* I and *Ti* II. The expression $[(S/s\Sigma s)]$ refers to theoretical intensities derived from the sum rule.[3]

The usefulness of equations (1-2) and (1-4) is not restricted to comparing lines belonging to the same element. Suppose two lines emitted by different elements happen to reach the same height, H_i. Then the abundance ratio of these elements in the chromosphere can be determined from equation (1-2) if the absolute values of the transition probabilities are known. Since the density gradients of the two elements may differ, the abundance ratio found by this process will, in general, apply only to a limited range in height around H_i.

B. GEOMETRIC RELATIONS

The transformation of the observed surface brightness of the chromosphere, which is proportional to $n_i(H_i)$, into the spatial density or concentration (dimension cm^{-3}) of the emitting atoms involves the solution of a certain integral equation of Abel's type.[4] In practice this integral equation does not need to be solved numerically if an appropriate interpolation formula is chosen which represents the observed radial distribution of the surface brightness.

As the simplest case, assume that the unknown spatial density, $c(x)$, of the emitting atoms follows a strictly exponential law:

$$c(x) = c_0 e^{-\beta x}. \tag{1-8}$$

The projected density of atoms $n(x)$ is found by integrating equation (1-8) along the entire line of sight (y-co-ordinate), thus:

$$n(x) = \int_{-\infty}^{\infty} c(y)\, dy = \left(\frac{2\pi R_\odot}{\beta} \right)^{1/2} c_0 e^{-\beta x}, \tag{1-9}$$

where $R_\odot$ denotes the solar radius; for the derivation of equation (1-9) see A. Unsöld.[4a]

[3] For notation and numerical values see H. N. Russell, *Ap. J.*, **83**, 129, 1936; L. Goldberg, *Ap. J.*, **82**, 1, 1935, and **84**, 11, 1936; D. H. Menzel and L. Goldberg, *Ap. J.*, **84**, 1, 1936.

[4] Cf. S. Rosseland, *Theoretical Astrophysics* (Oxford, 1936,) p. 262.

[4a] *Physik der Sternatmosphären* (Berlin, 1938), p. 395 and Fig. 130.

By another integration it is found that

$$N(H) = \int_H^\infty n(x)\,dx = \left(\frac{2\pi R_\odot}{\beta^3}\right)^{1/2} c_0 e^{-\beta H} = \left(\frac{2\pi R_\odot}{\beta^3}\right)^{1/2} c(H)\,. \quad (1\text{-}10)$$

Thus, in this simple case the functions $N(H)$ and $c(H)$ differ only by a constant factor.

A much more complicated density law, $c(x)$, may be represented by a sum of exponential terms. Write

$$c(x) = c_0[\,e^{-\beta_1 x} + B e^{-\beta_2 x} + \ldots.\,]\,, \quad (1\text{-}11)$$

from which follow

$$n(x) = c_0 (2\pi R_\odot)^{1/2} [\beta_1^{-1/2} e^{-\beta_1 x} + \beta_2^{-1/2} B e^{-\beta_2 x} + \ldots.\,] \quad (1\text{-}12)$$

and

$$N(H) = c_0 (2\pi R_\odot)^{1/2} [\beta_1^{-3/2} e^{-\beta_1 H} + \beta_2^{-3/2} B e^{-\beta_2 H} + \ldots.\,]\,. \quad (1\text{-}13)$$

Writing this equation in the form

$$N(H) = c_0 \left(\frac{2\pi R_\odot}{\beta_1^3}\right)^{1/2} \left[\, e^{-\beta_1 H} + \left(\frac{\beta_1}{\beta_2}\right)^{3/2} B e^{-\beta_2 H} + \ldots.\right] \quad (1\text{-}14)$$

brings to light its similarity with equation (1-11) and indicates how $N(H)$ can simply be transformed into $c(x)$ after the observed values of $N(H)$ have been represented by an empirical formula of the type of equation (1-14). This is a function of great flexibility and is likely to be applicable to practically all important cases. As a matter of fact, Mitchell and Williams found a two-term function of the type of equation (1-11) well suited for representing the emission gradient of the metals in the chromosphere. The emission gradient of hydrogen obeys the still simpler law corresponding to equation (1-9), as will be shown in Section II.

C. EXPOSURE-TIME EFFECT

The elementary theory outlined before is strictly valid only for an infinitesimally short exposure of the flash spectrum. The actual exposure times of flash spectrograms are of the order of 1 second; and, even during such a short interval, the motion of the moon will cover up, or uncover, a substantial part of the lower chromosphere. Consequently, the integration along any solar radius (see eq. [1-4]) should preferably take into account the varying exposure time of the aggregate of intensities recorded on the photographic plate as a narrow chromospheric crescent. The geometry of this exposure-time effect is quite complicated, and therefore a rigorous analysis can be carried out here only for the case of a total exclipse which is central at the same time. In fact, this is the case which prevailed at the site where Dr. Mitchell secured the flash spectrogram of the 1905 eclipse, which contributed the principal weight to his system of estimated heights.

Since the photographic density produced by an intensity, I, acting during a time interval, T, is a function of the argument IT^p, where p is the Schwarzschild exponent, equation (1-4) must be replaced by

$$\int_{H_i}^\infty I_i(x)\,[T(x)]^p dx = \text{const}\,. \quad (1\text{-}15)$$

Let $I_i(x)$ be

$$I_i(x) = \frac{A_i}{4\pi} h\nu_i c_{0i} f(x)\,, \quad (1\text{-}16)$$

where A_i is the downward transition probability from the atomic state, distinguished by the index i; ν_i is the associated frequency; and c_{0i} is the concentration (cm^{-3}) of atoms

in the state i at the solar surface, which is adopted as reference level ($x = 0$). Equation (1-16) defines the respective chromospheric heights, H_i, reached by a group of related lines, which all obey the same intensity law $f(x)$ and have theoretical intensities proportional to $A_i \nu_i c_{0i}$. At this point it is convenient to introduce a new variable, E_i, defined by

$$E_i = \frac{\text{const}}{A_i \nu_i c_{0i}} . \tag{1-17}$$

By plotting the estimated heights, H_i, against the theoretical intensities, $A_i \nu_i c_{0i}$, or rather against their reciprocals, E_i, a discontinuous graph is obtained at first, which, in practice, will be approximated by a continuous function $E(H)$. Therefore, the index i will be

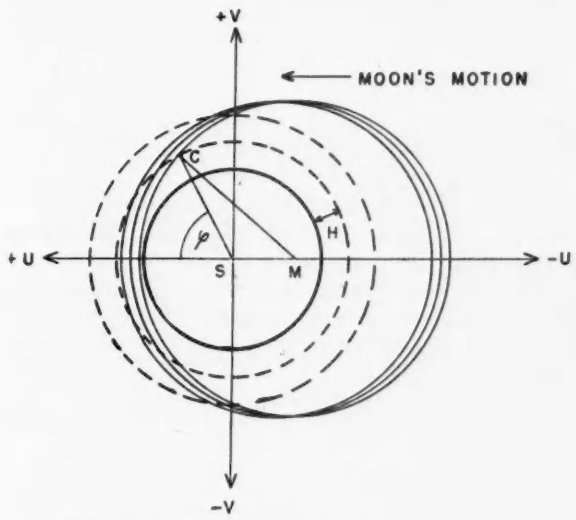

FIG. 1.—Geometric relations for a central total eclipse

omitted from now on. By substituting equations (1-16) and (1-17) into equation (1-15), it is found that

$$\int_H^\infty f(x)\,[T(x)]^n dx = E(H) . \tag{1-18}$$

In order to evaluate the variable exposure time, $T(x)$, consider the rate at which the moon's limb covers up the chromosphere. The diagram in Figure 1, which applies to a central eclipse, shows the position of the sun and of the moon at the exact time of the second contact, and two successive positions of the moon a short time later. Note the following expressions which define, respectively,

1. The limb of the sun: $u^2 + v^2 = R_\odot^2$, (1-19)
2. The isophotes of the chromosphere: $u^2 + v^2 = (R_\odot + h)^2$, (1-20)
3. The limb of the moon: $[u + D(t)]^2 + v^2 = R_\mathbb{C}^2$, (1-21)
4. The distance between the centers of sun and moon:

$$D(t) = R_\mathbb{C} - R_\odot - c\,(t - t_0) = 3.2 \times 10^9 \text{cm} - 3 \times 10^7\,(t - t_0)\ \text{cm} , \tag{1-22}$$

where $(t - t_0)$ is the time in seconds elapsed since the second contact. The numerical values of $R_{\mathbb{C}} - R_{\odot}$ and c refer to Dr. Mitchell's observations of the 1905 eclipse and will be used throughout this paper.

From the plane triangle, *CSM*, the following rigorous equation can be found for the rate at which the moon covers up the chromosphere:

$$h_2 - h_1 = \Delta h = + c\,(t_2 - t_1)\cos\varphi\,. \tag{1-23}$$

Here h_2 and h_1 denote the heights at which the moon's limb intersects, at the times t_2 and t_1, any ray φ = const. It is seen, then, that the rate of covering is uniform, though dependent on φ. From the same triangle, *CSM*, a simple approximate expression for the determination of φ can be derived, namely,

$$\cos\varphi = 1 - \frac{h}{R_{\mathbb{C}} - R_{\odot}} - \ldots\ldots \tag{1-24}$$

The neglected terms are of the order of $c(t_1 - t_0)/R_{\odot}$ and independent of h. By combining equation (1-24) with equation (1-23), we find

$$\Delta h = c\,(t_2 - t_1)\left[1 - \frac{h}{R_{\mathbb{C}} - R_{\odot}}\right], \qquad \frac{d\Delta h}{dh} = -\,c\,\frac{t_2 - t_1}{R_{\mathbb{C}} - R_{\odot}}, \qquad \frac{d^2\Delta h}{dh^2} \equiv 0\,. \tag{1-25}$$

The evaluation of the proper exposure time to be substituted in equation (18) is illustrated by Figure 2. The chromosphere outside the isophote $h = h_2$ receives the full exposure time $(t_2 - t_1)$, while over the range $h_1 < h < h_2$ there is only a fractional exposure of the duration

$$T = \frac{h - h_1}{h_2 - h_1}\,(t_2 - t_1)\,.$$

If we change the notation by putting

$$\begin{aligned} h_2 - h_1 &= \Delta h\,, \\ h_1 &= H\,, \\ h &= x\,, \end{aligned}$$

the exposure time becomes

$$\left.\begin{aligned} T\,(x) &= t_2 - t_1 \qquad \text{for} \qquad x > H + \Delta h \\ T\,(x) &= \frac{x - H}{\Delta h}\,(t_2 - t_1) \qquad \text{for} \qquad H < x < H + \Delta h\,. \end{aligned}\right\} \tag{1-26}$$

Equation (18) then assumes the form

$$(t_2 - t_1)^p \left\{\int_{H+\Delta h}^{\infty} f\,(x)\,dx + \int_{H}^{H+\Delta h} f\,(x)\left[\frac{x - H}{\Delta h}\right]^p dx\right\} = E\,(H)\,. \tag{1-27}$$

The factor $(t_2 - t_1)^p$ can be dropped, since $E(H)$ includes an undetermined constant factor, according to equation (1-17). Thus there results the following integral equation for the law of chromospheric surface brightness, $f(x)$, in terms of the function $E(H)$ given by the observations

$$E\,(H) = \int_{H+\Delta h}^{\infty} f\,(x)\,dx + \int_{H}^{H+\Delta h} f\,(x)\left[\frac{x - H}{\Delta h}\right]^p dx\,. \tag{1-28}$$

In the limiting case of an infinitesimally short exposure time, equation (1-28) reduces to the expression

$$\lim_{\Delta h \to 0} E(H) = \int_H^\infty f(x)\, dx, \tag{1-29}$$

which is identical with equation (1-4).

The further discussion of equation (1-28) is greatly simplified by putting the Schwarzschild exponent, p, equal to 1. According to laboratory evidence,[5] this is indeed the appropriate value for such high intensities (near the "optimal" intensity in the sense defined by Kron) as can be photographed with exposure times of from 0.1 to 10 seconds. Moreover, in a wide range around the "optimal" intensity the variation of p is quite small. It is believed, therefore, that no significant error is introduced into the following discussion by the assumption that $p = 1$.

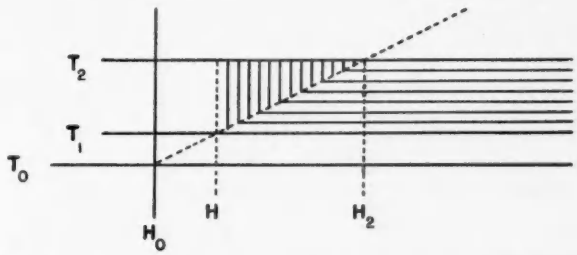

FIG. 2.—Variation of exposure time with height above the solar limb

Differentiation of equation (1-28) with respect to H now leads to

$$\frac{dE}{dH} = -\frac{1}{\Delta h}\int_H^{H+\Delta h} f(x)\left[1+\frac{x-H}{\Delta h}\frac{d\Delta h}{dH}\right]dx. \tag{1-30}$$

Note that, according to the theorem of the mean value of an integral, this equation is equivalent to the expression

$$E'(H) = -f(\bar{x})\left[1+\frac{1}{2}\frac{d\Delta h}{dH}\right], \qquad H \leqslant \bar{x} \leqslant H+\Delta h. \tag{1-31}$$

On differentiating equation (1-30) again with respect to H, we find, after some algebra,

$$\Delta h \frac{d^2E}{dH^2} = f(H) - f(H+\Delta h) - 2\frac{d\Delta h}{dH}\left[\frac{dE}{dH}+\left(1+\frac{1}{2}\frac{d\Delta h}{dH}\right)f(H+\Delta h)\right], \tag{1-32}$$

omitting a term

$$-\frac{d^2\Delta h}{dH^2}\int_H^{H+\Delta h} f(x)\left[\frac{x-H}{\Delta h}\right]dx,$$

because equation (1-25) stipulates

$$\frac{d^2\Delta h}{dH^2} \equiv 0.$$

[5] See C. E. K. Mees, *The Theory of the Photographic Process* (New York: Macmillan Co., 1942), pp. 242–43.

Write equation (1-32) as

$$\Delta h \frac{d^2E}{dH^2} + 2 \frac{d\Delta h}{dH} \frac{dE}{dH} \left[1 + \left(1 + \frac{1}{2} \frac{d\Delta h}{dH} \right) \frac{f(H+\Delta h)}{E'(H)} \right] = f(H) - f(H+\Delta h), \quad (1\text{-}33)$$

and substitute equation (1-31) for $E'(H)$ in the second term inside the brackets. Then

$$\Delta h \frac{d^2E}{dH^2} + 2 \frac{d\Delta h}{dH} \frac{dE}{dH} \left[1 - \frac{f(H+\Delta h)}{f(\bar{x})} \right] = f(H) - f(H+\Delta h) . \quad (1\text{-}34)$$

Since $f(x)$ is a monotonically decreasing function, the fraction $f(H + \Delta h)/f(\bar{x}) = \epsilon$ is confined to the range

$$0 \leqslant \epsilon \leqslant 1 . \quad (1\text{-}35)$$

Hence, equation (1-34) assumes the form

$$\Delta h \frac{d^2E}{dH^2} + 2(1-\epsilon) \frac{d\Delta h}{dH} \frac{dE}{dH} = f(H) - f(H+\Delta h) = F(H) , \quad (1\text{-}36)$$

where $F(H)$ is a monotonically decreasing, positive function of H, which for large values of H approaches zero asymptotically. Now form the following infinite series

$$\left.\begin{aligned} F(H) &= f(H) - f(H+\Delta h) , \\ F(H+\Delta h) &= f(H+\Delta h) - f(H+2\Delta h) , \\ &\cdots\cdots\cdots\cdots\cdots\cdots\cdots\cdots \\ F(H+n\Delta h) &= f(H+n\Delta h) - f(H+(n+1)\Delta h) , \end{aligned}\right\} \quad (1\text{-}37)$$

and perform a summation over n:

$$\sum_0^n F(H+n\Delta h) = f(H) - f(H+(n+1)\Delta h) . \quad (1\text{-}38)$$

The second term on the right side of this equation vanishes if the summation is extended to $n = \infty$. Therefore, if p be put equal to 1, the solution of the integral equation (1-28) is

$$f(H) = \sum_{n=0}^{\infty} \left\{ \Delta h \frac{d^2}{dH^2} E(H+n\Delta h) + 2(1-\epsilon) \frac{d\Delta h}{dH} \frac{d}{dH} E(H+n\Delta h) \right\} . \quad (1\text{-}39)$$

As an illustration, assume that the observed law of chromospheric emission along the solar radius can be represented by a purely exponential decay of the form

$$E(H) \sim e^{-\gamma H} . \quad (1\text{-}40)$$

With the differential quotients

$$E'(H+n\Delta h) \sim -\gamma e^{-\gamma(H+n\Delta h)}$$

and

$$E''(H+n\Delta h) \sim +\gamma^2 e^{-\gamma(H+n\Delta h)} ,$$

it follows that

$$f(H) \sim \left[\frac{\gamma^2 \Delta h\, e^{-\gamma H}}{1 - e^{-\gamma \Delta h}} - 2(1-\epsilon) \frac{d\Delta h}{dH} \frac{\gamma e^{-\gamma H}}{1 - e^{-\gamma \Delta h}} \right] , \quad (1\text{-}41)$$

or

$$f(H) \sim \frac{\gamma \Delta h}{1 - e^{-\gamma \Delta h}} \left[1 - \frac{2(1-\epsilon)}{\gamma \Delta h} \frac{d\Delta h}{dH} \right] \gamma e^{-\gamma H} . \quad (1\text{-}42)$$

With regard to the observed values of γ, which will be discussed later on, it may already be stated here that the second term in the brackets of equation (1-42) never exceeds $0.002(1-\epsilon)$ and can therefore be neglected altogether; for infinitesimally short exposures the quantity ϵ approaches $+1$, according to equation (1-35), and the term with the coefficient $(1-\epsilon)$ vanishes. Moreover, for infinitesimally short exposures, the quantity Δh vanishes, too, and equation (1-42) reduces to

$$\lim_{\Delta h \to 0} f(H) = \gamma e^{-\gamma H} . \tag{1-43}$$

This expression is indeed the correct limiting form of equation (1-30), for $E(H) \backsim \exp[-\gamma H]$, or

$$\lim_{\Delta h \to 0} \frac{dE(H)}{dH} = -f(H) . \tag{1-44}$$

If $E(H)$ can be represented as a sum of the form

$$E(H) \sim [e^{-\gamma_1 H} + b e^{-\gamma_2 H}] , \tag{1-45}$$

we find from equations (1-39) and (1-42), neglecting the terms proportional to $(1-\epsilon)$,

$$f(H) \sim \left[\frac{\gamma_1^2 \Delta h\, e^{-\gamma_1 H}}{1 - e^{-\gamma_1 \Delta h}} + b \frac{\gamma_2^2 \Delta h\, e^{-\gamma_2 H}}{1 - e^{-\gamma_2 \Delta h}}\right] . \tag{1-46}$$

If equation (1-40) is compared with (1-42) and (1-45) with (1-46), it is seen that eliminating the exposure-time effect does not preserve exactly the type of the original function, since $f(H)$ differs from $E(H)$, not by constant factors, but by the slowly varying functions

$$\frac{\gamma \Delta h}{1 - e^{-\gamma \Delta h}} \tag{1-47}$$

with (see eq. [1-25])

$$\Delta h = c\,(t_2 - t_1)\left[1 - \frac{H}{R_{\mathfrak{C}} - R_{\odot}}\right] .$$

However, the variation with H of the expression (1-47) is much smaller than that of $\exp[-\gamma H]$; and, in view of the limited accuracy of the observations determining $E(H)$, it may be assumed that it is always possible to fit to equation (1-42) a new curve of the form

$$f(H) \sim e^{-\beta H} \tag{1-48}$$

where β differs very little from γ. Likewise, a curve of the form

$$f(H) \sim [e^{-\beta_1 H} + b' e^{-\beta_2 H}] \tag{1-49}$$

can be fitted to the function (1-46).

D. THE EFFECT OF SCINTILLATION

The estimated heights of the flash lines correspond to angular elevations above the solar limb of a few seconds of arc. It so happens that the tremor disk, which is formed around every stellar image by the fluctuating refraction anomalies in the earth's atmosphere, has an angular diameter of the same order of magnitude. Hence it becomes necessary to examine to what extent atmospheric scintillation distorts the extra-terrestrial distribution of surface brightness over the chromosphere. Until the present investigation was far advanced, the writer had assumed that the influence of scintillation is automati-

cally included in equations (1-4) and (1-28), because the radial decay of intensity had been integrated from the lunar limb to infinite height. This procedure was suggested by the fact that on Dr. Mitchell's flash spectrograms (focal length of the concave grating = 180 cm) the entire radial decay of intensity is compressed, as it were, into a very narrow image; in other words, the width of the photographically recorded crescent is not much greater than the diameter of a focal stellar image.

There remains, nevertheless, a certain ambiguity in the interpretation of the estimated heights, which depends upon the answer to the following question: What is the physical quantity which defines the "termination" of a chromospheric crescent at a certain point and thereby the "height" assigned to the flash line by visual inspection of the photographic negative? Is it (*A*) the *radial integral* over the intensity, as implied by equations (1-4) and (1-28), or is it, perhaps, (*B*) the *maximum intensity* attained somewhere above the lunar limb? It does not appear obvious that these two hypotheses are equivalent in so far as the derivation of the extra-terrestrial intensity law $f(H)$ from the observed function $E(H)$ is concerned; and the situation is further obscured by the simultaneous action of varying exposure time and scintillation. But, in fact, the alternative definitions (*A*) and (*B*) of the termination of the chromospheric crescents lead to extra-terrestrial intensity laws that are identical for all practical purposes. Perhaps this will be taken as an indication that here subtlety has been carried too far. The real purpose of the following analysis is to insure that the remarkable difference between the chromospheric density gradient of hydrogen and that of the metals, which will require a physical explanation, is not the specious product of scintillation.

As a plausible representation of the intensity distribution throughout the tremor disk, T. M. Wanders[6] has introduced a scintillation function of bell-shaped type,

$$I(R) = I_0 \frac{s}{\pi} e^{-sR^2},$$

where I_0 is the extra-terrestrial intensity of a point source; R is the angular distance from the center of the tremor disk, measured in seconds of arc; and s is a scintillation parameter having the dimension [seconds of arc]$^{-2}$; the factor s/π normalizes the integral taken over the entire tremor disk. Numerical values of s[7] have been derived from measurements on large-scale photographs of the sharpness of the solar limb. The scintillation parameter s varies from 0.02 (strong scintillation) to 0.10 (excellent seeing), but it is well to remember that these figures refer to daytime observing conditions near the solar limb. Figure 3 illustrates the intensity distribution over the tremor disk for different conditions of seeing. It also contains a straight line, whose slope represents the emission gradient of hydrogen in the chromosphere, to be derived subsequently, which happens to be of the same order of magnitude as the average intensity gradient along the radius of the tremor disk. It is this suspicious similarity between the gradients portrayed on Figure 3 which prompted the present investigation of the scintillation effect. The emission gradients of the metals to be derived in Section III are, in the lower chromosphere, from ten to twenty times steeper than the emission gradient of hydrogen and, therefore, cannot well be reproduced on the scale of Figure 3.

The first step is to find the scintillation-distorted surface brightness, i, of the chromosphere for an infinitesimally short exposure time, during which the motion of the moon can be disregarded. In terms of $I(h)$, the extra-terrestrial surface brightness, the result is

$$i(h, H) = \int_{H-h}^{\infty} dx \int_{-\infty}^{\infty} I(h+x) \frac{s}{\pi} e^{-s(x^2+y^2)} dy = \left(\frac{s}{\pi}\right)^{1/2} \int_{H-h}^{\infty} I(h+x) e^{-sx^2} dx, \quad (1\text{-}50)$$

[6] *Zs. f. Ap.*, **8**, 108, 1934.

[7] *Ibid.*; P. ten Bruggencate and E. von der Pahlen, *Zs. f. Ap.*, **16**, 99, 1938; P. ten Bruggencate and J. Houtgast, *Zs. f. Ap.*, **20**, 152, 1940.

if two approximations to the true geometric situation (see Fig. 4) are introduced. As before, the curvature of the isophotes of the atmosphere has been neglected. Moreover, the angle α included between the isophotes $x = \text{const}$ and the moon's limb has been put equal to zero; the resulting error is negligible for present purposes, as can be shown by a rigorous analysis, which will be omitted here for sake of brevity. The integral (1-50) applies to all values of h, both greater and smaller than H, the height of the moon's limb above the sun's limb at the particular solar radius. Actually, a good deal of light is scattered into the field covered by the moon. If equation (1-50) is integrated over all heights, it follows that

$$\int_{-\infty}^{\infty} i\,(h,\,H)\,dh = \sqrt{\frac{s}{\pi}} \int_{-\infty}^{\infty} dh \int_{H-h}^{\infty} I\,(h+x)\; e^{-sx^2} dx = \int_{H}^{\infty} I\,(h)\,dh\,, \quad (1\text{-}51)$$

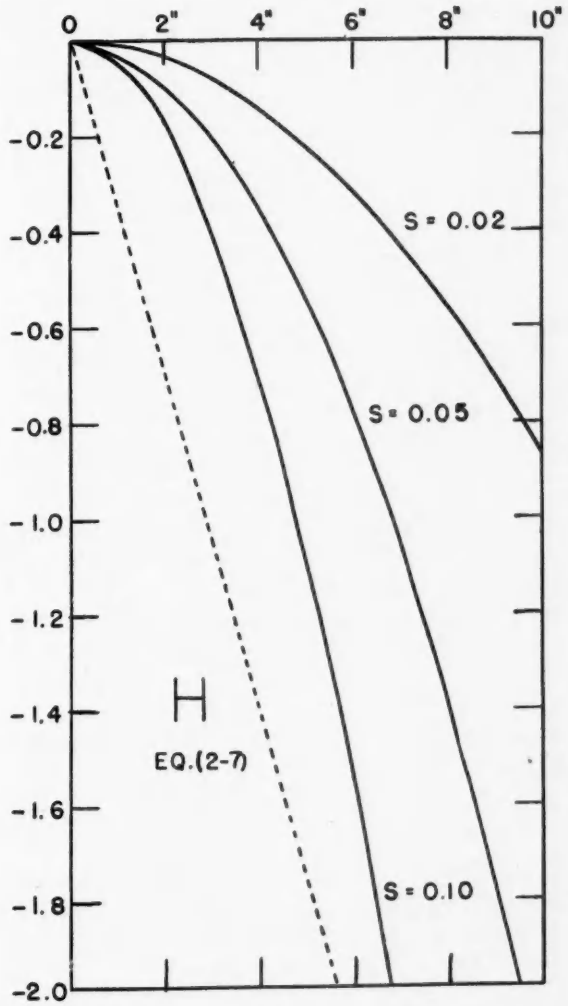

FIG. 3.—Intensity distribution in the tremor disk of an extra-terrestial point source. *Abscissae*, distance from center of tremor disk, in seconds of arc; *ordinates*, logarithm of intensity.

as it ought to be, since scintillation only redistributes the total intensity available. Equation (1-51) is the precise expression of the tacit assumption underlying equations (1-4) and (1-28)—that the entire radial decay of the chromospheric intensity is compressed into such a small, starlike image that the influence of scintillation is automatically taken care of.

During a finite exposure of the length $t_2 - t_1$, the photographic plate will record an aggregate of intensities which is given by the time integral over equation (1-51), or with respect to equations (1-16) and (1-17):

$$\int_{t_1}^{t_2} dt \int_{H}^{\infty} I(h)\, dh = \frac{\text{const}}{E_i(H_i)} \int_{t_1}^{t_2} dt \int_{H_i}^{\infty} f(x)\, dx . \tag{1-52}$$

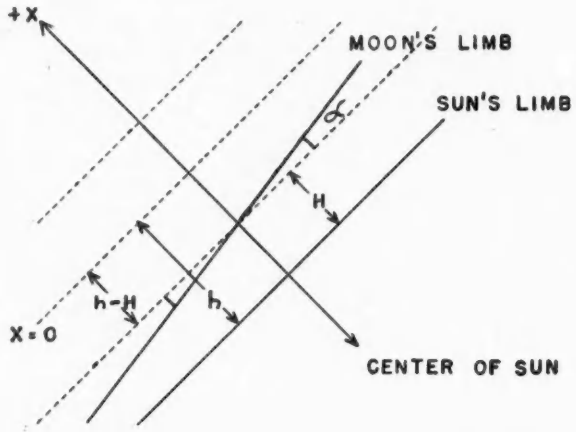

FIG. 4.—Geometry of the scintillation effect near the solar limb

Implicitly, the Schwarzschild exponent, p, has here again been put equal to 1. For any group of related lines which obey the same intensity law $f(x)$, but reach different heights H, it is found from equation (1-52) that

$$E(H) = \int_{t_1}^{t_2} dt \int_{H}^{\infty} f(x)\, dx . \tag{1-53}$$

If this expression, which corresponds to equation (1-18), is integrated by parts with respect to t, it follows that

$$\left.\begin{aligned} E(H) &= t_2 \int_{H_2}^{\infty} f(x)\, dx - t_1 \int_{H_1}^{\infty} f(x)\, dx - \int_{t_1}^{t_2} t \frac{\partial}{\partial t} \left[\int_{H}^{\infty} f(x)\, dx \right] dt \\ &= (t_2 - t_1) \int_{H_2}^{\infty} f(x)\, dx - t_1 \int_{H_1}^{H_2} f(x)\, dx + \int_{t_1}^{t_2} t f(H) \frac{dH}{dt}\, dt \\ &= (t_2 - t_1) \int_{H_2}^{\infty} f(x)\, dx + \int_{H_1}^{H_2} (t - t_1)\, f(x)\, dx . \end{aligned}\right\} \tag{1-54}$$

This last equation may be written as

$$\left.\begin{aligned}\frac{1}{t_2-t_1}E(H) &= \int_{H_2}^{\infty} f(x)\,dx + \int_{H_1}^{H_2} f(x)\left[\frac{t-t_1}{t_2-t_1}\right]dx \\ &= \int_{H+\Delta h}^{\infty} f(x)\,dx + \int_{H}^{H+\Delta h} f(x)\left[\frac{x-H}{\Delta h}\right]dx,\end{aligned}\right\} \quad (1\text{-}55)$$

which reveals its identity with equation (1-28), because of the relation

$$\frac{t-t_1}{t_2-t_1} = \frac{x-H_1}{H_2-H_1} = \frac{x-H}{\Delta h},$$

which was illustrated by Figure 2. The constant factor $(t_2 - t_1)^{-1}$ on the left side of equation (1-55) can be omitted as before because, by definition, $E(H)$ includes an undetermined constant of proportionality. Thus it is demonstrated that, on hypothesis A, the explicit combination of the effects of scintillation and varying exposure leads to the same integral equation as that which resulted from the straightforward analysis of the exposure-time effect alone.

On hypothesis B, it is equation (1-50) instead of equation (1-51) which has to be integrated with respect to t for an exposure of the duration $t_2 - t_1$. Let

$$J(h, H) = \left(\frac{s}{\pi}\right)^{1/2} \int_{t_1}^{t_2} dt \int_{H-h}^{\infty} I(h+x)\, e^{-sx^2} dx. \quad (1\text{-}56)$$

This function $J(h, H)$ represents the total energy producing the photographic image, if again the Schwarzschild exponent is put equal to 1; it has a maximum at a certain point $h = \bar{h}$, at which the photographic density of the chromospheric crescent assumes a peak value. According to hypothesis B, it is this maximum that the observer apprehends in estimating the point of termination of the crescent, which, in turn, fixes the "height" assigned to the line under inspection.

Now let equation (1-56) be subjected to the same series of transformations which lead from equation (1-52) to equation (1-55). After some algebra it is found that

$$\left.\begin{aligned}\frac{1}{t_2-t_1}\left(\frac{\pi}{s}\right)^{1/2} J(h, H) &= \int_{H+\Delta h-h}^{\infty} I(h+x)\, e^{-sx^2} dx \\ &\quad + \int_{H-h}^{H+h-h} \left[\frac{h+x-H}{\Delta h}\right] I(h+x)\, e^{-sx^2} dx\end{aligned}\right\} \quad (1\text{-}57)$$

or

$$\left.\begin{aligned}E(h, H) &= \int_{H+\Delta h-h}^{\infty} f(h+x)\, e^{-sx^2} dx \\ &\quad + \int_{H-h}^{H+\Delta h-h} \left[\frac{h+x-H}{\Delta h}\right] f(h+x)\, e^{-sx^2} dx.\end{aligned}\right\} \quad (1\text{-}58)$$

Since hypothesis B assumes that the observed function E has been established by focusing attention upon the peak value of the photographic density located at $h = \bar{h}$, it is appropriate to write the integral equation for the desired function $f(x)$ as

$$E^*(H) = \int_{H+\Delta h-\bar{h}}^{\infty} f(\bar{h}+x)\, e^{-sx^2} dx + \int_{H-\bar{h}}^{H+\Delta h-\bar{h}} \left[\frac{\bar{h}+x-H}{\Delta h}\right] f(\bar{h}+x)\, e^{-sx^2} dx. \quad (1\text{-}59)$$

Note that Δh has not been affected by this change, because it is a function of H only. After introducing a new variable, $u = \bar{h} + x$, equation (1-59) reads

$$E^*(H) = \int_{H+\Delta h}^{\infty} f(u)\, e^{-s(\bar{h}-u)^2} du + \int_{H}^{H+\Delta h} \left[\frac{u-H}{\Delta h}\right] f(u)\, e^{-s(\bar{h}-u)^2} du\,; \quad (1\text{-}60)$$

and, by the substitution

$$\psi(u) = f(u)\, e^{-s(\bar{h}-u)^2}, \quad (1\text{-}61)$$

it assumes the final form

$$E^*(H) = \int_{H+\Delta h}^{\infty} \psi(u)\, du + \int_{H}^{H+\Delta h} \left[\frac{u-H}{\Delta h}\right] \psi(u)\, du. \quad (1\text{-}62)$$

This integral equation is of the same type as equation (1-28), the solution of which was treated in the preceding section. Hence, from equation (1-39) and its subsequent discussion, it follows that

$$\psi(H) = \sum_{n=0}^{\infty} \left\{ \Delta h \frac{d^2}{dH^2} E^*(H + n\Delta h) \right\} = f(H)\, e^{-s(\bar{h}-H)^2}. \quad (1\text{-}63)$$

In other words, if the observed function $E(H)$ is transformed into the extra-terrestrial surface brightness by proceeding on the alternative hypotheses A and B, alternative functions $f(H)$ result, which are related by

$$f_A(H) = f_B(H)\, e^{-s(\bar{h}-H)^2}. \quad (1\text{-}64)$$

In order to test how far these two solutions differ, $\bar{h}$ must be evaluated from equation (1-57). Differentiating this equation with respect to h and putting the differential quotient equal to zero, it is found that

$$\int_{H+\Delta h-\bar{h}}^{\infty} I(\bar{h}+x)\, x\, e^{-sx^2} dx + \int_{H-\bar{h}}^{H+\Delta h-\bar{h}} \left[\frac{\bar{h}+x-H}{\Delta h}\right] I(\bar{h}+x)\, x\, e^{-sx^2} dx = 0, \quad (1\text{-}65)$$

or

$$\int_{H+\Delta h}^{\infty} I(u)\,(\bar{h}-u)\, e^{-s(\bar{h}-u)^2} du + \int_{H}^{H+\Delta h} \left[\frac{u-H}{\Delta h}\right] I(u)\,(\bar{h}-u)\, e^{-s(\bar{h}-u)^2} du = 0. \quad (1\text{-}66)$$

Substitute equation (1-61) into equation (1-66) and split the remaining factor $(\bar{h} - u)$ as follows:

$$\bar{h} - u = (\bar{h} - H) + (H - u).$$

Then $(\bar{h} - H)$ can be readily eliminated from the resulting equation, viz.,

$$\left.\begin{aligned} &(\bar{h}-H)\left\{\int_{H+\Delta h}^{\infty} \psi(u)\, du + \int_{H}^{H+\Delta h} \left[\frac{u-H}{\Delta h}\right] \psi(u)\, du\right\} \\ &+ \int_{H+\Delta h}^{\infty} (H-u)\,\psi(u)\, du + \int_{H}^{H+\Delta h} \left[\frac{u-H}{\Delta h}\right] (H-u)\,\psi(u)\, du = 0. \end{aligned}\right\} \quad (1\text{-}67)$$

Explicit expressions for $\bar{h} - H$ can now be obtained substituting $\psi(u)$ from equation (1-63) into equation (1-67) and evaluating the integrals. For instance, if $E^*(H)$ obeys equation (1-40), it follows from equation (1-42) that

$$\psi(H) = \frac{\gamma^2 \Delta h\, e^{-\gamma H}}{1 - e^{-\gamma \Delta h}}. \quad (1\text{-}68)$$

When this expression is substituted in equation (1-67), the factor in brackets can be placed outside the integrals, since, according to equation (1-25), Δh is practically a constant, except for very large values of H—in which case the exponential $e^{-\gamma H}$ is too small for Δh to affect the integration of $\psi(u)$. Hence to a very good approximation, it is found after integration of equation (1-67) that

$$\bar{h} - H = \frac{1}{\gamma}\left[1 - \frac{\gamma \Delta h}{e^{\gamma \Delta h} - 1}\right]; \tag{1-69}$$

and equation (1-64) becomes

$$f_A(H) = f_B(H) \exp\left\{-\frac{s}{\gamma^2}\left[1 - \frac{\gamma \Delta h}{e^{\gamma \Delta h} - 1}\right]^2\right\}. \tag{1-70}$$

It is then seen that the alternative functions, f_A and f_B, differ only by what amounts to a practically constant factor.

On the other hand, if $E^*(H)$ obeys the more complicated law (1-45), it follows from equation (1-46) that

$$\psi(H) \sim \left[\frac{\gamma_1^2 \Delta h\, e^{-\gamma_1 H}}{1 - e^{-\gamma_1 \Delta h}} + b\frac{\gamma_2^2 \Delta h\, e^{-\gamma_2 H}}{1 - e^{-\gamma_2 \Delta h}}\right], \tag{1-71}$$

and integration of equation (1-67) then leads to

$$\bar{h} - H = \frac{\frac{1}{\gamma_1}\left[1 - \frac{\gamma_1 \Delta h}{e^{\gamma_1 \Delta h} - 1}\right] e^{-\gamma_1 H} - \frac{1}{\gamma_2}\left[1 - \frac{\gamma_2 \Delta h}{e^{\gamma_2 \Delta h} - 1}\right] b\, e^{-\gamma_2 H}}{e^{-\gamma_1 H} + b\, e^{-\gamma_2 H}}. \tag{1-72}$$

In this case, $\bar{h} - H$ is essentially a weighted mean of $1/\gamma_1$ and $1/\gamma_2$. Although the weighting factors are functions of H, the resulting variation with H of the exponential in equation (1-64) is rather small. The factors in brackets in equations (1-69) and (1-72) are restricted to the range

$$0 \leqslant \left[1 - \frac{\gamma \Delta h}{e^{\gamma \Delta h} - 1}\right] \leqslant 1. \tag{1-73}$$

By combination of this inequality with equation (1-72) we find that

$$0 \leqslant \bar{h} - H \leqslant \frac{1}{\gamma_2}\left[1 - \frac{\gamma_2 \Delta h}{e^{\gamma_2 \Delta h} - 1}\right]$$

and

$$1 \geqslant \left[\frac{f_A(H)}{f_B(H)} = e^{-s(\bar{h} - H)^2}\right] \geqslant \exp\left\{-\frac{s}{\gamma_2^2}\left[1 - \frac{\gamma_2 \Delta h}{e^{\gamma_2 \Delta h} - 1}\right]^2\right\}. \tag{1-74}$$

For good seeing, the observations quoted above suggest the value

$$s = 0.05\ (1'')^{-2} \approx 0.10 \times 10^{-16} \mathrm{cm}^{-2},$$

since, at solar distance, $1''$ equals about 7.2×10^7 cm. An application of equations (1-64) and (1-74) will be given in Section III, where the density gradients of *Fe* I and *Ti* II are evaluated. As pointed out before, the divergence between the alternative solutions f_A and f_B will prove to be numerically insignificant.

II. THE HYDROGEN CHROMOSPHERE

The prominence of the Balmer series in the flash spectrum is a manifestation of the overwhelming abundance of hydrogen in the solar atmosphere. Indeed, as D. H. Menzel

has so aptly remarked, the outer envelope of the sun may be regarded as consisting of "chemically pure," though not "spectroscopically pure," hydrogen. The determination of the density gradient of hydrogen, therefore, should reveal the structure of the bulk of the chromosphere. Attempts in this direction have already been undertaken, among others by A. Pannekoek and M. G. J. Minnaert[8] and by G. G. Cillié and D. H. Menzel.[9] These investigations rely on the photometry of the total intensities of the Balmer lines in the flash spectrum—in other words, the emission integrated along the solar radius over all chromospheric levels; the interpretation of such measurements requires careful consideration of the phenomena of self-absorption in the Balmer lines.

A different approach to the problem of the hydrogen density gradient is afforded by the use of the estimated heights of the Balmer series as a measure of the energy emitted at the respective levels of termination. While this method turns out to be practically free from interference by the effect of self-absorption, an essentially hypothetical factor has to be introduced into the reduction of the observations, namely, the distribution of the hydrogen atoms over the various excited levels, according to equation (1-5). The assumption of thermodynamic equilibrium, with a constant temperature throughout the entire chromosphere, is the most convenient one. But its adoption should not be construed as a contention that thermodynamic equilibrium does prevail in the chromosphere. The following analysis is rather intended to test how far the interpretation of the observational data can be carried by such a schematic model.

From the intensities in the Balmer continuum, at λ 3540 and λ 3500, a temperature of about 10,000° K for the free electrons in the chromosphere has been deduced by G. G. Cillié and D. H. Menzel.[10] It appears, however, that in the numerical evaluation of equation (3.3) of their paper the factor $\log e = 0.434$ was omitted.[11] The results of two independent determinations of the electron temperature really are 5240° K and 4010° K; the individual exposures refer to moments when the moon's edge was 670 and 1700 km, respectively, beyond the sun's limb. The mean value $T = 4625°$ K does not differ very much from the theoretical boundary temperature of the sun, $T_0 = 4830°$ K, according to E. A. Milne;[12] the corresponding effective temperature is $T = 5740°$ K. More recently, G. F. W. Mulders has found $T_0 = 5050°$ K, taking into account the blanketing effect of the Fraunhofer lines.[13] For the present purpose it is preferable to retain Milne's value, because it was used by B. Strömgren for his analysis of the composition of the solar atmosphere.[14] The following investigations aim to establish a model of the chromosphere that merges into Strömgren's model pertaining to the deeper levels of the solar atmosphere.

A. THE DENSITY GRADIENT DERIVED FROM BALMER AND PASCHEN SERIES

In thermodynamic equilibrium a total concentration n_H of neutral hydrogen atoms is distributed over the excited levels according to the Boltzmann formula

$$c_n = \frac{2n^2}{u_0}\, c_H 10^{-\chi_n \vartheta_0}, \qquad (2\text{-}1)$$

where c_n denotes the concentration of atoms excited to the level, with the principal quantum number n, and χ_n is the corresponding excitation potential, measured in elec-

[8] *Verh. Kon. Akad. v. Wetensch., Amsterdam*, Vol. **13**, No. 5, 1928.

[9] *Harvard College Obs. Cir.*, No. 410, 1935.

[10] *Ap. J.*, **85**, 88, 1937.

[11] The writer is indebted to Dr. E. T. R. Williams for having brought this fact to his attention.

[12] *Phil. Trans. R. Soc. London*, A, **223**, 201, 1922.

[13] *Zs. f. Ap.*, **11**, 143, 1935.

[14] *Festschrift für E. Strömgren* (Copenhagen, 1940), p. 214.

tron-volts; the numerical value of the parameter $\theta_0 = 5040°/T_0$ is assumed to be 1.043 throughout the chromosphere ($T_0 = 4830°$ K). By combining equation (2-1) with that of the ionization equilibrium of hydrogen,

$$c_e c_{H+} = \frac{2u_1}{u_0} c_H \left(\frac{2\pi mkT_0}{h^2}\right)^{3/2} 10^{-13.54\theta_0}, \tag{2-2}$$

we can express the concentration of the excited atoms as function of the concentrations c_{H+} and c_e, of protons and electrons by

$$c_n = \frac{n^2}{u_1} c_e c_{H+} \left(\frac{h^2}{2\pi mkT_0}\right)^{3/2} 10^{(13.54-\chi)\theta_0}, \tag{2-3}$$

where the partition function u_1 of the hydrogen ion equals 1. Energy is emitted spontaneously by the population of excited atoms at the rate

$$E_{nn'} = A_{nn'} h\nu_{nn'} c_n \text{ [erg cm}^{-3} \text{ sec}^{-1}\text{]}. \tag{2-4}$$

The $A_{nn'}$'s are the Einstein coefficients of hydrogen, as tabulated by D. H. Menzel and C. L. Pekeris.[15] Expressed on a logarithmic scale, equation (2-4) becomes, after substitution of c_n from equation (3),

$$\log E_{nn'} = \log (A_{nn'} h\nu_{nn'}) + \log n^2 + (13.54 - \chi_n)\theta_0 + \log c_e c_{H+} - 20.91 . \tag{2-5}$$

Evidently, the rate of emission is practically independent of the assumed temperature of the chromosphere, for the higher members of the hydrogen series. Numerical values of the first three terms on the right side of equation (2-5) are listed in Table 1; their sum is the predicted rate of emission, tabulated as log $E_{nn'}$ in Figure 5. Table 1 also contains the estimated heights of the hydrogen lines, which are plotted against log $E_{nn'}$ in Figure 5. Inspection of this plot reveals that, up to elevations of about 3000 km, the logarithmic gradient of the emission has the constant value

$$\frac{d \log E}{dH} = -0.40 \times 10^{-8} \text{cm}^{-1}$$

or

$$E(H) \sim e^{-(0.92\times10^{-8}\text{cm}^{-1})H}, \tag{2-6}$$

which appears to be the same for the Balmer and the Paschen series. The two straight lines in Figure 5 represent this average gradient, constant throughout the lower chromosphere. The vertical distance of these two lines, which is about 0.50, happens to coincide approximately with the average of log E_{n2} − log E_{n3}, which is about 0.52; this numerical coincidence is fortuitous, because the heights of the Paschen series were estimated on a spectrogram (secured at the 1937 eclipse) taken with a different dispersion on infrared-sensitive film.

At elevations greater than 3000 km, the plot of the estimated heights begins to deviate from the straight lines shown in Figure 5. Strictly speaking, the ordinates of Figure 5 should be corrected for instrumental effects dependent on the wave length, such as atmospheric extinction, transmission loss in the optical system, and variation of the threshold sensibility of the photographic emulsion. This color correction has been determined empirically by a statistical analysis of numerous metallic multiplets, which will be described in Section III. Between the Balmer limit and λ 4000, the influence of the λ-correction on the gradient defined by equation (2-6) is quite negligible. Figure 6 shows a plot of the Balmer lines from *Hα* to *H*19 with the empirical color correction applied to the ordinates, and evidently the representation is now markedly improved, except

[15] *M.N.*, **96**, 77, 1935.

TABLE 1

THEORETICAL RATE OF EMISSION AND CHROMOSPHERIC HEIGHTS OF THE HYDROGEN SERIES

n	log $A_{nn'}h_{nn'}$ Unit [Erg Sec^{-1}]		log $n^2+(13.54-\chi_n)\theta_0$ $\theta_0=1.043$	Balmer Series				Paschen Series			
				λ	Height		log $E_{nn'}$ + Const.	λ	Height		log $E_{nn'}$ + Const.
	$n'=2$	$n'=3$			1905/25	1930/37			1937		
3	−3.88	.....	+2.52	6562.82	.....	12,000	−1.36	.....	.....		.....
4	4.47	−5.03	2.09	4861.33	8500	9000	2.39	.....	.....		−2.94
5	4.94	5.48	1.96	4340.47	8000	8000	2.98	12,818.05	.....		3.52
6	5.33	5.86	1.95	4101.74	8000	8000	3.38	10,938.09	.....		3.91
7	5.67	6.18	1.98	3970.07	8500	8000	3.69	10,049.38	.....		4.20
8	5.95	6.47	2.03	3889.05	8500	8000	3.92	9545.97	.....		4.44
9	6.21	6.73	2.08	3835.39	7000	7000	4.13	9229.02	.....		4.65
10	6.44	6.95	2.14	3797.90	6000	6000	4.30	9014.91	.....		4.81
11	6.64	7.16	2.20	3770.63	6000	6000	4.44	8862.79	.....		4.96
12	6.83	7.35	2.25	3750.15	6000	6000	4.58	8750.47	6500		5.10
13	7.01	7.52	2.31	3734.37	5600	6000	4.70	8665.02	.....		5.21
14	7.16	7.68	2.36	3721.94	5600	5500	4.80	8598.39	6000		5.32
15	7.31	7.85	2.41	3711.97	5000	4500	4.90	8545.38	.....		5.44
16	7.45	7.98	2.46	3703.86	4000	4000	4.99	8502.49	.....		5.52
17	7.59	8.10	2.51	3697.15	3500	3500	5.08	8467.26	4500		5.59
18	7.71	8.22	2.55	3691.56	3000	3500	5.16	8437.96	3500		5.67
19	7.83	8.36	2.60	3686.83	3000	3000	5.23	8413.32	3000		5.75
20	7.94	8.45	2.63	3682.81	2500	2500	5.31	8392.40	2500		5.82
21	8.05	8.56	2.67	3679.36	2500	2500	5.38	8374.48	2500		5.89
22	8.14	8.66	2.71	3676.36	2200	2500	5.43	8359.01	2500		5.95
23	8.24	8.76	2.75	3673.76	2000	2000	5.49	8345.55	2000		6.01
24	8.33	8.85	2.78	3671.48	2000	2000	5.55	8333.79	1800		6.07
25	8.42	8.94	2.82	3669.47	1800	1800	5.60	8323.43	2000		6.12
26	8.51	9.02	2.85	3667.68	1800	1800	5.66	8314.26	1800		6.17
27	8.59	9.10	2.88	3666.10	1500	1500	5.71	8306.11	1600		6.22
28	8.67	9.18	2.91	3664.68	1500	1500	5.76	8298.84	1500		6.27
29	8.75	9.26	2.94	3663.41	1200	1200	5.81	8292.31	1200		6.32
30	8.82	9.33	2.97	3662.26	1200	1500	5.85	8286.43	1000		6.36
31	8.89	9.40	2.99	3661.22	1000	1000	5.90	8281.13	1000		6.41
32	8.96	9.47	3.02	3660.28	.....	1000	5.94	8276.31	900		6.45
33	9.03	9.54	3.05	3659.42	.....	1000	5.98	8271.93	800		6.49
34	9.09	9.61	3.07	3658.64	750	800	6.02	8267.94	800		6.54
35	9.15	9.67	3.10	3657.93	750	800	6.05	8264.29	700		6.57
36	9.21:	9.73:	3.12	3657.27	500	600	6.08::	8260.94	600		6.61::
37	−9.27:	9.79:	3.15	3656.67	500	500	−6.11::	8257.86	600		6.64::
38	.....	9.84:	3.17	3656.14	.....	.....	.....	8255.15	500		6.67::
39	.....	9.89:	3.19	.....	.....	.....	.....	8252.3	500		6.70::
40	.....	−9.94	+3.21	.....	.....	.....	.....	8250.0	500		−6.73::
∞	.....	.....	.....	3645.98	.....	.....	.....	8203.57	.....		.....

for $H\beta$ and $H\gamma$. The lines $H\alpha$ and $H\delta$ lie very close to the extrapolated gradient defined by equation (2-6); and, since $H\epsilon$ and $H\zeta$ are blended with lines of *Ca* II and *He* I, their true heights should lie farther to the left on Figure 6. It is impossible to determine the variation of the λ-correction along the Paschen series, since no suitable metallic multiplets are available in this range. However, between λ 8400 and λ 8250 this variation should be much too small to be of any practical consequence; hence the emission gradient of the Paschen series should be unaffected up to elevations of about 3000 km. The earlier members of the Paschen series, which attain heights of between 3000 and 6000 km, fall into a region of the spectrum where the sensitivity of the emulsion (Eastman 1-F)

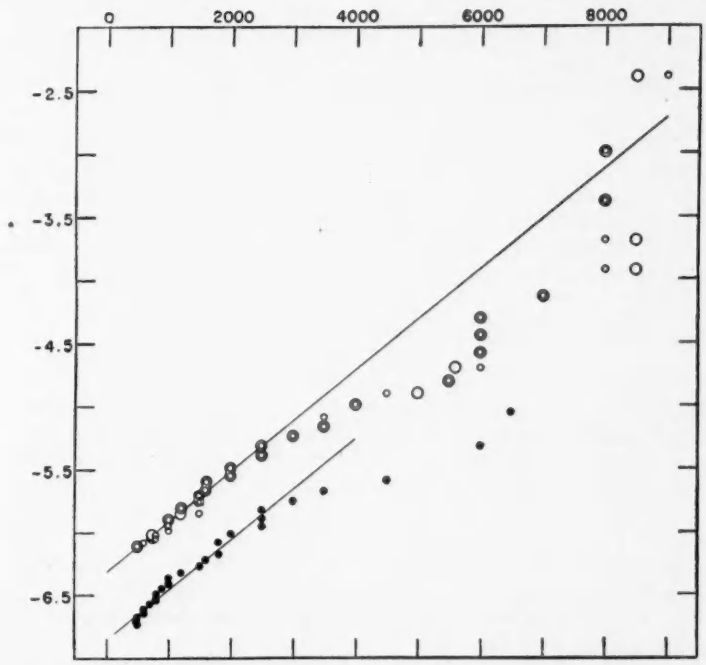

FIG. 5.—H − log I diagram of the Balmer series (*open circles*) and Paschen series (*filled circles*); the larger open circles refer to the heights estimated from the eclipse spectra of 1905 and 1925, and the smaller ones to the eclipses of 1930 and 1937.

gradually decreases toward greater wave lengths; the unknown correction for this effect would make the symbols of the earlier members of the Paschen series fall even more below the straight line shown in Figure 5.

The remaining deviations of the plot from a straight line can hardly be ascribed to irregularities of the moon's limb affecting the estimated heights, since the results obtained at different eclipses appear to be concordant. Formally, the deviation might be interpreted as a change of the excitation temperature at the higher levels of the chromosphere. Cillié and Menzel[16] have tried to determine from the integrated intensities of the Balmer series the numbers of hydrogen atoms occupying the several excited levels and have found, for the earlier series members, deviations of the order of 50 per cent from the distribution which would prevail in thermodynamic equilibrium. But they have not taken self-absorption into account, which would affect primarily the earlier

[16] *Harvard College Obs. Circ.*, No. 410, 1935.

series members. It will be demonstrated later on that the emission gradient derived from Figure 5 is free from distortion by self-absorption. It seems probable, therefore, that some of the remaining deviations from the gradient defined by equation (2-6) are caused by accidental errors in the estimated heights.

By substituting the observed emission gradient $E(H)$ given by equation (2-6) into equation (1-39), it is found from equation (1-42) that

$$f(H) \sim e^{-(0.92\times10^{-8}\,\mathrm{cm}^{-1})H},$$

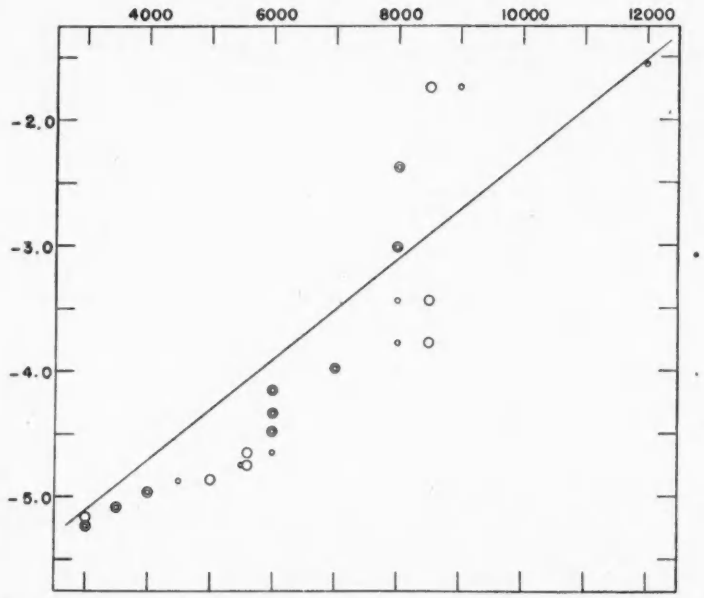

FIG. 6.—$H-\log I$ diagram of the Balmer series, based on the same observations as Fig. 5; the intensity logarithms of Fig. 5 have been corrected by adding the empirical color corrections ΔC, shown in Fig. 7.

because the variability of the factors dependent on Δh is negligibly small up to $H=$ 10,000 km. Furthermore, according to equations (1-16) and (1-9), the extra-terrestrial surface brightness of the chromosphere, $f(H)$, is in this case directly proportional to the spatial density of the emitting atoms. Hence

$$c_H = c_{H_0} e^{-(0.92\times10^{-8}\,\mathrm{cm}^{-1})H}, \qquad (2\text{-}7)$$

where c_{H_0} denotes the concentration (cm^{-3}) of hydrogen atoms at the level of the solar limb; and H is the elevation above the limb, measured in centimeters. In the next paragraph an attempt will be made to determine the constant c_{H_0}, without relying upon absolute measurements of the intensities of the hydrogen lines in the chromosphere.

B. THE ABSOLUTE DENSITY OF HYDROGEN IN THE CHROMOSPHERE

The electron pressure at the base of the chromosphere can be estimated from the theory of the termination of the Balmer series by intermolecular Stark effect. D. R. Inglis and E. Teller[17] have derived a simple relation between the principal quantum

[17] *Ap. J.*, **90**, 439, 1939.

number n of the last resolved Balmer line and the number, c^*, of broadening, charged particles per cubic centimeter:

$$\log c^* = 23.26 - 7.5 \log n \ . \tag{2-8}$$

At temperatures $T < 10^5/n$, c^* is the number of ions *plus* electrons, while at temperatures $T > 10^5/n$ the electrons make no contribution to the broadening because their velocities are too high. In the solar chromosphere the last observed member is $n = 37$ in the Balmer series and $n = 40$ in the Paschen series, according to Table 1. Hence the second case is realized, and, at the chromospheric level $H = 500$ km, the number per cubic centimeter of positive ions is

$$\log c^* = +11.50 \ , \qquad c^* = 3.16 \times 10^{11} \text{ (Balmer series)} \ ;$$

and

$$\log c^* = +11.24 \ , \qquad c^* = 1.74 \times 10^{11} \text{ (Paschen series)} \ .$$

The smaller of these two values, derived from the Paschen series, is to be preferred; that in the Balmer series the last resolved member has a smaller n may be attributed to the lesser separation (in angstrom units) of the successive members and to blending. On the assumption that the majority of particles are only singly ionized, these figures also represent the density of electrons; and with the boundary temperature of the sun ($T_0 = 4830°$ K) the electron pressure (from the Paschen series) is found to be, at the level $H = 500$ km,

$$\log p_e = -0.94 \ , \qquad p_e = 0.11 \text{ dynes cm}^{-2} \ . \tag{2-9}$$

These electrons are largely the product of the first ionization of the metals in the chromosphere. It is not possible, therefore, to substitute equation (2-9) in equation (2-2) for the purpose of finding the number of neutral hydrogen atoms. Rather, it becomes necessary to consider the simultaneous ionization of hydrogen and the metals, which will be treated as if they had all the same ionization potential of about 7.8 electron-volts.

There are, first, the two Saha equations,

$$p_e p_{H+} = K_H p_H \qquad \text{and} \qquad p_e p_{M+} = K_M p_M \tag{2-10}$$

and the equation of electric neutrality,

$$p_e = p_{H+} + p_{M+} \ . \tag{2-11}$$

Second, the abundance ratio A of hydrogen to metals is, by definition,

$$A = \frac{p_H + p_{H+}}{p_M + p_{M+}} \ . \tag{2-12}$$

By combining equations (2-10), (2-11), and (2-12), we find

$$p_H = \frac{p_e^2}{K_H} \left[1 + \frac{1}{A} \frac{1 + p_e/K_H}{1 + p_e/K_M} \right]^{-1} \ . \tag{2-13}$$

Thus the partial pressure of neutral hydrogen can be computed from the observed value (2-9) of the electron pressure and an assumed value of A. In the reversing layer, B. Strömgren[18] found $\log A = +3.90$. Since the chromosphere might well be relatively richer in hydrogen, A will be treated as a disposable constant.

With $\log K_H = -5.38$ and $\log K_M = +1.03$—this is the equilibrium constant for

[18] *Op. cit.*

the first ionization of iron (I.P. = 7.86 volts)[19]—there result pairs of A and $\log p_H$ listed in lines 1 and 2 of Table 2; in line 3, $\log c_H = \log p_H - 12.18$ (at $T_0 = 4830°$ K) are also given. These figures refer to the chromospheric level $H = 500$ km, since the electron pressure (2-9) was substituted in equation (2-13). By extrapolation with the observed density gradient (2-7), there results the hypothetical density c_{H_0} given in line 4 of Table 2. Application of the Boltzmann corrections,

$$\left.\begin{aligned} \log (4 \times 10^{-10.16 \times 1.043}) &= -9.99 \\ \log (9 \times 10^{-12.04 \times 1.043}) &= -11.60 , \end{aligned}\right\} \qquad (2\text{-}14)$$

leads to the densities c_{B_0} and c_{P_0} of atoms in the ground state of the Balmer and Paschen series, respectively, the logarithms of which are listed in lines 5 and 6 of Table 2. Lines 7 and 8 of the same table give the total numbers of atoms in the ground state of the

TABLE 2

MODEL OF HYDROGEN CHROMOSPHERE

1*	$\log A$	+ 3.90	+ 4.40	+ 4.90	+ 5.40	+ 5.90	+ 6.40	∞
2	$\log p_H$	2.85	3.18	3.37	3.45	3.48	3.50	+ 3.50
3	$\log c_H$	15.03	15.36	15.55	15.63	15.65	15.68	15.68
4	$\log c_{H_0}$	15.23	15.56	15.75	15.83	15.85	15.88	15.88
5	$\log c_{B_0}$	5.24	5.57	5.76	5.84	5.86	5.89	5.89
6	$\log c_{P_0}$	3.63	3.90	4.15	4.23	4.25	4.28	4.28
7	$\log \bar{c}_B$	13.28	13.61	13.80	13.88	13.90	13.93	13.93
8	$\log \bar{c}_P$	11.67	12.00	12.19	12.27	12.29	12.32	12.32
9	$\log n_{B_0}$	15.08	15.41	15.60	15.68	15.70	15.73	15.73
10	$\log n_{P_0}$	+13.47	+13.80	+13.99	+14.07	+14.09	+14.12	+14.12

* The numbered lines have the following values:
1, assumed abundance ratio of hydrogen to metals
2, partial pressure (dynes cm^{-2}) } of hydrogen atoms at level $H = 500$ km
3, partial density (cm^{-3}) }
4, 5, 6, density of atoms at level $H = 0$ km { hydrogen total; Balmer ground state; Paschen ground state
7, 8, total number of atoms in a radial column of 1 cm^2 cross-section, extending from base of chromosphere to infinite height
9, 10, total number of atoms in a transverse column of 1 cm^2 cross-section, passing the sun at the base of the chromosphere.

Balmer and Paschen series, respectively, that are contained in a radial column of 1 cm^2 cross-section, extending from the chromospheric level, $H = 0$ km, upward to infinity. These figures were obtained by integration of equation (1-8),

$$\log \bar{c}_B = \log c_{B_0} - \log \beta ,$$

where $\beta = 0.92 \times 10^{-8}$ cm^{-1} has been taken from equation (2-7). Finally, lines 9 and 10 of Table 2 bring the total numbers of atoms in the ground states of the Balmer and the Paschen series that are contained in a transverse column of 1 cm^2 cross-section, passing at the height $H = 0$ km above the solar limb; these figures, which were computed from equation (1-9) with

$$\log \sqrt{2\pi R_\odot / \beta} = +9.84 ,$$

[19] Russell and Moore, *Trans. Amer. Phil. Soc.*, **34**, 113, 1944.

will be required subsequently for evaluating the amount of self-absorption in the tips of the crescents of the chromospheric hydrogen lines.

If we anticipate some results to be derived later on, the abundance ratio of hydrogen to iron at the level $H = 500$ km is $\log Z(H : Fe) = +6.10$, according to the last line of Table 10. Furthermore, iron amounts to about 10–30 per cent, by numbers of atoms, of all the metals in the chromosphere, as will be shown in Section V, *B*. Hence, at the level $H = 500$ km, $\log A$ has a value of the order $+5.8$–5.1. Entering into the column headed $+5.40$ of Table 2, we find from lines 2 and 4 that

$$\left.\begin{aligned} \log p_H\,[\text{dynes cm}^{-2}] &= +3.45 \quad \text{at} \quad H = 500 \text{ km}, \\ \log c_H\,[\text{cm}^{-3}] &= +15.83 \quad \text{at} \quad H = 0 \text{ km}, \end{aligned}\right\} \tag{2-15}$$

and, by substitution of the last figure in equation (2-7), it follows, finally, that

$$\left.\begin{aligned} c_H &= (6.76 \times 10^{15}\text{cm}^{-3})\; e^{-(0.92\times10^{-8}\text{cm}^{-1})H}, \\ p_H &= (4.47 \times 10^{3} \text{ dynes cm}^{-2})\; e^{-(0.92\times10^{-8}\text{cm}^{-1})H} = 10^{+3.65-(0.40\times10^{-8}\text{cm}^{-1})H}. \end{aligned}\right\} \tag{2-16}$$

TABLE 3

DENSITY GRADIENT OF HYDROGEN FROM ELECTRON DENSITIES

1.....	$\log A$	3.90	4.40	4.90	5.40	5.90	6.40	∞
2.....	$\log p_H$	2.85	3.18	3.37	3.45	3.48	3.50	3.50
3.....	$\Delta \log p_H$	4.73	5.06	5.25	5.33	5.36	5.38	5.38
4.....	$\beta \times 10^8$	0.78	0.83	0.86	0.88	0.88	0.88	0.88

There is another indirect way of estimating the density gradient of hydrogen in the chromosphere: by combining the observed values of $\log p_H$ at the elevation $H = 500$ km (see l. 2 of Table 2) with values applying to the upper chromosphere, which can be derived, on certain assumptions, as follows:

Since K. Schwarzschild first made this suggestion, the continuous spectrum of the solar corona has generally been attributed to photospheric light scattered by free electrons. From a thorough discussion of numerous measurements of the brightness of the corona, S. Baumbach[20] has deduced the density of the free electrons in the corona as a function of the radial distance from the solar limb. The extrapolation of this curve right down to the solar limb would be somewhat risky, because its slope is quite steep. Therefore, Baumbach's curve will be extrapolated only from $H = 30''$ to $H = 20'' = 14{,}500$ km; this is about the "height" of the strongest chromospheric lines, like $H\alpha$ and H and K of *Ca* II. With $\log c_e = +8.55$ and $T_0 = 4830°$ K, or $\log p_e = -3.63$, the partial pressure of neutral hydrogen is found from equation (2-13) to be

$$\log p_H = -1.88 \quad \text{at} \quad H = 14{,}500 \text{ km}.$$

The first two lines of Table 3 are transferred from Table 2; they give $\log p_H$ at $H = 500$ km for different values of A. The next two lines give $\Delta \log p_H$, corresponding to $\Delta H = 14{,}500 - 500$ km, and the density gradient expressed as the exponent in equation (2-7), namely, $0.43\,\beta = \Delta \log p_H / \Delta H$. The computed values of β (in l. 4) deviate less than 5 per cent from 0.92×10^{-8} cm^{-1}, which is the slope of the straight lines drawn on Figure 5 through the Balmer and the Paschen series.

[20] *A.N.*, **263**, 121, 1937.

Conversely, if the partial pressure of hydrogen at $H = 14{,}500$ km is computed from equation (2-16), the result is $\log p_H = -2.15$; and, by equation (2-13), the corresponding electron pressure is $\log p_e = -3.76$, instead of the figure -3.63 derived above by slight extrapolation of Baumbach's curve. This discrepancy may be entirely attributed to the uncertainty of the extrapolation.

It is of interest, finally, to compare the density gradients of hydrogen deduced here with the earlier determinations based upon a photometry of the Balmer series (see the first three lines of Table 4). Only the second and third of the values of β in Table 4 have been corrected for self-absorption; their divergence has been taken by Cillié and Menzel as an indication that the structure of the chromosphere may vary from one eclipse to the next. In Section V, *C*, it will be shown that the fourth value does not require any correction for self-absorption.

III. METALS IN THE CHROMOSPHERE

In principle, the analysis of the density gradients of the metals follows the same lines as demonstrated for the case of hydrogen. But in practice, two obstacles are encountered: first, the lack of knowledge of the absolute, or even the relative, values of the transition

TABLE 4

COMPARISON OF DENSITY GRADIENTS OF HYDROGEN

β	Authors	Method
1.62×10^{-8} cm^{-1}	Pannekoek and Minnaert (1927)	Photometry
0.60×10^{-8}	Menzel (1930)	
1.60×10^{-8}	Cillié and Menzel (1932)	
0.92×10^{-8}	This paper, eq. (2–7), above	Estimated heights
0.88×10^{-8}	Baumbach (1937); and Table 3, above	Electron densities
6.9×10^{-8}	Hydrostatic equilibrium, $T_0=4830°$ K	Theoretical prediction

probabilities of many interesting lines and, second, the rather small heights of the majority of metallic lines and the narrow range in height covered by many multiplets. Very few metallic lines reach heights greater than 2000 km, and most of these are not suitable for combining with low-level lines of the same element, for one reason or another. A further restriction on combining lines for the derivation of density gradients is imposed by the necessity of avoiding large differences in excitation potential, which would require application of large Boltzmann corrections.

A. THE *H*-LOG *I* DIAGRAM FOR *Fe* I AND *Ti* II

There are only two spectra, *Fe* I and *Ti* II, that are well developed in the chromosphere and, at the same time, rich in lines whose *f*-values are known from experimental laboratory determinations.[21] The estimated heights of these lines were first plotted against the logarithms of the theoretical intensities, that is, $\log \nu^3 gf$, according to equation (1-7). Each multiplet in this plot defines the segment of a curve analogous to Figure 5. Then each segment had to be shifted parallel to the $\log I$ axis until all of them were joined up into a single curve, with the smallest possible scatter of the plotted points representing the individual lines. This task was accomplished in two steps.

It was soon noticed that in related multiplets having the upper level in common, but with the lower levels widely separated, lines with identical values of $\log \nu^3 gf$ did not reach the same chromospheric heights. But the respective plots of such multiplets, which, by definition, are located in widely separated regions of the spectrum, could be brought to

[21] R. B. and A. S. King, *Ap. J.*, **87**, 24, 1938; **94**, 27, 1941; **95**, 78, 1942.

coincidence by applying a shift ΔC parallel to the log I axis. This shift represents the combined effects of the variation, along the spectrum, of (1) the atmospheric extinction, (2) the transmission loss in the optical system, and (3) the threshold sensitivity of the photographic emulsion. By using suitable pairs of multiplets of all the metals, this shift ΔC was determined empirically as a function of the wave length and was then applied as "color correction" to each multiplet of *Fe* I and *Ti* II. The smoothed average curve of ΔC, shown in Figure 7, is not very reliable from λ 3500 to the ultraviolet end, and particularly so at wave lengths greater than λ 6000. These adopted quantities ΔC do not refer to any particular set of observational conditions prevailing at a certain eclipse, but rather characterize the composite system of chromospheric heights established by Dr. Mitchell's estimates on flash spectrograms secured with different instruments.

On the new plot (log $I + \Delta C$ against log v^3gf) the points fall clearly into different groups along parallel curves, according to the upper excitation potentials of the multiplets. The distances between these curves, measured parallel to the log I axis, are the differential Boltzmann corrections pertaining to the respective pairs of multiplets, or $\Delta E(5040/T)$, where T is the excitation temperature and E the excitation potential in volts. It is possible thus to determine the excitation temperatures by utilizing the esti-

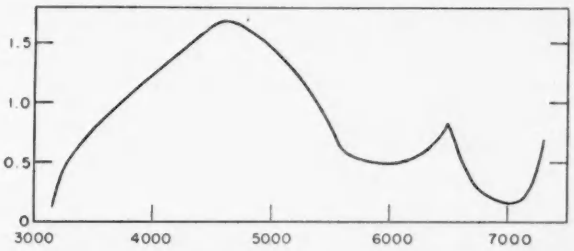

FIG. 7.—Empirical color correction, ΔC, comprising the variation along the spectrum of photographic sensitivity, reflection loss in the optical system and atmospheric extinction.

mated heights instead of the integrated photometric intensities of the chromospheric lines, as was done by W. Petrie.[22] The actual values of chromospheric excitation temperatures derived from estimated heights are given in Table 5; strictly speaking, these are average values of the excitation temperatures applying to a range in excitation potential of about 0.5–1.0 volt. The temperatures set down in Table 5 are sensitive to small variations in the adopted color corrections, ΔC, and their uncertainty is considerable, though difficult to evaluate numerically. Nevertheless, it is believed that the two principal features apparent in Table 5 are real, namely, the steady increase of the excitation temperature with increasing excitation potential and the fact that, for E.P. < 4 volts, the excitation temperature is definitely smaller than the boundary temperature of the sun. The results agree with Petrie's findings; average excitation temperatures, according to Petrie's mean curve for all elements, are given in the last column of Table 5, opposite *Fe* I.

By using these excitation temperatures, all the *Fe* I lines for which absolute f-values (King) were available (14 multiplets altogether) were combined into a single H-log I diagram, shown in Figure 7 as large dots. The same diagram contains five further multiplets ($z^7F^o-e^7D$, $z^7P^o-e^7D$, $z^5F^o-e^5F$, $z^5P^o-e^5D$, $z^3D^o-e^3D$) with higher excitation potentials, the lines marked by open circles; sum-rule intensities, checked by laboratory intensities in several cases, were used for these multiplets. Each of these five multiplets was first plotted separately, and the mean log I at $H = 800$ km was determined; these

[22] *J. R. Astr. Soc. Canada*, **38**, 137, 1944.

mean values then served to relate the individual log I scales to the scale defined by the King multiplets. The choice of the nineteen multiplets represented in Figure 7 was determined by a sufficient range in log I which they covered individually and by their largely being free from blends.

TABLE 5*

EXCITATION TEMPERATURES IN THE CHROMOSPHERE

Spectrum	Av. E.P. in Volts	5040/T	T° K	T_{Petrie}
Fe I	2.6	1.7::	3000	2700†
	3.1	1.6	3150	3000†
	3.8	1.5	3400	3350
	4.2	1.4	3600	3600
	4.5	1.25::	4000	3800
Ti II	3.8	1.5	3400	.....
	4.5	1.0::	5000	.....

* Uncertain values are marked by :: ; and figures extrapolated from Petrie's curve by a dagger.

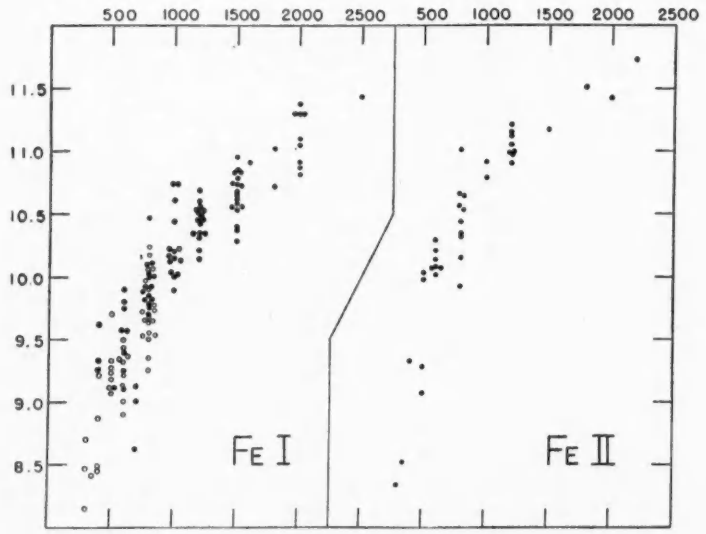

FIG. 8.—$H-\log I$ diagram of *Fe* I and *Fe* II

Figure 8 shows a plot of five multiplets of *Fe* II ($a^4G-z^4F^o$, $b^4F-z^4F^o$, $b^4F-z^4D^o$, $b^4P-z^4D^o$, $b^4D-z^4P^o$), with excitation potentials ranging from 5.5 to 5.8 volts. Sum-rule intensities were used, after checking them against some laboratory intensities[23] and Allen's solar gf-values; several lines with conspicuously discordant intensities were rejected. The several multiplets were fitted together between the heights of 800 and 1200 km.

[23] W. Clarkson, *Phil. Mag.*, **7**, 98, 1929.

The spectrum of *Ti* I is so weakly developed in the chromosphere and so heavily blended, too, that it is unsuitable for a derivation of the density gradient from the estimated heights, none of which exceed 800 km. The *H*-log *I* diagram of *Ti* II, based on eighteen multiplets and King's relative *gf*-values, is shown in Figure 9. The excitation temperatures determined from this spectrum (see Table 5) are rather poor, because the *Ti* II lines are clustered near the ultraviolet end of the flash spectrum; over this range the color correction ΔC changes rapidly with the wave length, so that the excitation temperatures are quite sensitive to the adopted values of ΔC. It was decided, therefore, to combine the different *Ti* II multiplets into a single curve by applying Boltzmann corrections, computed from the *Fe* I excitation temperatures given in Table 5. This procedure can perhaps be defended on the ground that Petrie[24] did not find systematic differences between the excitation temperatures derived from the several metals. Fortunately, the most interesting trait of the *Ti* II diagram, namely, the enormous height of 6000 km reached by three lines, is not affected by the uncertainty about the excitation temperatures. The excitation potentials of these three lines, which belong to the doublets $a^2F-z^2F^o$ and $a^2F-z^2D^o$, agree closely with that of the bulk of the *Ti* II lines, so that the Boltzmann corrections are insignificant.

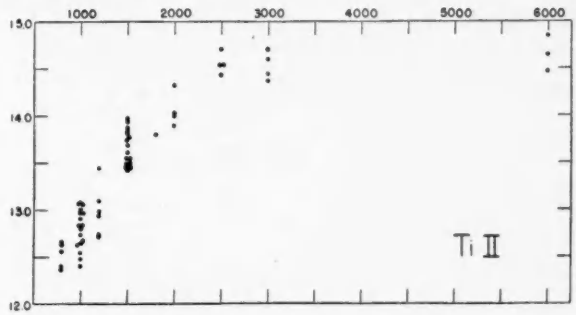

FIG. 9.—$H-\log I$ diagram of *Ti* II

B. EMISSION GRADIENTS FOR OTHER METALLIC SPECTRA

The results for the other metals are of inferior quality, compared with *Fe* I and *Ti* II, because for most of them only from one to three multiples were found suitable.

The spectra of *Sc* II and *Ca* I yield somewhat richer material. In Figure 10 is shown the *H*-log *I* diagram for *Sc* II, derived from the sum-rule intensities of the three triplets and the three singlets making up the transition array, 3d4s—3d4p. Note the height of 5000 km attained by the line λ 4246.8 ($a^1D-z^1D^o$), and the general similarity between this diagram and that of *Ti* II (see Fig. 9). These two spectra suggest that the emission gradient of the metals is much smaller between altitudes of 2000 and 5000 km than at altitudes less than 1500 km.

The full circles, or dots, in Figure 11 represent the lines of eight triplets of *Ca* I; sum-rule intensities were used for the individual multiples, and the separate plots of the several multiplets were superimposed in such a manner that a minimum spread at $H = 800$ km was obtained. The resonance line of *Ca* I, λ 4226.7, reaches a height of 4000 km; but, unfortunately, it is difficult to link it up with the fainter triplets. The absolute *f*-value of the resonance line is known from wave-mechanical computations.[25] Moreover, W. K. Prokofjew[26] has measured experimentally the ratio of the oscillator strength of the in-

[24] *Op. cit.*

[25] D. R. and W. Hartree, *Proc. R. Soc., London*, A, **164**, 167, 1938.

[26] *Zs. f. Phys.*, **50**, 701, 1928.

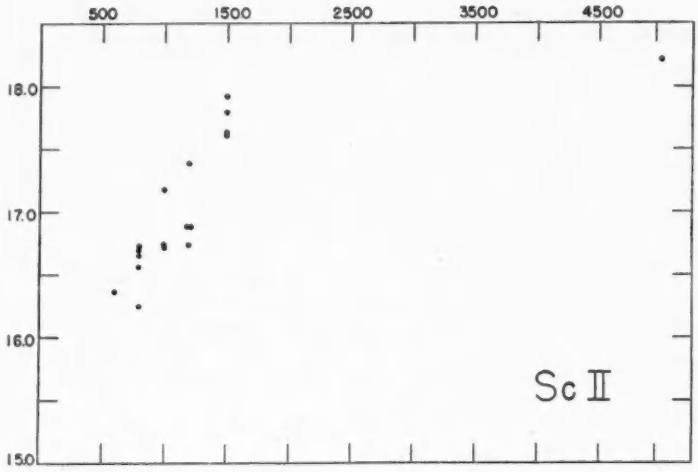

FIG. 10.—$H-\log I$ diagram of *Sc* II

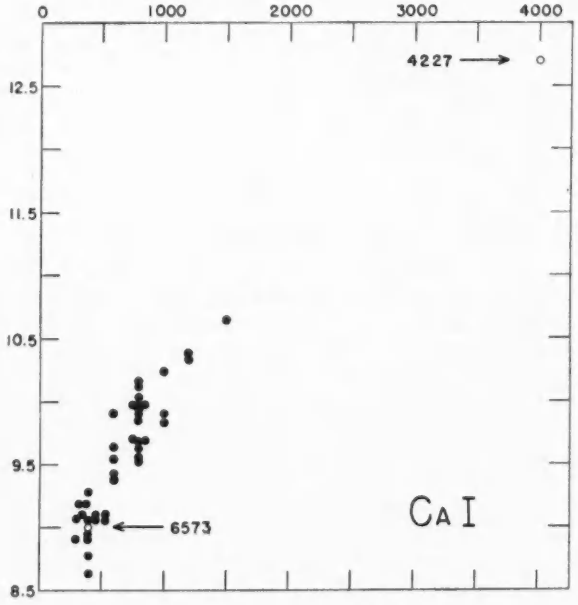

FIG. 11.—$H-\log I$ diagram of *Ca* I

tercombination line, λ 6572.8, to that of the resonance line. After the proper color and Boltzmann corrections had been applied, these two lines were entered in Figure 11 as open circles, the relative position of which is well established; though the location of this "doublet" with respect to the plot of the fainter triplet lines is rather uncertain. The intercombination line is exceedingly faint and reaches a height of only 400 km. Accordingly, it was plotted so as to coincide with the center of gravity, on the log I scale, of the other 400-km lines. But, since the emission gradient is quite steep and poorly determined for such small heights, the vertical position of the symbol for λ 6572.8 is quite uncertain, as well as that of λ 4226.7 for the same reason. Thus it may well be that the correct position of the symbol for λ 4226.7 is 1.0 or so lower on the scale of ordinates of Figure 11; in other words, the emission gradient of *Ca* I at heights greater than 2000 km may, after all, not differ much from that of *Ti* II and *Sc* II.

TABLE 6

CHROMOSPHERIC EMISSION GRADIENTS OF THE METALS

Spectrum	Av. Emission Gradient Δ log I per 100 km	Relevant Range in Height (Km)	Number of Multiplets
Sc II	0.16	800–1500	See Fig. 10
Ti II	.19	1000–1500	See Fig. 9
V II	.18	500–1200	2
Cr I	.20	500–1000	2
Cr II	.12::*	500–1200	2
Mn II	.14	800–1500	1
Fe I	.16	500–1200	See Fig. 7
Fe II	.18	500–1200	See Fig. 8
Ni I	.18	500–1000	3
Y II	.18	500–1200	2
Zr II	.18	500–1200	3
Mg I	.05	2000–6000	2
Ca I	.12	500–1200	See Fig. 11
Ca II	.04	10,000–14,000	2
Sr II	.07	1000–6000	2
Ba II	0.17::	1000–2500	2

* Uncertain values are marked by :: .

In Table 6 average emission gradients, referring to a limited range of heights as stated, are listed for the rest of the metals. Data for *Fe* I, *Fe* II, *Ti* II, *Sc* II, and *Ca* I, read from Figures 7–11, have been included to facilitate comparisons; for hydrogen, according to Figure 5, Δ log I/100 km has the value of 0.04. The figures given in the second column of Table 6 should be multiplied by 2.3×10^{-7} in order to transform them into the coefficients β, appearing in equation (1-9).

The elements in Table 6 fall into two natural groups: the metals of the long periods of the Periodic Table and the alkaline-earth metals (second column of the Periodic Table). The emission gradients of the metals of the first group agree closely with those derived for iron and titanium, at heights less than 1500 km. The second group of elements presents a less coherent picture. The emission gradients of *Ca* I and *Ba* II are about the same as the average one for the first group; note that the range in height covered is also about the same. The much smaller gradients derived for *Mg* I, *Ca* II, and *Sr* II apply to the upper chromosphere. Indeed, they tend to confirm the suggestion, based upon Figures 9 and 10, that, above 2000 km, the emission gradient of the metals is definitely smaller than that prevailing below the 1500-km elevation.

c. Determination of the density gradient of *Ti* and *Fe* atoms

Only the data for *Ti* II, *Fe* I, and *Fe* II are good enough to permit a detailed interpretation by the theory of chromospheric heights which was developed in Section I of this paper. The first step is the representation of the H-log I diagrams (see Figs. 7, 8, 9) by an empirical formula of the type adopted in equation (1-45):

$$E(H) \sim [e^{-\gamma_1 H} + b\, e^{-\gamma_2 H}] .$$

For each diagram two regression-curves were constructed, and normal points were obtained by taking the mean between these two curves. The normal points are listed in Tables 7 and 8 in the columns headed "log I." By definition (see eq. [1-17]), the quantities $E(H)$ are proportional to the reciprocals of the theoretical multiplet intensities, $I(H)$.

For the *Ti* II data two different sets of normal points were selected: (*a*) all lines shown in Figure 8, (*b*) all lines except the three lines reaching the height of 6000 km, which belong to the multiplets $a^2F - z^2F^o$ and $a^2F - z^2D^o$. By a process of trial and error the following curves were fitted to these normal points:

$$a) \qquad E(H) \sim [e^{-(4.60\times10^{-8}\,\mathrm{cm}^{-1})H} + 0.0126\, e^{-(0.138\times10^{-8}\,\mathrm{cm}^{-1})H}] , \tag{3-1}$$

$$b) \qquad E(H) \sim [e^{-(4.60\times10^{-8}\,\mathrm{cm}^{-1})H} + 0.0025\, e^{-(0.92\times10^{-8}\,\mathrm{cm}^{-1})H}] . \tag{3-2}$$

The quality of the representation of the *Ti* II data by these curves can be judged from the differences given in Table 7 under the head (O − C). The values shown in the column "log $E(H)$ comp." have been corrected by a constant in order to make them agree with log $E(H)$ obs. at $H = 800$ km.

The next step is to substitute the empirical equations (3-1) and (3-2) in equation (1-39), whereupon the function $f(H)$ is obtained in the form of equation (1-46). It is then a simple matter to transform, by a new curve-fitting, this expression for $f(H)$ into the more convenient one defined by equation (1-49). The results of this transformation are

$$a) \qquad f_A(H) \sim [e^{-(4.62\times10^{-8}\,\mathrm{cm}^{-1})H} + 0.00018\, e^{-(0.161\times10^{-8}\,\mathrm{cm}^{-1})H}] \tag{3-3}$$

and

$$b) \qquad f_A(H) \sim [e^{-(4.62\times10^{-8}\,\mathrm{cm}^{-1})H} + 0.00027\, e^{-(0.94\times10^{-8}\,\mathrm{cm}^{-1})H}] . \tag{3-4}$$

The subscript A has been affixed to $f(H)$ in order to indicate that this procedure is based on hypothesis A concerning the influence of atmospheric scintillation. The alternative function $f_B(H)$ differs imperceptibly from $f_A(H)$, because the numerical evaluation of equation (1-74) yields the following limits:

$$\left.\begin{matrix} a) & 0.9980 \\ b) & 0.9963 \end{matrix}\right\} \leqslant \frac{f_A(H)}{f_B(H)} \leqslant 1 . \tag{3-5}$$

The last step is the transition from the extra-terrestrial surface brightness of the chromosphere, which is proportional to $f(H)$, to the density distribution along the solar radius of the emitting atoms. From a comparison of equations (1-49) and (1-12), we obtain

$$f(H) \sim [e^{-\beta_1 H} + b' e^{-\beta_2 H}]$$

and

$$n(H) = c_0 \sqrt{2\pi R_\odot/\beta_1}\left[e^{-\beta_1 H} + \left(\frac{\beta_1}{\beta_2}\right)^{1/2} B\, e^{-\beta_2 H}\right] ,$$

from which follows the relation

$$B = \left(\frac{\beta_2}{\beta_1}\right)^{1/2} b' . \tag{3-6}$$

After the numerical values from equations (3-3) and (3-4) have been inserted into this expression, the spatial density, or concentration (cm^{-3}), of the emitting atoms is found from equation (1-11) as follows:

$$a) \qquad c\,(H)_{Ti\,II} \sim [\,e^{-(4.62\times10^{-8}cm^{-1})H} + 0.000034\,e^{-(0.16\times10^{-8}cm^{-1})H}] \qquad (3\text{-}7)$$

and

$$b) \qquad c\,(H)_{Ti\,II} \sim [\,e^{-(4.62\times10^{-8}cm^{-1})H} + 0.00012\,e^{-(0.94\times10^{-8}cm^{-1})H}]\,. \qquad (3\text{-}8)$$

The observational data for *Fe* I and *Fe* II, shown in Figures 7 and 8, cover a much greater range in height than those of *Ti* II. Therefore, no satisfactory representation by a two-term formula can be accomplished. After considerable numerical work, the following three-term formulas were obtained:

$$E\,(H)_{Fe\,I} \sim [\,e^{-(18.4\times10^{-8}cm^{-1})H} + 0.0155\,e^{-(6.21\times10^{-8}cm^{-1})H} + 0.000245\,e^{-(1.61\times18^{-8}cm^{-1})H}] \qquad (3\text{-}9)$$

and

$$E\,(H)_{Fe\,II} \sim [\,e^{-(18.4\times10^{-8}cm^{-1})H} + 0.00355\,e^{-(6.90\times10^{-8}cm^{-1})H} + 0.0000282\,e^{-(1.15\times10^{-8}cm^{-1})H}]\,. \qquad (3\text{-}10)$$

TABLE 7

Ti II CURVE-FITTING

H (Km)	log $I(H)$		log $E(H)$ Obs.		log $E(H)$ Comp.		O−C	
	a	*b*	*a*	*b*	*a*	*b*	*a*	*b*
800	12.40	12.40	0.00	0.00	0.00	0.00	0.00	0.00
1000	12.80	12.80	−0.40	−0.40	−0.39	−0.38	−0.01	−0.02
1200	13.16	13.16	0.76	0.76	0.77	0.74	+0.01	0.02
1500	13.62	13.62	1.22	1.22	1.30	1.21	+0.08	0.01
2000	14.23	14.13	1.83	1.73	1.87	1.72	+0.04	0.01
2500	14.40	14.43	2.00	2.03	2.03	2.00	+0.03	−0.03
3000	14.48	14.62	2.08	−2.22	2.08	−2.22	0.00	0.00
6000	14.66	.....	−2.26	.....	−2.26	.....	0.00	.....

The quality of this representation, according to Table 8, is quite satisfactory. The further reduction of equations (3-9) and (3-10) is carried out by the same steps as outlined for *Ti* II. It should be mentioned that the addition of a third exponential does not create any complications in solving the equations derived in Sections I, *D* and *C*. In fact, the interpolatory representation of $E(H)$ by a sum of exponentials was chosen for this very reason. Again, it is found that the functions $f_A(H)$ and $f_B(H)$ do not differ perceptibly, and the final results are

$$c\,(H)_{Fe\,I} \sim [\,e^{-(18.43\times10^{-8}cm^{-1})H} + 0.00102\,e^{-(6.24\times10^{-8}cm^{-1})H} + 0.00000118\,e^{-(1.64\times10^{-8}cm^{-1})H}] \qquad (3\text{-}11)$$

and

$$c\,(H)_{Fe\,II} \sim [\,e^{-(18.43\times10^{-8}cm^{-1})H} + 0.000328\,e^{-(6.93\times10^{-8}cm^{-1})H} + 0.000000733\,e^{-(1.18\times10^{-8}cm^{-1})H}]\,. \qquad (3\text{-}12)$$

The first term in each of these equations accounts for the gradient of $E(H)$ between 300 and 500 km, but the observations do not allow determining this steep decline with any

great precision. If the normal points at 300 and 400 km are rejected, the observations in the range from 500 to 2500 km lead to the following equations, which have been derived from an adjusted set of normal points differing slightly from the ones shown in Table 8:

$$c\,(H)_{Fe\,I} \sim [\,e^{-(8.09\times10^{-8}\mathrm{cm}^{-1})H} + 0.00020\,e^{-(1.76\times10^{-8}\mathrm{cm}^{-1})H}\,] \qquad (3\text{-}13)$$

and

$$c\,(H)_{Fe\,II} \sim [\,e^{-(11.53\times10^{-8}\mathrm{cm}^{-1})H} + 0.0000082\,e^{-(1.41\times10^{-8}\mathrm{cm}^{-1})H}\,]\,. \qquad (3\text{-}14)$$

TABLE 8

Fe I AND *Fe* II CURVE-FITTING

H (Km)	*Fe* I				*Fe* II			
	log *I*(*H*)	log *E*(*H*) Obs.	log *E*(*H*)	O−C	log *I*(*H*)	log *E*(*H*) Obs.	log *E*(*H*) Comp.	O−C
300	8.30	+0.85	+0.86	−0.01	13.75	+1.35	+1.29	+0.06
400	8.80	+0.35	+0.36	−0.01	14.50	+0.60	+0.58	+0.02
500	9.15	0.00	0.00	0.00	15.10	0.00	0.00	0.00
600	9.43	−0.28	−0.27	−0.01	15.55	−0.45	−0.43	−0.02
800	9.87	−0.72	−0.71	−0.01	16.00	−0.90	−0.95	+0.05
1000	10.20	−1.05	−1.05	0.00	16.33	−1.23	−1.26	+0.03
1200	10.46	−1.31	−1.30	−0.01	16.55	−1.45	−1.46	−0.01
1500	10.70	−1.55	−1.58	+0.03	16.75	−1.65	−1.65	0.00
2000	11.11	−1.96	−1.96	0.00	17.00	−1.90	−1.91	+0.01
2500	11.46	−2.31	−2.31	0.00	17.25	−2.15	−2.16	+0.01

TABLE 9

IONIZATION EQUILIBRIUM *Fe* I/*Fe* II

H (Km)	LOG $c_{Fe\,I}$		LOG $c_{Fe\,II}$		LOG $(c_{Fe\,I}/c_{Fe\,II})$			
	Eq. (3-11)	Eq. (3-13)	Eq. (3-12)	Eq. (3-14)	(3-11)/(3-12)	Δ	(3-13)/(3-14)	Δ
500	−3.81	−1.75	−3.97	−2.51	−0.16		−0.76	
1000	5.64	3.45	6.49	4.92	0.85	−0.69	1.47	−0.71
1500	6.72	4.70	7.67	5.93	0.95	0.10	1.23	0.24
2000	7.32	5.23	8.14	6.24	0.82	0.13	1.01	0.22
2500	7.72	5.62	8.41	6.54	0.69	0.13	0.92	0.09
3000	−8.07	−6.01	−8.66	−6.85	−0.59	−0.10	−0.84	−0.08

In Table 9 the ratios of the densities of *Fe* I and *Fe* II are given, both for the three-term and for the two-term formulas. If local ionization equilibrium exists at every level of the chromosphere, these ratios can be interpreted as a measure of the electron pressure:

$$\log \frac{c_{Fe\,I}}{c_{Fe\,II}} = \log p_e - \log K_{Fe} + \mathrm{const}\,. \qquad (3\text{-}15)$$

Here K_{Fe} denotes the equilibrium constant for the first ionization *Fe*, and the unknown constant on the right side appears because the absolute values of $c_{Fe\,I}$ and $c_{Fe\,II}$ are un-

known. If, moreover, the ionization temperature does not vary with height, it follows from equation (3-15) that

$$\frac{d}{dH}\log\frac{c_{Fe\,I}}{c_{Fe\,II}}=\frac{d\log p_e}{dH}.$$

Hence, the differences Δ, shown in Table 9, represent the quantities

$$\frac{\Delta\log p_e}{500\,\mathrm{km}}.$$

The enormous abundance of hydrogen in the solar atmosphere makes the gradient of the electron pressure independent of the density gradients of the metallic elements, at least for the small pressures prevailing at heights greater than 500 km; this conclusion is based upon equations (2-9) and (2-13). From equations (2-13) and (2-7) it is found that

$$\frac{d\log p_e}{dH}=\frac{1}{2}\frac{d\log p_H}{dH}=-0.20\times10^{-8}\mathrm{cm}^{-1}, \qquad (3\text{-}16)$$

and therefore the differences Δ shown in Table 9 should have the value of

$$\Delta=\frac{\Delta\log p_e}{500\,\mathrm{km}}=-0.10.$$

This value agrees as to order of magnitude with the observed values of Δ, between 1500 and 3000 km. Below 1000 km there is a big discrepancy, and the positive sign of the observed Δ would mean that the electron pressure increases upward. However, in this region the gradient of $E(H)$ is large, and the scatter of the observations is considerable (see Figs. 7 and 8), so that no physical significance need be attached to the positive Δ. Even the moderate agreement at greater heights should not be regarded as proof of the existence of ionization equilibrium. The intricacy of the reduction process, which involves a second differentiation in the determination of $c_{Fe\,I}$ as well as of $c_{Fe\,II}$, combined with the scatter of the observations, defeats any attempt to make such a delicate test. But it seems fair to say that at heights greater than 1500 km the observations are compatible with the assumption of ionization equilibrium.

IV. NONMETALS: HELIUM AND OXYGEN

The spectra of the nonmetallic elements are as poorly represented in the flash spectrum as they are in the Fraunhofer spectrum. The explanation is, of course, the same, namely, the high excitation potentials of the lines in the astrophysically accessible range of the spectrum.

At the 1937 eclipse, two multiplets of *O* I were recorded in the infrared of the flash spectrum, $3^5S^o-3^5P$ and $3^3S^o-3^3P$. The heights of the unresolved multiplets are 6000 km (quintet) and 3000 km (triplet), and the excitation potentials are 10.69 and 10.94 volts, respectively. Both multiplets are derived from the ground term, $2s^22p^3\,4S$, of *O* II, and the intensity ratio of the unresolved multiplets, predicted for LS-coupling is 15:9 (quintet : triplet); and, after multiplication by ν^4, it is found that $\Delta\log I$ (quintet : triplet) = 0.36. This quantity is to be increased by the differential color correction, ΔC, the amount of which is not well known but may be estimated to have the order of magnitude 0.5–1.0. Hence the average emission gradient of *O* I should be of the order of 0.03–0.05, in the same units as those used in Table 6; in other words, the average emission gradient of *O* I closely agrees with that of hydrogen, in the range from 3000 to 6000 km.

Observational data for the *He* I spectrum are more abundant, but transitions probabilities are available for only part of the lines observed in the chromosphere. The *f*-values

computed by L. Goldberg[27] were used, and in some cases those of A. Hylleraas.[28] In Figure 12 the logarithms of the theoretical line intensities, including the color correction but without Boltzmann correction, are plotted against the estimated heights of the *He* I lines. The symbols of some lines have an arrow pointing to the left, indicating that the line is blended and that the symbol of the unblended line would be located farther to the left. The lines plotted in Figure 12 comprise the series $2^3P^o-n^3D$, $2^1P^o-n^1D$, $2^3S-n^3P^o$, and $2^1S-n^1P^o$; for the $2P^o-nS$ series no reliable f-values are available. The several solid lines drawn in Figure 12 connect the symbols of lines having the same principal quantum number of the upper state; the lines thus forming the groups $n = 3$, $n = 4$, etc., have practically constant upper excitation potentials in each group, and hence the plots of the several groups should be brought to coincidence by applying the Boltzmann corrections $(5040/T)\Delta E$. It was expected that the several groups would form a regular progression on the diagram, with the graph of lines of higher excita-

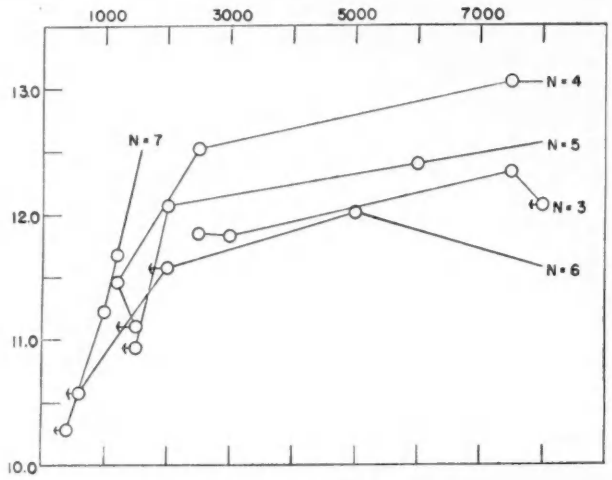

FIG. 12.—$H-\log I$ diagram of *He* I

tion potential located above that referring to lines of lower excitation potential, such as with the groups marked $n = 3$ (E.P. 22.97) and $n = 4$ (E.P. 23.63). It will be noticed, however, that the groups $n = 5$ and $n = 6$ are both lying lower than $n = 4$, and that $n = 6$ is even lower than $n = 3$. This result is somewhat puzzling. Formally, it could be interpreted as a change in excitation temperature with an excitation potential which is not progressive but goes through a maximum between $n = 4$ and $n = 5$. Such an explanation appears rather unsatisfactory because of the small range of excitation potential between the groups $n = 3$ and $n = 6$, which is only 1.1 volts. If the discordant groups, $n = 5$ and $n = 6$, are disregarded, an excitation temperature can be derived from $n = 3$ and $n = 4$; the result is $5040/T = 1.06$ or $T = 4750°$ K. This figure does not seem unreasonable and is about the same as Menzel's excitation temperature derived from the intensity distribution in the Balmer emission continuum. L. Goldberg[29] obtained excitation temperatures for *He* I from Menzel's photometry of the 1936 flash. His numerical results are: 4300° K at $H = 670$ km, and 6700° at $H = 2330$ km, on the assumption that self-absorption is negligible.

[27] *Ap. J.*, **90**, 414, 1939.

[28] *Zs. f. Phys.*, **106**, 395, 1935.

[29] *Ap. J.*, **89**, 673, 1939.

According to Figure 12, the general run of the graphs referring to the several groups is closely parallel. Therefore, it can be asserted with confidence that the average emission gradient of *He* I is of the order of 0.01/100 km between 2000 and 8000 km elevation, and much steeper below 2000 km, perhaps about 0.07/100 km; the corresponding values of the exponent β in equation (1-10) are 0.23×10^{-8} cm^{-1} and 1.61×10^{-8} cm^{-1}, respectively. It has already been noted by Mitchell and Williams, and by Cillié and Menzel,[30] too, that at altitudes greater than 2000 km the emission gradient of *He* I is smaller than that of any other element.

At the 1927 eclipse, A. Pannekoek and M. G. J. Minnaert[31] determined photometrically the decrease of the total intensity of the line λ 4471 after the second contact and evaluated the change along the solar radius of the surface brightness of the chromosphere in the light of this line. They found that, contrary to the behavior of the chromospheric hydrogen lines, λ 4471 attains a maximum of intensity at the height of about 1000 km; but they were not entirely certain of the reality of this result. Later, E. J. Perepelkin and O. A. Melnikov[32] investigated the radial-intensity distribution in the light of the D_3 line (λ 5876) on chromospheric spectra obtained without an eclipse. These observers also found a maximum of the *He* I emission, at an elevation of 1300 km. The average emission gradient between 3000 and 6000 km elevation is $\Delta \log I/\Delta H = 0.02/100$ km, that is, just twice the gradient given by Figure 12 but still only half of the hydrogen gradient, according to Figure 5. It would seem, then, that Figure 12 is in moderately good agreement with Perepelkin and Melnikov's result, in the range from 3000 to 6000 km. Below 2000 km, Figure 12 gives no indication of a reversal of the sign of the gradient, such as would be expected on the basis of the results of the Dutch and the Russian observers; however, most of the lines in that lower range are blended (note the arrows), and probably not much weight can be attached to the lack of agreement at lower altitudes.

V. THE ABUNDANCES OF THE ELEMENTS IN THE CHROMOSPHERE

Unless the chromosphere is continually kept in a well-mixed state by some "stirring" agency, there is no sense in speaking of relative abundances in "the" chromosphere. While the metals appear to have practically the same radial density gradient, hydrogen and helium behave in a conspicuously different manner. The work of Mitchell and Williams has revealed that the relative abundances of the metals in the flash parallel closely those derived by H. N. Russell from the Fraunhofer spectrum; and their results are in substantial agreement with Menzel's. However, hydrogen seems to be much more abundant in the chromosphere. Hence the determination of the abundance A of hydrogen relative to that of the metals becomes meaningless if the difference of their density gradients is not taken into account.

It is for this reason that the following determination of the quantity A makes use of the estimated heights of flash lines instead of the total intensities estimated on an intuitive scale and thereafter calibrated with the aid of multiplets, as Mitchell and Williams did, for it is impossible to free the estimated total intensities from the influence of the density gradients. On the contrary, by a comparison of lines reaching the same height in the chromosphere, the definite numbers of the respective emitting atoms are brought into a quantitative relation. The variation of A with height can thus readily be eliminated, and the extrapolated value of A at the zero level is then found to agree closely with the figure given by B. Strömgren for the photosphere. In other words, a physical continuity between photosphere and chromosphere is suggested.

[30] *Harvard Circ.*, No. 410.

[31] *Op. cit.*

[32] *Poulkovo Bull.*, No. 122, 1935.

A. THE ABUNDANCE RATIO OF HYDROGEN TO IRON

Since *Fe* I is the only metal in the lower chromosphere for which absolute *f*-values are available, this element will be used to fix the abundance ratio of hydrogen to the metals. The relative abundances of the several metals will be taken up thereafter.

For a comparison, choose any two lines of hydrogen and *Fe* I which reach the same estimated height, H. The equality of the estimated height implies, according to equations (1-5) and (1-7), the relation

$$[g f \nu^3]_B \frac{e^{-\chi_B/kT}}{u_B(T)} N_B(H) = [g f \nu^3]_{Fe} \frac{e^{-\chi_{Fe}/kT}}{u_{Fe}(T)} N_{Fe}(H) . \qquad (5\text{-}1)$$

The quantities on the left side of the equation refer to a line of the Balmer series, and those on the right to a line of *Fe* I. Since lines closely adjacent in the spectrum will be compared—in order to avoid systematic corrections depending on the wave length—the factor ν^3 can be dropped on either side. If the excitation energies are replaced by the excitation potentials measured in volts, equation (5-1) may be written as follows:

$$[g f]_B \frac{10^{-E_B(5040/T)}}{u_B(T)} N_B(H) = [g f]_{Fe} \frac{10^{-E_{Fe}(5040/T)}}{u_{Fe}(T)} N_{Fe}(H) . \qquad (5\text{-}2)$$

The quantities $N(H)$, which were defined by equation (1-3), are the total numbers of atoms contained in a slab, 1 cm thick, that extends from the height H upward to infinity. From equations (1-10) and (2-7) it is found that

$$N_B(H) = c_{B0} \sqrt{2\pi R_\odot/\beta^3}\, e^{-\beta H} , \qquad \beta = 0.92 \times 10^{-8}\text{cm}^{-1} . \qquad (5\text{-}3)$$

Similarly, it follows from equations (1-14) and (3-13) that

$$\left.\begin{aligned} N_{Fe}(H) &= c_{Fe0} \sqrt{2\pi R_\odot}\, [\beta_1^{-3/2} e^{-\beta_1 H} + \beta_2^{-3/2} B e^{-\beta_2 H}] ; \\ \beta_1 &= 8.09 \times 10^{-8}\text{cm}^{-1} ; \qquad \beta_2 = 1.76 \times 10^{-8}\text{cm}^{-1} ; \qquad B = 0.00020 . \end{aligned}\right\} \qquad (5\text{-}4)$$

If equation (3-11) is used instead of equation (3-13), the corresponding result is

$$\left.\begin{aligned} N_{Fe}(H) &= c_{Fe0} \sqrt{2\pi R_\odot}\, [\beta_1^{-3/2} e^{-\beta_1 H} + \beta_2^{-3/2} B e^{-\beta_2 H} + \beta_3^{-3/2} C e^{-\beta_3 H}] ; \\ \beta_1 &= 18.43 \times 10^{-8}\text{cm}^{-1} ; \qquad \beta_2 = 6.24 \times 10^{-8}\text{cm}^{-1} ; \qquad \beta_3 = 1.64 \times 10^{-8}\text{cm}^{-1} ; \\ B &= 0.000102 ; \qquad C = 0.00000118 . \end{aligned}\right\} \qquad (5\text{-}5)$$

By substituting equations (5-3) and (5-4) into equation (5-2), we can express the abundance ratio of neutral iron to neutral hydrogen at the zero level of the chromosphere as

$$\frac{c_{B0}}{c_{Fe0}} = \frac{[g f]_{Fe}}{[g f]_B} \frac{u_B(T)}{u_{Fe}(T)} 10^{-(E_{Fe}-E_B)(5040/T)} \left\{ \frac{\beta_1^{-3/2} e^{\beta_1 H} + \beta_2^{-3/2} B e^{-\beta_2 H}}{\beta^{-3/2} e^{-\beta H}} \right\} ; \qquad (5\text{-}6)$$

and, finally, the true abundance of hydrogen and iron is obtained by applying a further correction for the respective ionization degrees, α, of these two elements, namely,

$$Z = \frac{1-\alpha_{Fe}}{1-\alpha_B} \frac{c_{B0}}{c_{Fe0}} = \frac{1 + K_H/p_e}{1 + K_{Fe}/p_e} \frac{c_{B0}}{c_{Fe0}} , \qquad (5\text{-}7)$$

where $K_H = 10^{-5.38}$ and $K_{Fe} = 10^{+1.03}$ are the ionization constants of H and Fe at $T = 4830°$ K. The electron pressure, p_e, can be found from equations (2-9) and (3-16); the result is, for $H = 0$ km, $p_e = 10^{-0.94}$ dynes/cm², which gives

$$\frac{1-\alpha_{Fe}}{1-\alpha_B} = 10^{-1.97} .$$

At $T = 4830°$ K the partition functions of neutral hydrogen and neutral iron have the values $u_B(T) = +0.30$ and $u_{Fe}(T) = +1.43$. By substitution of these figures into equations (5-6) and (5-7), we find

$$Z(H:Fe) = \frac{[gf]_{Fe}}{[gf]_B} 10^{-3.10-(E_{Fe}-E_B)(5040/T)} \left\{ \frac{\beta_1^{-3/2} e^{-\beta_1 H} + \beta_2^{-3/2} B e^{-\beta_2 H}}{\beta^{-3/2} e^{-\beta H}} \right\}. \quad (5\text{-}8)$$

The successive steps of the numerical evaluation of equation (5-8) are listed in Table 10. Three strong *Fe* I multiplets located near the end of the Balmer series were compared with the two Balmer lines which reach a height of 1000 km; and the average *gf*-value, which corresponds to a height of 1000 km, was determined graphically for each multiplet. The value of the last factor in braces of equation (5-8), which appears in Table 10 in the line marked "log N_{Fe}/N_B," depends strongly on whether we choose to represent the density distribution of *Fe* I by the two-term formula (3-13) or the three-term formula (3-11). This divergence illustrates the uncertainty in extrapolating the density distribution of *Fe* I downward to the chromospheric zero level. Taking the average of the extreme values, it is found that $\log Z(H:Fe) = +3.53$. This figure is probably a lower limit, since the true density distribution may be presumed to be closer to equation (3-13) than to equation (3-11); perhaps $\log Z(H:Fe) = +4.5$ is as good a guess as possible under the circumstances. According to Table 11 and to Russell's and Menzel's work, iron constitutes perhaps 20–30 per cent, by numbers of

TABLE 10

ABUNDANCE RATIO OF HYDROGEN TO IRON

Description of Lines	*Fe* I			*H* I
	$a^5D - z^5F^o$	$a^5F - y^5F^o$	$a^5F - z^5G^o$	$B_{31} - B_{32}$
Estimated height in km	1000	1000	1000	1000
$\log gf$	− 1.86	− 0.70	− 1.05	− 3.05
E in electron-volt	3.25	4.25	4.35	13.53
$(E_B - E_{Fe})\theta$	+10.75	+ 9.70	+ 9.60	$\leftarrow\theta = 1.043$ from $T_0 = 4830°$ K
$\log \frac{[gf]_{Fe}}{[gf]_B}$	+ 1.21	+ 2.35	− 2.00	
$\log \frac{[gf]_{Fe}}{[gf]_B} 10^{-\theta\Delta E}$	+11.96	+12.05	+11.60	
Average	+11.87 ± 0.18			
See eq. (5-8)	− 3.10			
$\log \frac{N_{Fe}(1000\text{ km})}{N_B(1000\text{ km})}$	(3-13)	−4.21	−5.25 ± 1.04	
	(3-11)	−6.28		
$\log Z(H:Fe)$	(3-13)	+4.56	+3.53 ± 1.04 at $H = 0$ km	+6.11 at $H =$ 500 km
	(3-11)	+2.49		+6.10

atoms, of the elements with ionization potentials less than 13.5 volts, which are lumped together under the name of metals. Hence, log $Z(H : \text{Metals})$—or log A, to use Strömgren's notation—should have the order of 3.8–4.0, which accords well with Strömgren's figure for the photosphere, namely, log $A = +3.9$. Strömgren's figure itself now requires revision, since it is based on the absorption coefficients of H^- computed by Massey and Bates, which are superseded by Chandrasekhar's recent work. With due consideration of all the uncertainties involved, it appears justified to conclude that the abundance ratio of hydrogen to iron in the chromosphere, if extrapolated down to the solar limb, closely approaches that derived from the Fraunhofer spectrum.

It is worth noting that the uncertainties of the extrapolation stressed above do not affect the value of $Z(H : Fe)$ at $H = 500$ km, which has also been listed in the last line of Table 10; these figures have been obtained from Z at the zero level by applying the density gradients (2-7) and (3-13) or (3-11). The result has already been used in deriving equation (2-15), which fixes the absolute density of hydrogen.

TABLE 11

RELATIVE ABUNDANCES OF THE METALS
(By Numbers of Atoms)

Metal	log Z (1)	Menzel (2)	Russell (3)	Δ (1)−(2)	Δ (1)−(3)
Na	−0.8	+0.2	0.0	−1.0	−0.8
Mg	+0.6	+0.4	+0.6	+0.2	0.0
Al	−0.9	−0.8	−0.8	−0.1	−0.1
Ca	−0.7	−0.4	−0.5	−0.3	−0.2
Fe	0.0	0.0	0.0	0.0	0.0
Cu	−3.5	.....	−2.2	.....	−1.3
Sr	−3.6	−3.9	−3.9	+0.3	+0.3

B. THE RELATIVE ABUNDANCE OF THE METALS

In order to determine the relative abundance, by numbers of atoms, of any two metals, equations (5-6) and (5-7) have been combined into the expression

$$Z(1:2) = \frac{1 + K_1/p_e}{1 + K_2/p_e} \frac{[g f \nu^3]_2}{[g f \nu^3]_1} \frac{u_1}{u_2} 10^{-(E_2 - E_1)(5040/T)}. \qquad (5\text{-}9)$$

The last factor in equation (5-6) has been omitted on the assumption that all the metals obey the same density law. Such is probably a good first approximation, though it cannot be strictly correct because of the ionization which varies with height. It also should be noted that the factors ν^3, which were disregarded in equation (5-6), have been restored. Therefore, lines located in different parts of the spectrum can be compared, after the appropriate color corrections for sensitivity, extinction, etc., have been applied.

Numerical results obtained from equation (5-9) are given in Table 11; the number of entries is rather small because absolute transition probabilities are available for only a few elements. For the sake of comparison, Table 11 also lists the relative abundances, by numbers of atoms, in the chromosphere and photosphere according to D. H. Menzel[33] and H. N. Russell.[34] The agreement is satisfactory, except in the case of sodium. But the figure for sodium in column 1 is somewhat uncertain, as both the Boltzmann correction and the empirical color correction are large. On the whole, there appears to be good reason for believing that the relative abundances of the metals in the chromosphere are the same as in the photosphere.

[33] *Pub. Lick Obs.*, Vol. **17**, 1931.

[34] *Ap. J.*, **70**, 11, 1929.

C. TEST FOR SELF-ABSORPTION IN THE CHROMOSPHERE

The density gradients of the emitting atoms have been evaluated from predicted intensities which were tacitly assumed not to require any corrections for self-absorption in the chromosphere. This assumption will now be justified by computing the line-absorption coefficient in the tips of the chromospheric crescents from the total number of atoms in a column along the line of sight and the atomic absorption coefficient. The correction for self-absorption is then found from a table published in Pannekoek's theoretical investigation of the line emission in the chromosphere.[35]

The line-absorption coefficient, at the center of the line, is[36]

$$k = \frac{f\lambda}{\xi_0}\frac{\pi^{1/2}e^2}{m\,c}\,,$$

and

$$\log k = \log\frac{f\lambda}{\xi_0} - 1.83\,, \tag{5-10}$$

where λ is the wave length and f the absorption oscillator strength of this line; ξ_0 is the average velocity in the line of sight of the absorbing atom—as defined by Unsöld's equation (43.2)—which is the resultant of the thermal and turbulent velocity. According to W. H. McCrea's theory[37] of a chromosphere supported by turbulent pressure, ξ_0 is related to the observed density gradient β by the expression

$$\xi_0^2 = \frac{2g_\odot}{\beta}\,, \tag{5-11}$$

where $g_\odot$ is the acceleration of gravity at the solar surface. With $\log g_\odot = +4.44$ and $\log \beta_H = -8.04$ for hydrogen in the chromosphere, according to equation (2-7), it follows that

$$\log \xi_0 = +6.39\,, \qquad \xi_0 = 24.5\ \mathrm{km/sec^{-1}}\,. \tag{5-12}$$

It is interesting to note that this very figure was confirmed at the 1940 eclipse by O. R. Redman,[38] who measured the line profiles of $H\beta$, $H\gamma$, and $H\delta$ and carefully applied corrections for the instrumental pattern of the slit spectrograph.

The total number of atoms in a column of 1 cm^2 cross-section, extending along the line of sight and passing the chromosphere at an elevation H above the solar limit, is found from equations (1-9) or (1-12) by substituting the appropriate density law, that is to say, for the Balmer series,

$$n_B(H) = n_{B0}\,e^{-(0.92\times10^{-8}\mathrm{cm^{-1}})H}\,, \tag{5-13}$$

where n_{B0} is to be taken from line 9 of Table 2. By substituting (5-12) into (5-10) and multiplying with (5-13), the line-absorption coefficient, η, at the center of the line, for the entire column is found, viz.,

$$\log \eta(H) = \log n_{B0} - (0.40\times10^{-8}\mathrm{cm^{-1}})\,H + \log f\lambda - 8.22\,. \tag{5-14}$$

Numerical values of $\log \eta(H)$ are given in Table 12, for the different assumptions concerning the abundance ratio, A, of hydrogen to metals.

Entering into Pannekoek's table[39] with $\eta(H)$—or y_0 in Pannekoek's notation—the corrections for self-absorption all prove to be well below 1 per cent of the theoretical intensities of the Balmer lines. Consequently, the exponential in equation (2-7) represents

[35] A. Pannekoek, *B.A.N.*, **4**, 263, 1928.

[36] See A. Unsöld, *op. cit.*, p. 431 and eq. (98.15).

[37] *M.N.*, **89**, 718, 1929.

[38] *M.N.*, **102**, 140, 1942.

[39] *Op. cit.*

the true density gradient of hydrogen. An analogous demonstration for the Paschen series is unnecessary, because the values of f and n_{P_0} are even smaller than for the Balmer series.

Although hydrogen is enormously more abundant than the metals, it may be of interest to demonstrate in detail that the *Fe* I multiplets utilized in Table 10 are not affected by self-absorption. From equation (2-15) and the last line of Table 10 it follows that

$$\log c_{Fe} = +9.53 \qquad \text{at} \qquad H = 500 \text{ km} ;$$

and by multiplication with $(1 - \alpha_{Fe}) = 10^{-1.97}$ the concentration of the neutral iron atoms is found to be

$$\log c_{Fe\,I} = +7.56 \qquad \text{at} \qquad H = 500 \text{ km} .$$

TABLE 12

SELF-ABSORPTION IN THE BALMER SERIES

n	H (Km)	log $f\lambda$	$-0.40\times10^{-8}H$	log $\eta(H)$		
				log $A = +3.90$	log $A = +4.90$	log $A = +5.90$
37	500	−8.60::	−0.20	−1.96	−1.44	−1.34
31	1000	8.37	0.40	1.93	1.41	1.31
27/28	1500	7.21	0.60	1.97	1.45	1.35
23/24	2000	8.00	0.80	1.96	1.44	1.34
21	2500	7.85	1.00	2.01	1.49	1.39
18/19	3000	7.68	1.20	2.04	1.52	1.42
16	4000	7.49	1.60	2.25	1.73	1.63
14/15	5000	7.28	2.00	2.44	1.92	1.82
11	6000	6.97	2.40	2.53	2.01	1.91
9	7000	6.68	2.80	2.64	2.12	2.02
5/6	8000	5.85	3.20	2.21	1.69	1.59
4	9000	5.24	3.60	1.98	1.46	1.36
3	12,000	−4.38	−4.80	−2.34	−1.82	−1.72

If this figure is extrapolated, by equation (3-13), to the zero level, the result is

$$\log c_0 = +9.31 \qquad \text{at} \qquad H = 0 \text{ km} ;$$

so that equation (3-13) may be written as

$$\log c_{Fe\,I} = 10^{+9.31}\left[10^{-(0.35\times10^{-8}\text{cm}^{-1})H} + 10^{-3.37-(0.077\times10^{-8}\text{cm}^{-1}H)}\right] . \qquad (5\text{-}15)$$

This is the radial-density distribution of neutral iron atoms, from which the corresponding tangential distribution—the numbers of atoms in a column of 1 cm² cross-section along the line of sight—can be found from equation (1-12):

$$\log n_{Fe\,I} = 10^{+18.68}\left[10^{-(0.35\times10^{-8}\text{cm}^{-1})H} + 10^{-3.37-(0.077\times10^{-8}\text{cm}^{-1})H}\right] . \qquad (5\text{-}16)$$

Finally, by multiplying this expression with the appropriate Boltzmann correction, $(g/u_0)10^{-E\theta}$, and with equation (5-10), the absorption coefficient $\eta(H)$ is obtained:

$$\eta(H) = [gf]_{Fe\,I}\left(\frac{\lambda}{u_0}\right)10^{-8.22-E\theta}n_{Fe\,I}(H) . \qquad (5\text{-}17)$$

The quantity $n_{Fe\,I}$ has to be evaluated from equation (5-16) with $H = 1000$ km, since the values of $[gf]_{Fe\,I}$ in Table 10 refer to this height; the result is $\log n(1000) = +15.27$; and, for the three multiplets,

$$\log \eta\ (1000\ \text{km}) = \begin{matrix} a^5D - z^5F^o & a^5F - y^5F^o & a^5F - z^5G^o \\ -4.20 & -4.09 & -4.55 \end{matrix} \Bigg\}. \quad (5\text{-}18)$$

In computing these figures, the Doppler velocity of hydrogen, according to equation (5-12), has been used. Although the metals probably have smaller velocities, perhaps as low as 10 per cent of that of hydrogen, it is seen that in any case $\eta_{Fe\,I}$ is so much smaller than the η's of the Balmer series, listed in Table 12, that self-absorption cannot possibly be of any consequence for *Fe* I.

By analogy, this conclusion must apply to all the metals, most of which are less abundant than iron. While some of the metallic lines have f-values much higher than those of *Fe* I, particularly the resonance lines of the light metals, it seems extremely improbable that self-absorption would affect the emission from the tips of the chromospheric crescents, except possibly in singular cases like *Ca* II.

VI. REMARKS ON THE CONSTITUTION OF THE CHROMOSPHERE

The principal density gradients derived previously are illustrated by Figure 13, which reproduces all of them on the same scale. The zero points of ordinates for the several elements differ by arbitrary constants, because their relative abundances have not been taken into account; hence only the slopes of the different curves are comparable. Solid curves apply to the well-observed spectra which were subjected to a rigorous analysis. Besides, estimated gradients of poorly represented spectra are indicated by dashed lines; with the exception of *He* I, these data were taken from Table 6 without further reduction. Figure 13 also shows the density of atomic hydrogen for hydrostatic equilibrium at the boundary temperature of the sun, which is believed to prevail in deeper layers of the solar atmosphere where the Fraunhofer spectrum and the continuous emission originate. It is convenient, therefore, to refer to this gradient as the "photospheric gradient," and thereby to distinguish it from the chromospheric hydrogen gradient, defined by equation (2-7).

The general impression imparted by Figure 13 is that at altitudes less than 1000 km the density gradients of the metals are of the same order of magnitude as the photospheric hydrogen gradient but that between elevations of 3000 and 6000 km the metallic gradients appear to approach the chromospheric hydrogen gradient. This pronounced difference between the structure of the hydrogen chromosphere, on the one hand, and the structure of its metallic tributaries, on the other hand, calls for a physical explanation. In the absence of any generally accepted dynamical theory of chromospheric support, the only recourse available in the past was to the phenomenological theory proposed by W. H. McCrea, to which reference has already been made in Section V, *C*. McCrea's analysis has established a relation between the exponent β in the chromospheric density law embodied in equation (1-8) and the spatial velocities of the emitting atoms, which, with the notation used here, may be written as

$$\beta = \frac{g_\odot}{\xi_0^2/2} = g_\odot \left[\frac{kT}{m_0\mu} + \xi_t^2/2\right]^{-1}. \quad (6\text{-}1)$$

The atomic weight on the chemical scale has been designated by μ, so that m_0 is the mass unit corresponding to $\mu = 1$. If ξ, η, and ζ are the rectangular components of the space velocity of an individual atom, ξ_0 is defined by

$$(\xi^2 + \eta^2 + \zeta^2)_{\text{average}} = \tfrac{3}{2}\,\xi_0^2, \quad (6\text{-}2)$$

where ξ_0 is the resultant of the thermal velocities of the atoms corresponding to the gas temperature T and of a macroscopic turbulent velocity ξ_t of the gas; in other words,

$$\xi_0^2 = \frac{2kT}{m_0\mu} + \xi_t^2 . \tag{6-3}$$

Equation (6-1) can be tested by observation of the chromospheric line profiles on high-dispersion spectrograms. For hydrogen, McCrea's test was successful. As regards the metals, Unsöld[40] concluded that the line profiles measured by A. Pannekoek and

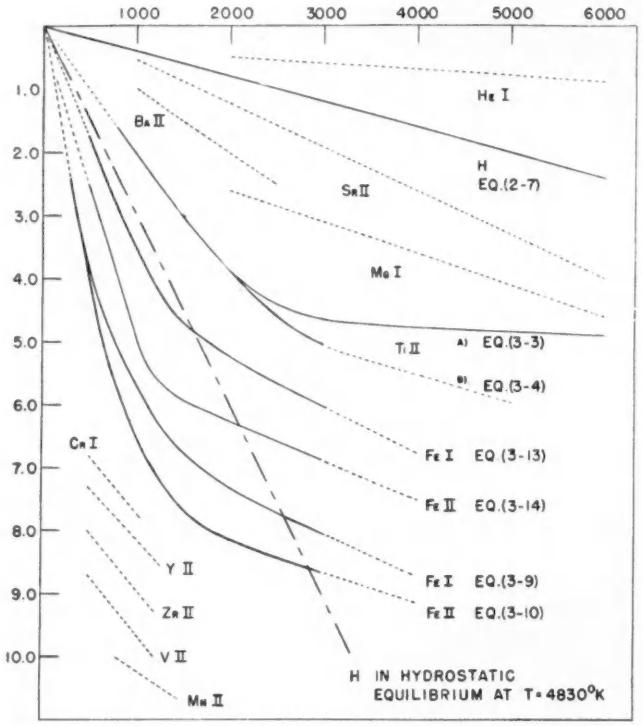

FIG. 13.—Density gradients in the chromosphere. *Abscissae*, heights above the solar limb, in kilometers; *ordinates*, logarithm of numbers of atoms per cubic centimeter.

M. Minnaert[41] and by D. H. Menzel[42] indicated turbulent velocities of the order of 10–15 km sec^{-1}. However, very likely these profiles were largely of instrumental origin. At the eclipse of 1940 October 1, R. O. Redman[43] measured numerous line profiles, which, after careful correction for the instrumental pattern, turn out to be much narrower. Redman expressed his measurements in terms of the average one-dimensional velocity, $\bar{v}$, which is related to ξ_0 by

$$\sqrt{\pi}\,\bar{v} = \xi_0 , \tag{6-4}$$

[40] *Op. cit.*, p. 437 and Table 74.

[41] *Verh. Kon. Akad. v. Wetensch. Amsterdam* (Sec. 1), **13**, No. 5, 1928.

[42] *Pub. Lick Obs.*, **7**, 1, 1931.

[43] *M.N.*, **102**, 140, 1942.

and gave the following numerical values and estimated heights, to which the profiles refer (see Table 13).

The principal conclusion Redman arrived at is based upon the fourth column of Table 13, which lists the thermal velocities of the heavier elements that would correspond to the observed hydrogen velocity $\bar{v} = 13.5$ kc on the assumption of a purely thermal origin of the latter; this assumption is equivalent to a kinetic temperature of about 35,000° K. Now the numerical agreement between the second and fourth columns of Table 13 is so close that the turbulent velocity ξ_t cannot exceed something of the order of 1 km sec^{-1}. In other words, Redman's observations discredit the current theory, inaugurated by McCrea's investigations, which supposes turbulence to provide the support of the chromosphere. Since Redman's surprising discovery depends entirely on the difficult determinations of line profiles, it is of particular interest that his chromospheric velocities lead to predicted density gradients which are in good agreement with the results obtained in this paper. The values of β given in the last column of Table 13 have been computed from equations (6-1) and (6-4). For hydrogen the agreement is perfect and for *He* I tolerably good (see Fig. 12). The predicted values of β for *La* II and the other heavy elements (mostly rare earths) are from three to four times larger than the observed values for iron and titanium. However, it does not seem impossible that such steep gradients could exist in the lower chromosphere to which the lines of the rare earths are restricted.

TABLE 13

R. O. REDMAN'S CHROMOSPHERIC LINE PROFILES

Line	$\bar{v}_{observed}$	Height	$\bar{v}_{thermal}$	$\beta_{computed}$
$H\beta$, $H\gamma$, $H\delta$	13.5 km/sec^{-1}	1500 km	[13.5] km/sec^{-1}	0.95×10^{-8} cm^{-1}
He I, λ 4471	8	1500	6.8	2.85
La II, λ 4333	1.6	Very low	1.9	69
Various heavy elements	1.75		1.1	58

The salient point is that, on McCrea's theory of turbulent support and with the high turbulent velocities accepted by Unsöld, it is impossible to account for the observationally well-established difference between the density gradients of hydrogen and the metals. On Redman's picture of the chromosphere, the conspicuous variation of the metallic gradients with height (see Fig. 13) would imply a corresponding variation of the kinetic temperature of the metallic atoms. The question of whether such a variation does exist in the chromosphere can be decided only by future simultaneous determinations of line profiles at different heights. Notwithstanding the technical difficulties involved in work of this nature, it appears that the solution of this problem would well repay the efforts of eclipse observers.

The high kinetic temperature found by Redman does not demand the existence of black-body radiation of corresponding composition or any approach to thermodynamical equilibrium for such a temperature. But it may legitimately be asked whether the density gradients derived here do not depend critically on the expedient, adhered to throughout this paper, of treating the chromosphere as a system in thermodynamical equilibrium with the theoretical boundary temperature of the sun, $T_0 = 4830°$ K. In the case of hydrogen, it is apparent from equation (2-5) and Table 1 that the excitation corrections are quite small for the higher series members and, therefore, cannot greatly affect the density gradient in the range below elevations of 3000 km; for the lowest members of the Balmer series, a change in the adopted excitation temperature would produce appreciable corrections. The chromospheric density gradient of hydrogen, defined by

equation (2-7) was, in fact, derived from the high-series members and, moreover, is supported by the evidence given in Table 3, which is wholly independent of any assumptions concerning the excitation. As regards *He* I, the observational data are presented in a form which does not involve excitation corrections at all; the excitation potentials of those lines shown in Figure 12 whose symbols are joined by heavy lines do not differ by more than a few tenths of 1 volt. Finally, for the metallic elements, excitation corrections were applied to the individual multiplets before combining them into a single H-log I diagram, as described in Section III, *A;* however, in this case the empirical excitation temperatures listed in Table 5 were used instead of the theoretical boundary temperature. It is believed, therefore, that the comparison of the several density gradients assembled in Figure 13 is not made illusory on account of debatable assumptions concerning the excitation.

The magnitude of the density gradient of hydrogen has an interesting bearing upon the problem of the sharpness of the apparent solar limb,[44] because the opacity of the solar atmosphere for visible light originates entirely from the ionization continuum of the negative hydrogen ion. As pointed out before, the hypothetical photospheric gradient of hydrogen is about seven times greater than the chromospheric one observed at elevations as little as 500 km above the solar limb. If this chromospheric gradient should extend downward, unaltered, right to the levels corresponding to the solar limb, the limb would be much more diffuse than in the case of hydrostatic equilibrium at those levels. The predicted difference in sharpness is so enormous that it ought to be possible to let observation decide between these alternatives.

The intensity distribution along the solar radius is given, at the extreme limb, by the expression

$$I = I_0 \, (1 - e^{-\tau'}) \, , \tag{6-5}$$

where I_0 is the surface brightness of the limb (emission according to Planck's law with the boundary temperature of the sun, $T_0 = 4830°$ K), and τ' is the optical thickness of the emitting layer measured along the radius of vision, which passes at an elevation H above a certain zero level. Moreover, let τ be the optical depth along the solar radius, measured inward, down to the same level H. The formulas for the respective optical thicknesses are

$$\tau' = 2 \int_0^\infty \kappa \rho d y \qquad \text{and} \qquad \tau = \int_H^\infty \kappa \rho d x \, , \tag{6-6}$$

where κ is the mass absorption coefficient and ρ is the density; dy is the line element along the line of vision; and dx the line element along the solar radius. For the solar atmosphere it is possible to express κ as a product $\kappa_0 p_e$, in which κ_0 is a function solely of the temperature. Write $p_e = cP^m$, where P is the total pressure and c and m are constants that have to be evaluated from an investigation of the ionization equilibrium. The equations (6-6) then assume the form (for $\mu = 1$)

$$\tau' = 2 \, \frac{\kappa_0 m_0}{kT_0} \, c \int_0^\infty P^{m+1} d y \qquad \text{and} \qquad \tau = \frac{\kappa_0 m_0}{kT_0} \, c \int_H^\infty P^{m+1} d x \, , \tag{6-7}$$

since, throughout the thin shell producing the phenomenon of the solar limb, the temperature may be regarded as constant and equal to the boundary temperature T_0. Because the ionization of hydrogen is negligible in the lower chromosphere, P can be put equal to the partial pressure of neutral hydrogen. Hence

$$P = P_0 e^{-\beta H} \, , \qquad \beta = 0.92 \times 10^{-8} \text{cm}^{-1} \, . \tag{6-8}$$

[44] Unsöld, *op. cit.*, p. 394; and A. Righini, *Memorie della Società Astronomica Italiana*, **15**, 217, 1943.

Then the result of the integration of (6-7) is[45]

$$\tau' = \frac{\kappa_0 m_0}{kT_0}\, cP_0^{m+1}\left[\frac{2\pi R_\odot}{\beta\,(m+1)}\right]^{1/2} e^{-\beta(m+1)H} \tag{6-9}$$

and

$$\tau = \frac{\kappa_0 m_0}{kT_0}\, cP_0^{m+1}\,\frac{1}{\beta\,(m+1)}\, e^{-\beta(m+1)H}\,. \tag{6-10}$$

It is convenient to fix the zero level from which H is counted in such a way that it corresponds to $\tau' = 1$; at this elevation the intensity distribution along the solar radius has its inversion point, as may readily be verified by differentiation of equation (6-5) with respect to H. Incidentally, this definition has the merit of according with the predictions of E. Mach's contrast theory,[46] which suggests that the human eye would represent the very locus of these inversion points as the optical limb of the solar disk.

In order to determine the constants c and m, the partial pressure of neutral hydrogen was computed from equation (2-13) as function of the electron pressure, by assuming $\log K_H = -5.38$ and $\log K_M = +1.03$; this was done for three different tentative values of the abundance ratio A of hydrogen to metals. Over the range $-1.0 < \log p_e < +1.0$, the results of the computations can be represented by the empirical formulas:

$$\log A = +2.90\,, \qquad \log p_e = -2.68 + {}_1{}^9{}_0 \log P\,; \tag{6-11}$$

$$\log A = +3.90\,, \qquad \log p_e = -3.17 + {}_1{}^8{}_0 \log P\,; \tag{6-12}$$

$$\log A = +4.90\,, \qquad \log p_e = -3.33 + {}_1{}^7{}_0 \log P\,. \tag{6-13}$$

The deviations of these interpolation formulas from the exact values are, at most, 0.04, or smaller than 10 per cent in p_e. For $\log A \geqslant +5.90$ and $\log p_e \leqslant -0.80$ the rigorous limiting expression

$$\log p_e = -2.69 + \tfrac{1}{2} \log P \tag{6-14}$$

may be used.

With respect to κ, S. Chandrasekhar has recently urged[47] that in a "gray" atmosphere the best way of choosing the mean absorption coefficient for continuous radiation is to define it as a straight mean of κ_ν, weighted according to the ratio $F_\nu(\tau)/F$ of the net monochromatic flux to the integrated flux, or

$$\kappa = \int_0^\infty \kappa_\nu \frac{F_\nu(\tau)}{F}\, d\nu\,. \tag{6-15}$$

The weighting factor F_ν/F is tabulated in Chandrasekhar's paper. The κ_ν were taken from Chandrasekhar's latest investigation, dealing with an improved evaluation of the absorption coefficients of the negative hydrogen ion.[48] The result of the integration of (6-15) for the outer boundary of the photosphere is $\log \kappa_0 = -1.20$; this quantity may be subject to later revision, for instance, after improved values of the absorption coefficient for the free-free transitions of H^- have become available. Any such revision would only cause the reference value of the pressure at the level $\tau' = 1$ to be slightly altered but will not affect the general argument about to be presented.

The radial intensity distribution at the extreme solar limb has been computed by combining equations (6-5) and (6-9) and using the expression (6-14) for the electron pressure. The resulting values of I/I_0 are plotted in Figure 14 for two different assumptions about the exponent β in the density law (6-8), namely, $\beta = 0.92\ 10^{-8}\text{cm}^{-1}$, as ob-

[45] Unsöld, *op. cit.*

[46] Cf. A. Kühl, *Festschrift für Hugo von Seeliger* (Berlin, 1924), p. 372.

[47] *Ap. J.*, **101**, 328, 1945.

[48] *Ap. J.*, **102**, 395, 1946.

served in the lower chromosphere according to equation (2-7), and $\beta = 6.9\ 10^{-8}\text{cm}^{-1} = g_{\odot} m_0 / kT_0$, which implies hydrostatic equilibrium at the theoretical boundary temperature of the sun. The behavior of these two curves is strikingly different. If the photospheric density gradient does prevail in the thin shell producing the phenomena of a "sharp" solar limb, the entire intensity drop is confined to a range of less than $0''.5t$, or about 300 km. Conversely, if the observed chromospheric density gradient should extend all the way down to the solar limb, the limb would be remarkably diffuse, cover-

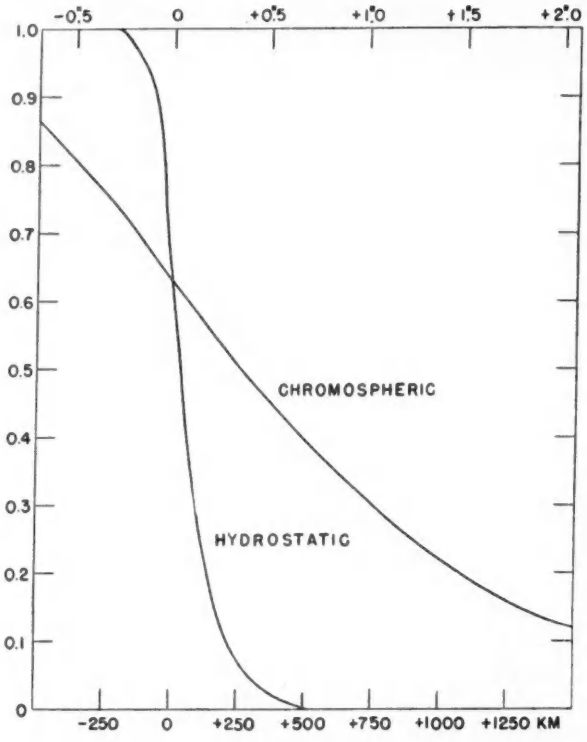

FIG. 14.—Predicted sharpness of the solar limb. *Abscissae*, radial distance from the solar limb; *ordinates*, intensities in units of the surface brightness of the solar limb at infinite optical thickness.

ing a range in height of at least $3''$, or 2000 km. Computations were also carried out with the expressions (6-11), (6-12), and (6-13) for the electron pressure. The resulting limb profiles diverge so little from that shown on Figure 14 that they were omitted for the sake of clarity. However, with these variant expressions, the electron and gas pressure at the reference level $H = 0$ km, i.e., $\tau' = 1$, assume quite different values; likewise the gradient of the electron pressure is altered. The ultimate choice between these different models of the solar atmosphere depends on considerations which will be sketched presently.

The writer is under great obligation to Professor B. Lindblad for his kind permission to quote from a recent letter of his the following passage which bears upon the question of the sharpness of the solar limb:

I wish to communicate to you that I have now the first results of a photometry of the rate of decrease of the continuous spectrum at the limb of the Sun from the cinematography of the flash spectrum which I undertook at the eclipse of July 9, 1945.

The measurements so far made refer to the last drop of the photosphere at the 2nd contact. The results are still preliminary, in so far as the density curve employed has to be tested for the influence of the difference in exposure time between the film camera and the sensitometer, but I do not think that the error can be large. The intensity fall shows such a striking agreement with your photospheric gradient that I hasten to send the results to you. They run as follows from an arbitrary I_0 which represents the highest measureable density. The spectrum has been measured near $H\beta$ where there are few chromospheric lines of any considerable intensity.

Elevation above Limb	I/I_0	Elevation above Limb	I/I_0
0".00	1.000	0".43	0.145
0.09	0.692	0.52	0.0938
0.17	0.437	0.60	0.0686
0.26	0.313	0.69	0.0453
0.35	0.211		

Comparing with your photospheric gradient, there is very good agreement for I/I_0 between 0.4 and 0.9.

It is true that I/I_0 is not with necessity the same in the two cases, but as the curves are nearly exponential in shape this is perhaps not so important.

There is a departure between the curves close to 1.00, as there must be, because in my case, when we reach the photospheric disk, the spectrum of a successively broader strip of the limb is photographed, so that the intensity must still increase rapidly with decreasing (negative) elevation.

At the small intensities there is a departure, my values being higher. This will partly be due to the background intensity, which has not been eliminated, but perhaps also to a transition to the "chromospheric gradient," as here the integrated intensity of the lines may become of some importance.

I have obtained material for a correction of the sensitometer scale on the film to the same exposure-time as that of the flash-film. On the film of the flash spectrum the sensitometer impressions were made with a few seconds' exposure, whereas the exposure-time of the flash spectrum is about 1/50 second. The correction will be small, and will tend to increase slightly the steepness of the observed gradient. It seems that it will rather improve the agreement with your theoretical photospheric gradient.

It rather seems as if we get in this way an experimental verification of the negative hydrogen ion as the main source of continuous absorption in the photosphere, which was really one of the principal aims of my cinematographic work on the flash spectrum.

In the present context, the significant conclusion to be drawn from Professor Lindblad's photometric work is that the transition from the photospheric to the chromospheric gradient must occur in the narrow interval between elevations of 200 and 500 km; in other words, the chromosphere has a rather well-defined lower boundary. With the definitive photometric profile at hand, it will become possible to make a study of more detailed models of the solar limb and the boundary layer of the chromosphere, by superimposing the two density laws of hydrogen in the form

$$P = P_0 \left[e^{-(0.92\times10^{-8}\mathrm{cm}^{-1})H} + B\, e^{-(6.9\times10^{-8}\mathrm{cm}^{-1})H} \right], \qquad (6\text{-}16)$$

instead of using equation (6-8), and then varying the constant B and the abundance ratio A. The aim would be to represent simultaneously the observed limb profile and the electron pressure of equations (2-9), which was obtained from the Inglis-Teller theory. If a satisfactory representation can be achieved, it would amount to an independent physical definition of the fiduciary level on which Dr. Mitchell's system of estimated heights is based.

Note added in proof:

Dr. Lyman Spitzer, Jr., has kindly pointed out that the influence of the Doppler width at $T = 35{,}000°$ K on the structure of the chromospheric crescents ought to be investigated before the density gradients here derived can be accepted, and that such an investigation can readily be carried out by the formalism already developed for the scintillation effect. The only change needed is to replace the scintillation parameter, s, by the appropriate parameter, s', representing the Doppler profile. For hydrogen the half-width at $T = 35{,}000°$ K is approximately $2\Delta\lambda = 0.65$ A, or 0.06 mm on the scale of Dr. Mitchell's flash spectrograms (dispersion, 10.8 A/mm); since the focal length of the concave grating was 1500 mm, $\Delta\lambda$ 0.03 mm corresponds to an elevation above the solar limb of about 4″. Hence, $s' = 0.693/(4'')^2 = 0.043('')^{-1}$. This value happens to agree closely with 0.05, the value of s adopted for evaluating the influence of scintillation upon the density gradients of *Fe* I and *Ti* II. However, for these heavy atoms the Doppler width is much smaller than for hydrogen, and its influence upon the density gradients must be negligible, because the scintillation effect for $s = 0.05$ has proved insignificant. Thus the previous conclusions remain unaffected.

A SEARCH FOR FAINT BLUE STARS*

M. L. HUMASON AND F. ZWICKY
Mount Wilson Observatory and California Institute of Technology
Received September 6, 1946

ABSTRACT

Four-color photography has been used in a search for faint blue stars with the 18-inch Schmidt telescope at Palomar, undertaken in the hope of finding new white dwarfs. In this *Contribution* the results are given for stars brighter than magnitude 15.0 pg in two regions: (*a*) the Hyades cluster; (*b*) the region of the north galactic pole. Spectroscopic observations have been made with the 100-inch reflector.

In the Hyades region fourteen blue stars were found, with spectral types ranging from B0 to B5. Proper motions are known for ten of these stars. From their motions and spectra, four are shown to be white dwarfs, three of them physical members of the cluster. Absorption lines are wide and shallow in the spectra of two others, whose motions are not known—an indication that they also may be white dwarfs.

In the region of the north galactic pole thirty-one blue stars were found. Their spectra range from B0 to A0. Proper motions are available for only four stars, one of which, from its motion and spectrum, is a white dwarf. Two other stars, whose motions are unknown, have spectra similar to those of the white dwarfs. The spectra of the remaining twenty-eight stars appear normal; if these objects are high-luminosity blue stars, their distances are exceedingly large. Possibly they belong to the type of stellar population shown in the Hertzsprung-Russell diagram for globular clusters and designated by Baade as "Type II." If so, their absolute magnitudes are about 0.0, and their distribution in space would be similar to that of the globular clusters and cluster-type variables.

I. GENERAL OUTLINE OF THE SEARCH PROGRAM

Schmidt telescopes of large apertures are well suited for search programs because they give uniform definition over considerable fields and because they are practically achromatic and allow the effective use of full-size objective prisms and gratings. As part of the work of the 18-inch Schmidt telescope at Palomar, a survey of the sky in different colors has been conducted during the past few years. Large areas of the sky were photographed in the infrared, red, yellow, blue, and near ultraviolet parts of the spectrum with the intention of selecting different types of interesting stars from the relative intensities in various parts of their spectra. In the present paper some results are given for a number of faint blue stars found during a search for white dwarfs. The search part of the program covered in this report was carried on during the years 1939–40 and was concentrated in two regions, namely, (*a*) the Hyades cluster of stars and (*b*) the neighborhood of the northern galactic pole. The reasons for these choices are as follows: J. M. Ramberg had announced the discovery of two white dwarfs among the physical members of the Hyades cluster.[1] A further search for white dwarfs among the faint members would be of particular interest in connection with the evolution of star clusters. It was expected also that, if apparently faint blue stars were found at the northern galactic pole, they might be white dwarfs, as the main-sequence stars of types O, B, and A are highly concentrated along the plane of the Milky Way.

For practical reasons the search was limited to stars brighter than about the fifteenth apparent photographic magnitude. To identify short-period variable stars, each field was photographed four times within a few hours on clear nights. The four types of photographs are as follows:

1. One exposure of 10 minutes on Agfa Supersensitive Panchromatic film with an intervening Minus Red 2 Gelatin filter, covering the region λλ 3500–5400.

* *Contributions from the Mount Wilson Observatory, Carnegie Institution of Washington*, No. 724.

[1] *A.N.*, **265**, 111, 1938; *Stockholms Obs. Medd.*, No. 37, 1938; *Stockholms Obs. Ann.*, **13**, No. 9, 90, 1941.

2. One exposure of 30 minutes on Agfa Supersensitive Panchromatic film with an Aero 2 Gelatin filter or a GG 11 glass filter of 2-mm thickness, covering the region λλ 4900–7000.

3. One exposure of 10 minutes on Agfa Commercial noncolor-sensitive film, covering the region λλ 3500–5200.

4. One exposure of 60 minutes on Agfa Supersensitive Panchromatic film with a 2-mm UGI glass filter, covering the region λλ 3500–3900.

All the films were developed for 7 minutes with Rodinal 1:20 at 65° F. The yellow exposure, No. 2, was then compared with the violet exposure, No. 4; blue stars could be identified with relative ease if no strong Balmer continuum in absorption was present. The blue exposures, Nos. 1 and 3, were compared to rule out short-period variable stars. A succession of fields was chosen, centered around guide stars 5° apart in right ascension and declination. Since the diameter of the field for the Schmidt telescope is slightly greater than 9°, most of the stars were included in different fields, and additional checks were obtained. This check is necessary because some of the photographs are not of the very best quality. The films sometimes move slightly in the plateholder because of the effects of humidity and differences in temperature, especially during the longer exposures. Also dust specks on the filters may interfere with a star image, and inequalities may occur in the process of development. Some difficulties were encountered because of variable red sensitivity of the panchromatic films.

II. PRELIMINARY LIST OF FAINT BLUE STARS

In Table 1 we give the results for fifteen stars in the region of the Hyades cluster and thirty-three stars near the northern galactic pole. Eighteen fields, each about 9° in diameter, were searched. The nine fields in the Hyades are centered on the intersections of three hour-circles having right ascensions 3^h56^m, 4^h16^m, and 4^h36^m, with three declination-circles at $+10°29'$, $+15°29'$, and $+20°29'$ (1940). The nine fields at the northern galactic pole are centered on the intersections of three hour-circles having right ascensions 12^h11^m, 12^h36^m, and 13^h1^m, with three declination-circles at $+31°18'$, $+36°18'$, and $+41°18'$ (1940). The apparent photographic magnitudes were estimated relative to the nearest available selected areas. The color classification is not quantitative but is divided into three classes: blue, decidedly blue, and very blue, referring to approximate ranges in the color index from +0.3 to −0.1, −0.1 to −0.3, and −0.3 to −0.6, respectively. These ranges were first established through tests on some brighter, unobscured A and B stars and later checked on fainter stars for which K. G. Malmquist[2] has determined the color indices. The co-ordinates given in Table 1 refer to the epoch 1855 and were measured relative to the nearest BD stars. Stars with known and large proper motions have been designated as white dwarfs by the letter "D," as proposed by W. J. Luyten.[3] Absorption lines in the spectra of stars referred to as having wide lines appear on our small-scale spectra to be from 20 to 80 angstroms wide.

In Table 2 is shown the distribution in colors and magnitudes of stars in the region of the Hyades cluster.

The distribution in colors and magnitudes of the stars near the northern galactic pole is shown in Table 3.

The list is complete to stars of about the fifteenth photographic magnitude. In view of the very small number of stars involved in these counts, the indicated increase in the number of stars per unit magnitude interval is probably not significant.

Spectra.—The spectral types of the forty-eight stars in Table 1 have been estimated from low-dispersion spectrograms obtained from 1940 to 1944 with the 100-inch reflector of the Mount Wilson Observatory. With the exception of seven stars, the dispersion used was 220 A/mm at $H\gamma$. Numbers 5, 7, 13, 28, 32, 33, and 34 were taken with a dispersion

[2] *Stockholm Obs. Ann.*, Vol. **12**, No. 7, 1936.

[3] *Ap. J.*, **101**, 131, 1945.

TABLE 1

PRELIMINARY LIST OF FAINT BLUE STARS

(Asterisks refer to notes on following page)

No.	R.A. 1855	Decl. 1855	m_{pg}	Color	Spectrum
	In the Region of the Hyades Cluster				
1	4^h41^m8	+17° 27′	12.7	Very blue	B2
2*	4 4.8	11 30	13.7	Very blue	B5
3*	3 45.6	10 19	13.0	Very blue	DB1
4*	3 47.4	9 20	14.8	Blue	DB3
5	3 44.0	6 43	14.7	Decidedly blue	B5
6	4 3.5	15 00	14.6	Blue	B3
7*	4 25.7	12 23	14.5	Decidedly blue	B3
8	4 41.0	13 35	14.6	Blue	B3
9*	4 24.0	17 26	14.1	Blue	DB3
10*	4 1.8	17 39	14.4	Decidedly blue	DB5
11	4 21.7	7 23	14.7	Decidedly blue	B2
12	4 16.3	8 12	12.8	Blue	B3
13*	4 39.8	7 33	14.6	Blue	G0
14	4 33.0	10 42	13.5	Decidedly blue	B2
15	4 32.8	+ 8 25	12.8	Blue	B5
	In the Region of the North Galactic Pole				
16	11^h50^m6	+30° 46′	14.4	Blue	A0
17	11 57.8	40 57	14.4	Blue	B2
18	12 1.6	37 51	15.1	Decidedly blue	B2
19*	12 5.5	34 42	12.8	Blue	B5
20*	12 5.4	43 28	14.9	Decidedly blue	B3
21	12 6.6	33 44	14.2	Very blue	B0
22	12 7.5	37 28	12.7	Decidedly blue	B3
23	12 10.1	32 58	14.2	Blue	A0
24	12 17.5	39 57	11.4	Blue	B8
25*	12 18.2	36 47	10.0	Very blue	B5
26	12 21.5	29 9	13.7	Blue	B5
27	12 24.6	39 48	12.5	Blue	A0
28*	12 25.4	42 17	15.2	Decidedly blue	B3
29*	12 27.8	38 26	13.6	Decidedly blue	B0
30	12 30.2	39 23	13.4	Decidedly blue	B5
31*	12 35.9	32 52	12.8	Blue	A0
32	12 44.1	37 58	15.2	Blue	B1
33	12 44.1	34 25	14.6	Blue	A0
34	12 48.4	38 20	14.7	Decidedly blue	B0
35	12 46.3	30 54	15.0	Decidedly blue	B2
36	12 49.4	33 13	14.3	Blue	A0
37	12 55.9	39 14	12.0	Decidedly blue	B8
38	12 52.4	28 20	13.9	Very blue	B0
39	12 57.8	28 54	14.8	Blue	B0
40	13 6.8	37 44	13.8	Decidedly blue	B2
41*	13 10.5	39 49	13.3	Blue	F0
42	13 6.4	32 8	14.2	Blue	B5
43*	13 9.5	29 52	12.5	Blue	DB0
44	13 17.0	36 53	11.0	Very blue	B2
45	13 19.3	40 53	12.4	Decidedly blue	B5
46*	12 50.0	33 13	14.7	Blue	F
47	12 52.4	28 8	14.7	Decidedly blue	B5
48	12 53.0	+41 48	13.6	Blue	A0

NOTES TO TABLE 1

No. 2.—Small proper motion in R.A. The spectral lines are shallow and very wide, indicating a white dwarf.

No. 3.—Van Maanen's measure of the proper motion indicates that this is a member of the Hyades cluster and therefore a white dwarf. The continuous spectrum extends far into the violet. Absorption lines are extremely weak and narrow.

No. 4.—Van Maanen's proper motion makes this a Hyades star and a white dwarf. Spectral lines are shallow and very wide.

No. 7.—Small proper motion in R.A. As the lines are shallow and very wide, the spectrum indicates a white dwarf.

No. 9.—Van Maanen and Luyten have both measured the proper motion; their results indicate that the star is a member of the Hyades cluster and therefore a white dwarf. Luyten's proper motion was measured previous to our discovery, and his designation is L 1239-16. Luyten informs us that E. G. Ebbighausen has measured a proper motion of 0".08 for this star. The spectral lines are very shallow and extremely wide. The continuous spectrum extends far into the violet. Suspected of being variable in light, and possibly in color.

No. 10.—Van Maanen's proper motion in R.A. is small. Luyten finds a measurable negative proper motion in both components. The spectrum lines are shallow and very wide. Probably white dwarf. Not a member of the Hyades cluster.

No. 13.—The indication that this star is blue may possibly be due to a defective spot on one film. Identification has been checked and found correct.

No. 19.—Malmquist No. 11.

No. 20.—Malmquist No. 33.

No. 25.—Malmquist No. 161; BD+36°2268.

No. 28.—The spectrum indicates that this star is possibly a white dwarf, as the lines are shallow and very wide.

No. 29.—Malmquist No. 132.

No. 31.—Malmquist No. 338.

No. 41.—Color measures show this star bluer than the spectrum would indicate.

No. 43.—Previously found by Luyten from the proper motion and designated by him as L 1409-4. The proper motion makes this star a white dwarf. The spectrum appears nearly continuous on small-scale spectrograms, which makes the classification uncertain. May be O type. A fifteenth-magnitude companion is 2" preceding.

No. 46.—Coincident with an anonymous extragalactic nebula.

TABLE 2

DISTRIBUTION IN COLOR AND MAGNITUDE OF FAINT BLUE STARS IN THE REGION OF THE HYADES CLUSTER

RANGE IN m_{pg}	NUMBER OF STARS			TOTAL
	Blue	Decidedly Blue	Very Blue	
10.0–10.5				
10.5–11.0				
11.0–11.5				
11.5–12.0				
12.0–12.5				
12.5–13.0	2		2	4
13.0–13.5		1		1
13.5–14.0			1	1
14.0–14.5	1	2		3
14.5–15.0	4	2		6
15.0–15.5				

of 500 A/mm at $H\gamma$. Classification was made by comparison with stars of known spectral type whose spectra had been obtained with the same dispersion and under the same conditions as those in the table. Comparison stars consisted of several high-luminosity stars of types O, B, and A, and known white dwarfs. The uncertainty in the spectral classification is probably not greater than three-tenths of a spectral division for those stars in Table 1 whose spectra appear normal. For several stars with shallow and very wide absorption lines or with spectra which appear nearly continuous, the uncertainty is greater. In some stars this uncertainty may be as large as a whole spectral division.

Of the forty-eight stars in Table 1, six—Nos. 2, 3, 4, 7, 9, and 10—in the Hyades region and two—Nos. 28 and 43—in the region of the north galactic pole have spectra similar in appearance to such well-known white dwarfs as Wolf 485, Wolf 1346, and AC+70°8247. Two stars—Nos. 13 (G0) and 41 (F0)—have types which do not correspond to the color indicated by the Schmidt photographs. The identifications of both stars have been checked and found correct, and the discrepancy is possibly due to defective spots on the Schmidt photographs. Star 46 is centrally superimposed on an anonymous extragalactic nebula, which may account for the overestimation of blueness.

TABLE 3

DISTRIBUTION IN COLOR AND MAGNITUDE OF FAINT BLUE STARS NEAR THE NORTHERN GALACTIC POLE

RANGE IN m_{pg}	NUMBER OF STARS			TOTAL
	Blue	Decidedly Blue	Very Blue	
10.0–10.5	.....	.....	1	1
10.5–11.0	.....	.....	1	1
11.0–11.5	1	.....	.....	1
11.5–12.0	.....	1	.....	1
12.0–12.5	2	1	.....	3
12.5–13.0	2	1	.....	3
13.0–13.5	1	1	.....	2
13.5–14.0	2	2	1	5
14.0–14.5	5	.....	1	6
14.5–15.0	3	4	.....	7
15.0–15.5	1	2	.....	3

Color.—Of the forty-five blue stars, thirty-six have been classified as B5 or earlier; two as B8; and seven as A0. The stars in the Hyades region show no correlation between color and spectral type. At the northern galactic pole, mean values of color and spectral type show only a slight correlation. Whether the lack of correlation between color and spectrum at the galactic pole indicates reddening in a region relatively free from absorbing material is doubtful. More likely the cause is a combination of errors in the assigned color values and spectral types.

Proper motions.—Preliminary measures of the proper motions of the first ten of our stars in the Hyades region were made by the late Dr. A. van Maanen on plates having an interval of from 1 to 3 years. Dr. W. J. Luyten, at the University of Minnesota, has measured the motions of four of our stars in the Hyades region and four in the region of the north galactic pole. Luyten's measures were made on Harvard plates having a scale of 60″ per mm and an interval of 30–35 years. The values obtained by van Maanen and Luyten are in Table 4.

Discussion.—In the region of the Hyades cluster, fourteen faint blue stars have been found. Three of these stars—Nos. 3, 4, and 9—have proper motions corresponding to that of the Hyades cluster and are therefore members of the cluster. Since their apparent magnitudes thus imply absolute magnitudes with values from approximately +11 to +12, they are undoubtedly white dwarfs. A fourth star—No. 10—has, according to Luyten, a considerable motion, but not in the direction of the cluster. Van Maanen's measure in μ_α yields a motion only one-third as great as Luyten's. These four stars all have spectra similar to those of known white dwarfs. All absorption lines are shallow and about 20–80 angstroms wide; or, as in star 3, the lines are so extremely weak that the spectrum appears almost continuous. The spectra of stars 2 and 7 might indicate that they, too, are white dwarfs, but van Maanen's measures of μ_α show no appreciable motion. As the interval for van Maanen's plates is only 1 year for star 2 and 2 years for star 7, it is possible that future measures on plates having a longer interval will show an appreciable proper motion. In the spectra of the remaining eight stars in the Hyades region, all the absorption lines appear to be slightly wider and weaker than normal. Because of the small scale of our spectra, it is difficult to decide whether this peculiarity is real. If real, it may be caused by rotation, since the lines of all elements are affected.

TABLE 4

KNOWN PROPER MOTIONS

	Star	van Maanen		Luyten	
		μ_α	μ_δ	μ_α	μ_δ
Hyades region	1	+0″.002 ± 0″.026		+0″.006	−0″.011
	2	− .021 ± .036			
	3	+ .090 ± .015	−0″.010 ± 0″.009		
	4	+ .140 ± .011	− .016 ± .011		
	5	+ .002 ± .011			
	6	− .020 ± .011		+ .004	− .008
	7	+ .018 ± .010			
	8	+ .014 ± .008			
	9	+ .104 ± .016	−0.020 ± 0.006	+ .101	− .038
	10	+0.027 ± 0.015		− .076	− .082
North galactic pole	16			+ .024::	− .019::
	26			+ .012	+ .011
	39			− .001	− .014
	43			−0.143	−0.072

In the fields searched at the north galactic pole, thirty-one faint blue stars were found. Of the four stars whose proper motions have been measured by Luyten, one—No. 43—has so large a motion that it is almost certainly a white dwarf. One other star whose proper motion is unknown—No. 28—may possibly be a white dwarf, as the absorption lines are wide and shallow. The spectra of the remaining twenty-nine stars appear normal. These stars form an interesting group if we consider their absolute magnitudes and distances. Unlike the objects found in the Hyades region, they appear in a region free from absorption and, although their motions are as yet unknown, their spectra indicate that they are not white dwarfs. If they are stars of normal luminosity, these distances would be very great. If the mean absolute magnitude of a normal B3 star is −2.2, as determined by Stebbins, Huffer, and Whitford,[4] the distance moduli for stars of twelfth and

[4] *Mt. W. Contr.*, No. 621; *Ap. J.*, **91**, 20, 1940.

fifteenth apparent magnitude are as shown in the accompanying tabulation. Consequently, a fifteenth-magnitude normal B3 star would be at the same distance as the Small Magellanic Cloud. Considering also that our observations go only to apparent magnitude 15 and that Table 3 indicates an increase in the number of stars per unit magnitude interval, we should expect to observe B stars as faint as the seventeenth and eighteenth magnitudes. Such stars would be as distant as the Andromeda galaxy, in which B-type stars actually appear in large numbers at the seventeenth and eighteenth apparent magnitudes. It is therefore obvious that any assumption that the luminosities of these B stars are normal is wrong. The difficulty just mentioned disappears, however, if we identify them with the B-type stars of Baade's population II, as shown in the Hertzsprung-Russell diagram for globular clusters.[5] These stars are at the blue end of the horizontal branch and have the absolute magnitude 0. Since they have the same absolute

Apparent Magnitude	Modulus	Distance
$m=12$	$m-M=14.2$	6,600 pc
$m=15$	$m-M=17.2$	27,000 pc

magnitude as the cluster-type variables, we should expect to find them scattered thinly in all directions, forming an almost spherical system. Additional evidence that these are stars of intermediate brightness is furnished by the observation by Baade and Minkowski of the spectra of two Type II blue stars in the globular star cluster M3. The spectral types of these two stars are O and B2, respectively, and the absolute magnitudes about 0.

The velocities of all the stars in Table 1 have been measured; but, because of the small dispersion used and the resulting large probable error, the results are not listed. Most of the velocities are small, however, and for that reason it seems improbable that the stars have moved out of the plane of the Milky Way. The outstanding exceptions are velocities of +200 km/sec for star 8 in the Hyades region, and −220 km/sec for star 17 in the region of the north galactic pole.

Because of the uncertainty in the absorption factor for the Hyades region, no assumption has been made in regard to the absolute magnitudes of stars with small proper motions in that region.

We wish to thank Dr. Luyten for his proper-motion measurements of four stars in the Hyades region and four in the region of the north galactic pole.

[5] *Mt. W. Contr.*, No. 696; *Ap. J.*, **100**, 137, 1944.

THE RELATIVE INTENSITIES OF THE CORONAL AND OTHER FORBIDDEN LINES*

I. S. BOWEN AND P. SWINGS
Mount Wilson Observatory
Received September 18, 1946

ABSTRACT

The behavior of the coronal lines in RS Ophiuchi, T Pyxidis, and T Coronae Borealis is in accord with the physical properties of these lines as predicted from Edlén's identifications. Observed anomalies in the relative abundance of certain ions in these and similar objects may be explained by irregularities in the intensity-curve of the primary exciting radiation of the central star, caused by *H* and *He* II continuous absorption. One line in the RS Oph spectrum is identified with [*K* XI].

In 1941, Bengt Edlén identified the coronal lines as forbidden lines of *A*, *Ca*, *Fe*, and *Ni* in the ninth to fifteenth stages of ionization. Strong evidence, from the physical side, for these identifications was provided by Edlén's own measurements of the extreme ultraviolet spectra of these ions.

From the astrophysical standpoint the presence of these extremely high stages of ionization in the neighborhood of the sun raised many difficult questions. Particularly disturbing was the presence of very highly ionized ions in the corona along with neutral and singly ionized atoms in the chromosphere and prominences, while all intermediate stages of ionization seemed to be absent.

The two strongest coronal lines, λ 5303 and λ 6374, have been observed in the three stars, RS Ophiuchi,[1] T Pyxidis,[2] and T Coronae Borealis;[3] three fainter coronal lines also have been detected in RS Oph. It becomes of interest, therefore, to consider whether the behavior of the coronal lines in these objects is in accord with the properties of the ions concerned, as predicted by physical theory. In particular, it is important to note whether this behavior throws any light on the difficulty already mentioned.

Table 1 lists all the coronal lines that have been definitely observed in at least one object besides the corona itself. The third column gives the transition probability A_m of each line; the fourth to seventh columns show the observed intensities in the various objects. For comparison, the transition probabilities and the intensities of the strongest lines of [*Fe* VII] and [*O* III] also are listed.

In passing from the *Fe* X of the coronal spectra to the lower stages of ionization of *Fe*, the first stage having forbidden transitions in the observable range is *Fe* VII. Aside from the difference in ionization, the chief difference between the lines of [*Fe* VII] and the strongest coronal lines assigned to [*Fe* X] and [*Fe* XIV] lies in the fact that the transition probabilities of the coronal lines are greater by a factor of about 100. One may, therefore, expect a marked decrease in the ratio of the intensities of [*Fe* VII] lines to coronal lines in passing to objects of increasing density. Such a decrease in the relative intensities may be observed if the objects in Table 1 are examined from right to left. That the change in density is a major cause of this shift in the relative intensities is

* *Contributions from the Mount Wilson Observatory, Carnegie Institution of Washington*, No. 725.

[1] Observed in 1933 but recently described in more detail by Joy and Swings, *Mt. W. Contr.*, No. 714; *Ap. J.*, **102**, 353, 1945.

[2] A. H. Joy, *Pub. A.S.P.*, **57**, 171, 1945.

[3] R. F. Sanford, *Pub. A.S.P.*, **58**, 156, 1946; D. B. McLaughlin, *Pub. A.S.P.*, **58**, 159, 1946; Herbig and Neubauer, *Pub. A.S.P.*, **58**, 196, 1946; J. Dufay, *I.A.U. Circular*, No. 1036 (Copenhagen, 1946).

shown by the behavior of the [*O* III] lines. In T Pyx the density was evidently very low, since the highly forbidden nebular pair at λ 5007 and λ 4959 was nearly as strong as λ 4363, which has a much higher transition probability. In RS Oph, however, increased density reduced the intensity of the lines of the nebular pair to less than one-tenth the intensity of λ 4363. In T CBr, λ 4363 was the only [*O* III] line observed, and it appeared only a short time before the disappearance of the coronal lines. No [*O* III] lines are observed in the corona. Indeed, with the exception of λ 4363 in T CBr and a few [*Fe* II] lines observed both in T CBr and in the chromosphere,[4] the coronal lines are the only forbidden lines observed either in the sun or in T CBr during the period under consideration. Although no direct calculations have been made, there is experimental evidence for believing that the transition probabilities of the [*Fe* II] lines are nearly as great as those of the coronal lines.[4, 5]

TABLE 1

INTENSITIES OF FORBIDDEN LINES IN VARIOUS SOURCES

Ion	λ	A_m (Sec^{-1})	Corona	T CBr	RS Oph	T Pyx
Ca XIII	4086.3	319	1.0	—	2	.....
Ni XII	4231.4	237	2.6	—	4	.....
Fe XIV	5302.86	60	100	P*	6	2
Fe XI	3986.9	9.5	0.7	—	4	.....
Fe X	6374.51	69	8.1	P*	20	1
Fe VII	6087.6	0.49	.....	—	3	5
	5722.6	0.30	.....	—	.....	M‡
	5163.2	0.21	.....	—	0	2
	3758.9	0.37	.....	—	4	2
O III	5006.84	0.016	.....	—	3	40
	4958.91	0.0056	.....	—	1	20
	4363.21	2.8	.....	†	35	50

* Present.

† Absent when the coronal lines first appeared, but present as a narrow line shortly before their disappearance.

‡ Masked.

The appearance of the coronal lines in these additional objects therefore provides definite evidence that, as the density varies, the coronal lines behave in just the manner that would be expected from Edlén's identifications. Furthermore, these additional observations give added weight to the suggestion originally made by Joy and Swings[1] that high density causes the absence of the forbidden lines of the intermediate stages of ionization in certain of these objects.

Other apparent anomalies in the relative abundance of certain ions in these objects may be caused by the operation of the primary mechanism of excitation of the gaseous envelopes. Presumably, the emission spectra of such objects as T CBr, RS Oph, and T Pyx come from a surrounding gaseous cloud excited by a mechanism similar to that which has proved effective in explaining the spectra of the planetary nebulae.[6] In this mechanism the primary step is the photo-ionization of the gas by the absorption of the continuous ultraviolet radiation of a very hot central star. Since approximately 99 per cent of the atoms in most astronomical objects are either *H* or *He*, these atoms will be the chief absorbers of radiation by this process. Furthermore, in the side of the cloud

[4] Bowen and Menzel, *Pub. A.S.P.*, **40**, 332, 1928.

[5] Swings and Struve, *Ap. J.*, **93**, 455, 1941.

[6] I. S. Bowen, *Ap. J.*, **81**, 1, 1935.

nearest the hot star this absorption will be limited largely to the ions *H* I and *He* II. The continuous stellar radiation entering the cloud will, therefore, be rapidly depleted in the regions of wave length shortward of the respective limits of absorption of these ions, 912 and 228 A. Throughout most of the cloud the primary exciting radiation will be greatly deficient in these two wave-length ranges. As a result, any ion whose ionization limit falls just short of 912 and 228 A will not be further ionized as rapidly as ions whose limits fall on either side of these deficient bands in the spectra. This should cause a substantial increase relative to adjacent stages of ionization in the population of ions whose limits fall in these deficient bands.

Because of the deficiency in radiation below 228 A, one would expect an unusual number of atoms in the stages *C* IV, *N* IV, *O* III, *Ne* III, *A* IV, *K* IV, *Fe* IV, etc., while the band below 912 A should cause an increase in the abundance of *O* I, *Si* II, and *Fe* II. One should, therefore, expect low-excitation-potential lines of these ions, either forbidden or permitted, to be abnormally strong where such lines exist in the observable range. High-excitation-potential lines, usually permitted, are normally formed in the course of recombination of the ion with an electron. This type of line should therefore appear with enhanced intensity for the next lower stage of ionization in each atom.

This effect will be still further enhanced by the presence in the gaseous envelope of strong emission lines of *H* and *He* II in the regions just longward of the respective limits, 912 and 228 A. Thus the absorption of these *H* and *He* II lines will cause an additional increase in the population of the ions whose absorption limits fall just shortward of 912 and 228 A at the expense of the next lower stage of ionization. For example, the population of *Fe* IV should be still further increased with respect to *Fe* III.

From the wide range of ionization in an object such as RS Oph, it would be inferred that the central star is surrounded by a layer of gas which is relatively thick in terms of the mean free path of the primary exciting radiation. Consequently, this mechanism should be particularly effective in RS Oph in modifying the normal distribution of ions between the various stages. It is, therefore, not surprising to find the lines of permitted *C* III and *N* III and forbidden *O* III, *Ne* III, and *Fe* II abnormally strong relative to the neighboring stages of ionization of these atoms. No forbidden or permitted lines of low excitation potential exist for *Fe* IV in the observable range. However, the transfer of most of the *Fe* in the lower stages of ionization to *Fe* II and *Fe* IV may account for the observed weakness of [*Fe* III], [*Fe* V], and [*Fe* VI], compared to [*Fe* II] and [*Fe* VII].

The same tendency to favor certain ions has been evident in varying degrees in the spectra of other objects, such as AX Per, CI Cyg, and RX Pup, which show a wide range of stages of ionization. The fact that [*Fe* II] and [*Fe* VII] are both strong at the same time, in comparison to the intervening stages, has long been particularly puzzling in these objects. Previously, the interpretation of these effects has been sought in the binary character of the objects or in stratification phenomena. If the present interpretation is correct, it may not be necessary to call on these older explanations.

The behavior of *Ca* II, *Fe* II, *Ti* II, etc., in the hotter stars suggests that the mechanism discussed in this *Contribution* may play a role in the excitation of the emission lines found in the spectra of many of these objects. Thus in the emission spectra of these stars the lines of *Ca* II, whose series limit at 1044 A is well outside the *H* absorption band, are relatively faint compared to the lines of such ions as *Fe* II and *Ti* II. This is in marked contrast with the absorption spectra of stars of early type, in which the *Ca* II lines are normally outstanding among the metallic lines.

Unfortunately, in many objects it is difficult to obtain a definite evaluation of the effectiveness of this mechanism through the determination of the relative populations in the various stages of ionization of a given element. Many of the higher stages of ionization of most elements have no lines of low excitation potential in the observable range. The few available lines of this type are almost invariably forbidden. Furthermore, the transition probabilities of the forbidden lines of successive stages of ionization often

differ in order of magnitude. As discussed on page 92, this causes the relative intensities to be subject to large variations, dependent upon the density in the region of emission. Thus, of the abundant elements, iron has probably the largest number of stages of ionization that are represented with low-excitation-potential lines in the observable range. However, no satisfactory lines are available for *Fe* IV, *Fe* VIII, *Fe* IX, and *Fe* XII. The transition probabilities of all forbidden lines of *Fe* VI and *Fe* VII are less than 1 sec^{-1}. The lines of [*Fe* X], [*Fe* XI], [*Fe* XIII], [*Fe* XIV], [*Fe* XV] and probably most of the lines of [*Fe* II] have values in the range from 9 to 100 sec^{-1}. The transition probabilities of the [*Fe* III], [*Fe* V] lines are unknown. Consequently, the [*Fe* II] lines, like the coronal lines, may in many cases owe to high density part of their enhancement relative to the lines of other stages of ionization. Because of these complications, it is often necessary, therefore, to rely on general trends among the ions of all available atoms for an evaluation of the effectiveness of this mechanism in shifting the distribution between various stages of ionization. In any case, the mechanism is one more factor that must be considered in a quantitative study of the physical conditions in emission-line objects.

In this discussion of the spectrum of RS Oph, one new identification should be noted. The $^2P_{3/2}-{}^2P_{1/2}$ transition of [*K* XI] was predicted by Edlén at λ 4258.7 but is not found in the corona. A line of intensity 1 has been observed in RS Oph at exactly this wave length, but it was identified by Joy and Swings as λ 4258.15 *Fe* II—an identification which is certainly insufficient and probably erroneous. The line λ 4258 *Fe* II is a component of laboratory intensity 3 in the $b^4P - z^4F^o$ multiplet. The strongest member of this multiplet at λ 4178.85 (lab. int. 8) is doubtfully attributed, as part of a blend, to a line of intensity 1 in RS Oph. The other components of the multiplet, λ 4296.57 (lab. int. 6), λ 4122.64 (lab. int. 4), and λ 4369.40 (lab. int. 2) are absent in RS Oph. Of the stronger $b^4P - z^4D^o$ multiplet, which has an excitation similar to that of $b^4P - z^4F^o$, several components, stronger than λ 4258.15 in the laboratory (or in α Cyg), are not found in RS Oph. It is thus probable that the line observed at λ 4258 in RS Oph is actually due to [*K* XI]. The star shows strong [*K* IV] and [*K* V].

RADIAL VELOCITIES AND SPECTRAL TYPES OF 181 DWARF STARS*

ALFRED H. JOY
Mount Wilson Observatory
Received September 19, 1946

ABSTRACT

Spectral types and radial velocities have been determined for 181 dwarf stars having for the most part proper motions greater than 0".35. The classification follows the Henry Draper system except that 21 subdwarfs have been recognized in types A, F, G, K, and M. Emission lines of *H* and *Ca* II (H and K) were observed in 41 stars, and of *Ca* II alone in 24 other stars.

The correlation between spectral type and absolute magnitude determined from trigonometric parallaxes is shown in Figure 1. If the subdwarfs are excluded, the average spread in luminosity is 1.6 mag.

Since the beginning of spectrographic work at the Mount Wilson Observatory, the observation of dwarf stars with large proper motions has been emphasized. A number of observers have taken part, and the results have been published from time to time. Dr. W. S. Adams has been largely responsible for the continued interest in this program.

The present paper gives the results of the observations of spectra of large-proper-motion stars for which one or more plates had been obtained prior to 1940, together with a few other stars of especial interest on account of their low luminosity. Except for five stars with emission lines, the proper motion of every star included is greater than 0".35. The early spectrograms were obtained by several observers (W. S. Adams, G. Strömberg, R. F. Sanford, R. E. Wilson, and A. H. Joy) and measured, for the most part, by members of the computing staff. The observations and measurements since 1940 have been made largely by the writer.

Most of the spectrograms were obtained with one-prism spectrographs at the 60- and 100-inch reflectors. Since 1940, at the 100-inch telescope, a two-prism spectrograph with a collimating mirror and a 6-inch Schmidt camera (dispersion 115 A/mm) has been used for the fainter stars.

The dispersions usually employed are:

Mag.	A/mm
8.0 or brighter	35
8.0—10.5	75
10.5—14	115

The average probable errors of the radial velocities for these three magnitude groups are 1.1, 1.7, and 2.1 km/sec, respectively.

The stars observed, with relevant data, are listed in Table 1. For stars not in the *Henry Draper Catalogue* the apparent visual magnitudes are generally Kuiper's estimates, although for some of the stars other sources have been used. The visual absolute magnitudes (M_v) of the seventh column were computed from the trigonometric parallaxes of the next column except that the absolute magnitudes of stars having no trigonometric parallaxes were read from the mean curve of the Russell diagram (Fig. 1) according to the estimated type. The parallaxes of such stars were computed from the apparent and absolute magnitudes and marked "(S)" in the eighth column. The measured radial velocities, corrected for the earth's orbital motion, are in the last column, together with their probable errors.

* *Contributions from the Mount Wilson Observatory, Carnegie Institution of Washington*, No. 726.

TABLE 1

SPECTROSCOPIC OBSERVATIONS OF DWARF STARS

STAR	α(1900)	δ(1900)	m_v	μ	SPECT.	M_v	π	VELOCITY	
								No. of Plates	Km/Sec
ADS 48A	0h 0m4	+45° 16′	9.4*	0″.86	dK6	9.2	0″.090(10)	3	0†
20 C 16	0 11.8	+40 24	8.7	0.55	dM0	8.3	.083(1)	3	+ 13±2.0
ADS 246A	0 12.8	+43 28	8.5*	2.89	dM2.5	10.7	.278(6)	11	+ 15† ...
ADS 246B	.....	.....	10.9	.....	sdM4e	13.1	.....	5	+ 22±0.8
GC 354	0 12.8	−14 1	6.6	0.41	dG0	4.7	.042(S)	3	+ 29±0.8
ADS 433A	0 26.3	+66 41	10.4	1.74	dM2.5	10.4	.099(3)	4	+ 18±2.6
GC 668A	0 28.8	−35 32	6.6	0.52	dG0	5.0	.049(1)	2	+ 28±0.2
20 C 40	0 33.5	+30 4	11.4	1.55	dM3.5†	11.0	.084(3)	3	+ 10±1.6
GC 873	0 38.2	+75 24	7.4	0.40	dG4	5.4	.039(2)	3	− 9±0.3
20 C 60	0 45.4	+57 45	11.5	1.58	dM2	10.4	.060(1)	3	− 19±1.1
GC 1058	0 48.1	−30 54	7.6*	0.63	dK5	7.7	.107(1)	3	− 5† ...
GC 1186	0 54.1	+31 57	7.0	0.36	dF5	4.7	.035(1)	3	+ 22±0.4
20 C 66	0 55.3	+71 9	9.9	1.78	dM3.5	10.1	.108(4)	3	+ 11±1.4
LPM 63	1 7.5	−17 32	11.6	1.33	dM5e	13.6	.251(S)	3	+ 28±3.6
GC 1752A	1 21.7	+44 53	5.0	0.36	F2	1.6	.021(3)	3	+ 12±0.9
GC 2050	1 35.7	+42 7	5.1	0.81	dG0	4.9	.091(2)	6	+ 1±0.6
GC 2280	1 48.0	−22 56	9.0	0.86	dM1.5	8.6	.082(2)	3	+ 25±2.6
20 C 153	2 7.3	+ 3 9	10.3	2.58	dM3	10.1	.088(2)	5	+ 7±1.7
ADS 2081B	2 37.4	+48 48	10.0	0.35	dM2.5	9.6	.081(5)	4	+ 25±2.5
20 C 187	2 46.0	+34 0	9.6	1.37	dM0	8.8	.068(3)	3	− 45±0.8
GC 3449	2 47.7	−13 11	6.1	0.42	dK0	6.8	.137(2)	3	+ 19±1.7
20 C 212	3 7.6	+18 28	14.4*	1.74	sdM0	13.1	.054(1)	3	−102† ...
GC 3901	3 8.3	+71 55	9.0	0.43	dG5	5.0	.016(1)	4	+ 9±3.1
20 C 217	3 9.9	+37 45	10.5	1.36	sdK5	8.7	.044(2)	3	−166±1.5
20 C 235	3 22.3	+37 3	10.6	1.58	sdK5	8.4	.036(2)	5	−174±4.1
ADS 2894A	3 52.4	− 1 27	8.6	0.27	dK5	8.6	.101(1)	4	+ 7±1.6
ADS 2894B	.....	.....	11.3*	.....	dM3e	11.3	.....	6	+ 15† ...
20 C 279	3 59.7	+32 42	9.2	1.08	dK4	6.9	.035(2)	3	+112±1.8
20 C 280	4 2.2	−21 6	9.7	0.78	dM0	8.5	.057(2)	3	+ 28±2.4
ADS 3093C	4 10.7	− 7 48	11.1	4.08	dM4.5e	12.6	.203(12)	3	− 45±1.7
20 C 303	4 37.0	+18 47	9.8	1.27	dM2.5	9.9	.106(3)	4	+ 33±1.9
BD+52°911	4 55.1	+53 3	9.8	1.96	dM0.5	8.7	.059(1)	2	+ 76±1.2
GC 6144	4 56.5	+13 57	8.3	0.41	dG8	6.7	.049(1)	3	− 27±1.4
20 C 318	5 7.0	+19 37	9.2	0.75	dK3	6.9	.035(2)	3	+ 7±1.3
ADS 4099B	5 23.3	+54 35	9.7	0.41	dK4	6.9	.028(7)	2	+ 27±0.2
CD−29°2277	5 25.0	−29 58	11.5	0.41	sdF6	6.2	.009(S)	5	+547±1.6†
Ross 42	5 26.7	+ 9 45	11.8*	0.30	dM4e	11.1	.073(2)	3	+ 17† ...
BD+62°780	5 36.3	+62 13	9.2	0.82	dK5	7.6	.048(S)	4	− 13±2.9
20 C 344	5 36.4	+12 28	11.7	2.53	sdM4.5	12.7	.161(2)	3	+103±1.9
20 C 347	5 39.5	+ 9 13	11.9	0.61	sdF7	6.1	.007(3)	3	− 1±5.8
20 C 377	6 6.4	−21 50	8.2	0.71	dM2.5	9.4	.172(3)	3	0±1.4
20 C 390	6 24.3	− 2 44	11.3	0.97	dM4.5e†	13.3	.253(4)	5	+ 24±2.7
BD+47°1355	6 44.1	+47 29	9.2	0.83	dK6	7.9	.055(S)	2	+ 28±1.4
20 C 400	6 48.3	+33 24	9.9	0.87	dM3.5	11.0	.162(2)	3	+ 41±2.0
20 C 402B	6 49.5	+40 13	10.7	0.44	dM1.5	8.7	0.041(2)	3	+ 61±1.8

TABLE 1—*Continued*

Star	α(1900)	δ(1900)	m_v	μ	Spect.	M_v	π	Velocity	
								No. of Plates	Km/Sec
Ross 986	7h 3m3	+38°43′	12.4*	1″.12	dM5e†	13.3	0″.151(1)	5	+ 52† ...
BD+5°1668	7 22.0	+ 5 35	10.0	3.75	dM4	12.1	.264(3)	3	+ 28±2.3
20 C 426	7 25.4	+36 26	11.2*	0.44	dM3.5e	10.9	.087(2)	9	+ 1† ...
Ross 989†	7 25.4	+36 27	12.2	0.41	dM4.5e	11.9	.087(2)	4	− 2±4.6
Ross 882	7 39.4	+ 3 48	11.6†	0.64	dM4.5e	12.4	.147(1)	5	+ 18±0.9
20 C 462	8 6.5	+ 9 9	12.5	5.40	dM5	13.4	.153(2)	2	− 35±0.1
20 C 475	8 27.3	+67 38	9.2	1.09	dM1	8.8	.089(3)	5	+ 18±2.1
20 C 489	8 43.1	+ 6 51	10.3	0.55	dM0	7.4	.026(3)	3	− 23±0.6
GC 12307	8 49.4	− 5 4	6.0	0.43	dG3	5.0	.063(S)	4	+ 30±1.9
20 C 498	8 50.0	+ 1 57	9.9	1.09	dM1	9.0	.066(1)	6	+ 3±2.6
20 C 500	8 52.8	+20 56	8.9	0.68	dK5	7.1	.045(2)	3	− 46±1.0
20 C 501	8 54.1	− 3 37	9.5	0.73	sdF3	6.7	.028(1)	5	+ 20±2.5
20 C 510	9 1.9	+51 12	8.1	0.43	dG6	5.6	.032(S)	3	+ 22±1.0
BD+1°2341	9 35.6	+ 1 28	11.0*	0.54	F0	2.7	.002(S)	4	− 65† ...
20 C 540	9 35.8	+13 40	10.6	0.77	dM2.5	9.7	.066(2)	3	+ 20±2.4
BD+75°403	10 1.7	+75 37	9.3	0.39	dK6	8.0	.055(1)	5	− 47±2.7
20 C 580	10 23.8	+ 1 22	9.6	0.96	dM2.5	10.1	.128(2)	3	+ 18±2.1
L 1113-55	10 30.9	+ 5 38	12.2	0.68	dM4e	11.4	.069(S)	3	+ 21±0.8
20 C 589	10 41.9	+28 57	10.3	0.83	sdF5	6.3	.016(1)	4	+ 77±1.7
20 C 591	10 45.7	+ 7 21	11.9*	1.23	dM5	12.6	.139(2)	3	+ 4† ...
GC 14964	10 46.8	+76 36	9.4	0.48	dK6	7.7	.045(1)	5	− 22±2.8
20 C 598	10 51.0	+70 8	10.2	0.64	dM0.5	8.4	.045(2)	4	+ 7 ±2.2
20 C 600	10 51.6	+ 7 36	13.5	4.67	dM6e†	16.5	.406(1)	4	+ 13±2.9
20 C 606B	11 0.5	+44 2	14.8†	4.54	dM5.5e	16.0	.176(2)	2†	... ...
GC 15365	11 5.2	+66 34	9.0	0.36	dG5	6.3	.029(1)	3	+ 27±3.2
BD−17°3336	11 10.3	−17 35	10.0	0.76	dM1	9.8	.056(3)	4	+ 5±2.4
BD−17°3337	11 10.3	−17 35	10.4*	0.76	dM1	9.5	.065(3)	5	+ 18† ...
20 C 632	11 18.6	+ 9 6	11.0	1.16	dM1	7.4	.019(1)	4	+ 58±1.0
20 C 641†	11 23.3	+ 8 6	9.7	1.21	dM0	8.0	.045(2)	3	+ 37±2.1
20 C 655	11 34.7	+67 52	12.3	3.20	sdM0.5	10.4	.042(2)	3	−118±1.7
GC 16044	11 36.2	−28 39	6.9*	0.38	dG0	3.9	.025(1)	4	− 20† ...
AC+79°3888	11 41.3	+79 14	11.0	0.87	sdM4	12.5	.198(2)	3	−115±3.1
20 C 662	11 42.6	+ 1 23	11.0	1.40	dM5	13.3	.292(1)	2	− 10±1.0
GC 16248	11 47.2	+10 30	7.8	0.36	dK1	6.5	.054(1)	3	+ 11±1.1
20 C 684	12 3.3	+ 0 4	10.8	0.96	dM1	9.8	.063(2)	2	+ 31±1.9
20 C 703	12 19.6	−17 38	11.7	2.49	dM4	11.8	.103(1)	4	+ 58±1.7
BD−6°3580	12 23.7	− 6 57	9.6	0.45	dK5	7.6	.040(S)	3	+ 27±1.7
20 C 716AB	12 28.4	+ 9 34	12.7	1.81	dM5.5e	14.5	.230(3)	6	− 5±3.0
20 C 717	12 28.8	−14 5	9.6	0.48	dK4	7.1	.032(2)	3	+ 7±1.0
20 C 726	12 34.0	+12 14	11.3	1.16	dM4	10.4	.065(1)	3	+ 8±0.2
GC 17308	12 38.4	−37 9	7.5	0.71	dG5	5.8	.038(2)	4	− 30±2.7
20 C 737	12 43.0	+10 18	11.1	1.09	dM4	11.3	.108(1)	3	+ 5±0.7
GC 17447	12 46.2	−12 56	8.1	0.41	dG2	5.3	.027(1)	5	+ 25±1.5
GC 17629	12 55.2	+69 19	8.6*	0.40	dG6	6.3	.034(1)	6	+ 7† ...
20 C 754	12 55.6	+ 6 13	13.6*	1.01	dM5e	13.6	0.100(S)	3	− 40† ...

TABLE 1—*Continued*

Star	α(1900)	δ(1900)	m_v	μ	Spect.	M_v	π	Velocity	
								No. of Plates	Km/Sec
20 C 755	12^h55^m8	+12°53′	9.9	0″.70	dM2e†	9.6	0″.087(S)	5	− 13±2.4
GC 17819	13 4.3	−21 39	7.3	0.40	dG7	6.7	.077(1)	4	− 6±1.7
GC 17966	13 11.6	+28 16	8.4	0.39	dG8	6.1	.035(S)	3	+ 16±0.8
ADS 8841B	13 11.9	+17 33	10.2	0.67	dM2	9.5	.072(2)	4	+ 10±2.0
20 C 770	13 13.9	− 2 33	9.8	0.71	dK5	8.1	.046(2)	3	+123±1.5
GC 18040	13 15.6	+38 41	8.3*	0.40	dG6	5.3	.025(1)	3	+ 1† ...
20 C 780A	13 23.2	− 1 50	11.4	0.50	dM4	11.4	.098(2)	3	− 26±1.4
20 C 782	13 24.9	+10 55	9.2	1.49	dM1	9.7	.124(1)	7	+ 19±1.4
AC+18°1204-96A	13 28.1	+17 16	11.0	0.38	dM4e	11.5	.126(S)	4	0±2.4
AC+18°1204-96B	.....	.....	11.5	.....	dM4.5e	12.4	.151(S)	3	+ 8±2.3
20 C 793	13 33.2	+75 1	9.8	0.43	dK6	8.0	.043(1)	3	− 1±1.2
GC 18520	13 37.2	+ 8 54	6.1	0.39	F4	3.9	.037(1)	5	− 11±1.1
20 C 806	13 42.2	− 5 38	9.6	0.67	dK4	7.0	.030(1)	3	− 46±0.5
ADS 9090A	13 58.5	+46 49	9.9	0.55	dM3	9.5	.085(8)	4	− 31±2.1
ADS 9090B	.....	.....	9.9	.....	dM3	9.5	.....	4	− 28±2.4
20 C 835	14 5.1	−13 27	9.7	0.42	sdF7	6.1	.019(S)	4	+126±2.8
20 C 837	14 7.8	−11 33	13.5	0.79	dM5.5e	14.7	.174(S)	1†	....
BD+21°2649	14 20.9	+21 3	8.0	0.64	F8	4.4	.019(S)	3	− 54±0.4
20 C 863	14 24.8	+15 57	10.5	1.74	dM3	9.9	.077(3)	3	+ 20±1.7
GC 19693	14 31.7	− 3 51	7.8	0.35	dG3	4.3	.020(2)	3	− 44±1.3
20 C 901	14 53.6	+31 45	11.1	1.50	dM1.5	9.2	.042(S)	3	+ 24±2.0
20 C 904	14 57.4	+45 49	9.0	0.43	dM0	8.3	.071(1)	3	− 14±1.4
CPD−21°5912	15 7.4	−21 36	10.5	0.70	dK5	8.0	.032(1)	3	− 72±2.1
L 1130-30A	16 1.6	+ 8 38	12.0*	0.48	dM3e	10.4	.048(S)	5	− 48† ...
L 1130-91	16 7.3	+ 5 46	12.1	0.69	dK4	7.0	.010(S)	4	− 15±3.0
ADS 9970AB	16 9.4	+39 36	8.7*	0.37	dG4	3.9	.011(1)	4	− 53±1.5
ADS 9982A	16 11.1	+ 7 35	9.4*	0.50	dK6	6.9	.032(1)	8	+ 7±2.1
BD+55°1823	16 14.9	+55 32	10.1	.....	dM1.5e†	9.2	.066(S)	3	− 28±0.6
20 C 986	16 21.1	+48 35	10.3	1.23	dM3	10.9	.132(2)	3	− 29±0.7
20 C 995	16 24.7	−12 25	10.2*	1.24	dM4.5	12.5	.288(4)	3	− 18† ...
GC 22255	16 27.9	+ 3 28	9.5*	0.40	dK0	7.6	.043(2)	5	− 58† ...
GC 22445	16 35.9	− 2 39	7.1	0.44	dG2	5.7	.051(3)	3	− 43±0.9
GC 22636	16 45.1	+37 12	8.2	0.38	dK0	7.1	.059(2)	4	+ 4±0.6
GC 22805AB	16 50.1	− 8 9	9.9	1.22	dM3e	11.0	.167(7)	26	+ 19† ...
GC 22805C	16 50.1	− 8 8	11.9*	1.22	sdM4	13.0	.162(4)	5	+ 25† ...
Ross 867	17 16.1	+26 36	13.4	0.47	dM5e	13.6	.110(S)	2†	....
Ross 868	17 16.1	+26 36	11.2	0.47	dM4e	11.4	.110(S)	4	− 28±1.9
ADS 10585AB	17 25.5	+29 29	9.9*	0.39	dM0	8.6	.055(3)	4	− 7±1.9
ADS 10786B	17 42.5	+27 47	10.4	0.82	dM4	10.6	.111(2)	4	− 13±1.9
LPM 661	17 50.3	−16 23	11.0	0.60	sdF8†	6.2	.011(S)	3	−216±2.2
20 C 1069	17 52.9	+ 4 25	9.7	10.25	sdM4.5†	13.4	.542(7)	12	−103±1.7†
BD−3°4233	17 59.8	− 3 2	9.2	0.53	dM2	9.9	.139(3)	3	+ 34±0.5
20 C 1091	18 27.9	−11 42	8.8	0.41	dM0	7.5	.054(3)	3	− 83±0.3
GC 25317	18 28.6	+44 57	8.1	0.36	F8	4.8	.022(1)	3	− 4±1.6
20 C 1095	18 32.4	+45 39	9.8	0.56	dM2	9.4	0.082(2)	3	− 23±2.9

TABLE 1—*Continued*

Star	α(1900)	δ(1900)	m_v	μ	Spect.	M_v	π	Velocity	
								No. of Plates	Km/Sec
20 C 1108....	18^h43^m6	−23°57	10.5	0".74	dM4.5e	13.3	0".355(3)	4	− 4±0.9
20 C 1129....	19 2.8	+20 44	10.7	0.57	sdM2	11.1	.122(4)	3	+ 34±2.2
Ross 731.....	19 2.9	+20 43	10.7	0.57	sdM2	11.1	.122(4)	3	+ 35±2.2
ADS 12061CD	19 3.7	+32 21	11.8	1.66	dM4	12.3	.127(4)	3	− 31±2.0
20 C 1136....	19 7.1	+ 2 44	11.3	1.88	dM4	11.4	.106(2)	3	− 40±0.7
20 C 1143....	19 12.0	+ 5 1	9.2	1.44	dM3	10.4	.171(4)	3	+ 33±1.1
ADS 12882A..	19 41.0	+ 4 0	7.0	0.1†	dG0	4.7	.035(S)	4	− 8±1.4
ADS 12882B..	.....	.....	11.4	.....	dM2e†	9.6	.044(S)	5	+ 5±2.8
20 C 1191....	20 2.7	+54 10	12.2*	1.62	dM3e	11.2	.063(3)	7	0† ...
CD −32°16135A	20 35.6	−32 47	10.9	0.45	dM4.5e†	11.1	.109(2)	5	− 4±2.4
CD −32°16135B	20 35.6	−32 47	11.1	0.45	dM4.5e	11.3	.109(2)	5	− 3±2.8
20 C 1223....	20 37.2	−19 16	10.3	1.15	dM2	9.4	.067(1)	3	+ 6±1.8
20 C 1225....	20 39.0	−31 42	8.7	0.45	dM2e	8.9	.111(1)	5	+ 5±3.0†
20 C 1227....	20 40.5	+54 57	15.3	1.87	dM5e	14.6	.072(1)	1	− 23† ...
20 C 1228....	20 41.4	+44 8	10.6	0.50	dM3	10.6	.102(1)	3	− 15±1.8
20 C 1242....	20 51.4	−10 49	11.5	1.14	dM3.5	10.2	.056(3)	3	+ 51±3.0
20 C 1253....	20 58.7	− 6 32	10.3	0.46	dK5	7.2	.024(2)	2	− 37±0.9
20 C 1263....	21 5.6	+59 21	13.4*	2.14	sdM1	11.5	.042(1)	5	−260† ...
20 C 1285....	21 24.8	+17 12	10.4	1.07	dM4	11.3	.150(1)	3	− 2±1.6
20 C 1288....	21 25.8	−10 14	11.5	1.19	dM4.5e	12.3	.147(2)	1†	....
GC 30918....	22 1.4	+ 1 22	7.5	0.37	F8	4.7	.028(2)	3	− 43±0.8
Ross 271.....	22 6.6	+17 55	10.4	0.51	dM2	9.4	.062(1)	3	− 41±2.3
20 C 1348....	22 9.1	− 9 13	11.5	0.68	dK4	7.3	.014(1)	4	− 18±4.1
GC 31109....	22 9.2	−16 18	6.6	0.36	dG8	4.3	.035(2)	3	+ 12±1.2
Wolf 1561A...	22 12.1	− 9 18	13.5	0.55	dM4.5e	13.5	.101(2)	3	+ 54±2.1
Wolf 1561B...	22 12.1	− 9 18	14.5	0.55	dM5e	14.5	.101(2)	1†	....
20 C 1363....	22 23.7	+ 5 19	14.4*	1.57	sdK6	9.8	.012(S)	2	−157† ...
ADS 15972B.	22 24.4	+57 12	11.3	0.86	dM4.5e	13.4	.258(7)	4	− 28±0.9
20 C 1368....	22 27.6	+49 11	9.3	0.41	dG8	6.1	.023(S)	3	+ 28±0.4
LPM 837.....	22 33.0	−15 53	12.3	3.27	dM5.5e	14.6	.286(2)	4	− 60±0.8
BD+9°5076..	22 33.6	+10 2	11.1*	0.57	dK0	6.8	.014(S)	3	− 70† ...
GC 31669....	22 37.5	+65 59	7.5	0.44	dG3	4.9	.030(1)	3	− 46±1.5
20 C 1382....	22 42.6	+43 49	10.2	0.84	dM4.5e	11.8	.205(4)	4	− 1±2.0
AC +31°70565†	22 47.2	+31 13	11.2	0.49	dM3.5e	9.6	.047(1)	4	0±2.0
20 C 1385....	22 47.3	+31 12	9.4	0.50	dK5	7.4	.040(2)	7	+ 3±1.5
20 C 1387....	22 47.9	−14 47	10.3	1.12	dM4.5	11.9	.212(4)	3	+ 13±1.3
GC 31978†...	22 50.8	−32 6	6.5	0.36	dK5	7.0	.128(2)	5	+ 12±1.6
20 C 1392....	22 51.7	+16 2	9.0*	1.09	dM2.5	10.1	.166(2)	6	− 19† ...
20 C 1404....	23 4.5	+ 0 12	10.2	1.29	sdG2	6.5	.018(S)	3	−112±0.7
GC 32541....	23 17.8	−11 19	8.0	0.50	dK2	6.9	.059(3)	3	+ 36±1.6
BD +19°5116A	23 26.7	+19 23	10.3	0.53	dM4e†	11.1	.146(1)	5	− 1±0.9
BD +19°5116B	.....	.....	12.8	.....	dM5.5e	13.6	.....	6	− 4±2.9
20 C 1445....	23 37.0	+43 39	12.2	1.82	dM5.5e†	14.7	.321(2)	3	− 81±2.5
GC 32998....	23 41.2	−42 7	7.5	0.88	sdA2S†	4.7	.027(2)	3	− 24±1.2
GC 33222....	23 52.4	−10 12	7.8	0.45	dG2	4.3	.020(2)	4	− 32±0.7
ADS 48F.....	23 59.9	+45 14	9.9	0.87	dM2	9.7	0.089(5)	4	+ 3±2.3

NOTES FOR TABLE 1

The magnitudes of all stars distinguished by an asterisk (*) in the fourth column have been corrected for a companion star. The correction for spectroscopic binaries is 0.4 mag.

The notes for stars marked with a dagger (†) follow:

ADS 48A	$0^h\ 0^m.4$	Spectroscopic binary, range −16 to +11 km/sec; the distant companion F and both stars of the close pair show strong emission H and K lines.
ADS 246A	0 12.8	This value of the radial velocity based on additional plates should replace values previously published; a range of from +2 to +28 km/sec indicates that the star is a spectroscopic binary; H and K appear in emission.
20 C 40	0 33.5	Luyten's estimates of early spectral type (*Pub. A.S.P.*, **34**, 132 and 356, 1922; *Lick Obs. Bull.*, **11**, 128, 1923) are obviously the result of misidentification.
GC 1058	0 48.1	Spectroscopic binary, range −20 to +14 km/sec.
20 C 212	3 7.6	Spectroscopic binary, range −140 to −76 km/sec; the spectral lines are greatly weakened.
ADS 2894B	3 52.4	Spectroscopic binary, range −1 to +34 km/sec; the emission lines were found by F. C. Leonard (*Pub. A.S.P.*, **56**, 38, 1944); the bright star has H and K in emission.
CD−29°2277	5 25.0	The high velocity found by D. M. Popper (*Ap. J.*, **98**, 210, 1943) is confirmed; the motion in the line of sight is by far the greatest yet found; the spectrum is characteristic of F-type subdwarfs.
Ross 42	5 26.7	Spectroscopic binary, range +5 to +48 km/sec.
20 C 390	6 24.3	Unseen companion reported by D. Reuyl (*A.J.*, **45**, 133, 1936); bright *H* lines were found by A. Vyssotsky (*Harvard Ann. Card*, No. 550, 1940).
Ross 986	7 3.3	Spectroscopic binary, range +27 to +85 km/sec; the emission lines were mentioned in a letter from W. J. Luyten, dated June 21, 1945.
20 C 426	7 25.4	Spectroscopic binary, range −26 to +25 km/sec.
Ross 989	7 25.4	39″ north of 20 C 426, which has nearly the same motion.
Ross 882	7 39.4	A. van Maanen reported 1.4 mag. increase in brightness on March 11, 1943 (*Pub. A.S.P.*, **57**, 216, 1945).
BD+1°2341	9 35.6	Spectroscopic binary, range −98 to −15 km/sec; the proper-motion star is the preceding of two stars in the field; the lines are poor and on one plate are suspected of being double.
20 C 591	10 45.7	Spectroscopic binary, range −18 to +16 km/sec.
20 C 600	10 51.6	The spectrum shows the strongest titanium oxide bands yet observed among dwarf stars.
20 C 606B	11 0.5	A. van Maanen reported 1.5 mag. increase in brightness on May 11, 1939 (*Mt. W. Contr.*, No. 630; *Ap. J.*, **91**, 503, 1940); two spectrograms with dispersion 440 A/mm were obtained by M. L. Humason.
BD−17°3337	11 10.3	Spectroscopic binary, range +3 to +43 km/sec.
20 C 641	11 23.3	South following of two stars; this identification is by A. N. Vyssotsky; the results given in *Mt. W. Contr.*, No. 387; *Ap. J.*, **70**, 219, 1929; and *Mt. W. Contr.*, No. 511; *Ap. J.*, **81**, 240, 1935, apply to the north preceding star.
GC 16044	11 36.2	Spectroscopic binary, range −32 to −10 km/sec.
GC 17629	12 55.2	Spectroscopic binary, range −12 to +21 km/sec.
20 C 754	12 55.6	Spectroscopic binary, range −76 to −22 km/sec.
20 C 755	12 55.8	Emission lines found by D. M. Popper (*Ap. J.*, **98**, 210, 1943).
GC 18040	13 15.6	Spectroscopic binary, range −19 to +19 km/sec.
20 C 837	14 7.8	One low-dispersion (220 A/mm) plate only.
L 1130-30A	16 1.6	Spectrographic binary, range −69 to −33 km/sec; the spectrum of the fourteenth-magnitude companion, distant 2″, has not been observed.
BD+55°1823	16 14.9	The emission lines were found by G. Münch (*Ap. J.*, **99**, 222, 1944).
20 C 995	16 24.7	Spectroscopic binary, range −26 to −7 km/sec.
GC 22255	16 27.9	Spectroscopic binary, range −76 to −39 km/sec.
GC 22805AB	16 50.1	Spectroscopic binary, range +4 to +30 km/sec.
GC 22805 C	16 50.1	Spectroscopic binary, range +13 to +46 km/sec.
Ross 867	17 16.1	Two low-dispersion (220 A/mm) plates only.
LPM 661	17 50.3	Lines very weak.
20 C 1069	17 52.9	Barnard's star; the weakness of the metallic lines indicates that this well-known star should be classed as a subdwarf; there is some evidence of a small variation in radial velocity.
ADS 12882A	19 41.0	The proper motion is estimated from the *A.G.* catalogue.
ADS 12882B	19 41.0	The emission lines were found by F. C. Leonard (*Pub. A.S.P.*, **56**, 202, 1944).
20 C 1191	20 2.7	Spectroscopic binary, range −97 to +71 km/sec.
CD−32°16135A	20 35.6	Variable intensity of the bright lines was suspected by W. J. Luyten (*Harvard Bull.*, No. 835, 1926).

(Notes for Table 1 continued on following page)

NOTES FOR TABLE 1—*Continued*

20 C 1225	20^h39^m0	The large range in the measures indicates that the star may be a spectroscopic binary.
20 C 1227	20 40.5	One low-dispersion (220 A/mm) plate only.
20 C 1263	21 5.6	Spectroscopic binary, range −292 to −242 km/sec.
20 C 1288	21 25.8	One low-dispersion (220 A/mm) plate only.
Wolf 1561B	22 12.1	One low-dispersion (220 A/mm) plate only.
20 C 1363	22 23.7	Spectroscopic binary, range −176 to −139 km/sec.
BD+9°5076	22 33.6	Spectroscopic binary, range −93 to −49 km/sec.
AC+31°70565	22 47.2	This star was found by accident near 20 C 1385 (*Pub. A.S.P.*, **55**, 242, 1943); according to McCormick observers, the two stars have about the same parallax and total proper motion, but direction of the cross-motion is quite different.
GC 31978	22 50.8	The motion is nearly the same as that of Fomalhaut.
20 C 1392	22 51.7	Spectroscopic binary, range −36 to −3 km/sec.
BD+19°5116A	23 26.7	The emission lines were found by Wirtanen (*Pub. A.S.P.*, **53**, 340, 1941).
20 C 1445	23 37.0	The absorption lines are poor and the bright *H* lines weak; probably a subdwarf.
GC 32998	23 41.2	In this subdwarf of early type the *H* absorption lines have deep cores and noticeable wings; λ 4481 *Mg* I is present but somewhat weakened.

THE RADIAL VELOCITIES

The radial velocities of 20 faint stars from Table 1 have been measured at the McDonald Observatory by D. M. Popper[1] and G. Münch.[2] A comparison of these velocities with the Mount Wilson values shows an average difference of 8.4 km/sec and a systematic difference (Mt. W. − McD.) of +3.3 km/sec.

For 7 bright stars of the list whose velocities were determined at the Lick Observatory, the systematic difference (Mt. W. − L.) is −0.2 km/sec. A comparison of Mount Wilson plates taken with different cameras and different slit-widths shows only insignificant mean differences.

Large velocities of over 75 km/sec were found for 19 stars of Table 1. As previously determined, the subdwarfs show the highest radial velocities. The average velocity for 21 subdwarfs of the list is 121 km/sec.

THE SPECTRA

The stars are classified according to the Henry Draper system. The types of the M dwarfs are based strictly upon the strength of the titanium oxide bands in the blue region of the spectrum. When obtained by this method, the types are comparable with those of the giants, supergiants, and M-type variables. The more detailed classification permitted by additional decimal half-subdivisions (M0.5, M1.5, etc.) seems justified.

Subdwarfs, formerly called "intermediate white dwarfs," have been recognized in late, as well as in early, types when the criteria are clearly marked. The spectroscopic features[3] which distinguish subdwarfs from ordinary dwarfs are: for types A–M, a general weakening of the absorption spectrum; A–G, a marked weakening and narrowing of hydrogen lines and of λ 4481 *Mg* II; F–G, a weakening of the G band; K–M, a strengthening of the Lindblad absorption band in the neighborhood of λ 4226 and a weakening of emission lines. According to Kuiper, the continuum at the head of the Balmer series is weakened in subdwarfs of early types, but this region of the spectrum has not been observed on our plates.

[1] *Ap. J.*, **95**, 308, 1942; **98**, 210, 1943.

[2] *Ap. J.*, **99**, 272, 1944.

[3] W. S. Adams, *Mt. W. Contr.*, No. 105; *Ap. J.*, **42**, 187, 1915. Adams, Joy, Humason, and Brayton, *Mt. W. Contr.*, No. 511; *Ap. J.*, **81**, 191, 1935. G. P. Kuiper, *Ap. J.*, **89**, 551, 1939; *Colloque internat. d'ap.*, III: *White Dwarfs* (Paris, 1941).

Emission lines of *Ca* II and *H* were observed in 41 stars of the list whose spectral types are M1.5 or later. Low luminosity and low temperature favor the production of emission lines in stars at the lower end of the main sequence, but emission lines are weak or absent in subdwarfs. The emergence of bright lines is rather definitely fixed at M4.5. Of the 32 stars with spectral type M4.5 or later, only 7 fail to show emission, and 3 of these are probably subdwarfs. Of 78 M-type stars with spectra earlier than M4.5, only 16 show emission *H* lines. Twenty-five additional stars (1 G0, 1 K0, 3 K5, 2 K6, and 18 M0-4), however, show bright H and K, but no blue or violet *H* lines in emission. The observations of H and K are not complete because many of the spectrograms are too weak in the violet region.

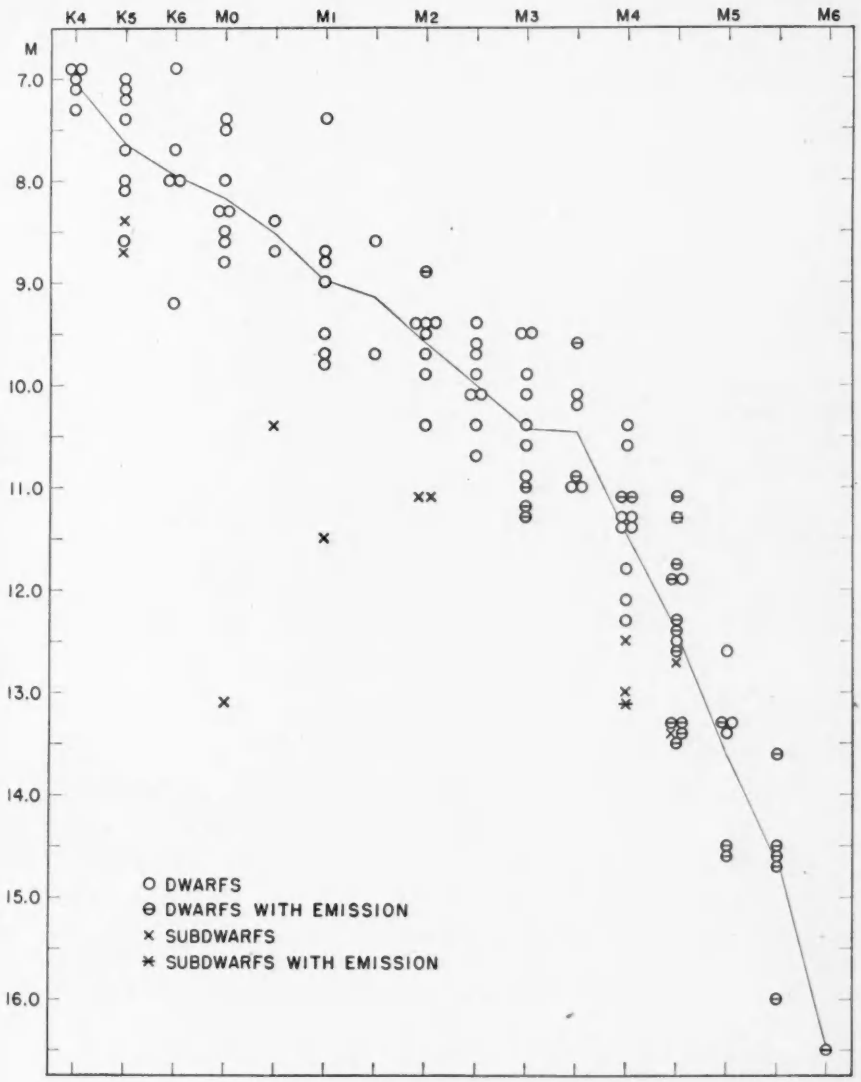

FIG. 1.—Russell diagram for late-type dwarfs with trigonometric parallaxes

Although 29 of the 66 stars showing emission are members of close pairs, the evidence seems to indicate that the bright lines result from low temperature or low luminosity rather than from duplicity.

ABSOLUTE MAGNITUDES

The absolute magnitudes determined from apparent magnitudes and trigonometric parallaxes are plotted against spectral type in Figure 1, and the mean values are given in Table 2.

TABLE 2

ABSOLUTE MAGNITUDES OF FAINT DWARF STARS

Spectral Type	M_v	Spectral Type	M_v	Spectral Type	M_v
K4	7.0	M1.0	9.0	M3.5	10.8
K5	7.6	M1.5	9.2	M4.0	11.5
K6	8.0	M2.0	9.6	M4.5	12.4
M0	8.2	M2.5	10.0	M5.0	13.6
M0.5	8.5	M3.0	10.4	M5.5	14.7

Because most of the stars were observed with low dispersion, no attempt was made to determine the spectroscopic absolute magnitude from the line intensities. If the stars recognized as subdwarfs are excluded, the average spread in luminosity is 1.6 mag. Since this value includes errors in apparent magnitude and trigonometric parallax, as well as errors in estimating spectral type, the results seem to indicate little dispersion in luminosity from the mean of the main sequence. The possibility of variations in apparent magnitude and type and the probability that some subdwarfs have been retained by mistake may account for some of the spread.

Kuiper's[4] success in classifying faint M-type spectra on panchromatic film suggests that the red region may offer possibilities of higher accuracy in estimating spectral types than the usual blue region. If the types could be estimated by employing criteria more sensitive than the blue *Ti* bands, it would be worth while to use decimals smaller than half-subdivisions in the classification, for, in the late spectral types, a difference of one subdivision in type corresponds to a difference of more than 2 mag. in the absolute magnitude.

[4] *Ap. J.*, **95**, 207, 1942.

ZEEMAN EFFECT IN STELLAR SPECTRA*

H. W. BABCOCK
Mount Wilson Observatory
Received September 23, 1946

ABSTRACT

Some stars of early spectral type which exhibit sharp metallic lines may be in rapid rotation, with their axes directed nearly toward the observer. On the possibility that strong magnetic fields are correlated with rapid rotation in such objects, the Zeeman effect for a normal triplet line, as observed through a circular analyzer, has been integrated over the visible hemisphere of the star. Reasonable assumptions are made regarding field distribution and limb darkening. It is found that the integrated Zeeman effect for a normal triplet should give a displacement of about 3×10^{-6} A/gauss at λ 4600.

Observations of the star 78 Vir (type A2p), made with a differential circular analyzer in front of the slit of the coudé spectrograph of the 100-inch telescope, show displacements of the metallic absorption lines that are interpreted as a Zeeman effect resulting from a general magnetic field having a strength of 1500 gauss at the pole. The control star ϵ Peg (type K0) shows no effect.

A comparison of the magnitude of the sun's general magnetic field[1] and its equatorial speed of rotation[2] (about 50 gauss and 2 km/sec, respectively) with the average equatorial speed[3] established for stars of type B, A, and early F (about 60 km/sec) suggests the possibility that the rapidly rotating stars may possess relatively strong magnetic fields. If the field strength be supposed to increase directly with the equatorial speed of rotation,[4] fields of the order of 1500 gauss may be predicted.

A small proportion of the early-type stars have very sharp lines, showing little or no rotational broadening; and some of these stars are presumably in rapid rotation, with their axes directed nearly toward the observer. If strong general magnetic fields occur in stars of this sort, the Zeeman effect may be sufficiently large to affect line widths perceptibly; moreover, if reasonable assumptions are made regarding the characteristics of the field, it can be shown that the integrated Zeeman effect for spectrum lines will be preferential in one direction, i.e., the components of the lines transmitted through analyzers for right-handed and left-handed circularly polarized light will be displaced in opposite directions by amounts proportional to the field strength and to the atomic Zeeman effects for the particular lines.

In making a preliminary calculation of the magnitude of the Zeeman effect that might possibly be observed in rapidly rotating stars, only absorption lines will be considered (the inverse Zeeman effect). Simplifying assumptions will be made as follows:

1. The rotational and magnetic axes of the star coincide and are directed toward the observer.
2. The star is spherical.
3. The coefficient of limb darkening[5,6] is 0.45.

* *Contributions from the Mount Wilson Observatory, Carnegie Institution of Washington*, No. 727.

[1] G. E. Hale, *Mt. W. Contr.*, No. 71; *Ap. J.*, **38**, 27, 1913: Hale, Seares, van Maanen, and Ellerman, *Mt. W. Contr.*, No. 148; *Ap. J.*, **47**, 206, 1918. In 1915, Hale expressed the hope that the 100-inch reflector would permit tests for stellar magnetism to be applied (*Ten Years Work of a Mountain Observatory* [Carnegie Institution of Washington, 1915], p. 45).

[2] W. S. Adams, *Mt. W. Contr.*, No. 33; *Ap. J.*, **29**, 110, 1909.

[3] C. T. Elvey, *Ap. J.*, **71**, 221, 1930.

[4] The association of magnetic fields with rotation in astronomical bodies appears to have been suggested first by Schuster (*Report B.A.A.S.* for 1892, p. 634; *Proc. Phys. Soc. London*, **24**, 121, 1912).

[5] A. Pannekoek, *M.N.*, **95**, 733, 1935.

[6] G. E. Kron, *Ap. J.*, **96**, 173, 1942.

4. The equivalent widths of the absorption lines are constant over the projected hemisphere of the star presented to the observer.

5. The distribution of the magnetic field over the surface of the star is similar to that of a uniformly magnetized sphere.

This last assumption was made by Hale and his collaborators in their investigation of the general magnetic field of the sun.[1] Their results depended upon the measurement of very small Zeeman displacements in a number of lines that differed considerably in intensity. The stronger lines, arising higher in the solar atmosphere, gave smaller measured displacements than did the weak lines, and this was provisionally taken to mean that the field decreased rapidly with increasing height. Hale noted, however, that "caution must be exercised in accepting the hypothesis that the general field decreases rapidly in intensity with increasing elevation inasmuch as the measures may perhaps be affected by systematic errors depending upon line intensity." S. Rosseland, later interpreting the Mount Wilson measurements to mean that the sun's general field differed very radically from that of a uniformly magnetized sphere, arrived at a value three times as great as Hale's for the horizontal component in the equatorial regions.[7] Recently, word has been received of the work of G. Thiessen,[8] who used a modification of an interference method described by H. D. Babcock.[9] To quote from the available summary of Thiessen's paper:

> The preliminary measurement of the iron line 6173.348 A gave a magnetic field strength at the poles of about 53 ± 12 gauss under the assumption of a dipole structure of the sun's field. The investigation of the chromium line 5247.576 A gave similar results. Thus, I was not able to confirm the very weak field of about 15 gauss found by Hale and collaborators from measurements of the same iron line 6173.348 A. This seems to be of some importance, because the hypothesis of the rapid decrease of the field strength with height in the solar atmosphere was partly based on these older measurements.

The best evidence at present, then, seems to favor the assumption that the field can reasonably be represented as similar to that of a uniformly magnetized sphere; but, if Rosseland's type of field were used in the following development, a result of the same order of magnitude would be obtained, although with reversed sign.

If we consider the distribution of the field of a uniformly magnetized sphere over its surface (equivalent to the field of a dipole at the center) according to the following formulae:

$$H = \tfrac{1}{2} H_p \, (1 + 3 \sin^2 \phi)^{\frac{1}{2}} , \qquad (1a)^{10}$$

$$H_x = \tfrac{3}{2} x z H_p , \qquad (1b)^{11}$$

$$H_y = \tfrac{3}{2} y z H_p , \qquad (1c)^{11}$$

$$H_z = \{ z^2 - \tfrac{1}{2} (x^2 + y^2) \} H_p , \qquad (1d)^{11}$$

where ϕ is the stellar latitude and z is the rectangular co-ordinate measured parallel to the axis from the equatorial plane, it will be seen that the field vector at the pole of the star is parallel to the axis and that, in passing from the pole to the equator, it turns through 180°, at the same time decreasing to one-half its value at the pole (Fig. 1). At latitude 35°.6, the field vector is perpendicular to the polar axis. From this we see that the component of the field vector parallel to the axis of the star, when integrated over the visible hemisphere, has a value different from zero, thus presenting the possibility of

[7] *Mt. W. Contr.*, No. 302; *Ap. J.*, **62**, 387, 1925; *Theoretical Astrophysics* (Oxford: Clarendon Press, 1936), p. 219.

[8] A summary of Thiessen's work is given by G. P. Kuiper, *Pop. Astr.*, **54**, 263, 1946, based on a report on file at the Yerkes Observatory.

[9] *Pub. A.S.P.*, **53**, 237, 1941.

[10] Foster and Porter, *Electricity and Magnetism* (London, 1903).

[11] Rosseland, *op. cit.*, p. 219. A common factor, $A(r)$, has been omitted, and the equations have been normalized.

observing the Zeeman effect in spectrum lines arising in the star's atmosphere. Limb darkening tends to suppress the contributions to the integrated Zeeman pattern arising in low latitudes, where the field is opposite and weaker than at the pole, and hence increases the net effect.

The Zeeman effect for a line exhibiting the normal triplet pattern, (0.00) 1.00, results in the appearance of two components equally displaced in opposite directions from the normal position of the line by an amount

$$\Delta\nu = 4.67 \times 10^{-5}\ \mathrm{cm}^{-1}\ \mathrm{gauss}^{-1}\ . \qquad (2)$$

These two components are characterized by circular polarization in opposite directions when the line of sight is parallel to the field. If the field vector is inclined to the line of sight, the undisplaced plane-polarized component of the normal triplet appears, while the displaced components are elliptically polarized, although their displacements remain

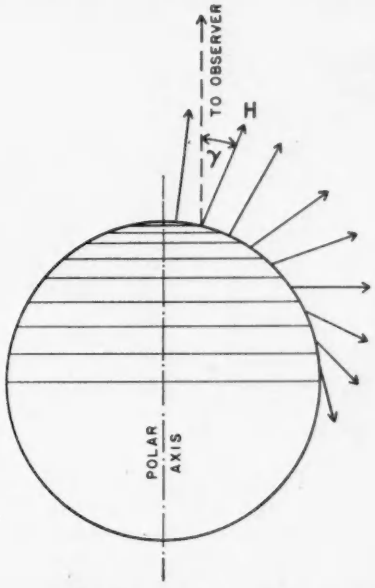

FIG. 1.—Variation of the direction and strength of the magnetic field with latitude on the surface of a star, on the assumption that the field is similar to that of a uniformly magnetized sphere. The field vector H makes an angle γ with the line of sight.

proportional to the field strength. The discovery of magnetic fields in sunspots by Hale[12] in 1908 stimulated interest in the variation of the intensities of the components of the pattern in the inverse Zeeman effect as the angle between the field vector and the line of sight is altered. This was the subject of investigations by P. Zeeman and B. Winawer,[13] W. Voigt,[14] and H. A. Lorentz,[15] among others. The problem becomes quite complex when the absorption is strong and when the magnetic field is not sufficiently intense to resolve the components completely. In the present investigation we shall apply only the more elementary theory that pertains to the relative intensities of Zeeman components in emission or in very weak absorption lines. This should be sufficient to permit an approximate calculation of the magnitude of the integrated effect to be expected in stars.

F. H. Seares has discussed the appearance of Zeeman patterns observed at discrete points at various latitudes on the surface of the sun, resulting from the sun's general

[12] *Mt. W. Contr.*, No. 30; *Ap. J.*, **28**, 315, 1908.

[13] *Ap. J.*, **32**, 329, 1910.

[14] *Magneto- und Elektrooptik* (1908).

[15] *Proc. R. Acad. Sci. Amsterdam*, **12**, 321, 1909.

magnetic field.[16] He expressed the relative intensities of the three components of a normal Zeeman triplet, as observed through an analyzer for circularly polarized light, as follows:

$$I_V = \tfrac{1}{4}(1 \pm \cos\gamma)^2\,; \qquad I_M = \tfrac{1}{2}\sin^2\gamma\,; \qquad I_R = \tfrac{1}{4}(1 \pm \cos\gamma)^2\,, \tag{3}$$

where γ is the angle between the magnetic field vector and the line of sight. These formulae are represented graphically in Figure 2, which has been taken from the *Handbuch der Astrophysik*, **4**, 189.

In the present case, where the resulting Zeeman pattern must be integrated over the whole visible hemisphere of the star and where the components are blended together by overlapping and low resolution, a small shift in the center of gravity of the blended pattern in changing from a right-handed to a left-handed circular analyzer may lend itself to detection and measurement if the stellar field is sufficiently strong. To obtain, first, a qualitative picture of the distorted components of the Zeeman pattern, we may consider the radiation emitted in the direction of the observer from zones equally wide in

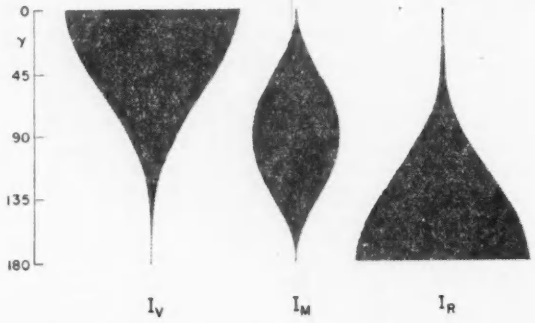

FIG. 2.—Relative intensities of the components of a Zeeman triplet, seen through a circular analyzer, as a function of the angle γ between the field vector and the line of sight (see eq. [3]). Intensity is represented by the width of each component.

stellar latitude. Bearing in mind the projected areas of the latitude zones, the limb darkening, and the variation in strength and direction of the field vector with latitude, we see that the Zeeman pattern for a normal triplet line will be distorted from that of Figure 2 to something resembling the pattern of Figure 3. The displacement, δ, of the center of gravity of the blended Zeeman pattern will evidently be only a fraction of the maximum displacement of the satellites from the normal position of the line.

In order to derive δ quantitatively, on the basis of the foregoing assumptions, for a star having a polar field strength H_p, use is made of the following additional relationships:

$$\text{Projected area of a latitude zone} = 2\pi r^2 \sin\phi\cos\phi\, d\phi\,, \tag{4}$$

$$\text{Projected surface brightness } I(\phi) = 0.55 + 0.45\sin\phi\,, \tag{5}$$

$$\cos\gamma = \frac{H_z}{H}. \tag{6}$$

Now (see Fig. 3) let the maximum displacement of the satellites of the normal triplet Zeeman pattern (at the pole) be aH_p. Then, for a zone of stellar latitude, $d\phi$, we set up, for the three parts of the distorted pattern, an equation of moments about the new center of gravity:

$$I_{V_\phi}(aH - \delta_\phi)\, d\phi - I_{M_\phi}\delta_\phi\, d\phi - I_{R_\phi}(aH + \delta_\phi)\, d\phi = 0\,, \tag{7}$$

[16] *Mt. W. Contr.*, No. 72; *Ap. J.*, **38**, 99, 1913.

whence

$$\delta_\phi = \frac{aH\,(I_{V_\phi} - I_{R_\phi})\,d\phi}{(I_{V_\phi} + I_{M_\phi} + I_{R_\phi})\,d\phi} = aH\cos\gamma\,. \tag{8}$$

We now desire to find the mean value of δ_ϕ over the hemisphere, taking account of the projection factor and projected surface brightness. Using equations (1*a*), (4), (5), and (8), we have

$$\delta = \frac{aH_p}{2}\,\frac{\int_0^{\pi/2} \sin\phi\cos\phi\,(1+3\sin^2\phi)^{\frac{1}{2}}\,(0.55+0.45\sin\phi)\cos\gamma\,d\phi}{\int_0^{\pi/2} \sin\phi\cos\phi\,(0.55+0.45\sin\phi)\,d\phi}\,. \tag{9}$$

Upon integrating the numerator numerically and the denominator directly, we obtain

$$\delta = \pm\,0.311\,aH_p\,.^* \tag{10}$$

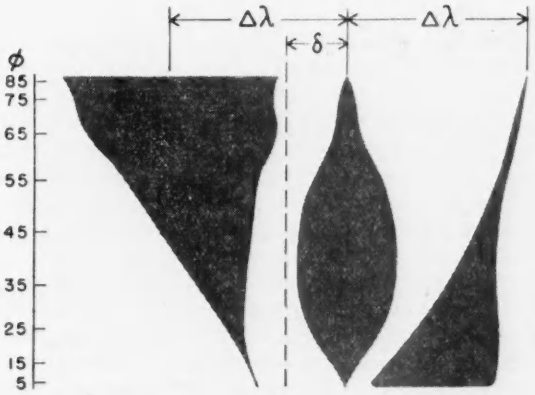

FIG. 3.—Intensities of the three analyzed Zeeman components, weighted according to projected areas of latitude zones, limb darkening, and variation in strength of magnetic field. The displacement of the center of gravity of the group from the normal position of the line is indicated by δ.

We should, therefore, expect the integrated effect to be about 31 per cent as great as that which would result if light from the pole of the star could be isolated.

From equations (2) and (10) we obtain

$$\Delta\lambda = 1.45\times10^{-5}\lambda^2 H \tag{11}$$

for the integrated case. If we assume that the wave length employed is λ 4600, the shift for a normal triplet integrated over the stellar hemisphere would be 3.1×10^{-6} A/gauss.

Thus far we have been concerned with the normal inverse Zeeman effect, the pattern of which is customarily designated (0.00) 1.00, where figures in parentheses represent the displacements of the "parallel" components from the normal position of the line and the following figures represent the displacements (positive and negative) of the "perpendicular" components, which, when viewed in the direction of the field, are circularly polarized. In the anomalous Zeeman effect, which is actually much more common than the normal effect, the several components are represented by their relative displacements, the most intense being printed in boldface type. For example, the notation for the Zeeman effect corresponding to the $^3D_1 - {}^3D_2^0$ transition is (**0.00**, 0.67) 0.50, 1.17, **1.83**. A discussion of the notation and a list of all common patterns are given by Kiess and

* The sign depends upon the use of a right- or a left-handed circular analyzer.

Meggers in "Tables of the Theoretical Zeeman Effect."[17] Occasional lines exhibit large Zeeman effects, two to three times as great as the normal; a few are unaffected.

For an emission line arising in a magnetic field, the direct Zeeman effect will be observed; and, as seen through a given circular analyzer, the displacement will be opposite to that found in the inverse effect.[18] In a stellar line exhibiting both emission and absorption components, this could lead to complications.

It is of interest to inquire whether the longitudinal Zeeman effect would be capable of giving the relationship between the polarity of a stellar magnetic field and the direction of rotation of the star. It appears that this might be possible if a measurable Zeeman effect can be found in one of the components of a visual binary where the direction of orbital motion is known, on the assumption that the sense of rotation of the star on its axis is the same as that of the revolution in its orbit.

We can now compute approximately the smallest stellar magnetic field that could possibly be detected with a suitable analyzer used in connection with the coudé spectrograph of the 100-inch telescope.[19] The long-focus (114-inch) camera of the coudé spectrograph has a dispersion of 2.9 A/mm in the second order. If two adjacent spectra of the star are photographed through right-handed and left-handed circular analyzers, the measurements can be made differentially, and any displacements will be effectively doubled. Finally, it is perhaps reasonable to assume that lines can be chosen having Zeeman effects 1.5 times the normal and that differential displacements of 0.001–0.002 mm on the plate can be detected if a number of lines are available for measurement. The minimum polar field observable is then found to be of the order of 500 gauss. Since the Zeeman effect increases with the square of the wave length, a considerable gain can be expected in going to the red or perhaps the infrared region of the spectrum, if other factors remain constant. With the grating currently in use in the coudé spectrograph, this is not feasible; but the restriction is only temporary.

In the optical system of the 100-inch telescope, all reflections are essentially at normal incidence, with the exception of the reflection from the coudé flat. Here the angle of incidence is 45° for an object on the celestial equator. This reflection alters somewhat the ellipticity of any reflected elliptically polarized light; the amount of the change will depend to some extent upon the condition of the reflecting surface, as well as upon the angle of incidence. For the coudé flat mirror the effect is small for objects not too far north of the celestial equator. The result will be to decrease somewhat any observed Zeeman effects; the displacement equation (11) should properly be written

$$\Delta\lambda = 1.45 \times 10^{-5} \epsilon \lambda^2 H \ , \qquad (12)$$

where ϵ is a polarization factor, generally a little less than unity.

ANALYZERS

Two slightly different analyzers for circularly polarized light have been used in making observations with the coudé spectrograph. In each analyzer the optical parts are held in a metal mounting directly in front of the slit. The analyzer generally used consists of a suitably oriented quarter-wave plate of mica, of a thickness chosen as correct for λ 4600, followed by a plane-parallel crystal of calcite. The calcite divides the incident beam into two beams that emerge parallel and are separated by a distance proportional to the thickness of the crystal. The calcite is so oriented that both transmitted images of the star fall on the slit, while its thickness is so chosen that the separation of

[17] *Bureau Standards J. Research*, **1**, 641, 1928.

[18] This point is discussed in Jenkins and White, *Physical Optics* (1st ed.; New York: McGraw-Hill, 1937), p. 425.

[19] W. S. Adams, *Mt. W. Contr.*, No. 638; *Ap. J.*, **93**, 11, 1941.

the images yields two closely adjacent spectra on the plate. If any right-handed circularly polarized light is received by the analyzer, it will be directed into only one of the photographed spectra, while left-handed circularly polarized light will be directed into the other. Unpolarized light will be equally divided between the two. This type of analyzer was described and used by Zeeman.[20] It is found that the grating of the coudé spectrograph does not exhibit preferential effects for plane-polarized light parallel or normal to the slit; hence the two spectra are of very nearly equal intensity. The deviation of light transmitted by the analyzer is not over 1 minute of arc. The *Fe* comparison spectrum, extending relatively far on either side of the stellar spectra, is photographed in the ordinary way.

A second type of analyzer used for a few plates differs from the first in that the calcite is replaced by two pieces of Polaroid with their axes perpendicular to each other and mounted with the dividing line perpendicular to the slit. The mica quarter-wave plate is used as before. This analyzer produces essentially the same effect as the calcite analyzer if the star is trailed along the slit, yielding two contiguous spectra having the desired properties, but it is much more wasteful of light.

A Fresnel rhomb might replace the mica quarter-wave plate to advantage, but greater care would have to be exercised to insure proper optical alignment.

OBSERVATIONS

The only previous accounts known to the writer of attempts to observe the Zeeman effect, or circularly polarized light, in stellar spectra are those of W. H. Wright[21] and of P. W. Merrill.[22] They used plane and circular analyzers in connection with the Mills spectrograph attached to the 36-inch refractor of the Lick Observatory. Attention was directed mainly to components of bright hydrogen lines; no positive results were obtained.

Beginning in April, 1946, a number of selected stars have been observed by the writer, using the analyzers described, with the 32-inch (10 A/mm) and 114-inch (2.9 A/mm) cameras of the coudé spectrograph of the 100-inch telescope. In general, the stars selected have been members of types B, A, and F that exhibit sharp absorption lines (apart from *H* and *He* lines, which may be broadened by Stark effect). The observing list included several stars listed by W. W. Morgan[23] as belonging to a peculiar branch of the spectral sequence in the interval B8–F0. It is desired, of course, to select stars that are probably in rapid rotation about axes directed nearly toward the observer, even though there may be no direct basis for such a selection. The proportion of early-type stars which have sharp lines is small and, according to Miss Christine Westgate,[24] is in agreement with the assumption of random distribution of the direction of their axes. A small inclination of the axis, resulting in a slight rotational broadening of the lines, would not be expected to interfere seriously with the search for the Zeeman effect. A few early-type stars exhibiting emission lines, in addition to sharp absorption lines, have been placed on the observing program, as O. Struve[25] has shown that emission may indicate the existence of an extended ring or shell resulting possibly from rapid rotation.

The present discussion is confined primarily to the star 78 Virginis ($\alpha = 13^h31^m35^s$; $\delta = +3°55'$ [1950]; mag. 4.93; spectral type A2p), of which observations were made as shown in Table 1. The lines are quite sharp, even with a dispersion of 2.9 A/mm. The region λλ 3800–4800 is covered on the well-exposed plates.

[20] *Researches in Magneto-optics* (New York: Macmillan Co., 1913), p. 47.

[21] *Lick Obs. Bull.*, **6**, 60, 1910.

[22] *Lick Obs. Bull.*, **7**, 162, 1913.

[23] *Ap. J.*, **77**, 330, 1933.

[24] *Ap. J.*, **77**, 141, 1933.

[25] *Ap. J.*, **72**, 1, 1930; **73**, 94, 1931.

From the first, relative displacements between the right-handed and left-handed spectra were suspected for some of the lines in this star. On some of the plates taken with rather poor seeing, the image of the star on the slit was so large that the two spectra appear partially blended, with no dividing line between them. Under these conditions the affected lines appear very slightly inclined. The plates were measured by carefully aligning the vertical wire of the measuring machine with the arc lines of the comparison spectrum; settings were then made on the stellar lines, first on the upper part and then on the lower, and the scale difference was noted for each line. After the wave lengths were computed and the lines identified, the term designations were found by reference to Miss C. E. Moore's *Revised Multiplet Table*.[26] Then the mean Zeeman effects for the perpendicular components of each pattern were determined with the aid of "Tables of Theoretical Zeeman Effects," by Kiess and Meggers.[17] For the anomalous effect Russell's rule was used, that the center of gravity of an asymmetrical blended pattern may be taken to lie one-quarter of the way from the strong component to the extreme weak component. Finally, the results for each plate were represented by plotting the measured differential displacement for each line, in angstroms, against the theoretical Zeeman

TABLE 1

OBSERVATIONS OF 78 VIRGINIS

1946	Plate No.	Camera	Analyzer		Remarks
			Type	Position	
April 24	Ce 4254	114 inch	Mica-calcite	Erect	Weak
May 7	4257	32	Mica-Polaroid	Erect	
May 8	4262	32	Mica-calcite	Erect	
May 8	4263	114	Mica-Polaroid	Erect	Weak
June 15	4293	114	Mica-calcite	Inverted	
June 16	4299	114	Mica-calcite	Erect	

effect for the line. The measured displacements were found to be predominantly in one direction, even on the plates of lower dispersion. For Ce 4262, made with the mica-calcite analyzer, 86 lines were measured; for Ce 4257, made with the mica-Polaroid analyzer, 59 lines were measured. After rejecting a few lines from each plate for uncertain identification or blends, it was found that for 28 lines common to the two plates the measured displacements agreed within 0.002 mm. The mean values for these lines are plotted in the diagram of Figure 4.

The two best plates of high dispersion (2.9 A/mm), Ce 4293 and Ce 4299, were then measured in the same way. Table 2 lists the measured stellar wave lengths corrected for velocity, the measured differential displacements for the lines on each plate in microns, and the mean value of the displacements corrected to λ 4600 on the assumption that the displacements are due to a cause varying as the square of the wave length. A minor correction is also made for the decrease in efficiency of the quarter-wave plate toward the ends of the measured spectrum. This is necessary because the phase retardation for wave lengths other than λ_0, for which the plate is designed, is approximately

$$\delta = \frac{\pi}{2}\frac{\lambda_0}{\lambda},$$

and the undesired component of circularly polarized light will be transmitted with an intensity nearly proportional to $\sin^2(\delta - [\pi/2])$. The fifth column of Table 2 gives the

[26] *Contr. Princeton U. Obs.*, No. 20, 1945.

shift in angstroms corresponding to the measured displacements. The laboratory wave lengths and identification are then listed, followed in the last column by the theoretical Zeeman effect for the perpendicular component.

Figure 5 is the characteristic plot of displacement against Zeeman effect, where a few lines have been omitted because of blending. The encircled points are those for which agreement was closest between results from the two plates. It is perhaps not surprising that there should be considerable dispersion in the measured quantities, since these quantities are so small and are affected by the grain of the plate. Furthermore, the dispersion might yet be somewhat reduced by a more exhaustive study of blending effects. I am grateful to Dr. O. C. Wilson for independently measuring a few of the lines showing the largest displacements. Figure 6 is a microphotometer tracing of the region near λ 4177 on a plate (Ce 4299) of 78 Vir.

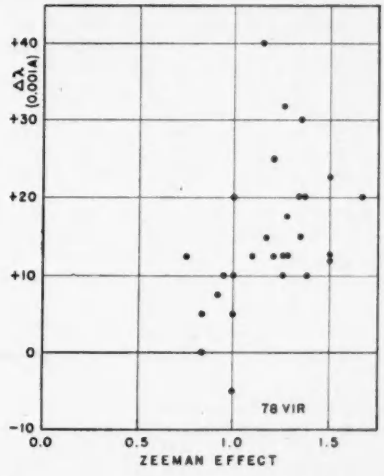

FIG. 4.—Differential displacements plotted against Zeeman effect for 78 Vir. Each point represents the mean value for a line measured on two plates having a dispersion of 10 A/mm.

As indicated in Table 1, Ce 4293 was made with the analyzer "inverted," while Ce 4299 was made with the analyzer "erect." This means that the analyzer was rotated through 180° between the two exposures so that the right- and left-handed properties of the analyzer were interchanged with respect to the upper and lower spectra on each plate. The sign of the differential displacements was found to be different on the two plates, as would be expected for the Zeeman effect. Furthermore, the measured displacements in angstroms were found to be essentially the same for the mica-calcite and the mica-Polaroid analyzers and for the 32- and 114-inch cameras. As a check, an exposure was made in which, instead of photographing the spectrum of a star, light from the iron arc was reflected diffusely into the slit through the analyzer; no outstanding displacements were found.

To provide a further check on the reality of the results for 78 Vir, a plate (Ce 4328) of the K0 star, ε Pegasi, was taken with the mica-calcite analyzer and the 114-inch camera. Since no appreciable rotation has been detected for stars of types as late as G and K, it is to be expected that ε Pegasi would possess no strong general magnetic field[27] and that the Zeeman effect should not be observed in its spectrum. This plate was

[27] ε Peg is listed by Aitken (A15268) as possessing two fainter companions at distances of 82″ and 141″, respectively. The observed changes in position angle are, at most, a few tenths of a degree in thirty-one years. This is entirely compatible with our assumption of a low rate of rotation.

TABLE 2

MEASUREMENTS IN THE SPECTRUM OF 78 VIRGINIS

λ	ΔS Ce 4299	$-\Delta S$ Ce 4293	Mean $\lvert\Delta S\rvert$ (λ 4600)	Δλ	Identification	Zeeman Effect
3878.66	0	.....	0	0.000	8.663 *Fe* I	0.88
3899.72	9	.....	12	.035	9.709 *Fe* I	1.50
3900.55	0	.....	0	.000	0.546 *Ti* II	1.11
3902.95	4	.....	6	.017	2.948 *Fe* I	1.20
3913.50	4	.....	6	.017	3.464 *Ti* II; 3.635 *Fe* I	0.89; 1.50
3920.26	8	.....	11	.032	0.260 *Fe* I	1.50
3922.93	2	.....	3	.009	2.914 *Fe* I	1.50
3926.00	− 1	.....	− 1	− .003	6.001 *Fe* I	1.38
3933.67	1	.....	1	.003	3.664 *Ca* II	1.33
3935.93	− 2	.....	− 3	− .009	5.942 *Fe* II	1.05
3938.34	0	.....	0	.000	8.00 *Mg* I	1.00
3939.01	1	.....	1	.003	8.969 *Fe* II	0.90
3945.21	8	.....	11	.032	5.119 *Fe* I; 5.21 *Fe* II (*P*)	1.78; 1.80
3948.80	2	.....	3	.009	8.779 *Fe* I; 8.901 *Ca* I	1.01; 2.00
3951.16	1	.....	1	.003	1.154 *Nd* II	1.04
3983.95	2	.....	3	.009	3.960 *Fe* I	1.00
3997.42	3	8	7	.020	7.43 *Y* II; 7.394 *Fe* I	1.04; 1.00
4002.54	7	.....	9	.026	2.549 *Fe* II	1.07
4003.30	.....	10	13	.038	3.33 *Cr* II	0.95
4005.26	4	.....	5	.014	5.246 *Fe* I	1.50
4012.47	0	0	0	.000	2.467 *Fe* II	0.40
4020.05	.....	3	4	.012	0.05 *Fe* I (*P*)	1.50
4020.91	.....	8	11	.032	0.898 *Co* I	1.33
4033.00	7	.....	9	.026	3.073 *Mn* I	1.94
4037.99	0	5	3	.009	8.03 *Cr* II	1.04
4045.82	7	.....	9	.026	5.815 *Fe* I	1.25
4051.94	1	.....	1	.003	1.923 *Fe* I; 1.97 *Cr* II	0.67; 1.14
4063.60	3	3	4	.012	3.597 *Fe* I	1.08
4070.82	3	.....	4	.012	0.766 *Fe* I; 0.90 *Cr* II	1.50; 1.05
4071.74	4	0	3	.009	1.740 *Fe* I	0.67
4072.56	1	2	2	.006	2.56 *Cr* II	0.83
4086.14	2	.....	3	.009	6.14 *Cr* II	1.33
4110.98	0	.....	0	.000	1.01 *Cr* II	1.10
4122.64	0	1	1	.003	2.638 *Fe* II	1.31
4128.12	1	.....	1	.003	8.14 *Mn* II	0.87
4128.74	8:	5	7	.020	8.735 *Fe* II	1.80
4132.05	1:	5	5	.014	2.060 *Fe* I	1.50
4136.96	4	.....	5	.014	7.002 *Fe* I	1.00
4143.43	0	.....	0	.000	3.418 *Fe* I	1.00
4145.78	2	3	3	.009	5.77 *Cr* II	1.20
4150.99	.....	1	1	.003	0.97 *Zr* II	1.29
4153.89	− 2	8	4	.012	3.906 *Fe* I	1.50
4163.65	4	0	2	.006	3.655 *V* II; 3.658 *Cb* I; 3.644 *Ti* II	0.84; 1.47; 1.07
4173.48	1	2	2	.006	3.450 *Fe* II	1.48
4177.66	15	1:	13	.038	7.70 *Fe* II; 7.597 *Fe* I; 7.59 *Co* I	1.66; 1.30; 2.28
4178.88	0	5	3	.009	8.855 *Fe* II	0.80
4179.41	− 3	5	1	.003	9.43 *Cr* II; 9.419 *V* I	1.21; 1.41
4195.42	1	7	5	.014	5.41 *Cr* II	1.40
4202.02	3	− 1	1	.003	2.031 *Fe* I	1.15
4210.34	11	4	9	.026	0.352 *Fe* I; 0.352 *Sm* II	3.00; .....
4217.08	.....	1	1	.003	7.07 *Cr* II	0.84
4219.36	0:	4	4	.012	9.364 *Fe* I; 9.383 *W* I	1.08; 1.50
4224.13	11	10	13	.038	4.09 *Cr* II (*P*); 4.176 *Fe* I	1.93; 1.80
4224.85	.....	10	12	.035	4.85 *Cr* II	0.80
4227.39	1	.....	1	0.003	7.42 *Fe* I (*P*)	0.75

TABLE 2—*Continued*

λ	ΔS Ce 4299	$-\Delta S$ Ce 4293	Mean $\lvert\Delta S\rvert$ (λ 4600)	Δλ	Identification	Zeeman Effect
4229.83	.....	16	19	0.055	9.81 *Cr* II	1.90
4233.17	8	− 2	4	.012	3.167 *Fe* II	1.22
4242.34	1	1	1	.003	2.38 *Cr* II	1.17
4250.78	0	8	5	.014	0.790 *Fe* I	0.91
4252.62	.....	3	4	.012	2.62 *Cr* II	1.20
4261.90	− 4	5	1	.003	1.92 *Cr* II	1.07
4269.27	2	3	3	.009	9.28 *Cr* II	0.80
4271.12	− 1	10	5	.014	1.159 *Fe* I	1.50
4274.80	.....	4	5	.014	4.803 *Cr* I	1.96
4275.54	.....	4	5	.014	5.57 *Cr* II	0.91
4278.14	.....	1	1	.003	8.128 *Fe* II	0.21
4289.71	8	2	6	.017	9.721 *Cr* I	1.67
4294.10	3	8	6	.017	4.101 *Ti* II; 4.128 *Fe* I	1.20; 1.20
4303.18	5	7	7	.020	3.166 *Fe* II	1.47
4307.91	5	2	4	.012	7.906 *Fe* I	1.00
4312.91	.....	6	7	.020	2.861 *Ti* II	1.37
4383.56	3	.....	3	.009	3.547 *Fe* I	1.28
4385.40	2	.....	2	.006	5.381 *Fe* II	1.33
4395.05	− 5	5	0	.000	5.031 *Ti* II	1.07
4404.78	4	8	7	.020	4.752 *Fe* I; 4.81 *Zr* II	1.25; 1.26
4443.82	0	5	3	.009	3.802 *Ti* II	0.94
4447.74	3	.....	3	.009	7.722 *Fe* I	2.00
4451.57	3	3	3	.009	1.566 *Nd* II; 1.586 *Mn* I	0.97; 1.43
4466.59	2	7	5	.013	6.57 *Fe* I	1.50
4468.53	1	2	2	.006	8.493 *Ti* II	1.05
4476.08	6	1	4	.010	6.082 *Fe* I	1.51
4481.26	5	4	5	.013	1.261 *Ti* I; 1.327 *Mg* II; 1.273 *Tm* II	1.67; 0.89; ....
4489.18	0	5	3	.009	9.185 *Fe* II	1.50
4501.31	7	.....	7	.020	1.270 *Ti* II	0.93
4508.30	4	1	3	.009	8.26 *Fe* II (*P*)	1.25
4522.65	3	3	3	.009	2.634 *Fe* II	0.91
4528.62	− 3	.....	− 3	− .009	8.619 *Fe* I	1.25
4541.54	3	1:	3	.009	1.523 *Fe* II	0.80
4555.00	3	0	2	.006	5.02 *Cr* II	1.33
4558.70	5	− 6:	0	.000	8.659 *Cr* II	1.17
4563.78	− 4	.....	− 4	− .011	3.761 *Ti* II	0.83
4565.76	3	.....	3	.009	5.78 *Cr* II; 5.73 *Mn* I	0.60; 2.40
4576.34	2	4	3	.009	6.331 *Fe* II	1.20
4580.07	5	.....	5	.014	0.055 *Fe* II; 0.056 *Cr* I	1.86; 1.75
4588.21	.....	9	9	.026	8.217 *Cr* II	1.07
4589.94	7	2	5	.014	9.961 *Ti* II; 9.89 *Cr* II	1.07; 2.06
4592.07	− 2	2	0	.000	2.09 *Cr* II	1.20
4616.64	− 1	4:	2	.006	6.64 *Cr* II	0.80
4618.65	− 2	.....	− 2	− .006	8.568 *Fe* I; 8.765 *Fe* I	.... ; 1.50
4620.52	2	8	5	.014	0.513 *Fe* II	1.33
4629.31	2	5	4	.010	9.336 *Fe* II	1.33
4634.05	0	.....	0	.000	4.11 *Cr* II	0.50
4652.14	6	.....	6	.017	2.158 *Cr* I	1.17
4684.75	− 2	.....	− 2	− .006	4.77 *Cr* II	1.10
4780.06	2	.....	2	.006	9.986 *Ti* II	1.33
4805.20	1	.....	1	0.003	5.18 *Cr* II	1.31

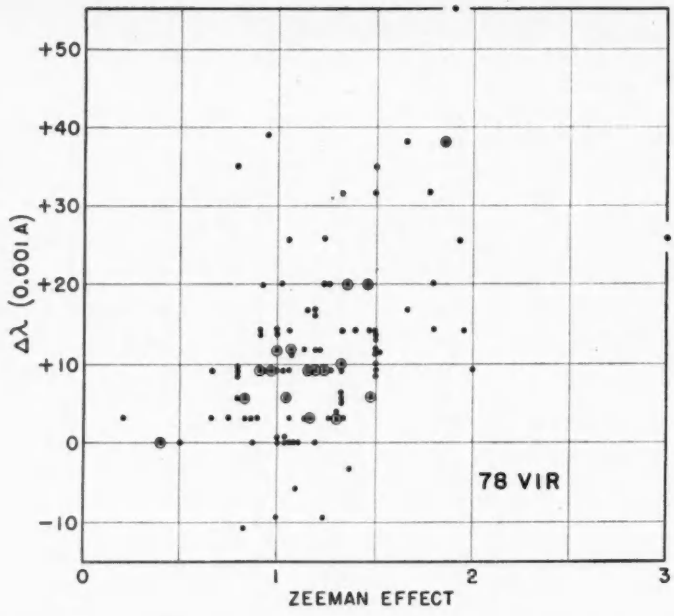

FIG. 5.—Differential displacements plotted against theoretical Zeeman effects for individual lines in high-dispersion spectra (2.9 A/mm) of 78 Vir. Data are from Table 2. Encircled dots represent mean values where the displacements from the two plates agree within 0.003 mm.

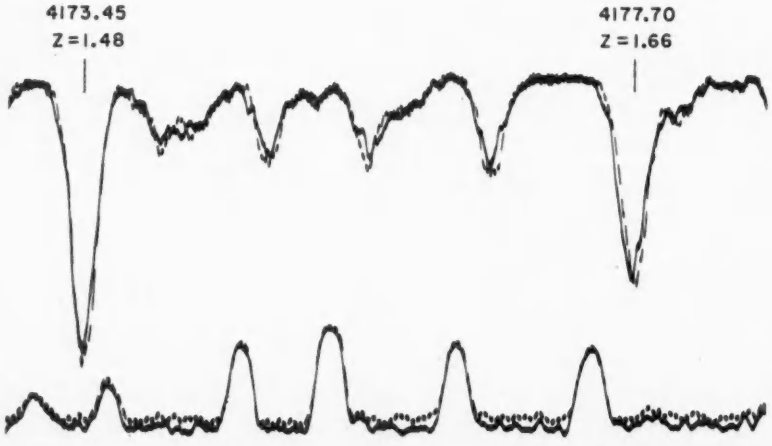

FIG. 6.—Microphotometer tracing of a small section of the spectrum of 78 Vir. The plate was scanned four times, always in the same direction and with no change in the adjustments other than the lateral position of the plate. The two sides of the stellar spectrum (analyzed for right- and left-handed polarization) were scanned separately; for one side the recording beam was interrupted by a light-chopper to give a dotted trace. Note the displacements for the two strong absorption lines (*top*). The Zeeman effect for λ 4173 (*Fe* II) is 1.48; λ 4177 may be a blend of three lines having Zeeman effects of 1.66, 1.30, and 2.28, respectively (see Table 2). The two parts of the comparison spectrum, on opposite sides of the stellar spectrum, were likewise scanned separately; the superposition of the traces (*bottom*) shows that the plate was properly oriented with respect to the slit of the microphotometer.

measured in the same way as the others, settings being made on the upper and lower parts of each line. For 62 lines selected at random, the numbers of positive and negative displacements were about equal, and the average displacement (with regard to sign) was 0.0003 A compared to 0.0110 A for 78 Vir. A plot of measured displacement against Zeeman effect for the lines in ϵ Peg is given in Figure 7. It seems obvious that the measurements in the spectrum of this star merely reflect the usual photographic and personal errors. We conclude that there is no measurable Zeeman effect in ϵ Peg and that no spurious effect is introduced by the apparatus.

A most significant point is the appearance of a definite correlation between the magnitude of the measured displacements and the Zeeman effect in 78 Vir (Figs. 4 and 5), although the Zeeman effects for the lines were unknown to the measurer at the time the measures were made. However, an unlooked-for effect is that a line representing the data, if passed through the origin, would not be straight; the displacements appear to in-

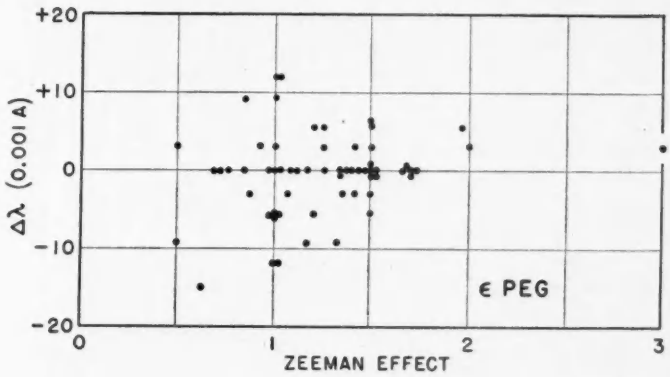

FIG. 7.—Measured displacements plotted against Zeeman effect for lines in the spectrum of the control star ϵ Peg (type K0), for which no detectable general magnetic field would be expected. The vertical dispersion of the points represents ordinary errors of measurement. Compare with Fig. 5.

crease more rapidly than would be expected for the larger Zeeman patterns. A plausible explanation for this apparent lack of linearity is found in Seares's discussion of the measurement of small Zeeman displacements in solar spectra.[16] Seares points out that, for very small displacements in a comparatively diffuse line where the components are unresolved, settings will probably be made on the center of gravity of the pattern, but that if the pattern is partially resolved, as in a sharper line having a large displacement, there will be a tendency to set on the most intense component of the pattern rather than on the center of gravity. This will apply to the pattern of Figure 3 for the triplet and also to the multiple components of the pattern in the anomalous effect, for which Russell's blending rule was used in computing the mean Zeeman effects.

Since the data appear to satisfy criteria for the Zeeman effect and since no other reason for the occurrence of the displacements in the spectrum of 78 Vir has been found, one feels justified in interpreting the data according to the foregoing theory. The 114-inch camera plates give a differential (double) shift of about 0.009 A for a Zeeman effect of 1.00. This shift is found to be equivalent to a polar-field strength of about 1500 gauss for 78 Vir. It is, of course, pure coincidence that this value is identical with the prediction made in the first paragraph of this paper.

The distribution of points in the characteristic diagram for 78 Vir (Fig. 5), deserves further comment, particularly as the dispersion in measured displacements appears to be

somewhat greater than the corresponding dispersion for ϵ Peg. The available data are probably insufficient to permit definite conclusions; but, if more precise results can be obtained in the future, either through the discovery of stars with stronger fields or through improved apparatus, and if careful attention is given to blending effects, the distribution of points in the characteristic diagram may yield a clue to the variation of physical conditions in the stellar atmosphere as a function of latitude or as a function of height. For a given line, let the measured shift be denoted by Δ and the atomic Zeeman effect by Z. The ratio Δ/Z for various points in the diagram may then be of interest. It was shown earlier in this paper that for spectrum lines having uniform intensity as a function of latitude the ratio Δ/Z will be constant in a given star. If a weak absorption line arises dominantly in the polar region of a star (which we assume to be rotating rapid-

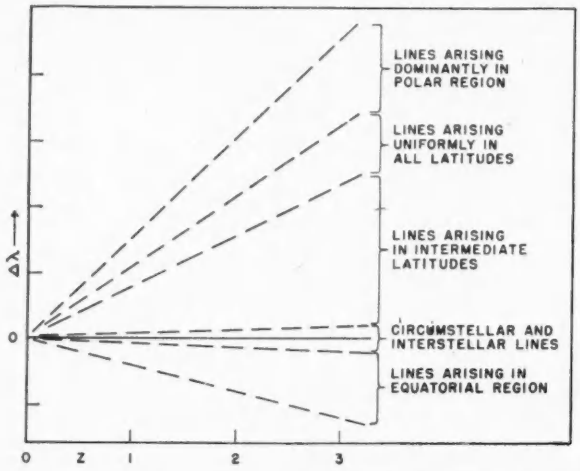

FIG. 8.—Schematic diagram showing for a weak line the relationship between the ratio Δ/Z and the latitude or height at which it arises.

ly about an axis directed nearly toward the observer), its ratio of Δ/Z may be expected to be about twice as great as the normal. On the other hand, a line arising dominantly in the equatorial region, where the surface gravity may be notably lower than at the pole, will have a ratio Δ/Z smaller than the normal and possibly even reversed in sign, since at latitude 35° the component of the field parallel to the line of sight reverses, becoming negative for lower latitudes. Particularly in extended stellar atmospheres, the variation of Δ/Z with height may outweigh any variation with latitude. Circumstellar or shell lines will naturally have a ratio Δ/Z approximately equal to zero, since the field strength (according to our model) decreases as the cube of the distance from the center of the star. The ratio for interstellar lines should, of course, be exactly zero. The diagram of Figure 8 shows these relationships schematically. Some of the physical effects of rapid stellar rotation have been discussed by P. Swings and S. Chandrasekhar,[28] J. A. Hynek,[29] and R. B. Baldwin.[30] In addition to these, a considerable body of literature exists on the

[28] *M.N.*, **96**, 883, 1936.

[29] *Ap. J.*, **83**, 476, 1936.

[30] *Pop. Astr.*, **52**, 134, 1944.

theory of rotationally distorted stars as developed from the study of close binary systems.[31]

The demonstration that some of the absorption lines in the spectrum of 78 Vir exhibit circular polarization interpretable in terms of Zeeman effect opens interesting possibilities for further investigations. The profiles and visibilities of stellar lines may be altered by magnetic fields, and, particularly if varying fields occur, it is possible that the key is at hand to some of the peculiar phenomena of stellar spectra. Further discussion can well be deferred until the results of additional observations become available.

It is a pleasure to express my indebtedness to my father, H. D. Babcock, for much helpful advice.

Note added in proof:

An additional spectrogram of 78 Vir, obtained with the analyzer and 32-inch camera on 1947 Jan. 7, confirms the existence and approximate magnitude of the displacements.

[31] For discussion and bibliography see Z. Kopal, *An Introduction to the Study of Eclipsing Variables* (Harvard University Press, 1946), p. 123.

THE SPECTRUM OF Z ANDROMEDAE IN AUGUST, 1946*

PAUL W. MERRILL
Mount Wilson Observatory
Received October 19, 1946

ABSTRACT

Spectrograms from λλ 3450–5000, 10 A/mm, and from λλ 4300–6650, 20 A/mm, taken on August 16, 17, and 18, 1946, show a dark-line shell spectrum plus sixty bright lines. Traces of *TiO* bands are visible. The photographic magnitude was 10.7.

The most striking *dark lines* are those of *H* and ionized metals, particularly *Ti* II. Lines of *Fe* I are numerous, although very few lines of other neutral metals are seen. The shell is nearly stationary, not expanding as in 1939–1940.

The principal *bright lines* are those of *H*, *He* I, *He* II, *N* III, *O* III, [*O* I], [*O* III], [*Ne* III], [*Ne* V], [*Fe* II], [*Fe* V], [*Fe* VII]. All the bright lines are more or less diffuse. A few of the stronger ones have two components of unequal intensity; in the *H* lines the weaker component is longward, but in lines of *He* I, *He* II, [*O* III], [*Ne* III], and [*Ne* V] it is shortward.

The spectrum of Z Andromedae, 232848, known for its remarkable "combination" of a low-temperature absorption spectrum with bright lines requiring high excitation, was photographed on three successive nights in August, 1946, with the coudé spectrograph of the 100-inch reflector (Table 1). The dispersion was higher than that previously em-

TABLE 1

JOURNAL OF OBSERVATIONS

Plate	Date	Dispersion (A/mm)	Emulsion	Exp.	Continuous Spectrum
Ce 4370	1946 Aug. 16	10.3	IIA-O	430^m	λλ 3450–5000
4373	Aug. 17	20.6	103A-D	450	λλ 4300–6300
4376	Aug. 18	20.6	103A-E	366	λλ 6100–6650

ployed on this object. Many lines, both bright and dark, can be studied in more detail than on my earlier plates.

According to Dr. Sergei Gaposchkin, of the Harvard College Observatory, the light-curve was rising rapidly during August. At the time of my spectroscopic observations the photographic magnitude was 10.7.

The last column of Table 1 indicates the approximate limits of the continuous spectrum recorded on each plate. In the yellow, green, and extreme ultraviolet the continuous spectrum is weak, the photographic contrast low. In these regions only fairly strong lines are distinctly shown, and many faint ones are undoubtedly lost.

More than two hundred sharp dark lines constitute a well-developed early-type shell spectrum. The only M-type features readily recognizable are traces of *TiO* band structure near λ 4600 and weak *TiO* bands extending longward from heads at λ 4955 and λ 6158. About sixty bright lines from λ 3312 to λ 6678 include those repeatedly photographed in the spectrum of this object.[1]

* *Contributions from the Mount Wilson Observatory, Carnegie Institution of Washington*, No. 728.

[1] H. H. Plaskett, *Pub. Dom. Ap. Obs.*, **4**, 119, 1928; Swings and Struve, *Ap. J.*, **93**, 356, 1941; P. W. Merrill, *Mt. W. Contr.*, No. 688; *Ap. J.*, **99**, 15, 1944; O. Struve, *Ap. J.*, **99**, 205, 1944; Swings and Struve, *Ap. J.*, **101**, 224, 1945. *Contribution* No. 688 includes a brief history of the spectroscopic observations of Z And, with numerous references.

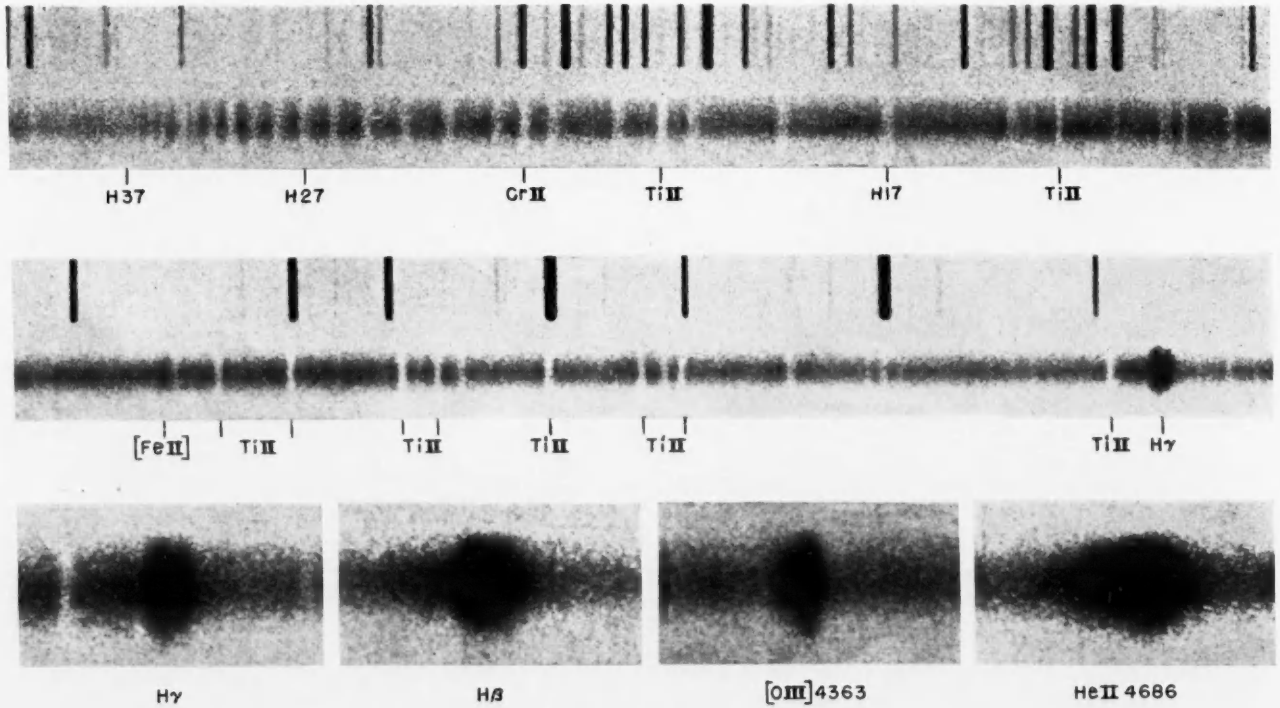

FIG. 1.—Portions of the Spectrum of Z Andromedae, Plate Ce 4370, 1946, August 16. *Upper*, λλ 3650–3720; *center*, λλ 4280–4350

HYDROGEN LINES

The lines of the Balmer series are complex and interesting. The *Hα* line is an extremely intense emission line, but, because of a rapid decrement of intensity along the series, emission was measured only to *Hη*. Absorption components, on the other hand, were measured from *Hγ* to *H* 37. Thus, an emission series with a rapid decrement appears to be superposed on a dark series with a slow decrement. Both bright and dark components were measured in lines *Hγ*–*Hη*, except in *Hζ*, which is blended with *He* I λ 3888.

The intensities of the dark lines vary along the series in a remarkable manner. In those lines with obvious emission, *Hα*–*Hη*, the intensities are low; in the shortward lines the intensities increase to a flat maximum at about *H* 23, with a final rapid decrease beyond *H* 32 (see Fig. 1). In comparison with the corresponding lines in the spectrum of 48 Librae (Plate Ce 4320, July 13, 1946), where the absorption series as a whole is very strong and obvious emission is confined to two or three lines of longest wave length, the estimated relative intensities (Z And : 48 Lib) are: *H* 12, 0.2; *H* 18, 0.4; *H* 22, 0.6; *H* 25, 0.8; *H* 28–*H* 37, 1.0. Although at *H* 12 the dark lines of Z And are only about one-fifth as intense as those of 48 Lib, from *H* 28 to *H* 37 they are fully equal.

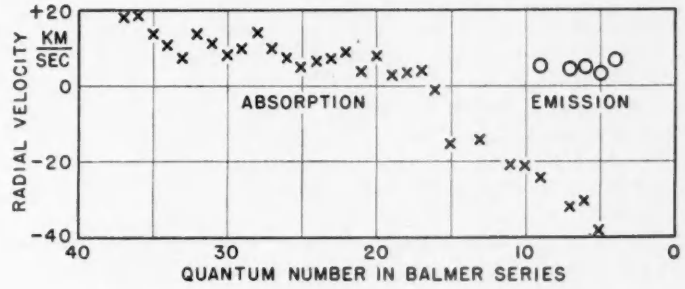

FIG. 2.—Radial velocities derived from hydrogen lines

This fact may indicate that the gaseous layer producing the lines in Z And has a lower electron pressure than that in 48 Lib, but stratification in the stellar atmosphere could invalidate this conclusion.

The measured displacements of the hydrogen lines are plotted in Figure 2; *Hζ*, *H* 12, and *H* 14 are omitted because they are blended with other lines. The mean velocity derived from the emission components *Hβ*–*Hη*, excepting *Hζ*, is +4.9 km/sec, which is nearly the same as that for the dark components *H* 17–*H* 25, and 6 km/sec less than that for the dark components *H* 26–*H* 37, which presumably are little affected by bright edges. Thus the bright lines and the undisturbed dark lines yield nearly the same velocity, the dark lines having a very slight relative displacement longward. In the lines *Hγ*–*H* 15, with both emission and absorption, the bright lines occupy nearly their normal positions, while the dark components are weakened and greatly displaced, as if only their shortward edges were left uncovered by the emission. These facts indicate that the bright hydrogen lines are not subject to the absorption of the hydrogen atoms which produce the dark Balmer series in the photospheric spectrum. Hence the origin of the hydrogen emission must be outside rather than inside the stratum which produces the dark lines; it might be in the star's outer atmosphere, in a companion star, or in large volumes of gas quite outside the star or stars. This conclusion concerning the origin of the emission does not necessarily apply to all Be or Ae spectra. In fact, in the spectra of certain stars the absorption cores seem to cut through the emission lines as well as through the photospheric continuum—a phenomenon resembling self-reversal

in a laboratory arc, which indicates that the absorbing layer overlies the region where emission occurs.

The bright lines $H\beta$, $H\gamma$, and $H\delta$ have two components not distinctly separated; the velocity of the stronger is +5 km/sec, that of the weaker +40 km/sec. The weaker components have the more rapid decrement. The measured displacements of the strong components probably correspond to the motion of the star as a whole, while the weaker components are displaced redward by the equivalent of 35 km/sec.

The peculiarities of the hydrogen lines have been recorded in some detail to illustrate the difficulties that may beset interpretation of measured displacements and equivalent widths. Similar complexities may be present in less extreme form in many stellar spectra. Progressive changes along the Balmer series somewhat similar to those in Z And had previously been found in 48 Lib[2] and other shell stars.

HELIUM LINES

The lines λλ 5876, 4471, and 4026 of the $^3P-^3D$ series of *He* I are bright; the mean velocity derived from them is +16 km/sec. There is a trace of emission at λ 3819 and possibly at λ 3705. Very weak dark components yield the following velocities: λ 4471, −25 km/sec; λ 4026, −14; λ 3819, −11; λ 3705, −9.

The lines λλ 6678, 4922, and 4387 of the $^1P-^1D$ series are bright; the mean velocity derived from them is +4 km/sec. The line λ 4922 is complex, with a faint emission component 0.7 A (43 km/sec) shortward from the main component. No dark components were measured. The line λ 5015 of the series $^1S-^1P$ is bright, but the observations are poor. Nothing was measured at λ 3965. The bright line λ 3888 of the series $^3S-^3P$ is blended with $H\zeta$; the strong dark component yields the velocity −34 km/sec. The relatively great intensity of this dark line indicates that the helium lines are produced in a region of low density.

The bright line of *He* II λ 4686 is very strong. The main component yields a velocity of −10 km/sec; a weaker component lies 1.2 A (76 km/sec) shortward. A trace of the bright line λ 5411 is visible.

PERMITTED METALLIC LINES

The dark lines of the shell spectrum are narrow and well defined; the most striking are those of hydrogen and ionized metals (see Fig. 1). Among the ionized lines, those of *Ti* II are outstanding. A number of the *Fe* II lines have bright edges. The lines of *Si* I λ 3905 and λ 4103 (blended with *N* III), together with λλ 3853, 3856, 3862 of *Si* II, are faintly present in emission; λ 4128 and λ 4130 of *Si* II are weak dark lines. A trace of bright λ 4267 of *C* II is seen. Very few neutral metallic lines, except those of *Fe* I, are visible.

The measured displacements of various groups of lines are collected in Table 2. The mean velocity derived from neutral lines is 2 km/sec greater than that from ionized lines. The velocities from *Na* I and *Ca* II and that from λ 3888 *He* I differ markedly from the general mean.

FORBIDDEN METALLIC LINES

Seven or eight lines of [*Fe* II] from multiplets (6F), (7F), (10F)?, and (21F) are bright; the mean radial velocity is +4 km/sec. Multiplet (3F) of [*Fe* V] is represented by λ 3839 and λ 3892; multiplet (3F) of [*Fe* VII] by λ 3587 and λ 3760 (see Table 3).

A diffuse bright line of moderate intensity was measured at λ 6086.7. If we assume a velocity displacement of −0.2 A, the normal wave length becomes λ 6086.9. The identification is probably [*Fe* VII] multiplet (1F), since (3F) is definitely present. The other members of (1F), λ 5721 and λ 6600, are not seen. It is improbable that the line

[2] Merrill and Sanford, *Mt. W. Contr.*, No. 690; *Ap. J.*, **100**, 14, 1944.

TABLE 2

DISPLACEMENTS OF ABSORPTION LINES

Element	Rad. V.	Wt.*	Element	Rad. V.	Wt.
H	+ 9.3	17	*Si* II	+12.3	0.5
			Sc II	7.4	8
Mg I	8.7	3	*Ti* II	7.1	45
Cr I	12.3	0.5	*V* II	7.8	9
Fe I	+ 9.4	27	*Cr* II	7.3	12
			Mn II	6.8	1.5
Mean	+ 9.4	30.5	*Fe* II	8.0	12
			Ni II	6.4	2
Na I	− 9	1	*Sr* II	+ 8.4	1
Ca II	14	1			
He I (λ 3888)	−34	1	Mean	+ 7.4	91

* Lines accurately measurable have weight 1; others, weight 0.5. The weights are thus equal to, or less than, the number of lines measured.

TABLE 3

BRIGHT LINES

λ	Int.	Ident.	λ	Int.	Ident.
3312	1	*O* III	4233	1	*Fe* II
3341	2	*O* III	4244	2	[*Fe* II]
3346	1, 3n*	[*Ne* V]	4267	1	*C* II
3426	2, 6n	[*Ne* V]	4277	1.5	[*Fe* II]
3429	1−	*O* III	4287	2	[*Fe* II]
3444	3	*O* III	4341	7, 4	*Hγ*
3586	1n	[*Fe* VII]	4359	1.5	[*Fe* II]
3737	1	.....	4363	2, 7	[*O* III]
3759	1	.....	4388	2n	*He* I
3760	2	[*Fe* VII], *O* III	4416	1.5	[*Fe* II]
3835	1	*Hη*	4458	1	[*Fe* II]
3839	1.5	[*Fe* V]	4471	4	*He* I
3853	tr. n	*Si* II	4488	1	[*Fe* II]
3856	1n	*Si* II	4634	2n	*N* III
3863	1−n	*Si* II	4641	5n	*N* III
3869	2, 6	[*Ne* III]	4642	tr. n	*N* III
3889	3, 2	*He* I, *Hζ*	4686	6, 15n	*He* II
3891	2	[*Fe* V]	4861	10, 6	*Hβ*
3895	0.5	[*Fe* V]	4922	2, 4n	*He* I
3967	0.5, 3	[*Ne* III]	4959	1, 3	[*O* III]
3970	2.5	*Hε*	5007	2, 5	[*O* III]
4026	1	*He* I	5015	2	*He* I
4068	0.5	[*S* II]	5412	tr	*He* II
4097	3n	*N* III	5876	8	*He* I
4101	5, 2	*Hδ*	6086	3n	[*Fe* VII]
4103	1	*N* III, *Si* I	6300	1	[*O* I]
4177	1	[*Fe* II]	6563	100	*Hα*
4178	1	*Fe* II	6678	8	*He* I

* Two components with intensities 1 and 3. All the lines in Table 3 are somewhat diffuse; the widest ones are marked "n."

λ 6086 of [*Ca* v] makes any contribution because the other (stronger) line, λ 5309, of multiplet (1F) is weak or absent.

NEBULAR LINES

Numerous bright lines of *N*, *O*, *Ne*, and *S* are included in Table 3. Displacements and widths are recorded in Tables 4 and 5. The permitted lines of *He* II, *N* III, and *O* III exhibit the peculiar relative intensities characteristic of gaseous nebulae. Hence it is

TABLE 4

DISPLACEMENTS OF BRIGHT LINES

Element	Line or Mult.	Rad. V. Str. Comp. (Km/Sec)	Rel. Displ. Wkr. Comp. (Km/Sec)	Element	Line or Mult.	Rad. V. Str. Comp. (Km/Sec)	Rel. Displ. Wkr. Comp. (Km/Sec)
H	*Hβ*, *Hγ*, *Hδ*	+ 5	+35	[*O* I]	λ 6300	+ 5	.....
He I	$^3P-^3D$	16	.....	[*O* III]	(1F), (2F)	3	−34
	$^1P-^1D$	4	.....	[*Ne* III]	(1F)	8	−36
	λ 4922	6	−43	[*Ne* V]	(1F)	24	−72
He II	λ 4686	3	−76	[*Fe* II]	(6F), (7F), (21F)	4	.....
N III	(1), (2)	(9)	.....				
O III	(3)	(17)	.....	[*Fe* V]	(3F)	16	.....
	(15)	+ 6	.....	[*Fe* VII]	(3F)	+ 6	.....

TABLE 5

WIDTHS OF BRIGHT LINES

λ	Ident.	Width		Remarks
		A	Km/Sec	
3345	[*Ne* V]	0.84	76	
3425	[*Ne* V]	0.79	69	Main component
		1.67	146	Over-all
4686	*He* II	3.21	205	Over-all
4861	*Hβ*	1.78	110	Longward portion
		2.78	172	Over-all
5876	*He* I	1.42	73	
6085	[*Fe* VII]	2.26	111	

probable that in Z And the lines are produced in the same way as in the nebulae, namely, by an atomic mechanism described by I. S. Bowen[3] that depends on the coincidence at λ 304 of strong ground-level lines of *O* III and *He* II.

The list of lines in Table 3 is not complete. Many other weak ones are suspected in the underexposed continuous spectrum in the visual region; some of these would probably be measurable with reasonable accuracy on a stronger exposure.

STRUCTURE AND DISPLACEMENT OF BRIGHT LINES

All the bright lines are more or less diffuse. The approximate widths of several are recorded in Table 5. A few of the stronger ones have two components of unequal intensity; in the *H* lines the weaker component is longward, but in lines of *He* I, *He* II,

[3] *Ap. J.*, **81**, 1, 1935.

[*O* III], [*Ne* III], [*Ne* V] it is shortward (see Fig. 1). No wonder that, with low dispersion, the radial velocities derived from various lines present a baffling complexity.

On the present spectrograms nearly all the single lines, as well as the stronger components of double lines, yield a velocity close to +5 km/sec (Table 4). The *He* I lines of the $^3P-^3D$ series, which yield somewhat larger velocities, are probably displaced by dark components on their shortward edges. In [*Ne* V] and [*Fe* V] the adopted wave lengths may be in error. In view of the diffuseness and duplicity of the lines in Z And, I doubt whether the present plates would yield reliable values for the normal wave lengths of these lines. Possibly stellar spectra better adapted to the purpose may be obtained in the future.

The spectrum of Z And usually consists of numerous bright lines superposed on a continuous spectrum in which absorption bands of *TiO* can be detected. The occasions on which the star exhibits a shell spectrum appear to be rather rare; the only previous observations to show a shell spectrum are those in 1939–1940 by Swings and Struve[4] and by P. W. Merrill.[5] At that time the shell lines yielded large negative velocities, which decreased (arithmetically) considerably during the period of observation. Thus it appears that on various occasions the shell may be either stationary or expanding.

The spectrograms discussed in this *Contribution* show that the bright lines are diffuse and that the widths of lines of various elements do not decrease with increasing atomic weight. Moreover, some of the lines appear double. The structure of the lines cannot be due to kinetic motions; it probably arises either (1) in gross motions of portions of the star's extended atmosphere (possibly comparable to the rising and falling motions in solar flares and prominences) or (2) in motions of streams of gas coursing about in a system containing more than one star. Previous data[5] suggest a possible period of 650–680 days in the displacements of bright lines. It would be interesting to know whether the structure changes in the same period. It is hoped that a few more high-dispersion spectrograms of Z And may be obtained and that further information concerning this object and its enigmatic variations may be extracted from them.

[4] *Ap. J.*, **91**, 546, 1940.

[5] *Mt. W. Contr.*, No. 688; *Ap. J.*, **99**, 15, 1944.

EXTENDED SUM RULES FOR TRANSITION ARRAYS

DONALD H. MENZEL
Harvard College Observatory
Received September 21, 1946

ABSTRACT

It is shown that the sums of multiplet strengths over a transition array is equal to

$$S(\gamma, nl \rightarrow \gamma n'l') = \frac{\varpi_\gamma}{2}[2(2l+1) - k][2(2l'+1) - k']l''\sigma^2 ,$$

where γ denotes the parent-configuration of statistical weight ϖ_γ; l'' is the larger of the angular momentum l-values of the jumping electron; k and k' are the number of electrons in γ to which the jumping electron is equivalent; σ is the radial quantum integral, characteristic of the array. This sum is independent of the type of coupling, as long as configuration interaction is negligible.

Other sum rules have been derived for extended transition arrays, i.e., comprising all possible transitions from various arrangements of M electrons within a given n shell.

It is shown, finally, that the oscillator strength, $f_{n'n}$, for all possible transitions from shell n to shell n' is

$$f_{nn'} = \frac{1}{3}\frac{\nu}{R}\frac{M}{2n^2}\{B\} ,$$

where ν is the frequency, R the Rydberg constant, and

$$\{B\} = \{(\rho_{01} + \rho_{10}) + 2(\rho_{12} + \rho_{21}) + \ldots . n\rho_{n-1,\, n}\} ,$$

where ρ^{l_2} is the radial quantum integral,

$$\rho_{ll'}^{l_2} = \int_0^\infty r\, R(nl)\, R(n'l')\, dr .$$

Apart from the factor M, the value for $f_{nn'}$ agrees with that for hydrogen.

Goldberg[1] has shown that the summation of multiplet strengths over a complete transition array, where the jumping electron is not equivalent to others in either the lower or the upper configuration, is

$$\Sigma S\,(\gamma, nl \rightarrow \gamma, n'l') = \frac{[\varpi_\gamma 2\,(2l+1)]\,[\varpi_\gamma 2\,(2l'+1)]}{2\varpi_\gamma}\, l''\sigma^2 , \qquad (1)$$

where ϖ_γ is the statistical weight of the ionic parent-configuration γ; l'' is the higher of the two l-values of the jumping electron; and σ is the radial quantum integral defined by

$$\sigma = \frac{-\epsilon}{\sqrt{(2l+1)(2l'+1)}} \int_0^\infty r \cdot R\,(n, l)\, R\,(n', l')\, d\,r . \qquad (2)$$

The R's denote the normalized eigenfunctions of the jumping electron, and ϵ is the electronic charge.

For a nonequivalent jumping electron coupled to a core of weight ϖ_γ, the resultant configuration has a weight, $\varpi_\gamma 2(2l+1)$. The factor $2\,\varpi_\gamma$ is merely the product of the electronic weight and the weight of the ion.

To get an equation applicable to transitions involving equivalent electrons, we must replace the brackets of equation (1) by the true weight factors and multiply the formula by the numbers of equivalent electrons in the initial and final configurations. If k and k'

[1] *Ap. J.*, **84**, 11, 1936. A check of Goldberg's Table 1, has shown that the factor, a, for $d^2p^2-d^3p$ should be $\frac{1}{3}$ and not $\frac{1}{21}$.

are the numbers of electrons, in the parent-ion, equivalent to the jumping electron in the initial and final configurations, we multiply by the factor $(k+1)\,(k'+1)$. For example, in the transition array $d^3p^4-d^2p^5$, we regard d^2p^4 as the ionic configuration γ and take $k = 2, k' = 4$. For the array $d^3s - d^2sp$, we take d^2s as γ, with $k = 2, k' = 0$. We shall postpone until later a detailed proof of the general formula.

Thus, denoting initial and final configurations as α and α', we can write

$$\Sigma S\,(\alpha \rightarrow \alpha') = (k+1)\,(k'+1)\,\frac{\varpi_\alpha \varpi_{\alpha'}}{2\varpi_\gamma}\,l''\sigma^2\,. \tag{3}$$

This formula can be simplified.

To calculate the weights when equivalence occurs for either or both the initial or final configurations, we calculate, first, the ϖ_γ of the parent-ion. Each nl shell, containing k equivalent electrons, contributes a factor,

$$\frac{[2\,(2l+1)]!}{k!\,[2\,(2l+1)-k]!}, \tag{4}$$

to the total weight. Each complete or empty shell contributes a factor of unity, so that only incomplete shells come under consideration.

TABLE 1

s	2	d	10	d^9	10	f^7	3432
s^2	1	d^2	45	d^{10}	1	f^8	3003
p	6	d^3	120	f	14	f^9	2002
p^2	15	d^4	210	f^2	91	f^{10}	1001
p^3	20	d^5	252	f^3	364	f^{11}	364
p^4	15	d^6	210	f^4	1001	f^{12}	91
p^5	6	d^7	120	f^5	2002	f^{13}	14
p^6	1	d^8	45	f^6	3003	f^{14}	1

Individual weight factors are given in Table 1. The factors are independent of n. Thus, for the (very improbable) configurations

$$1s2s^22p^43s^22p^63d^74s^04p4d^{10}4f^4\,,$$

the factors are

$$2\cdot 1\cdot 15\cdot 1\cdot 1\cdot 120\cdot 1\cdot 6\cdot 1\cdot 1001 = 21{,}621{,}600\,.$$

This configuration thus comprises almost twenty-two million states.

The configuration α differs from γ in having one more electron, which may or may not be equivalent. In general, we may write

$$\frac{\varpi_\alpha}{\varpi_\gamma} = \frac{[2\,(2l+1)]!}{(k+1)\,![2\,(2l+1)-k-1]!} \div \frac{[2\,(2l+1)]!}{k![2\,(2l+1)-k]!} = \frac{2\,(2l+1)-k}{k+1}, \tag{5}$$

and similarly for α'. Thus we may set

$$S\,(\gamma, nl \rightarrow \gamma, n'l') = \frac{\varpi_\gamma}{2}[2\,(2l+1)-k]\,[2\,(2l'+1)-k']\,l''\sigma^2\,. \tag{6}$$

I repeat that k and k' represent the number of electrons in the initial or final parent-configuration to which the jumping electron is equivalent. If k and k' are both zero, so that no equivalence is involved, we recover Goldberg's formula (1). It should be further mentioned that these sums are independent of the assumption of LS coupling, and hold as long as configuration interaction is negligible.[2]

[2] For other related papers on the subject of multiplet strengths cf. Condon and Shortley, *The Theory of Atomic Spectra;* Leo Goldberg, *Ap. J.*, **82**, 1, 1935; and Menzel and Goldberg, *Ap. J.*, **84**, 1, 1936.

This result should find useful applications in astrophysics; it provides a new standard for relating line strengths in different arrays, once the factor σ has been determined from quantum mechanics.

It is possible to derive still further extended sum rules. To take a specific example, the transition arrays between the following configurations have the radial quantum integrals in common:

$$
\begin{array}{llll}
1s^2 2s^2 2p^6 3s^2 3p^2 & \rightarrow & 1s^2 2s^2 2p^6 3s 3p^2 \cdot np \\
\gamma' \quad 3s^2 3p\ 3d & \rightarrow & \gamma' \quad 3s 3p\ 3d & \cdot np \\
\gamma' \quad 3s^2 \quad 3d^2 & \rightarrow & \gamma' \quad 3s \quad 3d^2 & \cdot np \\
\gamma' \quad 3s\ 3p^3 & \rightarrow & \gamma' \quad 3p^3 & \cdot np \\
\gamma' \quad 3s\ 3p^2 3d & \rightarrow & \gamma' \quad 3p^2 3d & \cdot np \\
\gamma' \quad 3s\ 3p\ 3d^2 & \rightarrow & \gamma' \quad 3p\ 3d^2 & \cdot np \\
\gamma' \quad 3s \quad 3d^3 & \rightarrow & \gamma' \quad 3d^3 & \cdot np
\end{array}
$$

Each of the foregoing configurations has a specified number of electrons (four) in the three-quantum shell, at least one of which is in the s-orbit, the remainder covering all possible configurations within the three-quantum shell. Denote the constant configuration by the symbol γ'. Vertical columns of configurations, like the two listed above, we shall call an "extended" configuration. All transitions involved we shall call a "configuration array."

Re-write equation (6) as follows:

$$S = 2\varpi_\gamma \frac{[2(2l+1) - k][2(2l'+1) - k']}{2(2l+1)\,2(2l'+1)} l''\rho\,, \tag{7}$$

where

$$\rho^{\frac{1}{2}} = -\int_0^\infty r R(nl) R(n'l')\, dr\,. \tag{8}$$

I have suppressed the factor ϵ, so that S is now given in atomic units. It is not difficult to prove that the desired extended sum is

$$S_e = \Sigma S = 2\varpi_{\gamma'} \frac{(2n^2-1)!}{(2n^2-M)!\,(M-1)!} \frac{2(2l'+1) - k'}{2(2l'+1)} l''\rho\,, \tag{9}$$

where ϖ_γ is the statistical weight of the constant portion of the configurations and M the number of electrons assigned to the n quantum shell, with no specification concerning the l-values.

This formula, with appropriate definitions of l', l'', and ρ, applies to other configuration arrays within the same limitations of assigning M-electrons to a given n-shell. As a continuation of the foregoing example, we may write the extended array for a jumping p-electron as follows:

$$
\begin{array}{llll}
\gamma' \quad 3p^4 & \rightarrow \gamma' \quad 3p^3 & \cdot nd \text{ (or ns)} \\
\gamma' 3s\ 3p^3 & \rightarrow \gamma' 3s\ 3p^2 & \cdot nd \text{ (or ns)} \\
\gamma' \quad 3p^3 3d & \rightarrow \gamma' \quad 3p^2 3d & \cdot nd \text{ (or ns)} \\
\gamma' 3s^2 3p^2 & \rightarrow \gamma' 3s\ 3p & \cdot nd \text{ (or ns)} \\
\gamma' 3s\ 3p^2 3d & \rightarrow \gamma' 3s\ 3p\ 3d & \cdot nd \text{ (or ns)} \\
\gamma' \quad 3p^2 3d^2 & \rightarrow \gamma' \quad 3p\ 3d^2 & \cdot nd \text{ (or ns)} \\
\gamma' 3s^2 3p\ 3d & \rightarrow \gamma' 3s^2 \quad 3d & \cdot nd \text{ (or ns)} \\
\gamma' 3s\ 3p\ 3d^2 & \rightarrow \gamma' 3s \quad 3d^2 & \cdot nd \text{ (or ns)} \\
\gamma' \quad 3p\ 3d^3 & \rightarrow \gamma' \quad 3d^3 & \cdot nd \text{ (or ns)}
\end{array}
$$

A similar configuration array holds for a jumping d-electron.

The radial integral is a function of nl and $n'l'$ and should be written $\rho(nl, n'l')$. We shall, however, consider n and n' as specified and write ρ_{ll}, as sufficient identification

for our present problem. In most cases the excited electron will go to an unfilled shell, so that $k' = 0$. In this instance we can write a still further extension of the transition array, termed, for convenience, a "shell array." This sum is

$$\left.\begin{aligned} S_u = \Sigma S_e = 2\varpi_{\gamma'} \frac{(2n^2-1)\,!}{(2n^2-M)\,!\,(M-1)\,!} \\ \{(\rho_{01}+\rho_{10}) + 2(\rho_{12}+\rho_{21}) + 3(\rho_{13}+\rho_{31}) + \ldots . n\rho_{n-1,n}\}, \end{aligned}\right\} \quad (10)$$

in which equation n is less than n'. For hydrogen, $M = 1$, and $\tilde{\omega}_\gamma = 1$ the equation reduces to

$$S_u = 2\{B\}, \quad (11)$$

where the bracket, B, has the same significance as in equation (10).

A shell array covers all transitions from electrons in shell n to positions in shell n'. One significance of this equation is that the shell-array sums display the radial quantum integrals in the same algebraic combination as for hydrogen.

The total number of states comprising the shell is

$$\varpi_\gamma = \frac{\varpi_{\gamma'}(2n^2)\,!}{M!\,(2n^2-M)\,!}. \quad (12)$$

Defining the oscillator strength in the usual manner as

$$f_{BA} = \frac{1}{3}\frac{\nu}{R}\frac{S(AB)}{\varpi_A}, \quad (13)$$

where ν is the frequency and R the Rydberg constant, we get, for the $f_{n'n}$ of the ultra-array,

$$f_{n'n} = \frac{1}{3}\frac{\nu}{R}\frac{M}{2n^2}\,2\{B\}. \quad (14)$$

S is to be expressed in atomic units.

Thus, apart from the factor M, the equation for the f-value for an ultra-array is identical with that for hydrogen, although the ρ's will, in general, be different. The result should be independent of configuration interaction within a given n shell.

The approximation made in this treatment implies that the radial-wave functions describing an n,l-electron are unchanged in different arrangements of the electrons in the given n-shell. When the states of a given shell are not degenerate, the frequency introduced for equation (14) should be the mean weighted frequency for all transitions.

Although equation (10) was worked out on the assumption that the shell n' is empty, considerations of symmetry require the introduction of the factor

$$\frac{(2n'^2-1)\,!}{(2n'^2-M')\,(M'-1)\,!}, \quad (15)$$

when the shell n' contains M'-electrons. In this case we must consider all possible arrangements of electrons within both the initial and the final configurations and interpret γ' as applying to the configuration exclusive of the shells n and n'.

Equation (14) is useful in discussions of general opacity in stellar interiors. I shall return to this problem in a later paper.

The derivation of the basic sum-rule (6) is elementary. The only nonvanishing strengths, or square of the electric moment joining two zero-order states,[3] are the following:

$$S(\gamma, n, l, m_l, m_s; \gamma, n', l', m_l \pm 1, m_s) = \tfrac{1}{2}(l'' \pm m_l)(l'' \pm m_l - 1)\,\sigma^2, \quad (16)$$

and

$$S(\gamma, n, l, m_l, m_s; \gamma\ n', l', m_l, m_s) = l''^2 - m_l^2)\,\sigma^2, \quad (17)$$

[3] Cf. Goldberg, *Ap. J.*, **82**, 1, 1935, eqs. (7) and (8).

where l'' denotes, as in equation (1), the larger of the quantum numbers l, or l'. We are required to sum these strengths over all initial and final zero-order states of the array. The number of such initial states in configurations α and α' is given by equation (5), i.e.,

$$\varpi_\alpha = \varpi_\gamma \frac{2\,(2l+1) - k}{k+1} \quad \text{and} \quad \varpi_\alpha = \varpi_\gamma \frac{2\,(2l'+1) - k'}{k'+1}. \tag{18}$$

Suppose, for simplicity, that $l' = l - 1 = l''$. Then each zero-order state in the l-configuration will connect with three possible states in the l'-configuration, viz., those for which $\Delta m_l = \pm 1, 0$. The sum of these three strengths is

$$\sum_{m'_l} S = (2l''+1)\, l''\sigma^2, \tag{19}$$

independent of m_l.

There are $k+1$ equivalent jumping electrons in each zero-order state of the initial configuration. If $k' = 0$, we can sum equation (19) merely by multiplying it by $(k+1)\,\tilde{\omega}_\alpha$. But, if there are equivalent electrons in the final configuration as well, the number of states is reduced from the nonequivalent value of $2(2l'+1)\tilde{\omega}_\gamma$ to $\tilde{\omega}_\alpha$, i.e., by the ratio

$$\frac{2\,(2l'+1) - k'}{2\,(2l'+1)\,(k'+1)}. \tag{20}$$

But, in the final listing of permissible transitions, each final state will appear $(k'+1)$ times.

The total strength is thus the product of equation (19) by $\tilde{\omega}_\alpha$, the exclusion factor (20), and $(k+1)\,(k'+1)$. The final result is given by equation (6), which is equivalent, in turn, to equation (3). Since the strengths are symmetrical, the results are independent of our previous assumption of $l' = l + 1$, as long as we define l'' as in equation (3). These sums of strengths over the zero-order states are, by the principle of spectroscopic stability, equal to the sums in any type of coupling where configuration interaction is negligible.

I wish to express appreciation to Dr. George H. Shortley and Dr. Leo Goldberg for reading this paper in manuscript.

THE ELECTRON VELOCITY DISTRIBUTION IN GASEOUS NEBULAE AND STELLAR ENVELOPES

DAVID BOHM AND LAWRENCE H. ALLER
University of California, Berkeley, California, and
Kirkwood Observatory, Indiana University
Received October 18, 1945; revised October 15, 1946

ABSTRACT

A general method is given for solving Boltzmann's equation for the steady-state velocity distribution of electron-ion gases, such as those present in gaseous nebulae or stellar atmospheres. In a typical planetary nebula it is found that the velocity distribution is very close to Maxwellian. Because the average lifetime of an electron in the assembly is about 10 years and because its energy is reshuffled nearly every second by electrostatic encounters, the deviations from the equilibrium Maxwellian distribution must be very small. The non-Maxwellian distributions obtained by Hagihara are merely first approximations to an expansion of a Maxwellian distribution in terms of the wrong temperature.

Section I gives a general summary of the results and the physical picture behind them. Section II lists the formulae for the probabilities of all processes involved; in Section III Boltzmann's equation is set down, and Hagihara's work is discussed. Section IV gives a general method for solving Boltzmann's equation when electrostatic interaction is the dominating term.

I. INTRODUCTION

In a gaseous nebula, electrons arising from photoemission are responsible for the excitation of forbidden lines, such as those of *O* III. In the process of excitation, the electronic energy is reduced, and, finally, the electrons are recaptured. The steady state of electron velocity distribution is determined by the condition of balance of all processes tending to change it. Since the assembly is clearly not in thermodynamic equilibrium, the velocity distribution may deviate from the Maxwellian. Nevertheless, it has usually been assumed that the deviations were small, although it has never been clearly proved that this is true. In fact, Hagihara[1] has suggested that the distribution need not be even approximately Maxwellian. If this is true, a great deal of existing work must be re-examined. For example, since the estimation of abundances of elements from line intensities requires a knowledge of the velocity distribution, particularly of the high-energy portion usually associated with the "tail" of the Maxwellian curve, a careful investigation of this point is required. Not only is a detailed study of the mechanisms involved in producing a steady state needed for an understanding of the microscopic processes, but it also must lie at the basis of any treatment of macroscopic problems, such as the diffusion of concentrations of matter.

Hagihara has maintained not only that the distribution may deviate widely from the Maxwellian but also that the precise extent of this deviation is not completely determined by specifying the distribution of the intensity of the incident radiation and the density of matter. In fact, he states that, for any temperature, he can obtain a distribution (generally non-Maxwellian) which is a solution of the equations involved. It would certainly seem that the distribution would be defined by the physical conditions mentioned above. Hence, if it is really ambiguous, as maintained by Hagihara, there is something about the physical processes involved that we do not understand.

To clarify some of these points, we have solved Boltzmann's equation by a method especially designed to treat the high-velocity portion of the distribution with the neces-

[1] *Tokyo Astr. Bull.*, Nos. 525, 542, 571, 1941; see also a series of papers entitled "Electron Velocity Distribution in a Planetary Nebula," *Jap. Jour. Astr. and Geophys.*, **17**, 199, 417, 1940; **18**, 89, 149, 1941; **19**, 9, 75, 1941; **20**, 1, 37, 59, 67, 1943.

sary accuracy. Our results show that the distribution must actually be very close to Maxwellian and that the non-Maxwellian distributions considered by Hagihara are really the first approximations to Maxwellian distributions of another temperature. Thus the apparent ambiguity in the electron temperature turns out to have a purely formal character.

A brief physical picture of how the steady state is actually brought about may be helpful here. Neutral atoms, principally hydrogen, are ionized photoelectrically by ultraviolet radiation arising ultimately from the central star. Electrons are emitted with a kinetic energy equal to the difference between the photon energy and the ionization energy. The number emitted with a given energy is determined by the frequency distribution of the radiation and the absorption coefficient as a function of the energy. Now consider what happens to an electron after it is emitted. It can undergo elastic scattering by other electrons, ions, or neutrals; inelastic scattering by ions, giving rise to excitation of metastable ions; or collisions of the second kind with metastable ions, emission of radiation in free-free transitions, or recapture with the emission of radiation. A steady state results from the balance of all these processes. Fortunately, they do not all occur with the same frequency. In fact, elastic scattering by other electrons and ions is enormously more probable than any of the others. Estimates made in Section II show that the average electron exchanges its energy with other electrons by elastic collisions about once a second if the electron density has the typical value of about $10^4/\text{cm}^3$. The next most frequent process is the excitation of *O* III ions to a metastable level. Even if an electron has the optimum energy for excitation, this process happens only once in 4 months. If it does occur, however, a great deal of energy is absorbed, so that the temperature of the electron gas is lowered. The average lifetime of an electron before it is recaptured is about 10 years, while free-free emissions would require 40 years to dissipate the average electronic energy at a typical electron temperature of 10,000° K.

If electrons remain in the gas 10 years, suffer inelastic collisions once in 4 months, and exchange energy with one another every second, the distribution must certainly approach the equilibrium Maxwellian form. Since the high-energy portion of the distribution, which is responsible for the excitation of the forbidden lines, must result from the boiling-up of low-energy electrons, all traces of the initial stellar energy distribution will have been wiped out, except in so far as it has contributed to the total energy supply in the thermodynamic sense. The calculations of Menzel and others who have used a Maxwellian distribution are thus justified. In Sections II, III, and IV we solve the problem mathematically, in order to present a general method useful in treating stellar envelopes and interstellar space and also to justify the physically evident conclusion that the distribution must be very close to the Maxwellian.

Under what circumstances, if any, would we expect appreciable deviations from a Maxwellian distribution? In general, deviations become appreciable when the probability of inelastic scattering or recombination begins to be comparable with that of elastic scattering. The high-energy ranges of the distribution are more likely to be affected than the low-energy ranges.[2] If, as in typical nebulae, inelastic collisions occur every 10^8 seconds and a redistribution of energy by electrostatic forces takes place every second, the deviations must be negligible. Even in a nebula consisting entirely of doubly ionized oxygen atoms and electrons, where we might expect the inelastic collisional processes to be about ten thousand times more frequent, the velocity distribution would scarcely deviate from the Maxwellian. In a pure hydrogen nebula of so high a temperature that most of the Balmer-line excitation took place by collisions rather than by recombination, the velocity distribution would still be nearly Maxwellian. At the very low densities of interstellar space, where the collisional reshuffling of electrons proceeds very slowly, it

[2] It may be shown that the distribution does not deviate appreciably from the Maxwellian for ratios of E/kT below a critical value, of the order of the square root of the ratio of the probability of elastic encounters to that of the most likely type of inelastic encounter.

is still doubtful that detectable deviations exist, since the radiative processes would occur also at a very slow pace. In general, we are tempted to conclude that deviations of electronic velocities from a Maxwellian distribution are likely to be very small in all stellar and interstellar media accessible to observation.

II. CROSS-SECTIONS FOR THE VARIOUS PHYSICAL PROCESSES

We shall now collect the expressions for the cross-sections of the various processes that occur in a gaseous nebular shell exposed to dilute high-temperature radiation. Many of the formulae have been given elsewhere,[3] but we shall need them here in slightly different forms.

A. PHOTO-IONIZATION

The number of transitions from the ground level (essentially all ionizations take place from the lowest level) arising from the absorption of radiation in a frequency interval ν to $\nu + d\nu$ is given by

$$F_{1\kappa}d\nu = 4\pi N_1 I_\nu a(\nu)\frac{d\nu}{h\nu}, \tag{1}$$

where N_1 is the number of atoms in the ground level and I_ν is the intensity of radiation, and by

$$W\frac{2h\nu^3}{c^2}\frac{1}{e^{h\nu/kT_1}-1},$$

where W represents the effect of the dilution of the radiation by geometric and other factors and may be a function of ν. For convenience, we may choose T_1 as the color temperature of the central star in the ultraviolet. The absorption coefficient is

$$a(\nu) = \frac{\pi\epsilon^2}{mc} f_{1\kappa}, \tag{2}$$

where $f_{1\kappa}$ is the Ladenburg f, or oscillator strength, for the transition involved. Here $h\nu$ is the energy absorbed in the transition. Normally, formulae for f are given for discrete transitions (n–n' in hydrogen). To develop the proper expressions for the transitions involving the continuum, Menzel and Pekeris[4] have introduced the quantum number, κ, by replacing n by $i\kappa$ where κ is a real and continuous variable. Then frequencies of transitions from a lower level n' in hydrogen to the continuum are given by the Balmer formula,

$$\nu = RZ^2\left(\frac{1}{n'^2}+\frac{1}{\kappa^2}\right). \tag{3}$$

The velocity of a free electron V is related to κ by $\frac{1}{2}mV^2 = \mathrm{hR}Z^2/\kappa^2$, so that

$$mV\,dV = hd\nu = -\frac{2hRZ^2}{\kappa^3}d\kappa. \tag{4}$$

For convenience we may express the number of neutrals in any level n in terms of the number of ions and electrons, the equilibrium value given by the Saha equation and the

[3] See the series entitled "Physical Processes in Gaseous Nebulae": *Ap. J.* (I) **85**, 330, 1937; (II) **86**, 70, 1937; (III) **88**, 52, 1938; (*IV*) **86**, 313, 1938; (V) **88**, 423, 1938; (X) **92**, 408, 1940; (XI) **93**, 178, 1941; (XII) **93**, 195, 1941; (XIII) **93**, 230, 1941; (XVI) **94**, 30, 1941; (XVII) **94**, 436, 1941; (XVIII) **102**, 239, 1945. The papers of the series are referred to in the text as Paper I, Paper II, etc. Equations are referred to by paper and number. Thus (I-4) means eq. 4 of Paper I.

[4] *M.N.*, **96**, 78, 1935.

Boltzmann law, and a correction factor which takes into account the deviation from thermodynamic equilibrium, according to (I-4),

$$N_n = b_n N_i N_\epsilon \frac{h^3}{(2\pi m k T_\epsilon)^{3/2}} e^{hRZ^2/n^2kT} \frac{\varpi_n}{2}, \tag{5}$$

where N_n is the number of atoms in level n in each cm,^{3} N_1 is the number of ions per cm,^{3} N_ϵ is the number of electrons per cm^3, ϖ_n is the statistical weight of level n, and b_n is the correction factor. By combining the above formulae, we obtain an expression for the number of electrons entering the range $d\nu$ at ν per cm^3 per second,

$$F_{1\kappa}d\nu = N_i N_\epsilon \frac{KZ^4}{T_\epsilon^{3/2}} b_1 \frac{W e^{h\nu_1/kT_\epsilon}}{e^{h\nu/kT_1}1} \frac{g d\nu}{\nu}, \tag{6}$$

where K is a numerical constant equal to 3.202×10^{-6}; g is the Gaunt correction factor, which may be tabulated as a function of the frequency ν; and b_1 is a correction factor for the ground level. An expression for b_1 has been given in (V-2), viz.,

$$b_1 = \frac{G_{T_\epsilon}}{e^{X_1}\int_{y_1}^{\infty} W_{1\kappa} \frac{dy}{y(e^y - 1)}}, \tag{7}$$

where

$$X_1 = \frac{hRZ^2}{kT_\epsilon} = \frac{h\nu_1}{kT_\epsilon} = \frac{1.5703 \times 10^5}{T_\epsilon}, \qquad y = \frac{h\nu}{kT_1},$$

and G_{T_ϵ} has been given graphically in Paper XVI. It is of the order of 0.1 for $T_\epsilon \sim 10^{4°}$ K. If W is constant with frequency, we have

$$F_{1\kappa}d\nu = N_i N_\epsilon \frac{3.202 \times 10^{-6}}{T^{3/2}} \frac{G_{T_\epsilon} \frac{d\nu}{\nu}}{(e^y - 1)\int_{y_1}^{\infty} \frac{dy}{y(e^y - 1)}}. \tag{8}$$

It is clear that N_i, N_ϵ, and T_ϵ will adjust themselves so that the total number of ionizations will equal the total number of recombinations. In fact, this is one of the relations used in Paper V to determine T_ϵ.

B. RECOMBINATION

The target area for the capture of an electron on a level n with an energy corresponding to κ is

$$\sigma_{\kappa n} = \frac{2^4}{3\sqrt{3}} \frac{\epsilon^2 h}{m^2 c^3} \frac{1}{\left(\frac{1}{n'^2} + \frac{1}{\kappa^2}\right)} \frac{\kappa^2}{n'^3} g_{II}, \tag{9}$$

where g_{II} is a correction factor. The total number of captures to a single ion is obtained simply by summing over n and multiplying by the velocity V. If we write the energy in terms of electron volts as a convenient unit, we obtain, for the total number of captures on all levels of an ion,

$$\frac{2^4}{3\sqrt{3}} \frac{\epsilon^2 h}{m^2 c^3} \sqrt{\frac{\mathfrak{V}\epsilon}{150m}} \frac{\mathfrak{V}_i}{\mathfrak{V}} \Sigma \frac{1}{\left(\frac{1}{n'^2} + \frac{\mathfrak{V}}{\mathfrak{V}_i}\right)} \frac{g_{II}}{n'^3} = 1.24 \times 10^{-14} \frac{\mathfrak{V}_i}{\sqrt{\mathfrak{V}}} \Sigma \frac{1}{\left(\frac{1}{n'^2} + \frac{\mathfrak{V}}{\mathfrak{V}_i}\right)} \frac{1}{n'^3},$$

where $\mathfrak{V}_i$ here denotes the ionization potential of hydrogen. If, however, we use c.g.s. units which are more convenient in some cases, we get, for the total number of captures per cm³/sec,

$$V f(V) N_e^2 \Sigma \sigma_{\kappa n} = 2.08 \times 10^{-22} N_e^2 f(V) V \Sigma \frac{1}{\left(\frac{1}{n'^2} + \frac{\mathfrak{V}}{\mathfrak{V}_i}\right)} \frac{1}{n'^3} \frac{E_i}{E}. \qquad (10)$$

Thus the cross-section varies slowly with the energy. To estimate its magnitude, let us consider, for example, an electron of energy 1.35 volts, for which $\mathfrak{V}_i/\mathfrak{V}$ is equal to 10. The sum then is about 1.7, and we get $\sigma = 10 \times 1.7 \times 2.1 \times 10^{-22} = 3.57 \times 10^{-21}/\text{cm}^2$. The rate of recombination, $N_i V \sigma$, for $N_i \sim 10^4$ and $V = 6.9 \times 10^7$ cm/sec, will be simply 2.5×10^{-9} sec. This result means that a single electron, of energy 1.35 volts, will take 4×10^8 sec, or about 13 years, to be captured. A slower electron, of, say, 0.5 volt of energy, will be recaptured in the order of 8 years. We shall adopt 10 years as the order of magnitude of the lifetime of an electron in the nebula.

C. INELASTIC COLLISIONS

The target area for the collisional excitation of the ^{1}D metastable level of *O* III by an electron moving with velocity V is[5]

$$\sigma = \frac{1}{\varpi_A} \frac{h}{4\pi m^2} \frac{\Omega(AB)}{V^2} = \frac{4.17}{2J_A + 1} \frac{\Omega(AB)}{V^2}, \qquad (11)$$

since ϖ_A, the statistical weight of the ground term of *O* III, is 9. If we express the energy in volts, we get

$$\sigma_{AB} = \frac{2.6 \times 10^{-15}}{\mathfrak{V}} \text{ cm}^2. \qquad (12)$$

In order to produce an inelastic collision with an *O* III ion, an electron must have at least 2.48 volts of energy, so that $\sigma = 0$ when $\mathfrak{V}$ is less than $\mathfrak{V}_0 = 2.48$ volts. An electron with slightly greater energy than $\mathfrak{V}_0$ has the maximum probability of suffering an inelastic collision. Let us estimate the average time taken for such an electron to produce an excitation. The probability of excitation per electron is $N_A \sigma V$, where N_A is the number of *O* III ions per cm³. In most bright nebulae, N_A is of the order of unity. Now $V \sim 9.35 \times 10^7$, and $\sigma = 1.105 \times 10^{-15}$; hence $N\sigma V \sim 9.7 \times 10^{-8}$. The mean time required for an excitation will be 1.03×10^7 seconds, or about 4 months, and this is at the most favorable energy for such a process.

The superelastic collisons are even less important, since they take place only with excited ions which are present in lower than equilibrium concentrations. The target areas for the two inverse processes are related by

$$\varpi_A \sigma_{AB} = \varpi_B \sigma_{BA}, \qquad (13)$$

in virtue of the principle of detailed balancing in thermodynamic equilibrium.

To find the number of superelastic collisions, we must know the number of excited ions, a quantity determined by the balance between the production by collisional excitation and destruction by radiation and superelastic collisions. To a first approximation, we may assume a Maxwellian distribution to calculate this balance; it will soon be evident that this assumption in this step introduces a very small error. The results of Paper XIII enable us to work out the relevant expressions as we want them. Under typical conditions the ratio of superelastic to total de-excitations will be about 0.1.

[5] See (X-26).

D. FREE-FREE TRANSITIONS

The target area for a free-free transition from a state κ to a state lying between κ' and $\kappa' + d\kappa'$ is given by

$$\sigma_{\kappa\kappa'} d\kappa' = \frac{2^4}{3\sqrt{3}} \frac{\epsilon^2 h}{m^2 c^3} \frac{1}{\left(\frac{1}{\kappa^2} - \frac{1}{\kappa'^2}\right)} \frac{\kappa^2}{\kappa'^3} g d\kappa' . \tag{14}$$ [6]

Since $E = hR/\kappa^2$ and since $Z = 1$ for hydrogen, the loss in energy is $\Delta E = hR(1/\kappa^2 - 1/\kappa'^2)$. To find the mean rate of energy loss, we multiply the probability of collision by the energy lost per collision,

$$N_i \sigma_{\kappa\kappa'} V d\kappa' dE = \frac{2^4}{3\sqrt{3}} \frac{\epsilon^2 h^2 R}{m^2 c^3} N_i V \frac{\kappa^2}{\kappa'^3} g d\kappa' . \tag{15}$$

To obtain the total energy loss, we integrate over all values of κ' larger than κ. Thus

$$\frac{d\bar{E}}{dt} = \frac{2^4}{3\sqrt{3}} \frac{\epsilon^2 h^2 R}{m^2 c^3} \tfrac{1}{2} V g N_i . \tag{16}$$

This is the mean rate of energy loss. To find the mean time required to dissipate an energy equal to the initial energy, divide by E and take the reciprocal,

$$\frac{F}{\frac{d\bar{E}}{dt}} = \frac{\tfrac{1}{2} m V^2}{2.10 \times 10^{-22} n R \tfrac{1}{2} V g N_i} . \tag{17}$$

Expressing the energy, E, in volts, we get

$$\frac{E}{\frac{d\bar{E}}{dt}} = 1.2 \times 10^9 \sqrt{\mathfrak{V}} \text{ seconds} .$$

For electron energies in the neighborhood of 1 volt, this interval amounts to about 40 years. Hence, at prevailing electron temperatures in gaseous nebulae, free-free emissions dissipate energy very slowly.

E. COULOMBIC ENCOUNTERS

The coulombic scattering, which arises from the electrostatic interactions between charged particles, may be estimated with the aid of the Rutherford expression[7] for the cross-section for scattering of a particle of energy, E, through an angle, θ, thus:

$$\sigma = \frac{\epsilon^4}{16 E^2 \sin^4 \frac{\theta}{2}} . \tag{18}$$

The total number of particles scattered into angles between θ and $\theta + d\theta$ is

$$dn = 2\pi N_e V \frac{\epsilon^4}{16E^2} \frac{\sin \theta d\theta}{\sin^4 \frac{\theta}{2}} . \tag{19}$$

[6] If we write Menzel and Pekeris' formula (1.53) for a continuous state of width $d\kappa$ at κ' instead of for a discrete lower level n', we get our equation (14).

[7] This is the Rutherford scattering formula. A discussion along the lines in which we are interested may be found in Kennard, *Kinetic Theory of Gases* (New York: McGraw-Hill Book Co., 1938).

Since the cross-section is so large for small angle deflections, these will play the dominant role, and we may replace sin θ by θ for the vast majority of collisions. Then

$$dn = \frac{2\pi N_e v\epsilon^4}{E^4} \frac{d\theta}{\theta^3}. \tag{20}$$

Because an ion is so very much heavier than an electron, we may neglect energy transfers to it. To estimate the mean energy transfer in electron-electron encounters, we must note that the Rutherford formula applies only in the frame of reference in which the center of gravity is at rest. Since the angle of scattering in the fixed co-ordinate system is one-half that in the center-of-mass system[7] and since the relative energy is one-half that of the incident electron, the above formula is unchanged if θ is allowed to refer to the actual angle of scattering in the fixed system and E to the incident energy. For the time being we shall assume that the scattering particle is moving at a negligible velocity. In Section IV the effect of its finite velocity will be considered. To a first approximation the energy gained by the scattering electron is given by

$$E = E \sin^2 \theta \sim E\theta^2 . \tag{21}$$

The mean rate of energy transfer then is

$$\Delta E dn = \frac{2\pi N_e v\epsilon^4}{E} \frac{d\theta}{\theta}. \tag{22}$$

We obtain the total energy transfer by integrating from some appropriate minimum value of θ to the maximum value of θ, which is π, thus:

$$\frac{dE}{at} = \frac{2\pi N_e v\epsilon^4}{E} ln \left(\frac{\pi}{\theta_{\min}}\right). \tag{23}$$

The scattering cross-section increases without bound as the angle of deflection approaches zero. Hence, if the formula is to be physically significant, there must be some process or processes which serve to fix a minimum angle for which the scattering expression can be applied.

The minimum angle is determined by the maximum distance for which the electrostatic field of the electron is not seriously modified by the presence of all the other electrons in the gas. In fact, the more distant encounters must be regarded as many-body collisions. At any instant many distant electrons are pulling on any given electron, some in one way, some in another. The average force tends to cancel out; but, because the density fluctuates, there are small residual energy transfers, the effects of which should, in a completely rigorous treatment, be added to the effects of the close encounters. The same problem arises in the determination of the time of relaxation in stellar systems. Spitzer[8] and Chandrasekhar[9] suggest that the assumption of a single encounter, leading to the Rutherford cross-section, breaks down at a collision distance of about two or three times the mean distance between stars. At greater distances they believe that the complex many-body interactions will effectively cause the mean force to be much less than the coulomb force. In fact, the contribution of more distant encounters is so small that it can be ignored by choosing an appropriate maximum value of b, the cutoff distance, beyond which the scattering is negligible. Because the result depends only on the logarithm of this value, it will not depend critically on the cutoff, which may be taken as b_0, the mean distance between stars.

[8] *M.N.*, **100**, 387, 1940.

[9] *Principles of Stellar Dynamics* (University of Chicago Press, 1942), see esp. pp. 56 ff.

The plasma problem differs from the stellar problem in two respects; first, there are repulsive, as well as attractive, forces, and, second, there is plenty of time for equilibrium to be set up. On the other hand, Chandrasekhar and Spitzer have shown that the time of relaxation of the stellar system is much greater than the probable age of the universe. In the plasma there is a tendency to establish an equilibrium state in which every charge is shielded by charges of the opposite sign. This shielding tendency is resisted by the random motion, which tends to mix charges regardless of sign. As a result of the balance of these two tendencies, there is a critical distance at which shielding, on the average, becomes effective. An exact treatment of this problem is complicated, and it will suffice to establish an upper limit to the cutoff distance (i.e., a lower limit to the scattering angle.)

To calculate this distance we may use the methods of Debye. The potential around any charge is determined by Poisson's equation:

$$\nabla^2\phi = 4\pi\epsilon\,(N_\epsilon - N_i)\,. \tag{24}$$

The electronic and ionic densities, N_ϵ and N_i, are determined by the Boltzmann equations

$$N_\epsilon = N_0 e^{\epsilon\phi/kT}\,, \qquad N_i = N_0 e^{-\epsilon\phi/kT}\,.$$

If $\epsilon\phi/kT$ is not too large, the first term of the expansion for the exponentials is adequate. We have

$$\nabla^2\phi = \frac{8\pi\epsilon^2 N_0}{kT}\,\phi\,.$$

The solution corresponding to a unit charge at short distance and finite potential at infinity is

$$\phi = \frac{\epsilon e^{-r/h}}{r}\,,$$

where

$$h^2 = \frac{kT}{8\pi N_0\epsilon^2}\,. \tag{25}$$

Now h is the distance at which the potential begins to deviate appreciably from the coulombic; it is therefore the distance at which shielding becomes appreciable. Below this distance the potential is roughly coulombic, and the Rutherford cross-section applies; while above this value the potential soon becomes negligible, so that one may take h as the cutoff. This should certainly give at least an upper estimate.

When the value of h is computed for our problem, we find that it is much larger than the mean distance between electrons. Because this quantity appears in the logarithm, the replacement of b_0 by h changes the result by a factor of 2 or less; hence, in practice, the question of cutoff is not critical and certainly does not affect the qualitative validity of our results. At worst, we can say that the true value for the cutoff lies somewhere between b_0 and h.

The relation between the maximum encounter distance, b, and the angle $\theta_{\min}$ is given by the expression

$$\theta_{\min} = 2\,\arctan\frac{\epsilon^2}{2Eb} \sim \frac{\epsilon^2}{Eb}\,; \tag{26}$$

and it makes very little difference whether or not we employ for b the mean distance between electrons of the Debye encounter limit, h. At an electron density of $10^4/\text{cm}^3$ and a temperature of 10,000° K, h will be 5 cm, while the mean interelectronic distance, b_0, will be of the order of 0.05 cm. Under these conditions the log $(\pi/\theta_{\min})$ factor in equation (23) will amount to 16.5 or 12, depending on our choice of b; hence the two results for

dE/dt will differ by a factor of less than 2. For a numerical example, let us choose the log factor to be 15. To find the mean time required for an electron to dissipate its energy, we divide the mean rate of energy loss given in equation (23) by E and take the reciprocal, thus:

$$T \sim \frac{E^2}{30\pi N_e v \epsilon^4}. \tag{27}$$

In an example where $E = 3.3$ volts and $N_e \sim 10^4$, the corresponding velocity, v, will be 1.07×10^8 cm/sec, and the time will be of the order of 4 seconds. That is, a 3.3-volt electron loses most of its energy to the other electrons in only 4 seconds. Since most electrons have even less energy than this, they may redistribute what they have in an even shorter time. Therefore, 1 second is the order of the time involved in shuffling the energy among the electrons.

Thus it is clear that interelectronic collisions are the main processes acting to determine the distribution among the velocities and that the other physical processes, such as recombination, etc., amount to only small perturbations. An electron liberated within the nebula loses half its initial energy within a few seconds and thereafter obtains an energy primarily determined by the velocities of all the other electrons. Since the distribution cannot differ much from the equilibrium form that it would have if all other processes were absent, it must be very close to the Maxwellian. A method for the calculation of the slight deviations will be considered in the next section.

Spitzer[8] and, more recently, Chandrasekhar[9] have treated the problem of coulombic-type encounters for the corresponding stellar case in great detail. Chandrasekhar has derived general expressions for inverse-square law deflections, valid for all angles of encounter. In the present treatment we have confined our attention to small angles, so that our expressions are somewhat simpler than those of Chandrasekhar. For the detailed theory of encounters, the reader is referred to the excellent treatment given in *Principles of Stellar Dynamics*.

III. BOLTZMANN'S EQUATION FOR THE ASSEMBLY

A. SOLUTION WITH ELASTIC COLLISIONS ONLY

In order to calculate the deviations from Maxwell's formula, we must solve the Boltzmann integrodifferential equation,[10] which determines the distribution. Let $N_e = N_i$ denote the number of electrons per cm^3; $f_2(u, v, w)$ denotes the distribution function specifying the fraction of all electrons in the range between u and $u + du$, v and $v + dv$, and w and $w + dw$. We normalize f_2 so that its integral over all velocity space is unity, viz.,

$$\int\int\int_{-\infty}^{+\infty} f_2(u, v, w)\, du\, dv\, dw = 1. \tag{28}$$

If the distribution function is isotropic in velocity space, then f_2 is a function only of the absolute value of the velocity V, and the normalization reduces to

$$4\pi \int_{-\infty}^{+\infty} f_2(V)\, V^2 dV = 1. \tag{29}$$

Our $f_2(V)$ is related to the $f(v)$ used by Menzel through the relation

$$f(v) = 4\pi V^2 f_2(V) \tag{30}$$

[10] See, e.g., Kennard, *op. cit.*, p. 89.

(notice that we use a V to denote the total speed and v for the y-component). The total number of electrons in any specified interval of velocity space is given by the formula

$$dN = N_e f_2(V)\, du\, dv\, dw\,. \tag{31}$$

Boltzmann's equation simply expresses the rate of change of the distribution function arising from the various processes, such as collision, excitation, recombination, etc., which are occurring in the assembly. The equation is

$$\left.\begin{aligned}\frac{\partial (N_e f_2)}{\partial t} = &- (\boldsymbol{V}\cdot\nabla)(N_e f_2) - (\dot{\boldsymbol{V}}\cdot\nabla_V)(N_e f_2) + \left[\frac{\partial}{\partial t}(N_e f_2)\right]_{\text{coll}} \\ &+ \left[\frac{\partial}{\partial t}(N_e f_2)\right]_p,\end{aligned}\right\} \tag{32}$$

wherein $(\dot{\boldsymbol{V}}\cdot\nabla_V)$ signifies the operator

$$\dot{u}\frac{\partial}{\partial u} + \dot{v}\frac{\partial}{\partial v} + \dot{w}\frac{\partial}{\partial w},$$

$$\left[\frac{\partial}{\partial t}(N_e f_2)\right]_{\text{coll}}$$

signifies the rate of change of $(N_e f_2)$ arising from encounters, while

$$\left[\frac{\partial}{\partial t}(N_e f_2)\right]_p$$

signifies the rate of change of $N_e f_2$ arising from all other processes, such as recombination, inelastic collisions, free-free emissions, etc., discussed in Section II.

The first two terms represent the effects of hydrodynamical flow in phase space, as a result of which the density and velocity distribution are changing simply because of the motions and macroscopic accelerations undergone by the particles involved. If the distribution is independent of the spatial co-ordinates and if there are no macroscopic body forces, these two terms vanish. For the present we shall assume that these simple conditions prevail in a nebula, at least over moderate distances. At some time it may be advisable to consider spatial diffusions and the effects of radiation pressure over large distances, which will appear as a body force. These forces could introduce but small corrections to the main collisional terms.

Because elastic collisions have been shown to be far more frequent than any other event, the distribution will differ only slightly from what it would be if they were the only processes. It is therefore worth while, first, to consider the distribution arising from elastic collisions alone. It will be shown presently that the only solutions to Boltzmann's equation for this case must be Maxwellian. Thus we may write

$$f_2(V) = \left(\frac{m}{2\pi kT}\right)^{3/2} e^{-mv^2/2kT}. \tag{33}$$

Later, when the effect of other processes is considered, we shall find that the distribution differs slightly from the Maxwellian; but we can write

$$f_2(V) = b(V)\left(\frac{m}{2\pi kT}\right)^{3/2} e^{-mv^2/2kT}, \tag{34}$$

where $b(V)$ is a correction factor close to unity.

Hagihara states that there is an approximate solution to Boltzmann's equation for the isotropic case with elastic collisions that is more general than the Maxwellian distribution, viz.,

$$f_2(V) = \left(\frac{m}{2\pi kT}\right)^{3/2} [c + d\,V^2]\; e^{-mv^2/2kT}. \tag{35}$$

For any given temperature, T, and for any assigned spectral energy distribution and matter density, the condition for a radiative steady state and the condition for constant populations in each level determined c and d. But the temperature itself apparently is not determined by any physical process, and the result is ambiguous. To prove that the V^2 term may be present, Hagihara[11] expands the most general solution in a series of Hermite polynomials

$$f_2(u,\ v,\ w) = \left(\frac{m}{kT}\right)^{1/2} \sum_{ijk} f_{ijk}\varphi_{ijk}, \tag{36}$$

with

$$\varphi_{000} = \frac{1}{(2\pi)^{3/2}}\; e^{-\frac{u^2+v^2+w^2}{2kT/m}}, \qquad \varphi_{ijk} = (-1)^{i+j+k} H_{ijk}\varphi_{000},$$

and

$$H_i = H_i\left(u\sqrt{\frac{m}{kT}}\right), \qquad H_j = H_j\left(v\sqrt{\frac{m}{kT}}\right), \qquad H_k = H_k\left(w\sqrt{\frac{m}{kT}}\right),$$

$$H_0(X) = 1, \qquad H_1(X) = X \qquad \text{and} \qquad H_2(X) = X^2 - 1.$$

The solution with $H_0(X)$ refers to the Maxwellian distribution, while that with $H_1(X)$ refers to mass motion. Since we are considering the case in which there is no mass motion, the H_1 terms must vanish. The only isotropic term of second order is

$$H_{200} + H_{020} + H_{002} = V^2 - 3, \qquad \text{where} \qquad V^2 = u^2 + v^2 + w^2.$$

The total number of particles is found by integrating f_2 over all velocities. Because of the orthogonality properties of the Hermite polynomials, the only contribution to this number is made by H_0. As for the total energy, it is readily shown that only H_0 and $H_{200} + H_{020} + H_{002}$ contribute. Since neither the number of particles nor the total energy can be changed by elastic collisions and since the number and energy together determine the coefficients of these two terms, the coefficients of H_{000} and $H_{200} + H_{020} + H_{002}$ are not changed by collisions. Thus, to the second order the $V^2 - 3$ term is also a steady-state solution of Boltzmann's equation. A direct substitution in the precise form of the equation, however, shows that this latter term is not a solution to higher orders. Yet, if we wish to know the tail of the distribution function, the higher-order terms are essential, and therefore the approximate solution given by Hagihara cannot be applied unless the very high-order polynomials are also considered. The greater the velocities in which we are interested, the further the expansion must be carried.

It is possible, however, to go further and to show that, for the case of elastic collisions, all steady-state solutions to Boltzmann's equation must be Maxwellian. Boltzmann's H theorem[12] serves to establish this result. The method employed is to show that the function, $H = \Sigma f_2 \ln f_2$, which is summed over all parts of phase space, must have a negative derivative unless the distribution is Maxwellian. Since a steady state requires that all functions of the distribution be constant, it can exist only for the Maxwellian case. In the light of this result, as well as that of the previous considerations, showing that the V^2 term is a bad approximation for the high-energy range, Hagihara's approximate solution

[11] *Tokyo Astr. Bull.*, No. 525, eq. (2).

[12] Kennard, *op. cit.*, p. 53.

must be thought of simply as the first term of a Maxwellian distribution expanded about another temperature, thus

$$e^{-mV^2/2kT'} = e^{-mV^2/2kT}\left(1 - \left[\frac{m}{2kT} - \frac{m}{2kT'}\right]V^2 + \dots\right).$$

When the distribution is not in equilibrium, there is no unique temperature; this is the essential content of Hagihara's result. Yet, from the facts discussed above, we may define a best temperature which makes the correction factor as close as possible to unity. It is clear that the best Maxwellian distribution is that which, by itself and without a correction factor, represents correctly the total number of particles and the total energy. This means that the best temperature is the one in which the V^2 term is absent. We shall see that Boltzmann's equation requires a boundary condition specifying a value of $b(0)$ and the coefficient of the V^2 term in the expansion of $b(V)$. By choosing $b(0) = 1$ and the coefficient of the V^2 term zero, we satisfy our boundary conditions with the best possible temperature. Thus the temperature is made unique, and the ambiguity mentioned above is shown to be merely the consequence of the choice of an inappropriate temperature.

Since a Maxwellian distribution of any temperature is the most general solution of Boltzmann's equation when only elastic collisions are considered, it is clear that the temperature must be determined by processes other than elastic collisions. In the nebular case the distribution is very close to an equilibrium one, and to a first approximation we may assume a Maxwellian distribution, and then determine the temperature and the density by setting up the condition for a balance of the emission and recapture of electrons and for the balance of energy. Menzel and his collaborators have done this in Papers V and XVI of the nebular series.

B. GENERAL FORMULATION OF BOLTZMANN'S EQUATION

Let us now turn to the problem of the detailed formulation of Boltzmann's equation. We shall find it convenient to re-express all quantities as functions of the energy. Let the fraction of particles between E and $E + dE$ be denoted by $f_3(E)dE$. Since $E = \frac{1}{2}mV^2$ and $dE = mVdV$, we have

$$f_3(E)\,dE = f_3(E)\,mV\,dV = f(V)\,dV \qquad \text{or} \qquad f_3(E) = \frac{f(v)}{mV}. \tag{37}$$

The Maxwellian distribution in energy may be written as

$$f_3(E) = \frac{2E^{1/2}}{\sqrt{\pi}\,(kT)^{3/2}}\,e^{-E/kT}. \tag{38}$$

We shall also find it convenient to write the deviation from the Maxwellian form with the aid of the factor $b(E) = 1 + \delta(E)$ where $\delta(E)$ is small. Furthermore, since the best temperature is chosen with $b(0) = 1$ and the coefficient of E in the expansion of $b(E) = 0$, we also have $b'(0) = 0$ and

$$f_3(E) = \frac{2}{\sqrt{\pi}\,(kT)^{3/2}}[1 + \delta(E)]E^{1/2}e^{-E/kT}. \tag{39}$$

We shall now collect the expressions for the noncoulombic contributions to $(\partial N_e f_2/\partial t)$.

a) Photo-ionization.—The number of electrons emitted per second in the energy range dE is given by equation (8), with ν replaced by $E/h + E_a/h$, where E_a is the ionization energy of hydrogen, or 13.54 volts,

$$F_{1E}dE = \frac{3.202 \times 10^{-6}}{T_e^{3/2}}\,N_e^2 h G_{T_e}\frac{dE}{E+E_a}\frac{1}{(e^y-1)}\int_{y_1}^{\infty}\frac{dy}{y\,(e^y-1)}. \tag{40}$$

b) Recombinations.—The number of electrons possessing energy between E_1 and $E_1 + dE_1$ that are recaptured on all levels is found by multiplying the probability of recapture of electron and ion by the number of electrons and ions concerned. The number of electrons is $N_e f_3(E_1)dE_1$, and the number of ions is $N_i = N_e$. We get

$$\left[\frac{\partial (N_e f_3)}{\partial t}\right]_{\text{recomb}} = 1.24 \times 10^{-14} N_e^2 f_3(E_1) \frac{\mathfrak{V}_i}{\sqrt{\mathfrak{V}_1}} \Sigma \frac{1}{\left(\frac{1}{n'^2} + \frac{\mathfrak{V}}{\mathfrak{V}_i}\right) n_1^3} \tag{41}$$

if we express E in volts, $\mathfrak{V}$, in this formula. In absolute units the result is

$$\left[\frac{\partial (N_e f_3)}{\partial t}\right]_{\text{recomb}} = 2.08 \times 10^{-22} N_e^2 f_3(E_1)\, V\, \Sigma \frac{1}{n_1^3 \left(\frac{1}{n'^2} + \frac{E}{E_a}\right)} \frac{E_a}{E}. \tag{42}$$

c) Inelastic collisions.—Inelastic collisions cause electrons to be transferred from a given energy range to a lower one. Provided $E_1 > E_0$, the rate at which electrons leave a given energy range is $dE_1 \sigma(E_1) V(E_1) N_A N_e f_3(E_1)$, and the rate at which they are caused to enter from an energy exceeding E_1 by the excitation energy, E_0, is $f_3(E_1 + E_0)\sigma(E_1 + E_0) N_A N_e V(E_1 + E_0)$. In a typical planetary nebula, where the green *O* III lines are the strongest, N_A denotes the number of *O* III ions in the ground ^3P term, and N_B the number in the ^1D level, while E_0 denotes the excitation energy. The total change is

$$\left[\frac{\partial (N_e f_3)}{\partial t}\right]_{\text{inel}} = N_A N_e \left[f_3(E+E_0)\, V(E_1+E_0)\, \sigma(E_1+E_0) - f_3(E_1)\, V(E_1) \times \sigma(E_1)\, Q(E_1) \right], \tag{43}$$

where $Q(E_1) = 0$ when $E < E_0$ and $Q(E_1) = 1$ when $E > E_0$. By similar reasoning, we obtain for the superelastic collisions

$$\left[\frac{\partial (N_e f_3)}{\partial t}\right]_{\text{superel}} = N_B N_e \left[f_3(E_1 - E_0)\, \sigma(E_1 - E_0)\, V(E_1 - E_0)\, Q(E_1 - E_0) - f_3(E_1)\, \sigma(E_1)\, V(E_1) \right].$$

If E_1 is less than E_0, there can be no gains from superelastic collisions.

d) Free-free emissions.—Free-free emissions arise from electron-ion encounters and will cause electrons to leave a given energy range and be transferred to a lower one, differing by the energy of the photon emitted. The rate of loss is calculated from equation (14) thus:

$$N^2 f_3(E_1)\, V(E_1) \int_0^\infty \frac{2^4}{3\sqrt{3}} \frac{\epsilon^2 h}{m c^3} \frac{1}{\left(\frac{1}{\kappa^2} - \frac{1}{\kappa'^2}\right)} \frac{\kappa^2}{\kappa'^3}\, g\, d\kappa'. \tag{44}$$

The rate of gain of electrons will be

$$N_e^2 \frac{2^4 \epsilon^2 h}{3\sqrt{3} m c^3} \int_0^\infty f_3\left[E + hR\left(\frac{1}{\kappa^2} - \frac{1}{\kappa'^2}\right)\right] \frac{V\left[E_1 + hR\left(\frac{1}{\kappa^2} - \frac{1}{\kappa'^2}\right)\right]}{\left(\frac{1}{\kappa^2} - \frac{1}{\kappa'^2}\right)} \frac{\kappa^2}{\kappa'^3}\, g\, d\kappa', \tag{45}$$

and the net rate of change is just the difference between the latter and the former expressions.

e) Coulombic terms.—Let us now consider the contribution of the coulombic terms. The rate of change of the distribution resulting from scattering is determined from the

coulomb cross-section (cf. Sec. II). The problem, however, is complicated by the fact that both of the electrons involved in the collision are moving. Therefore, we must sum up the contributions to the change of distribution resulting from electrons of all different velocities. When an electron collides with another electron which is moving, it may lose or gain energy, depending on the relative velocities and the angle of collision. It is from those collisions that produce a gain of energy that the high-velocity portion of the Maxwellian distribution arises.

For the present we shall denote the fact that the collision cross-section depends on the energies of both colliding particles by writing it $\sigma = \sigma(E_1, E_2, \Delta E)$, where E_1 is the electron under consideration, E_2 is the electron with which it collides, and ΔE is the energy given to the first electron as a result of collision. The precise form of σ will be derived in Section IV; the number of collisions per second by electrons of energy E with electrons of energy E_2 and energy exchange, ΔE, then is

$$d(\Delta E) \int_0^\infty (dE_2)\ v_r N_e^2 f_3(E_1)\ f_3(E_2)\ \sigma(E_1, E_2, \Delta E)\,, \tag{46}$$

where v_r is the relative velocity of the two electrons. To find the rate at which the distribution function is changed by collision, let us consider electrons in a given energy range from E_1 to $E_1 + dE_1$. Electrons of energy $(E_1 - \Delta E)$ are scattered into this range by collisions with an exchange of ΔE in the positive sense, as defined above. On the other hand, collisions also cause electrons to leave this range. The net change in the distribution is found by summing over all ΔE's. Although ΔE cannot be greater than E_2, the cross-section decreases so rapidly with E that we may make our limits $-\infty$ to $+\infty$. We obtain

$$\left[\frac{\partial(N_e f_3)}{\partial t}\right]_{\text{coll}} = N_e^2 \int_0^\infty dE_2 \int_{-\infty}^{+\infty} d(\Delta E)\,[\,v_r(E_1 - \Delta E, E_2)\,\sigma(E_1 - \Delta E, E_2, \Delta E) \times f_3(E_1 - \Delta E)\ f_3(E_2) - v_r(E_1, E_2)\,\sigma(E_1, E_2, \Delta E)\ f_3(E_1)\ f_3(E_2)\,]\,. \tag{47}$$

We now have all the terms that enter into Boltzmann's equation.

IV. THE SOLUTION OF BOLTZMANN'S EQUATION

We shall begin by considering the coulomb terms only, which, as we have seen, represent the main processes involved. The term $[\partial N_e f_3/\partial t]_{\text{coll}}$, in its complete form, is too complicated to allow a solution. It is possible, however, to obtain an approximation which takes advantage of the fact that coulomb scattering involves mainly very small angles and, therefore, very small changes of energy. This is made possible by the fact that the coulomb cross-section, $\sigma(E_1, E_2, \Delta E)$, becomes very large as ΔE goes to zero. Because σ varies continuously as a function of E_1, we can expand $\sigma(E_1 - \Delta E, E_2, \Delta E)$ as a series of powers of ΔE about E_1. This means that, in so far as σ depends on ΔE through E_1, we can expand it, but, in so far as it depends on ΔE directly, we do not expand it. For convenience we shall write

$$v_r \sigma = \Omega(E_1, E_2, \Delta E)\,. \tag{48}$$

Then $[\partial N_e f_3/\partial t)_{\text{coll}}$ can be expanded up to the second power in ΔE as follows:

$$\left[\frac{\partial(N_e f_3)}{\partial t}\right]_{\text{coll}} = N_e^2 \int_0^\infty dE_2 \int_{-\infty}^{+\infty} d\Delta E \left[\,(-\Delta E)\frac{\partial}{\partial E}\Omega(E_1, E_2, \Delta E)\ f_3(E_1) + \frac{(\Delta E)^2}{2}\frac{\partial^2}{\partial E_1^2}\Omega(E_1, E_2, \Delta E)\ f_3(E_1)\right] f_3(E_2)\,. \tag{49}$$

Because the explicit dependence of Ω on ΔE is such that Ω is large only for very small ΔE, the higher terms in the expansion integrate out to a negligible value. This expansion results in an equation very similar to the Fokker-Planck equation.[13] The difference is that the terms are to be calculated directly from the known collision cross-sections and not semi-empirically, as is usually done. This procedure is possible only because the cross-section for this case is both known and simple.

If we now introduce equation (39) for $f_3(E)$ and neglect all terms involving $\delta(E)$ twice as a factor (as they are of the second order), we obtain

$$\left[\frac{\partial (N_\epsilon f_3)}{\partial t}\right]_{\text{coll}} = (I) + (II) + (III),$$

where

$$\left.\begin{aligned}
(I) &= \frac{2}{\sqrt{\pi}\,(kT)^{3/2}} N_\epsilon^2 \int_0^\infty dE_2 \int_{-\infty}^{+\infty} d(\Delta E)\left[(-\Delta E)\frac{\partial}{\partial E_1}\left(\frac{\Omega E^{1/2} e^{-E/kT}}{(kT)^{3/2}}\right)\right. \\
&\quad \left. + \frac{(\Delta E)^2}{2}\frac{\partial^2}{\partial E^2}\Omega E^{1/2} e^{-E_1/kT}\right]\left[e^{-E_2/kT} E_2^{1/2}\right]\frac{2}{\sqrt{\pi}\,(kT)^{3/2}}; \\
(II) &= \frac{2N_\epsilon^2}{\sqrt{\pi}\,(kT)^{3/2}} \int_0^\infty dE_2 \int_{-\infty}^{+\infty} d\Delta E\left[-\Delta E \frac{\partial}{\partial E}\Omega E_1^{1/2} e^{-E_1/kT}\delta(E_1)\right. \\
&\quad \left. + \frac{(\Delta E)^2}{2}\frac{\partial^2}{\partial E_1^2}\Omega E_1^{1/2} e^{-E_1/kT}\delta(E_1)\right]\left[e^{-E_2/kT} E_2^{1/2}\frac{2}{\sqrt{\pi}\,(kT)^{3/2}}\right]; \\
(III) &= \frac{2N_\epsilon^2}{\sqrt{\pi}\,(kT)^{3/2}} \int_0^\infty dE_2 \int_{-\infty}^{+\infty} d\Delta E\left[-(\Delta E)\frac{\partial}{\partial E_1}(\Omega E_1^{1/2} e^{-E/kT})\right. \\
&\quad \left. + \frac{(\Delta E)^2}{2}\frac{\partial^2}{\partial E_1^2}(\Omega E_1^{1/2} e^{-E_1/kT})\right]\left[e^{-E_2/kT} E_2^{1/2}\delta(E_2)\right]\frac{2}{\sqrt{\pi}\,(kT)^{3/2}}.
\end{aligned}\right\} \quad (50)$$

Term (I) would be present even if we had a Maxwellian distribution with $\delta(E) = 0$. Therefore, since a Maxwellian distribution is known to be in equilibrium for scattering alone, term (I) must be zero. In the course of the calculation we shall find it convenient to prove this. Term (II) represents the change in the deviation of the distribution from the Maxwellian, brought about by collision of the non-Maxwellian portion with the much larger Maxwellian component of the distribution which is the principal term. Term (III) represents the change in the Maxwellian component brought about by energy exchange with the small non-Maxwellian component. Terms involving $\delta(E)$ twice as factors represent the changes brought about by the small non-Maxwellian component with itself and are therefore negligible.

The first step in solving the problem is to carry out the integrations over ΔE, which are the same in all three terms. Inspection of these terms shows that they contain as factors the following two quantities:

$$A = \int_{-\infty}^{+\infty} d(\Delta E)\,\Delta E \Omega(E_1, E_2, \Delta E); \qquad B = \int_{-\infty}^{+\infty} d(\Delta E)\,(\Delta E)^2 \Omega(E_1, E_2, \Delta E). \quad (51)$$

A is proportional to the mean rate at which an electron of energy E_1 gains energy from electrons of energy E_2, while B is proportional to the dispersion of this rate about its mean. Terms containing A represent the change in the distribution function arising from the mean rate of energy transfer among the individual electrons, while terms containing

[13] Chandrasekhar, "Stochastic Problems in Physics and Astronomy," *Rev. Mod. Phys.* **15**, 1, 1943.

B represent the modifications introduced by the fact that the rate of energy transfer is not equal to its average but fluctuates in a more or less random way. The question of when it is adequate to represent all effects of a set of collision processes by their mean effects and by the mean deviation from the mean is essentially the same as in the treatment of the Fokker-Planck equation.[13] The mathematical justification for this procedure in our case is that, because the collision cross-section is such a rapidly decreasing function of ΔE, powers of ΔE higher than the second make a negligible contribution.

In order to evaluate A and B, we must first obtain an expression for the energy transfer ΔE as a function of the angle of scattering and of the angle between the motion of the two particles. Let us consider two colliding electrons, labeled "1" and "2," respectively. The velocity of the first particle is represented by V_1 and that of the second by V_2. Let us choose the z-axis in the direction of motion of the first particle, and let the angle between V_1 and V_2 be represented by the polar angle ω. We shall take the azimuthal angle as zero. To find the average value of ΔE, we must integrate over all possible angles of scattering, weighted with the scattering cross-section;[14] the result is

$$A(\omega) = -\frac{4\pi\epsilon^4 S(V_1^2 - V_2^2}{m(V_1^2 + V_2^2 - 2V_1V_2\cos\omega)^{3/2}}, \tag{52}$$

where (cf. eq. [27])

$$S = ln\left[\left(\frac{\pi}{\theta}\right)_{\min}\right].$$

Because S is such a slowly varying function of V, it is practically constant and is shown in Section II; its value is about 10 or 20 for the densities and temperatures of typical nebulae. Further,

$$B(\omega) = \frac{4\pi S\epsilon^4 V_1^2 V_2^2 \sin^2\omega}{(V_1^2 + V_2^2 - 2V_1V_2\cos\omega)^{3/2}}. \tag{53}$$

Inspection of A shows that, if $V_1 > V_2$, the average energy transfer is negative, while if $V_1 < V_2$, it is positive. This result simply means that a particle tends to lose energy on collisions with less energetic particles and to gain energy on collision with more energetic ones.

Since the distribution is isotropic, we must now average over ω, the angle between the motion of the two colliding particles, weighting according to the element of solid angle. Since all azimuthal angles are equally probable, we need merely weight over polar angles ω, with the factor $\frac{1}{2}\sin\omega d\omega$ (which is normalized when integrated over ω from 0 to π). Although these integrals are continuous functions of V_1 and V_2, their analytical form undergoes a change at $V_1 = V_2$. Thus it is necessary to consider the two possibilities: the first in which $V_1 > V_2$ and the second in which $V_2 > V_1$. We get[14]

$$\left.\begin{aligned} &(I) \quad (V_1 > V_2) \qquad A = -\frac{4\pi\epsilon^4 S}{mV_1}; \qquad B = \frac{8\pi S\epsilon^4 V_2^2}{3V_1}, \\ &(II) \quad (V_2 > V_1) \qquad A = \frac{4\pi\epsilon^4 S}{mV_2}; \qquad B = \frac{8\pi S\epsilon^4 V_1^2}{3V_2}. \end{aligned}\right\} \tag{54}$$

This result means that the average rate of energy loss to a slower particle is inversely proportional to the velocity of the faster particle only. On the other hand, in collisions with a faster particle, a slower particle gains energy at a rate inversely proportional to the

[14] For discussion of a closely analogous stellar problem see Chandrasekhar, *Ap. J.*, **93**, 326, 1941.

velocity of the faster particle only. Obviously, these two results are necessary for each other's consistency. We may now re-write $[\partial N_\epsilon f_3/\partial t]_{\text{coll}}$ in terms of A and B, viz.,

$$\left.\begin{aligned}\left[\frac{\partial}{\partial t}(N_\epsilon f_3)\right]_{\text{coll}} &= \frac{4N_\epsilon^2}{\pi(kT)^3}\int_0^\infty dE_2 E_2^{1/2} e^{-E_2/kT}\left[-\frac{\partial}{\partial E_1}A(E_1, E_2)E_1^{1/2}e^{-E_1/kT}\right.\\ &\left.+\frac{1}{2}\frac{\partial^2}{\partial E_1^2}B(E_1, E_2)E_1^{1/2}e^{-E_1/kT}\right]\frac{4N_\epsilon^2}{\pi(kT)^3}\int_0^\infty dE_2 E_2^{1/2}e^{-E_2/kT}\left[-\frac{\partial}{\partial E_1}\right.\\ &\left.\times AE_1^{1/2}e^{-E_1/kT}\delta(E_1)+\frac{1}{2}\frac{\partial^2}{\partial E_1^2}BE_1^{1/2}e^{-E_1/kT}\delta(E_1)\right]\frac{4N_\epsilon^2}{\pi(kT)^3}\\ &\times\int_0^\infty dE_2 E_2^{1/2}e^{-E_2/kT}\delta(E_2)\left[-\frac{\partial}{\partial E}AE_1^{1/2}e^{-E_1/kT}+\frac{1}{2}\frac{\partial^2}{\partial E_1^2}BE_1^{1/2}e^{-E_1/kT}\right].\end{aligned}\right\} \quad (55)$$

The next step is to carry out integrations over E_2. For integrals (I) and (II) this operation is possible, since all dependence on E_1 is explicit in terms of known functions. In integral (III), however, E_2 occurs through the unknown $\delta(E_2)$. This raises a serious difficulty in obtaining a complete solution in a straightforward way. We shall see presently, however, that a systematic approximation procedure can be adopted, in which the value of $\delta(E_2)$ to be inserted in integral (III) is always to be obtained from the next lower approximation. Meanwhile, we shall direct our attention to integrals (I) and (II), both of which require the evaluation of exactly the same integrals; these integrals have been evaluated by Chandrasekhar and others. We find

$$\left.\begin{aligned}C(E_1) &= \frac{4N_\epsilon^2}{\pi(kT)^3}\int_0^\infty dE_2 E^{1/2}e^{-E_2/kT}A(E_1, E_2) = \frac{2N_\epsilon^2 8\pi S\epsilon^4}{\pi(kT)^{3/2}(2\pi mkT)^{1/2}}\\ &\times\left[2e^{-E_1/kT}-\frac{W\left(\sqrt{\frac{E_1}{kT}}\right)}{\sqrt{\frac{E_1}{kT}}}\right]\end{aligned}\right\} \quad (56)$$

and

$$\left.\begin{aligned}D(E_1) &= \frac{4N_\epsilon^2}{\pi(kT)^3}\int_0^\infty dE_2 E_2^{1/2}e^{-E_2/kT}B(E_1, E_2) = \frac{2N_\epsilon^2 8\pi S\epsilon^4(2kT)}{\pi(kT)^3(2\pi mkT)}\\ &\times\left[\frac{W\left(\sqrt{\frac{E_1}{kT}}\right)}{\sqrt{\frac{E_1}{kT}}}-e^{-E_1/kT}\right],\end{aligned}\right\} \quad (57)$$

where

$$W(t) = \int_0^t e^{-x^2}dx.$$

In order to show that a Maxwellian distribution obtained by setting $\delta(E) = 0$ is a steady state for the case of coulomb collisions alone, we must show that term (I) is zero. We can do this most conveniently by showing that its integral is zero, or that

$$-C(E_1)E_1^{1/2}e^{-E_1/kT}+\frac{1}{2}\frac{\partial}{\partial E_1}D(E_1)E_1e^{-E_1/kT}=0. \quad (58)$$

Direct substitution of the formulae for C and D into the above expression shows that it is actually zero. This provides a check on the calculation. With the aid of equation (58) we may now simplify term (II) in Boltzmann's equation thus:

$$\left[\frac{\partial}{\partial t}(N_e f_3)\right]_{\text{coll}} - \text{term}(III) = \frac{1}{2}\frac{\partial}{\partial E_1} D(E_1)\, e^{-E_1/kT} \frac{E_1^{1/2}\partial\delta(E_1)}{\partial E_1}. \quad (58a)$$

Thus terms (I) and (II) together reduce to simply the expression above.

AN APPROXIMATION METHOD FOR THE SOLUTION OF BOLTZMANN'S EQUATION

Boltzmann's equation may be written thus for a steady state:

$$\left[\frac{\partial(N_e f_3)}{\partial t}\right] = \left[\frac{\partial(N_e f_3)}{\partial t}\right]_{\text{coll}} + \left[\frac{\partial(N_e f_3)}{\partial t}\right]_p. \quad (59)$$

Because $(\partial N_e f_3/\partial t)_{\text{coll}}$ is so large, we start with a zeroth approximation, in which $(\partial N_e f_3/\partial t)_p$ is neglected altogether. The solution for the zeroth approximation is simply a Maxwellian distribution with the temperature and particle density chosen to satisfy the conditions that the total number of electrons emitted is equal to those recaptured and that the total energy absorbed is equal to that going into the various dissipative processes such as excitation, radiation, etc. This is essentially the procedure used by most investigators in the past.

The next step is to solve for the higher approximations by an iterative process. We insert the zeroth-order Maxwellian approximation for $f_3(E)$ into $(\partial N_e f_3/\partial t)_p$ and then obtain an integrodifferential equation for the correction factor. The justification for this procedure is that $(\partial N_e f_3/\partial t)_p$ is already multiplied by relatively small coefficients, which are of the first order, so that, to the first order, it may be evaluated by replacing $f_3(E)$ by its zeroth-order approximation wherever it occurs. On the other hand, $(\partial N_e f_3/\partial t)_{\text{coll}}$ is so large that we cannot do this. Once we obtain a first-order solution, this procedure may be repeated to obtain higher-order approximations if desired. In general, this method is good only when the main part of the distribution is not too far from Maxwellian. For the nebular case this criterion is usually satisfied fairly well. For the first approximation our equation takes the form

$$\left.\begin{aligned}\frac{1}{2}\frac{\partial}{\partial E_1} D(E_1)\, e^{-E_1/kT} E_1^{1/2} \frac{\partial\delta(E_1)}{\partial E_1} + \frac{4N_e^2}{\pi(kT)^3}\int_0^\infty dE_2 E_2^{1/2} e^{-E_2/kT}\delta(E_2) \\ \times\left[-\frac{\partial}{\partial E_1} AE_1 e^{-E_1/kT} + \frac{1}{2}\frac{\partial^2}{\partial E_1^2} BE_1^{1/2} e^{-E_1/kT}\right] = -\left[\frac{\partial(N_e f_3)}{\partial t}\right]_{p_0},\end{aligned}\right\} \quad (60)$$

where $[\partial(N_e f_3)\partial t]_{p_0}$ signifies $[\partial(N_e f_3)\partial t]_p$ evaluated with the assumption of a suitable Maxwellian distribution.

In this form the equation is still difficult to solve, because the unknown variable occurs under the integral sign. If desired, it could be solved as a series of powers of E_1, but, in general, this is not necessary. The reason is that, if the distribution is close to the Maxwellian, the integrand can be shown to be very small. Remembering that our boundary conditions on $\delta(E)$ are that $\delta(0) = 0$, $\delta'(0) = 0$, we see from the differential equation that $\delta(E)$ can become appreciable only at rather large values of E, since it cannot begin to grow until its derivative has grown. The rate of change of its derivative, however, is small because it involves the ratio of probabilities of inelastic to coulomb encounters. But when E_2 is large, the factor $e^{-E_2/kT}$ makes the integrand negligible. Thus the integral itself is much smaller than term (II), and we may regard it as a second-order term, neglecting it altogether in the first approximation.

Because the distribution is so close to the Maxwellian that it is not worth while to find its precise departure therefrom, we shall be content to find an upper limit to this deviation. The processes of photoelectric ionization, excitation of the *O* III lines, and recombination are most rapid; hence it suffices to consider these alone.

We shall find it convenient to transform to the dimensionless variable

$$\frac{E}{kT} = \lambda . \tag{61}$$

Let us define a new distribution function as

$$dn = f_3(E)\, dE = f_4(\lambda)\, d\lambda = kT f_3(E)\, d\lambda ; \tag{62}$$

thus

$$f_3(E) = \frac{f_4(\lambda)}{kT} . \tag{63}$$

With f_4, the normalized Maxwellian distribution is

$$f_4 = \frac{2}{\sqrt{\pi}} \lambda^{1/2} e^{-\lambda} , \tag{64}$$

and the complete distribution is

$$f_4 = \frac{2}{\sqrt{\pi}} \lambda^{1/2} e^{-\lambda} [1 + \delta(\lambda)] . \tag{65}$$

In evaluating the noncollisional terms, let us first consider the one due to the photoionization (cf. eq. [40]). We want to find the rate of emission per unit of λ. Now equation (40) gives

$$F_{1E} dE = F_{1E} kT\, d\lambda . \tag{66}$$

Thus

$$\left[\frac{\partial (N_e f_4)}{\partial t}\right]_{\text{emis}} = \frac{3.202 \times 10^{-6}}{T_e^{3/2}} \frac{N_e^2 G_{T_e}}{\lambda + \lambda_a} \frac{1}{e^y - 1} \int_{y_1}^{\infty} \frac{dy}{y(e^y - 1)} . \tag{67}$$

The term due to recombination is found from equation (9) by multiplyiug the rate of recombination for a single electron by the electron density in λ-space for the approximate Maxwellian distribution, which we are using in the noncoulomb terms, as follows:

$$\left[\frac{\partial (N_e f_4)}{\partial t}\right]_{0\ \text{recomb}} = 2.097 \times 10^{-22} \frac{2}{\sqrt{\pi}} V(\lambda) \frac{\lambda_a}{\lambda} N_e^2 e^{-\lambda} \lambda^{1/2} \Sigma \frac{1}{\left(\frac{1}{n'^2} + \frac{\lambda_a}{\lambda}\right)} \frac{g}{n^3} . \tag{68}$$

Since $V = \sqrt{2kT\lambda/m}$, we get

$$\left[\frac{\partial (N_e f_4)}{\partial t}\right]_{0\ \text{recomb}} = \frac{2}{\sqrt{\pi}} \times 2.097 \times 10^{-22} \sqrt{\frac{2kT}{m}} \lambda_a N_e^2 e^{-\lambda} \Sigma \frac{1}{\left(\frac{1}{n'^2} + \frac{\lambda_a}{\lambda}\right)} \frac{g}{n^3} . \tag{69}$$

For excitation terms we refer to Section III, equations (42) and (11), where $(\partial N_e f_4/\partial t)_{\text{inel}}$ is given by

$$9.28 N_A N_e \frac{f_4(\lambda + \lambda_a)}{v(\lambda + \lambda_a)} - \frac{f_4(\lambda)}{V(\lambda)} Q(\lambda) , \tag{70}$$

where $Q(\lambda) = 0$, when $\lambda < \lambda_0$; and $Q(\lambda) = 1$ when $\lambda > \lambda_0$. With

$$f \sim \frac{2}{\sqrt{\pi}} e^{-\lambda} \lambda^{1/2}$$

we get

$$\left[\frac{\partial (N_e f_4)}{\partial t}\right]_{\text{inel}} = \frac{9.28}{\sqrt{\frac{2\pi kT}{m}}} \times 2 N_A N_e e^{-\lambda} \left[e^{-\lambda_0} - Q(\lambda) \right]. \tag{71}$$

Finally, the coulomb collisions must be considered. The term we have worked out is $(\partial N_e f_3/\partial t)_{\text{coll}}$. What we want is

$$\left[\frac{\partial}{\partial t}(N_e f_4)\right]_{\text{coll}} = kT\left[\frac{\partial}{\partial t}(N_e f_3)\right]_{\text{coll}} = \frac{(kT)}{2} \frac{\partial}{\partial E_1} D(E_1)\, e^{-E/kT} E_1^{1/2} \frac{\partial \delta}{\partial E}. \tag{72}$$

If we replace E_1 by kT and D by its value given in equation (57) and use equation (58*a*), we get

$$\left[\frac{\partial}{\partial t}(N_e f_4)\right]_{\text{coll}} = \frac{16\pi S\epsilon^4}{(kT)^{3/2}\sqrt{\pi}\sqrt{2\pi m}} \frac{\partial}{\partial \lambda}\left[e^{-\lambda} \lambda^{1/2} \frac{W(\sqrt{\lambda})}{\sqrt{\lambda}} - e^{-\lambda} \frac{\partial \delta}{\partial \lambda}\right]. \tag{73}$$

Finally, equating $-(\partial N_e f_4/\partial t)_{\text{coll}}$ and $(\partial N_e f_4/\partial t)_{0/p}$, we obtain

$$\left.\begin{aligned} -\frac{\partial}{\partial \lambda}\left(e^{-\lambda}\lambda^{1/2}\left[\frac{W(\sqrt{\lambda})}{\sqrt{\lambda}} - e^{-\lambda}\right]\right)\frac{\partial \delta}{\partial \lambda} = {} & \frac{3.202\times 10^{-6}\sqrt{2m}\,(kT)^{3/2} G_{T_e}}{T_e^{3/2} 16 S\epsilon^4 (\lambda + \lambda_a)(e^y - 1)} \\ & \times \int_{y_1}^{\infty} \frac{dy}{y(e^y - 1)} - \frac{(kT)^2 \times 2.1 \times 10^{-22} \lambda_a e^{-\lambda}}{4\sqrt{\pi} S\epsilon^4} \Sigma \frac{1}{\left(\frac{1}{n'^2} + \frac{\lambda_a}{\lambda}\right)} \frac{g}{n'^3} \\ & + 9.28 \frac{N_A}{N} \frac{kTm}{8\sqrt{\pi} S\epsilon^4} e^{-\lambda} \left[e^{-\lambda_0} - Q(\lambda) \right]. \end{aligned}\right\} \tag{74}$$

In a typical example, with $T_e = 10{,}000°$ K, $N_A \sim 1$, $N_e \sim 10^4$, $y_1 \sim 2$, $\lambda + \lambda_a \sim 14.5$, and $G_{T_e} \sim 0.1$, the value of the integral on the right turns out to be about 0.04, and

$$\left.\begin{aligned} -\frac{\partial}{\partial \lambda}\left(e^{-\lambda}\lambda^{1/2}\left[\frac{W(\sqrt{\lambda})}{\sqrt{\lambda}} - e^{-\lambda}\right]\right)\frac{\partial \delta}{\partial \lambda} = {} & 4\times 10^{-10} - 1.4\times 10^{-9} e^{-\lambda} \\ & + 7.6\times 10^{-8} e^{-\lambda} \left[e^{-\lambda} - Q(\lambda) \right]. \end{aligned}\right\} \tag{75}$$

Since λ varies between 0 and 5 over the range of interest and since the coefficient $(e^{-\lambda}\lambda^{1/2}[W(\sqrt{\lambda})/\sqrt{\lambda} - e^{-\lambda}])$ is not much less than 0.01 over most of the range of interest, we see immediately that $\delta(\lambda)$ cannot possibly become large. Some difficulties arise from a zero of the quantity $\lambda^{1/2}[W(\sqrt{\lambda})/\sqrt{\lambda} - e^{-\lambda}]$ at the origin which leads to an infinity in the value of $\partial\delta/\partial\lambda$ there. This infinity is spurious, however, because the approximation breaks down when the derivative of δ gets large. Because the coefficients on the right-hand side are so small, the region in which the derivative is large is confined to a small region close to the origin. Thus the equation is in error in this very small region where it predicts large values of δ'. We may neglect this region altogether, however, because it is so narrow that it cannot possibly affect the high-energy tail. Essentially, this singularity arises from the infinite cross-section for recombination at low energies. This cross-section, it will be recalled, integrates out to a finite value in all cases.

From the foregoing discussion it is clear that the inelastic terms could be at least a million times larger than they are now, before there was any doubt that the distribution was Maxwellian.

We are grateful to Dr. S. Chandrasekhar and Dr. Lyman Spitzer, who read the manuscript and made a number of valuable suggestions.

ON THE RADIATIVE EQUILIBRIUM OF A STELLAR ATMOSPHERE. XIII

S. CHANDRASEKHAR
Yerkes Observatory
Received October 28, 1946

ABSTRACT

In this paper the problem of diffuse reflection, which was considered in Paper XI, is extended to include the case of reflection of a partially polarized beam. It is shown that this extension leads us to consider that a *scattering matrix* $\mathbf{S}$ in terms of which Helmholtz' principle of reciprocity admits a simple mathematical formulation.

1. *Introduction.*—In Paper XI[1] of this series the general equations of transfer for an atmosphere scattering radiation in accordance with Rayleigh's law[2] and allowing for the imperfect polarization of the scattered radiation have been formulated and solved for the problem of diffuse reflection of a parallel beam of unpolarized radiation by a semi-infinite plane-parallel atmosphere. In this paper we shall extend this discussion to include the case of reflection of an incident partially polarized beam, principally with the object of clarifying and reformulating Helmholtz' principle of reciprocity[3] in terms of the symmetry properties of a certain *scattering matrix*, $\mathbf{S}$, which the theory naturally leads us to consider. Moreover, this notion of a scattering matrix is basic for the further developments contained in the paper following this one.

2. *The reduction of the equations of transfer for the problem of diffuse reflection of a parallel beam of partially plane-polarized radiation by a plane-parallel atmosphere.*—According to the ideas outlined in Paper XI, § 2, we can characterize a pencil of partially plane-polarized light by the quantities I_l, I_r, and U, where I_l and I_r are the intensities in two directions at right angles to each other in the plane of vibration of the electric vector and $U = (I_l - I_r) \tan 2\chi$, where χ denotes the inclination of the plane of polarization to the direction to which I_l refers. An incident parallel beam of partially plane-polarized light can therefore be defined in terms of the three fluxes, πF_l, πF_r, and πU_0 per unit area normal to the beam, the indices l and r now referring to directions in the meridian plane and at right angles to it.[4]

Let the beam be incident at an angle β normal to the boundary. Then, as in Paper XI, § 5, we can distinguish at any level between a field of diffuse radiation (which has arisen as a result of multiple scattering and which we shall characterize by I_l, I_r, and U) and the incident radiation reduced by the factor $e^{-\tau \sec \beta}$, where τ denotes the optical depth of the level under consideration. Similarly, we can also distinguish at any level between the contributions to the various source functions arising from the scattering of the reduced incident radiation and the diffuse radiation. The equations of transfer can then be written as in Paper XI, equations (53)–(55), $\mathfrak{I}_l^{(i)}$, $\mathfrak{I}_r^{(i)}$, and $\mathfrak{I}_U^{(i)}$ now representing the contributions to the respective source functions arising from the scattering of the re-

[1] *Ap. J.*, **104**, 110, 1946. This paper will be referred to as "Paper XI." The earlier paper (*Ap. J.*, **103**, 351, 1946) will be referred to as "Paper X."

[2] As in Paper XI, we include under "Rayleigh's law" only that part of it which pertains to the state of polarization and the angular distribution of the scattered radiation.

[3] Cf. M. Minneart, *Ap. J.*, **93**, 403, 1941.

[4] Cf. Fig. 1 in Paper X.

duced incident fluxes $\pi F_l e^{-\tau \sec\beta}$, $\pi F_r e^{-\tau \sec\beta}$, and $\pi U_0 e^{-\tau \sec\beta}$ prevailing at τ. Accordingly, in place of Paper XI, equations (56)–(58), we now have

$$\left.\begin{aligned}\mathfrak{I}_l^{(i)}(\tau, \mu, \varphi) = {}& \tfrac{3}{16}F_l e^{-\tau\sec\beta}\{2\sin^2\beta + \mu^2(3\cos^2\beta - 2) - 4\mu(1-\mu^2)^{\frac{1}{2}} \\ & \times\cos\beta\sin\beta\cos\varphi + \mu^2\cos^2\beta\cos 2\varphi\} + \tfrac{3}{16}F_r e^{-\tau\sec\beta}\mu^2(1-\cos 2\varphi) \\ & + \tfrac{3}{16}U_0\, e^{-\tau\sec\beta}\{-2\mu(1-\mu^2)^{\frac{1}{2}}\sin\beta\sin\varphi + \mu^2\cos\beta\sin 2\varphi\},\end{aligned}\right\} \quad (1)$$

$$\left.\begin{aligned}\mathfrak{I}_r^{(i)}(\tau, \mu, \varphi) = {}& \tfrac{3}{16}F_l e^{-\tau\sec\beta}\cos^2\beta(1-\cos 2\varphi) + \tfrac{3}{16}F_r e^{-\tau\sec\beta}(1+\cos 2\varphi) \\ & - \tfrac{3}{16}U_0 e^{-\tau\sec\beta}\cos\beta\sin 2\varphi,\end{aligned}\right\} \quad (2)$$

and

$$\left.\begin{aligned}\mathfrak{I}_U^{(i)}(\tau, \mu, \varphi) = {}& \tfrac{3}{8}F_l e^{-\tau\sec\beta}\{-2(1-\mu^2)^{\frac{1}{2}}\cos\beta\sin\beta\sin\varphi + \mu\cos^2\beta\sin 2\varphi\} \\ & - \tfrac{3}{8}F_r e^{-\tau\sec\beta}\mu\sin 2\varphi + \tfrac{3}{8}U_0 e^{-\tau\sec\beta}\{(1-\mu^2)^{\frac{1}{2}}\sin\beta\cos\varphi - \mu\cos\beta\cos 2\varphi\}.\end{aligned}\right\} \quad (3)$$

Combining Paper XI, equations (49)–(55), and the foregoing equations (1)–(3), we have the required equations of transfer. An examination of these equations indicates that the solutions for $I_l(\tau, \mu, \varphi)$, $I_r(\tau, \mu, \varphi)$, and $U(\tau, \mu, \varphi)$ must be expressible in the forms

$$\left.\begin{aligned}I_l(\tau, \mu, \varphi) = {}& I_l^{(0)}(\tau, \mu) + I_l^{(1)}(\tau, \mu)\cos\varphi + I_l^{(-1)}(\tau, \mu)\sin\varphi \\ & + I_l^{(2)}(\tau, \mu)\cos 2\varphi + I_l^{(-2)}(\tau, \mu)\sin 2\varphi,\end{aligned}\right\} \quad (4)$$

$$I_r(\tau, \mu, \varphi) = I_r^{(0)}(\tau, \mu) + I_r^{(2)}(\tau, \mu)\cos 2\varphi + I_r^{(-2)}(\tau, \mu)\sin 2\varphi, \quad (5)$$

and

$$\begin{aligned}U(\tau, \mu, \varphi) = {}& U^{(1)}(\tau, \mu)\sin\varphi + U^{(-1)}(\tau, \mu)\cos\varphi + U^{(2)}(\tau, \mu)\sin 2\varphi \\ & + U^{(-2)}(\tau, \mu)\sin 2\varphi.\end{aligned} \quad (6)$$

As the notation indicates, $I_l^{(0)}$, $I_l^{(1)}$, etc., are all functions of τ and μ only. Substituting these forms for the solution in the equations of transfer, we find that they break up into the following five sets of equations:

$$\left.\begin{aligned}
\mu\frac{dI_l^{(0)}}{d\tau} &= I_l^{(0)} - \frac{3}{8}\Big[\int_{-1}^{+1} I_l^{(0)}(\tau,\mu')\,[\![2(1-\mu'^2)+\mu^2(3\mu'^2-2)]\!]\,d\mu' \\
&\quad + \mu^2\int_{-1}^{+1} I_r^{(0)}(\tau,\mu')\,d\mu'\Big] - \tfrac{3}{16}F_l e^{-\tau\sec\beta}\,[2\sin^2\beta+\mu^2(3\cos^2\beta-2)] \\
&\quad - \tfrac{3}{16}F_r e^{-\tau\sec\beta}\,\mu^2, \\
\mu\frac{dI_r^{(0)}}{d\tau} &= I_r^{(0)} - \frac{3}{8}\Big[\int_{-1}^{+1} I_l^{(0)}(\tau,\mu')\,\mu'^2 d\mu' + \int_{-1}^{+1} I_r^{(0)}(\tau,\mu')\,d\mu'\Big] \\
&\quad - \tfrac{3}{16}F_l e^{-\tau\sec\beta}\cos^2\beta - \tfrac{3}{16}F_r e^{-\tau\sec\beta};
\end{aligned}\right\} \text{(I)}$$

$$\left.\begin{aligned}
\mu\frac{dI_l^{(1)}}{d\tau} &= I_l^{(1)} - \tfrac{3}{4}\mu(1-\mu^2)^{\frac{1}{2}}\int_{-1}^{+1} I_l^{(1)}(\tau,\mu')\,\mu'(1-\mu'^2)^{\frac{1}{2}}\,d\mu' - \tfrac{3}{8}\mu(1-\mu^2)^{\frac{1}{2}} \\
&\quad \times\int_{-1}^{+1} U^{(1)}(\tau,\mu')(1-\mu'^2)^{\frac{1}{2}}d\mu' + \tfrac{3}{4}F_l e^{-\tau\sec\beta}\mu(1-\mu^2)^{\frac{1}{2}}\cos\beta\sin\beta, \\
\mu\frac{dU^{(1)}}{d\tau} &= U^{(1)} - \tfrac{3}{4}(1-\mu^2)^{\frac{1}{2}}\int_{-1}^{+1} I_l^{(1)}(\tau,\mu')\,\mu'(1-\mu'^2)^{\frac{1}{2}}d\mu' - \tfrac{3}{8}(1-\mu^2)^{\frac{1}{2}} \\
&\quad \times\int_{-1}^{+1} U^{(1)}(\tau,\mu')(1-\mu'^2)^{\frac{1}{2}}d\mu' + \tfrac{3}{4}F_l e^{-\tau\sec\beta}(1-\mu^2)^{\frac{1}{2}}\cos\beta\sin\beta;
\end{aligned}\right\} \text{(II)}$$

$$\left.\begin{aligned}
\mu\frac{dI_l^{(-1)}}{d\tau} &= I_l^{(-1)} - \tfrac{3}{4}\mu(1-\mu^2)^{\frac{1}{2}}\int_{-1}^{+1} I_l^{(-1)}(\tau,\mu')\,\mu'(1-\mu'^2)^{\frac{1}{2}}\,d\mu' \\
&\quad + \tfrac{3}{8}\mu(1-\mu^2)^{\frac{1}{2}}\int_{-1}^{+1} U^{(-1)}(\tau,\mu')(1-\mu'^2)^{\frac{1}{2}}d\mu' + \tfrac{3}{8}U_0 e^{-\tau\sec\beta}\mu(1-\mu^2)^{\frac{1}{2}}\sin\beta, \\
\mu\frac{dU^{(-1)}}{d\tau} &= U^{(-1)} + \tfrac{3}{4}(1-\mu^2)^{\frac{1}{2}}\int_{-1}^{+1} I_l^{(-1)}(\tau,\mu')\,\mu'(1-\mu'^2)^{\frac{1}{2}}d\mu' \\
&\quad - \tfrac{3}{8}(1-\mu^2)^{\frac{1}{2}}\int_{-1}^{+1} U^{(-1)}(\tau,\mu')(1-\mu'^2)^{\frac{1}{2}}d\mu' - \tfrac{3}{8}U_0 e^{-\tau\sec\beta}(1-\mu^2)^{\frac{1}{2}}\sin\beta;
\end{aligned}\right\} \text{(III)}$$

$$\left.\begin{aligned}
\mu\frac{dI_l^{(2)}}{d\tau} &= I_l^{(2)} - \tfrac{3}{16}\mu^2\int_{-1}^{+1} I_l^{(2)}(\tau,\mu')\,\mu'^2 d\mu' + \tfrac{3}{16}\mu^2\int_{-1}^{+1} I_r^{(2)}(\tau,\mu')\,d\mu' \\
&\quad - \tfrac{3}{16}\mu^2\int_{-1}^{+1} U^{(2)}(\tau,\mu')\,\mu' d\mu' - \tfrac{3}{16}F_l e^{-\tau\sec\beta}\mu^2\cos^2\beta + \tfrac{3}{16}F_r e^{-\tau\sec\beta}\mu^2, \\
\mu\frac{dI_r^{(2)}}{d\tau} &= I_r^{(2)} + \tfrac{3}{16}\int_{-1}^{+1} I_l^{(2)}(\tau,\mu')\,\mu'^2 d\mu' - \tfrac{3}{16}\int_{-1}^{+1} I_r^{(2)}(\tau,\mu')\,d\mu' \\
&\quad + \tfrac{3}{16}\int_{-1}^{+1} U^{(2)}(\tau,\mu')\,\mu' d\mu' + \tfrac{3}{16}F_l e^{-\tau\sec\beta}\cos^2\beta - \tfrac{3}{16}F_r e^{-\tau\sec\beta}, \\
\mu\frac{dU^{(2)}}{d\tau} &= U^{(2)} - \tfrac{3}{8}\mu\int_{-1}^{+1} I_l^{(2)}(\tau,\mu')\,\mu'^2 d\mu' + \tfrac{3}{8}\mu\int_{-1}^{+1} I_r^{(2)}(\tau,\mu')\,d\mu' \\
&\quad - \tfrac{3}{8}\mu\int_{-1}^{+1} U^{(2)}(\tau,\mu')\,\mu' d\mu' - \tfrac{3}{8}F_l e^{-\tau\sec\beta}\mu\cos^2\beta + \tfrac{3}{8}F_r e^{-\tau\sec\beta}\mu;
\end{aligned}\right\} \text{(IV)}$$

and

$$\left.\begin{aligned}
\mu\frac{dI_l^{(-2)}}{d\tau} &= I_l^{(-2)} - \tfrac{3}{16}\mu^2\int_{-1}^{+1} I_l^{(-2)}(\tau,\mu')\,\mu'^2 d\mu' + \tfrac{3}{16}\mu^2\int_{-1}^{+1} I_r^{(-2)}(\tau,\mu')\,d\mu' \\
&\quad + \tfrac{3}{16}\mu^2\int_{-1}^{+1} U^{(-2)}(\tau,\mu')\,\mu' d\mu' - \tfrac{3}{16}U_0 e^{-\tau\sec\beta}\,\mu^2\cos\beta\,, \\
\mu\frac{dI_r^{(-2)}}{d\tau} &= I_r^{(-2)} + \tfrac{3}{16}\int_{-1}^{+1} I_l^{(-2)}(\tau,\mu')\,\mu'^2 d\mu' - \tfrac{3}{16}\int_{-1}^{+1} I_r^{(-2)}(\tau,\mu')\,d\mu' \\
&\quad - \tfrac{3}{16}\int_{-1}^{+1} U^{(-2)}(\tau,\mu')\,\mu' d\mu' + \tfrac{3}{16}U_0 e^{-\tau\sec\beta}\cos\beta\,, \\
\mu\frac{dU^{(-2)}}{d\tau} &= U^{(-2)} + \tfrac{3}{8}\mu\int_{-1}^{+1} I_l^{(-2)}(\tau,\mu')\,\mu'^2 d\mu' - \tfrac{3}{8}\mu\int_{-1}^{+1} I_r^{(-2)}(\tau,\mu')\,d\mu' \\
&\quad - \tfrac{3}{8}\mu\int_{-1}^{+1} U^{(-2)}(\tau,\mu')\,\mu' d\mu' + \tfrac{3}{8}U_0 e^{-\tau\sec\beta}\,\mu\cos\beta\,.
\end{aligned}\right\} \quad \text{(V)}$$

We now proceed to the solution of these equations appropriately for the problem of diffuse reflection by a semi-infinite plane-parallel atmosphere.

3. *The solution of the equations of transfer.*—Of the five systems to which we reduced the equations of transfer in § 2, the only one which requires any detailed consideration is the first; the others are equivalent to the systems already considered in Paper XI, §§ 7 and 8.

Considering, then, System (I), we observe that, as the inhomogeneous parts consist of two terms proportional, respectively, to F_l and F_r, we can express $I_l^{(0)}$ and $I_r^{(0)}$ as the sum of the appropriate solutions of

$$\left.\begin{aligned}
\mu\frac{dI_l^{(0)}}{d\tau} &= I_l^{(0)} - \frac{3}{8}\Big[\int_{-1}^{+1} I_l^{(0)}(\tau,\mu')\,[\![\,2(1-\mu'^2) + \mu^2(3\mu'^2-2)\,]\!]\,d\mu' \\
&\quad + \mu^2\int_{-1}^{+1} I_r^{(0)}(\tau,\mu')\,d\mu'\Big] - \tfrac{3}{16}F_l e^{-\tau\sec\beta}\,[\,2\sin^2\beta + \mu^2(3\cos^2\beta - 2)\,]\,, \\
\mu\frac{dI_r^{(0)}}{d\tau} &= I_r^{(0)} - \frac{3}{8}\Big[\int_{-1}^{+1} I_l^{(0)}(\tau,\mu')\,\mu'^2 d\mu' + \int_{-1}^{+1} I_r^{(0)}(\tau,\mu')\,d\mu'\Big] \\
&\quad - \tfrac{3}{16}F_l e^{-\tau\sec\beta}\cos^2\beta\,;
\end{aligned}\right\} \quad \text{(I}_a\text{)}$$

and

$$\left.\begin{aligned}
\mu\frac{dI_l^{(0)}}{d\tau} &= I_l^{(0)} - \frac{3}{8}\Big[\int_{-1}^{+1} I_l^{(0)}(\tau,\mu')\,[\![\,2(1-\mu'^2) + \mu^2(3\mu'^2-2)\,]\!]\,d\mu' \\
&\quad + \mu^2\int_{-1}^{+1} I_r^{(0)}(\tau,\mu')\,d\mu'\Big] - \tfrac{3}{16}F_r e^{-\tau\sec\beta}\,\mu^2\,, \\
\mu\frac{dI_r^{(0)}}{d\tau} &= I_r^{(0)} - \frac{3}{8}\Big[\int_{-1}^{+1} I_l^{(0)}(\tau,\mu')\,\mu'^2 d\mu' + \int_{-1}^{+1} I_r^{(0)}(\tau,\mu')\,d\mu'\Big] \\
&\quad - \tfrac{3}{16}F_r e^{-\tau\sec\beta}\,.
\end{aligned}\right\} \quad \text{(I}_b\text{)}$$

i) *Solution of System* (I_a).—Replacing the equations of System (I_a) by an equivalent system of $4n$ linear equations in the usual manner, we find that the equations admit particular integrals of the form

$$I_{l,i}^{(0)} = \tfrac{3}{16}F_l e^{-\tau \sec\beta}\frac{2(1-\mu_i^2)\,\Gamma}{1+\mu_i \sec\beta} \qquad (i = \pm 1, \ldots, \pm n), \quad (7)$$

and

$$I_{r,i}^{(0)} \equiv 0 \qquad (i = \pm 1, \ldots, \pm n), \quad (8)$$

where Γ has the same meaning as in Paper XI, equation (81). Combining these particular integrals for $I_{l,i}^{(0)}$ and $I_{r,i}^{(0)}$ with the corresponding solutions (Paper X, eqs. [87] and [88]) of the homogeneous equations and which are further compatible with our present requirement of the boundedness of the solution for $\tau \to \infty$, we have

$$\left.\begin{aligned} I_{l,i}^{(0)} = \tfrac{3}{16}F_l\Big[\,(1-\mu_i^2)\sum_{\beta=1}^{n-1}\frac{L_\beta e^{-\kappa_\beta \tau}}{1+\mu_i\kappa_\beta} + \sum_{a=1}^{n} M_a(1-k_a\mu)\,e^{-k_a\tau} + Q \\ + e^{-\tau\sec\beta}\,\frac{2(1-\mu_i^2)\,\Gamma}{1+\mu_i\sec\beta}\Big] \qquad (i = \pm 1, \ldots, \pm n) \end{aligned}\right\} \quad (9)$$

and

$$I_{r,i}^{(0)} = \tfrac{3}{16}F_l\Big[Q - \sum_{a=1}^{n}\frac{M_a(k_a^2-1)}{1+\mu_i k_a}e^{-k_a\tau}\Big] \quad (i = \pm 1, \ldots, \pm n), \quad (10)$$

where $L_\beta (\beta = 1, \ldots, n-1)$, $M_a (a = 1, \ldots, n)$, and Q are $2n$ constants of integration to be determined from the boundary conditions

$$I_{l,i}^{(0)} = I_{r,i}^{(0)} = 0 \qquad \text{at} \qquad \tau = 0 \qquad (i = -1, \ldots, -n). \quad (11)$$

In terms of the functions

$$\left.\begin{aligned} S_l(\mu) = (1-\mu^2)\sum_{\beta=1}^{n-1}\frac{L_\beta}{1-\mu\kappa_\beta} + \sum_{a=1}^{n} M_a(1+k_a\mu) + Q \\ + (1-\mu^2)\,\frac{2\Gamma}{1-\mu\sec\beta} \end{aligned}\right\} \quad (12)$$

and

$$S_r(\mu) = Q - \sum_{a=1}^{n}\frac{M_a(k_a^2-1)}{1-\mu k_a}, \quad (13)$$

the boundary conditions are

$$S_l(\mu_i) = S_r(\mu_i) = 0 \qquad (i = 1, \ldots, n), \quad (14)$$

while the angular distributions of the corresponding emergent intensities at $\tau = 0$ are expressible in the forms

$$I_l^{(0)}(0, \mu) = \tfrac{3}{16}F_l S_l(-\mu) \qquad \text{and} \qquad I_r^{(0)}(0, \mu) = \tfrac{3}{16}F_l S_r(-\mu). \quad (15)$$

To obtain explicit formulae for the functions $S_l(\mu)$ and $S_r(\mu)$, we proceed as in Paper XI in a similar evaluation.

We first show that the functions $S_l(\mu)$ and $S_r(\mu)$ must have the forms

$$S_l(\mu) = \frac{2\sin^2\beta}{\mu_1^2 \ldots \mu_n^2} \frac{P(-\cos\beta)}{\rho(-\cos\beta)} \frac{P(\mu)}{\rho(\mu)} \frac{\mu + a}{(\cos\beta + a)(1 - \mu\sec\beta)} \tag{16}$$

and

$$S_r(\mu) = \frac{X\cos\beta}{\mu_1^2 \ldots \mu_n^2} \frac{P(-\cos\beta)}{R(-\cos\beta)} \frac{P(\mu)}{R(\mu)}, \tag{17}$$

where a and X are certain constants to be determined and the functions R, ρ, and P have the same meanings as in Paper X, equations (129), (132), and (133). From equations (13) and (17) it now follows that

$$M_\alpha = -\frac{X\cos\beta}{\mu_1^2 \ldots \mu_n^2} \frac{P(-\cos\beta)}{R(-\cos\beta)} \frac{P(1/k_\alpha)}{R_\alpha(1/k_\alpha)(k_\alpha^2 - 1)} \qquad (\alpha = 1, \ldots, n), \tag{18}$$

where $R_\alpha(x)$ is defined as in Paper X, equation (129).

To determine the constants X and a, we make use of the relations (Paper XI, eqs. [100] and [102])

$$\sum_{\alpha=1}^{n} M_\alpha k_\alpha = \tfrac{1}{2}[S_l(+1) - S_l(-1)] \tag{19}$$

and

$$\sum_{\alpha=1}^{n} M_\alpha k_\alpha^2 = \tfrac{1}{2}[S_l(+1) + S_l(-1)] - S_r(0), \tag{20}$$

which follow from the definitions of the functions S_l and S_r.

Substituting for $S_l(+1)$, $S_l(-1)$, $S_r(0)$, and M_α according to equations (16)–(18) in equations (19) and (20), we find after some minor reductions that

$$\left.\begin{aligned} X\sum_{\alpha=1}^{n} \frac{P(1/k_\alpha)\,k_\alpha}{R_\alpha(1/k_\alpha)(k_\alpha^2 - 1)} = \frac{R(-\cos\beta)}{\rho(-\cos\beta)(a + \cos\beta)} \Bigg[& (a+1)(1+\cos\beta)\frac{P(1)}{\rho(1)} \\ & + (a-1)(1-\cos\beta)\frac{P(-1)}{\rho(-1)}\Bigg] \end{aligned}\right\} \tag{21}$$

and

$$\left.\begin{aligned} X\sum_{\alpha=1}^{n} \frac{P(1/k_\alpha)\,k_\alpha^2}{R_\alpha(1/k_\alpha)(k_\alpha^2 - 1)} - X(-1)^n \mu_1 \ldots \mu_n = \frac{R(-\cos\beta)}{\rho(-\cos\beta)(a+\cos\beta)} \\ \times\Bigg[(a+1)(1+\cos\beta)\frac{P(1)}{\rho(1)} - (a-1)(1-\cos\beta)\frac{P(-1)}{\rho(-1)}\Bigg]. \end{aligned}\right\} \tag{22}$$

The summations which occur on the left-hand side of these equations have been evaluated in Paper X. We have (cf. Paper X, eqs. [149], [162], and [163])

$$\sum_{\alpha=1}^{n} \frac{P(1/k_\alpha)\,k_\alpha}{R_\alpha(1/k_\alpha)(k_\alpha^2 - 1)} = -\frac{1}{2}\left[\frac{P(1)}{R(1)} - \frac{P(-1)}{R(-1)}\right] \tag{23}$$

and

$$\sum_{\alpha=1}^{n} \frac{P(1/k_\alpha)\,k_\alpha^2}{R_\alpha(1/k_\alpha)(k_\alpha^2 - 1)} = -\frac{1}{2}\left[\frac{P(1)}{R(1)} + \frac{P(-1)}{R(-1)}\right] + (-1)^n \mu_1 \ldots \mu_n. \tag{24}$$

Using these results in equations (21) and (22), we obtain, after some further reductions,

$$\frac{X}{R(1)R(-\cos\beta)} = -\frac{2}{\rho(1)\,\rho(-\cos\beta)}\,\frac{(a+1)(1+\cos\beta)}{a+\cos\beta} \tag{25}$$

and

$$\frac{X}{R(-1)R(-\cos\beta)} = +\frac{2}{\rho(-1)\,\rho(-\cos\beta)}\,\frac{(a-1)(1-\cos\beta)}{a+\cos\beta}. \tag{26}$$

Solving these equations for X and a, we find that

$$X = q\,\frac{R(-\cos\beta)}{\rho(-\cos\beta)} \tag{27}$$

and

$$\frac{a+\mu}{a+\cos\beta}\sin^2\beta = 1-\mu\cos\beta - c\,(\cos\beta-\mu)\,, \tag{28}$$

where q and c are two constants having the same values as in Paper XI, equations (130) and (134).

Combining equations (16), (17), (27), and (28), we finally have

$$S_l(\mu) = \frac{2}{\mu_1^2\ldots\mu_n^2}\,\frac{P(-\cos\beta)}{\rho(-\cos\beta)}\,\frac{P(\mu)}{\rho(\mu)}\,\frac{1-\mu\cos\beta-c\,(\cos\beta-\mu)}{1-\mu\sec\beta} \tag{29}$$

and

$$S_r(\mu) = \frac{q\cos\beta}{\mu_1^2\ldots\mu_n^2}\,\frac{P(-\cos\beta)}{\rho(-\cos\beta)}\,\frac{P(\mu)}{R(\mu)}\,. \tag{30}$$

The corresponding laws of the emergent distributions are

$$I_l^{(0)}(0,\mu) = \tfrac{3}{16}F_l\{2H_l(\mu)\,H_l(\mu')\,[1+\mu\mu'-c\,(\mu+\mu')]\}\,\frac{\mu'}{\mu+\mu'} \tag{31}$$

and

$$I_r^{(0)}(0,\mu) = \tfrac{3}{16}F_l q H_r(\mu)\,H_l(\mu')\,\mu'\,, \tag{32}$$

where the functions $H_l(\mu)$ and $H_r(\mu)$ are defined as in Paper XI, equations (141) and (142). Further, in equations (31) and (32) we have written $\mu' = \cos\beta$.

ii) *Solution of System* (I_b).—The discussion of this system proceeds quite analogously. Thus we find that, for this system also, the boundary conditions and the angular distribution of the emergent radiation can be expressed in terms of the positive zeros of certain functions and their values for the negative arguments, respectively. The functions we have to consider in this case are (cf. Paper XI, eqs. [87] and [88])

$$\left.\begin{aligned} S_l(\mu) = (1-\mu^2)\sum_{\beta=1}^{n-1}\frac{L_\beta}{1-\mu\kappa_\beta} + \sum_{a=1}^{n}M_a\,(1+k_a\mu) + Q \\ - C\,(1+\mu\sec\beta)\cos^2\beta \end{aligned}\right\} \tag{33}$$

and

$$S_r(\mu) = Q - \sum_{a=1}^{n}\frac{M_a\,(k_a^2-1)}{1-\mu k_a} + \frac{C\sin^2\beta}{1-\mu\sec\beta}, \tag{34}$$

where C has the same meaning as in Paper XI, equation (80).

To obtain explicit formulae for the functions $S_l(\mu)$ and $S_r(\mu)$ defined as in equations (33) and (34), we first observe that they must have the forms

$$S_l(\mu) = \frac{2Y}{\mu_1^2 \ldots . \mu_n^2} \frac{P(-\cos\beta)}{\rho(-\cos\beta)} \frac{P(\mu)}{\rho(\mu)} \cos\beta \tag{35}$$

and

$$S_r(\mu) = \frac{\sin^2\beta}{\mu_1^2 \ldots . \mu_n^2} \frac{P(-\cos\beta)}{R(-\cos\beta)} \frac{P(\mu)}{R(\mu)} \frac{\mu + b}{(\cos\beta + b)(1 - \mu \sec\beta)}, \tag{36}$$

where Y and b are certain constants to be determined. The reductions now required to determine these constants are very similar to those used in Paper XI, pp. 122–27. Following this procedure, we find that the equations which determine Y and b can be brought to the forms (cf. eqs. [25] and [26])

$$\frac{2Y}{\rho(1)\,\rho(-\cos\beta)} = -\frac{1}{R(1)R(-\cos\beta)} \frac{(b+1)(1+\cos\beta)}{b+\cos\beta} \tag{37}$$

and

$$\frac{2Y}{\rho(-1)\,\rho(-\cos\beta)} = +\frac{1}{R(-1)R(-\cos\beta)} \frac{(b-1)(1-\cos\beta)}{b+\cos\beta}. \tag{38}$$

Solving these equations, we find that

$$Y = \tfrac{1}{2} q \frac{\rho(-\cos\beta)}{R(-\cos\beta)} \tag{39}$$

and

$$\frac{b+\mu}{b+\cos\beta} \sin^2\beta = 1 - \mu\cos\beta + c(\cos\beta - \mu). \tag{40}$$

Substituting these equations in our expressions for $S_l(\mu)$ and $S_r(\mu)$, we have

$$S_l(\mu) = \frac{q\cos\beta}{\mu_1^2 \ldots . \mu_n^2} \frac{P(-\cos\beta)}{R(-\cos\beta)} \frac{P(\mu)}{\rho(\mu)} \tag{41}$$

and

$$S_r(\mu) = \frac{1}{\mu_1^2 \ldots . \mu_n^2} \frac{P(-\cos\beta)}{R(-\cos\beta)} \frac{P(\mu)}{R(\mu)} \frac{1 - \mu\cos\beta + c(\cos\beta - \mu)}{1 - \mu\sec\beta}. \tag{42}$$

The angular distributions of the emergent radiation now take the forms

$$I_l^{(0)}(0, \mu) = \tfrac{3}{16} F_r q H_l(\mu) H_r(\mu') \mu' \tag{43}$$

and

$$I_r^{(0)}(0, \mu) = \tfrac{3}{16} F_r \{H_r(\mu) H_r(\mu')[1 + \mu\mu' + c(\mu + \mu')]\} \frac{\mu'}{\mu + \mu'}. \tag{44}$$

This completes our discussion of Systems (I_a) and (I_b).

Combining solutions (31), (32), (43), and (44) of Systems (I_a) and (I_b), we obtain the required solution of System (I). We have,

$$\left.\begin{aligned} I_l^{(0)}(0, \mu) = \tfrac{3}{16}\{2H_l(\mu) H_l(\mu')[1 + \mu\mu' - c(\mu + \mu')] F_l \\ + q H_l(\mu) H_r(\mu')(\mu + \mu') F_r\} \frac{\mu'}{\mu + \mu'} \end{aligned}\right\} \tag{45}$$

and

$$I_r^{(0)}(0,\mu) = \tfrac{3}{16}\{qH_r(\mu)\,H_l(\mu')(\mu+\mu')F_l + H_r(\mu)\,H_r(\mu')[1+\mu\mu'+c(\mu+\mu')F_r]\}\frac{\mu'}{\mu+\mu'}. \tag{46}$$

Turning our attention, next, to the remaining Systems (II)–(V), we observe that they are essentially equivalent to the systems considered in Paper XI, §§ 7 and 8; and the solutions for the angular distribution of the emergent intensities can be written down after a simple inspection. We have

$$I_l^{(1)}(0,\mu) = \mu U^{(1)}(0,\mu) = -\tfrac{3}{4}F_l\mu\mu'(1-\mu^2)^{\frac{1}{2}}(1-\mu'^2)^{\frac{1}{2}}H^{(1)}(\mu)\,H^{(1)}(\mu')\frac{\mu'}{\mu+\mu'}; \tag{47}$$

$$I_l^{(-1)}(0,\mu) = -\mu U^{(-1)}(0,\mu) = -\tfrac{3}{8}U_0\mu(1-\mu^2)^{\frac{1}{2}}(1-\mu'^2)^{\frac{1}{2}}H^{(1)}(\mu)\,H^{(1)}(\mu')\frac{\mu'}{\mu+\mu'}; \tag{48}$$

$$I_l^{(2)}(0,\mu) = -\mu^2 I_r^{(2)}(0,\mu) = \tfrac{1}{2}\mu U^{(2)}(0,\mu) = \tfrac{3}{16}(F_l\mu'^2 - F_r)\,\mu^2 H^{(2)}(\mu)\,H^{(2)}(\mu')\frac{\mu'}{\mu+\mu'}; \tag{49}$$

and

$$I_l^{(-2)}(0,\mu) = -\mu^2 I_r^{(-2)}(0,\mu) = -\tfrac{1}{2}\mu U^{(-2)}(0,\mu) = \tfrac{3}{16}U_0\mu^2\mu' H^{(2)}(\mu)\,H^{(2)}(\mu')\frac{\mu'}{\mu+\mu'}. \tag{50}$$

In the foregoing equations the functions $H^{(1)}(\mu)$ and $H^{(2)}(\mu)$ are defined in the same way as in Paper XI, equations (149) and (157).

Finally, combining solutions (45)–(50) in accordance with equations (4)–(6), we obtain the complete set of equations which determine the polarization and the angular distribution of the radiation diffusely reflected by a semi-infinite plane-parallel atmosphere. We have

$$\begin{aligned} I_l(0,\mu,\varphi) = \tfrac{3}{16}[&F_l\{2H_l(\mu)\,H_l(\mu')[\![1+\mu\mu'-c(\mu+\mu')]\!] - 4\mu\mu' \\ &\times(1-\mu^2)^{\frac{1}{2}}(1-\mu'^2)^{\frac{1}{2}}H^{(1)}(\mu)\,H^{(1)}(\mu')\cos\varphi + \mu^2\mu'^2H^{(2)}(\mu)\,H^{(2)}(\mu')\cos 2\varphi\} \\ &+F_r\{qH_l(\mu)\,H_r(\mu')(\mu+\mu') - \mu^2H^{(2)}(\mu)\,H^{(2)}(\mu')\cos 2\varphi\} \\ &+U_0\{-2\mu(1-\mu^2)^{\frac{1}{2}}(1-\mu'^2)^{\frac{1}{2}}H^{(1)}(\mu)\,H^{(1)}(\mu')\sin\varphi \\ &+\mu^2\mu'H^{(2)}(\mu)\,H^{(2)}(\mu')\sin 2\varphi\}]\frac{\mu'}{\mu+\mu'}; \end{aligned} \tag{51}$$

$$\begin{aligned} I_r(0,\mu,\varphi) = \tfrac{3}{16}[&F_l\{qH_r(\mu)\,H_l(\mu')(\mu+\mu') - \mu'^2H^{(2)}(\mu)\,H^{(2)}(\mu')\cos 2\varphi\} \\ &+F_r\{H_r(\mu)\,H_r(\mu')[\![1+\mu\mu'+c(\mu+\mu')]\!] + H^{(2)}(\mu)\,H^{(2)}(\mu')\cos 2\varphi\} \\ &-U_0\mu'H^{(2)}(\mu)\,H^{(2)}(\mu')\sin 2\varphi]\frac{\mu'}{\mu+\mu'}; \end{aligned} \tag{52}$$

and

$$\left.\begin{aligned} U(0,\mu,\varphi) &= \tfrac{3}{8}\,[F_l\{-2\mu'(1-\mu'^2)^{\frac{1}{2}}(1-\mu^2)^{\frac{1}{2}}H^{(1)}(\mu)\,H^{(1)}(\mu')\sin\varphi+\mu\mu'^2 \\ &\times H^{(2)}(\mu)\,H^{(2)}(\mu')\sin 2\varphi\}-F_r\mu H^{(2)}(\mu)\,H^{(2)}(\mu')\sin 2\varphi+U_0\{(1-\mu^2)^{\frac{1}{2}} \\ &\times(1-\mu'^2)^{\frac{1}{2}}H^{(1)}(\mu)\,H^{(1)}(\mu')\cos\varphi-\mu\mu' H^{(2)}(\mu)\,H^{(2)}(\mu')\cos 2\varphi\}]\,\frac{\mu'}{\mu+\mu'}\,. \end{aligned}\right\} \quad (53)$$

For the case of an incident beam of unpolarized light,

$$F_l = F_r = \tfrac{1}{2}F, \qquad \text{and} \qquad U_0 = 0\,, \tag{54}$$

and the solutions reduce to the ones given in Paper XI, § 9.

4. *The principle of reciprocity; the scattering matrix.*—The solution for the problem of diffuse reflection given in the preceding section allows us to verify Helmholtz' principle of reciprocity when polarization accompanying scattering is taken into account. Stated for our problem in its conventional form, the principle asserts that the intensity diffusely reflected in a direction (μ, φ) and in a direction in the plane of vibration of the electric vector, which is inclined at an angle ψ with the meridian plane from a parallel beam incident in the direction $(-\mu', \varphi')$ and which is plane-polarized in a direction inclined at an angle χ with the meridian plane, must be expressible in the form

$$I(0;\psi,\mu,\varphi;\chi,\mu',\varphi') = \mu' H(\psi,\mu;\chi,\mu';\varphi-\varphi')\,, \tag{55}$$

where H is a symmetrical function in the variable pair (ψ, μ) and (χ, μ'). To verify this, we first observe that, for an incident plane-polarized beam in which the plane of polarization is inclined at an angle χ with the meridian plane,

$$F_l = F\cos^2\chi; \qquad F_r = F\sin^2\chi; \qquad \text{and} \qquad U_0 = F\sin 2\chi\,, \tag{56}$$

where πF denotes the total net flux in the beam per unit area normal to itself. Further, to obtain the intensity scattered in a direction (μ, φ) and inclined at an angle ψ with the meridian plane, we must combine the solutions given in § 3 according to (cf. Paper XI, eq. [7])

$$I(0;\psi,\mu,\varphi) = I_l(0,\mu,\varphi)\cos^2\psi + I_r(0,\mu,\varphi)\sin^2\psi + \tfrac{1}{2}U(0,\mu,\varphi)\sin 2\psi\,. \tag{57}$$

In this manner we obtain

$$\left.\begin{aligned} I(0;\psi,\mu,\varphi;\chi,\mu',\varphi') &= \tfrac{3}{16}F\,[H_l(\mu;\mu')\cos^2\chi\cos^2\psi + H_r(\mu;\mu')\sin^2\chi\sin^2\psi \\ &+ q(\mu+\mu')\{H_l(\mu)\,H_r(\mu')\cos^2\psi\sin^2\chi + H_r(\mu)\,H_l(\mu')\cos^2\chi\sin^2\psi\} \\ &+ H^{(1)}(\mu)H^{(1)}(\mu')(1-\mu^2)^{\frac{1}{2}}(1-\mu'^2)^{\frac{1}{2}}\{(-4\mu\mu'\cos^2\chi\cos^2\psi+\sin 2\psi\sin 2\chi) \\ &\times\cos(\varphi-\varphi') - 2(\mu\cos^2\psi\sin 2\chi+\mu'\cos^2\chi\sin 2\psi)\sin(\varphi-\varphi')\} \\ &+ H^{(2)}(\mu)\,H^{(2)}(\mu')\{(\mu^2\mu'^2\cos^2\chi\cos^2\psi+\sin^2\chi\sin^2\psi-\mu^2\sin^2\chi\cos^2\psi \\ &- \mu'^2\cos^2\chi\sin^2\psi-\mu\mu'\sin 2\chi\sin 2\psi)\cos 2(\varphi-\varphi') + (\mu^2\mu'\cos^2\psi\sin 2\chi \\ &+ \mu\mu'^2\cos^2\chi\sin 2\psi-\mu'\sin^2\psi\sin 2\chi-\mu\sin^2\chi\sin 2\psi)\sin 2(\varphi-\varphi')\}] \\ &\times\frac{\mu'}{\mu+\mu'} \end{aligned}\right\} \quad (58)$$

where we have written

$$H_l(\mu;\mu') = 2H_l(\mu)\,H_l(\mu')\,[1+\mu\mu'-c\,(\mu+\mu')] \tag{59}$$

and

$$H_r(\mu;\mu') = H_r(\mu)\,H_r(\mu')\,[1+\mu\mu'+c\,(\mu+\mu')]\,. \tag{60}$$

It is seen that this expression has indeed the symmetry property required by the reciprocity principle. It may be further pointed out in this connection that the *total* reflected intensity,

$$I(0,\mu,\varphi) = I_l(0,\mu,\varphi) + I_r(0,\mu,\varphi)\,, \tag{61}$$

has also the symmetry required by the reciprocity principle only for the case of an incident unpolarized beam. In no other case can the principle be applied for total intensities.

The demonstration of the reciprocity principle that we have just given makes it apparent that a precise mathematical formulation of the principle as generally stated will be involved and will lack simplicity. However, we shall show that there is an alternative formulation of the principle which has a simple mathematical expression. For this purpose it is convenient to replace the subscripts l, r, and U by the indices 1, 2, and 3 and let

$$I_l = I_1\,; \qquad I_r = I_2\,; \qquad \text{and} \qquad U = I_3\,. \tag{62}$$

An incident partially polarized beam will then be characterized by the fluxes $\pi F_k (k = 1, 2, 3)$, and the solutions for the emergent intensities given in § 3 can be abbreviated in the form

$$I_i(0,\mu,\varphi) = \frac{3}{16\mu}\,q_i \sum_{k=1}^{3} S_{ik}(\mu,\varphi;\mu',\varphi')\,F_k\,, \tag{63}$$

where

$$q_1 = q_2 = 1 \qquad \text{and} \qquad q_3 = 2\,, \tag{64}$$

and S_{ik} are certain coefficients which we can directly read from equations (51)–(53). Moreover, these coefficients may be regarded as the elements of matrix $\mathbf{S}$:

$$\left(\frac{1}{\mu}+\frac{1}{\mu'}\right)\boldsymbol{S}(\mu,\varphi;\mu',\varphi')=$$

$$\left|\begin{array}{lll}
2H_l(\mu)H_l(\mu')[1+\mu\mu'-c(\mu+\mu')] & qH_l(\mu)H_r(\mu')(\mu+\mu') & \\
-4\mu\mu'(1-\mu^2)^{\frac{1}{2}}(1-\mu'^2)^{\frac{1}{2}}H^{(1)}(\mu)H^{(1)}(\mu') & & -2\mu(1-\mu^2)^{\frac{1}{2}}(1-\mu'^2)^{\frac{1}{2}}H^{(1)}(\mu)H^{(1)}(\mu') \\
\quad\times\cos(\varphi-\varphi') & & \quad\times\sin(\varphi-\varphi') \\
+\mu^2\mu'^2H^{(2)}(\mu)H^{(2)}(\mu')\cos 2(\varphi-\varphi') & -\mu^2H^{(2)}(\mu)H^{(2)}(\mu') & +\mu^2\mu'H^{(2)}(\mu)H^{(2)}(\mu')\sin 2(\varphi-\varphi') \\
 & \quad\times\cos 2(\varphi-\varphi') & \\
qH_r(\mu)H_l(\mu')(\mu+\mu') & H_r(\mu)H_r(\mu')[1+\mu\mu' & \\
 & \quad+c(\mu+\mu')] & \\
-\mu'^2H^{(2)}(\mu)H^{(2)}(\mu')\cos 2(\varphi-\varphi') & +H^{(2)}(\mu)H^{(2)}(\mu') & -\mu'H^{(2)}(\mu)H^{(2)}(\mu')\sin 2(\varphi-\varphi') \\
 & \quad\times\cos 2(\varphi-\varphi') & \\
-2\mu'(1-\mu'^2)^{\frac{1}{2}}(1-\mu^2)^{\frac{1}{2}}H^{(1)}(\mu)H^{(1)}(\mu') & & (1-\mu^2)^{\frac{1}{2}}(1-\mu'^2)^{\frac{1}{2}}H^{(1)}(\mu)H^{(1)}(\mu') \\
\quad\times\sin(\varphi-\varphi') & & \quad\times\cos(\varphi-\varphi') \\
+\mu\mu'^2H^{(2)}(\mu)H^{(2)}(\mu')\sin 2(\varphi-\varphi') & -\mu H^{(2)}(\mu)H^{(2)}(\mu') & -\mu\mu'H^{(2)}(\mu)H^{(2)}(\mu')\cos 2(\varphi-\varphi') \\
 & \quad\times\sin 2(\varphi-\varphi') &
\end{array}\right| \tag{65}$$

We shall call this the *scattering matrix;* for in terms of it the angular distribution and the state of polarization of the reflected radiation can always be specified.

We now see that among the elements of the matrix $\boldsymbol{S}$ we have the relations

$$S_{ik}(\mu, \varphi; \mu', \varphi') = S_{ki}(\mu', \varphi; \mu, \varphi') . \tag{66}$$

In other words, if $\tilde{\boldsymbol{S}}$ denotes the transposed matrix of $\boldsymbol{S}$, then

$$\tilde{\boldsymbol{S}}(\mu, \varphi; \mu', \varphi') = \boldsymbol{S}(\mu', \varphi; \mu, \varphi') . \tag{67}$$

It is on account of this symmetry property of $\boldsymbol{S}$ that the reciprocity principle arises. Conversely, we may regard this symmetry of the matrix $\boldsymbol{S}$ as the expression of the reciprocity principle.

In conclusion I wish to record that this investigation was stimulated by a series of lectures which Dr. M. Minneart gave at the Yerkes Observatory during the summer of 1946.

ON THE RADIATIVE EQUILIBRIUM OF A STELLAR ATMOSPHERE. XIV

S. CHANDRASEKHAR
Yerkes Observatory
Received October 28, 1946

ABSTRACT

The main object of this paper is to show how, by incorporating into the methods developed in the earlier papers of this series a basic idea of Ambarzumian, we are able to solve exactly a large class of problems in the theory of radiative transfer. More specifically, we show that, when the solutions for the emergent (or the reflected) radiation (obtained in the nth approximation of the earlier papers) involve H-functions of the form

$$H(\mu) = \frac{1}{\mu_1 \ldots \mu_n} \frac{\prod_i (\mu + \mu_i)}{\prod_a (1 + k_a \mu)}, \tag{i}$$

where the μ_i's are the positive zeros of the Legendre polynomial $P_{2n}(\mu)$ and the k_a's are the roots of a characteristic equation

$$1 = 2 \sum_{j=1}^{n} \frac{a_j \Psi(\mu_j)}{1 - k^2 \mu_j^2} \qquad (\Psi \text{ an even polynomial in } \mu \text{ and } \int_0^1 \Psi(\mu) d\mu \leqslant \tfrac{1}{2}), \tag{ii}$$

then, in the limit of infinite approximation, the H-functions become solutions of functional equations of a certain standard form, namely,

$$H(\mu) = 1 + \mu H(\mu) \int_0^1 \frac{H(\mu')\Psi(\mu')}{\mu + \mu'} d\mu' . \tag{iii}$$

Further, when the solution involves, in addition to the H-functions, certain constants, then in the exact solution these constants are related in a determinate way with the moments of the H-functions themselves.

The paper is divided into five main sections. In Section I we derive (following Ambarzumian's general ideas) the functional equations for the problem of diffuse reflection when allowance is also made for the polarization of the scattered radiation in accordance with Rayleigh's law. This problem requires us to find a functional equation for the scattering matrix $\boldsymbol{S}$ introduced in Paper XIII. In Section II the functional equation for $\boldsymbol{S}$ is solved and the solution expressed in terms of four functional equations, all of type (iii). The exact solutions for the laws of darkening in the two states of polarization for an electron-scattering atmosphere are also given in this section. Section III is devoted to a general study of functional equations of the form (iii). The basic theorem relating the H-function as defined in terms of the Gaussian division and the characteristic roots and as defined as the solution of the associated functional equation is proved in this section. In Section IV the problem of diffuse reflection in accordance with the phase function $\lambda(1 + x \cos \Theta)$ is treated. And, finally, in Section V we give the exact solutions for transfer problems involving Rayleigh's phase function.

1. *Introduction.*—The problem of diffuse reflection by a semi-infinite plane-parallel atmosphere has been considered under a variety of circumstances in earlier papers of this series.[1] And it has been shown for many of the problems considered that the angular distribution (and in some cases, also, the state of polarization) of the reflected radiation can be given in closed forms in a general nth approximation. The essential feature of

[1] *Ap. J.*, **101**, 348, 1945; **103**, 165, 1946; **104**, 110, 191, 1946; and **105**, 151, 1947. These papers will be referred to as Papers VIII, IX, XI, XII, and XIII, respectively. Other papers of this series to which we shall have occasion to refer are Papers II (*Ap. J.*, **100**, 76, 1944), III (*ibid.*, **100**, 117, 1944), and X (*ibid.*, **103**, 351, 1946).

these solutions is that, in addition to certain constants, they involve only certain "H-functions" of the form

$$H(\mu) = \frac{1}{\mu_1 \cdot \cdots \cdot \mu_n} \frac{\prod_i (\mu + \mu_i)}{\prod_a (1 + k_a \mu)}, \tag{1}$$

where the μ_i's are the positive zeros of the Legendre polynomial $P_{2n}(\mu)$ and the k_a's are the positive roots of a characteristic equation of the form

$$1 = 2 \sum_{j=1}^{n} \frac{a_j \Psi(\mu_j)}{1 - k^2 \mu_j^2}, \tag{2}$$

where the a_j's are the Gaussian weights and $\Psi(\mu)$ is an even polynomial in μ, satisfying the condition[2]

$$\int_0^1 \Psi(\mu)\, d\mu \leqslant \tfrac{1}{2}. \tag{3}$$

Now the solutions we have found for the various problems of diffuse reflection were obtained by directly solving the appropriate equations of transfer, in contrast to a method recently devised by V. A. Ambarzumian[3] in which an explicit solution of the transfer problem is avoided by deriving functional equations for the reflection functions $\sigma(\mu, \varphi; \mu_0, \varphi_0)$, which give the intensity reflected in a given direction (μ, φ) when a parallel beam of unit flux per unit area normal to itself is incident in the direction $(-\mu_0, \varphi_0)$. These functional equations of Ambarzumian are of rather complicated forms, even in cases in which our method gives closed solutions of relatively simple forms.[4] This is somewhat surprising, and a close examination of the correspondence between the two methods undertaken in this paper reveals that a knowledge of the *forms* of the solutions obtained by our method enables us, in most cases, to reduce Ambarzumian's type of functional equations to the following standard form:

$$H(\mu) = 1 + \mu H(\mu) \int_0^1 \frac{H(\mu')\Psi(\mu')}{\mu + \mu'}\, d\mu'. \tag{4}$$

Indeed, we shall show that in a certain nth approximation the solution of the functional equation (4) is, in fact, our H-function. More precisely, it will appear that $H(\mu)$, as we have defined it in equations (1) and (2), is an exact solution of the associated *difference equation*

$$H(\mu) = 1 + \mu H(\mu) \sum_{j=1}^{n} \frac{a_j H(\mu_j)\Psi(\mu_j)}{\mu + \mu_j}. \tag{5}$$

It would therefore appear that, with the solutions in the forms we have given them, we can pass directly to the limit of infinite approximation by letting the H-functions become solutions of functional equations of the form (4) rather than of the associated difference equations. And as for the constants which appear in our solutions, they can be shown to be related in some way with the moments of the H-functions themselves. The conclusions we have just stated are of practical importance as well; for, on the basis of

[2] This condition is necessary for $H(\mu)$ to be real (see theorem 3, corollary 1, § 12).

[3] *J. Phys. Acad. Sci. U.S.S.R.*, **8**, 64, 1944.

[4] Thus compare his pair of functional equations on p. 72, eq. (30) (*op. cit.*), with our solution (108) in Paper IX. Both refer to the same physical problem.

tests that we have made, it appears that, starting with a solution for $H(\mu)$ in the third approximation, we can derive by a rapid method of iteration the exact function numerically. Thus, by incorporating Ambarzumian's basic idea in the methods developed in this series of papers, we are able to solve a very large class of transfer problems *exactly*.

The plan of this paper is as follows:

In Section I we derive, following Ambarzumian's general ideas, the functional equations for the problem of diffuse reflection when allowance is also made for the polarization of the scattered radiation in accordance with Rayleigh's law. As we shall see, this problem requires us to find a functional equation for the scattering matrix $\boldsymbol{S}$, which we introduced in the preceding paper. The problem is, accordingly, more advanced than the ones considered by Ambarzumian; but it serves to illustrate the power of his fundamental idea. In Section II we show that the solution of the functional equations (which, for the most important set of functions, is a simultaneous system of order 4) derived in Section I can all be expressed in terms of four independent functional equations of the standard type (4) and a constant, which is expressible in terms of the moments of two of these functions. Section III is devoted to a general study of functional equations of the form (4). In particular, we prove in this section the basic theorem relating the H-function as defined by equations (1) and (2) and the solution of the functional equation (4). The analysis of these sections throws some interesting sidelights on integrals of the type of Hopf-Bronstein. Several other theorems relating to this type of functional equation are also proved. In Section IV we treat a problem considered by Ambarzumian and show how the solution of a pair of simultaneous functional equations which he had derived can also be reduced to a single functional equation of the form (4). Finally, in Section V we solve the functional equations for the problem of diffuse reflection with Rayleigh's phase function (without allowing for polarization).

I. FUNCTIONAL EQUATION FOR THE SCATTERING MATRIX DESCRIBING THE DIFFUSE REFLECTION FROM A SEMI-INFINITE ATMOSPHERE, SCATTERING RADIATION ACCORDING TO RAYLEIGH'S LAW

2. *The vector form of the equations of transfer.*—For the purpose of deriving the functional equations for the problem of diffuse reflection according to Rayleigh's law and allowing for the polarization of the scattered radiation, we must first re-write the equations of transfer given in Papers XI and XIII in more suitable forms. First, it is convenient to introduce subscripts 1, 2, and 3 instead of the letters l, r, and U and to let

$$I_l = I_1\,, \qquad I_r = I_2\,, \qquad \text{and} \qquad U = I_3\,. \tag{6}$$

Now suppose that a parallel beam of partially polarized light, characterized by the fluxes

$$\pi F_k \qquad (k = 1,\ 2,\ 3)\,, \tag{7}$$

is incident on the atmosphere in the direction $(-\mu_0,\ \varphi_0)$. The equation of transfer for I_i can be written in the form

$$\mu \frac{dI_i}{d\tau} = I_i - B_i(\tau,\ \mu,\ \varphi) \qquad (i = 1,\ 2,\ 3)\,, \tag{8}$$

where the source-function, B_i, can be regarded as the sum of two source-functions, one arising from the scattering of the diffuse radiation at τ and the other arising from the scattering of the reduced incident radiation, $\pi F_k e^{-\tau/\mu_0}$, prevailing at τ. According to Paper XIII, equations (1)–(3), we can write

$$B_i(\tau,\ \mu,\ \varphi) = \mathfrak{J}_i(\tau,\ \mu,\ \varphi) + \tfrac{3}{16} q_i \sum_{k=1}^{3} j_{ik}(\mu,\ \varphi;\ \mu_0,\ \varphi_0)\, F_k e^{-\tau/\mu_0} \qquad (i = 1,\ 2,\ 3)\,, \tag{9}$$

where $\mathfrak{J}_i(\tau, \mu, \varphi)$ denotes the contribution to the source-function arising from the diffuse radiation field at τ and $j_{ik}(\mu, \varphi; \mu_0, \varphi_0)$ are certain coefficients which can be regarded as the elements of the matrix

$$J(\mu, \varphi; \mu_0, \varphi_0) = \left| \begin{array}{cccc} 2(1-\mu^2)(1-\mu_0^2) + \mu^2\mu_0^2 & & & -2\mu(1-\mu^2)^{\frac{1}{2}}(1-\mu_0^2)^{\frac{1}{2}} \sin(\varphi-\varphi_0) \\ -4\mu\mu_0(1-\mu^2)^{\frac{1}{2}}(1-\mu_0^2)^{\frac{1}{2}} \cos(\varphi-\varphi_0) & & & +\mu^2\mu_0 \sin 2(\varphi-\varphi_0) \\ +\mu^2\mu_0^2 \cos 2(\varphi-\varphi_0) & \mu^2-\mu^2 \cos 2(\varphi-\varphi_0) & & \\ \mu_0^2-\mu_0^2 \cos 2(\varphi-\varphi_0) & 1+\cos 2(\varphi-\varphi_0) & & -\mu_0 \sin 2(\varphi-\varphi_0) \\ -2\mu_0(1-\mu_0^2)^{\frac{1}{2}}(1-\mu^2)^{\frac{1}{2}} \sin(\varphi-\varphi_0) & & & (1-\mu^2)^{\frac{1}{2}}(1-\mu_0^2)^{\frac{1}{2}} \cos(\varphi-\varphi_0) \\ +\mu\mu_0^2 \sin 2(\varphi-\varphi_0) & & -\mu \sin 2(\varphi-\varphi_0) & -\mu\mu_0 \cos 2(\varphi-\varphi_0) \end{array} \right| \tag{10}$$

Further, in equation (9)

$$q_1 = q_2 = 1\ , \qquad \text{and} \qquad q_3 = 2\ . \tag{11}$$

It will be observed that the matrix $\boldsymbol{J}$ (which is appropriate for *single scattering*) has the same symmetry that we have noted for the scattering matrix $\boldsymbol{S}$ in Paper XIII (eq. [67]). Thus,

$$\tilde{\boldsymbol{J}}(\mu, \varphi; \mu_0, \varphi_0) = \boldsymbol{J}(\mu_0, \varphi; \mu, \varphi_0)\ . \tag{12}$$

Returning to the source-functions $\mathfrak{J}_i(\tau, \mu, \varphi)$, we verify that the expressions given for these functions in Paper XI (eqs. [49]–[52]) can be abbreviated in the form

$$\left.\begin{aligned}\mathfrak{J}_i(\tau, \mu, \varphi) = \frac{3}{16\pi}\, q_i \int_{-1}^{+1}\int_0^{2\pi} \sum_{k=1}^{3} j_{ik}(\mu, \varphi; -\mu', \varphi')\, I_k(\tau, \mu', \varphi')\, d\mu' d\varphi' \\ (i = 1, 2, 3)\ .\end{aligned}\right\} \tag{13}$$

Combining equations (8), (9), and (13), we have

$$\left.\begin{aligned}\mu \frac{dI_i}{d\tau} = I_i - \frac{3}{16\pi}\, q_i \int_{-1}^{+1}\int_0^{2\pi} \sum_{k=1}^{3} j_{ik}(\mu, \varphi; -\mu', \varphi')\, I_k(\tau, \mu', \varphi')\, d\mu' d\varphi' \\ - \tfrac{3}{16} q_i \sum_{k=1}^{3} j_{ik}(\mu, \varphi; \mu_0, \varphi_0)\, F_k e^{-\tau/\mu_0} \qquad (i = 1, 2, 3)\ .\end{aligned}\right\} \tag{14}$$

If we now regard the intensities $I_i (i = 1, 2, 3)$ as the components of a vector $\boldsymbol{I}$, we can re-write the three equations of transfer which equation (14) represents as a single vector equation of the form

$$\left.\begin{aligned}\mu \frac{d\boldsymbol{I}}{d\tau} = \boldsymbol{I} - \frac{3}{16\pi}\boldsymbol{Q} \int_{-1}^{+1}\int_0^{2\pi} \boldsymbol{J}(\mu, \varphi; -\mu', \varphi')\, \boldsymbol{I}(\tau, \mu', \varphi')\, d\mu' d\varphi' \\ - \tfrac{3}{16}\boldsymbol{Q}\boldsymbol{J}(\mu, \varphi; \mu_0, \varphi_0)\, \boldsymbol{F} e^{-\tau/\mu_0}\ ,\end{aligned}\right\} \tag{15}$$

where

$$\boldsymbol{F} = (F_1, F_2, F_3) \tag{16}$$

and

$$\boldsymbol{Q} = \begin{vmatrix} 1 & 0 & 0 \\ 0 & 1 & 0 \\ 0 & 0 & 2 \end{vmatrix}\ . \tag{17}$$

Since the equation of transfer is linear in $\boldsymbol{F}$, it is clear that the intensity $I_i(\mu, \varphi; \mu_0, \varphi_0)$, diffusely reflected by the atmosphere in the direction (μ, φ), must be expressible in the form

$$I_i(\mu, \varphi; \mu_0, \varphi_0) = \tfrac{3}{16} q_i \sum_{k=1}^{3} \sigma_{ik}(\mu, \varphi; \mu_0, \varphi_0)\, F_k \qquad (i = 1, 2, 3) \tag{18}$$

or as a vector equation,

$$\boldsymbol{I}(\mu, \varphi; \mu_0, \varphi_0) = \tfrac{3}{16}\boldsymbol{Q}\boldsymbol{\Sigma}(\mu, \varphi; \mu_0, \varphi_0)\, \boldsymbol{F}\ . \tag{19}$$

3. *The functional equation for the scattering matrix.*—To obtain the functional equations for the quantities $\sigma_{ik}(\mu, \varphi; \mu_0, \varphi_0)$, introduced in § 2, the procedure is as follows:

Consider the case when the incident beam has only one nonvanishing component in $\boldsymbol{F}$, say F_k. Denote the corresponding intensities by $I_i^{(k)} (i = 1, 2, 3)$. The equations of transfer now reduce to

$$\mu \frac{dI_i^{(k)}}{d\tau} = I_i^{(k)} - B_i^{(k)}(\tau, \mu, \varphi) \qquad (i = 1, 2, 3)\ , \tag{20}$$

where

$$B_i^{(k)}(\tau, \mu, \varphi) = \mathfrak{I}_i^{(k)}(\tau, \mu, \varphi) + \tfrac{3}{16} q_i j_{ik}(\mu, \varphi; \mu_0, \varphi_0) F_k e^{-\tau/\mu_0} \qquad (i = 1, 2, 3). \quad (21)$$

However, in general, there will be nonvanishing intensities in all three components in the reflected light. In fact, according to equation (18), we must have

$$I_i^{(k)}(\mu, \varphi; \mu_0, \varphi_0) = \tfrac{3}{16} q_i \sigma_{ik}(\mu, \varphi; \mu_0, \varphi_0) F_k \qquad (i = 1, 2, 3). \quad (22)$$

Now consider a level at depth $d\tau$ below the boundary of the atmosphere at $\tau = 0$. At this level the radiation field present can be decomposed into two parts: first, there is the reduced incident flux of amount

$$\pi F_k \left(1 - \frac{d\tau}{\mu_0}\right), \quad (23)$$

and, second, there is a diffuse radiation field. The amount of this diffuse radiation field which is directed inward can be inferred from the equation of transfer: for, since at $\tau = 0$ there is no inward intensity, at the level $d\tau$ we must have an inward intensity (cf. eq. [20]),

$$I_i^{(k)}(d\tau, -\mu', \varphi') = \frac{1}{\mu'} B_i^{(k)}(0, -\mu', \varphi')\, d\tau \qquad (i = 1, 2, 3), \quad (24)$$

in the direction $(-\mu', \varphi')$. Both the radiation fields (23) and (24) will be reflected by the atmosphere below $d\tau$ by the *same laws* as those by which the atmosphere below $\tau = 0$ reflects. The reason for this invariance is simply that the removal of a layer of arbitrary optical thickness from an infinite atmosphere cannot alter its reflecting-power. This is Ambarzumian's basic idea. Accordingly, the reflection of radiations (23) and (24) by the atmosphere below $d\tau$ will contribute to an *outward* intensity in the direction (μ, φ) the amount

$$\left.\begin{aligned} I_i^{(k)}(d\tau, \mu, \varphi) &= \tfrac{3}{16} q_i \sigma_{ik}(\mu, \varphi; \mu_0, \varphi_0)\left(1 - \frac{d\tau}{\mu_0}\right) F_k \\ &\quad + \frac{3}{16\pi} q_i d\tau \int_0^1 \int_0^{2\pi} \sum_{l=1}^{3} \sigma_{il}(\mu, \varphi; \mu', \varphi') B_l^{(k)}(0, -\mu', \varphi') \frac{d\mu'}{\mu'} d\varphi'. \end{aligned}\right\} \quad (25)$$

On the other hand, from the equation of transfer, we can directly conclude that

$$\left.\begin{aligned} I_i^{(k)}(d\tau, \mu, \varphi) &= I_i^{(k)}(0, \mu, \varphi) + \frac{d\tau}{\mu}\left[I_i^{(k)}(0, \mu, \varphi) - B_i^{(k)}(0, \mu, \varphi)\right] \\ &= \tfrac{3}{16} q_i \left(1 + \frac{d\tau}{\mu}\right) \sigma_{ik}(\mu, \varphi; \mu_0, \varphi_0) F_k - \frac{d\tau}{\mu} B_i^{(k)}(0, \mu, \varphi). \end{aligned}\right\} \quad (26)$$

Combining equations (25) and (26) and passing to the limit $d\tau = 0$, we have

$$\left.\begin{aligned} \tfrac{3}{16} q_i \left(\frac{1}{\mu} + \frac{1}{\mu_0}\right) \sigma_{ik}(\mu, \varphi; \mu_0, \varphi_3) F_k &= \frac{1}{\mu} B_i^{(k)}(0, \mu, \varphi) \\ &\quad + \frac{3}{16\pi} q_i \int_0^1 \int_0^{2\pi} \sum_{l=1}^{3} \sigma_{il}(\mu, \varphi; \mu', \varphi') B_l^{(k)}(0, -\mu', \varphi') \frac{d\mu'}{\mu'} d\varphi'. \end{aligned}\right\} \quad (27)$$

But, according to equations (13) and (21),

$$\left.\begin{aligned} B_i^{(k)}(0, \mu, \varphi) &= \mathfrak{I}_i^{(k)}(0, \mu, \varphi) + \tfrac{3}{16} q_i j_{ik}(\mu, \varphi; \mu_0, \varphi_0) F_k \\ &= \tfrac{3}{16} q_i j_{ik}(\mu, \varphi; \mu_0, \varphi_0) F_k + \frac{3}{16\pi} q_i \int_0^1 \int_0^{2\pi} \sum_{m=1}^{3} j_{im}(\mu, \varphi; -\mu', \varphi') \\ &\quad \times I_m^{(k)}(0, \mu', \varphi')\, d\mu' d\varphi' = \tfrac{3}{16} q_i F_k \Big[j_{ik}(\mu, \varphi; \mu_0, \varphi_0) \\ &\quad + \frac{3}{16\pi} \int_0^1 \int_0^{2\pi} \sum_{m=1}^{3} j_{im}(\mu, \varphi; -\mu', \varphi')\, q_m \sigma_{mk}(\mu', \varphi'; \mu_0, \varphi_0)\, d\mu' d\varphi' \Big]. \end{aligned}\right\} \quad (28)$$

Using equation (28) in equation (27) and writing

$$\mu\sigma_{ik}(\mu, \varphi; \mu_0, \varphi_0) = S_{ik}(\mu, \varphi; \mu_0, \varphi_0), \tag{29}$$

we obtain, after some further reductions,

$$\begin{aligned}
&\left(\frac{1}{\mu}+\frac{1}{\mu_0}\right) S_{ik}(\mu, \varphi; \mu_0, \varphi_0) = j_{ik}(\mu, \varphi; \mu_0, \varphi_0) \\
&+\frac{3}{16\pi}\int_0^1\int_0^{2\pi}\sum_{m=1}^{3} j_{im}(\mu, \varphi; -\mu'', \varphi'')\, q_m S_{mk}(\mu'', \varphi''; \mu_0, \varphi_0)\frac{d\mu''}{\mu''}\, d\varphi'' \\
&+\frac{3}{16\pi}\int_0^1\int_0^{2\pi}\sum_{l=1}^{3} S_{il}(\mu, \varphi; \mu', \varphi')\, q_l j_{lk}(-\mu', \varphi'; \mu_0, \varphi_0)\frac{d\mu'}{\mu'}\, d\varphi' \\
&+\frac{9}{256\pi^2}\int_0^1\int_0^{2\pi}\int_0^1\int_0^{2\pi}\sum_{l=1}^{3}\sum_{m=1}^{3} S_{il}(\mu, \varphi; \mu', \varphi')\, q_l j_{lm}(-\mu', \varphi'; -\mu'', \varphi'') \\
&\qquad\times q_m S_{mk}(\mu'', \varphi''; \mu_0, \varphi_0)\frac{d\mu'}{\mu'}\, d\varphi'\frac{d\mu''}{\mu''}\, d\varphi''.
\end{aligned} \tag{30}$$

Equation (30) can be written as a matrix equation in the form

$$\begin{aligned}
&\left(\frac{1}{\mu}+\frac{1}{\mu_0}\right)\boldsymbol{S}(\mu, \varphi; \mu_0, \varphi_0) = \boldsymbol{J}(\mu, \varphi; \mu_0, \varphi_0) \\
&\quad+\frac{3}{16\pi}\int_0^1\int_0^{2\pi}\boldsymbol{J}(\mu, \varphi; -\mu'', \varphi'')\boldsymbol{Q}\boldsymbol{S}(\mu'', \varphi''; \mu_0, \varphi_0)\frac{d\mu''}{\mu''}\, d\varphi'' \\
&\quad+\frac{3}{16\pi}\int_0^1\int_0^{2\pi}\boldsymbol{S}(\mu, \varphi; \mu', \varphi')\boldsymbol{Q}\boldsymbol{J}(-\mu', \varphi'; \mu_0, \varphi_0)\frac{d\mu'}{\mu'}\, d\varphi' \\
&\quad+\frac{9}{256\pi^2}\int_0^1\int_0^{2\pi}\int_0^1\int_0^{2\pi}\boldsymbol{S}(\mu, \varphi; \mu', \varphi')\boldsymbol{Q}\boldsymbol{J}(-\mu', \varphi'; -\mu'', \varphi'')\boldsymbol{Q} \\
&\qquad\times\boldsymbol{S}(\mu'', \varphi''; \mu_0, \varphi_0)\frac{d\mu'}{\mu'}\, d\varphi'\frac{d\mu''}{\mu''}\, d\varphi''.
\end{aligned} \tag{31}$$

This is the required functional equation for the scattering matrix.

From equation (31) it readily follows that the scattering matrix $\boldsymbol{S}$ must have the same properties for transposition as the matrix $\boldsymbol{J}$. Hence,

$$\tilde{\boldsymbol{S}}(\mu, \varphi; \mu_0, \varphi_0) = \boldsymbol{S}(\mu_0, \varphi; \mu, \varphi_0). \tag{32}$$

In other words, we are able to deduce very simply the reciprocity principle in the form in which we reformulated it in Paper XIII (§ 4).

II. THE SOLUTION OF THE FUNCTIONAL EQUATION FOR THE SCATTERING MATRIX

4. *The reduction of the functional equation for* **S.**—From the form of the functional equation for $\boldsymbol{S}$ and the manner of its relation to $\boldsymbol{J}$, it is evident that in a Fourier analysis of the elements of $\boldsymbol{S}$ in $(\varphi - \varphi_0)$ we must have the same nonvanishing components as in the corresponding elements of $\boldsymbol{J}$. We may accordingly assume without loss of generality that $\boldsymbol{S}$ has the form

$$\boldsymbol{S}(\mu, \varphi; \mu_0, \varphi_0) =$$

$$\begin{vmatrix}
S_{11}^{(0)}(\mu, \mu_0) & S_{12}^{(0)}(\mu, \mu_0) & \\
-4\mu\mu_0(1-\mu^2)^{\frac{1}{2}}(1-\mu_0^2)^{\frac{1}{2}}S_{11}^{(1)}(\mu, \mu_0)\cos(\varphi-\varphi_0) & & -2\mu(1-\mu^2)^{\frac{1}{2}}(1-\mu_0^2)^{\frac{1}{2}}S_{13}^{(1)}(\mu, \mu_0)\sin(\varphi-\varphi_0) \\
+\mu^2\mu_0^2S_{11}^{(2)}(\mu, \mu_0)\cos 2(\varphi-\varphi_0) & -\mu^2S_{21}^{(2)}(\mu, \mu_0)\cos 2(\varphi-\varphi_0) & +\mu^2\mu_0S_{13}^{(2)}(\mu, \mu_0)\sin 2(\varphi-\varphi_0) \\
\\
S_{21}^{(0)}(\mu, \mu_0) & S_{22}^{(0)}(\mu, \mu_0) & \\
-\mu_0^2S_{21}^{(2)}(\mu, \mu_0)\cos 2(\varphi-\varphi_0) & +S_{22}^{(2)}(\mu, \mu_0)\cos 2(\varphi-\varphi_0) & -\mu_0S_{23}^{(2)}(\mu, \mu_0)\sin 2(\varphi-\varphi_0) \\
\\
-2\mu_0(1-\mu_0^2)^{\frac{1}{2}}(1-\mu^2)^{\frac{1}{2}}S_{31}^{(1)}(\mu, \mu_0)\sin(\varphi-\varphi_0) & & (1-\mu^2)^{\frac{1}{2}}(1-\mu_0^2)^{\frac{1}{2}}S_{33}^{(1)}(\mu, \mu_0)\cos(\varphi-\varphi_0) \\
+\mu_0^2\mu S_{31}^{(2)}(\mu, \mu_0)\sin 2(\varphi-\varphi_0) & -\mu S_{32}^{(2)}(\mu, \mu_0)\sin 2(\varphi-\varphi_0) & -\mu\mu_0S_{33}^{(2)}(\mu, \mu_0)\cos 2(\varphi-\varphi_0),
\end{vmatrix} \tag{33}$$

where, as the notation indicates, $S_{11}^{(0)}$, etc., are all functions of μ and μ_0 only. From the property (32) of $\boldsymbol{S}$ for transposition, we now conclude that

$$S_{jk}^{(i)}(\mu, \mu_0) = S_{kj}^{(i)}(\mu_0, \mu) . \tag{34}$$

Substituting in equation (31) the form (33) for $\boldsymbol{S}$ and equating the different Fourier components of the various elements, we find, after a long but straightforward series of reductions, that we are led to the following three systems of equations:

$$
\left.
\begin{aligned}
&\left(\frac{1}{\mu}+\frac{1}{\mu_0}\right) S_{11}^{(0)}(\mu,\mu_0) = j_{11}^{(0)}(\mu,\mu_0) + \frac{3}{8}\int_0^1 \frac{d\mu''}{\mu''}\left\{ j_{11}^{(0)}(\mu,\mu'') S_{11}^{(0)}(\mu'',\mu_0)\right.\\
&\quad\left. + \mu^2 S_{21}^{(0)}(\mu'',\mu_0)\right\} + \frac{3}{8}\int_0^1 \frac{d\mu'}{\mu'}\left\{ j_{11}^{(0)}(\mu',\mu_0) S_{11}^{(0)}(\mu,\mu') + \mu_0^2 S_{12}^{(0)}(\mu,\mu')\right\}\\
&\quad + \frac{9}{64}\int_0^1\int_0^1 \frac{d\mu''}{\mu''}\frac{d\mu'}{\mu'}\{S_{11}^{(0)}(\mu,\mu')[j_{11}^{(0)}(\mu',\mu'') S_{11}^{(0)}(\mu'',\mu_0) + \mu'^2 S_{21}^{(0)}(\mu'',\mu_0)]\\
&\qquad + S_{12}^{(0)}(\mu,\mu')[\mu''^2 S_{11}^{(0)}(\mu'',\mu_0) + S_{21}^{(0)}(\mu'',\mu_0)]\},\\
&\left(\frac{1}{\mu}+\frac{1}{\mu_0}\right) S_{12}^{(0)}(\mu,\mu_0) = \mu^2 + \frac{3}{8}\int_0^1 \frac{d\mu''}{\mu''}\left\{ j_{11}^{(0)}(\mu,\mu'') S_{12}^{(0)}(\mu'',\mu_0) + \mu^2 S_{22}^{(0)}(\mu'',\mu_0)\right\}\\
&\quad + \frac{3}{8}\int_0^1 \frac{d\mu'}{\mu'}\{S_{11}^{(0)}(\mu,\mu')\mu'^2 + S_{12}^{(0)}(\mu,\mu')\}\\
&\quad + \frac{9}{64}\int_0^1\int_0^1 \frac{d\mu''}{\mu''}\frac{d\mu'}{\mu'}\{S_{12}^{(0)}(\mu,\mu')[\mu''^2 S_{12}^{(0)}(\mu'',\mu_0) + S_{22}^{(0)}(\mu'',\mu_0)]\\
&\qquad + S_{11}^{(0)}(\mu,\mu')[j_{11}^{(0)}(\mu',\mu'') S_{12}^{(0)}(\mu'',\mu_0) + \mu'^2 S_{22}^{(0)}(\mu'',\mu_0)]\},\\
&\left(\frac{1}{\mu}+\frac{1}{\mu_0}\right) S_{21}^{(0)}(\mu,\mu_0) = \mu_0^2 + \frac{3}{8}\int_0^1 \frac{d\mu''}{\mu''}\{\mu''^2 S_{11}^{(0)}(\mu'',\mu_0) + S_{21}^{(0)}(\mu'',\mu_0)\}\\
&\quad + \frac{3}{8}\int_0^1 \frac{d\mu'}{\mu'}\{S_{21}^{(0)}(\mu,\mu') j_{11}^{(0)}(\mu',\mu_0) + S_{22}^{(0)}(\mu,\mu')\mu_0^2\}\\
&\quad + \frac{9}{64}\int_0^1\int_0^1 \frac{d\mu''}{\mu''}\frac{d\mu'}{\mu'}\{S_{21}^{(0)}(\mu'',\mu_0)[S_{21}^{(0)}(\mu,\mu')\mu'^2 + S_{22}^{(0)}(\mu,\mu')]\\
&\qquad + S_{11}^{(0)}(\mu'',\mu_0)[S_{21}^{(0)}(\mu,\mu') j_{11}^{(0)}(\mu',\mu'') + S_{22}^{(0)}(\mu,\mu')\mu''^2]\},\\
&\left(\frac{1}{\mu}+\frac{1}{\mu_0}\right) S_{22}^{(0)}(\mu,\mu_0) = 1 + \frac{3}{8}\int_0^1 \frac{d\mu''}{\mu''}\{\mu''^2 S_{12}^{(0)}(\mu'',\mu_0) + S_{22}^{(0)}(\mu'',\mu_0)\}\\
&\quad + \frac{3}{8}\int_0^1 \frac{d\mu'}{\mu'}\{S_{21}^{(0)}(\mu,\mu')\mu'^2 + S_{22}^{(0)}(\mu,\mu')\}\\
&\quad + \frac{9}{64}\int_0^1\int_0^1 \frac{d\mu''}{\mu''}\frac{d\mu'}{\mu'}\{S_{22}^{(0)}(\mu,\mu')[\mu''^2 S_{12}^{(0)}(\mu'',\mu_0) + S_{22}^{(0)}(\mu'',\mu_0)]\\
&\qquad + S_{21}^{(0)}(\mu,\mu')[j_{11}^{(0)}(\mu',\mu'') S_{12}^{(0)}(\mu'',\mu_0) + \mu'^2 S_{22}^{(0)}(\mu'',\mu_0)]\},
\end{aligned}
\right\} \quad \text{(I)}
$$

where we have used the abbreviation

$$
j_{11}^{(0)}(\mu,\mu') = 2(1-\mu^2)(1-\mu'^2) + \mu^2\mu'^2 ; \tag{35}
$$

$$
\left.
\begin{aligned}
&\left(\frac{1}{\mu}+\frac{1}{\mu_0}\right) S_{11}^{(1)}(\mu,\mu_0) = \left\{1 + \frac{3}{8}\int_0^1 \frac{d\mu''}{\mu''}(1-\mu''^2)[S_{31}^{(1)}(\mu'',\mu_0) + 2\mu''^2 S_{11}^{(1)}(\mu'',\mu_0)]\right\}\\
&\qquad \times\left\{1 + \frac{3}{8}\int_0^1 \frac{d\mu'}{\mu'}(1-\mu'^2)[S_{13}^{(1)}(\mu,\mu') + 2\mu'^2 S_{11}^{(1)}(\mu,\mu')]\right\},\\
&\left(\frac{1}{\mu}+\frac{1}{\mu_0}\right) S_{13}^{(1)}(\mu,\mu_0) = \left\{1 + \frac{3}{8}\int_0^1 \frac{d\mu''}{\mu''}(1-\mu''^2)[S_{33}^{(1)}(\mu'',\mu_0) + 2\mu''^2 S_{13}^{(1)}(\mu'',\mu_0)]\right\}\\
&\qquad \times\left\{1 + \frac{3}{8}\int_0^1 \frac{d\mu'}{\mu'}(1-\mu'^2)[S_{13}^{(1)}(\mu,\mu') + 2\mu'^2 S_{11}^{(1)}(\mu,\mu')]\right\},\\
&\left(\frac{1}{\mu}+\frac{1}{\mu_0}\right) S_{31}^{(1)}(\mu,\mu_0) = \left\{1 + \frac{3}{8}\int_0^1 \frac{d\mu''}{\mu''}(1-\mu''^2)[S_{31}^{(1)}(\mu'',\mu_0) + 2\mu''^2 S_{11}^{(1)}(\mu'',\mu_0)]\right\}\\
&\qquad \times\left\{1 + \frac{3}{8}\int_0^1 \frac{d\mu'}{\mu'}(1-\mu'^2)[S_{33}^{(1)}(\mu,\mu') + 2\mu'^2 S_{31}^{(1)}(\mu,\mu')]\right\},\\
&\left(\frac{1}{\mu}+\frac{1}{\mu_0}\right) S_{33}^{(1)}(\mu,\mu_0) = \left\{1 + \frac{3}{8}\int_0^1 \frac{d\mu''}{\mu''}(1-\mu''^2)[S_{33}^{(1)}(\mu'',\mu_0) + 2\mu''^2 S_{13}^{(1)}(\mu'',\mu_0)]\right\}\\
&\qquad \times\left\{1 + \frac{3}{8}\int_0^1 \frac{d\mu'}{\mu'}(1-\mu'^2)[S_{33}^{(1)}(\mu,\mu') + 2\mu'^2 S_{31}^{(1)}(\mu,\mu')]\right\};
\end{aligned}
\right\} \quad \text{(II)}
$$

and

$$\left(\frac{1}{\mu}+\frac{1}{\mu_0}\right)S_{11}^{(2)}(\mu,\mu_0)=\left\{1+\frac{3}{16}\int_0^1\frac{d\mu''}{\mu''}\left[\mu''^4S_{11}^{(2)}(\mu'',\mu_0)+2\mu''^2S_{31}^{(2)}(\mu'',\mu_0)\right.\right.$$
$$\left.\left.+S_{21}^{(2)}(\mu'',\mu_0)\right]\right\}\left\{1+\frac{3}{16}\int_0^1\frac{d\mu'}{\mu'}\left[\mu'^4S_{11}^{(2)}(\mu,\mu')+2\mu'^2S_{13}^{(2)}(\mu,\mu')+S_{12}^{(2)}(\mu,\mu')\right]\right\},$$

$$\left(\frac{1}{\mu}+\frac{1}{\mu_0}\right)S_{22}^{(2)}(\mu,\mu_0)=\left\{1+\frac{3}{16}\int_0^1\frac{d\mu''}{\mu''}\left[\mu''^4S_{12}^{(2)}(\mu'',\mu_0)+2\mu''^2S_{32}^{(2)}(\mu'',\mu_0)\right.\right.$$
$$\left.\left.+S_{22}^{(2)}(\mu'',\mu_0)\right]\right\}\left\{1+\frac{3}{16}\int_0^1\frac{d\mu'}{\mu'}\left[\mu'^4S_{21}^{(2)}(\mu,\mu')+2\mu'^2S_{23}^{(2)}(\mu,\mu')+S_{22}^{(2)}(\mu,\mu')\right]\right\},$$

$$\left(\frac{1}{\mu}+\frac{1}{\mu_0}\right)S_{33}^{(2)}(\mu,\mu_0)=\left\{1+\frac{3}{16}\int_0^1\frac{d\mu''}{\mu''}\left[\mu''^4S_{13}^{(2)}(\mu'',\mu_0)+2\mu''^2S_{33}^{(2)}(\mu'',\mu_0)\right.\right.$$
$$\left.\left.+S_{23}^{(2)}(\mu'',\mu_0)\right]\right\}\left\{1+\frac{3}{16}\int_0^1\frac{d\mu'}{\mu'}\left[\mu'^4S_{31}^{(2)}(\mu,\mu')+2\mu'^2S_{33}^{(2)}(\mu,\mu')+S_{32}^{(2)}(\mu,\mu')\right]\right\},$$

$$\left(\frac{1}{\mu}+\frac{1}{\mu_0}\right)S_{12}^{(2)}(\mu,\mu_0)=\left\{1+\frac{3}{16}\int_0^1\frac{d\mu''}{\mu''}\left[\mu''^4S_{12}^{(2)}(\mu'',\mu_0)+2\mu''^2S_{32}^{(2)}(\mu'',\mu_0)\right.\right.$$
$$\left.\left.+S_{22}^{(2)}(\mu'',\mu_0)\right]\right\}\left\{1+\frac{3}{16}\int_0^1\frac{d\mu'}{\mu'}\left[\mu'^4S_{11}^{(2)}(\mu,\mu')+2\mu'^2S_{13}^{(2)}(\mu,\mu')+S_{12}^{(2)}(\mu,\mu')\right]\right\},$$

$$\left(\frac{1}{\mu}+\frac{1}{\mu_0}\right)S_{21}^{(2)}(\mu,\mu_0)=\left\{1+\frac{3}{16}\int_0^1\frac{d\mu''}{\mu''}\left[\mu''^4S_{11}^{(2)}(\mu'',\mu_0)+2\mu''^2S_{31}^{(2)}(\mu'',\mu_0)\right.\right.$$
$$\left.\left.+S_{21}^{(2)}(\mu'',\mu_0)\right]\right\}\left\{1+\frac{3}{16}\int_0^1\frac{d\mu'}{\mu'}\left[\mu'^4S_{21}^{(2)}(\mu,\mu')+2\mu'^2S_{23}^{(2)}(\mu,\mu')+S_{22}^{(2)}(\mu,\mu')\right]\right\},$$

$$\left(\frac{1}{\mu}+\frac{1}{\mu_0}\right)S_{23}^{(2)}(\mu,\mu_0)=\left\{1+\frac{3}{16}\int_0^1\frac{d\mu''}{\mu''}\left[\mu''^4S_{13}^{(2)}(\mu'',\mu_0)+2\mu''^2S_{33}^{(2)}(\mu'',\mu_0)\right.\right.$$
$$\left.\left.+S_{23}^{(2)}(\mu'',\mu_0)\right]\right\}\left\{1+\frac{3}{16}\int_0^1\frac{d\mu'}{\mu'}\left[\mu'^4S_{21}^{(2)}(\mu,\mu')+2\mu'^2S_{23}^{(2)}(\mu,\mu')+S_{22}^{(2)}(\mu,\mu')\right]\right\},$$

$$\left(\frac{1}{\mu}+\frac{1}{\mu_0}\right)S_{32}^{(2)}(\mu,\mu_0)=\left\{1+\frac{3}{16}\int_0^1\frac{d\mu''}{\mu''}\left[\mu''^4S_{12}^{(2)}(\mu'',\mu_0)+2\mu''^2S_{32}^{(2)}(\mu'',\mu_0)\right.\right.$$
$$\left.\left.+S_{22}^{(2)}(\mu'',\mu_0)\right]\right\}\left\{1+\frac{3}{16}\int_0^1\frac{d\mu'}{\mu'}\left[\mu'^4S_{31}^{(2)}(\mu,\mu')+2\mu'^2S_{33}^{(2)}(\mu,\mu')+S_{32}^{(2)}(\mu,\mu')\right]\right\},$$

$$\left(\frac{1}{\mu}+\frac{1}{\mu_0}\right)S_{31}^{(2)}(\mu,\mu_0)=\left\{1+\frac{3}{16}\int_0^1\frac{d\mu''}{\mu''}\left[\mu''^4S_{11}^{(2)}(\mu'',\mu_0)+2\mu''^2S_{31}^{(2)}(\mu'',\mu_0)\right.\right.$$
$$\left.\left.+S_{21}^{(2)}(\mu'',\mu_0)\right]\right\}\left\{1+\frac{3}{16}\int_0^1\frac{d\mu'}{\mu'}\left[\mu'^4S_{31}^{(2)}(\mu,\mu')+2\mu'^2S_{33}^{(2)}(\mu,\mu')+S_{32}^{(2)}(\mu,\mu')\right]\right\},$$

$$\left(\frac{1}{\mu}+\frac{1}{\mu_0}\right)S_{13}^{(2)}(\mu,\mu_0)=\left\{1+\frac{3}{16}\int_0^1\frac{d\mu''}{\mu''}\left[\mu''^4S_{13}^{(2)}(\mu'',\mu_0)+2\mu''^2S_{33}^{(2)}(\mu'',\mu_0)\right.\right.$$
$$\left.\left.+S_{23}^{(2)}(\mu'',\mu_0)\right]\right\}\left\{1+\frac{3}{16}\int_0^1\frac{d\mu'}{\mu'}\left[\mu'^4S_{11}^{(2)}(\mu,\mu')+2\mu'^2S_{13}^{(2)}(\mu,\mu')+S_{12}^{(2)}(\mu,\mu')\right]\right\}.$$

5. *The functional equations for* $S_{11}^{(0)}$, $S_{12}^{(0)}$, $S_{21}^{(0)}$, *and* $S_{22}^{(0)}$.—The first of the three systems of equations to which we have reduced the functional equation for $\boldsymbol{S}$ is the most important and, at the same time, the most difficult. We shall accordingly consider this system in some detail.

Substituting for $j_{11}^{(0)}$, according to equation (35) in the equations of System (I), we find on examination that they can be brought to the forms

$$\left.\begin{aligned}\left(\frac{1}{\mu}+\frac{1}{\mu_0}\right)S_{11}^{(0)}(\mu,\mu_0) &= \left\{\mu^2+\frac{3}{8}\int_0^1\frac{d\mu'}{\mu'}\left[\mu'^2S_{11}^{(0)}(\mu,\mu')+S_{12}^{(0)}(\mu,\mu')\right]\right\}\\ &\times\left\{\mu_0^2+\frac{3}{8}\int_0^1\frac{d\mu''}{\mu''}\left[\mu''^2S_{11}^{(0)}(\mu'',\mu_0)+S_{21}^{(0)}(\mu'',\mu_0)\right]\right\}\\ &+2\left\{1-\mu^2+\frac{3}{8}\int_0^1\frac{d\mu'}{\mu'}(1-\mu'^2)S_{11}^{(0)}(\mu,\mu')\right\}\\ &\times\left\{1-\mu_0^2+\frac{3}{8}\int_0^1\frac{d\mu''}{\mu''}(1-\mu''^2)S_{11}^{(0)}(\mu'',\mu_0)\right\};\end{aligned}\right\}\quad(36)$$

$$\left.\begin{aligned}\left(\frac{1}{\mu}+\frac{1}{\mu_0}\right)S_{12}^{(0)}(\mu,\mu_0) &= \left\{\mu^2+\frac{3}{8}\int_0^1\frac{d\mu'}{\mu'}\left[\mu'^2S_{11}^{(0)}(\mu,\mu')+S_{12}^{(0)}(\mu,\mu')\right]\right\}\\ &\times\left\{1+\frac{3}{8}\int_0^1\frac{d\mu''}{\mu''}\left[\mu''^2S_{12}^{(0)}(\mu'',\mu_0)+S_{22}^{(0)}(\mu'',\mu_0)\right]\right\}\\ &+2\left\{\frac{3}{8}\int_0^1\frac{d\mu''}{\mu''}(1-\mu''^2)S_{12}^{(0)}(\mu'',\mu_0)\right\}\\ &\times\left\{1-\mu^2+\frac{3}{8}\int_0^1\frac{d\mu'}{\mu'}(1-\mu'^2)S_{11}^{(0)}(\mu,\mu')\right\};\end{aligned}\right\}\quad(37)$$

$$\left.\begin{aligned}\left(\frac{1}{\mu}+\frac{1}{\mu_0}\right)S_{21}^{(0)}(\mu,\mu_0) &= \left\{\mu_0^2+\frac{3}{8}\int_0^1\frac{d\mu''}{\mu''}\left[\mu''^2S_{11}^{(0)}(\mu'',\mu_0)+S_{21}^{(0)}(\mu'',\mu_0)\right]\right\}\\ &\times\left\{1+\frac{3}{8}\int_0^1\frac{d\mu'}{\mu'}\left[\mu'^2S_{21}^{(0)}(\mu,\mu')+S_{22}^{(0)}(\mu,\mu')\right]\right\}\\ &+2\left\{\frac{3}{8}\int_0^1\frac{d\mu'}{\mu'}(1-\mu'^2)S_{21}^{(0)}(\mu,\mu')\right\}\\ &\times\left\{1-\mu_0^2+\frac{3}{8}\int_0^1\frac{d\mu''}{\mu''}(1-\mu''^2)S_{11}^{(0)}(\mu'',\mu_0)\right\};\end{aligned}\right\}\quad(38)$$

and

$$\left.\begin{aligned}\left(\frac{1}{\mu}+\frac{1}{\mu_0}\right)S_{22}^{(0)}(\mu,\mu_0) &= \left\{1+\frac{3}{8}\int_0^1\frac{d\mu''}{\mu''}\left[\mu''^2S_{12}^{(0)}(\mu'',\mu_0)+S_{22}^{(0)}(\mu'',\mu_0)\right]\right\}\\ &\times\left\{1+\frac{3}{8}\int_0^1\frac{d\mu'}{\mu'}\left[\mu'^2S_{21}^{(0)}(\mu,\mu')+S_{22}^{(0)}(\mu,\mu')\right]\right\}\\ &+\frac{9}{32}\int_0^1\frac{d\mu'}{\mu'}(1-\mu'^2)S_{21}^{(0)}(\mu,\mu')\int_0^1\frac{d\mu''}{\mu''}(1-\mu''^2)S_{12}^{(0)}(\mu'',\mu_0).\end{aligned}\right\}\quad(39)$$

An inspection of these equations shows what we have already seen directly from the functional equation for $\boldsymbol{S}$, that, among these functions of "zero order," the relation (34) must hold in particular. In other words,

$$S_{11}^{(0)}(\mu,\mu_0)=S_{11}^{(0)}(\mu_0,\mu);\ S_{12}^{(0)}(\mu,\mu_0)=S_{21}^{(0)}(\mu_0,\mu);\ S_{22}^{(0)}(\mu,\mu_0)=S_{22}^{(0)}(\mu_0,\mu).\quad(40)$$

In view of these relations, it follows from equations (36)–(39) that we can express the functions $S_{11}^{(0)}$, $S_{12}^{(0)}$, $S_{21}^{(0)}$ and $S_{22}^{(0)}$ in the forms

$$\left(\frac{1}{\mu}+\frac{1}{\mu_0}\right) S_{11}^{(0)}(\mu, \mu_0) = \psi(\mu)\,\psi(\mu_0) + 2\phi(\mu)\,\phi(\mu_0), \tag{41}$$

$$\left(\frac{1}{\mu}+\frac{1}{\mu_0}\right) S_{12}^{(0)}(\mu, \mu_0) = \psi(\mu)\,\chi(\mu_0) + 2\phi(\mu)\,\zeta(\mu_0), \tag{42}$$

$$\left(\frac{1}{\mu}+\frac{1}{\mu_0}\right) S_{21}^{(0)}(\mu, \mu_0) = \psi(\mu_0)\,\chi(\mu) + 2\phi(\mu_0)\,\zeta(\mu), \tag{43}$$

and

$$\left(\frac{1}{\mu}+\frac{1}{\mu_0}\right) S_{22}^{(0)}(\mu, \mu_0) = \chi(\mu)\,\chi(\mu_0) + 2\zeta(\mu)\,\zeta(\mu_0), \tag{44}$$

where

$$\psi(\mu) = \mu^2 + \frac{3}{8}\int_0^1 \frac{d\mu'}{\mu'}\left[\mu'^2 S_{11}^{(0)}(\mu, \mu') + S_{12}^{(0)}(\mu, \mu')\right], \tag{45}$$

$$\phi(\mu) = 1 - \mu^2 + \frac{3}{8}\int_0^1 \frac{d\mu'}{\mu'}(1-\mu'^2)\, S_{11}^{(0)}(\mu, \mu'), \tag{46}$$

$$\chi(\mu) = 1 + \frac{3}{8}\int_0^1 \frac{d\mu'}{\mu'}\left[\mu'^2 S_{21}^{(0)}(\mu, \mu') + S_{22}^{(0)}(\mu, \mu')\right], \tag{47}$$

and

$$\zeta(\mu) = \frac{3}{8}\int_0^1 \frac{d\mu'}{\mu'}(1-\mu'^2)\, S_{21}^{(0)}(\mu, \mu'). \tag{48}$$

Substituting for $S_{11}^{(0)}$, etc., from equations (41)–(44) back into equations (45)–(48), we obtain the functional equations for our problem in their normal forms. We have

$$\left.\begin{aligned}\psi(\mu) = \mu^2 + \tfrac{3}{8}\mu\psi(\mu)\int_0^1 \frac{d\mu'}{\mu+\mu'}\left[\mu'^2\psi(\mu') + \chi(\mu')\right] \\ + \tfrac{3}{4}\mu\phi(\mu)\int_0^1 \frac{d\mu'}{\mu+\mu'}\left[\mu'^2\phi(\mu') + \zeta(\mu')\right],\end{aligned}\right\} \tag{49}$$

$$\left.\begin{aligned}\phi(\mu) = 1 - \mu^2 + \tfrac{3}{8}\mu\psi(\mu)\int_0^1 \frac{d\mu'}{\mu+\mu'}(1-\mu'^2)\,\psi(\mu') \\ + \tfrac{3}{4}\mu\phi(\mu)\int_0^1 \frac{d\mu'}{\mu+\mu'}(1-\mu'^2)\,\phi(\mu'),\end{aligned}\right\} \tag{50}$$

$$\left.\begin{aligned}\chi(\mu) = 1 + \tfrac{3}{8}\mu\chi(\mu)\int_0^1 \frac{d\mu'}{\mu+\mu'}\left[\mu'^2\psi(\mu') + \chi(\mu')\right] \\ + \tfrac{3}{4}\mu\zeta(\mu)\int_0^1 \frac{d\mu'}{\mu+\mu'}\left[\mu'^2\phi(\mu') + \zeta(\mu')\right],\end{aligned}\right\} \tag{51}$$

and

$$\zeta(\mu) = \tfrac{3}{8}\mu\chi(\mu)\int_0^1 \frac{d\mu'}{\mu+\mu'}(1-\mu'^2)\,\psi(\mu') + \tfrac{3}{4}\mu\zeta(\mu)\int_0^1 \frac{d\mu'}{\mu+\mu'}(1-\mu'^2)\,\phi(\mu'). \tag{52}$$

Equations (49)–(52) represent a nonlinear, nonhomogeneous system of four simultaneous functional equations. The solution of such a system would seem, on first sight,

to be an impossible task. But we shall show how a knowledge of the forms of the solutions gained from the analysis in Papers XI and XIII enables us to reduce the solution of equations (49)–(52) to two simple functional equations, each of form (4). And, as we have already indicated in § 1, such functional equations can be solved quite readily by a rapidly converging method of iteration.

6. *The forms of the solutions of the functional equations* (49)–(52).—In solving the functional equations (49)–(52), we shall be guided by the forms of the solutions which we have obtained by directly solving the relevant equations of transfer. We shall, therefore, first re-write the solutions given in Papers XI and XIII in forms which can be compared with equations (41)–(44).

From the expression for the scattering matrix given in Paper XIII (eq. [65]) we see, for example, that

$$\left(\frac{1}{\mu}+\frac{1}{\mu_0}\right) S_{11}^{(0)}(\mu, \mu_0) = 2H_l(\mu)\, H_l(\mu_0)\,[1+\mu\mu_0 - c\,(\mu+\mu_0)], \tag{53}$$

$$\left(\frac{1}{\mu}+\frac{1}{\mu_0}\right) S_{12}^{(0)}(\mu, \mu_0) = qH_l(\mu)\, H_r(\mu_0)\,(\mu+\mu_0), \tag{54}$$

$$\left(\frac{1}{\mu}+\frac{1}{\mu_0}\right) S_{21}^{(0)}(\mu, \mu_0) = qH_r(\mu)\, H_l(\mu_0)\,(\mu+\mu_0), \tag{55}$$

and

$$\left(\frac{1}{\mu}+\frac{1}{\mu_0}\right) S_{22}^{(0)}(\mu, \mu_0) = H_r(\mu)\, H_r(\mu_0)\,[1+\mu\mu_0 + c\,(\mu+\mu_0)]. \tag{56}$$

Here q and c are two constants which are defined in Paper XI, equations (130) and (134); and $H_l(\mu)$ and $H_r(\mu)$ are H-functions defined in terms of the roots of the characteristic equations

$$1 = \frac{3}{2}\sum_{j=1}^{n} \frac{a_j\,(1-\mu_j^2)}{1-k^2\mu_j^2} \tag{57}$$

and

$$1 = \frac{3}{4}\sum_{j=1}^{n} \frac{a_j\,(1-\mu_j^2)}{1-k^2\mu_j^2}, \tag{58}$$

respectively.

Now, between the constants q and c there exists the relation

$$q^2 = 2\,(1-c^2). \tag{59}$$[5]

Hence

$$1+\mu\mu_0 \pm c\,(\mu+\mu_0) = (1\pm c\mu)(1\pm c\mu_0) + \tfrac{1}{2}q^2\mu\mu_0. \tag{60}$$

[5] This follows from the definitions of the constants q and c. Thus, from Paper XI, eq. (130), we find that

$$2(1-c^2) = -8\,\frac{R(1)R(-1)\rho(1)\rho(-1)}{[R(-1)\rho(1)-R(1)\rho(-1)]^2};$$

or, using Paper XI, eqs. (133) and (134), we have

$$2(1-c^2) = \left\{\frac{2\rho(1)\rho(-1)}{R(-1)\rho(1)-R(1)\rho(-1)}\right\}^2 = q^2.$$

We may accordingly re-write equations (53)–(56) in the forms

$$\left(\frac{1}{\mu}+\frac{1}{\mu_0}\right)S_{11}^{(0)}(\mu,\mu_0) = [q\mu H_l(\mu)][q\mu_0 H_l(\mu_0)] + 2[H_l(\mu)(1-c\mu)][H_l(\mu_0)(1-c\mu_0)], \tag{61}$$

$$\left(\frac{1}{\mu}+\frac{1}{\mu_0}\right)S_{12}^{(0)}(\mu,\mu_0) = [q\mu H_l(\mu)][H_r(\mu_0)(1+c\mu_0)] + 2[H_l(\mu)(1-c\mu)][\tfrac{1}{2}q\mu_0 H_r(\mu_0)], \tag{62}$$

$$\left(\frac{1}{\mu}+\frac{1}{\mu_0}\right)S_{21}^{(0)}(\mu,\mu_0) = [q\mu_0 H_l(\mu_0)][H_r(\mu)(1+c\mu)] + 2[H_l(\mu_0)(1-c\mu_0)][\tfrac{1}{2}q\mu H_r(\mu)], \tag{63}$$

and

$$\left(\frac{1}{\mu}+\frac{1}{\mu_0}\right)S_{22}^{(0)}(\mu,\mu_0) = [H_r(\mu)(1+c\mu)][H_r(\mu_0)(1+c\mu_0)] + 2[\tfrac{1}{2}q\mu H_r(\mu)][\tfrac{1}{2}q\mu_0 H_r(\mu_0)]. \tag{64}$$

The similarity of equations (61)–(64) to (41)–(44) is apparent. While the solutions (53)–(56) can be brought into such a correspondence with equations (41)–(44) in a variety of ways, it appeared after some examination that the particular choice we have made is the correct one. Indeed, we shall prove in § 8 that the solutions of the functional equations (49)–(52) are of the forms

$$\psi(\mu) = q\mu H_l(\mu), \tag{65}$$

$$\phi(\mu) = H_l(\mu)(1-c\mu), \tag{66}$$

$$\chi(\mu) = H_r(\mu)(1+c\mu) \tag{67}$$

and

$$\zeta(\mu) = \tfrac{1}{2}q\mu H_r(\mu), \tag{68}$$

where $H_l(\mu)$ and $H_r(\mu)$ are defined as the solutions of the functional equations (cf. our remarks in § 1)

$$H_l(\mu) = 1+\tfrac{3}{4}\mu H_l(\mu)\int_0^1 \frac{H_l(\mu')(1-\mu'^2)}{\mu+\mu'}\,d\mu', \tag{69}$$

and

$$H_r(\mu) = 1+\tfrac{3}{8}\mu H_r(\mu)\int_0^1 \frac{H_r(\mu')(1-\mu'^2)}{\mu+\mu'}\,d\mu', \tag{70}$$

and q and c are two constants satisfying the relation (59) and related in a way that we shall later specify with the moments of $H_l(\mu)$ and $H_r(\mu)$.

7. *Some integral properties of the functions* $H_l(\mu)$ *and* $H_r(\mu)$.—Before we can prove that the solutions of the functional equations (49)–(52) are as we have stated them in § 6, it is necessary to establish certain integral properties of the functions $H_l(\mu)$ and $H_r(\mu)$ which satisfy the functional equations (69) and (70).

We shall state and prove the required properties in the form of three lemmas.

Lemma 1.—
$$\int_0^1 H_l(\mu)(1-\mu^2)\,d\mu = \tfrac{4}{3}, \tag{71}$$

and

$$\int_0^1 H_r(\mu)(1-\mu^2)\,d\mu = \tfrac{4}{3}(2-\sqrt{2}). \tag{72}$$

To prove equation (71), for example, we multiply the functional equation satisfied by $H_l(\mu)$ by $(1-\mu^2)$ and integrate over the range of μ. We obtain

$$\left.\begin{aligned}\int_0^1 H_l(\mu)(1-\mu^2)\,d\mu = \tfrac{2}{3} + \frac{3}{4}\int_0^1\int_0^1 \frac{\mu}{\mu+\mu'} H_l(\mu)(1-\mu^2) \\ \times H_l(\mu')(1-\mu'^2)\,d\mu d\mu'\,.\end{aligned}\right\} \quad (73)$$

Interchanging μ and μ' in the double integral in equation (73) and taking the average of the two equations, we have

$$\int_0^1 H_l(\mu)(1-\mu^2)\,d\mu = \tfrac{2}{3} + \frac{3}{8}\int_0^1\int_0^1 H_l(\mu)(1-\mu^2)\,H_l(\mu')(1-\mu'^2)\,d\mu d\mu' \quad (74)$$

or, alternatively,

$$\frac{3}{8}\left[\int_0^1 H_l(\mu)(1-\mu^2)\,d\mu\right]^2 - \int_0^1 H_l(\mu)(1-\mu^2)\,d\mu + \tfrac{2}{3} = 0\,. \quad (75)$$

From equation (75) the relation in question follows.

In a similar way, from the functional equation satisfied by $H_r(\mu)$ we obtain (cf. eq. [75])

$$\frac{3}{16}\left[\int_0^1 H_r(\mu)(1-\mu^2)\,d\mu\right]^2 - \int_0^1 H_r(\mu)(1-\mu^2)\,d\mu + \tfrac{2}{3} = 0\,. \quad (76)$$

Solving this equation, we find

$$\int_0^1 H_r(\mu)(1-\mu^2)\,d\mu = \tfrac{4}{3}(2 \pm \sqrt{2})\,. \quad (77)$$

The ambiguity in sign in the foregoing equation can be removed by considerations which we shall not go into here. But it may be stated that the positive sign in the quantity in parenthesis on the right-hand side of equation (77) is excluded on the ground that

$$H_r(\mu) < H_l(\mu) \qquad (\mu < 1)\,. \quad (78)$$

Corollary.—The functional equations for $H_l(\mu)$ and $H_r(\mu)$ have the alternative forms

$$1 = \tfrac{3}{4} H_l(\mu)\int_0^1 H_l(\mu')(1-\mu'^2)\frac{\mu'}{\mu+\mu'}\,d\mu' \quad (79)$$

and

$$1 = H_r(\mu)\left[\frac{1}{\sqrt{2}} + \frac{3}{8}\int_0^1 H_r(\mu')(1-\mu'^2)\frac{\mu'}{\mu+\mu'}\,d\mu'\right]. \quad (80)$$

Equation (80) can be proved in the following manner:

$$\left.\begin{aligned}&\tfrac{3}{8} H_r(\mu)\int^1 H_r(\mu')(1-\mu'^2)\frac{\mu'}{\mu+\mu'}\,d\mu' \\ &\quad = \tfrac{3}{8} H_r(\mu)\int_0^1 H_r(\mu')(1-\mu'^2)\left[1-\frac{\mu}{\mu+\mu'}\right]d\mu \\ &\quad = H_r(\mu)\left(1-\frac{1}{\sqrt{2}}\right) - \tfrac{3}{8}\mu H_r(\mu)\int_0^1 \frac{H_r(\mu')(1-\mu'^2)}{\mu+\mu'}\,d\mu' \\ &\quad = H_r(\mu)\left(1-\frac{1}{\sqrt{2}}\right) - H_r(\mu) + 1 \\ &\quad = 1 - \frac{1}{\sqrt{2}} H_r(\mu)\,.\end{aligned}\right\} \quad (81)$$

Equation (79) can be established in a similar way.

Lemma 2.—If a_0 and a_1 are the moments of orders zero and one, respectively, of the function $H_l(\mu)$, then

$$a_0 = 1 + \tfrac{3}{8}\,(a_0^2 - a_1^2)\,. \tag{82}$$

Similarly, if A_0 and A_1 are the zero and first moments of $H_r(\mu)$, then

$$A_0 = 1 + \tfrac{3}{16}\,(A_0^2 - A_1^2)\,. \tag{83}$$

To prove equation (82) we simply integrate over μ the functional equation defining $H_l(\mu)$. We find

$$\left.\begin{aligned}
\int_0^1 H_l(\mu)\,d\mu &= 1 + \frac{3}{4}\int_0^1\int_0^1 \frac{H_l(\mu)\,H_l(\mu')}{\mu+\mu'}\,\mu\,(1-\mu'^2)\,d\mu d\mu' \\
&= 1 + \frac{3}{8}\int_0^1\int_0^1 \frac{H_l(\mu)\,H_l(\mu')}{\mu+\mu'}\,[\mu(1-\mu'^2) + \mu'(1-\mu^2)]\,d\mu d\mu' \\
&= 1 + \frac{3}{8}\int_0^1\int_0^1 H_l(\mu)\,H_l(\mu')\,(1-\mu\mu')\,d\mu d\mu' \\
&= 1 + \frac{3}{8}\Big[\int_0^1 H_l(\mu)\,d\mu\Big]^2 - \frac{3}{8}\Big[\int_0^1 H_l(\mu)\,\mu d\mu\Big]^2,
\end{aligned}\right\} \tag{84}$$

from which the relation in question follows.

Relation (83) between the moments of $H_r(\mu)$ can be similarly proved.

Lemma 3.—
$$(1-\mu^2)\int_0^1 \frac{H_l(\mu')}{\mu+\mu'}\,d\mu' = \frac{H_l(\mu)-1}{\frac{3}{4}\mu H_l(\mu)} + (a_1 - \mu a_0)\,, \tag{85}$$

and

$$(1-\mu^2)\int_0^1 \frac{H_r(\mu')}{\mu+\mu'}\,d\mu' = \frac{H_r(\mu)-1}{\frac{3}{8}\mu H_r(\mu)} + (A_1 - \mu A_0)\,, \tag{86}$$

where a_0, a_1, A_0, and A_1 have the same meanings as in lemma 2.

The integral relation (85) can be proved in the following manner:

$$\left.\begin{aligned}
\int_0^1 \frac{H_l(\mu')}{\mu+\mu'}\,d\mu' &= \int_0^1 \frac{H_l(\mu')\,(1-\mu'^2)}{\mu+\mu'}\,d\mu' + \int_0^1 \frac{H_l(\mu')\,\mu'^2}{\mu+\mu'}\,d\mu' \\
&= \frac{H_l(\mu)-1}{\frac{3}{4}\mu H_l(\mu)} + \int_0^1 H_l(\mu')\left[\mu' - \mu + \frac{\mu^2}{\mu+\mu'}\right]d\mu' \\
&= \frac{H_l(\mu)-1}{\frac{3}{4}\mu H_l(\mu)} + (a_1 - \mu a_0) + \mu^2\int_0^1 \frac{H_l(\mu')}{\mu+\mu'}\,d\mu'.
\end{aligned}\right\} \tag{87}$$

Hence, the result. Equation (86) follows quite similarly.

8. *Verification of the solution.*—We shall now show that the solutions of the functional equations (49)–(52) are as stated in § 6. First, we may observe that if the constants q and c are related as in equation (59), then equations (41)–(44) and (65)–(68) will together lead to expressions for $S_{11}^{(0)}$, etc., which will be formally identical with equations (53)–(56); however, $H_l(\mu)$ and $H_r(\mu)$ will have to be understood (here as elsewhere) as satisfying the functional equations (69) and (70).[6] The proof that equations (65)–(68)

[6] We shall not repeat this every time. The expressions for the functions as products involving the Gaussian division of the interval (0, 1) and the relevant characteristic roots is only an approximation. As our discussion in Sec. III will emphasize, the exact H-functions always satisfy functional equations of the form (4), and in this paper we are seeking only exact solutions.

do represent the solution of equations (49)–(52) will therefore consist in showing that, with a suitable choice of q and c (compatible with eq. [59]), the substitution of $S_{11}^{(0)}$, etc., according to equations (53)–(56), in equations (45)–(48) will lead to ψ, ϕ, etc., which will be in agreement with equations (65)–(68).

Considering, first, $\phi(\mu)$, we have (cf. eqs. [46] and [53])

$$\left.\begin{aligned}\phi(\mu) &= 1-\mu^2+\tfrac{3}{4}\mu H_l(\mu)\int_0^1 \frac{d\mu'}{\mu+\mu'}(1-\mu'^2)\,H_l(\mu')\,[1-c\,(\mu+\mu')+\mu\mu'] \\ &= 1-\mu^2+\tfrac{3}{4}\mu H_l(\mu)\int_0^1 d\mu'\,(1-\mu'^2)\,H_l(\mu')\left[\mu-c+\frac{1-\mu^2}{\mu+\mu'}\right] \\ &= 1-\mu^2+\tfrac{3}{4}\mu\,(\mu-c)\,H_l(\mu)\int_0^1 H_l(\mu')\,(1-\mu'^2)\,d\mu' \\ &\qquad +\tfrac{3}{4}\mu\,(1-\mu^2)\,H_l(\mu)\int_0^1 \frac{H_l(\mu')\,(1-\mu'^2)}{\mu+\mu'}\,d\mu'.\end{aligned}\right\} \tag{88}$$

Using lemma 1 (eq. [71]) and recalling the functional equation satisfied by $H_l(\mu)$, we find

$$\phi(\mu) = 1-\mu^2+\mu\,(\mu-c)\,H_l(\mu)+(1-\mu^2)\,[H_l(\mu)-1] \tag{89}$$

or

$$\phi(\mu) = H_l(\mu)\,(1-c\mu)\,. \tag{90}$$

This is in agreement with equation (66).

Considering, next, $\phi+\psi$, we have (cf. eqs. [45] and [46])

$$\left.\begin{aligned}\phi(\mu)+\psi(\mu) &= 1+\frac{3}{8}\int_0^1 \frac{d\mu'}{\mu'}\,[S_{11}^{(0)}(\mu,\mu')+S_{12}^{(0)}(\mu,\mu')] \\ &= 1+\tfrac{3}{8}\mu H_l(\mu)\int_0^1 \frac{d\mu'}{\mu+\mu'}\Big[2H_l(\mu')\,[\![1-c\,(\mu+\mu')+\mu\mu']\!] \\ &\qquad +qH_r(\mu')\,(\mu+\mu')\Big] \\ &= 1+\tfrac{3}{8}q\mu H_l(\mu)\,A_0+\tfrac{3}{4}\mu H_l(\mu)\int_0^1 d\mu' H_l(\mu') \\ &\qquad \times\left[\mu-c+\frac{1-\mu^2}{\mu+\mu'}\right] \\ &= 1+\tfrac{3}{8}q\mu H_l(\mu)\,A_0+\tfrac{3}{4}\mu\,(\mu-c)\,H_l(\mu)\,a_0 \\ &\qquad +\tfrac{3}{4}\mu\,(1-\mu^2)\,H_l(\mu)\int_0^1 \frac{H_l(\mu')\,d\mu'}{\mu+\mu'},\end{aligned}\right\} \tag{91}$$

where, as in lemmas 2 and 3 (§ 7), a_0 and A_0 are the zero-order moments of $H_l(\mu)$ and $H_r(\mu)$. Using lemma 3 (eq. [85]) in the last step of the preceding reduction, we find

$$\phi(\mu)+\psi(\mu) = H_l(\mu)+\mu H_l(\mu)\,[\tfrac{3}{8}qA_0+\tfrac{3}{4}\,(a_1-a_0c)]\,. \tag{92}$$

From equations (90) and (92) we now obtain

$$\psi(\mu) = \mu H_l(\mu)\,[\tfrac{3}{8}qA_0+\tfrac{3}{4}\,(a_1-a_0c)+c]\,. \tag{93}$$

In order that this last equation may be in agreement with equation (65), we must require that

$$q = \tfrac{3}{8}qA_0+\tfrac{3}{4}\,(a_1-a_0c)+c\,. \tag{94}$$

Turning our attention next to $\zeta(\mu)$, we have (cf. eqs. [48] and [55])

$$\zeta(\mu) = \tfrac{3}{8} q\mu H_r(\mu) \int_0^1 H_l(\mu')(1-\mu'^2)\, d\mu', \tag{95}$$

or, using lemma 1 (eq. [71]), we obtain

$$\zeta(\mu) = \tfrac{1}{2} q\mu H_r(\mu), \tag{96}$$

in agreement with equation (68).

Finally, considering $\zeta(\mu) + \chi(\mu)$, we have (cf. eqs. [47] and [48])

$$\left.\begin{aligned}
\zeta(\mu) + \chi(\mu) &= 1 + \frac{3}{8}\int_0^1 \frac{d\mu'}{\mu'}\,[S_{21}^{(0)}(\mu,\mu') + S_{22}^{(0)}(\mu,\mu')] \\
&= 1 + \tfrac{3}{8}\mu H_r(\mu)\int_0^1 \frac{d\mu'}{\mu+\mu'}\,[qH_l(\mu')(\mu+\mu') + H_r(\mu') \\
&\qquad \times [\![1 + c(\mu+\mu') + \mu\mu']\!]] \\
&= 1 + \tfrac{3}{8} q\mu H_r(\mu)\, a_0 + \tfrac{3}{8}\mu(\mu+c) H_r(\mu)\, A_0 + \tfrac{3}{8}\mu(1-\mu^2) \\
&\qquad \times H_r(\mu)\int_0^1 \frac{H_r(\mu')}{\mu+\mu'}\, d\mu'.
\end{aligned}\right\} \tag{97}$$

Using lemma 3 (eq. [86]) and equation (96), we find, after some minor reductions, that

$$\chi(\mu) = H_r(\mu) + \mu H_r(\mu)\,[\tfrac{3}{8} q a_0 + \tfrac{3}{8}(A_1 + A_0 c) - \tfrac{1}{2} q]. \tag{98}$$

In order, now, that equation (98) may agree with equation (67), we must require that

$$c = \tfrac{3}{8} q a_0 + \tfrac{3}{8}(A_1 + A_0 c) - \tfrac{1}{2} q. \tag{99}$$

Equations (94) and (99), for the determination of the constants q and c, can be rewritten in the forms

$$(3A_0 - 8)\, q - 2(3a_0 - 4)\, c + 6a_1 = 0 \tag{100}$$

and

$$(3a_0 - 4)\, q + (3A_0 - 8)\, c + 3A_1 = 0. \tag{101}$$

Solving these equations, we find

$$q = -6\,\frac{a_1(3A_0 - 8) + A_1(3a_0 - 4)}{(3A_0 - 8)^2 + 2(3a_0 - 4)^2} \tag{102}$$

and

$$c = +3\,\frac{2a_1(3a_0 - 4) - A_1(3A_0 - 8)}{(3A_0 - 8)^2 + 2(3a_0 - 4)^2}. \tag{103}$$

It remains to prove that q and c, as given by equations (102) and (103), are compatible with the condition (eq. [59])

$$2(1 - c^2) = q^2, \tag{104}$$

which we have assumed. To show that this is the case, we evaluate $2(1 - c^2) - q^2$ according to equations (102) and (103). We find

$$2(1 - c^2) - q^2 = 2\,\frac{[(3A_0 - 8)^2 - 9A_1^2] - 2[9a_1^2 - (3a_0 - 4)^2]}{(3A_0 - 8)^2 + 2(3a_0 - 4)^2}. \tag{105}$$

On the other hand, using lemma 2 (eq. [82]), we find

$$(3A_0 - 8)^2 - 9A_1^2 = 9(A_0^2 - A_1^2) - 48A_0 + 64 = 16 . \tag{106}$$

Similarly, using equation (83), we find

$$9a_1^2 - (3a_0 - 4)^2 = 9(a_1^2 - a_0^2) + 24a_0 - 16 = 8 . \tag{107}$$

Hence, the right-hand side of equation (105) vanishes, and q and c are indeed related, as required.

This completes the verification.

It may be noted that, since we have incidentally shown that

$$(3A_0 - 8)^2 + 2(3a_0 - 4)^2 = 9(A_1^2 + 2a_1^2) , \tag{108}$$

the expressions (102) and (103) for q and c have the alternative forms

$$q = 2\,\frac{4(A_1 + 2a_1) - 3(A_0a_1 + a_0A_1)}{3(A_1^2 + 2a_1^2)} \tag{109}$$

and

$$c = \frac{8(A_1 - a_1) + 3(2a_1a_0 - A_0A_1)}{3(A_1^2 + 2a_1^2)} . \tag{110}$$

9. *The solutions of Systems (II) and (III).*—In contrast to System (I), the solutions of Systems (II) and (III) can be found without any difficulty, since an inspection of the equations of these two systems shows that all the functions $S^{(1)}$ are equal to each other, and similarly all the functions $S^{(2)}$ are equal to each other. Therefore, writing

$$S_{ij}^{(1)}(\mu, \mu_0) = S^{(1)}(\mu, \mu_0) \qquad (i, j = 1, 3) \tag{111}$$

and

$$S_{ij}^{(2)}(\mu, \mu_0) = S^{(2)}(\mu, \mu_0) \qquad (i, j = 1, 2, 3) , \tag{112}$$

we find that the equations of Systems (II) and (III) reduce to a single equation each for the two functions $S^{(1)}(\mu, \mu_0)$ and $S^{(2)}(\mu, \mu_0)$. We have

$$\left(\frac{1}{\mu} + \frac{1}{\mu_0}\right) S^{(1)}(\mu, \mu_0) = \left\{1 + \frac{3}{8}\int_0^1 \frac{d\mu''}{\mu''}(1 - \mu''^2)(1 + 2\mu''^2) S^{(1)}(\mu'', \mu_0)\right\} \times \left\{1 + \frac{3}{8}\int_0^1 \frac{d\mu'}{\mu'}(1 - \mu'^2)(1 + 2\mu'^2) S^{(1)}(\mu, \mu')\right\} \tag{113}$$

and

$$\left(\frac{1}{\mu} + \frac{1}{\mu_0}\right) S^{(2)}(\mu, \mu_0) = \left\{1 + \frac{3}{16}\int_0^1 \frac{d\mu''}{\mu''}(1 + \mu''^2)^2 S^{(2)}(\mu'', \mu_0)\right\} \times \left\{1 + \frac{3}{16}\int_0^1 \frac{d\mu'}{\mu'}(1 + \mu'^2)^2 S^{(2)}(\mu, \mu')\right\} . \tag{114}$$

From equations (113) and (114) it follows that the functions $S^{(1)}(\mu, \mu_0)$ and $S^{(2)}(\mu, \mu_0)$ are symmetrical in the variables μ and μ_0 and that they are expressible in the forms

$$\left(\frac{1}{\mu} + \frac{1}{\mu_0}\right) S^{(1)}(\mu, \mu_0) = H^{(1)}(\mu) H^{(1)}(\mu_0) \tag{115}$$

and

$$\left(\frac{1}{\mu}+\frac{1}{\mu_0}\right) S^{(2)}(\mu, \mu_0) = H^{(2)}(\mu)\, H^{(2)}(\mu_0)\,, \tag{116}$$

where $H^{(1)}(\mu)$ and $H^{(2)}(\mu)$ are solutions of the functional equations

$$H^{(1)}(\mu) = 1 + \tfrac{3}{8}\mu H^{(1)}(\mu) \int_0^1 \frac{H^{(1)}(\mu')}{\mu+\mu'} (1-\mu'^2)(1+2\mu'^2)\, d\mu \tag{117}$$

and

$$H^{(2)}(\mu) = 1 + \tfrac{3}{16}\mu H^{(2)}(\mu) \int_0^1 \frac{H^{(2)}(\mu')}{\mu+\mu'} (1+\mu'^2)^2 d\mu'\,. \tag{118}$$

It will be noticed that these functional equations for $H^{(1)}(\mu)$ and $H^{(2)}(\mu)$ again illustrate the correspondence between the functional equations which define them exactly and the approximate forms in terms of the Gaussian division and characteristic roots in which they appear in the method of solution of the earlier papers of this series.

We have now completed the solution of the functional equation for the scattering matrix $\boldsymbol{S}$. It will be observed that the solution for $\boldsymbol{S}$ which we have now obtained is of exactly the same form as that given in Paper XIII (eq. [65]), with the only difference that the four H-functions which appear in the solution are now defined in terms of the exact functional equations which they satisfy; further, the two constants, q and c, are shown to be related in a definite way with the moments of $H_l(\mu)$ and $H_r(\mu)$.

10. *The exact laws of darkening in the two states of polarization in an electron-scattering atmosphere.*—In Paper X we worked out a detailed theory of the radiative equilibrium of an atmosphere in which the Thomson scattering by free electrons governs the transfer of radiation. It was predicted that, under the circumstances considered, the emergent radiation should be polarized, the intensities in the two states of polarization showing different laws of darkening. We shall now see how an exact solution for this latter problem can be written down, using the results of the preceding sections.

In Paper X we showed that the emergent intensities $I_l(0, \mu)$ and $I_r(0, \mu)$ in the two states of polarization can be expressed in the forms (cf. Paper X, eqs. [128], [170], and [171] and nn. 15 and 17 in Paper XI)

$$I_l(0, \mu) = \tfrac{3}{8} F \frac{q}{\sqrt{2}} H_l(\mu) \tag{119}$$

and

$$I_r(0, \mu) = \tfrac{3}{8} F \frac{1}{\sqrt{2}} H_r(\mu)(\mu + c)\,, \tag{120}$$

where the constants q and c have the same meanings as in the problem of diffuse reflection which we have just considered. It therefore follows that the exact solutions for the emergent intensities $I_l(0, \mu)$ and $I_r(0, \mu)$ can be obtained by simply redefining the functions $H_l(\mu)$ and $H_r(\mu)$ as satisfying the functional equations (69) and (70) and determining the constants q and c according to equations (109) and (110). That we are justified in doing this is further confirmed by the fact that the total emergent flux given by equations (119) and (120) is exactly πF, as it should be; for, in order for this to be the case, it is clearly necessary that

$$\left.\begin{aligned} F = F_l + F_r &= 2\int_0^1 [I_l(0, \mu) + I_r(0, \mu)]\, \mu d\mu \\ &= \frac{3}{4\sqrt{2}} F (q a_1 + A_2 + c A_1) \end{aligned}\right\} \tag{121}$$

or that

$$q a_1 + A_2 + c A_1 = \tfrac{4}{3}\sqrt{2}\,. \tag{122}$$

The validity of equation (122) can be established as follows:
Evaluating $qa_1 + cA_1$ according to equations (109) and (110), we find that

$$qa_1 + cA_1 = \tfrac{8}{3} - A_0 . \tag{123}$$

Hence

$$qa_1 + A_2 + cA_1 = \tfrac{8}{3} + (A_2 - A_0) . \tag{124}$$

But lemma 1, equation (72), is equivalent to

$$A_0 - A_2 = \tfrac{4}{3}(2 - \sqrt{2}) ; \tag{125}$$

using this result in equation (124), we prove that equation (122) is, in fact, true.

III. ON A CLASS OF FUNCTIONAL EQUATIONS WHICH OCCURS IN THE THEORY OF RADIATIVE TRANSFER

11. The basic theorems.—The discussion of the problem of diffuse reflection from the point of view of the functional equation satisfied by the scattering matrix has disclosed two things: first, that there exists a class of functional equations of the form

$$H(\mu) = 1 + \mu H(\mu) \int_0^1 \frac{H(\mu')}{\mu + \mu'} \Psi(\mu')\, d\mu' , \tag{126}$$

which plays an important role in the theory of radiative transfer, and, second, that in a certain nth approximation the solution of equation (126) is given by equations (1) and (2). In Section III, we propose to examine this correspondence and establish some general theorems relating to functional equations of the type (126).

We shall begin our discussion by proving the following theorem, which appears to be the basic one in this subject.

Theorem 1.—Let $\Psi(\mu)$ be an even polynomial of degree $2m$ in μ, such that

$$\int_0^1 \Psi(\mu)\, d\mu \leqslant \tfrac{1}{2} . \tag{127}$$

Let $\mu_j (j = \pm 1, \ldots, \pm n)$ denote the division of the interval $(-1, +1)$ according to the zeros of the Legendre polynomial of order $2n (> m)$; further, let $a_j (= a_{-j})$ denote the corresponding Gaussian weights. Finally, let $k_\alpha (\alpha = 1, \ldots, n)$ denote the distinct positive (or zero) roots of the characteristic equation

$$1 = \sum_j \frac{a_j \Psi(\mu_j)}{1 + k\mu_j} = 2 \sum_{j=1}^{n} \frac{a_j \Psi(\mu_j)}{1 - k^2 \mu_j^2} . \tag{128}$$

Then the function

$$H(\mu) = \frac{1}{\mu_1 \ldots \mu_n} \frac{\prod_i (\mu + \mu_i)}{\prod_\alpha (1 + k_\alpha \mu)} \tag{129}$$

satisfies the equation

$$H(\mu) \equiv 1 + \mu H(\mu) \sum_{j=1}^{n} \frac{a_j H(\mu_j) \Psi(\mu_j)}{\mu + \mu_j} . \tag{130}$$

Proof.—Let us first consider the case

$$\int_0^1 \Psi(\mu)\, d\mu < \tfrac{1}{2} . \tag{131}$$

In this case the characteristic equation admits of n distinct nonvanishing positive roots, and we consider the function

$$S(\mu) = \sum_{\alpha=1}^{n} \frac{L_\alpha}{1 - k_\alpha \mu} + 1 , \tag{132}$$

where $L_\alpha (\alpha = 1, \ldots, n)$ are certain constants to be determined from the equations

$$\sum_{\alpha=1}^{n} \frac{L_\alpha}{1 - k_\alpha \mu_i} + 1 = 0 \qquad (i = 1, \ldots, n) , \tag{133}$$

or, equivalently,

$$S(\mu_i) = 0 \qquad (i = 1, \ldots, n) . \tag{134}$$

By considerations of a type that we are now familiar with, it can be shown that

$$S(\mu) = k_1 \ldots k_n \mu_1 \ldots \mu_n \frac{(-1)^n}{\mu_1 \ldots \mu_n} \frac{\prod_i (\mu - \mu_i)}{\prod_\alpha (1 - k_\alpha \mu)} . \tag{135}$$

In other words,

$$S(\mu) = k_1 \ldots k_n \mu_1 \ldots \mu_n H(-\mu) . \tag{136}$$

Since $H(0) = 1$, we can re-write equation (136) alternatively in the form

$$S(\mu) = S(0) H(-\mu) , \tag{137}$$

where

$$S(0) = \sum_{\alpha=1}^{n} L_\alpha + 1 = k_1 \ldots k_n \mu_1 \ldots \mu_n . \tag{138}$$

Now, since $\Psi(\mu)$ is even in μ, we can write the equation which a characteristic root satisfies in either of the forms

$$1 = \sum_j \frac{a_j \Psi(\mu_j)}{1 + k\mu_j} \tag{139}$$

or

$$1 = \sum_j \frac{a_j \Psi(\mu_j)}{1 - k\mu_j} . \tag{140}$$

Let k_α denote a particular characteristic root. Then, on account of equations (139) and (140), which are satisfied by any of the characteristic roots, we can clearly write:

$$\left.\begin{aligned} S(0) &= \sum_{\beta=1}^{n} L_\beta + 1 \\ &= \sum_{\beta=1}^{n} \frac{L_\beta}{k_\alpha + k_\beta} \left[\sum_j a_j \Psi(\mu_j) \left\{ \frac{k_\alpha}{1 + k_\alpha \mu_j} + \frac{k_\beta}{1 - k_\beta \mu_j} \right\} \right] \\ &\qquad + \sum_j \frac{a_j \Psi(\mu_j)}{1 + k_\alpha \mu_j} . \end{aligned}\right\} \tag{141}$$

Simplifying the quantity in brackets in the foregoing equation, we have

$$S(0) = \sum_{\beta=1}^{n} L_\beta \Big[\sum_j \frac{a_j \Psi(\mu_j)}{(1+k_\alpha \mu_j)(1-k_\beta \mu_j)} \Big] + \sum_j \frac{a_j \Psi(\mu_j)}{1+k_\alpha \mu_j}, \tag{142}$$

or, inverting the order of the summation,

$$S(0) = \sum_j \frac{a_j \Psi(\mu_j)}{1+k_\alpha \mu_j} \Big[\sum_{\beta=1}^{n} \frac{L_\beta}{1-k_\beta \mu_j} + 1 \Big]. \tag{143}$$

But the quantity in brackets in equation (143) is $S(\mu_j)$ (cf. eq. [132]). Hence

$$S(0) = \sum_j \frac{a_j S(\mu_j) \Psi(\mu_j)}{1+k_\alpha \mu_j}. \tag{144}$$

In equation (144) (as in eqs. [139]–[143]) the summation is, of course, extended over all values of j, positive and negative. However, since $S(\mu_j) = 0$ (eq. [134]), in equation (144), only the terms with negative j make a nonzero contribution. We can therefore write

$$S(0) = \sum_{j=1}^{n} \frac{a_j S(-\mu_j) \Psi(\mu_j)}{1-k_\alpha \mu_j} \qquad (\alpha = 1, \ldots, n), \tag{145}$$

or, in view of equation (137),

$$1 = \sum_{j=1}^{n} \frac{a_j H(\mu_j) \Psi(\mu_j)}{1-k_\alpha \mu_j} \qquad (\alpha = 1, \ldots, n). \tag{146}$$

Now consider the function

$$1 - \mu \sum_{j=1}^{n} \frac{a_j H(\mu_j) \Psi(\mu_j)}{\mu + \mu_j}. \tag{147}$$

According to equation (146), this vanishes for $\mu = -1/k_\alpha$ ($\alpha = 1, \ldots, n$); for

$$1 + \frac{1}{k_\alpha} \sum_{j=1}^{n} \frac{a_j H(\mu_j) \Psi(\mu_j)}{(-1/k_\alpha) + \mu_j} = 1 - \sum_{j=1}^{n} \frac{a_j H(\mu_j) \Psi(\mu_j)}{1-k_\alpha \mu_j} = 0. \tag{148}$$

Hence

$$\prod_{j=1}^{n} (\mu + \mu_j) - \mu \sum_{j=1}^{n} a_j H(\mu_j) \Psi(\mu_j) \prod_{i \neq j} (\mu + \mu_i) \tag{149}$$

also vanishes for

$$\mu = -\frac{1}{k_\alpha} \qquad (\alpha = 1, \ldots, n). \tag{150}$$

But the expression (149) is a polynomial of degree n in μ. It cannot, therefore, differ from

$$\prod_{\alpha=1}^{n} (1 + k_\alpha \mu) \tag{151}$$

by more than a constant factor; and the constant of proportionality is seen to be

$$\mu_1 \ldots \mu_n \tag{152}$$

from a comparison of the two functions at $\mu = 0$. It therefore follows that

$$1 - \mu \sum_{j=1}^{n} \frac{a_j H(\mu_j)\Psi(\mu_j)}{\mu + \mu_j} = \mu_1 \ldots \mu_n \frac{\prod_{a=1}^{n} (1 + k_a\mu)}{\prod_{j=1}^{n} (\mu + \mu_j)} = \frac{1}{H(\mu)}. \tag{153}$$

Hence

$$H(\mu) = 1 + \mu H(\mu) \sum_{j=1}^{n} \frac{a_j H(\mu_j)\Psi(\mu_j)}{\mu + \mu_j}, \tag{154}$$

which proves the theorem for the case (131).

Turning, now, to the case

$$\int_0^1 \Psi(\mu)\, d\mu = \tfrac{1}{2}, \tag{155}$$

we observe that, in this case, $k = 0$ is a root of the characteristic equation, and we are left with only $(n - 1)$ positive roots. We therefore consider in this case the function

$$S(\mu) = \sum_{a=1}^{n-1} \frac{L_a}{1 - k_a\mu} + L_0 - \mu \tag{156}$$

in place of equation (132). However, the constants L_0 and L_a $(a = 1, \ldots, n-1)$ are again to be determined by the conditions

$$S(\mu_i) = 0 \qquad (i = 1, \ldots, n). \tag{157}$$

With this definition of $S(\mu)$, equation (137) continues to be valid, and the rest of the proof follows on similar lines. The only essential point of departure that needs to be noted is that, at the stage of the proof corresponding to equation (142) and before inverting the order of the summation, we must add the extra term

$$-\sum_j \frac{a_j \Psi(\mu_j)\, \mu_j}{1 + k_a\mu_j} \tag{158}$$

to the right-hand side of the equation. We can do this without altering anything, since the quantity we thus add is zero; for

$$\left.\begin{aligned} \sum_j \frac{a_j \Psi(\mu_j)\, \mu_j}{1 + k_a\mu_j} &= \frac{1}{k_a}\Big[\sum_j a_j \Psi(\mu_j) \Big\{1 - \frac{1}{1 + k_a\mu_j}\Big\}\Big] \\ &= \frac{1}{k_a}\Big[1 - \sum_j \frac{a_j \Psi(\mu_j)}{1 + k_a\mu_j}\Big] = 0. \end{aligned}\right\} \tag{159}$$[7]

For the rest, the proof is exactly the same as in case (127).

This completes the proof of the theorem.

[7] Note that we are permitted to set $\sum_j a_j \Psi(\mu_j) = 1$, since the Gauss sum in the "nth approximation" evaluates the integrals exactly for all polynomials of degree less than or equal to $4n - 1$; and we have assumed that $2n > m$.

Theorem 2.—The solution of the functional equation

$$H(\mu) = 1 + \mu H(\mu) \int_0^1 \frac{H(\mu')\Psi(\mu')}{\mu + \mu'} d\mu', \tag{160}$$

where $\Psi(\mu)$ is an even polynomial satisfying the condition

$$\int_0^1 \Psi(\mu)\, d\mu \leqslant \tfrac{1}{2}, \tag{161}$$

is the limit function

$$\lim_{n \to \infty} \frac{1}{\mu_1 \cdot \cdots \cdot \mu_n} \frac{\prod_{i=1}^{n} (\mu + \mu_i)}{\prod_a (1 + k_a \mu)}, \tag{162}$$

where the μ_i's and the k_a's have the same meanings as in theorem 1.

Proof.—The theorem arises in the following way: It is known that the integral of a bounded function over the interval (0, 1) can be approximated by a Gauss sum with any desired degree of accuracy by choosing a division of the interval according to the zeros of a Legendre polynomial of a sufficiently high degree. The integral which occurs on the right-hand side of equation (160) can therefore be replaced by the Gauss sum

$$\sum_{j=1}^{n} \frac{a_j H(\mu_j)\Psi(\mu_j)}{\mu + \mu_j} \tag{163}$$

to any desired accuracy by choosing a sufficiently large n. But by theorem 1, for a finite n, no matter how large, the solution of the equation

$$H(\mu) = 1 + \mu H(\mu) \sum_{j=1}^{n} \frac{a_j H(\mu_j)\Psi(\mu_j)}{\mu + \mu_j} \tag{164}$$

is always given by equation (129). Hence, if we now let $n \to \infty$, equation (164) becomes equation (160), and the solution for $H(\mu)$ is recovered as the limit function (162).

It is realized that the proof of theorem 2 which we have given is only a sketch and that it does not meet the full demands of a rigorous mathematical demonstration. But there can be hardly any doubt that a proof meeting such demands could be constructed, if one so desired, along the lines indicated.[8]

12. *Some integral properties of the functions* $H(\mu)$.—There are a number of integral theorems (of an essentially elementary kind) which can be proved for functions satisfying equations of the form (126). These theorems have applications in the further development of the theory, but they have also some physical interest.

Theorem 3.— $$\int_0^1 H(\mu)\Psi(\mu)\, d\mu = 1 - \left[1 - 2\int_0^1 \Psi(\mu)\, d\mu\right]^{1/2}. \tag{165}$$

[8] It is probable that questions of "uniqueness" and "existence" will cause the principal difficulties in the construction of a rigorous mathematical proof. In our discussion we have implicitly assumed both, since the equations arise in a physical context and the physical situations are such as to leave no room for ambiguity. In any event, to go into mathematical subtleties here will be to go beyond the scope of a physical investigation.

Proof.—Multiplying the equation satisfied by $H(\mu)$ by $\Psi(\mu)$ and integrating over the range of μ, we have

$$\left.\begin{aligned}\int_0^1 H(\mu)\Psi(\mu)\,d\mu \\ = \int_0^1 \Psi(\mu)\,d\mu + \int_0^1\int_0^1 \frac{\mu}{\mu+\mu'} H(\mu)\Psi(\mu)\,H(\mu')\Psi(\mu')\,d\mu d\mu'.\end{aligned}\right\} \quad (166)$$

Interchanging μ and μ' in the double integral in equation (166) and taking the average of the two equations, we obtain

$$\left.\begin{aligned}\int_0^1 H(\mu)\Psi(\mu)\,d\mu \\ = \int_0^1 \Psi(\mu)\,d\mu + \frac{1}{2}\int_0^1\int_0^1 H(\mu)\Psi(\mu)\,H(\mu')\Psi(\mu')\,d\mu d\mu'\end{aligned}\right\} \quad (167)$$

or, alternatively,

$$\frac{1}{2}\Big[\int_0^1 H(\mu)\Psi(\mu)\,d\mu\Big]^2 - \int_0^1 H(\mu)\Psi(\mu)\,d\mu + \int_0^1 \Psi(\mu)\,d\mu = 0. \quad (168)$$

Solving this equation for the integral in question, we have

$$\int_0^1 H(\mu)\Psi(\mu)\,d\mu = 1 \pm \Big[1 - 2\int_0^1 \Psi(\mu)\,d\mu\Big]^{1/2}. \quad (169)$$

The ambiguity in the sign in equation (169) can be removed by the consideration that the integral on the left-hand side must uniformly converge to zero when $\Psi(\mu)$ tends to zero uniformly in the interval (0, 1). This requires us to choose the negative sign in equation (169), and the result stated follows.

Corollary 1.—A necessary and sufficient condition that $H(\mu)$ be real is

$$\int_0^1 \Psi(\mu)\,d\mu \leqslant \tfrac{1}{2}. \quad (170)$$

This is, of course, an immediate consequence of the theorem.

The physical meaning of the limitation (170) is interesting; for it is really equivalent to the condition that, on each scattering, more radiation should not be emitted than was incident. Further, it may be noted that we have the equality sign in (170) only in the *conservative case*, i.e., only when there is no absorption and the efficiency of scattering is unity.

Corollary 2.—An alternative form of the functional equation satisfied by $H(\mu)$ is

$$1 = H(\mu)\left\{\Big[1 - 2\int_0^1 \Psi(\mu)\,d\mu\Big]^{1/2} + \int_0^1 \frac{\mu'}{\mu+\mu'} H(\mu')\Psi(\mu')\,d\mu'\right\}. \quad (171)$$

Proof.—This can be proved as follows: Using the result of theorem 3 and recalling the functional equation satisfied by $H(\mu)$, we have

$$\left.\begin{aligned}H(\mu)\int_0^1 \frac{\mu'}{\mu+\mu'} H(\mu')\Psi(\mu')\,d\mu' &= H(\mu)\int_0^1 H(\mu')\Psi(\mu')\Big[1 - \frac{\mu}{\mu+\mu'}\Big]d\mu' \\ &= H(\mu)\left\{1 - \Big[1 - 2\int_0^1 \Psi(\mu)\,d\mu\Big]^{1/2}\right\} - H(\mu) + 1 \\ &= 1 - H(\mu)\Big[1 - 2\int_0^1 \Psi(\mu)\,d\mu\Big]^{1/2},\end{aligned}\right\} \quad (172)$$

which is equivalent to equation (171).

We may note in this connection that for the practical purposes of iterating known approximate solutions of $H(\mu)$, the equation in the form (171) is more efficient than the original.

Theorem 4.—
$$\left.\begin{aligned}\left[1-2\int_0^1\Psi(\mu)\,d\mu\right]^{1/2}\int_0^1 H(\mu)\Psi(\mu)\,\mu^2 d\mu \\ +\frac{1}{2}\left[\int_0^1 H(\mu)\Psi(\mu)\,\mu d\mu\right]^2=\int_0^1\Psi(\mu)\,\mu^2 d\mu\,.\end{aligned}\right\}\quad(173)$$

Proof.—To prove equation (173) we multiply the equation defining $H(\mu)$ by $\Psi(\mu)\mu^2$ and integrate over the range of μ. We find

$$\left.\begin{aligned}&\int_0^1 H(\mu)\Psi(\mu)\,\mu^2 d\mu \\ &=\int_0^1\Psi(\mu)\,\mu^2 d\mu+\int_0^1\int_0^1\frac{H(\mu)H(\mu')\Psi(\mu)\Psi(\mu')}{\mu+\mu'}\,\mu^3 d\mu d\mu' \\ &=\int_0^1\Psi(\mu)\,\mu^2 d\mu+\frac{1}{2}\int_0^1\int_0^1\frac{H(\mu)H(\mu')\Psi(\mu)\Psi(\mu')}{\mu+\mu'}\,(\mu^3+\mu'^3)\,d\mu d\mu' \\ &=\int_0^1\Psi(\mu)\,\mu^2 d\mu+\frac{1}{2}\int_0^1\int_0^1 H(\mu)H(\mu')\Psi(\mu)\Psi(\mu')\,(\mu^2-\mu\mu'+\mu'^2)\,d\mu d\mu' \\ &=\int_0^1\Psi(\mu)\,\mu^2 d\mu+\left[\int_0^1 H(\mu)\Psi(\mu)\,\mu^2 d\mu\right]\left[\int_0^1 H(\mu)\Psi(\mu)\,d\mu\right] \\ &\qquad-\frac{1}{2}\left[\int_0^1 H(\mu)\Psi(\mu)\,\mu d\mu\right]^2.\end{aligned}\right\}\quad(174)$$

Using theorem 3, we obtain, after some minor reductions,

$$\left.\begin{aligned}\left[1-2\int_0^1\Psi(\mu)\,d\mu\right]^{1/2}\int_0^1 H(\mu)\Psi(\mu)\,\mu^2 d\mu+\frac{1}{2}\left[\int_0^1 H(\mu)\Psi(\mu)\,\mu d\mu\right]^2 \\ =\int_0^1\Psi(\mu)\,\mu^2 d\mu\,,\end{aligned}\right\}\quad(175)$$

which is the required result.

Corollary 1.—For the conservative case

$$\int_0^1\Psi(\mu)\,d\mu=\tfrac{1}{2}\,,\qquad(176)$$

we have the further integral,

$$\int_0^1 H(\mu)\Psi(\mu)\,\mu d\mu=\left[2\int_0^1\Psi(\mu)\,\mu^2 d\mu\right]^{1/2}.\qquad(177)$$

This last relation (177) throws some interesting light on the Hopf-Bronstein relation (Paper II, eq. [71]) between the boundary and the effective temperatures in a gray atmosphere in radiative equilibrium; for, in this case, the appropriate functional equation is

$$H(\mu)=1+\tfrac{1}{2}\mu H(\mu)\int_0^1\frac{H(\mu')}{\mu+\mu'}\,d\mu'.\qquad(178)$$

Consequently,

$$\Psi(\mu)=\text{constant}=\tfrac{1}{2}\,,\qquad(179)$$

and the case is a conservative one. We have, accordingly, the two integrals,[9]

$$\int_0^1 H(\mu)\, d\mu = 2 \tag{180}$$

and

$$\int_0^1 H(\mu)\, \mu d\mu = \frac{2}{\sqrt{3}}. \tag{181}$$

On the other hand, since for this problem (cf. Paper II)

$$I(0, \mu) \propto H(\mu), \tag{182}$$

we have

$$\frac{J(0)}{F} = \frac{\int_0^1 H(\mu)\, d\mu}{4\int_0^1 H(\mu)\, \mu d\mu} = \frac{\sqrt{3}}{4}, \tag{183}$$

which is the Hopf-Bronstein integral. We therefore conclude that for all conservative cases of radiative transfer we have an integral of the Hopf-Bronstein type, which is essentially that given by equation (177). We may give two further examples of such integrals.

i) Considering, first, the case of a semi-infinite atmosphere in radiative equilibrium (with no incident radiation) and scattering radiation in accordance with Rayleigh's phase function, we have a functional equation of our standard form with (cf. Sec. V)

$$\Psi(\mu) = \tfrac{3}{16}(3 - \mu^2). \tag{184}$$

The integral of this function over μ is $\frac{1}{2}$, and we have a conservative case. The two integrals are

$$\int_0^1 H(\mu)(3 - \mu^2)\, d\mu = \tfrac{16}{3} \tag{185}$$

and

$$\int_0^1 H(\mu)(3 - \mu^2)\, \mu d\mu = \tfrac{16}{3}\ \sqrt{0.3}. \tag{186}$$

These equations imply that

$$\frac{\int_0^1 I(0, \mu)(3 - \mu^2)\, d\mu}{\int_0^1 I(0, \mu)(3 - \mu^2)\, \mu d\mu} = \frac{1}{\sqrt{0.3}}. \tag{187}$$

It can be shown that equation (187) is equivalent to a curious relation which was established in Paper III (eq. [67]).

ii) The equation for $H_l(\mu)$, which we have discussed in Section II, also corresponds to a conservative case, since this equation is characterized by (cf. eq. [69])

$$\Psi(\mu) = \tfrac{3}{4}(1 - \mu^2), \tag{188}$$

and the integral of this over μ is $\frac{1}{2}$. The two integrals now are

$$\int_0^1 H_l(\mu)(1 - \mu^2)\, d\mu = \tfrac{4}{3} \tag{189}$$

and

$$\int_0^1 H_l(\mu)(1 - \mu^2)\, \mu d\mu = \tfrac{4}{3}\sqrt{0.2}. \tag{189'}$$

[9] The first of these is contained in Ambarzumian's paper (*op. cit.*), but the second is not.

Hence, for the problem of an electron-scattering atmosphere,

$$\frac{\int_0^1 I_l(0,\mu)(1-\mu^2)\,d\mu}{\int_0^1 I_l(0,\mu)(1-\mu^2)\,\mu d\mu} = \sqrt{5}. \tag{190}$$

Corollary 2.—For the conservative case, an alternative form of the functional equation satisfied by $H(\mu)$ is

$$H(\mu)\left\{\left[2\int_0^1 \Psi(\mu)\,\mu^2 d\mu\right]^{1/2} - \int_0^1 \frac{\mu'^2}{\mu+\mu'} H(\mu')\Psi(\mu')\,d\mu'\right\} = \mu. \tag{191}$$

This readily follows from equations (165) and (177).

Theorem 5.—

$$\left.\begin{aligned}\int_0^1 H(\mu)\Psi(\mu)\,\mu^{2n}d\mu &= \int_0^1 \Psi(\mu)\,\mu^{2n}d\mu + \tfrac{1}{2}(-1)^n\left[\int_0^1 H(\mu)\Psi(\mu)\,\mu^n d\mu\right]^2 \\ &+ \sum_{m=0}^{n-1}(-1)^m\left[\int_0^1 H(\mu)\Psi(\mu)\,\mu^{2n-m}d\mu\right]\left[\int_0^1 H(\mu)\Psi(\mu)\,\mu^m d\mu\right].\end{aligned}\right\} \tag{192}$$

This is a generalization of theorem 4, and the proof follows on similar lines.

Theorem 6.—For a function $H(\mu)$ satisfying a functional equation of the form

$$H(\mu) = 1 + \mu H(\mu)\int_0^1 \frac{H(\mu')(a+b\mu'^2)}{\mu+\mu'}\,d\mu', \tag{193}$$

where a and b are two constants, we have the relations

$$\alpha_0 = 1 + \tfrac{1}{2}(a\alpha_0^2 + b\alpha_1^2) \tag{194}$$

and

$$(a+b\mu^2)\int_0^1 \frac{H(\mu')}{\mu+\mu'}\,d\mu' = \frac{H(\mu)-1}{\mu H(\mu)} - b(\alpha_1 - \mu\alpha_0), \tag{195}$$

where α_0 and α_1 are the moments of order zero and one of $H(\mu)$.

The proof of this theorem follows on exactly the same lines as those of lemmas 2 and 3 (§ 7).

IV. THE SOLUTION OF THE FUNCTIONAL EQUATIONS FOR THE PROBLEM OF DIFFUSE REFLECTION IN ACCORDANCE WITH THE PHASE FUNCTION $\lambda(1 + x\cos\Theta)$

13. *The functional equations of the problem.*—The problem of diffuse reflection in accordance with the phase function $\lambda(1 + x\cos\Theta)$ ($\lambda \leqslant 1$ and $-1 \leqslant x \leqslant 1$) was treated in Paper IX, and Ambarzumian (*op. cit.*) derived the relevant functional equations of the problem by his method. However, our object in considering this problem again is principally to show how a knowledge of the form of the solution gained from our analysis in Paper IX enables us to reduce a pair of functional equations, which Ambarzumian has derived for the azimuth independent term in the *scattering function*, to a single functional equation of the standard form.

Now, if we express the intensity $I(\mu, \varphi; \mu_0, \varphi_0)$ reflected in the direction (μ, φ) when a parallel beam of radiation of net flux πF per unit area normal to itself is incident in the direction $(-\mu_0, \varphi_0)$ in the form

$$I(\mu, \varphi; \mu_0, \varphi_0) = \frac{\lambda}{4\mu} S(\mu, \varphi; \mu_0, \varphi_0) F, \tag{196}$$

the scattering function $S(\mu, \varphi; \mu_0, \varphi_0)$ satisfies the functional equation (cf. Ambarzumian, *op. cit.*, eq. [10])

$$\left.\begin{aligned}\left(\frac{1}{\mu}+\frac{1}{\mu_0}\right)S(\mu,\varphi;\mu_0,\varphi_0) = j(\mu,\varphi;\mu_0,\varphi_0)+\frac{\lambda}{4\pi}\int_0^1\int_0^{2\pi} j(\mu,\varphi;-\mu'',\varphi'')\\ \times S(\mu'',\varphi'';\mu_0,\varphi_0)\frac{d\mu''}{\mu''}\,d\varphi''+\frac{\lambda}{4\pi}\int_0^1\int_0^{2\pi} S(\mu,\varphi;\mu',\varphi')\\ \times j(-\mu',\varphi';\mu_0,\varphi_0)\frac{d\mu'}{\mu'}\,d\varphi'+\frac{\lambda^2}{16\pi^2}\int_0^1\int_0^{2\pi}\int_0^1\int_0^{2\pi} S(\mu,\varphi;\mu',\varphi')\\ \times j(-\mu',\varphi';-\mu'',\varphi'')\,S(\mu'',\varphi'';\mu_0,\varphi_0)\frac{d\mu'}{\mu'}\,d\varphi'\,\frac{d\mu''}{\mu''}\,d\varphi'',\end{aligned}\right\} \tag{197}$$

where, to exhibit the analogy with the equation for the scattering matrix derived in Section I (eq. [31]), we have written

$$j(\mu,\varphi;\mu_0,\varphi_0) = 1-x\mu\mu_0+x(1-\mu^2)^{\frac{1}{2}}(1-\mu_0^2)^{\frac{1}{2}}\cos(\varphi-\varphi_0)\,. \tag{198}$$

An examination of equation (197) shows that we can express the scattering function in the form

$$S(\mu,\varphi;\mu_0,\varphi_0) = S^{(0)}(\mu,\mu_0)+x(1-\mu^2)^{\frac{1}{2}}(1-\mu_0^2)^{\frac{1}{2}}S^{(1)}(\mu,\mu_0)\cos(\varphi-\varphi_0)\,, \tag{199}$$

where, as the notation indicates, $S^{(0)}$ and $S^{(1)}$ are functions of μ and μ_0 only. Substituting this form for S in equation (197), we obtain the two equations

$$\left.\begin{aligned}\left(\frac{1}{\mu}+\frac{1}{\mu_0}\right)S^{(0)}(\mu,\mu_0) = 1-x\mu\mu_0+\tfrac{1}{2}\lambda\int_0^1(1+x\mu\mu'')\,S^{(0)}(\mu'',\mu_0)\frac{d\mu''}{\mu''}\\ +\tfrac{1}{2}\lambda\int_0^1 S^{(0)}(\mu,\mu')(1+x\mu'\mu_0)\frac{d\mu'}{\mu'}+\tfrac{1}{4}\lambda^2\int_0^1\int_0^1 S^{(0)}(\mu,\mu')(1-x\mu'\mu'')\\ \times S^{(0)}(\mu'',\mu_0)\frac{d\mu'}{\mu'}\frac{d\mu''}{\mu''}\end{aligned}\right\} \tag{200}$$

and

$$\left.\begin{aligned}\left(\frac{1}{\mu}+\frac{1}{\mu_0}\right)S^{(1)}(\mu,\mu_0) = \left\{1+\tfrac{1}{4}x\lambda\int_0^1\frac{d\mu''}{\mu''}(1-\mu''^2)\,S^{(1)}(\mu'',\mu_0)\right\}\\ \times\left\{1+\tfrac{1}{4}x\lambda\int_0^1\frac{d\mu'}{\mu'}(1-\mu'^2)\,S^{(1)}(\mu,\mu')\right\}.\end{aligned}\right\} \tag{201}$$

Of these two functional equations, only equation (200) requires any detailed consideration, since it is at once apparent that the solution of equation (201) must be of the form

$$\left(\frac{1}{\mu}+\frac{1}{\mu_0}\right)S^{(1)}(\mu,\mu_0) = H^{(1)}(\mu)\,H^{(1)}(\mu_0)\,, \tag{202}$$

where $H^{(1)}(\mu)$ satisfies the equation

$$H^{(1)}(\mu) = 1+\tfrac{1}{4}x\lambda\mu H^{(1)}(\mu)\int_0^1\frac{H^{(1)}(\mu')}{\mu+\mu'}(1-\mu'^2)\,d\mu'\,. \tag{203}$$

Our subsequent discussions in this section will therefore be concerned with only equation (200).

14. *The reduction of the functional equation for* $S^{(0)}(\mu, \mu_0)$ *to their normal forms.*—On examination it is seen that equation (200) can be written in the form

$$\left(\frac{1}{\mu}+\frac{1}{\mu_0}\right) S^{(0)}(\mu, \mu_0) = \left\{1+\tfrac{1}{2}\lambda\int_0^1 S^{(0)}(\mu'', \mu_0)\frac{d\mu''}{\mu''}\right\} \times \left\{1+\tfrac{1}{2}\lambda\int_0^1 S^{(0)}(\mu, \mu')\frac{d\mu'}{\mu'}\right\} - x\left\{\mu_0-\tfrac{1}{2}\lambda\int_0^1 S^{(0)}(\mu'', \mu_0)\,d\mu''\right\}\left\{\mu-\tfrac{1}{2}\lambda\int_0^1 S^{(0)}(\mu, \mu')\,d\mu'\right\}. \quad (204)$$

From this equation it follows that $S^{(0)}(\mu, \mu_0)$ is symmetrical in μ and μ_0 and, further, that it can be expressed in the form

$$\left(\frac{1}{\mu}+\frac{1}{\mu_0}\right) S^{(0)}(\mu, \mu_0) = \psi(\mu)\psi(\mu_0) - x\phi(\mu)\phi(\mu_0), \quad (205)$$

where

$$\psi(\mu) = 1+\tfrac{1}{2}\lambda\int_0^1 S^{(0)}(\mu, \mu')\frac{d\mu'}{\mu'} \quad (206)$$

and

$$\phi(\mu) = \mu-\tfrac{1}{2}\lambda\int_0^1 S^{(0)}(\mu, \mu')\,d\mu'. \quad (207)$$

Now, substituting for $S^{(0)}$ from equation (205) back into equations (206) and (207), we obtain the functional equations in their normal forms. We have

$$\psi(\mu) = 1+\tfrac{1}{2}\lambda\mu\psi(\mu)\int_0^1 \frac{\psi(\mu')}{\mu+\mu'}\,d\mu' - \tfrac{1}{2}x\lambda\mu\phi(\mu)\int_0^1 \frac{\phi(\mu')}{\mu+\mu'}\,d\mu' \quad (208)$$

and

$$\phi(\mu) = \mu-\tfrac{1}{2}\lambda\mu\psi(\mu)\int_0^1 \frac{\psi(\mu')}{\mu+\mu'}\,\mu'd\mu' + \tfrac{1}{2}x\lambda\mu\phi(\mu)\int_0^1 \frac{\phi(\mu')}{\mu+\mu'}\,\mu'd\mu'. \quad (209)$$

These equations agree with those given by Ambarzumian (*op. cit.*).

15. *The solutions of the functional equations (208) and (209).*—As in our discussion of the functional equations (49)–(52) in Section II, we shall be guided in the present instance also by the form of the solutions obtained by directly solving the relevant equation of transfer. We shall, therefore, first re-write the solution given in Paper IX in a form in which it can be compared with equation (205).

Now the solution for $I^{(0)}(0, \mu)$ given in Paper IX (eq. [108]) is equivalent to

$$\left(\frac{1}{\mu}+\frac{1}{\mu_0}\right) S^{(0)}(\mu, \mu_0) = H^{(0)}(\mu)\,H^{(0)}(\mu_0)\,[1-c(\mu+\mu_0)-x(1-\lambda)\mu\mu_0], \quad (210)$$

where $H^{(0)}(\mu)$ is defined in terms of the roots of the characteristic equation (Paper IX, eq. [26])

$$1 = \lambda\sum_{j=1}^{n}\frac{a_j[1+x(1-\lambda)\mu_j^2]}{1-k^2\mu_j^2}. \quad (211)$$

Further, in equation (210), we have written c in place of $x(1-\lambda)\sigma/\rho$, which occurs in Paper IX, equation (108).

We now re-write solution (210) in the form

$$\left(\frac{1}{\mu}+\frac{1}{\mu_0}\right) S^{(0)}(\mu,\mu_0) = [H^{(0)}(\mu)(1-c\mu)]\,[H^{(0)}(\mu_0)(1-c\mu_0)] - x\,[q\mu H^{(0)}(\mu)]\,[q\mu_0 H^{(0)}(\mu_0)]\,, \tag{212}$$

where

$$xq^2 = c^2 + x(1-\lambda)\,. \tag{213}$$

The similarity of equations (212) and (205) is evident. Again, though solution (208) can be brought into such a correspondence with equation (205) in other ways, it will appear that we have made the correct choice in writing it as we have done. Indeed, we shall presently prove that the solution of the functional equations (208) and (209) are of the forms

$$\psi(\mu) = H^{(0)}(\mu)(1-c\mu) \tag{214}$$

and

$$\phi(\mu) = q\mu H^{(0)}(\mu)\,, \tag{215}$$

where $H^{(0)}(\mu)$ is now defined as the solution of the functional equation

$$H^{(0)}(\mu) = 1 + \tfrac{1}{2}\lambda\mu H^{(0)}(\mu)\int_0^1 \frac{H^{(0)}(\mu')}{\mu+\mu'}\,[1+x(1-\lambda)\,\mu'^2]\,d\mu'\,, \tag{216}$$

and q and c are two constants related in the manner of equation (213) and expressible in terms of the moments of $H^{(0)}(\mu)$.

16. *The verification of the solution.*—Before we proceed to prove that the solution of equations (208) and (209) is as we have stated it in § 15, we may note that, since the functional equation (216) is of the form considered in theorem 6 (§ 12), we have the relations

$$\alpha_0 = 1 + \tfrac{1}{4}\lambda\,[\alpha_0^2 + x(1-\lambda)\,\alpha_1^2] \tag{217}$$

and

$$[1+x(1-\lambda)\,\mu^2]\int_0^1 \frac{H^{(0)}(\mu')}{\mu+\mu'}\,d\mu' = \frac{H^{(0)}(\mu)-1}{\tfrac{1}{2}\lambda\mu H^{(0)}(\mu)} - x(1-\lambda)(\alpha_1-\mu\alpha_0)\,, \tag{218}$$

where α_0 and α_1 are the moments of order zero and one of $H^{(0)}(\mu)$.

Our proof that equations (214) and (215) do represent the solution of equations (208) and (209) will consist in showing that, with a suitable choice of q and c (compatible with eq. [213]), the substitution of $S^{(0)}$ according to equation (210) (with $H^{(0)}$ now defined as the solution of eq. [216]) in equations (206) and (207) leads to ψ and ϕ, which are in agreement with equations (214) and (215).

Considering, first, $\psi(\mu)$, we have

$$\begin{aligned}\psi(\mu) &= 1 + \tfrac{1}{2}\lambda\mu H^{(0)}(\mu)\int_0^1 \frac{d\mu'}{\mu+\mu'}\,H^{(0)}(\mu')\,[1-c(\mu+\mu') - x(1-\lambda)\,\mu\mu'] \\ &= 1 + \tfrac{1}{2}\lambda\mu H^{(0)}(\mu)\int_0^1 d\mu' H^{(0)}(\mu')\left[\frac{1+x(1-\lambda)\,\mu^2}{\mu+\mu'} - c - x(1-\lambda)\,\mu\right].\end{aligned} \tag{219}$$

The right-hand side of equation (219) can be simplified by using equation (218). We find in this manner that

$$\psi(\mu) = H^{(0)}(\mu)\,[1 - \tfrac{1}{2}\lambda\mu\{c\alpha_0 + x(1-\lambda)\,\alpha_1\}]\,. \tag{220}$$

In order that equation (220) may be in agreement with equation (214), we must require that

$$c = \tfrac{1}{2}\lambda\,[c a_0 + x\,(1-\lambda)\,a_1] \tag{221}$$

or that

$$c = x\lambda\,(1-\lambda)\,\frac{a_1}{2-\lambda a_0}. \tag{222}$$

Considering, next, $\phi(\mu)$, we find in a similar way from equations (207) and (210) that

$$\phi(\mu) = [1 + \tfrac{1}{2}\lambda\,(c a_1 - a_0)]\,\mu H^{(0)}(\mu). \tag{223}$$

The agreement of equations (215) and (223) now requires that

$$q = 1 + \tfrac{1}{2}\lambda\,(c a_1 - a_0). \tag{224}$$

Substituting for c from equation (22) in equation (224), we find, after some minor rearranging of the terms, that

$$q = \frac{4 - 4a_0\lambda + \lambda^2\,[a_0^2 + x\,(1-\lambda)\,a_1^2]}{2\,(2-\lambda a_0)}. \tag{225}$$

The term in brackets in the numerator of equation (225) can be simplified by using relation (217) between the moments of $H^{(0)}(\mu)$. We find that

$$q = \frac{2\,(1-\lambda)}{2-\lambda a_0}. \tag{226}$$

It remains to verify that q and c, as given by equations (222) and (226), are consistent with relation (213), which we have assumed. To show that this is the case, we evaluate

$$q^2 - \frac{c^2}{x} \tag{227}$$

according to equations (222) and (226). We find that

$$\left.\begin{aligned} q^2 - \frac{c^2}{x} &= \frac{1}{(2-\lambda a_0)^2}\left[4\,(1-\lambda)^2 - x\lambda^2\,(1-\lambda^2)\,a_1^2\right] \\ &= \frac{1-\lambda}{(2-\lambda a_0)^2}\left[4\,(1-\lambda) - x\lambda^2\,(1-\lambda)\,a_1^2\right]. \end{aligned}\right\} \tag{228}$$

But (cf. eq. [217])

$$-x\lambda^2\,(1-\lambda)\,a_1^2 = 4\lambda\,(1 - a_0 + \tfrac{1}{4}\lambda a_0^2); \tag{229}$$

using this relation in equation (228), we find that

$$q^2 - \frac{c^2}{x} = 1 - \lambda, \tag{230}$$

which shows that q and c, as defined by equations (222) and (226), are indeed related, as required.

This completes the verification.

V. THE SOLUTION OF THE FUNCTIONAL EQUATIONS FOR THE PROBLEM OF DIFFUSE REFLECTION IN ACCORDANCE WITH RAYLEIGH'S PHASE FUNCTION

17. *The functional equations of the problem.*—For this problem we write the reflected intensity $I(\mu, \varphi; \mu_0, \varphi_0)$ in the form

$$\left.\begin{aligned} \mu I(\mu, \varphi; \mu_0, \varphi_0) &= \tfrac{3}{32} F [S^{(0)}(\mu, \mu_0) - 4\mu\mu_0 (1-\mu^2)^{\frac{1}{2}} (1-\mu_0^2)^{\frac{1}{2}} \\ &\times S^{(1)}(\mu, \mu_0) \cos(\varphi - \varphi_0) + (1-\mu^2)(1-\mu_0^2) S^{(2)}(\mu, \mu_0) \cos 2(\varphi - \varphi_0)], \end{aligned}\right\} \quad (231)$$

and find for $S^{(0)}(\mu, \mu_0)$, $S^{(1)}(\mu, \mu_0)$, and $S^{(2)}(\mu, \mu_0)$ the functional equations

$$\left.\begin{aligned} \left(\frac{1}{\mu} + \frac{1}{\mu_0}\right) S^{(0)}(\mu, \mu_0) &= j^{(0)}(\mu, \mu_0) + \tfrac{3}{16} \int_0^1 j^{(0)}(\mu, \mu'') S^{(0)}(\mu'', \mu_0) \frac{d\mu''}{\mu''} \\ &+ \tfrac{3}{16} \int_0^1 S^{(0)}(\mu, \mu') j^{(0)}(\mu', \mu_0) \frac{d\mu'}{\mu'} + \frac{9}{256} \int_0^1 \int_0^1 S^{(0)}(\mu, \mu') j^{(0)}(\mu', \mu'') \\ &\times S^{(0)}(\mu'', \mu_0) \frac{d\mu'}{\mu'} \frac{d\mu''}{\mu''}, \end{aligned}\right\} \quad (232)$$

$$\left.\begin{aligned} \left(\frac{1}{\mu} + \frac{1}{\mu_0}\right) S^{(1)}(\mu, \mu_0) &= \left\{1 + \frac{3}{8} \int_0^1 \mu''^2 (1-\mu''^2) S^{(1)}(\mu'', \mu_0) \frac{d\mu''}{\mu''}\right\} \\ &\times \left\{1 + \frac{3}{8} \int_0^1 \mu'^2 (1-\mu'^2) S^{(1)}(\mu, \mu') \frac{d\mu'}{\mu'}\right\}, \end{aligned}\right\} \quad (233)$$

and

$$\left.\begin{aligned} \left(\frac{1}{\mu} + \frac{1}{\mu_0}\right) S^{(2)}(\mu, \mu_0) &= \left\{1 + \frac{3}{32} \int_0^1 (1-\mu''^2)^2 S^{(2)}(\mu'', \mu_0) \frac{d\mu''}{\mu''}\right\} \\ &\times \left\{1 + \frac{3}{32} \int_0^1 (1-\mu'^2) S^{(2)}(\mu, \mu') \frac{d\mu'}{\mu'}\right\}, \end{aligned}\right\} \quad (234)$$

where in equation (231) we have written

$$\left.\begin{aligned} j^{(0)}(\mu, \mu_0) &= 3 - \mu^2 - \mu_0^2 + 3\mu^2\mu_0^2 \\ &= \tfrac{1}{3}(3-\mu^2)(3-\mu_0^2) + \tfrac{8}{3}\mu^2\mu_0^2. \end{aligned}\right\} \quad (235)$$

Of the three functional equations, (231)–(233), only the first need be considered in any detail, since it is at once apparent that the solutions for the other two must be of the forms

$$\left(\frac{1}{\mu} + \frac{1}{\mu_0}\right) S^{(1)}(\mu, \mu_0) = H^{(1)}(\mu) H^{(1)}(\mu_0) \quad (236)$$

and

$$\left(\frac{1}{\mu} + \frac{1}{\mu_0}\right) S^{(2)}(\mu, \mu_0) = H^{(2)}(\mu) H^{(2)}(\mu_0), \quad (237)$$

where $H^{(1)}(\mu)$ and $H^{(2)}(\mu)$ satisfy the functional equations

$$H^{(1)}(\mu) = 1 + \tfrac{3}{8}\mu H^{(1)}(\mu) \int_0^1 \frac{H^{(1)}(\mu')}{\mu + \mu'} \mu'^2 (1-\mu'^2)\, d\mu' \quad (238)$$

and

$$H^{(2)}(\mu) = 1 + \tfrac{3}{32}\mu H^{(2)}(\mu) \int_0^1 \frac{H^{(2)}(\mu')}{\mu + \mu'} (1-\mu'^2)^2 d\mu'. \quad (239)$$

Returning to equation (231), we find, on examination, that this equation can be written in the form

$$\left.\begin{aligned}\left(\frac{1}{\mu}+\frac{1}{\mu_0}\right)S^{(0)}(\mu,\mu_0) &= \frac{1}{3}\left\{3-\mu^2+\frac{3}{16}\int_0^1 (3-\mu'^2)\,S^{(0)}(\mu,\mu')\,\frac{d\mu'}{\mu'}\right\}\\ &\quad\times\left\{3-\mu_0^2+\frac{3}{16}\int_0^1 (3-\mu''^2)\,S^{(0)}(\mu'',\mu_0)\,\frac{d\mu''}{\mu''}\right\}\\ &\quad+\frac{8}{3}\left\{\mu^2+\frac{3}{16}\int_0^1 S^{(0)}(\mu,\mu')\,\mu'\,d\mu'\right\}\left\{\mu_0^2+\frac{3}{16}\int_0^1 S^{(0)}(\mu'',\mu_0)\,\mu''\,d\mu''\right\}.\end{aligned}\right\} \quad (240)$$

From equation (240) it follows that $S^{(0)}(\mu, \mu_0)$ is symmetrical in μ, μ_0 and, further, that it can be expressed in the form

$$\left(\frac{1}{\mu}+\frac{1}{\mu_0}\right)S^{(0)}(\mu,\mu_0) = \tfrac{1}{3}\psi(\mu)\,\psi(\mu_0)+\tfrac{8}{3}\phi(\mu)\,\phi(\mu_0), \quad (241)$$

where

$$\psi(\mu) = 3-\mu^2+\frac{3}{16}\int_0^1 (3-\mu'^2)\,S^{(0)}(\mu,\mu')\,\frac{d\mu'}{\mu'} \quad (242)$$

and

$$\phi(\mu) = \mu^2+\frac{3}{16}\int_0^1 \mu'^2 S^{(0)}(\mu,\mu')\,\frac{d\mu'}{\mu'}. \quad (243)$$

Now, substituting for $S^{(0)}$ according to equation (241) in equations (242) and (243), we obtain the functional equations

$$\left.\begin{aligned}\psi(\mu) = 3-\mu^2+{}_1^1{}_6\,\mu\psi(\mu)\int_0^1 \frac{\psi(\mu')}{\mu+\mu'}(3-\mu'^2)\,d\mu'\\ +\tfrac{1}{2}\mu\phi(\mu)\int_0^1 \frac{\phi(\mu')}{\mu+\mu'}(3-\mu'^2)\,d\mu'\end{aligned}\right\} \quad (244)$$

and

$$\phi(\mu) = \mu^2+{}_1^1{}_6\,\mu\psi(\mu)\int_0^1 \frac{\psi(\mu')}{\mu+\mu'}\,\mu'^2 d\mu'+\tfrac{1}{2}\mu\phi(\mu)\int_0^1 \frac{\phi(\mu')}{\mu+\mu'}\,\mu'^2 d\mu', \quad (245)$$

which are now in their normal forms.

18. *The solution of the functional equations (244) and (245).*—As in our earlier discussion of similar systems of functional equations, we shall again be guided by the form of the solution obtained by the direct solution of the equation of transfer.

Now, the solution for $I^{(0)}(0, \mu)$ given in Paper IX, equation (189), is readily seen to be equivalent to

$$\left(\frac{1}{\mu}+\frac{1}{\mu_0}\right)S^{(0)}(\mu,\mu_0) = H^{(0)}(\mu)\,H^{(0)}(\mu_0)\,[3-c(\mu+\mu_0)+\mu\mu_0], \quad (246)$$

where $H^{(0)}(\mu)$ is defined in terms of the roots of the characteristic equation

$$1 = \frac{3}{8}\sum_{j=1}^{n}\frac{a_j(3-\mu_j^2)}{1-k^2\mu_j^2}. \quad (247)$$

Further, in equation (246) we have written

$$c = (1-2\xi)\sqrt{3}, \quad (248)$$

ξ being defined as in Paper IX, equations (184) and (188).

We now re-write solution (246) in the form

$$\left.\begin{aligned}\left(\frac{1}{\mu}+\frac{1}{\mu_0}\right) S^{(0)}(\mu,\,\mu_0) &= \tfrac{1}{3}\,[H^{(0)}(\mu)\,(3-c\mu)]\,[H^{(0)}(\mu_0)\,(3-c\mu_0)] \\ &\quad + \tfrac{8}{3}\,[q\mu H^{(0)}(\mu)]\,[q\mu_0 H^{(0)}(\mu^0)]\,,\end{aligned}\right\} \tag{249}$$

where

$$q^2 = \tfrac{1}{8}\,(3-c^2)\,. \tag{250}$$

The similarity of equations (241) and (249) is apparent, and, though solution (246) can be brought into this correspondence with equation (241) in other ways, it is nevertheless true that

$$\psi(\mu) = H^{(0)}(\mu)\,(3-c\mu) \tag{251}$$

and

$$\phi(\mu) = q\mu H^{(0)}(\mu) \tag{252}$$

represent the solution of the functional equations (244) and (245) if we define $H^{(0)}(\mu)$ as satisfying the equation

$$H^{(0)}(\mu) = 1 + \tfrac{3}{16}\mu H^{(0)}(\mu)\int_0^1 \frac{H^{(0)}(\mu')}{\mu+\mu'}\,(3-\mu'^2)\,d\mu' \tag{253}$$

and choose q and c consistent with equation (250) and in a manner we shall specify.

The proof that the solutions of equations (244) and (245) are as we have just stated proceeds as in the earlier cases, use now being made of the following relations:

$$\int_0^1 H^{(0)}(\mu)\,(3-\mu^2)\,d\mu = \tfrac{16}{3}\,, \tag{254}$$

$$a_0 = 1 + \tfrac{3}{8}\tfrac{3}{2}\,(3a_0^2 - a_1^2)\,, \tag{255}$$

and

$$(3-\mu^2)\int_0^1 \frac{H^{(0)}(\mu')}{\mu+\mu'}\,d\mu' = \frac{H^{(0)}(\mu)-1}{\frac{3}{16}\mu H^{(0)}(\mu)} + (a_1 - \mu a_0)\,, \tag{256}$$

where a_0 and a_1 are the moments of order zero and one of $H^{(0)}(\mu)$. Relations (254)–(256) follow from theorems 3 and 6 (§ 12) for the particular case of equation (253).

First, considering $\psi(\mu)$ as defined in equation (242), we find that the substitution of $S^{(0)}$ according to equation (246) leads to an expression for ψ which is in agreement with equation (251). On the other hand, if we evaluate $\phi(\mu)$ in a similar fashion, we find that

$$\phi(\mu) = \mu H^{(0)}(\mu)\,[\tfrac{9}{16}a_1 - c\,(\tfrac{9}{16}a_0 - 1)]\,. \tag{257}$$

To bring this into agreement with equation (252), we must set

$$q = \tfrac{9}{16}a_1 - c\,(\tfrac{9}{16}a_0 - 1)\,. \tag{258}$$

But, as we have already assumed that q and c are related as in equation (250), we must require that

$$\left(\frac{3-c^2}{8}\right)^{\frac{1}{2}} = \tfrac{9}{16}a_1 - c\,(\tfrac{9}{16}a_0 - 1) \tag{259}$$

or that

$$32\,(3-c^2) = [9a_1 - c\,(9a_0 - 16)]^2\,. \tag{260}$$

Expanding this last equation, we find

$$(288 - 288a_0 + 81a_0^2)\,c^2 - 18\,(9a_0 - 16)\,a_1 c + 81a_1^2 - 96 = 0\,. \tag{261}$$

The coefficient of c^2 in equation (261) can be simplified by using equation (255). We find

$$9a_1^2c^2 - 6(9a_0 - 16)a_1c + 27a_1^2 - 32 = 0. \tag{262}$$

The discriminant of this equation is

$$36a_1^2[(9a_0 - 16)^2 - 27a_1^2 + 32] = 36a_1^2[(288 - 288a_0 + 81a_0^2) - 27a_1^2]; \tag{263}$$

but this vanishes because of equation (255). Hence the quantity on the left-hand side of equation (262) is a perfect square, and we conclude that

$$c = \left(3 - \frac{32}{9a_1^2}\right)^{\frac{1}{2}} \quad \text{and} \quad q = \frac{2}{3a_1}. \tag{264}$$ [10]

Thus, with q and c as defined in equation (264), equations (251) and (252) do represent the solution of the functional equations (244) and (245).

19. *The exact law of darkening for an atmosphere with a constant net flux and scattering radiation in accordance with Rayleigh's phase function.*—In Paper III we worked out the theory of the radiative equilibrium of an atmosphere (with no incident radiation) in which scattering in accordance with Rayleigh's phase function governs the transfer of radiation. And in the appendix to Paper IX we gave the law of darkening for such an atmosphere in closed form. We have (Paper IX, appendix, eq. [9])

$$I(0, \mu) = \lambda F H^{(0)}(\mu), \tag{265}$$

where $H^{(0)}(\mu)$ has the same meaning as in the problem of diffuse reflection which we have just considered. But the constant λ, defined in the following manner (Paper IX, appendix, eq. [10]):

$$\lambda = (-1)^n \mu_1 \ldots \mu_n \frac{3\sqrt{3}}{2(B - A)}, \tag{266}$$

appears to bear no relation to the constant c of § 18 (eq. [248]). However, it can be shown that, in the framework of the theory of Papers III and IX, there is, in fact, a simple relation between λ and c. To show this, we must make use of the relation

$$\frac{P(\sqrt{3})P(-\sqrt{3})}{R(\sqrt{3})R(-\sqrt{3})} = -8\mu_1^2 \ldots \mu_n^2, \tag{267}$$

which follows from the identity[11]

$$1 - \frac{3}{8}\sum_{j=1}^{n} \frac{a_j(3 - \mu_j^2)}{1 - \mu_j^2 x} = (-1)^n \mu_1^2 \ldots \mu_n^2 \frac{x\prod_{\alpha=1}^{n-1}(x - k_\alpha^2)}{\prod_{j=1}^{n}(1 - \mu_j^2 x)} \tag{268}$$

when we set $x = \frac{1}{3}$. Now, from the definition of ξ, we have (cf. Paper IX, eqs. [184] and [188])

$$\xi(1 - \xi) = -\frac{AB}{(A - B)^2} = -\frac{1}{(A - B)^2} \frac{P(\sqrt{3})P(-\sqrt{3})}{R(\sqrt{3})R(-\sqrt{3})} \tag{269}$$

or

$$\xi(1 - \xi) = \frac{8\mu_1^2 \ldots \mu_n^2}{(A - B)^2}. \tag{270}$$

[10] In eq. (264) we have chosen the positive sign for c, since it is found that $9a_0 > 16$.

[11] Cf. Papers VIII, eqs. (41) and (46), and XI, n. 16.

Using this last relation in equation (266), we have

$$\lambda = [\tfrac{3}{8}\tfrac{7}{2}\xi(1-\xi)]^{\frac{1}{2}}; \tag{271}$$

or, expressing ξ in terms of c in accordance with equation (248), we find

$$\lambda = [\tfrac{9}{1}\tfrac{9}{2}\tfrac{}{8}(3-c^2)]^{\frac{1}{2}} = \tfrac{3}{4}q. \tag{272}$$

With this value of λ, the law of darkening (265) becomes

$$I(0, \mu) = \tfrac{3}{4}qFH^{(0)}(\mu). \tag{273}$$

In the form (273) the law of darkening involves only constants and functions which also appear in the associated problem of diffuse reflection and for which exact expressions have been given. The exact law of darkening for our present problem is therefore obtained by simply redefining $H^{(0)}(\mu)$ in terms of the functional equation (253) and determining q as in equation (264). Thus, substituting for q from equation (264), we have

$$I(0, \mu) = \frac{1}{2a_1}FH^{(0)}(\mu), \tag{274}$$

in which form it is evident that solution (274) provides for the emergent radiation an outward flux which is exactly πF. Finally, we may note that for this problem there is an equivalent of the Hopf-Bronstein relation which is given by equation (187).

20. *Remarks on future work.*—The analyses of the various problems presented in this paper have served to illustrate and amplify the statement made in the introduction, that exact solutions for a large class of problems in the theory of radiative transfer can be obtained by letting the H-functions (defined in terms of the Gaussian division and characteristic roots) which appear in their solution become solutions of associated functional equations. And, as we have already indicated, the task of determining these exact H-functions by a process of iteration is considerably lightened by starting with as good an approximation as our "third approximation" provides. Mrs. Frances H. Breen and the writer have started on this work of evaluating the exact forms of the various H-functions which have been tabulated in their second or third approximations in earlier papers. We hope to have these calculations completed in the near future. But, apart from this matter of getting the exact numerical forms of the solutions of problems which have already been solved in principle, there are a number of other directions in which the theory developed in these papers can be extended. We may briefly indicate the nature of some of these.

First, there is the problem of scattering on laws more general than Rayleigh's. It would appear that in these more general cases the equations of transfer could still be written in vector form, like equation (15), the physical problem being one of determining the analogue of the matrix $\boldsymbol{QJ}$ which will describe the result of a single scattering. Second, there is the related question of what the equations of transfer are in cases in which the radiation field is one of general elliptic polarization. Under these circumstances it would follow from Stokes's considerations[12] that four intensities will be required to characterize the field (instead of three, as in the case of partial plane polarization) and that the equations of transfer could be expressed as a single vector equation in four-dimensional space. Scattering and diffuse reflection will then be described by matrices of order 4. These generalizations of the theory developed in Papers XI and XIII are likely to be fairly straightforward ones; but it would be of interest to have at least these formal developments completed.

[12] *Mathematical and Physical Papers of Sir George Stokes* (Cambridge, England, 1901), **3**, 233.

Third, there is the problem of transfer in plane-parallel atmospheres of finite thicknesses. It is not difficult to write down the formal solutions for such problems (e.g., Paper XII, eqs. [45] and [74]); the main difficulty (if such it is!) is that, in the forms in which the solutions have been written down, they involve constants of integration explicitly. And the problem of the elimination of the constants is not far advanced. But, once we can accomplish the elimination of the constants, we shall also be in a position to reduce the Ambarzumian type of functional equations to manageable proportions. However, it is not impossible that some deep generalizations of the methods of the earlier papers will be necessary before significant advances can be made in these directions.

Finally, there is the whole field of time-dependent transfer problems which requires to be explored. So far there has been only one investigation in this subject, namely, that by E. A. Milne.[13] In view of our present enormously increased resources for solving transfer problems, it would clearly be profitable to reconsider time-dependent situations and formulate problems of interest.

It is our intention to examine these and other problems in the near future.

[13] *J. London Math. Soc.*, **1**, 40, 1926.

SPECTRAL TYPES OF STARS IN THE GLOBULAR CLUSTERS MESSIER 3 AND MESSIER 13*

DANIEL M. POPPER
Yerkes and McDonald Observatories
Received October 28, 1946

ABSTRACT

Spectral classifications have been obtained for fourteen stars in Messier 3 and for twenty-one stars in Messier 13. The brightest stars, which have absolute photovisual magnitudes between −2 and −3 and color indices principally between +0.9 and +1.6 mag., are of spectral type G5–K0 and luminosity class *Ib*. They are peculiar in that the *CN* absorption shortward from λ 4215 is weak. This result is in agreement with an early observation by Lindblad and with Baade's grouping of the globular-cluster stars in the same population group as the high-velocity stars. Among the brightest members of each cluster is at least one O or B star. Approximate magnitudes and colors have been obtained for the brightest stars in the central regions of the two clusters. These observations augment Shapley's photometry and show that a large fraction of the brightest stars are to be found in the central regions. The dispersion in radial velocity of the most massive stars in Messier 13 is not more than a few kilometers per second.

INTRODUCTION

There have been a few early investigations of the spectra of stars in globular clusters. Pease and Adams observed thirty-nine stars in Messier 13[1] with low dispersion. The choice of stars appears to have been a matter of chance, since a long slit was held stationary at a random position in the cluster. The estimated spectral types range from A0 to G0 with maximum frequency at F0. The brightest stars of the cluster, which are yellow-red, do not appear to have been picked up by this method. Sanford observed seven stars in Messier 3 and measured their radial velocities.[2] Neither the identifications of the stars nor their spectral types were given.[3] Sanford also observed the bright red variable, Messier 3, No. 95, twice, finding changes in the spectrum.

Lindblad extended his spectrophotometric investigations of stellar-luminosity effects during a stay at Mount Wilson.[4] In the course of this work he obtained a slitless spectrogram of Messier 13. Three of the bright yellow-red stars were sufficiently detached from the body of the cluster to enable Lindblad to examine their spectra. He also reported on one of the stars of Messier 3 observed by Sanford. Lindblad concluded that these stars are of type near K0, with the peculiarity that the cyanogen absorption shortward from λ 4215 is weaker than normal if the stars are giants or brighter. The significance of this peculiar observation was somewhat obscured because Lindblad was of the opinion that "pseudo-cepheids" (i.e., supergiants) have weak *CN* absorption. Hence he concluded that the brightest cluster stars are "pseudo-cepheids," a result not discordant with their absolute magnitudes. Keenan has shown,[5] however, that, from G2 to K0, *CN* is enhanced in the spectra of supergiants. This effect may be verified by an examination of the prints in the Yerkes *Atlas of Stellar Spectra*.

* *Contributions from the McDonald Observatory, University of Texas*, No. 131.

[1] *Pub. A.S.P.*, **25**, 260, 1913; **26**, 204, 1914.

[2] *Annual Report of the Director of the Mount Wilson Observatory for the Year 1918; Pop. Astr.*, **27**, 99, 1919.

[3] In his photometric study of Messier 3 (Shapley and Davis, *Ap. J.*, **51**, 140, 1920), Shapley identifies three of Sanford's stars.

[4] *Ap. J.*, **55**, 85, 1922; see esp. p. 116.

[5] *Ap. J.*, **93**, 475, 1941.

More recently, Joy obtained a series of spectrograms of the 15-day Cepheid in Messier 3.[6]

Ten Bruggencate[7] appears to have been the first to recognize the fundamental difference between the color-magnitude diagrams for globular clusters and those for galactic clusters and stars in the neighborhood of the sun. Later, Hachenberg[8] and Greenstein[9] emphasized the differences more explicitly. They are shown schematically in a diagram by Baade.[10] The feature that will be of particular interest to us is the apparent restriction of the brighter stars to a narrow range of colors in the vicinity of color classes g and k.

In his stimulating paper,[10] Baade suggests that other groups of stars belong to the same family (his population type II) as the globular-cluster stars. Among these groups is that of the high-velocity stars and, in particular, the small group of high-velocity giants of spectral types G5–K2. Morgan and his co-workers at the Yerkes Observatory have found that the *CN* absorption at λ 4215 in the spectra of these stars is considerably weaker than in the spectra of other stars of the same spectral type and absolute magnitude.[11] If Baade's suggestion is correct, we might expect the spectra of stars in the proper range of spectral types in globular clusters to show weak *CN* absorption. Lindblad's early observations, mentioned above, have already indicated that this is indeed the case.

The present investigation was undertaken in order to determine what spectral types and peculiarities are found among the brightest stars in the globular clusters and, in particular, to check and extend Lindblad's result.

THE OBSERVATIONS

Spectrograms of stars in Messier 3 and Messier 13 were obtained with the Cassegrain spectrograph of the McDonald Observatory. The *f*/1 Schmidt camera was used in combination with glass prisms, giving a dispersion of 150 A/mm at $H\gamma$. This dispersion is perhaps a bit low for the most accurate spectral classification, but for types G and K it is adequate. The width of the stellar spectra is 0.2 mm, and the projected slit width 0.018 mm. The standard exposure time on 103*a*-O film is 1 hour for a star of photographic magnitude 13.5. The iron-arc comparison was placed on only one side of each stellar spectrum to facilitate matching of standard and cluster spectra. The question of membership of each star in its cluster can be answered from a glance at its spectrum, since both clusters have large radial velocities, −150 km/sec for Messier 3 and −230 km/sec for Messier 13.

The stars observed were chosen from Shapley's lists,[12] with the addition of a few of the brighter stars nearer the centers of the clusters than Shapley's photometry reaches. Most of the stars are among the thirty brightest in each cluster, though a few fainter ones have also been observed. In general, one good spectrogram per star was obtained. The plots of Barnard's micrometer measures contained in *Yerkes Publications*, Volume 6, serve as ideal finding-charts.

Standard stars for spectral classification were selected from the Yerkes *Atlas*. A few additions and revisions have been supplied through the courtesy of W. W. Morgan. An average of three spectrograms per standard star was obtained in order to insure a good density match with each cluster spectrogram.

[6] *Ap. J.*, **92**, 396, 1940.

[7] *Sternhaufen* (Berlin, 1927), pp. 129 ff.

[8] *Zs. f. Ap.*, **18**, 49, 1939 (investigation of Messier 92).

[9] *Ap. J.*, **90**, 387, 1939 (investigation of Messier 4).

[10] *Ap. J.*, **100**, 137, 1944.

[11] *An Atlas of Stellar Spectra* (Chicago, 1943), pp. 24, 25, 26, 35. In an unpublished investigation, G. Münch has added a considerable number of stars to this group.

[12] Messier 3: Shapley and Davis, *op. cit.* Messier 13: Shapley, *Mt. W. Contr.*, **6**, 225, 1919.

Because of the crowding of stars in the central regions of the clusters, Shapley did not consider his photometry reliable at distances less than 2′ from the centers and hence did not publish magnitudes for the central regions. These regions contain most of the stars in the clusters. It is of interest to see the extent to which the color-magnitude diagrams are affected by the inclusion of the brightest stars in the central parts.[13] The scale of 7″.4/mm at the Cassegrain focus of the 82-inch reflector is sufficient to separate most of the brighter stars completely from their neighbors on short exposures with good seeing. Photovisual and photographic magnitudes for some of these stars in Messier 3 and Messier 13 were estimated on one pair of plates for each cluster. Shapley's magnitudes for stars farther from the center were used as standards. The uncertainty of a single magnitude is probably about $0^m.1$ or $0^m.2$ on Shapley's system. These magnitudes include the effect of a number of close fainter stars, although their images are invisible on the short exposures used. The magnitude per square second (the approximate size of the stellar images) contributed by these "background" stars may be estimated in two independent ways. First, from Stebbins and Whitford's determination of the integrated magnitude of the central region of each cluster[14] and, second, from the relative exposure times for spectrograms of stars and of the background. The two methods are in good agreement and indicate that the background effect should not exceed 0.05 mag. for the faintest stars considered in any of the four cases. Hence we may neglect it. The results of these estimates are included in Figures 2 and 3. They are not necessarily complete for the central regions to any magnitude limit, but they do include most of the brightest stars. It is not surprising that a large fraction of the brightest stars of the clusters are found in the most densely populated parts. That these stars appear, on the average, a bit bluer than the bright stars outside the center may be an observational effect.

Relatively few of these central stars could be observed spectrographically because of the nearly continuous background of fainter stars. An occulting device is needed. When there was some question as to how much the background might be affecting the stellar spectrogram, the slit was lengthened to twice its normal length, and the star trailed over only the normal length. Then the spectrum of the background alone appears on one-half of the spectrogram. Those spectrograms affected appreciably by background are not included in the discussion below.

RESULTS

All the results in this paper are based on one spectrogram per star. Hence outstanding or peculiar characteristics of individual stars must be considered tentative. Those conclusions that depend on a number of stars, on the other hand, are definitive. The reader should keep this distinction in mind.

Most of the cluster stars observed have color indices between +0.9 and +1.6 mag. and absolute photovisual magnitudes between −2 and −3 (for details see Tables 1 and 2). Casual inspection of the spectra of these stars, principally between $H\delta$ and $H\gamma$, reveals immediately (1) that the stars are of type G and early K and (2) that the hydrogen lines and λ 4290 are conspicuously stronger than in the spectra of normal giants (luminosity class III) of approximately the same spectral type and have more nearly their strength in supergiants (luminosity class I*b*).[15] The spectra of the individual stars were classified by comparison with standard stars of luminosity classes I*b*–III and spectral types G0–K3 in the wave-length region λ 4200 to $H\gamma$. The luminosity class is determined

[13] The only cluster for which photometry has been carried out right up to the center is Messier 4 (Greenstein, see n. 8). This cluster is closer to us, is much more open, and contains fewer stars than Messier 3 and Messier 13. No significant difference in the color-magnitude diagram was found between the central and the outer regions.

[14] *Ap. J.*, **84**, 132, 1936.

[15] See the plates of the Yerkes *Atlas* for a confirmation of these effects in the spectra of standard stars, as well as of other spectroscopic features mentioned.

OF MICH.

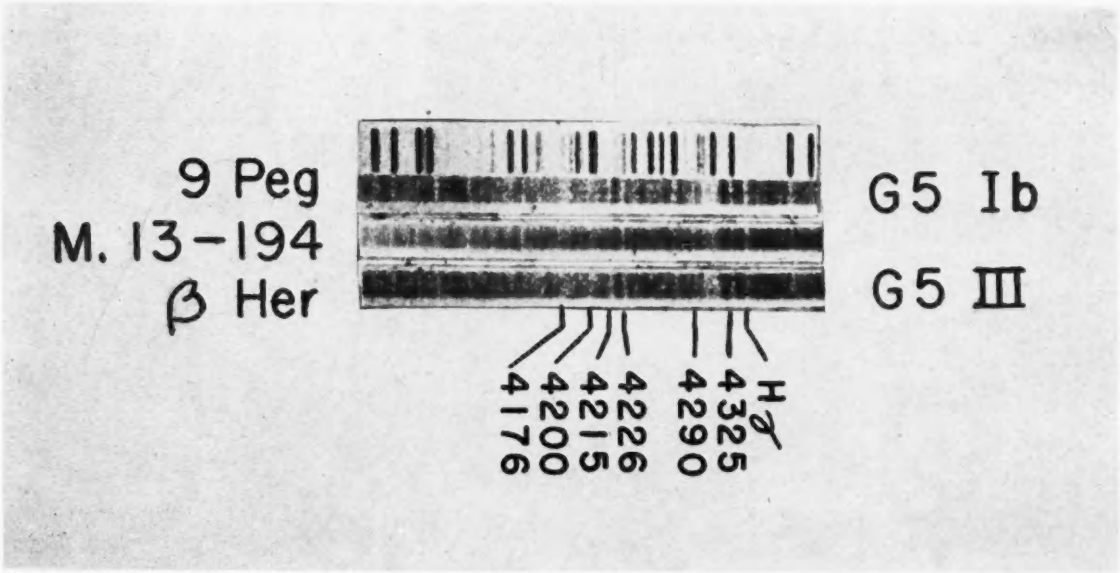

FIG. 1.—Messier 13, No. 194, is classified as G5 Ib, with *CN* intensity corresponding to luminosity class III–IV

from the ratio λ 4290: λ 4325. Within any luminosity class the spectral type is established from the ratio λ 4226: $H\gamma$. Checks on the classification are furnished by ratios of various other pairs of lines in the group λλ 4226, 4271, 4290, 4325, and $H\gamma$. Shorter wave-length regions were not used because the spectrograms tend to be underexposed there. Attempts to use λ 4077 for luminosity separation among the standard stars were less successful than the use of λ 4290. The results of the classification are included in Tables 1 and 2.

The most obvious peculiarity in the spectra of these bright yellow-red stars, when photographed with a dispersion of 150 A/mm, is the weakness of the broad feature around λ 4176 relative to the broad feature around λ 4200. In the spectra of the standard supergiants, λ 4176 is the stronger, whereas the two features are of about equal intensity in the spectra of normal giants. The explanation of this peculiarity lies in the abnormal weakness of *CN* absorption in the cluster stars. Its detection is an independent confirmation of the effect noted by Lindblad[4] and predicted on the basis of Baade's discussion[10] of Morgan's observations.

Lindblad's determination of *CN* strength consisted of spectrophotometric comparison of the region λλ 4144–4184 with the region λλ 4227–4272. Morgan's estimates of *CN* strength, on the other hand, are obtained by visual comparison of the intensity of the continuum on either side of λ 4215. It is the weakness of this "break" in the continuum that was found by him to be abnormal in the high-velocity giants. The anomalous intensity ratio of the blends at λ 4176 and λ 4200, observed in the cluster stars, is an additional manifestation of the weakness of *CN*. In the spectra of supergiants between G5 and K2 and, to a lesser extent, in the spectra of giants, the blend near λ 4176 and, in particular, its longward extension to λ 4181 are composed largely of the (2, 3) band of the violet *CN* system. A more detailed comparison of the cluster spectrograms with those of standard stars was effected by bringing them immediately adjacent to each other. In this way it could be seen that the *CN* "break" at λ 4215 is definitely weaker than in the spectra of supergiants and that the apparent weakness of the λ 4176 blend is caused in large part by the weakness of its longward side. An attempt to show these effects is made in Figure 1. The same effects at a lower luminosity can be seen in the reproductions of spectrograms of B2527 and δ Lep on Plates 42 and 45 of the Yerkes *Atlas*.

For each cluster star of luminosity class I*b* estimated as type G5 or later, an attempt was made to determine the luminosity class of the standard star of the same spectral type that has equal *CN* absorption. For all but three of the stars the *CN* was weaker than in luminosity class III, averaging class IV or a bit brighter. For one star (Messier 13, No. 199) the *CN* intensity appeared to correspond to class II–III. Additional spectrograms are required to check the reality of this difference.

In the spectra of high-velocity giants, the λ 3883 ($\Delta v = 0$) and λ 3590 ($\Delta v = +1$) bands of *CN* are also anomalously weak.[16] One cluster star (Messier 13, No. 414) was observed in the λ 3883 region with quartz prisms. Although adequate standards are not available, it is evident that the λ 3883 *CN* absorption also is weak in cluster stars.

Those stars observed that are not included in the group discussed above, principally bluer and/or fainter stars, were also classified by comparison with standards selected from the Yerkes *Atlas*. Classifications for the A stars are considerably less reliable than for the later types, the luminosity classifications being particularly uncertain. The spectral type is determined only from the ratio of K to the *H* lines, and the luminosity from the appearance of the *H* lines. It is not possible to draw from these spectrograms any conclusions about the metallic-line spectra of A-type cluster stars.

Classifications of all the stars are given in Tables 1 and 2 and are shown in Figures 2 and 3. In the tables the first column gives the designation of the star according to Von Zeipel[17] (Messier 3) or to Ludendorff[18] (Messier 13). The next two columns contain Shap-

[16] Unpublished material.

[17] *Ann. de l'obs. de Paris, Mém.*, **25**, Part F, 1908.

[18] *Pub. d. Ap. Obs. zu Potsdam*, Vol. **15**, Part VI (No. 50), 1905.

ley's photovisual magnitudes and color indices.[12] The fourth column gives the spectral classifications discussed above, and the last column refers to notes following the tables.

Figures 2 and 3 show the color magnitude diagrams for all stars measured by Shapley brighter than $m_{pv} = 14.0$. Plotted in addition are the bright stars in the centers of the clusters and fainter stars of which spectrograms have been obtained. The spectral types listed in Tables 1 and 2 are also indicated in the diagrams. The photographic distance

TABLE 1

SPECTRAL TYPES OF STARS IN MESSIER 3

$m_{pv} - M_{pv} = 15.5$

Star	m_{pv}	Color Index	Spectrum	Notes
205	12.7	$+1^m1$	G8 I*b*	
206*	10.3	+1.0	K3 V	
238	12.5	+1.8	K0 I*b*	
318	var.	.....	M	1
420	13.4:	+0.2:	F8–G0p	2
490	12.3	+1.8	G5 I*b*	
589	12.8	+0.9	G5 I*b*	
612	12.6	+1.4	K0 I*b*	3
716†	13.5	+1.1	G5 I*b*	
740*	13.4	+0.7	G5 IV–V	
752	12.5	+1.4	G8–K0 I*b*	4
837	12.5	+1.4	G8 I*b*	
1053†	12.3	+1.5	G5 I*b*	
1127	12.6	+1.3	G8 I*b*	
1128	14.7	−0.6	O8	5
1219	12.6	+1.4	G8 I*b*	
1397	12.6	+1.7	K0: I*b*	6
Nucleus	.....	.....	F6–F8 III–V	7

* Not a member of the cluster.

† In central region. Magnitude and color determined here.

NOTES TO TABLE 1

1. 318—Variable 95, period 103.2 days. Observed spectrographically by Sanford. According to Greenstein's elements (*Harvard Bull.*, No. 901, 1935), my observation was made 16 days after minimum light. No emission lines present.
2. 420—Magnitudes uncertain (Shapley). Spectrum washed out.
3. 612—Observed by Sanford.
4. 752—Observed by Sanford and studied by Lindblad.
5. 1128—Good *H* and *He* I lines; λ 4541 of *He* II appears strong and gives the correct radial velocity, but no other O-type lines are visible.
6. 1397—Weak spectrogram.
7. Nucleus—Slit set on brightest region of cluster nucleus, conspicuously bright stars being avoided.

modulus of Messier 3, 15.6 mag., is well established from the large number of cluster-type variables. That of Messier 13, 14.8 mag., depends on only one cluster-type variable and three Cepheids of longer period and is less reliable.[19] One-tenth of a magnitude has been subtracted from the photographic moduli to obtain photovisual moduli, this being the approximate reddening for both clusters according to the cosecant law. Both are at high galactic latitudes. On the basis of these moduli, the brightest stars in Messier 3 are about 0.4 mag. brighter than those in Messier 13.

[19] Helen B. Sawyer, *Pub. David Dunlap Obs.*, Vol. 1, No. 11, 1942.

The bright yellow-red stars in globular clusters, then, are supergiants of type G2–K0, with M_{pv} between -2 and -3 and color indices between $+0.9$ and $+1.6$ mag., and they have the peculiarity that the *CN* absorption is weak. That there is only a slight correlation between spectral type and color index for these stars probably reflects uncertainties both in the colors and in the spectral types. According to R. E. Wilson's calibration of the absolute magnitudes of galactic supergiants,[20] those of type G2–K0 have M_{pv} between -2.5 and -3.5. Greenstein obtains similar values.[21] They find, however, that the stars of earlier type are brighter, while in the clusters the bluer stars are fainter, as they are for galactic Cepheids.

TABLE 2

SPECTRAL TYPES OF STARS IN MESSIER 13

$m_{pv} - M_{pv} = 14.7$

Star	m_{pv}	Color Index	Spectrum	Notes	Star	m_{pv}	Color Index	Spectrum	Notes
15*	12.8	$+0^m3$	F8 V		324†	var.	.....	K0 *Ib*	4
70	12.0	+1.4	K2 *Ib*	1	353	12.9	$+1^m0$	G5 *Ib*	
96	12.5	+1.2	G5 *Ib*	1	414	12.1	+1.4	G8 *Ib*	
158	12.7	+1.2	G5 *Ib*		481†	12.4	+1.0	G2 *Ib*	
174	13.9	+0.7	F8p	2	773	13.1	+0.8	G5 *Ib*–II	
194	12.2	+1.4	G5 *Ib*	1	835	12.2	+1.1	G2–G5 *Ib*	
199	12.2	+1.4	G5–G8 *Ib*		935	14.5	0.0	A3 III	
222	13.1	−0.5	B5 V	3	973	12.1	+1.3	K0 *Ib*	
258	13.4	+1.2	G2 III		978	15.4	−0.4	A3 III	
262†	12.4	+1.1	G5 *Ib*		993	13.9	0.0	A5 III–V	
267	13.9	−0.2	A3 II		1019*	12.6	+0.4	G2 III	
274	14.0	+1.0	G0–G2 III		Nucleus	.....	.....	F8 III–V	5
296†	12.7	+0.8	G2–G5 *Ib*						

* Not a member of the cluster.

† In central region. Magnitude and color determined here

NOTES TO TABLE 2

1. 70, 96, 194—Stars observed by Lindblad.
2. 174—λ 4307 appears unusually strong.
3. 222—*H* lines strong; weak λ 4026 of *He* I gives correct radial velocity.
4. 324—Variable 11. Range in m_{pg} 12.9–13.8, apparently irregular (Sawyer, *Pub. David Dunlap Obs.*, Vol. **1**, No. 5, 1940). At the time of exposure of spectrogram, m_{pg} was about 13.0. At the time of direct photographs, m_{pg} was about 13.8 and color index +1.8 mag.
5. Nucleus—Observed as in Messier 3.

Among the brighter stars of the clusters are a few that fall in regions of the color-magnitude diagrams avoided by population group II,[10] lying principally to the blue side of the supergiant group (see Figs. 2 and 3). Table 3 lists the most pronounced of such cases among the brightest stars of each cluster. These stars are of particular interest when they are cluster members.

We note that in each cluster there is at least one early-type star among the brightest stars. The B5 star in Messier 13 has about the absolute magnitude of a normal B5 dwarf. The O star in Messier 3 is much fainter than a normal O star. The tentative nature of results based on only one spectrogram per star is again emphasized.

[20] *Ap. J.*, **93**, 212, 1941.

[21] *Proc. Nat. Acad.*, **26**, 259, 1940.

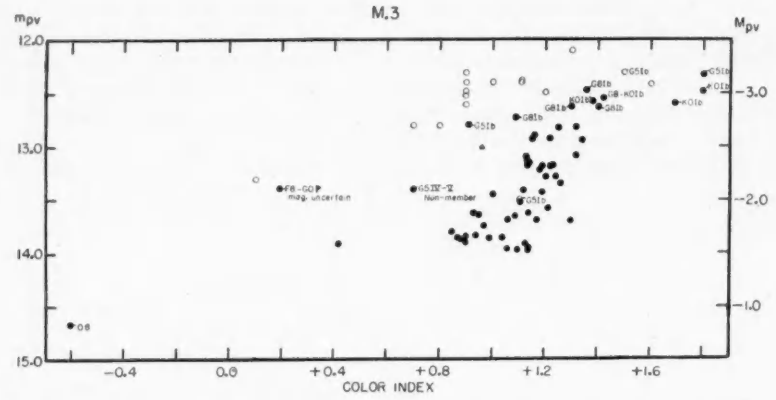

FIG. 2.—Color-magnitude diagram for Messier 3. *Filled circles:* All Shapley's stars brighter than $m_{pv} = 14.0$ within 9′ of center of cluster and fainter star with spectrum obtained. *Open circles:* Brightest stars in central region.

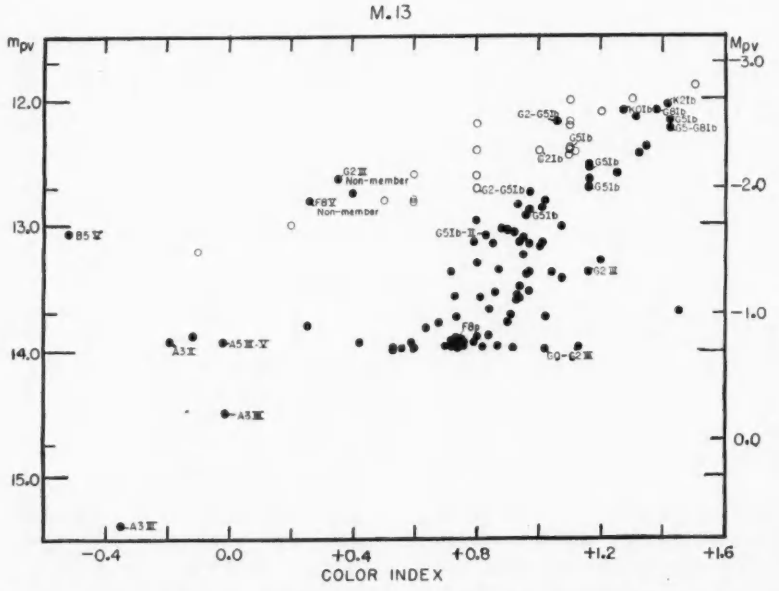

FIG. 3.—Color-magnitude diagram for Messier 13. *Filled circles:* All Shapley's stars brighter than $m_{pv} = 14.0$ and fainter stars with spectra observed. *Open circles:* Brightest stars in central region.

Shapley has objected[22] to a detailed subdivision of his observed magnitudes and colors. Since I am observing individual stars, however, it is necessary to consider the individual magnitudes and colors. The nonmember foreground stars furnish checks on Shapley's color system. In each of the cases observed (see Table 3), his color is near the value expected for a normal star of the observed spectral type. These results indicate that Shapley's observations are essentially reliable.

The velocity dispersion in a globular cluster is an important dynamical quantity. The material obtained here is, however, not well suited for the determination of this quantity,

TABLE 3

BRIGHT STARS NOT IN THE SUPERGIANT BRANCHES

Star	m_{pv}	Color Index	Spectrum	Remarks
	Messier 3, $m-M=15.5$			
206	10.3	$+1^m0$	K3 V	Not a member
237	13.9	+0.4	.....	Not observed
420	13.4:	+0.2:	F8–G0p	Magnitude and color uncertain; spectrum peculiarly washed out
740	13.4	+0.7	G5 IV–V	Not a member
746	13.3	+0.1	.....	Near center of cluster; much the bluest bright star there; too crowded to obtain spectrogram
1128	14.7	−0.6	O8	If the classification is correct, this star is bolometrically one of the brightest in the cluster
	Messier 13, $m-M=14.7$			
15	12.8	$+0^m3$	F8 V	Not a member
222	13.1	−0.5	B5 V	Brightest star in the cluster photographically
267	13.9	−0.2	A3 II	
326	13.9	−0.1	.....	Not observed
610	13.0	+0.2	.....	Bluest bright stars in central region; spectrograms not obtained
780	13.2	−0.1	.....	
993	13.9	0.0	A5 III–V	
1019	12.6	+0.4	G2 III	Not a member
1087	12.7	+0.4	.....	Not observed

since there is only one low-dispersion spectrogram each for a few of the most massive cluster stars and, further, since the comparison spectrum is on only one side of each stellar spectrum. Nevertheless, fourteen spectrograms of the thirteen I*b* stars observed in Messier 13 were measured to see if the dispersion is very large. The mean error of a single spectrogram, from the internal agreement of the different lines, is about ± 10 km/sec. For only three spectrograms does the measured velocity differ by more than 10 km/sec from the mean for all spectrograms. Of these three, one is a second spectrogram of a star for which the first gives a very small velocity difference; another has an overexposed comparison. About all we may conclude from the evidence on hand is that the dispersion for the brightest stars is not more than a few kilometers per second.

It is a pleasure to acknowledge the advice of Dr. W. W. Morgan on problems of spectral classification, and the assistance of Mr. Charles Heyduck at the telescope.

[22] *Star Clusters* (New York, 1930), p. 26.

INFRARED SPECTRA OF EARLY-TYPE STARS*

W. A. HILTNER
Yerkes and McDonald Observatories
Received November 4, 1946

ABSTRACT

A descriptive discussion of the infrared spectra of early-type stars, with emphasis on shell and emission-line stars, is given.

Spectrographic investigations in the near infrared region of the spectrum have been necessarily limited in the past to relatively bright stars. The pioneer investigations were made by Merrill,[1] who observed a large number of bright stars of all spectral types with a grating spectrograph at Mount Wilson Observatory, and by Merrill and Wilson,[2] who made a comparative study of the Paschen and Balmer series of hydrogen. With the recent development of faster emulsions, investigations have been extended to relatively faint stars with moderately high dispersion.[3] In April, 1946, a grating spectrograph was placed in service at the McDonald Observatory in conjunction with the 82-inch reflector. The optical system consists of an off-axis parabolic collimator with a focal length of 1300 mm, an off-axis Schmidt camera with a focal length of 300 mm, and an aluminum-on-Pyrex grating supplied by Professor R. W. Wood. The diameter of the collimated bundle is 100 mm. The dispersion in the first order is 48 A/mm. Normally, photographic plates instead of film are employed in the spectrograph, and a region of approximately 1000 A can be obtained simultaneously on the flat plate with good focus.

The first order on one side of the grating is especially bright in the red and the infrared, and the exposure times necessary are not excessive. For a 4.0-mag. B-type star a 20-minute exposure is required to obtain a spectrogram 0.4 mm wide on an Eastman *I*-N emulsion, hypersensitized with ammonia. The projected slit width is 0.015 mm. For a fourth-magnitude M-type star the exposure time is of the order of 1 minute.

During parts of April and May and one night in September, 1946, the spectrograph was used to obtain spectra in the spectral region λλ 8300–8700 of early-type stars, with emphasis on shell and emission-line stars. In addition, a few eclipsing variables were included. The spectra of the more interesting objects are reproduced in Figures 1–4, and the plate numbers of the spectrograms and the dates of observation are given in Table 1. The spectrograms are arranged in the reproductions according to the type and character of the spectrum.

The early-type stars which show emission lines in the infrared region appear to fall into four groups, as follows: (1) double emission of *O* I 8446 with central absorption; (2) single emission of *Ca* II 8498, 8542, 8662; (3) double emission with possible central absorption of *O* I 8446, *Ca* II 8498, 8542, 8662 and the Paschen series; (4) single emission of *O* I 8446 and the Paschen series.

The first group is well represented by 48 Lib, ζ Tau, 28 Tau, and MWC 394. In addition, 66 Cyg has weak *O* I 8446 emission. MWC 394 possesses double emission of the Paschen series with the violet component somewhat stronger, the same as is observed

* *Contributions from the McDonald Observatory, University of Texas*, No. 132.

[1] *Ap. J.*, **79**, 183, 1934; see also *Pub. A.S.P.*, **37**, 272, 1925.

[2] *Ap. J.*, **80**, 19, 1934.

[3] See *Ap. J.*, **98**, 131, 1943; Swings, *Pub. A.S.P.*, **56**, 238, 1944; Keenan and Hynek, *Ap. J.*, **101**, 265 and 270, 1945; Greenstein and Merrill, *Ap. J.*, **104**, 177, 1946.

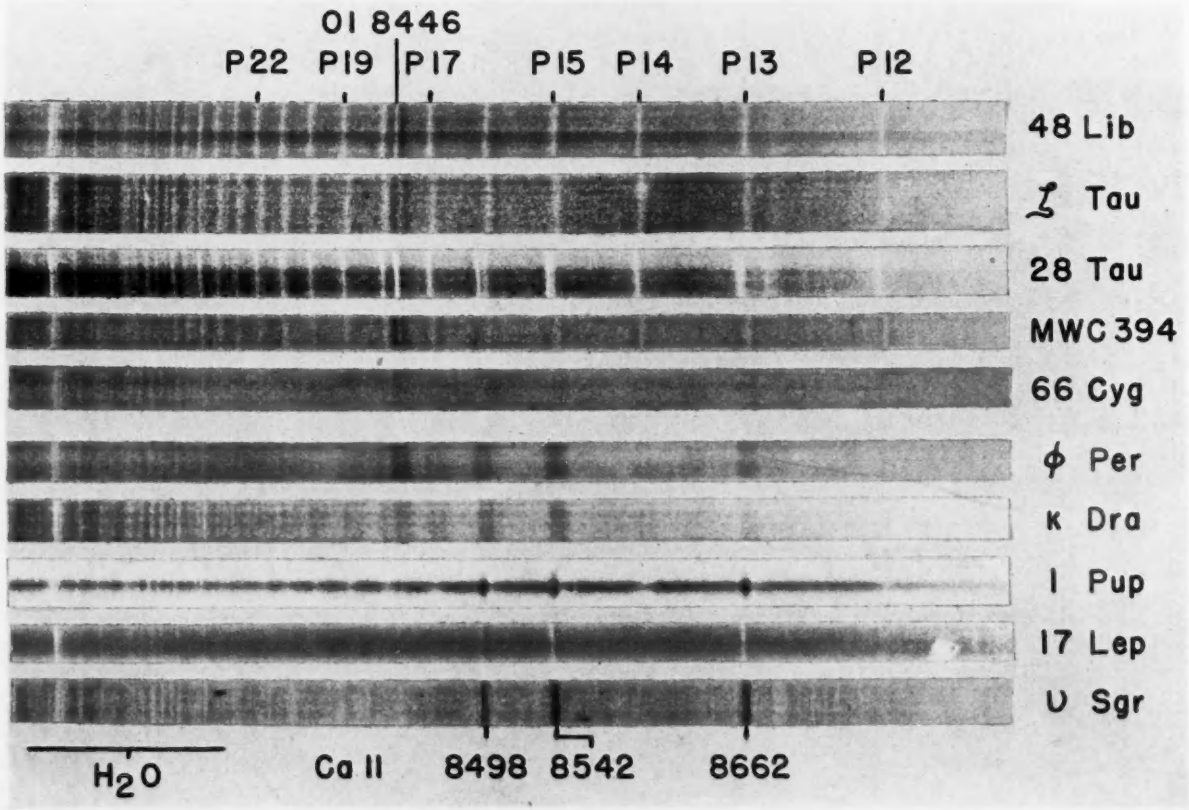
O I 8446
P22
P19
P17
P15
P14
P13
P12
48 Lib
ζ Tau
28 Tau
MWC 394
66 Cyg
φ Per
κ Dra
I Pup
17 Lep
υ Sgr
H2O
Ca II
8498
8542
8662

FIG. 1

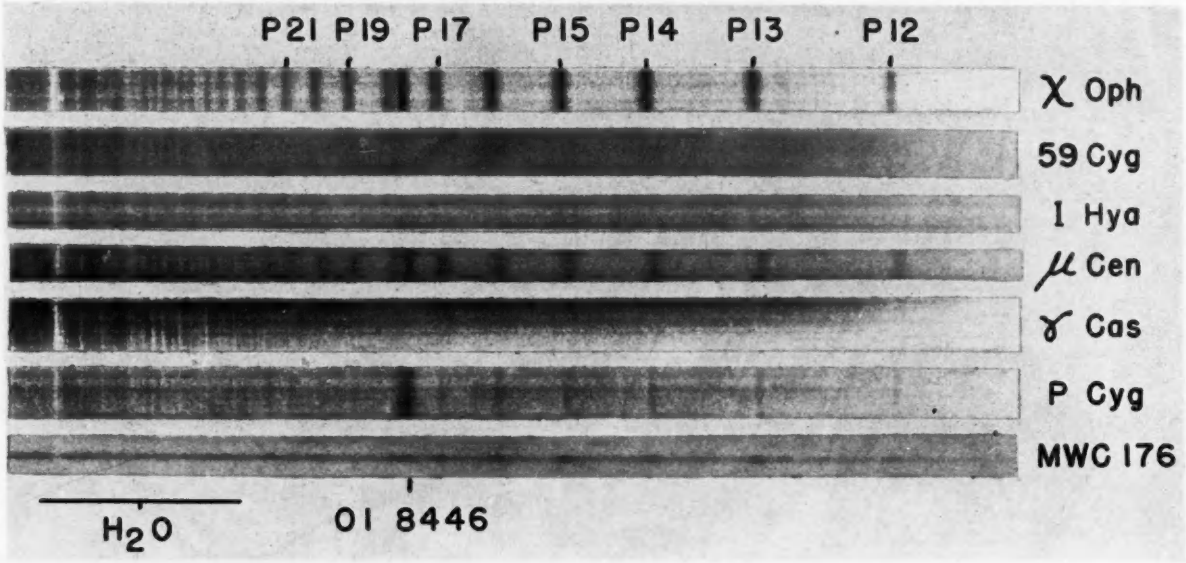
P21 P19 P17 P15 P14 P13 P12
χ Oph
59 Cyg
1 Hya
μ Cen
γ Cas
P Cyg
MWC 176
H2O
O1 8446

FIG. 2

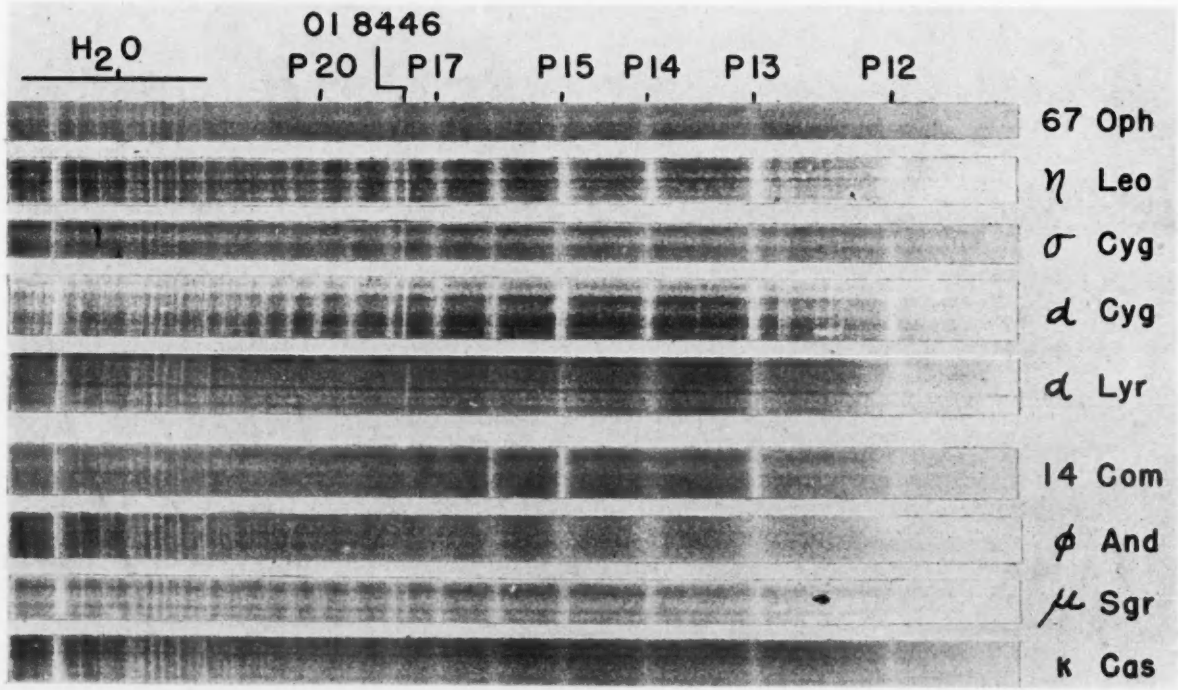
H2O
01 8446
P20
P17
P15
P14
P13
P12
67 Oph
η Leo
σ Cyg
d Cyg
α Lyr
14 Com
φ And
μ Sgr
κ Cas

FIG. 3

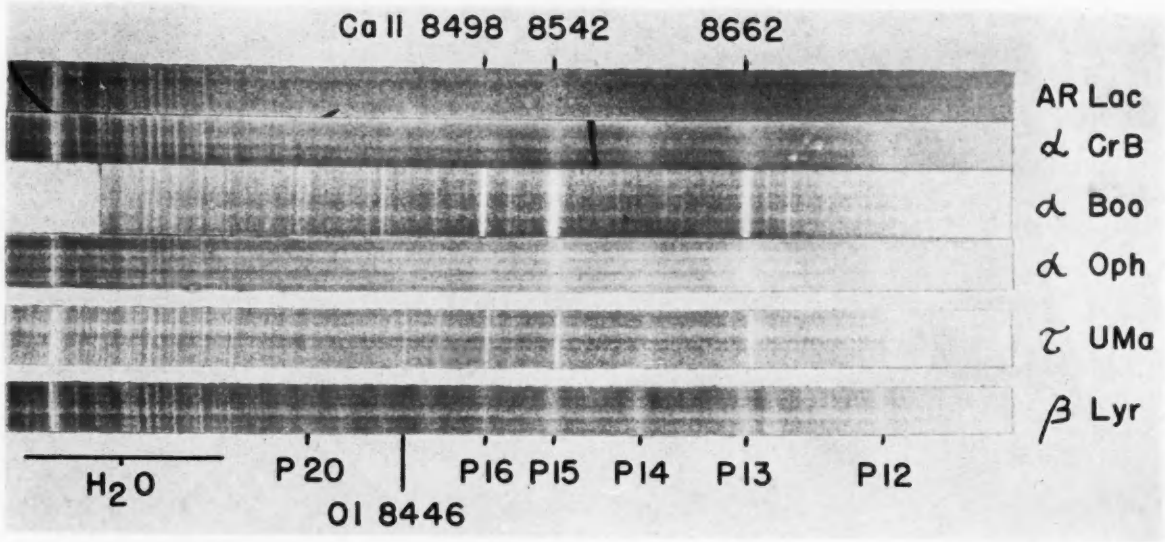
Ca II 8498
8542
8662
AR Lac
α CrB
α Boo
α Oph
τ UMa
β Lyr
H2O
P20
O1 8446
P16
P15
P14
P13
P12

FIG. 4

for *O* I 8446. In the two cases investigated (48 Lib and ζ Tau), the *O* I 7773 blend was present strongly in absorption without emission. Attention should be called to the relatively diffuse character of the Paschen series of hydrogen in the shells of 28 Tau, 48 Lib, and ζ Tau, relative to the Balmer series.[4]

The second group of stars is represented by l Pup, 17 Lep, and v Sgr. In the last star *Ca* II emission was first announced by Weaver.[5] In 17 Lep the *Ca* II emission is accompanied by strong violet absorption, and *O* I 8446 is in absorption. The spectrogram of 17 Lep did not reproduce well because the original spectrogram was overexposed.

The third group, showing emission of both *O* I and *Ca* II is represented by ϕ Per and κ Dra. The infrared spectra of the two stars are almost identical, except that *O* I 8446 is somewhat stronger in ϕ Per than in κ Dra. Both stars show weak hydrogen emission and possibly other emission features. In ϕ Per, *O* I 7773 is in absorption, flanked on either side with weak emission. *O* I 7773 is very weak in emission in κ Dra.

TABLE 1

JOURNAL OF OBSERVATION

Plate	Date	Objects	Plate	Date	Objects
Cir 5....	1946 Apr. 22	α Boo	Cir 78....	1946 May 11	l Pup
15....	24	ζ Tau	91....	14	σ Cyg, α Oph, MWC 394
29....	27	α Cyg, α Lyr			
34....	29	τ UMa	101....	16	I Hya, μ Cen
42....	30	48 Lib	117....	20	MWC 176
47....	May 1	P Cyg, 14 Com	152....	Sept. 12	β Lyr, α CrB
59....	6	χ Oph, μ Sgr, 59 Cyg, ϕ Per	153....	12	κ Cas, AR Lac
			154....	12	28 Tau, ϕ And, γ Cas
62....	7	η Leo, κ Dra			
64....	7	66 Cyg	155....	12	17 Lep
69....	9	67 Oph, v Sgr			

The last group of stars has single *O* I emission, in addition to emission in the Paschen series. Typical examples are χ Oph, μ Cen, and MWC 176. Other stars with less well-defined emission are 59 Cyg, I Hya, and γ Cas. The structure of the emission in these stars is not well defined, but the Paschen emission in I Hya and γ Cas is probably double. P Cyg is shown on the reproduction for comparison purposes. The stars χ Oph and μ Cen were investigated in the region where *O* I 7773 is located, and in both cases the emission at *O* I 7773 is much weaker than *O* I 8446. This is in agreement with estimated intensities in P Cyg, published by Swings,[6] when allowance is made for the greater blending of the emission and absorption at O I 7773 in our spectrograms than those used by Swings.

The presence of *Ca* II 8498, 8542, 8662 emission when the *Ca* II H and K lines are in absorption; the presence of *O* I 8446 emission when *O* I 7773 is in absorption; and the presence of very strong *O* I 8446 absorption in a shell spectrum, especially 28 Tau, are all intriguing problems. An attempt was made by Wyse[7] to explain the presence of the *Ca* II triplet emission in Me variables[8] when H and K were in absorption. The mechanics is that of depopulation of the ^{2}D state by ionization by Lyman-α quanta. This process has been discussed recently by Greenstein and Merrill[9] in connection with v Sgr. In this con-

[4] For reproductions of the spectra of 28 Tau and 48 Lib see Struve and Swings, *Ap. J.*, **97**, 426, 1943; and Struve, *Ap. J.*, **98**, 98, 1943.

[5] *Ap. J.*, **98**, 131, 1943.

[6] *Pub. A.S.P.*, **56**, 238, 1944.

[7] *Pub. A.S.P.*, **53**, 184, 1941.

[8] Merrill, *Ap. J.*, **79**, 197, 1934.

[9] *Op. cit.*, p. 188.

nection attention must be called to the paper recently published by Keenan and Hynek[10] on the presence of absorption lines of *O* I in VV Cep. The presence of *O* I absorption in VV Cep is anomalous, and Keenan and Hynek explained its presence by assuming that the *O* I atoms were excited by the intense continuous ultraviolet diluted radiation from the B-type star. The question now arises as to why the *Ca* II triplet is so strong in absorption in VV Cep if the radiation field from the B-type companion is so intense in the far ultraviolet and if the mechanism proposed by Wyse is operating. From the present observations of the behavior of *O* I and *Ca* II in shell and emission-line stars, we can conclude that the mechanisms involved are not at present understood. For example, the nonmetastable *O* I 8446 is remarkably strong in absorption in the shell of 28 Tau. Also, in χ Oph and μ Cen, *O* I 8446 is much stronger in emission than *O* I 7773. This may be a consequence of the partial metastability[11] of the lower level of *O* I 7773, which tends to favor *O* I 7773 in absorption relative to *O* I 8446. This does not, of course, account for the absence of emission on either side of the *O* I 7773 absorption in such stars as ζ Tau and 48 Lib; a recombination process is present where the 3^3P state is favored relative to the 3^5P state.

Figure 3 shows a number of high-luminosity stars of early spectral type. For comparison purposes α Lyr is also shown. The diffuse character of the Paschen series in the high-luminosity stars is noteworthy. On the same plate three stars (ϕ And, μ Sgr, κ Cas) with bright $H\alpha$ are shown. The shell star of latest type, 14 Com, is also shown in Figure 3. The characteristic features are strong absorption lines of the *Ca* II triplet and diffuse absorption lines of the Paschen series.

Figure 4 shows a spectrogram of τ UMa, a metallic-line A star. In general, the infrared spectrum agrees well with that of the photographic region. There is, however, possibly one exception. The intensity of the *Ca* II triplet has been compared with β Leo, A3V; and the triplet appears to be more intense in τ UMa, although the intensity of the K line in τ UMa corresponds to an A3 star.

In late-type stars the *Ca* II triplet is very strong in absorption and may provide an opportunity to observe the late-type companions of binary systems, especially eclipsing stars, where it is particularly important to know the mass ratios.[12] A spectrogram of α CrB was obtained during maximum light and is reproduced in Figure 4, along with spectra of α Boo and α Oph. There is slight evidence that *Ca* II 8542, the strongest line of the triplet, is present. The lines *Ca* II 8542 and *O* I 8446 are certainly present in β Per (spectrum not reproduced), but they probably have their origin in the primary star. The two stars α CrB and β Per are not favorable cases because of the relative faintness of the companions (in the photographic region the secondary star of β Per[13] contributes 7.5 per cent of the total light; the secondary of α CrB contributes even less); and positive results may be obtained when more favorable systems are investigated.

A spectrogram of AR Lac was obtained which is of interest. This eclipsing variable consists of two late-type stars, a K0 and a G5, and has a period of 2.0 days. The lines *Ca* II H and K are strong in absorption, with a sharp, moderately strong emission arising from the secondary star. The *Ca* II triplet, however, is much weaker in absorption than anticipated, suggesting that the *Ca* II triplet lines are nearly filled with emission. The spectrograms reproduced in Figure 4 were taken during maximum light.

A spectrogram of β Lyr taken at phase 2.1 days is reproduced in Figure 4. The Paschen series is well defined, and *N* I is well represented. A second spectrogram of poorer quality taken on May 1, phase 11.4 days, shows the Paschen series to be more diffuse, but the character of *N* I remained the same. The line *O* I 8446 is very weak, if present.

[10] *Op. cit.*, p. 270.

[11] *Ibid.*, p. 272.

[12] For a discussion of the mass ratios of eclipsing binaries see O. Struve, *Ap. J.*, **104**, 279, 1946.

[13] See Stebbins, *Ap. J.*, **53**, 116, 1921.

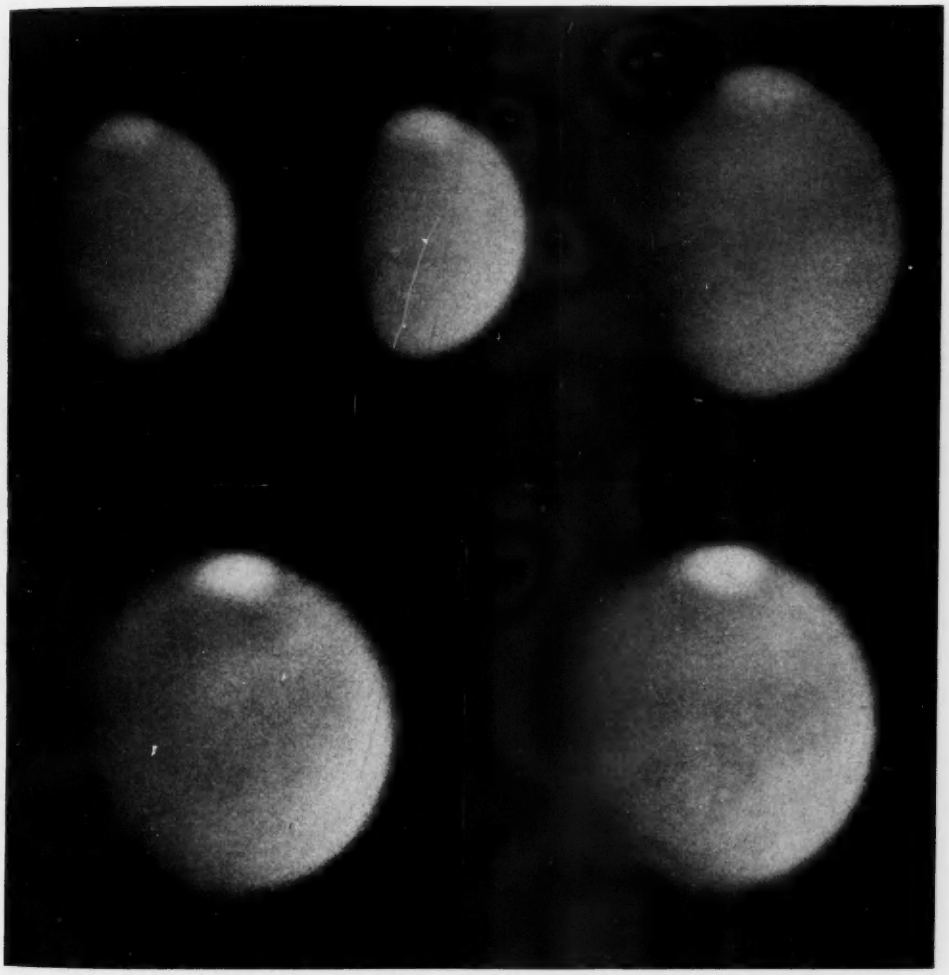

FIG. 1.—*Above:* 1909, July 14, $10^h \pm$ U.T. (4), (4); 1909, Aug. 16, $9^h \pm$ U.T. (3). *Below:* 1909, Aug. 18, 7:27 U.T. (3); 1909, Aug. 18, 8:08 U.T. (5). *1*, visual observations show detached part of polar cap to left; *2*, detached spot suspected on photographs of this date but seen plainly visually.

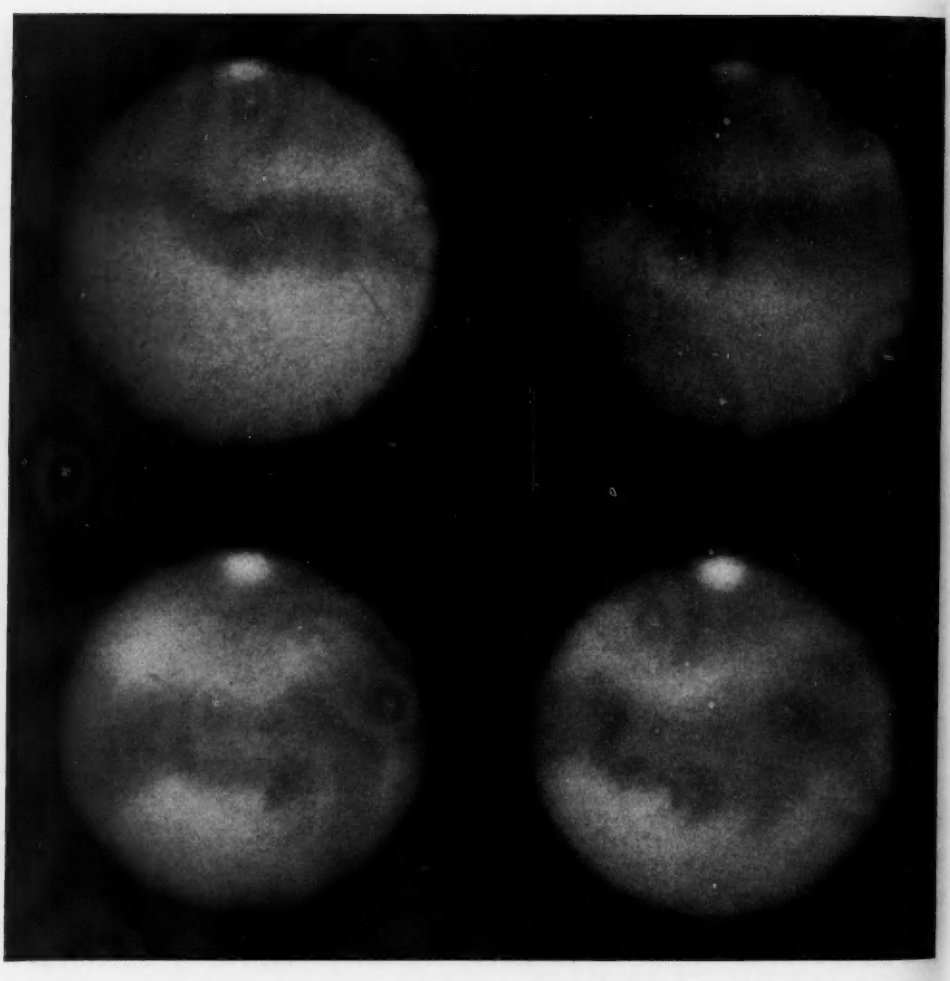

FIG. 2.—*Above:* 1909, Sept. 8, 7:32 U.T. (3), (4). *Below:* 1909, Sept. 25, 4:55 U.T. (3); 1909, Sept. 25, 6:17 U.T. (3).

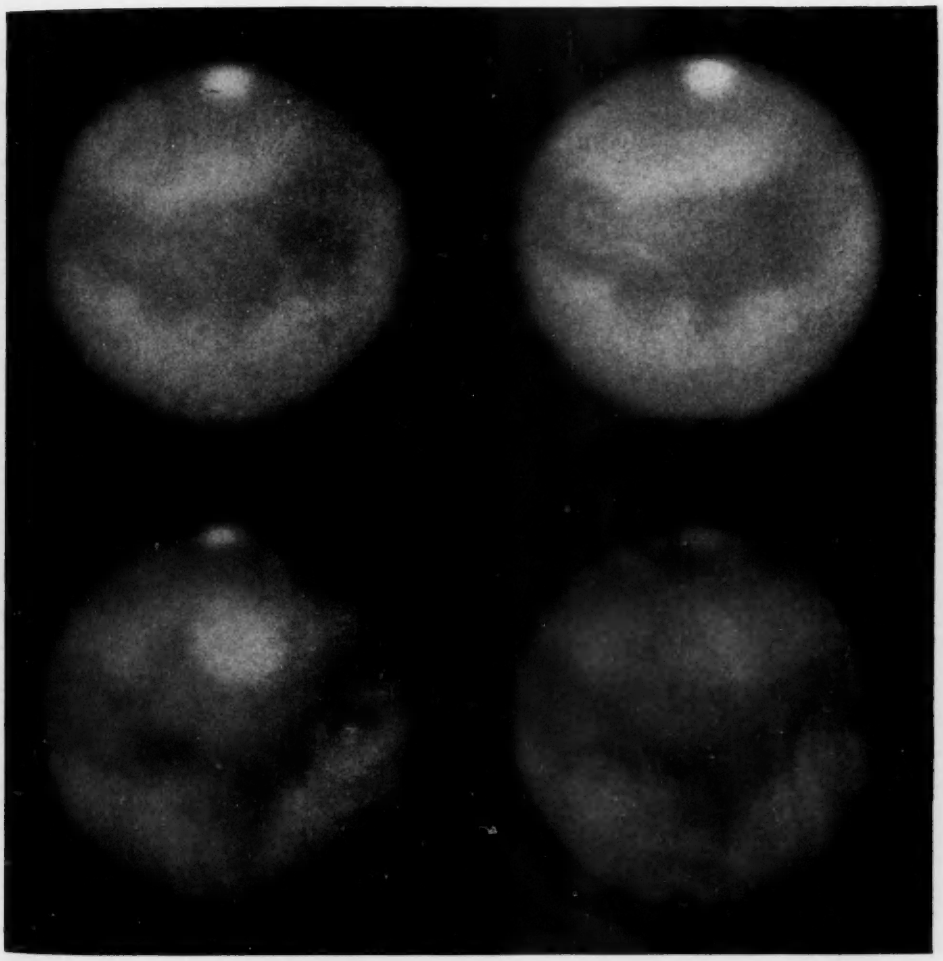

FIG 3.—*Above:* 1909, Sept. 25, 7:10 U.T. (3), (3). *Below:* 1909, Sept. 29, 3:25 U.T. (5), (4)

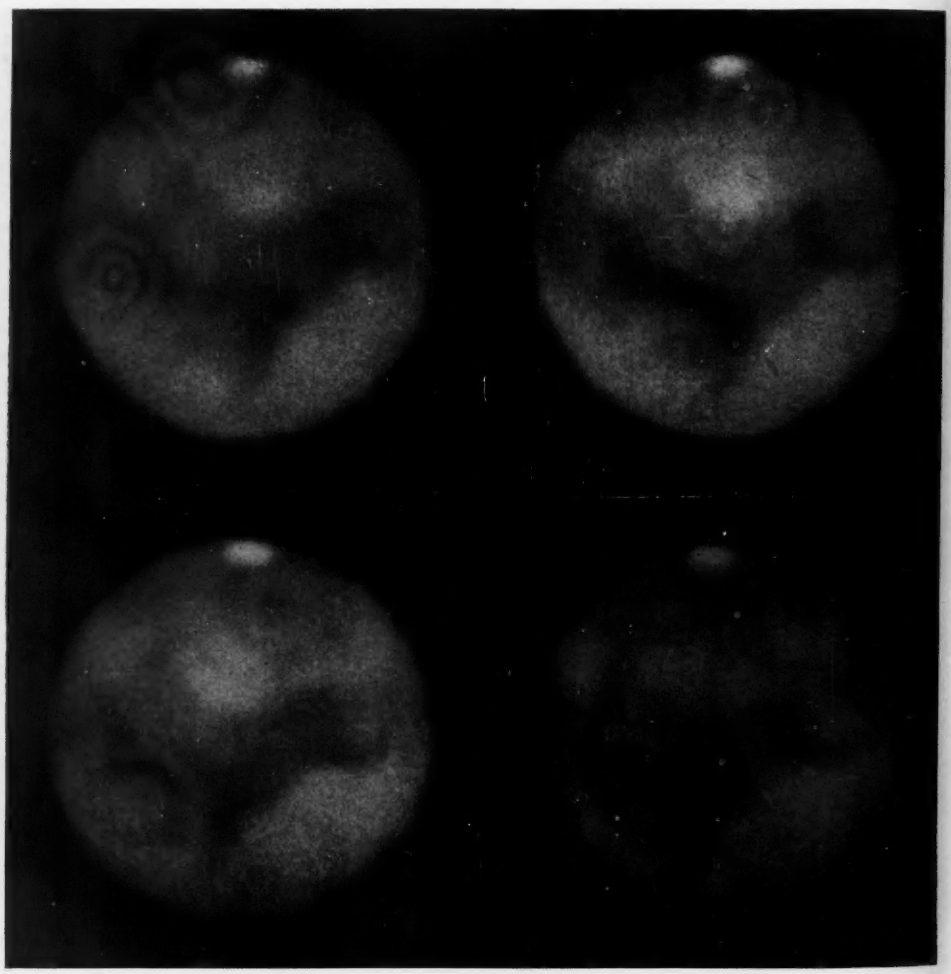

FIG. 4.—*Above:* 1909, Sept. 29, 3:45 U.T. (3), (3). *Below:* 1909, Sept. 29, 4:25 U.T. (4), (3)

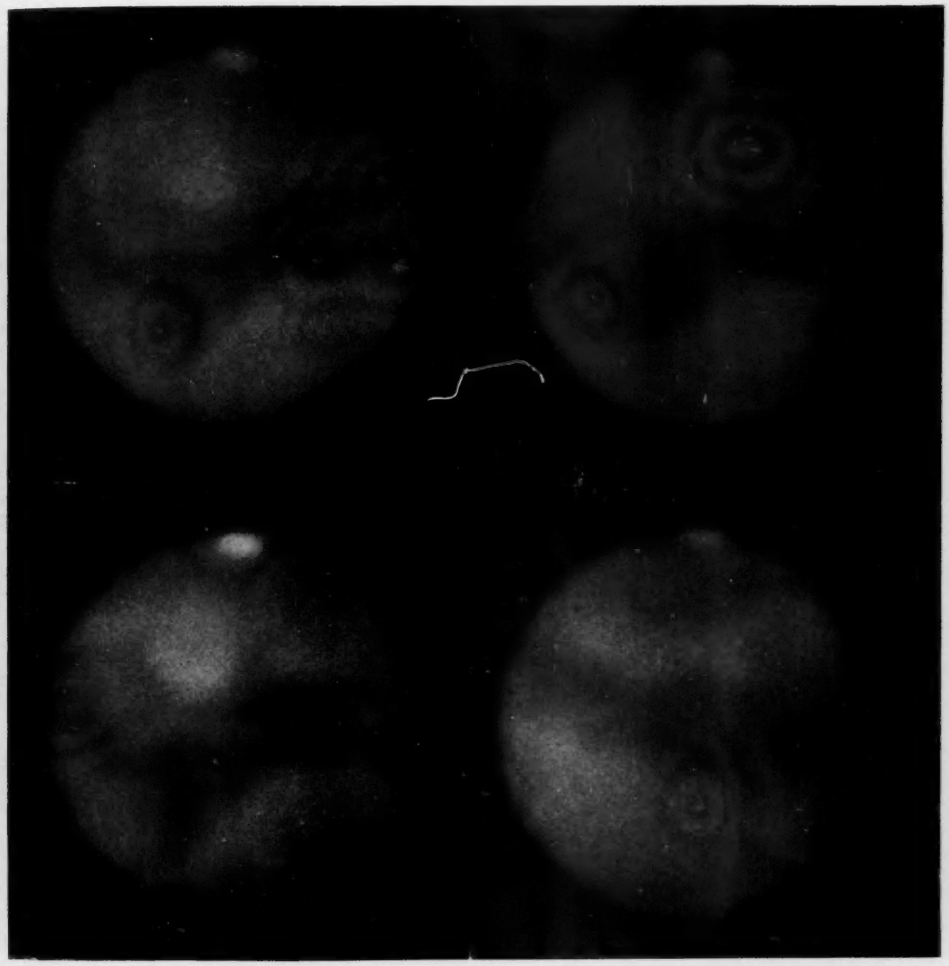

FIG. 5.—*Above:* 1909, Sept. 29, 4:47 U.T. (4); 1909, Sept. 29, 5:00 U.T. (4). *Below:* 1909, Sept. 29, 5:00 U.T. (5); 1909, Oct. 6, 4:15 U.T. (3).

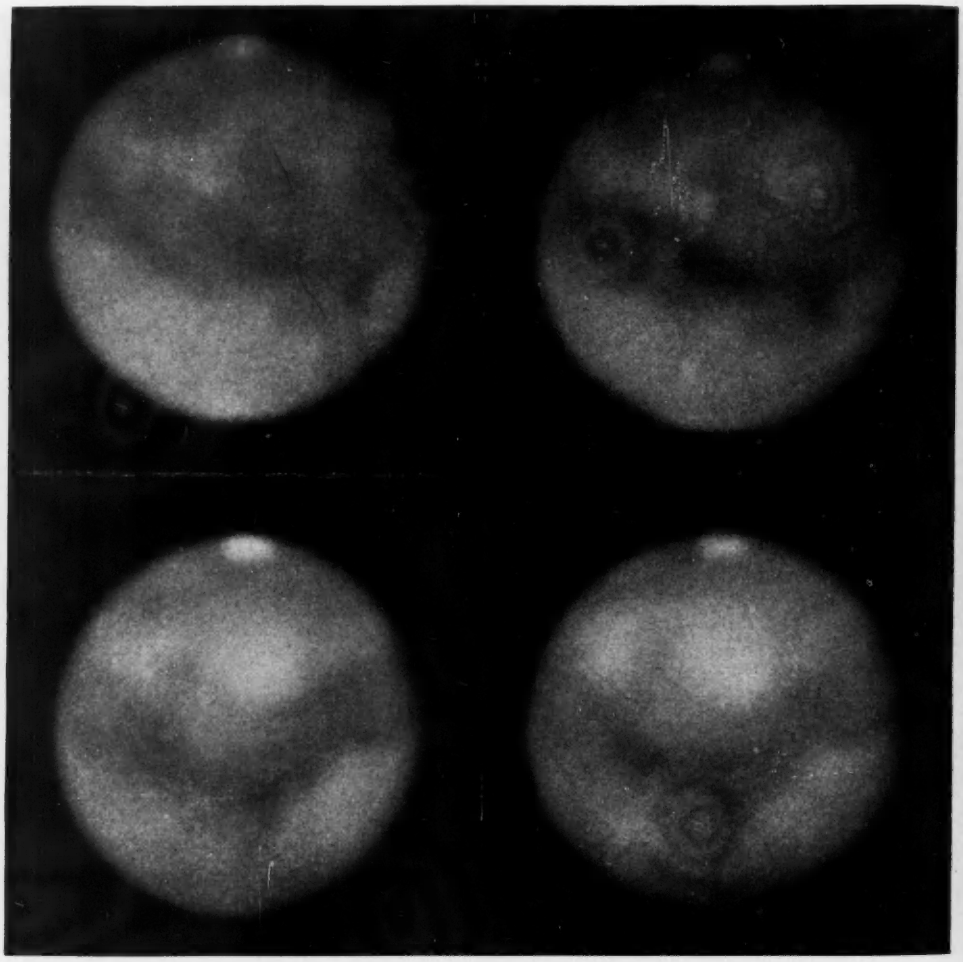

FIG. 6.—1909, Oct. 2. *Above:* 3:25 U.T. (3); 3:52 U.T. (3). *Below:* 5:17 U.T. (3); 5:35 U.T. (3)

NOTES

BARNARD'S PHOTOGRAPHS OF MARS

During the 1909 opposition of Mars, Professor Barnard obtained a fine series of Mars photographs with the Yerkes refractor. He published copies for two dates only, September 24 and 28, 1909,[1] which have been widely reproduced in textbooks. In view of the improvements which may be made by combining several images into a single reproduction, it was considered desirable to present a more complete account of Barnard's photographs.

The negatives were Cramer Isonon or Cramer Instantaneous Iso plates exposed through a yellow filter made by Wallace. A Brashear enlarging lens magnified the 40-inch image about two and a half times on the plate. The reproductions shown here make the angular scale of all images about the same. The legends give the date and approximate U.T.; in some cases no precise time record was available. The number of images combined into each print is given in parentheses.

Barnard's original Plate 9[1] corresponds to our Figure 2 (3); his Plate 10 to our Figure 5 (1). The present reproductions are viewed best from a distance of 3–4 feet, giving a magnification of about 400 diameters; a similar power is the optimum for seeing the half-tones visually. Figures 1–6 show the gradual shrinking of the polar cap, as well as the fact that it is not centered on 90° (Fig. 2), and also the general haze in the Mars atmosphere, lasting until nearly the end of September.[2]

The most important contribution of the photographs is, of course, the correct representation of the half-tones, which drawings rarely bring out. For comparison purposes, reference is made to the fine drawings by Antoniadi,[2,3] which include four made from photographs of the same opposition, sent to him by Barnard and Hale.[4]

GERARD P. KUIPER
MARY R. CALVERT

YERKES OBSERVATORY
November 18, 1946

[1] *M.N.*, **71**, 471, 1911.

[2] Cf. E. M. Antoniadi, "Report on Mars, 1909," *Mem. B.A.A.*, **20**, 34, 1916.

[3] *La Planète Mars*, Pl. VI, 1930.

[4] *M.N.*, **71**, 714, 1911. Figs. 1 and 2 correspond to our Figs. 2–5.

REVIEWS

The Earth and the Stars. By C. G. ABBOT. New York: D. Van Nostrand Co., Inc., 1946. Pp. 288+xii. $3.75.

This is the second revised edition of a popular book published by its distinguished author in 1925.

Higher Mathematics for Students of Chemistry and Physics. By J. W. MELLOR. New York: Dover Publications, 1946. Pp. 641+xxi. $4.50.

This is a reprint of a well-known work which has served generations of physicists, chemists, and astronomers in their introduction to mathematical methods and reasoning. Since there are now other competing books in the field which also include the mathematical methods of the quantum theory, it is possible that the value of the book is not so great as it was when it was first published early in this century. But it is always nice to have a classic, such as the one under review, available.

Scientific Instruments. Edited by HERBERT J. COOPER. New York: Chemical Publishing Co., Inc., 1946. Pp. 304. $6.00.

As the title implies, this book gives a brief discussion of many scientific instruments and can be adequately reviewed by quoting from the Preface.

"Scientific instruments are here described in a way that may be understood by the non-specialist, so that the worker in one field may get a useful idea of the instruments used in another. The book does not set out to tell the specialist about his own equipment but about the other man's."

It is the reviewer's opinion that the goal outlined in the Preface has, in general, been achieved. The book is divided into five sections. The first section, on optical instruments, contains a chapter each on lenses, cameras, the microscope and electron microscope, polarimeters, photometers, range finders, refractometers and interferometers, spectroscopes and telescopes. The second section is on measuring instruments, with chapters on density, dimension, electrical, fluid, pressure, temperature, time, speed, and weight. The third section, consisting of six chapters, pertains to navigational and surveying instruments. The fourth section is on liquid-testing and viscosity measurements. The fifth section is reserved for miscellaneous instruments.

Astronomers are familiar with most of the instruments discussed, and the volume will probably not be especially useful to the professional astronomer. It should, however, be valuable to beginning students in astronomy or the other physical sciences.

W. A. HILTNER

Yerkes Observatory

ERRATUM

In Volume **104,** page 272, seventh line from the bottom, instead of "violet," read "red."